A STUDY OF CHARGE MOTION IN ROTARY MILLS,

WITH PARTICULAR REFERENCE TO THE GRINDING ACTION

MALCOLM S. POWELL

A STUDY OF CHARGE MOTION IN ROTARY MILLS,

WITH PARTICULAR REFERENCE TO THE GRINDING ACTION

MALCOLM S. POWELL

Thesis presented for the degree of

DOCTOR OF PHILOSOPHY

In the Department of Mechanical Engineering

UNIVERSITY OF CAPE TOWN

March 1993

ACKNOWLEDGEMENTS

Thanks are due to Mintek, and especially Dr P.T. Wedepohl, the support of whom has been extensive and essential to this work. Mr F.S Cornelius, Mr W. Dibetso, and Miss M. Coetzee assisted with the experimental work, for which I am most grateful. Dr L.A. Vermeulen is to be thanked for his considerable interest and his suggestions on data analysis, especially with the milling trials. Dr Hinde has also contributed suggestions and provided support. The staff of the Engineering Services Division of Mintek are thanked for their patience with constructing and amending the experimental apparatus, and for the high quality of their work.

The staff of Groote Schuur Hospital were very helpful, and especial thanks must go to Miss N. Blythey of cardiology, and Mr J. Boniaszczyk of nuclear medicine for their enthusiasm and hours of assistance. Ms S. Brock and Prof. P.J. Commerford of cardiology also rendered extensive and generous assistance. Without their assistance this work would not have been possible. I am also indebted to my wife, Frances, and father, Terence, and to N. Cowley for their assistance with the final compilation. Finally thanks are due to my supervisor, Prof. G.N. Nurick, for his assistance and suggestions.

ABSTRACT

The objective of this study was to develop a fundamental understanding of the action of the grinding charge in a mill, and to then correlate this with the metallurgical performance of different mill-liners. To achieve these overall objectives it was first necessary to develop suitable experimental techniques, and the development of these techniques became a large part of the objective of the study.

The motion of balls deep within the charge of a rotary grinding mill was investigated. Novel investigative techniques were used to track the motion of the balls, including X-ray filming at 50 frames per second of both the front and side views of a transparent mill, and gamma-camera filming of a radioactive ball. Analysis of the trajectories of the balls revealed several phenomena in the milling action that have not been reported until now.

It was observed that the paths of the balls are smooth, that they spiral in and out of the charge, and that the grinding does not take place by rotary nipping of the ore between the balls. The centre of mass of the entire charge was determined, and was found to provide the correct form of the torque curve when the simple torque-arm method was used. The angle of repose of the charge was found to be uniquely defined by the centre of circulation of the charge. The face angle of the lifter bars was found to influence both the maximum impact energy and the amount of work done by the charge. Radial segregation takes place throughout the charge according to both the mass and size of the balls, even in a mill with smooth end faces.

Milling trials were conducted in a 1.8 m diameter batch mill run in the autogenous mode, in an attempt to assess the influence of the liner design on the rate of production of fines. The results of the milling experiments were then correlated with the motion of the grinding media in a mill. It was established that changes in liner design can cause variations of up to 40% in the rate of production of fines and the energy efficiency of a mill. The correct height and spacing of the lifters are intimately interrelated, and different configurations to those reported in the literature were found

to be optimal. With the correct liner design, it should be possible to minimize the energy consumption while maximizing the milling rate.

SUMMARY

The objective of this study was to develop a fundamental understanding of the action of the grinding charge in a mill, and to then correlate this with the metallurgical performance of different mill-liners. To achieve these overall objectives it was first necessary to develop suitable experimental techniques, and the development of these techniques became a large part of the objective of the study.

The motion of balls deep within the charge of a rotary grinding mill was analyzed. This was an extension of earlier work in which the influence of liner design on the motion of the outer grinding media was modelled. Novel investigative techniques were used to track the motion of the balls, including X-ray filming at 50 frames per second of both the front and side views of a transparent mill, and gamma-camera filming of a radioactive ball. These films enabled the trajectories of the balls to be tracked over many revolutions of the mill, and for a wide range of mill speeds and liner configurations. The interactions within the charge and the location and shape of the charge are described. Analysis of the trajectories revealed several phenomena in the milling action that have not been reported until now.

The trajectories of the balls are surprisingly smooth, even for those deep within the charge. It was found that the balls do not rotate about their own axes, and therefore grinding does not take place by rotary nipping of the ore between the balls. The balls spiral in and out of the charge in a way that implies good mixing of the charge. The actual centre of mass of the charge was determined, and was found to provide the correct form of the torque curve when the simple torque-arm method of calculation was used. The amount of slip within the charge is independent of the liner configuration once the charge is keyed into the rotary motion of the mill. The angle of repose of the charge was found to be uniquely defined by the centre of circulation of the charge. The face angle of the lifter bars was found to influence both the maximum impact energy and the amount of work done by the charge. The maximum work was done by the balls in the inner half of the cascading region, which corresponds to the region of maximum interaction between the balls. It was found that radial segregation

takes place throughout the charge according to both the mass and the size of the balls, even in a mill with smooth end faces. This effect depends strongly on the mill speed, and there are different 'neutral' speeds at which no segregation by size or mass is apparent. The design of the liner appears to influence the segregation of the charge to some extent.

Milling trials were conducted in a 1.8 m diameter batch mill run in the autogenous mode, to assess the influence of liner design on the rate of production of fines. A reproducible sampling technique was established for assessing the mass of fines in the mill at any time during the run. The torque of the mill was measured by strain gauges attached to the drive shaft. The results of the milling experiments were then correlated with the motion of the grinding media.

It was established that changes in the liner design can cause variations of up to 40% in the rate of production of fines and the energy efficiency of a mill. The height and spacing of the lifters are intimately interrelated, and different configurations to those reported in the literature were found to be optimal. The torque drawn by the mill changed dramatically during a batch test, and this was concluded to arise from the substantial change in the composition of the charge with milling time. The power draw was concluded to be principally a function of the mass of grinding media, when in the 'normal' operating range, as opposed to the total mass of the charge. With the correct liner design, it should be possible to minimize the energy consumption while maximizing the milling rate. The liner must have a sufficiently high profile to key in the outer layer of charge to the rotary motion of the mill, but a profile that is too high reduces the efficiency of the mill. The profile of the lining can also be designed to optimize the impact point of the charge, which will increase the maximum impact energy and the work done by the charge.

NOMENCLATURE

THEORETICAL STUDY

General variables

a	Rod radius
α	Angular acceleration of the ball
D	Internal diameter of the mill
δ	$\sin\alpha(R-h) - a \equiv$ a constant
f	Frictional force between ball and lifter face
F	Resultant force on the ball
g	Gravitational acceleration (9.8 $m.s^{-2}$)
h	Radial height of lifter bar
h'	Perpendicular height of lifter bar
h''	Perpendicular distance from mill shell to top of lifter bar
I	Moment of inertia of ball
m	Mass of ball
N	Normal force exerted by lifter on ball
R	Internal radius of mill
r	Radial location of the centre of the ball
$\vec{r}$	Vector from centre of mill to centre of ball
r_o	R - a
s	$r.\cos\beta$
$\vec{s}$	Vector directed from tip to base of lifter bar
$\dot{s}$	Linear velocity of ball up lifter face
$\ddot{s}$	Linear acceleration of ball up lifter face
t	time
T	Torque
μ_s	Static coefficient of friction, between ball and lifter bar
μ_k	Kinetic coefficient of friction, between ball and lifter bar
v	Net velocity of the ball, in cartesian coordinate system
Ω	Angular velocity of the mill
x	horizontal cartesian coordinate of the centre of the ball

y	vertical cartesian coordinate of the centre of the ball
Y	Half the width of the base of the lifter bar
$\perp$	Perpendicular
$\parallel$	Parallel

Angles

α	Between lifter face and radial line passing through the tip of the lifter
β	Between radius vector to ball and lifter face
ε	At base of lifter, between radial vector and lifter face
γ	Dynamic angle of lifter face, subtended by s and x axis
ϕ	Angular location of the ball.
ψ	Subtended at centre of mill, between lifter tip and lifter centre
ρ	Face angle of lifter, From the base of the lifter to the face.
σ	Angle of ball's velocity vector
θ	Angular displacement of the tip of the lifter
ξ	Subtended at mill centre, between lifter tip and the centre of the ball

Subscripts

$_o$	Point of equilibrium
$_L$	Tip of lifter
$_{cm}$	Centre of mass
$_m$	Maximum
$_l$	Transition point from rolling to sliding
$_p$	Point of contact between ball and lifter face
$_x$	In x direction
$_y$	In y direction
$_E$	Point at which ball strikes mill shell
$_\parallel$	Parallel to
$_\perp$	Perpendicular to
$_r$	Radial component

MILLING TRIALS

γ	Fraction of fines in the sand
fines	Material finer than 75μm
F	Fractional slurry filling just sufficient to fill the voids
m	Mass of sample
M	Mass of solids in the mill
P	Percentage filling of the mill with charge
ρ	Density of the slurry
ρ_R	Density of the rock
sands	Solids small enough to pass through the sampling valve
t	Milling time
θ	Time constant for production of fines
τ	Time constant for the decay of the torque
T	Torque
v	Volume of sample
V	Volume of material in the whole mill

Subscripts

$_\infty$	infinite time
$_f$	Fines
$_o$	At zero time, the beginning of the batch milling run
$_R$	Rocks
$_{sample}$	Sample of slurry taken from the mill
$_{sands}$	Sands in the sample
$_T$	With reference to the torque

GLOSSARY

Centre of circulation, CoC The axial line about which the charge rotates, this is off-set from the centre of the mill.

Charge The grinding media and slurry in a mill.

Critical speed The rotational speed of the mill at which the gravitational and centrifugal forces acting on a particle against the mill shell, at the top of the mill, just balance. The particle would theoretically centrifuge at this speed.

Equilibrium surface The zone that separates the ascending and descending media in the mill.

Fines The ground material that is of the desired final size, < 75μm in this work.

Fractional slurry filling Volumetric fraction of the total charge that is slurry.

Grid liner A pocketed liner block that traps balls or pebbles to form a composite type lining.

Lifter, lifter bar A narrow bar of liner protruding into the mill. This forms a profile to the lining that keys in the charge. The bars run along the length of the mill, and can either be separate or integral to the mill lining blocks.

Percentage critical The rotary speed of the mill expressed as a percentage of the critical speed. This is a useful terminology, as mills of different sizes can be directly compared on this basis.

DH ratio The ratio of the inner diameter of the mill to the height of the lifter bar.

SH ratio The ratio of the spacing between lifter bars to their height.

RoM mills Run-of-mine mills, the South African term for autogenous grinding mills.

Shoulder of charge The uppermost section of the bulk en-masse charge, from which point the media is projected into flight, or cascades down on the charge.

Toe of charge The highly active zone at the base of the cascading region where the descending media impacts upon the rest of the charge and is drawn back into the rotary motion of the mill.

Trommel A rotary screen used for sorting rocks into separate size fractions.

CONTENTS

LIST OF FIGURES

LIST OF TABLES

CHAPTER 1
INTRODUCTION

1.1. OVERVIEW

The comminution of ores is a vital link in the processing and extraction of the world's minerals. Rotary mills are a commonly used comminution device, and the many thousands of mills in the world, which all operate on the same principle, must span the range from coarse primary grinding to fine tertiary reduction. Primary autogenous or semi-autogenous mills are capable of carrying out reduction of 300 mm rocks down to 80% passing a final size anywhere in the range from 75 μm to 2000 μm, depending upon the application. Tertiary mills, on the other hand, are used to grind 500 μm material down to a final product of 20 μm.

Mills vary in both diameter and length in the range from 12 m down to less than 2 m. The aspect ratio, ratio of diameter to length, varies from 3:1 right to the other extreme of 1:5. The grinding media in the mills can be anything from 25 mm to 125 mm steel balls, to 300 mm rocks, to rods running the length of the mill. The mills can be run dry, or wet with a wide range of slurry viscosities. The speeds of the mills, expressed in percentage of critical speed (where 100% is the speed at which the outer charge would theoretically centrifuge), vary from 60% to 100%. The mills discharge through central trunnions, peripheral grates or pebble ports, or even fully open-end screens. The ore can pass through once in an open-circuit mill, or the oversize material can be recirculated in a closed-circuit mill, or the mill can even be run in a batch mode. The filling of the mills can range from 20% of mill volume up to 50%.

The development of this wide variety of mills has mainly been via step-wise increments, based on operator experience and empirical results derived from testwork on both full-scale and pilot mills. Extensive work has been carried out on establishing an understanding of the fundamentals of the fracture of ore, so as to improve the understanding of comminution. However, mill design still cannot be carried out from first principles and is based on previous experience or pilot work. The scale-up from small pilot mills to full size production mills introduces a significant degree of

uncertainty, despite the great deal of research that has been conducted in this area. This is essentially because of the wide gaps in knowledge of the fundamental forces active in the milling process.

Milling is in essence carried out by a large number of random interactions within the tumbling media in the mill. These can range from relatively soft rubbing of the surface of a rock, to high-stress compression of particles, to severe impacts from falling media. It is the frequency, severity, and relative intensity between the different forms of reduction, that ultimately determine the reduction action of the mill. However, this aspect of milling is poorly understood, and without this knowledge one cannot reliably predict the breakage characteristics of a particular ore in a mill. It remains for pilot-scale testwork to be carried out on every ore-body to be able to design a mill for a particular application with any degree of certainty.

The motion of the grinding media in the mill determines the balance of the grinding forces. This charge motion is primarily a function of the speed and size of the mill, the type of media, the slurry viscosity, and the design of the mill liners. It was felt that this fundamental aspect of milling represented a large gap in knowledge, that would always hamper the search for a full understanding of how comminution takes place in rotary mills. This in turn would limit the ability to design mills reliably, increasing the cost of testwork and adding to the cost of mill construction, as a considerable safety margin must always be built in to the mill sizing and power. Without a proper understanding of how they function it is also more difficult to optimise the efficiency of mills, which in turn increases the power cost and limits the throughput of existing milling plants.

To help fill this gap in knowledge a research programme was set up to study the motion of the grinding media in a mill, and the influence of liner design and mill speed upon this. The work was initiated with an analysis of the influence of liner design upon the motion of the outer grinding media in a mill[1,2], and then continued in the present study to consider the motion within the bulk of the charge.

The initial study successfully derived the motion of the outer grinding media from Newtonian mechanics. The trajectories predicted by the model were fitted to observed data from a model mill and found to correlate very well. The model has been developed into a computer program, which has been used to assist in the designing of mill liners, based upon their effect on the impact point of the grinding media on the mill liner or bulk charge. An updated summary of this work is given in the present study.

The feeling was that to develop a real understanding of the action in a mill, it was necessary to delve into the charge motion deep within the mill. What was the action of a single ball within that randomly rotating mass? How was its motion affected by changes in the mill parameters? What, if any, influence could one have upon the action of a ball by changing the mill-liner configuration? It was intriguing questions such as these, coupled with a realisation that very little work had been carried out in this field, that led to the initiation of a thorough study of the charge motion within the bulk of the charge - with the hope that a fundamental approach of this kind might throw light upon some of the mysteries of milling. It was felt that if such a study could be successfully carried out, then it would add a keystone to the understanding and application of milling of minerals.

1.2. OBJECTIVES

The areas that were of interest were condensed into a set of more specific objectives, that may be attained in the duration of the study.

1. To track the motion of balls at any point within the charge body of a model mill.
2. Analyze the ball motion to derive the kinetics of the charge motion, and to reveal the influence of different liner designs upon this motion.
3. To conduct milling trials to assess the influence of liner design upon the rate of production of final product. This would concentrate on autogenous milling.
4. To attempt to correlate the results of the milling trials with the kinetics of the charge motion.

A number of papers addressing the motion of the grinding media in a mill, and the effects of liner design on this, are reviewed. Some papers on the influence of liner design on the grinding action of mills are also selected for review. No attempt is made to delve into breakage and selection functions, as it is not the objective of this work to analyze the kinetics of breakage. This work concentrates on the net output of the mill, as affected by the design of the liners.

The work is divided into two distinct sections: the analysis of the charge motion in a mill, and the associated theoretical derivations; and practical milling trials to assess the effect of changing the liner design on the milling rate. Each section follows the progression of determining the objectives of the experiments, developing suitable experimental techniques, conducting the experiments, presenting the derived results, conducting a detailed analysis of the data, and discussing the results. An attempt is made to interlink the theoretical predictions, charge motion analyses, and practical trials. The conclusions cover the progress made in this work, and the practical applicability of the results.

CHAPTER 2
LITERATURE SURVEY

Papers dealing with charge motion, techniques of investigating it, and the effect of liner design on charge motion are considered. From the few that actually cover work on charge motion, out of the many papers available on milling, it was apparent that this fundamental aspect of milling has not been extensively studied. Investigations on the effect of liner configuration on the performance of mills are also reviewed. The papers are discussed in chronological order so as to highlight the development of this study over the years. A résumé of each paper is given, then a critical analysis of its usefulness to this work is made. Only those aspects of the papers that are relevant to the present study are reviewed; other aspects of the papers may be omitted from the review. Where a paper presents a summary of or improves upon the work of an earlier paper by any author, only the latter paper may be reviewed. The views expressed in the discussion of each paper are those of this author, unless otherwise specified.

The review of the literature acted as a guide to the experimental work that was conducted in this study. Papers presenting relevant experimental techniques and results of direct interest are highlighted. Of necessity many papers with a bearing on the topic are omitted. The articles that are reviewed should, however, provide a general overview of the current status of work in this field. In particular, only a few of the numerous studies on milling are reviewed. These primarily cover the influence of liner design on milling. Work on breakage and selection functions is not covered, as the modelling of breakage is not tackled in this study. The primary emphasis is on the effect of liner design and charge motion on the net performance of mills, and a mechanistic approach is taken.

2.1 PAPERS REVIEWED

2.1.1 The theory of the tube mill
by H.A. White[3] (1905)

White based his work on the premise that in a tube mill the balls generally keep to the same layers, thus the motion was that of rows of balls within each other. His experimental work was carried out on tubes of up to 230 mm in diameter with glass plates on the ends and a hole through which water could be added or extracted.

A "circle of reference" representing the path followed by the centres of the outermost balls is used. The balls travel up this circle until the gravitational and centrifugal forces acting upon them balance. They are then projected into free flight and follow a parabolic path until the circle is intersected at the opposite side of the mill, whereupon this circular path is resumed. The curve that defines the surface of departure for different layers of balls forms a semi-circle, and the curve that defines the surface of impact is found to be a limacon and trisectrix. The optimum conditions for maximum impact are derived from the trajectory that yields the maximum height of fall, which is in fact the one that passes through the centre of the circle.

The cycle time of each layer, according to its radius, is worked out. This is then integrated over all layers to yield the average cycle time and time in flight of the charge as a whole. The average height of fall of a ball, allowing for the relative number of balls in each layer, can then be derived. Inserting an approximate average ball size relative to the mill diameter, the optimum speed for the greatest average fall is found.

In his experimental work, White always had to use higher speeds than theoretically predicted to produce a given charge motion, so he concluded "It is clear that a sufficient quantity of balls must be present or friction between them and the rim will be insufficient and there will be relative slip. Here may also be observed one of the factors causing undue wear of the liners and wasted energy".

White proposed that the outer layer of balls be maintained in a state of centrifuging so as to protect the liner against wear, and the load be held at 66 per cent of the internal mill volume to allow an efficient falling distance. For crushing to be effective the water level should be maintained below the depth of charge at the bottom of the tube mill, otherwise falling balls waste their energy in passing through the water. He proposed a much lower speed and load if attrition grinding was concluded to be of greater importance than crushing, in wet milling. The relative importance of each mode of reduction was rather controversial, so he could not make a firm proposal. He also advised that a practical method of determining the best speed at which to run a mill would be to find that speed at which the highest power per revolution is absorbed.

A supporting comment in an accompanying discussion of the paper was that at Glen Deep mine, in the Witwatersrand, the mills ran most efficiently when charged with a minimum of water.

Discussion

This is the first mathematical study of charge motion that has been found and it is certainly a thorough and useful piece of work. White assumes perfect keying-in of material within the body of the charge, but acknowledges slip on the liner as being important. His observations of fairly short-length model mills loaded with balls all of the same diameter lead White to the conclusion that "... balls keep to their own layer". However, when looking at such a mill one is observing the motion of the end row, that is firmly packed against the glass. These balls would be neatly stacked upon one another in concentric circles, so they are likely to retain their rows. Within the body of a real mill there is a wide range of ball sizes which will be unevenly packed so the formation of neat, well defined rows that are maintained with the cyclic motion of the charge is improbable.

Although this is an idealized model, the analysis and its conclusions are generally valid. It helps considerably in the understanding of and improving of the milling operation, as the predicted trends are based upon the fundamental laws of physics and are therefore transferable between different mills. In his own words White claimed

that "The true use of theoretical considerations is to shape the course of practical trials". He acknowledged his work as a guide to rather than the solution of milling practice.

2.1.2 Fine crushing in ball mills
by E.W. Davis[4] (1919)

From the large volume of available data on milling almost any theory of charge motion can be "proved" by careful selection of data. So "... a consideration which is entirely theoretical and devoid of any personal element would seem to be desirable and instructive". This led Davis to carry out the second - but seemingly quite independent of White's work - mathematical study of the mechanics of the ball mill, upon which most other work on the subject is based.

He analyzed ball motion under the same conditions as White, assuming zero slip between the mill shell and the charge, but carried out his derivations slightly differently. He obtained a charge profile and ball trajectories identical to those derived by White.

In carrying out impact grinding the most effective blow struck by a falling ball is found by determining the ball's velocity relative to the lining, or another layer of balls, and maximizing it for given conditions. This was found to be for a departure angle (measured to the point at which the ball is projected off the shoulder of the charge and into flight) of 54° from the vertical. But as the angle of departure varies with radius from the mill centre, the radius of gyration of the charge is used to work out the optimum conditions for the charge as a whole. From this is derived the relationship between the inner and outer radii of the charge, on its circular path, for optimum operating conditions of the mill. The correlation between these radii and the charge volume then have to be determined. The sum of a ball's circular and parabolic path times, taken at the radius of gyration, are deemed to be the charge's cycle time. From this it is derived that the ball has 1,44 cycles per mill revolution. This leads to the ball spending 56% of its time in the circular path resulting in that same percentage of total

charge being in this region. This gives the correlation between the inner and outer radii and the charge volume.

Davis used his equations to determine the charge profile, velocity of ball strike, number of ball strikes, and the relation between speed, diameter and charge volume for best theoretical efficiency.

He then tested his theories by comparing them with the charge motion observed in a small (76 mm diameter by 51 mm long) mill loaded with fine sand. He claimed a good correlation, with differences due to interference between particles. This, he argued, arose because the initial velocity vectors of two adjacent particles at their points of departure intersected when extrapolated a short distance. He also pointed out that his calculated best speed was for impact crushing, not attrition grinding.

Discussion

A mathematical treatment does not entirely eliminate the personal factor Davis referred to, due to the simplifications and assumptions that are of necessity introduced. He has assumed that no slip takes place against the liner or within the body of the charge, but extensive slip surely occurs at the upper end of the circular path. This is important, as the velocity of departure determines the subsequent trajectory of the particle.

Davis shows that his derived parabolic paths do not intersect, then he claims that the intersection of the paths of the particles cause interference which results in the differences between his observed and calculated paths. Thus to substantiate his calculations he introduces a self-contradiction.

In a discussion of the paper White pointed out that the inner layers of balls have a far shorter cyclic time than the outer layers so that an estimation of this time using the centre of gyration is too inaccurate: it should in fact be calculated by summing over all radii. White also raised the point that maximum efficiency and capacity appear to occur at different mill speeds, for on Witwatersrand mills the maximum capacity is found at a higher speed than that predicted.

The simplifications in Davis' derivations limit the applicability of the conclusions, but the basic approach is useful, being founded on the fundamental laws of motion. Thus his theories can be used as a basis upon which further work can be developed.

2.1.3 Ball paths in tube mills
by H.E.T. Haultain and F.C. Dyer[5] (1922)

This work was inspired by Davis' theories, but it argued that Davis' theory of ball motion was incorrect. The study was experimental with purely qualitative conclusions.

Two glass-ended mills each 12.7 mm long, one 610 and the other 152 mm in diameter, were used in the experimental work. These were loaded with brass discs, seeds, or crushed marble, in both wet and dry mixtures. The discs had four projections on either side to prevent them sticking to the glass when used wet. By recording the charge motion with still photographs and high speed film (120 frames per second) it was clearly observed that extensive slippage, or adjustment of position, took place between the discs and lining and layers of discs. Black radial lines on the ends of the discs clearly showed the rotation of the discs relative to each other as this adjusting of position took place. This slip resulted in Davis' theoretical paths of motion not being attained. In addition, segregation of the charge into small discs in the centre and large discs at the periphery at low speeds, and the reverse at high speeds in the cataracting regime, was observed. This led the authors to conclude that a speed just below cataracting would be optimum for even mixing, thus avoiding a central section of under-utilized large balls. The authors admit that these mills do not reflect real conditions, but rather are a guide, or indication, of the motion in a real mill.

Upon receiving this paper Davis requested the experiments to be carried out with the addition of a quartz charge. This did reduce the slip against the shell dramatically, even to zero, for the main part of the circular path. The observed paths still did not fully correlate with those predicted by Davis, although the correlation was certainly far better than previously. Davis claimed this remaining non-correlation to be entirely due to slip near the top of the circular path of the particles. Haultain, however, maintained

his standpoint that there were significant differences between Davis' theory and observation, with slip being the important factor not taken into account in his calculations, especially as the effect of slurries was unknown.

Discussion

This work serves well to illustrate the importance of slip in charge motion, both against the mill shell and within the charge. It thus demonstrates the incompleteness of Davis' theory, showing that his basic assumption of no slip is invalid. An important point, as suggested by Davis, is the large effect of slip just near the top of the circular path, which is most likely due to a loss in charge pressure (see Vermeulen[14]). The end effects in this mill were acknowledged to decrease the effect of slip and therefore would have tended to work against, rather than for, the authors claims. The effects of charge segregation are of interest, for as is pointed out, this could have a detrimental effect on milling.

2.1.4 A laboratory investigation of ball milling
by A.M. Gow, A.B. Campbell, W.H. Coghill[6] (1929)

The authors carried out experimental work on a laboratory mill of 914 mm diameter and 152 mm long, firstly with grids and then with glass screens at either end. According to their observations the balls were thrown further than predicted by the parabolic path theory. This, they concluded, was because the balls do not act independently when they leave the shell but continue in contact, pushing those ahead until passing the apex of flight. Due to the intimate contact between balls, this stream of balls can't lose velocity; thus they have a horizontal speed at their apex equal to their peripheral speed against the shell.

Segregation of large and small balls was also observed, with the large balls near the outside for slow speeds and in the middle for high speeds. This was determined to be purely a function of size as the same result was obtained for wooden balls. It was concluded that the centre of mass of the small balls is closer to the mill shell; therefore they cataract further across the mill, thus tending to migrate to the outside of the mill

at speeds high enough for cataracting to occur. No explanation was given for the opposite occurring at low speeds.

As a result of the longer path length the authors had observed, it was concluded that slower mill speeds than previously predicted as optimum should be used. Speeds of 50% to 65% instead of 75% of the critical speed were recommended. The grinding tests carried out to substantiate these claims were also carried out on 152 mm long mills. They stated that a short mill was used so as to reduce slippage of the charge.

In a discussion of the paper, Davis mentioned that due to end grid effects it was entirely possible for the 25 mm grids being only 152 mm apart to hold the 32 mm balls locked effectively between them, thus carrying the balls much further than they would otherwise travel. Davis also mentioned that photographs by Haultain and Dyer showed trajectories similar to his results, in fact indicating less lift than predicted by his theories and therefore indicating the presence of some slip, a factor of about 9 per cent fitting his predictions.

Discussion

The end effect mentioned by Davis is undoubtedly the major shortcoming of this work. This is substantiated by White, who pointed out that the grinding characteristics obtained were quite different to those of real mills. In addition, if one considers the range of ball sizes and their random packing it is highly improbable, except possibly for brief bursts, that the balls could form neat integral rows that remain intact during the upward part of the flight of the balls. It therefore seems reasonable to discount this explanation, and others similar to it. The real value of this paper is that it shows the importance of realistic experimental designs.

2.1.5 Ball mill studies

by A.W. Fahrenwald and H.E. Lee[7] (1931)

This ball path analysis is based on the work of Davis, with some slight modifications and additions. The influence of ball size on mill efficiency was appreciated and a formula for optimizing it was derived, assuming a single sized ball. For mills of different size, but maintaining the same angles of departure of the outer layer, the theory predicts identical charge motion. So it was concluded that all mills should run at the same optimum percentage of critical speed. From the consideration of the outer layer of balls, the authors decided that when extrapolating to a full charge the effects must be modified, but that presumably the trends in behaviour accompanying changes in the variables remain the same.

The 'new theories' of Gow *et al*[6] were found to predict paths that projected the balls too far, with the parabolic theory giving closer correlation. It was noted that the work of Gow *et al.* was based on the abnormal conditions that promoted jamming of the charge between the mill ends, so those observations and consequent formulae should not be accepted as representing true paths of balls in a normal mill.

In the words of the authors "The large number of variables prevailing in this study prevent a complete statement of the conditions in mathematical form". So they felt the trends could be predicted but that the optimum points for best operation of mills had to be found experimentally. If the optimum conditions for one mill are know, then these conditions may be approximately calculated for any other mill.

In the experimental study, power was monitored for variations in mill speed, ball size, and load. It was found that the power draw of a mill peaked at a definite combination of these variables. The authors concluded that this peaking occurred when the charge consumed the most energy, and the mill was thus operating at its maximum efficiency. A factor of slip between the charge and the lining was indicated: this was assumed to impart a rolling action to the balls that resulted in a radial component of force which

led to them departing from the liner sooner than expected. A formula for the modified velocity was derived.

The coefficient of friction for different size quartz particles at varying moisture was found by dragging balls across a wrought-iron surface with a layer of slurry on it. A decrease in the coefficient of sliding friction from dry to wet was found, which dominated the increase in viscosity. As the frictional factor dropped, a higher pressure, and therefore load, would be required to maintain the same charge motion.

Discussion

Conclusions on the effect of balls rolling due to slip on the liner do not consider the retarding effect of the surrounding charge which would most probably prevent any such independent rolling. The observations and comments in this work are useful; however most of the conclusions are not confirmed by firm experimental results, so they cannot be taken as fact, but rather as suggestions. Comments on the effect of slurries are useful, as very few papers mention the influence of slurry addition on charge motion. This is also the first paper that considers the importance and effect of varying coefficients of friction, on the charge motion. Experimentally derived optimum points for one mill cannot necessarily be transferred to another, especially when the size of the mill, or the type of ore changes. It is also not clear that all mills should operate at the same critical speed, especially over a range of different applications.

2.1.6 Technical design of autogenous mills
by R.C. Meaders and A.R. MacPherson[8] (1964)

The authors felt that a fundamental study of the complex nature of autogenous grinding mills was required as these mills had to carry out quite a different form of grinding to the conventional ball and pebble mills. The mill had to carry out both crushing of the larger rocks, and fine grinding to final product size. Experimental work was carried out on a pilot mill, with a diameter of 1670 mm and length of 66 mm. The mill was run in closed circuit (the oversize in the discharge being returned to the mill), and the parameters that were considered to be primarily responsible for determining

the operating efficiency of the mill were varied. These parameters are the height and spacing of lifter-bars, the method of product discharge, and the length and speed of the mill. The tests were carried out on a uniform limestone, that was taken from a single blast, and used for all 105 tests. After each variable had been optimized, the tests were repeated to ensure that the set of conditions for maximum efficiency had not changed the optimum settings that had been previously established for the individual parameters. The energy used to produce one unit of new surface area was used as the basis for comparison of the results.

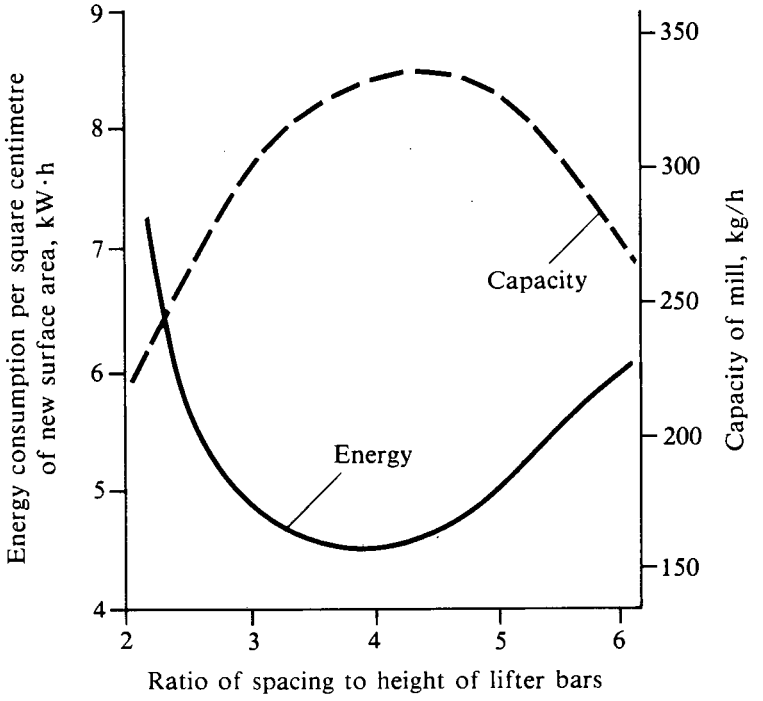

Figure 1. The ratio of spacing to height of lifter-bars, and its effect on the performance of a mill (after Meaders and MacPherson)

Variations in the ratio of spacing to height of the lifter-bars were found to have a marked influence on the operation of the mill. Figure 1 shows that a distinct peak in mill capacity and a minimum in the energy per unit of surface area produced was obtained at a ratio of spacing to height of between 4.0 and 4.5.

It was also found that the optimum height of the lifter-bars depends on the speed of the mill. A mill with a smooth lining has to be operated at over 90% of the critical

speed, whereas at slower speeds the height of the lifters has to be increased to maintain optimum conditions. For each lifter height there was found to be a definite peak in performance at a particular speed, an example of which is given in Figure 2. The best overall operation was obtained at a speed of around 77% of the critical speed, with a ratio of mill diameter to lifter-bar height of 17.6. The circulating load was found to be of major importance, and it varied widely with the operating conditions.

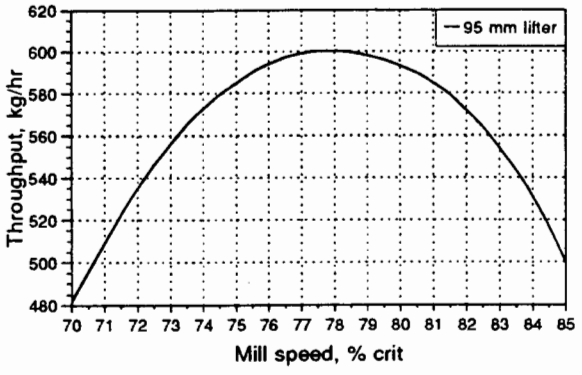

Figure 2. Effect of speed on throughput for a given lifter height (after Meaders and MacPherson)

Discussion

This is a well-planned and carefully executed piece of experimental work, and confidence can be placed in the authors' findings. The important conclusions that can be drawn from this work are that the overall efficiency of a mill can be optimized at a certain speed with lifter-bars of the correct height, and that, for a given speed, there is an optimum height for the lifter-bars. These heights must also then be related to the spacing between the lifter-bars. Changes in liner configuration can have an effect of over 15% on the total milling capacity or energy usage, indicating the importance of such considerations.

2.1.7 Contribution to a study of quasi-autogenous milling
by B. Marechal[9] (1968)
Third part: Internal mechanics of the aerofall mill

The three theories on trajectories of solids within a mill upon which this paper was based were those of E.W. Davis (1905)[4], R. von Steiger (1929) and A. Joissel (1951). The simple theory of Davis, of particles following circular paths then being projected

into parabolic trajectories, was chosen. Although the 'transcendent trajectories' and 'conservation of volume' theories of Von Steiger and Joissel respectively were each considered to be slightly more accurate, this difference was considered too slight to warrant the extra complications introduced into the subsequent analysis. The main results of Davis' theory that were used are: solids move perpendicular to the axis of rotation of the mill; there is no slip on the mill shell; air resistance can be neglected. It was assumed that slippage takes place only at the free surface of the charge (zone of descending balls); it was claimed that this can be verified for slippage against the mill shell being negligible. From this the curve of equilibrium of the charge surface is calculated. It is found that mill speed and degree of filling has little effect on the equilibrium slope (angle of repose) but that coefficient of friction of the charge has a large effect. It was concluded that this surface does not represent the free surface of the charge, but rather the surface below which solids rotate without slipping (*en masse region*) and above which they fall or roll in cascade.

The role of lifter-bars is then considered. In calculating the lift of a lifter-bar the following assumptions and approximations are made: the lifter is of negligible height relative to the mill radius; the sides of the lifter are parallel to the radius vector; the particles are released into free parabolic motion at the moment they begin to slip. Based on these assumptions, it is calculated that the lifter-bars promote only a slight increase in lift relative to a smooth non-slip liner, so particles lying in the spaces between lifters are lifted slightly higher than the rest of the charge. However, the greater the diameter of the mill, the less effect this has on the general motion within the body of the charge. It is thus considered that the only effect of lifter-bars is to produce a zone of higher peripheral trajectories of particles that lie between the lifter-bars, the motion of the rest of the charge being that produced by a non-slipping mill liner.

Discussion

The assumption of no slip between the charge and liner appears to be justified by assuming the use of low lifter-bars, the lifters being considered as perfect keying-in agents. This is could be valid for the circular path below the main bulk of the charge,

but is an inadequate assumption for the last part of the path where charge pressure is too low to key-in the charge effectively - a region which is critical in determining the subsequent trajectory of the particles. The assumption that there is no slip between a smooth liner and the charge, does not justify the conclusion that there is no slip within the body of the charge, this was conclusively shown by Vermeulen and Howat[22]. The equilibrium surface that is derived is not likely to be correct, as it is based on invalid assumptions. The calculations of the charge motion and of the equilibrium surface are based upon the spiral-circular path predicted by Davis' theory, but not observed in practice.

In the analysis of the effect of lifter-bars they must be just high enough to hold a particle, as it is assumed that the particle is set into free flight the moment it begins to slip. In actual fact a particle will slip or roll down the face of a lifter until it reaches the tip of the lifter, only then being projected into flight. This is due to the lifter-bar maintaining a constant radial velocity and therefore remaining in contact with the particle until it reaches the tip of the lifter-bar, as shown by Vermeulen[15]. Vermeulen also showed that it is invalid to assume that the sides of rectangular lifters are parallel to the radius vector, as this is a factor influencing the charge motion.

The statement that lifters have little effect on the general charge motion, especially as the mill gets larger, should be borne in mind when conducting studies of charge motion. The extent to which the lifters key-in the charge is important but their actual profile may have little effect on the bulk motion of the charge. The existence of a surface of equilibrium within the charge body is also of interest.

This work is based to a large extent on that published in the book by Rose and Sullivan[10], and reaches the same conclusions. However, as Marechal points out, the book contains a few errors in its analyses. So although it is relevant to the topic it is not reviewed, as the work of Marechal provides a summary of the derivations, that are relevant to this study, which are contained in the book.

2.1.8 Measurement of impact forces in ball mills
by D.J. Dunn and R.G. Martin[11] 1978

A ball was instrumented to the measure impact forces in a production mill, with the specific aim of assessing the stresses induced in the liner material by direct ball impacts. A ball was manufactured with a hollow centre, and divided into two halves that screwed together. Accelerometers were mounted inside the cavity.

Preliminary drop tests, designed to simulate the conditions in a mill, produced a linear relationship between velocity at impact and impact acceleration. The acceleration at impact was measured at up to 600g (g = gravitational acceleration), at a velocity of $5.2 m.s^{-2}$. The impact acceleration was about half of that on steel when there was a thin bed of ore on the liner. The maximum stress measured in a 2.74 m diameter mill, containing a normal ore charge, was in the range 200 to 250g. When the mill charge was ground down until it was devoid of ore, the impact stresses increased to well over 350g, and beyond the measurement capability of the accelerometers. Ball-on-liner impact severity increases with mill diameter and speed.

The Influence of increased severity of impacts when the liner is not cushioned by a layer of ore is discussed, with a particular emphasis on correct mill operating procedures.

Discussion

This work provides valuable practical data on the impact forces present in mills, and shows that the acceleration at impact can be very high. Knowing the acceleration, the impact time can then be calculated if the velocity of the ball immediately prior to and after impact are known. This factor should be of use in the present work. The paper highlights the importance of ensuring that the balls do not impact directly on the mill liner, which in itself justifies being able to predict, and thereby control, the motion of the outer grinding media.

2.1.9 The effect of liner design on the performance of a continuous wet ball mill
By R.S.C. Rogers, K.Shoji, A.M. Hukki, and R.J. Linn[12] (1982)

Three distinct types of movement in a mill are identified:

Rising - balls locked together, with little relative movement.

Cascading - balls roll down the surface, with many ball-ball impacts, and a nipping action that favours the breakage of the smaller lumps and particles.

Cataracting - balls thrown clear of the surface and falling a greater distance before impacting, so favouring the breakage of larger and stronger lumps of material.

The authors selected liners perceived to favour particular types of ball movement:

Corrugated (C) - a wave pattern with a 16 mm height, and 70 mm radius of curvature: to provide a gentle cascading motion.

Bar lifter (B) - lifter bars 41 mm high, with a face angle of 40°: to provide a violent cataracting motion.

Angular spiral (A) - A series of square sections arranged in a spiral along the axis of the mill: to concentrate larger balls at the feed end of the mill.

The performance of a 0.91 m diameter by 1.52 m long mill run in open-circuit, with the different liners installed, was tested.

Mill Power

This was measured through a torque transducer on the drive pinion. Allowance was made for the power losses of the mill both empty and loaded to 100% of its capacity, at the full range of speeds, so that the net power draw could be calculated. The mill was charged to 35% of its volume with a range of ball sizes, resulting in different masses of ball charge, dependent upon the volume occupied by the different sets of lifter bars. Sufficient sand was loaded to just fill the interstices. The power was measured, once it had stabilised, for each of the range of speeds. The heavier the ball loading, the higher the maximum power draw was, and the C liner resulted in a peak power at a higher critical speed. So the C liner gives maximum tumbling at a higher critical speed, and the more rapid circulation of balls in cascading gives a higher maximum power.

Breakage kinetics

First-order breakage kinetics were used for each $\sqrt{2}$ size interval, and the specific rate of breakage for each size interval, s_i, was taken as a precise index of the ease of grindability of each size of particle. A quartzite that had previously been well quantified in terms of an empirical relationship for the s_i values, was used. The mill was run at 73% of the critical speed and for each liner configuration it was loaded with a fixed mass of balls and sand. Three different size intervals of sand were used, and one interval was ground at a time. Then from the mass of sand remaining after given time intervals, the values of three of the variables in the empirical equation could be determined. The derived values of s_i were then plotted for each liner type. It was found that the C liner produced the highest rate of breakage for small particles. Liners B and A produced very similar breakage characteristics, so it was concluded that these two liners must cause very similar tumbling actions under the operating conditions tested.

Residence time distributions (RTD)

The residence times of different sizes of particles vary in a continuous mill, giving rise to a residence time distribution curve. It was felt that the different tumbling actions arising from each liner may bring about different RTD's, so these were assessed with the short-lived radioactive tracer method. It was found that the mean residence times varied substantially for low feed rates, but was the same at high feed rates. The reverse spiral of liner A probably caused it to have the higher hold-up, and thus longer residence time at low feed rates. The dimensionless RTD was also found to vary slightly for the different liners.

Open circuit grinding

During RTD testing the mill feed and product size distributions and the net mill power were determined. To aid in assessing the data, steady state simulation models were developed. These models required values that were not measured directly, but were estimated from tests conducted on a small laboratory mill, so as to reduce the required research input. By the use of correction factors good correlations were obtained, using curves fitted to data to back-calculate the actual values. The simulation models were checked by comparing their predicted values with actual product size distribution data,

and the fits were found to be excellent. The results indicated that liner C should provide greater efficiency and higher mill product rates under these test conditions. Liner B had a lower specific energy usage than liner A, but A had a higher production rate.

Conclusions

The conclusion was drawn that the use of breakage kinetics and RTD concepts in mass-size balance equations, and net mill power measurements, can provide a quantitative means of evaluating liner design effects on ball mill performance. Modelling also provides accurate simulations of test conditions, and assists in extrapolating of data. The liner that favoured cascading provided superior mill performance, for the conditions tested, in terms of both energy efficiency and productivity. The optimal form of liner is condition dependent and will vary with the speed of the mill and size reduction required. This test considered fine grinding of a relatively fine feed material, so it favoured cascading grinding.

Discussion

This work was very comprehensive in its approach, and care was taken to cover all the variables of test work. A methodology based on modelling of the breakage characteristics was successfully developed for carrying out comparative work on different liner designs. The comprehensive nature of the test work limited the range of conditions that could be tested, so that only very limited conclusions could be drawn on the effect of the liner design. However, continued work of this nature would certainly build up valuable knowledge on the effect of liner design on milling efficiency. The modelling approach would certainly assist in extending the applicability of the work to production mills.

As this work used linear breakage functions, this approach would not be applicable to the thousand-fold reductions experienced in autogenous milling. The comprehensive nature of the work also restricts the range of conditions that can realistically be tested in an experimental program. So it was felt that these techniques would be of limited use in the type of study being contemplated.

2.1.10 Effects of speed and liner configuration on ball mill performance by R.E. McIvor[13] (1983)

This investigation of the effect of liners upon the power consumption of mills is based on the analysis of previous experimental work and on theoretical modelling. The paper begins by presenting some general facts about grinding, including the observations that a large circulating load decreases over-grinding, and that large balls are preferable for coarse grinding, while small balls favour fine grinding. Impact breakage is defined as the action of a particle being crushed into many smaller pieces, by such mechanisms as being smashed between balls or ball and lining, and slow compression fracturing or crushing. Attrition grinding is defined as either abrasion, the surface removal of grains by rubbing action, or chipping, where pieces are removed by forces that fail to break the whole particle.

The author states that "The outer row of balls being acted upon directly by the mill shell is prominent in determining the motion of the entire charge. Besides dissipating a significant fraction of the total energy consumed by the mill, the outer row is the only portion of the charge in direct contact with the shell and so forms the key link for energy transmission to the remainder of the charge."

The downfall of previous experiments (Gow, *et al*[6], Fahrenwald and Lee[7]) due to interference or wedging of balls between the end liners of short-length laboratory mills was also mentioned, thus throwing doubt on the validity of their refinements to earlier theories. Because McIvor wanted to avoid similar experimental pitfalls and had found no analyses of the effects of lifters on charge motion, he carried out a theoretical analysis of particle motion in a mill. This consisted of considering a flat bar at any given angle to the liner. The particle take-off point was determined to occur at the moment the gravitational, centrifugal, and frictional forces balance out. The particle was then assumed to follow an unobstructed free fall. From these computations it was found that the trajectory of a particle is independent of the size of a mill. This indicated that the percentage of critical speed at which a mill is operated should be constant for any size of mill. The particle trajectories are shown to be highly sensitive to the lifter-

bar leading face angle. Although this is not directly revealed by the computations, it is concluded that power draw will vary with different original liner designs and vary throughout the liner-wear life as the profile of the liner changes.

The author decided that extension of the theory to the entire charge is too complex. However, he noted the following general observations: the ball charge level has a significant effect on overall charge motion; radial segregation of ball sizes exists, as observed by previous researchers; increased lifter height or decreased ball diameter results in higher trajectories of the outer row of balls; if the ball diameter is approximately equal to the lifter height, then the trajectories of the outer row of balls are relatively unaffected by subsequent rows due to their lack of direct lift on the outer row and lower percentage critical speed at the reduced diameter of the inner rows.

In conclusion, it is stated that due to the complexity of milling, past experience and empirical relationships are important, but that they do not promote understanding of the fundamental processes and so are of little help in promoting basic improvements. Thus the author states that "While investigations of grinding mechanisms and charge motion require further refinement, they can provide basic knowledge useful for improving the design and operating performance of grinding circuits".

Discussion

This investigation illustrates the important effect of the profile of the liner on the motion of the charge and on the power usage of a mill. The outer layer of the charge consumes a significant proportion of the total input of power to the mill, and is responsible for the transfer of energy to the bulk of the charge. The motion of the outer layer of the charge also has a significant effect on the motion of the bulk of the charge.

This is one of the first comprehensive analyses of the effect of lifter-bars on charge motion. Its main drawback is that the height of the lifter-bars is not taken into account, despite the experimental observation that the height has a significant effect on the lifting action. Although incomplete, the analysis forms a useful basis upon which to

develop further work, and it gives some good guidelines upon which to base liner design.

2.1.11 Fluctuations in the slip of the Grinding Charge in Rotary Mills with Smooth Liners

by L.A. Vermeulen and D.D. Howat[14] (1984)

In this study, the motion of grinding elements in contact with the smooth liner of an experimental mill was investigated. A model mill with transparent ends was loaded with rods to a charge level of over 40% of capacity. The motion of the rods during operation of the mill was filmed, and the velocities of the rods were calculated from measurements made on successive frames of the film. Although the mill was run at a constant speed, large fluctuations in the velocities of the rods occurred, varying from less than 50% to almost 100% of the peripheral speed of the mill, with an average velocity in the region of 60% of the velocity of the mill shell.

Surging of the charge consisted of alternating phases of cataracting, as the charge reached its maximum angle of repose, and of cascading, as the charge slipped back. From this observation it was concluded that when cataracting takes place, with at least 20% of the rods in flight, the charge pressure decreases, which leads to slip of the charge; then with the resumption of cascading the charge pressure increases, so the charge keys-in again to the motion of the mill, thus increasing the charge's angle of repose until cataracting again takes place.

An expression for the slip is given, which along with an estimate for charge pressure at the mill shell, is used to test the postulate that fluctuations in mean speed, and therefore slip, are proportional to fluctuations in dynamic pressure. This is achieved by calculating rod speeds and comparing these to those observed in the model mill. An excellent correlation, within 5%, is found, which provides good evidence in support of the postulate.

Therefore, in the case of a smooth lining, there is a minimum pressure of charge required for an adequate keying-in action of the rods on the shell, and at any lower pressure, extensive slip takes place. This slip represents a large loss of energy, since the motion of the mill is not transferred effectively to the charge. In addition, extensive wear of the lining results from the intense sliding motion of the charge across the surface of the lining, a conclusion that is corroborated by the circumferential grooving that is observed on smooth linings in ball mills.

Discussion

This paper highlights the importance of maintaining sufficient charge pressure to key in the charge to the rotary motion of the mill, when a smooth lining is used. It is also evident that the charge pressure may have to be incorporated into any models of the bulk charge motion.

2.1.12 The lifting action of lifter bars in rotary mills

by L.A. Vermeulen[15] (1984)

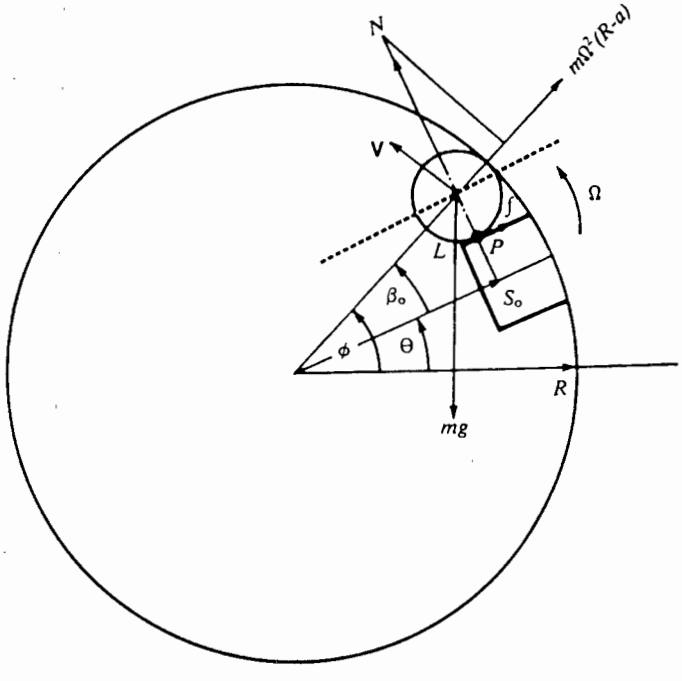

Figure 3. The forces acting on a ball resting on a lifter bar (after Vermeulen)

A standard rectangular cross-section lifter-bar was considered. By exaggerating the scale of the bar and grinding element (in this case a rod was chosen), some

previously unappreciated factors are illustrated (Figure 3). Due to the width of the bar, its leading edge is not perpendicular to the mill shell, thus the normal reaction of the bar has a radial component. It is also noted that the rod could not be free of the bar once the equilibrium conditions are reached, as the rod and ball initially have the same velocity, and the rod can only experience a decrease in tangential velocity due to the force of gravity, once in flight. Therefore the bar remains in contact with the rod, causing it to roll or slide down the lifter face. This factor was found to have a significant added effect on the computed lift and to introduce a substantial radial component to the rod's initial velocity once it was projected into flight.

The lift is defined as the final angle of departure from the lifter minus the departure angle from a smooth non-slip liner. The analysis involves finding the angle at which the gravitational, normal, and centrifugal forces balance. From this point of equilibrium the rod slides along the lifter bar, which is equivalent to sliding down a plane of constantly changing inclination. The calculations are thorough and errorless with only one assumption introduced in the theoretical derivations: that the final rolling/sliding interaction at the tip of the lifter is sufficiently small to be ignored. This assumption was subsequently found to be correct[2].

A filmed study was made of rod motion in an experimental mill fitted with various height lifters. Images of the cine' film strips were projected onto graph paper and the positions of rods in successive frames were plotted, thus tracing their paths of motion. These were compared with the calculated trajectories, the two being found to correlate very well for the coefficient of friction being chosen as zero. The motion of the rod down the lifter is concluded to be sliding as opposed to rolling, which produces more lift than that experimentally found. The coefficient of friction must be finite and thus produce some rolling action but that this factor would, according to the correlation found, be small. The relationship between spin-frequency of the rods, as leaving the lifter, and the coefficient of friction is determined, so the friction can be derived by measuring the spin. It is also pointed out that as the lifter-bar wears the angle of its leading edge is reduced, thus reducing the lift.

Discussion

This is a thorough and correct analysis of the outer charge motion. The coefficient of friction was not measured, but used as an adjustable variable to fit the predicted to the observed results. This can cast some doubt upon the exact correlation between the theory and the measured results. The sound mathematics make this study an ideal one upon which to base further work. Important points, such as the effect of lifter height and leading face angle, are shown for the first time in this paper. It is fairly certain that the presence of ore will have a significant effect on the coefficient of friction, thus changing the degree of lift in real mills, but once this factor has been experimentally determined, it can be accounted for in the calculations.

2.1.13 Physical information from the inside of a rotary mill

by L.A. Vermeulen, M.J. Ohlson de Fine, and F. Shakowski[16] (1984)

The bolts used to clamp the mill liners to the shell of an industrial pebble mill were instrumented to continuously relay information about internal conditions of the mill to external receivers. The impact bolt consisted of a piezo-electric sensor inserted into the end of a hole drilled up most of the length of the bolt. The conduction bolt was drilled right through its length and an electrically insulated electrode inserted; this experienced enhanced conduction when immersed in the mineral pulp. Periodic and largely reproducible signals were obtained from each of the bolts.

The structure of each piezo-electric signal indicates the presence of five distinct impact zones of material onto the shell of the mill. Theoretical impact points were calculated based on the assumptions of: spherical pebbles; keying of the charge into the rotary motion of the mill; no pebble interactions in the neighbourhood of departure; the body of the charge consisting of concentric rows of pebbles. A complete mismatch was found between these calculated and piezo-indicated impact points, the calculated ones yielding less lift and far shorter paths for the trajectories.

The possible action of the lifter-bars was considered. These can lift the smaller pebbles up to 30° further, but can only act on two or possibly three layers. These

cannot account for the five impact zones spread over an angular range of 60°. The interaction of pebbles can only occasionally be sufficiently large to produce the required extra lift, thus failing to explain the ever-present structure within the peaks.

The action of the pulp in providing a possible weak adhesion sufficient to carry the pebbles much further was then considered. Supposing that the adhesive force was proportional to the centrifugal force, a relationship between the radius of a row of charge and the effect of adhesion was developed. Inserting values for the arbitrary constant and average pebble radius, that were required to solve the relationship, reasonable predictions of the indicated impact positions were obtained.

The conduction signal indicates the angles of entry to and departure from the charge. There is considerable noise in the signal before the point of entry, due to material impacting onto the liner. The entry and exit points are considered to give an indication of the charge repose angle and the mill load.

Discussion

This work presents a useful method of analyzing charge motion within a real mill. It has shown the possible effect of the adhesive action of the pulp in producing higher flight paths than predicted by the simple theories of charge motion that are generally used. There is no conclusive indication, however, that this is the correct explanation of the observed impact points. The work emphasises the importance of studying charge motion under realistic conditions. An indication is also given of the information that may be deduced from measurements with these instrumented bolts. The experimental techniques presented here would certainly be useful in any work on charge motion.

2.1.14 Measurement of energy distributions in ball mills
by L. Rolf and T. Vongluekiet[17] (1984)

Direct measurements of the impact forces in a mill were obtained by mounting a movable pestle into a rubber spring, such that it was flush with the surface of the ball.

Impact forces on the pestle had to exceed a value determined by the stiffness of the rubber, to depress the pestle and activate an electronic counter. Six 40 mm balls were used simultaneously, with threshold impact values ranging from 20 to 100 mJ. The mill had to be run without slurry, otherwise the pestle became jammed. An 800 mm diameter mill was run with either a smooth lining or with 12 rectangular lifters, 40 mm high. The mill speed was varied from 55 to 130% of the critical, and the load volume of balls varied from 7.2 to 17.9% of the mill volume. The results were reduced to the impacts for a single ball, per revolution of the mill. The data gave cumulative frequency distributions of the number of impacts. This was differentiated to give the frequency distribution of impact energy.

For the mill equipped with lifter bars, the number of impacts per revolution decreased with increasing mill speed, markedly so above the critical speed. For speeds below the critical, there was a maximum in the impact frequency distribution at 40 mJ, corresponding to a height of fall of 15 mm. This did not occur for the high speeds, which must have a maximum below the minimum measured value of 20 mJ. Because the curve passes through the origin, i.e. there are no impacts with zero energy, the frequency distribution curve must pass through a maximum. The difference between the measured total energy input to the mill, and that converted by impacts, decreased very slightly with increasing mill speed, for the higher ball charges. The maximum quotient of the two was 70%, indicating a high proportion of impactive action.

In the smooth lined mill the number of impacts increases with increasing mill speed. This is explained by the reduced slip at higher speeds, which thus increases the speed of the charge relative to that of the mill. The smooth mill has a high number of impacts at the low energies, and the frequency maximum was indicated to be below the minimum measured impact value. The maximum value of the ratio of measured impact energy to total energy is only 0.36, half of that for the mill with lifters.

Discussion

This is considered to be a highly informative experimental technique, with general practical applicability. It should be possible to relate the impact frequency curves to

the measured milling action and to observed charge motion. This was not done in this work, but certainly could be if accompanied by the appropriate experiments. The results show that most of the energy is dissipated in the lower energy impacts, concentrated around a certain value. If these impact forces are related to grinding resulting from such forces, it should be possible to derive the source of the majority of the grinding work under various milling conditions. The drop off in impact forces with increasing speed can be related to the decreasing impact velocities predicted for the outer balls in a mill with rectangular lifters, according to this author's theory of charge motion[1,2]. It would be interesting for further analysis of this work to be presented by the authors, as a lot more information could be derived from the experiments, than that presented in this paper.

2.1.15 Scale up of lifters in ball mills

by D.W. Fuerstenau and A.Z.M. Abouzeid[18] (1985)

A study was made of how lifters in a batch ball mill affect comminution, through their effect on the parameters of the batch-grinding equation. A mill of 254 mm diameter by 279 mm long had eight lifters mounted in it. Four different sizes: 3.2, 6.4, 12.7, and 25.4 mm in height, and of an identical wedge-shape, were used in turn. Monosized dolomite samples were dry ground for 0.5 to 8 min, with 25.4 mm balls. The ball load was adjusted to maintain a 50% volumetric filling, the number of balls used varying from 365 to 457. The load of feed material was varied to maintain a 100% filling of the ball interstices, the feed weight ranging from 24 to 30 kg.

The lower lifters resulted in a higher rate of disappearance of the feed material (for tests with the same quantity of balls). It was concluded that this was because the lower lifters would result in a greater height of fall of the balls, which would lead to more energy being imparted to the material. The rate of production of fines was 26% higher with the lower lifters. The grinding rate was appreciably less with smooth liners than with the 3.2 mm lifters (these had the same mass of balls and of media). The breakage distribution function was independent of lifter size. The size of the lifters had no effect on the rate of grinding as a function of the specific energy consumption, i.e.

the Kw.hr/t was invariant for any product size. This figure was higher when the mill was run with no lifters.

Discussion

An interesting finding of the paper was that the product size distribution, and the energy in kW.hr/t required to produce the finely ground product, were invariant for different size lifters, despite a wide range of production rates. It was also noted that a smooth lining produced quite different results to the lifter bar lining.

It is felt that the work suffers from some basic design flaws, that cast doubt on the reliability of the conclusions on the effect of lifters on the rate of production of fine material. The design of the lifters was unrealistic, in relation to production mills. The large lifters were very close together - not even 2 balls could fit between them - and they occupied 20% of the mill volume. As a result of the wide sloping faces of the lifters, the spacing between them increased from 30 mm to 92 mm as the height of the lifters was reduced, changing the height to spacing ratio from 1.2 to 28. This ratio is reported by Meaders and MacPherson[8] to have a substantial effect on the milling efficiency, they recorded differences of the order of 50% in both capacity and energy consumption. It therefore cannot be ascertained which factor was primarily responsible for the change in rate of production.

The comment that the lower lifters result in a greater height of drop of the balls, appears to be based on the total mill filling being about 18% less for the mill with low lifters. The balls therefore fell further to impact on the toe region. It is not clear that this comment is correct, but in any case this would not apply to production mills, where a change in the height of the lifters would, at most, change the volume of the mill occupied by the lifters by 3%.

It is difficult to simulate the conditions in a production mill when testing on a pilot mill, especially with regard to scaling down in proportion, as the grinding media needs to be sufficiently large and heavy to carry out the grinding. However, with lifters the ratios of height and spacing must be retained, along with face angle and size relative to the

media, for realistic comparisons to be made with production mills. This problem is possibly best solved by scaling-up the model mills used for experimental work.

2.1.16 Estimation of milling parameters by use of a conductivity bolt by L.A. Vermeulen[19] (1985)

The information that could be deduced from conductivity bolt measurements was worked out, based on the existence of an equilibrium surface within the charge. This BHF (Barth-Hinsley-Fobelets)[20],10 surface is considered to separate the *en masse* material keyed-into the rotary motion of the mill from the loose material cascading and rolling down. By considering a mass in equilibrium under the action of gravitational and centrifugal forces with a friction term along the tangent of this surface, the form of the BHF surface is derived. The volume between the mill shell and this surface can then also be calculated. From measurements of the angle of entry and departure of a bolt into and out of the charge and with the mill speed known, the two constants in the equations can be determined. Estimates of the dynamic angle of repose of the load and of the mill power were then made, based on the profile of the BHF surface.

The correlation between calculated and measured values was then investigated, on both experimental and real mills. Although the measured values were not the same as the calculated values of mill charge volume, there was found to be a linear relationship. The larger calculated values are thought to be due to expansion of the charge when in motion. Calculations of power were about 20% higher than the measured values, thought also to result from using the static instead of dynamic charge density.

The BHF surface is considered to be well defined from the kidney to where the material departs from the charge, but ill-defined towards the toe of the charge where impacting and cascading result in many more than the three basic forces considered being present. It was concluded that the most information that can be deduced from conductivity bolt measurements are: estimates of mill load and power; dynamic angle of charge repose; and dynamic density of the charge.

Discussion

It is somewhat doubtful that the BHF surface can be accurately predicted from simple equilibrium conditions. The calculated surface is unlikely to coincide with the equilibrium surface observed to pass through the kidney of a rotating charge. The major reason for this is that the forces exerted by the material tumbling down over this surface are not taken into account. This notion is backed up by the BHF surface giving over-estimates of charge volume, when in fact there is material in-flight in mills rotating at the speeds that were considered. However, from the linear relationship between calculated and actual values it is apparent that consideration of this surface is useful. This paper also gives a good idea of the scope of application of a conductivity bolt as an investigative tool.

2.1.17 The effects of mill speed and filling on the behaviour of the load in a rotary grinding mill

by Liddell and Moys[21] (1988)

It is stated that "The motion and position of the load have the major influence on the power drawn by a mill". The existing equations were considered to be over-simplifications, and not based on direct observations of the action in a mill, so the authors conducted some measurements of the location of the mill load.

A mill 545 mm in diameter by 308 mm long, with a 13 mm mesh liner was used for the test work. The mill had an accurate torque measuring mechanism, and was run in batch mode with a load of balls and slurry. A conductivity probe, consisting of an insulated central plate that registered when the presence of grinding media shorted it through to the mill shell, was mounted in the mill. A threshold current was set to indicate when the probe entered and exited the charge, and this was fed to a monitoring computer. The mill was operated at loads of 30, 40, and 50% filling, and at speeds ranging from 50% to 95% of critical.

For the higher fillings the torque increases gradually and then drops off sharply from a peak value, as the speed is increased. The height of the shoulder steadily increases

with speed. The shoulder rises with mill filling, and is considerably higher than predicted by Davis's theory, except at low fillings and speeds above 80% critical, when the charge suffers from slip against the liner. The position of the toe is hardly affected by the mill speed, until above 80%, when the toe rises rapidly up the descending side of the mill. This indicates that the charge is impacting directly on the liner, and corresponds with the rapid drop in torque. It is concluded that the impacting charge returns some of its kinetic energy to the mill. The position of the toe is linearly dependent on the mill filling.

The effect of pulp friction in the load was examined by running it with glycerine, glycerine and sand, and a standard slurry. With pure glycerine and balls the torque steadily increased with speed, whereas with the sand and slurry it reached a peak at 78% critical speed. Readings from the probe indicated that the glycerine media caused the load to slump. Thus running a mill without a realistic slurry will give misleading torque measurements.

Measured mill power was compared to that predicted by three commonly used power equations, which are all based on the concept of a simple load profile given by the chord joining the toe and shoulder of the charge. These were found to overestimate the power by a factor of between 10 and 50%, when the measured values of the load position were used. The equations do not make adequate allowance for the drop in torque at higher speeds, nor do they allow for the effect of mill filling on the torque. It is concluded that until the motion of the load can be characterised mathematically, the power draw of a mill cannot be realistically calculated.

Discussion

This paper clearly illustrates the inadequacies of the power models based on simplistic charge profiles, and indicates a need for proper modelling of the charge motion in a mill. The interrelation between mill speed, charge filling, and the charge profile indicates the important effect of these on the action of the load. The importance of the friction in the charge was well demonstrated by the charge slumping with a low-friction

'slurry'. This shows that a realistic slurry is required if useful torque measurements are to be taken.

2.1.18 Effects of lifter bars on the motion of *en-masse* grinding media in milling
by L.A. Vermeulen, and D.D. Howat[22] (1988)

A model mill, 263 mm in diameter, was charged to 45% capacity with 9.5 mm rods, and the motion filmed through an end window. The mill was run at 73% critical speed with and without lifters, to study their effect on the motion of the rods within the bulk of the charge. Lifters of a height 1.3 and 4.3 times the rod radius were used. The paths of successive layers of rods were analyzed, and compensation was made for a perspective error that gave rise to a slight ovality of the mill image.

The centre of circulation of the charge was located at a radius of 65 mm, and layers of rods up to this central region were tracked. By plotting the angular positions of the rods as a function of time, their mean angular velocity, when in the upward-moving bulk of the charge, could be calculated from the slope of the lines. From plots of the radial position as a function of the angular position, the average radius of each layer of rods was derived. Nine to ten sets of data were analyzed for each test condition.

Figure 4 shows the derived results, with the shell of the mill on the right, and the angular velocities ranging up to Ω_{mill}. Error bars corresponding to one standard deviation indicate the variability of the results. With both heights of lifter bars, the first two layers of rods are keyed into the rotary motion of the mill, and the angular velocities of successive layers decreases systematically. The extrapolation of the fitted curve intersects the x axis (zero angular velocity) at about 65 mm, which corresponds to the earlier measured location of the centre of circulation. With a smooth lining there is extensive slip of the first two layers, with markedly reduced slip between successive layers of rods. The slip between successive layers of rods, from layer 2 inwards, is approximately constant, and the line again intersects the x axis at 65 mm. So the charge has the same radius to its centre of circulation as for lifter bars.

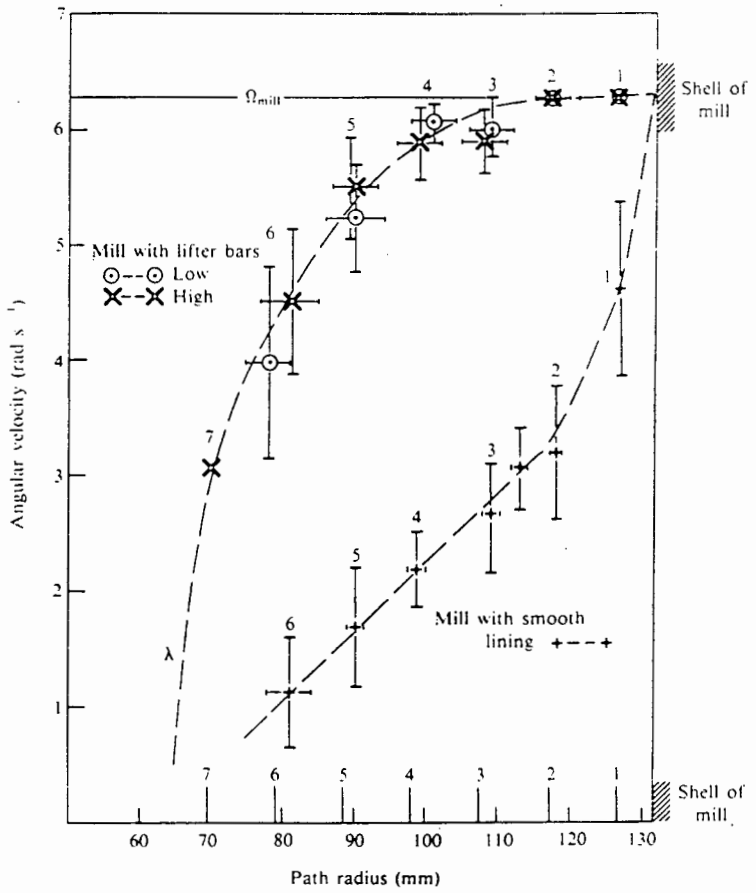

Figure 4. The mean angular velocities of rods in the various layers in a mill (after Vermeulen and Howat)

From the fact that the second layer doesn't slip for the lower lifter bars, but that the third layer slips for both sets of lifters, the conclusion was drawn that the dynamic charge pressure was insufficient to key in the third layer fully. The dynamic pressure was taken to consist of two components, the weight of the charge and the centrifugal force, and is given by:

$$p = \alpha \rho g R + \beta \rho \omega^2 R^2 \qquad (1)$$

Where p is the dynamic pressure, ρ the mean dynamic density, ω the angular velocity of the rod about the centre of the mill and at a distance R from the mill centre, g the gravitational constant, and α and B dimensionless constants. By expressing this as a fractional change in pressure between successive layers, it was possible to calculate the limiting pressure required to prevent slip and the pressure between the layers of

charge. The pressures at the interfaces between the layers of rods were substantially larger in the mill with lifters, as compared to those without.

Abrasive interactions can be assessed from the shear forces between layers of rods. The difference in angular velocities multiplied by the radius at the interface, gives the difference in velocities between two layers. The shear stress is assumed to be proportional to the mean dynamic pressure, and taking abrasion (A) as the rate at which work is done by the shear stress on unit of area of the interface:

$$A = \mu p R \Delta\omega \quad \text{for a given interface}$$

Where μ is in effect a coefficient of friction between the layers.
The values of A for the smooth mill are much higher than for the lining with lifters, mainly due to the high slip in the outer two layers.

The rates at which rods are transported through the *en-masse* regime, and their kinetic energies were then calculated. For a mill with lifters the rate of rod transport is more than doubled, the kinetic energy increased fourfold, and the rate at which the energy is transported though the en-masse regime increased fivefold, compared to the smooth lining.

Discussion
This is the first extensive investigation into the interactions within the bulk of the charge in a mill, and some interesting results are derived. The data is analyzed in a mathematically correct and straightforward manner, with all equations having a physical basis. The results can thus be viewed with confidence. The comparative slip in the charge and the rate of transport of energy into the grinding media are of particular interest to the present study.

2.1.19 Measurement of kinetic energy of grinding media in a tumbling ball mill by S. Yashima, H. Hashimoto, Y. Kanda, and S. Sano[23] (1988)

Three load sensors were mounted into the shell of a 300 mm diameter model mill, and the compressive loading of impacting balls measured. The kinetic energy at impact

was calculated using a formulation developed by Tomishenko, involving the Youngs moduli and Poisson's ratios of the ball and sensor. It was assumed that the balls impacted perpendicularly on the sensor. The mill was run at 90% of the critical speed, and charged separately with three different ball sizes (36.5, 30.2, 25.4 mm), each at three loadings. Tests were also conducted with two lifters fixed in the mill, either 25 or 50 mm in height, and sloping 15° forward of radial. The sensors were fixed in 11 different radial positions.

Both the kinetic energy of the balls, E_k, and the energy input to the mill, E_i, per unit time, increased with ball loading. The efficiency of energy conversion, the ratio of E_k to E_i, increased with loading, as did the frequency of impacts from balls falling from higher up. This was assumed to be due to better keying-in of the balls, and consequent higher lift. The lifters greatly improved the efficiency of energy conversion, up to three-fold for the 50 mm lifters. The assumption was made that the lifters prevented energy losses arising from the surging motion present without them.

A model of breakage processes was developed on the assumption that breakage takes place when the balls impact on a bed of particles against the mill shell. A number of simplifications had to be introduced, such as an empirical relationship for the number of particles in the crushing zone, for the theory of elasticity to be used to express the compression force on the particles. The probability of breakage of a particle under a given compressive force was calculated, and the experimental values of kinetic energy of impacts used, to assess the probability of a particle undergoing fracture.

Three size intervals of quartz sand were fed independently to the mill, and breakage and selection parameters obtained from first-order plots of the grinding data. The calculated and experimental data differed hugely, by factors from 2 to 200 fold. The experiments showed that the lifters had no influence on grinding, whereas the theory predicted very large differences in grinding efficiency. Subsequently a comprehensive range of fillings, from 0.01 to 0.48, were tested, for the smooth lining and with the 50

mm lifters. The lifters gave a fairly constant specific rate of breakage, and the smooth lining a fluctuating rate, depending on the mill filling.

It was concluded from the work that frictional crushing, or surface grinding, played a far larger role in grinding than did impact crushing.

Discussion

A great deal of effort went into taking very careful measurements of impact forces, and correlating them to breakage kinetics. However, the work appears to have suffered from flaws which limited the usefulness of the results. The original assumption was that all the grinding takes place by impact crushing against the shell of the mill, and this cannot be the case when these are only a small fraction of the interactions taking place in the mill. The very strange arrangement of only two lifters, very high, and sloping forward, would have resulted in the balls in contact with them basically centrifuging at the test speed. Because of the large size of the balls, the bulk of them were most probably quite well keyed-in by these lifters, and stacked up in rows. A ball resting upon another is the equivalent situation to a radial lifter, and at 90% critical speed the theory developed in previous work[1,2] predicts that the ball would be projected well across the mill, and impact on the lining. This would account for the high efficiency in terms of impacts on the mill shell. This ball-on-shell impacting is generally considered to be undesirable, as it leads to rapid liner wear, and a reduced rate of grinding.

The results of the work indicate that conclusions about the entire action of a mill cannot be drawn from measurements of outer interactions only. But such measurements could undoubtedly be of use in building up a comprehensive picture of the interactions in a tumbling mill. It is also felt that experimental conditions should be as realistic as possible, to be able to supply useful data.

2.1.20 Charge motion in a semi-autogenous grinding mill
by Z. Rogovin and J.A. Herbst[24] (1989)

A 610 mm diameter by 305 mm long mill was constructed of plexiglass, so that the action of the media inside the mill could be observed. It could be run in a continuous throughput mode through a 150 mm inlet and grate discharge end wall. It was loaded with 19 and 9.5 mm ceramic, and 9.5 mm steel balls, to simulate a semi-autogenous charge. The mill was charged to 20 and 35% of its volume, and the speed set at 75, 44, and 24% of the critical. Water and a limestone slurry were used in the tests.

With water, the angle of repose was found to increase from 30° to 60° as the speed was increased. There was no water pool at the toe, and the ball interstices were never completely filled with water. With the slurry feed, there was a hold-up of limestone at the feed-end for high feed rates, and a build-up at the discharge end for low feed rates.

Charge segregation effects were observed in some detail. At low speeds, 44% of the critical and lower, the smaller and the heavier balls concentrated in the centre. At the top (shoulder) of the charge the added lift from the end walls results in a concave cascading surface, i.e. one that is higher at the end walls and lower at the centre. This causes the balls to roll in towards the centre of the mill, away from the ends. At the toe the charge has a convex profile, so the balls roll towards the end walls. The charge segregation was explained by the tendency of small balls to shift downwards, and big particles upwards, as they roll down a free surface. The heavier balls also tend to concentrate in the lower part of the stream. At high speeds (75% critical) the reverse was observed, with small balls concentrating towards the outside of the charge. At this higher speed the balls are projected into flight, so they don't roll down the free surface. In flight it is more likely that the heavier and larger balls will be in the lower layers of the particle steam, thus concentrating them towards the centre. In addition the small balls concentrate towards the ends of the mill. The balls roll down the end lifters, which form a V-shape towards the centre, and thus cause the larger balls to fall off at a greater radius than the small balls, which can continue rolling

between the lifters towards the centre. The large balls are thus subjected to the inward forces in the upper regions, as discussed earlier, so they tend towards the axial centre of the mill. It was concluded that the end walls have a tremendous effect on the charge segregation, especially in short mills. With a high feed rate of slurry, the limestone packs between the feed end lifters, and thus prevents the occurrence of the segregation mechanism. So at low and high speeds the large balls concentrate at the periphery.

The conical shape of the end walls and the end lifters are concluded to have a significant effect on the grinding. The concentration of steel balls near the centre is unfavourable for grinding. The packing of small balls near the discharge could slow the exit of fine material. Since the mill charge is not homogenously mixed, it will not give uniform grinding along its length. Careful end-liner design that takes these segregation effects into account should be able to achieve more efficient grinding.

Discussion

This paper is of interest to the present study, especially as regards the effects of charge segregation. The segregation was explained mainly in terms of the effect of the end liners, in the short mill used. It would be of interest to note whether such segregation occurs in long mills, where the effects of the end liners are very small. It is clear that segregation of the charge can have a detrimental effect on the grinding action, especially if large or heavy balls are concentrated at the centre.

2.1.21 A multi-torque model for the affects of dispersants and slurry viscosity on ball milling

by D.W. Fuerstenau, P.C. Kapur, and B. Velamakanni[25] (1990)

A model of the torque drawn by the mill was developed on the basis of results of tests using viscosity modifiers. In batch milling, the torque dropped as more fines were produced, and the slurry viscosity increased, but this drop in torque could be avoided by adding a viscosity reducing agent. It was inferred from this result that the charge splits into two distinct zones as the slurry thickens. The standard charge profile of the

cascading region, and a layer of centrifuging/cataracting charge on the periphery of the mill, form the two zones. The centrifuging layer was assumed to arise from the high viscosity of the slurry gluing the balls to the mill shell. As a centrifuging charge has a much lower power draw, this would account for the lowering of the torque of the mill.

In some of their previous work the authors had shown that slurry viscosity varied with time in the following manner:

$$\eta = \eta_{\infty}(1 - \exp[-X(t - t_o)]) \qquad (2)$$

where η_{∞} = limiting viscosity after extended grinding.

t_o = threshold time after which viscosity begins to rise.

X = function of the mill-material system.

A third component in the power function was taken to arise from a friction factor in the charge. From models for the three independent components of the torque, and using the viscosity factor, a six-parameter torque model was derived. At higher viscosities only four of the parameters needed to be used. These were derived from standard parameter estimation techniques, based on long records of torque as a function of time. The components arising from each individual contributor to the torque could then be calculated.

A reasonable correlation with experimental results was obtained. Discrepancies were accounted for by the simplification of an even thickness of centrifuging balls, and the end effects of the mill. When divided into individual components, the cascading torque was found to drop slightly during the test, and the cataracting torque to reach a peak and then drop off rapidly, reaching a negative value.

The dimensionless size factor, taken as a ratio of the median size, was found to give a constant size distribution curve with grinding time. It was concluded from this that the median size is an unambiguous measure of the fineness of grind, and that the grinding mechanism is invariant with time, despite large changes in viscosity and

charge motion. An exception to this was the size distribution after 70 min with the viscosity reducer. The assumption was made that the grinding kinetics no longer conformed to first order kinetics with such a high percentage of fine material. The extent of grinding was deduced to only be dependent on the amount of energy used. The grinding rate would therefore reach a maximum when the torque peaks.

Discussion

This work presents an interesting extension to the basic theories on torque prediction; however, the mechanical basis of the theory is derived from inferred results, not from actual observation or direct measurement of the separate effects. An exceedingly viscous slurry would be required to stick a layer of balls to the shell of the mill, especially at the tested speed of 65% of critical. It is felt that the model is not well substantiated but that by having a number of variable parameters in the equation it could be made to give a general fit to the data. The fitted curve lay within 10% of the measured values, but it does not actually seem to follow the trends displayed by the values. When the net torque was divided into the computed components of cascading and cataracting torque, the cataracting component became negative as grinding time progressed. It seems highly unlikely that the outer cataracting layer could impart more energy to the mill than was required to lift it from the shoulder to the top of the mill. The possibility of cataracting balls returning some energy to the mill upon impacting on the shell is not considered. Neither is the effect of the changing slurry on the coefficient of friction between the charge and the smooth mill shell taken into account.

Fahrenwald and Lee[7] had found that the coefficient of friction between rocks and a metal surface dropped substantially with a slurry interface. This would result in a greater degree of slipping between the charge and the liner, and lower the angle of repose of the charge, thus also lowering the power draft. Arguments of this nature indicate the possible flaws in the multi-torque model, and those in models that are developed upon assumed mechanisms. These mechanisms can be 'proved' to exist by fitting multi-parameter models, but upon further analysis it is often found that quite different mechanisms can be made to fit such models equally well. It is felt that care should be taken to avoid such pitfalls in any modelling that is carried out. The

applicability of the simple torque arm model may be limited, but a more careful mechanistic approach is required to correctly modify it. Such a model is likely to have a number of separate components that will vary in magnitude with milling conditions, and these should each be determined independently.

2.1.22 Simulation of ball charge motion in ball mills

by B.K. Mishra, R.K. Rajamani, and W.G. Pariseau[26] (1990)

The proposal was made that the charge motion in a mill is of considerable practical importance because the following can be accurately predicted from the motion: power draw; distribution of forces, and hence the wear rates of the balls and liners; and mass transport of the product. The theories used to predict power draft in mills make over-simplified assumptions, and hence are inadequate. The discrete element method (DEM), which is capable of handling multi-body collisions, was used to accurately establish the motion of the balls inside a mill.

The mill was viewed from end-on as a two-dimensional plane loaded with discs. The normal and shear forces imparted on each disc by its neighbours were used to compute the net force acting on the disc, by assuming the disc was in equilibrium with its immediate neighbours. From this was derived the acceleration of the ball in the horizontal and vertical planes, and its rotational acceleration. This was done for every ball, and integrated over sufficiently small time steps to limit disturbances to a ball's immediate neighbours. An existing program for studying soil dynamics was modified to accommodate the mill geometry and provide a visual result. Laboratory experiments were conducted to measure the basic material properties required by the model, such as stiffness, coefficient of friction, and coefficient of restitution. The motion of balls in a model mill was tracked using video camera filming and a frame grabber system to transfer images of all the balls to a computer.

In a smooth-lined mill, increasing the coefficient of friction from 0.2 to 0.9 changed the ball motion from cascading to cataracting, and increased the energy input by 50%. Changing the angle of lifter bars had a considerable effect on the trajectory of a single

ball against the lining. Decreasing the face angle of the lifter by 21° reduced the angle of impact of the ball on the lining by about 90°, at 63% of the critical speed. The observation was made that the trajectories could be controlled by changing the face angle and height of the lifter bars. For analyzing the effect of mill speed, six equally spaced rectangular lifters were used (approximately a ball diameter in height), and the mill run at 50, 62, 75, and 90% of the critical speed. The height of the shoulder increased, and the charge pressure reduced with speed. At 90% critical speed the balls tended to centrifuge.

From laboratory experiments the torque was found to increase for speeds up to about 100% of the critical, and then drop off. The effect of mill filling on torque was measured, and concluded to pass through a peak. The conclusion was drawn that the model predicts power draft very accurately, and so was being extended to three dimensions.

Discussion

The work presented in this paper takes a huge step forward, compared with all previous work, towards predicting the overall charge motion in a mill. The results were presented rather sketchily, so one could not always be sure whether they were experimental or predicted data, or both. The predicted charge motion did seem to follow the correct trends, for example with changing the lifter bar angle. However, the technique requires intensive computations, so powerful computer systems must be utilised. This makes it difficult to carry out numerous predictions, and in fact not possible at all without very powerful computers. This might unfortunately limit its application, unless valid simplifications (substantiated by experimental work) can be found, or until the required computing power becomes more commonly available. The bulk motion modelling technique used holds great promise, but it did not seem to give an accurate prediction of the observed ball trajectories. Observations were made of balls against the end window, so it cannot be deduced whether the discrepancies arose from modelling inadequacies or experimental distortion. The required facilities were beyond the scope of the present work, but the results from future work in this field will be watched with interest.

2.1.23 Prediction of grinding-mill power
by S. Morrell[27] (1992)

Generally, the simpler power models are used in the design of milling plants, but these models ".. predict either invariant power peaks with respect to filling and speed or no power maxima at all". This does not correlate with practical experience. The more complex models have not been substantiated on operating plants. Motivated by these observations the author attempted to build up a more accurate model, that would take into account the speed and loading of the mill, the type of lining and the rheology of the slurry.

Experimental tests were conducted to determine how the profile of the charge changed with mill speed and loading. A model mill was loaded with an autogenous charge that was scaled down from the equilibrium charge of a 1.8 m pilot mill. Brightly coloured tracers were added to the mill charge, and these were photographed though the end window, using still photography with a slow shutter speed. The resultant trace lines outlined the shape of the charge, and the length of the lines indicated the speed of the particles. It was assumed that the end-effects were negligible, and that the charge did not segregate along the length of the mill. The mill load was varied from 15 to 60% of the mill volume, and the mill speed varied from 55% to 85% of the critical speed.

The mill was run with a smooth lining. The angular position of the toe was found to rise with increasing mill filling, and be unaffected by mill speed. The shoulder moved substantially upwards with increased mill filling, and for the higher loads the angular position rose with increasing mill speed. This was in accordance with the work conducted by Liddell and Moys[21]. The tangential velocities of the particles were determined from the lengths of the trace lines, for a known shutter speed of the camera. The velocities decreased in a linear manner, from nearly that of the mill shell at the periphery of the mill, to zero at the eye (centre of circulation) of the charge.

A mill power model was developed on the basis of a charge profile in the form of an annular ring. Radial lines intersecting the ring of charge at the toe and shoulder

defined the extent of the charge body. The torque arm of each element in the charge was calculated from the tangential component of the gravitational force acting on each element. Multiplying by the mill speed, and integrating over the volume of the charge gave the total power delivered to the charge. The effect of slip between layers of the charge was taken into account by incorporating an empirical equation for slip as a function of radial displacement, derived from the filmed charge motion. The entire charge is assumed to occupy the annular charge sector.

The effects of mill speed and filling were incorporated as empirical relationships, determined from the filmed study. The charge is assumed to consist of a coarse fraction, rocks or balls, and a slurry fraction with a solids content the same as that at the mill discharge. The charge density can then be calculated, with assumed values of charge porosity, and fraction of solids in the slurry. An empirical equation, based on the no-load power draw of some industrial mills, was used to provide a measure of the difference between net and gross power draw.

The energy recovered by the mill from impacting particles was considered to be negligible because the particles generally impact perpendicular to the mill shell, except at very high mill speeds. Allowance is made for the energy required to accelerate the charge from zero tangential velocity, as it enters the mill charge, to the average charge velocity. This is determined to be in the region of 3 to 4% of the total power draw.

The model was applied to a database of 45 different production mill configurations. A correction factor of 1.03 was applied to overflow mills, and 1.22 to grate discharge mills. The model predicts the variation of mill peak power with different mill speeds and filling, but suitable plant data was not available to compare to the predictions. It is concluded that the model successfully predicts the mill power draw for a wide range of industrial conditions. The model will be extended to include the effect of lifter bars, pulp rheology and the size distribution of the mill load.

Discussion

This work takes the approach of using the observed motion in the mill to predict mill power draw. Even with the simple models developed a reasonable power prediction is obtained for a wide variety of mills, indicating the general validity of this mechanistic approach. It cannot be assumed that the end-effects of the windows are negligible, so the motion observed in the experiments would not have been representative of the bulk charge motion. However, the trends were likely to have been correct, which were used to develop the simple models. When the charge impacts on the lining there is a substantial tangential component, as shown by the charge trajectories in this authors earlier work[1,2], so it is invalid to assume there is no return of energy to the mill by the impacting balls.

The concepts upon which this work is based are useful for further development of theories on mill power draw.

2.1.24 Measurement of the forces exerted by the load on a liner in a ball mill, as a function of liner profile, load volume and mill speed

by M.H. Moys and J. Skorupa[28] (1992)

The general motion of the grinding media in a mill is outlined. It is pointed out the centre of motion of the charge (the point about which the charge circulates), is not the same as the centre of gravity of the charge. The work is based on the proposal that if the tangential force exerted by the load on a liner segment can be measured, then the total torque drawn by the mill can be calculated.

One element of the liner was mounted independently of the shell and other liners, on two loadbeams. The loadbeams monitored the radial and tangential forces exerted on the liner, and the pivoting system was carefully designed and constructed to allow free movement of the liner element. The element was electrically isolated from the mill, to also be used as a conductivity probe, for measuring the location of the charge. The forces on the liner were monitored while it was in the charge, and the speed of the mill, and mill loading varied.

The results are given for a double wave type liner. Good reproducibility of the measured forces was obtained. The radial force rose rapidly to a peak at about 30° before the bottom of the mill was reached, then dropped off at an increasing rate until disappearing at about 30° above the horizontal. The radial location of the peak moved towards the toe as the speed was increased. The peak value dropped off rapidly at speeds from 100% critical upwards. The tangential force had a bimodal form, peaking near the base of the mill, as the balls were accelerated up to the radial velocity of the mill, and again at the horizontal position, when the force of gravity is a maximum. The value of the first peak increased with increasing speed, until dropping off at speeds above 90% critical, and becoming negative for supercritical speeds.

For speeds between 60 and 90% of the critical, the torque calculated from the tangential force measurements gives a torque prediction within 5% of that measured. The torque was not measured for the full rotation of the mill, so was inadequate for calculating the torque at high speeds, when the charge was close to centrifuging.

Discussion

This innovative measurement gives a most useful insight into the forces acting in a mill, and a reasonable prediction of the power draw in a mill. It will be of particular interest to see how different liner designs affect these forces, and thus the transfer of energy to the charge.

2.1.25 The slip of a particle on the inside of a rotating cylinder

by Nates, Nurick, and Reddy[29] (1993)

Part 1 - Theoretical analysis

The force equations acting on an isolated particle on the shell of a smooth-lined mill are solved. For a mill rotating at 102% of the critical speed, different modes of motion of the particle were predicted, depending on the coefficient of friction, μ :

$\mu = 0.2$ Oscillating about the base of the mill, but not being projected into flight.

$\mu = 1$ The particle travels above the horizontal, from where it departs from the liner and is projected into flight.

$\mu = 3$ The particle can slip relative to the liner, but still be lifted to the top of the mill and thus centrifuge. This was named slip centrifuging. The calculated degree of slip relative to the mill was less than 1%. The minimum particle velocity is at 83° to the horizontal, after which the frictional force dominates, and the particle begins to accelerate back up to the velocity of the mill shell. The minimum μ required for centrifuging decreases as the speed of the mill increases.

$\mu > 3$ Toppling over of the block can occur for high coefficients of friction, combined with a low mill speed. The block then tumbles down the mill shell.

For a given mill speed, the particle is lifted higher, and projected further across the mill as μ increases. The trajectories as predicted by the theory of Davis are only obtained for infinite friction. For a given coefficient of friction, the lift and extent of projection increase with mill speed.

Part 2 - Experimental investigation

An open-ended drum, with a diameter of 404 mm and length of 100 mm, was mounted on a central shaft. The exclusion of a front window eliminated possible end-effects acting on the block. The static and kinetic coefficients of friction were measured, and found to be very close: bare steel $\mu = 0{,}20 \pm 0.04$; and cloth lining $\mu = 0.44 \pm 0.04$. The speed of the mill was varied from 30% to the speed at which the block centrifuged, and the angles of slip and departure were determined from analyzing video films taken of the mill.

It was demonstrated that the angle of rise is independent of the mass of the block, as predicted by the theory. The data for angle of departure as a function of mill speed, fell within the band of uncertainty of the theoretically predicted angles, with the uncertainty arising from the error range of measured values of μ. It was determined that the error in measuring from the video film when the block began to slip relative to the mill was very large, around 37°. This was a function of the limitation of being able to detect relative movement of the surfaces, which is very slight to begin with. The experimental error in the measurement of this factor is not relevant to the other

measurements. It was demonstrated that the model successfully predicted the onset of centrifuging, which is dependent upon μ.

It was pointed out that the experimental underestimation of the slip zone is inherent in this type of measurement, and that it would have led to previous investigators also underestimating this factor. The consequence of this is that the abrasion zone may be larger than previously estimated.

Discussion

This paper presents an in-depth analysis of the influence of the coefficient of friction on the degree of slip, and subsequent trajectories of particles in a mill. The theory may be able to predict the trajectories of the outer balls in a mill loaded with a charge of balls. It is also possible that this theory could be extended to successive layers within the mill, considering each layer to be a rough surface, with a bulk average coefficient of friction between layers. The assumption of no rolling will be valid for balls in the bulk of the charge, as the surrounding balls will inhibit rotational motion.

2.2 GENERAL DISCUSSION OF THE PAPERS REVIEWED

The papers considered present a variety of ideas upon which to base both experimental and theoretical work. That simplifications have to be made is quite apparent, but the shortcomings of unrealistic simplifications and assumptions are also clear. The interactions of the grinding media within the bulk of the charge have not been experimentally investigated, only those apparent at the end window of a mill. One would expect a far greater degree of randomness in the action of the media not in contact with constraining plane of the mill end face. The bulk motion modelling technique used by Mishra *et al*[26] holds great promise, but it has not yet been adequately checked against observed charge trajectories. It can be seen that there is a great deal of scope for improvement in the present theories of charge motion, thus making a study of this nature a valid and useful pursuit.

There are a number of theories on the power draw of the mill, with the mechanistic approaches, based on analyses of the charge motion, giving some good results, but

none presenting a complete picture. The energy distributions and impact forces have been given some attention, but have not been well related to the actual grinding action in mills. Possibly a combination of the required forces for fracture, calculated by Yashima *et al* [23], and the distribution of impact forces measured by Rolf and Vongluekiet[17], could shed further light on the source of the grinding in a mill.

CHAPTER 3
PREVIOUS WORK

The present study is an extension of an earlier set of work[1,2], and the two are intimately linked. The theory is used in the present work, so a summary of the earlier work is presented.

A theoretical model, which is based on the fundamental laws of motion, was developed to describe the motion of an isolated rod or ball in a rotary mill, as affected by the geometry of the mill lining. This model takes into account both the static and the kinetic coefficients of friction that act between the grinding element and the lifter, and allowance is made for the rolling and slipping of the element. The model examines flat-faced lifters of any face-angle and of any height. The full derivations are presented in Appendix I. These include some modifications and additions made during the current work. Only the outermost layer of charge is considered. However, this is an important indicator of the charge motion since it yields the outermost limits of the bulk charge motion.

The charge motion of rods in a glass-ended mill was filmed with a high-speed camera. The mill was fitted with a variety of lifters with different face-angles and heights, and was run at a wide range of speeds. The trajectories of the rods on film were then tracked. The coefficients of friction between the rods and the lifter material were measured under the vibrating conditions that are found in the mill.

It was found that there was a good correlation between the theoretical predictions and experimental results over a wide range of conditions. A comparison of the experimentally determined, and theoretically derived trajectories is shown in Figure 5. Once it was established that the theory provided a good prediction of the influence of lifters and mill speed upon the rod trajectories, the theory was analyzed to provide a deeper insight into the effects that were observed.

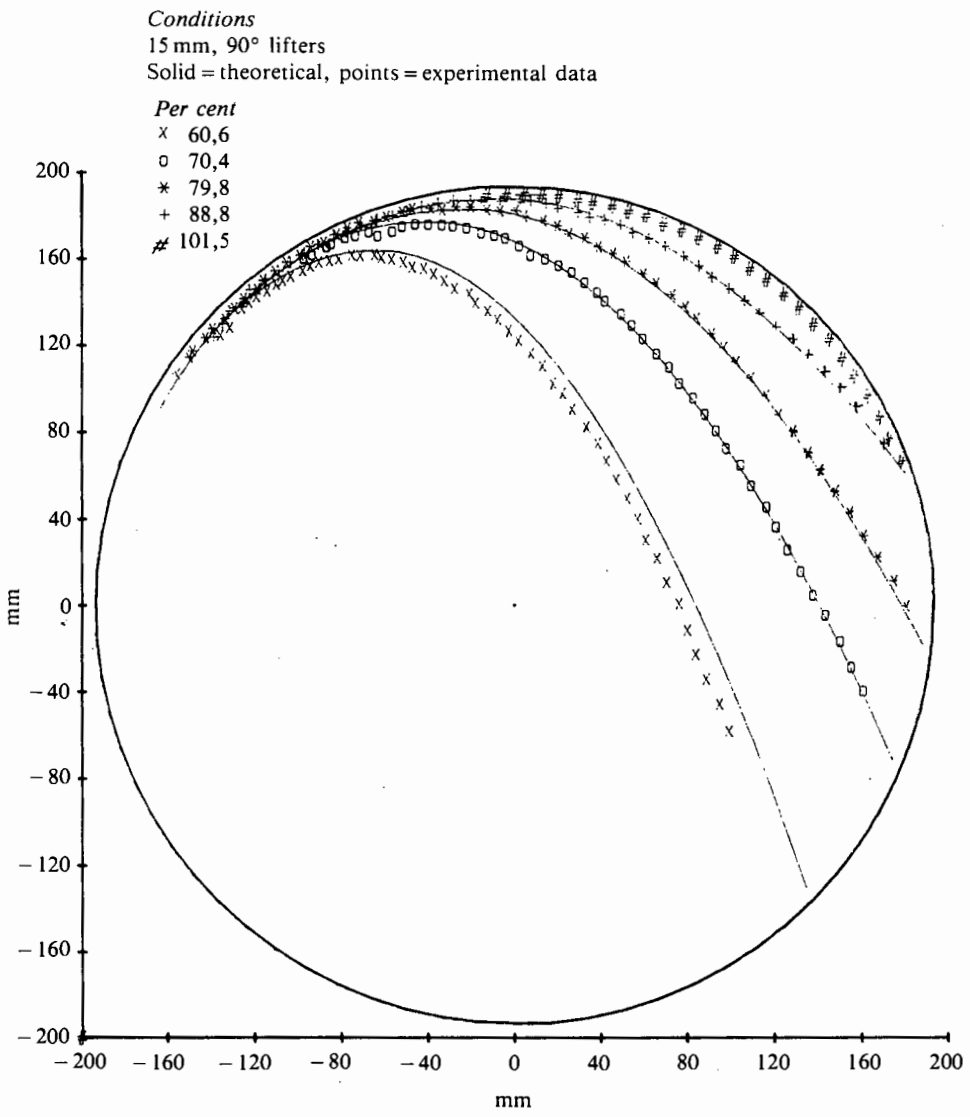

Figure 5. Comparison of theoretical and experimental trajectories over a wide range of speeds

Work by other authors had examined the effect that lifters have upon the charge motion only to the point up to which the charge is lifted[13,15]. However, both the full trajectory, and especially the impact point of the charge, are of great importance. In milling, it is desirable to key-in the charge to the rotary motion of the mill, but in so doing the charge should not be projected onto the shell of the mill. If the grinding element impacts directly onto the lining, then accelerated wear of the lining and rapid degradation of the grinding media take place, without achieving any milling of the ore. It is therefore important that the grinding elements are projected onto the toe of the charge; taking this into consideration, the impact point at which the grinding element

strikes the shell of the mill was emphasised in this work. Figure 6 illustrates the key points in the charge trajectory, which are referred to in the following discussion.

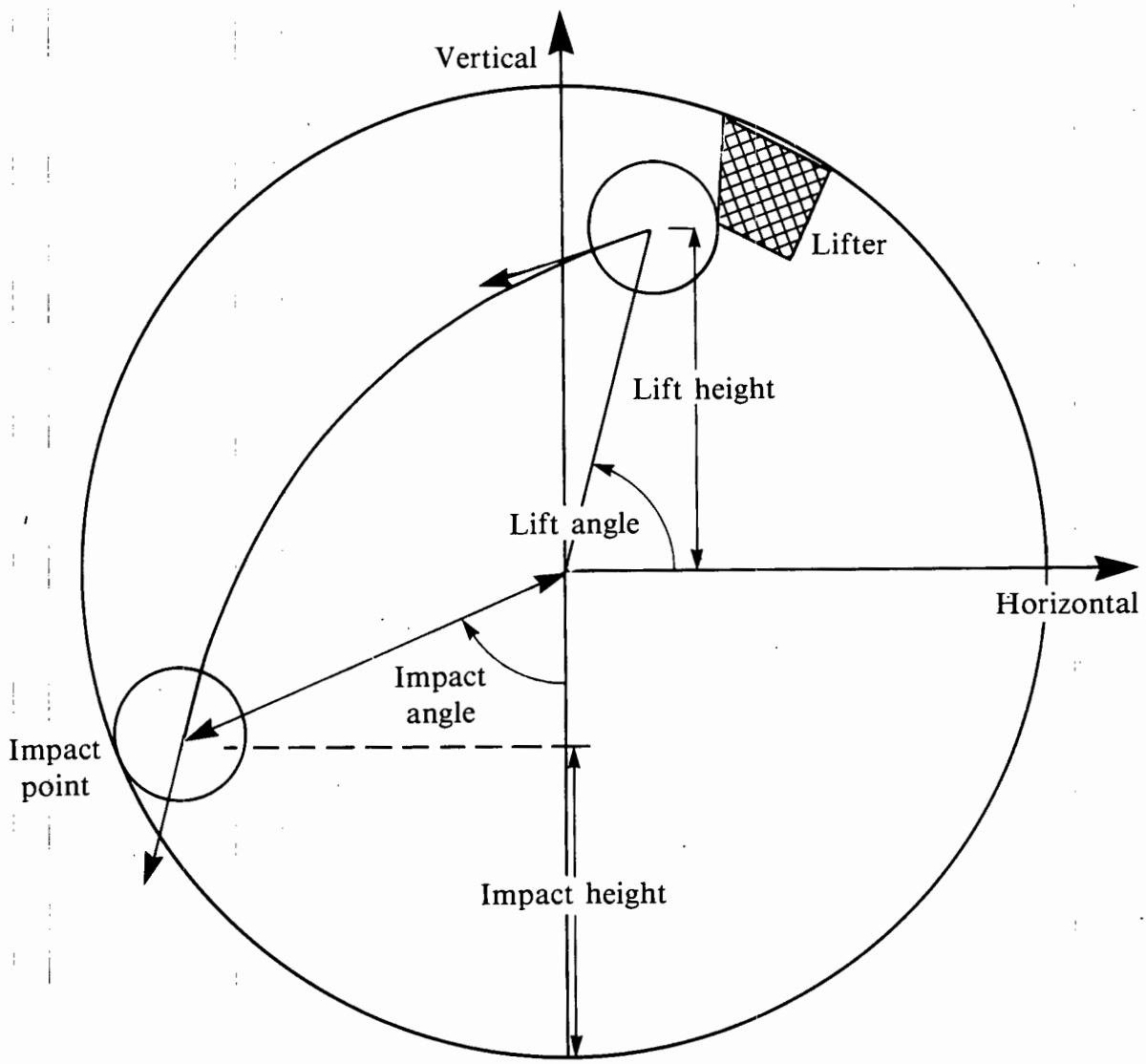

Figure 6. The lift and impact points of a ball

The influence of lifter height and face-angle, and the speed of the mill on the impact point of the grinding element are summarised in three-dimensional plots (Figure 7 to Figure 9), that show the combined influence of two of the variables upon the impact point. These are for the 387 mm model mill loaded with 12 mm diameter rods, used in this experimental work.

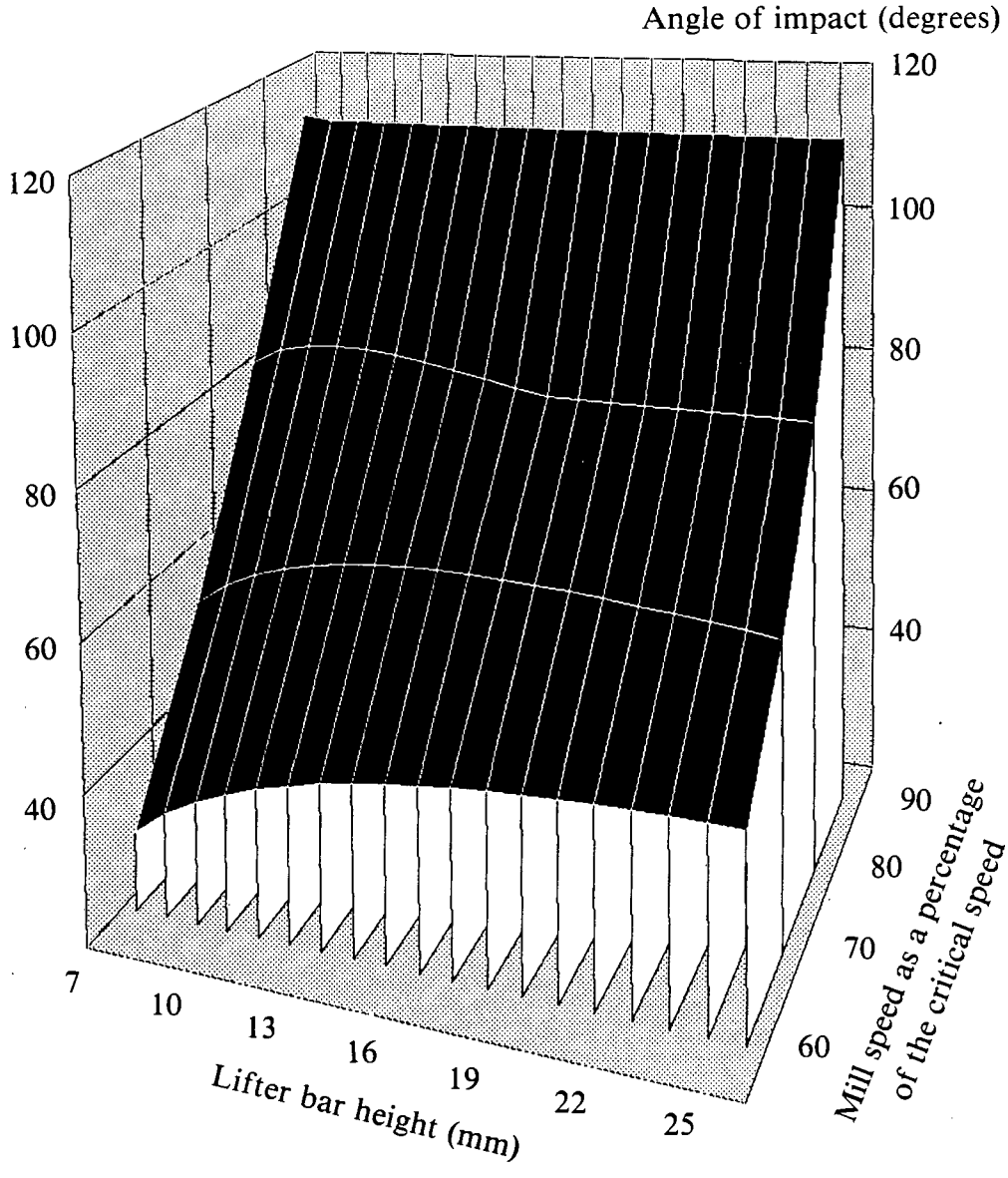

Figure 7. The combined influence of the height of the lifter and the speed of the mill upon the angle of impact.

It was found that as the height of the lifter increases from zero to slightly greater than one charge radius, the height has a strong influence on charge trajectories. For most lifter heights the angle of departure increases steadily with an increase in the height of the lifter, which is to be expected. However, above a critical lifter height, which is dependent upon the speed of the mill and the face-angle of the lifter, the balls follow identical trajectories which are independent of the height of the lifter. This occurs because the ball is projected off the face of the lifter prior to reaching the tip. This condition arises when the face of the lifter is close to perpendicular, and so the

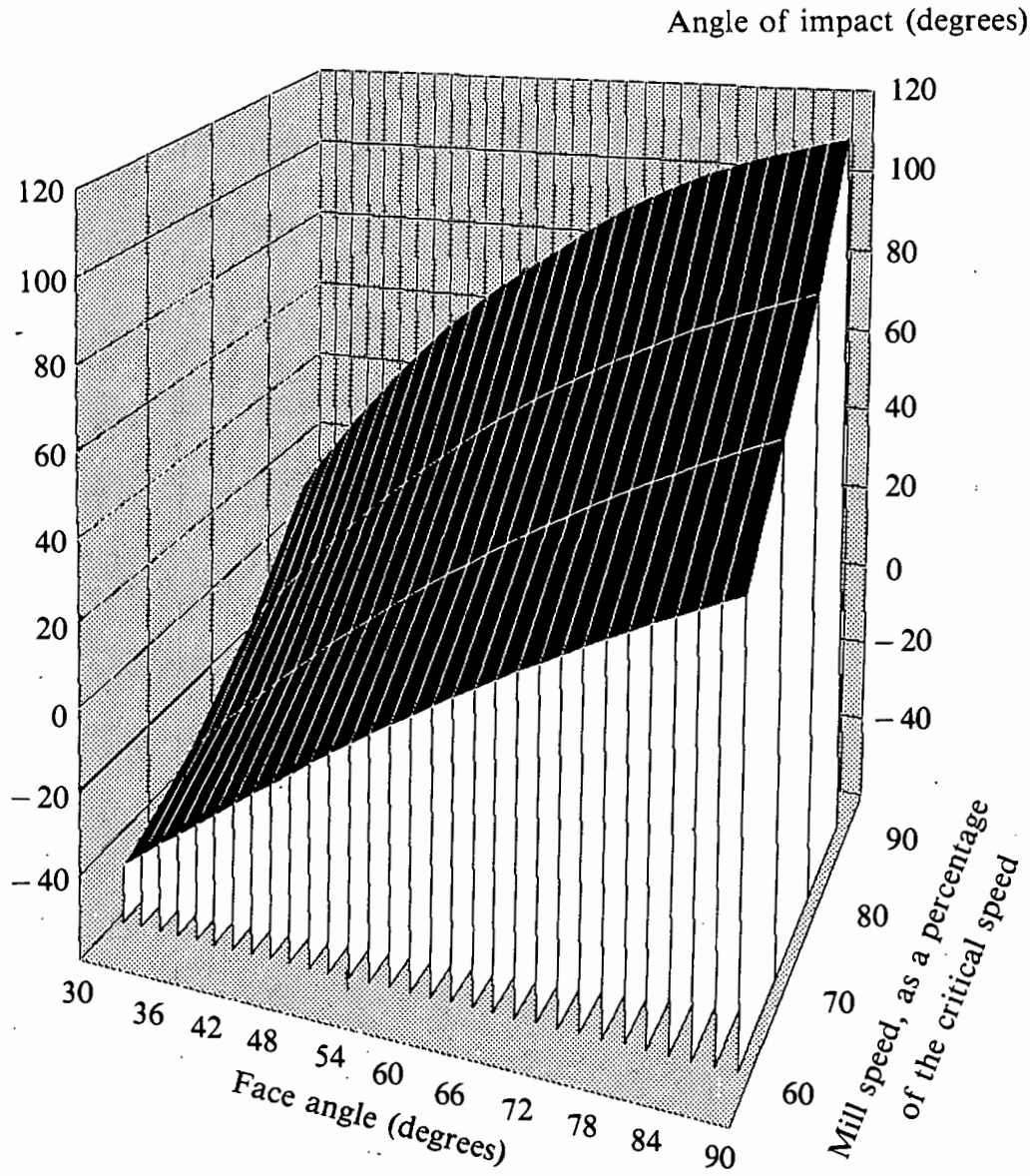

Figure 8. The combined influence of the face angle of the lifter and the speed of the mill upon the angle of impact.

gravitational acceleration acting on the ball is directed away from the face of the lifter, thus causing the ball to accelerate away from the face. The escape of the ball from the face of the lifter is facilitated by the fact that, in moving towards the tip of the lifter, the tangential velocity of the face decreases as a result of its decreasing radius of rotation. As the tangential component of the ball's velocity increases due to the gravitational acceleration, the ball moves free of the lifter face.

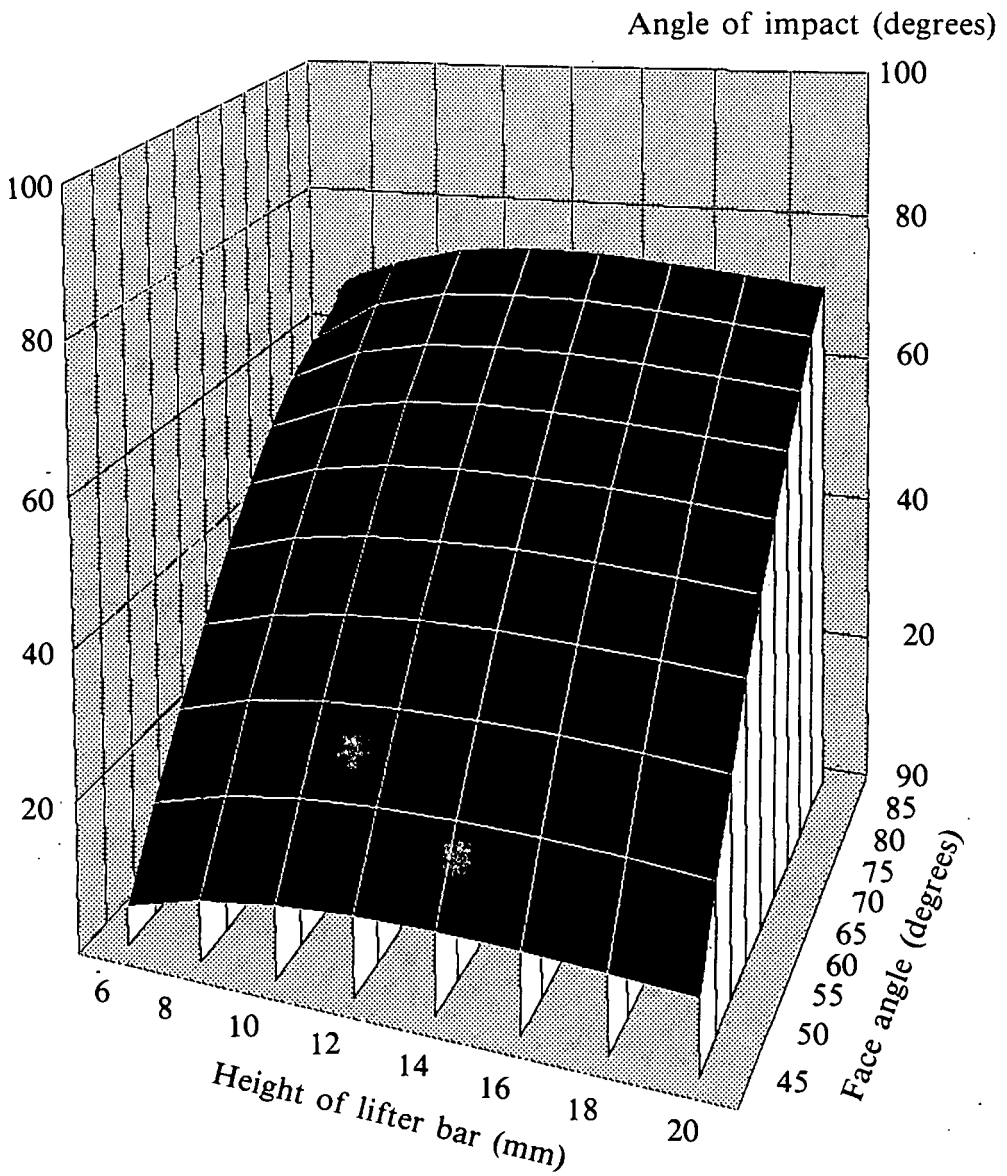

Figure 9. The combined influence of the height and the face angle of the lifter upon the angle of impact.

Once the height of a lifter is greater than the radius of the ball, it exerts only a small effect upon the trajectory of the balls, as shown in Figure 7. There is a peak in the projected angle of impact for a lifter height that is about equal to a ball diameter, after which the angle of impact drops off slightly. The underlying cause of this drop-off in the height of the trajectory is the radial acceleration of the ball. As the ball slides along the face of the lifter, the radial velocity increases relative to the tangential component of the velocity. In addition, the face of the lifter becomes progressively more vertical as it lifts the ball higher, and the ball is projected off at a more horizontal angle. Thus,

although the net velocity at the moment of projection off the lifter increases with an increase in the height of the lifter, the initial velocity vector of the free-flight trajectory is progressively directed further downwards. The direction factor gradually dominates the velocity factor, and leads to a shallower trajectory. The horizontal region on the impact-angle curve corresponds with the region of constant trajectories, when the ball leaves the lifter before reaching the tip. The influence of the height of the lifter on the angle of impact is dependent upon the speed of the mill. At 60% of the critical speed, the angle of impact gradually increases and then levels out, without passing through a maximum. This was corroborated by the experimental results.

The change in the height of the impact point is very small, however, so, in practical terms, an increase in lifter-bar height - once it is higher than the radius of the grinding element - has only a slight effect upon the charge trajectories.

An increase in the angle of the lifters was found to have a strong influence upon the height of the charge trajectories. In the case of a high-speed mill, running at 90% of the critical speed, a perpendicular lifter projects the outer layer of charge high up onto the opposing face of the mill, at 110°, as shown in Figure 8. The angle of the lifters can be tuned to project this outer layer onto the toe of the charge. In this instance, a lifter of 54° would be ideal; resulting in an impact point of 60°. By use of this technique, lifters can be used to key in the bulk of the charge, without the projection of the outer layers onto the shell of the mill. This is especially important in high-speed mills, such as are found on the South African gold mines, as lifters can be installed to key-in the charge without the projection of the charge onto the shell of the mill. A curved or round-tipped lifter yields an outer charge motion that is equivalent to that of a flat-faced lifter with a height that corresponds to the point at which the curvature starts. This height is equivalent to the minimum critical height, if the bar curves from its base.

A linear relationship was discovered between the speed of the mill and the angle of impact, and changes in the mill speed strongly influence the charge trajectories.

The relative influence of lifter height and face angle upon the impact point are shown in Figure 9. The lifter angle clearly has a far bigger influence on the charge trajectories than the lifter height.

Because the theoretical model is based on the fundamental laws of motion, it can be applied to a mill of any size. All trajectories and angles of departure and impact are independent of the size, and can be directly scaled-up. However, it must be borne in mind that the pressures in the charge and the forces of impact increase with an increase in the size of the mill. So, for identical charge motions, different grinding characteristics apply for mills of different sizes.

Some surprising effects of lifter geometry upon the charge trajectories were revealed by the study, and are of practical importance. The theoretical model is an improvement on all previous models, and agrees well with experimental results over a wide range of conditions.

CHAPTER 4
EXTENSION OF THE THEORY

4.1 GENERAL DESCRIPTION OF THE CHARGE

Many investigators have used the line joining the shoulder and toe of the charge to represent the angle of repose of the charge. This seems reasonable at low speeds, but as the mill speed is increased above 80% of the critical speed, this line becomes an unrealistic measure of both the angle of repose and the line defining the surface of the *en masse* charge. Vermeulen[19] has used the BHF surface to define the limits of the *en masse* region, and this surface provides, in principle, the correct description of the equilibrium surface of the charge. The equilibrium surface is the surface that divides the ascending, *en masse* charge from the descending charge. The surface starts at the toe and ends at the shoulder of the charge, and passes through the turning point of the ball paths at the top and bottom of each concentric path of the charge. The surface must also pass through the centre of circulation (CoC) of the charge. In an end-on view of the mill this surface is seen as a line.

As illustrated in Figure 10, the equilibrium surface can be superimposed onto the paths of the balls and the CoC easily located. The dashed line joining the toe and shoulder illustrates how meaningless it is to define the angle of repose and the *en masse* region by this line. The angle κ defines the angular location of the CoC. The tangent to the equilibrium surface at the CoC is perpendicular to the radial line passing through the CoC. This condition is uniquely defined because the equilibrium surface has a different curvature to the mill shell, so only one point on the surface can have a tangent perpendicular to a radial line. The paths of the balls in the *en masse* region form concentric circular paths of decreasing radii that converge on the CoC. So it is apparent that the tangent to the ball path at the CoC is perpendicular to the radial line passing through the CoC, and this is a fundamental property of the CoC. The tangential line subtends the same angle κ with the horizontal, as the angle of repose of the CoC. The CoC gives a good measure of the location of the charge, so the angle κ will be defined in this work to be the angle of repose of the charge.

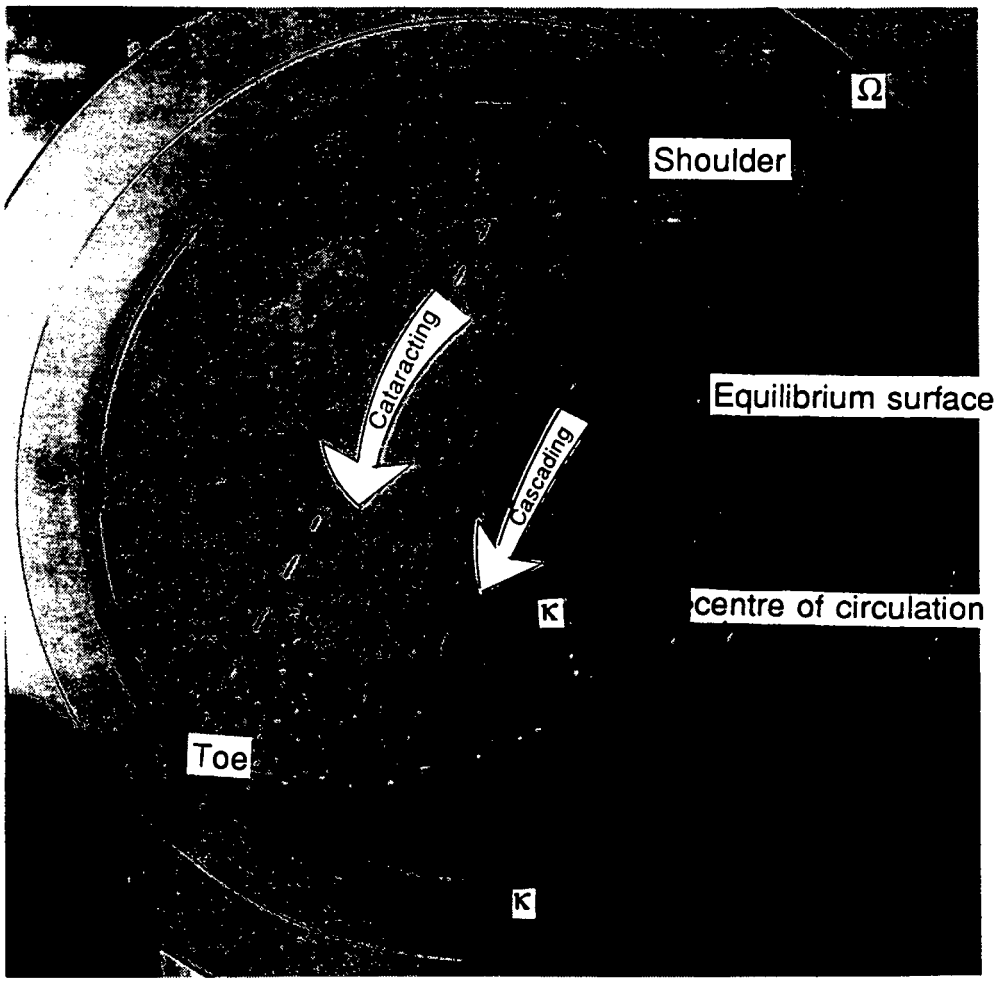

Figure 10. Definitions of the defined regions of the mill charge

This definition of the angle of repose is an extension of another conventional definition, i.e. the static angle of repose of a slowly tilted mill charge just at the point of slipping. The new definition accounts for the angle of repose under dynamic conditions, and that the angle of slip is not uniquely defined for a cascading/cataracting charge. For the condition of definition of the conventional definition, the charge just slipping, the two angles are identical.

The radial location of the CoC must vary with the speed of the mill, for a fixed charge filling. When the mill is stationary, the surface of the charge is horizontal, and the CoC is not defined, because the charge is not circulating. When the mill is set in motion, the charge is lifted up the side of the mill until it reaches the angle of static equilibrium

of the charge, which is an intrinsic property of any particular mill charge. The media will then begin to cascade down the surface of the charge, circulation of the charge begins and the CoC becomes defined. The minimum radius of the CoC is the distance to the surface of the charge plus one ball diameter, as there must be at least one layer of charge tumbling down the free surface for circulation of the charge to occur. There is thus a minimum angle of repose of the charge, and an initial radius of circulation, defined by the material properties of the charge and the volumetric filling of the mill. As the speed of the mill is increased, the angle of repose of the CoC increases. The radial location moves outwards because there is an increasing fraction of the grinding media cascading and cataracting on the inside of the CoC and correspondingly less media on the outside of the CoC. However, beyond a certain critical speed of the mill the radius of the CoC begins to move back in towards the centre of the mill. This corresponds with the CoC moving out of the bulk of the charge into a central hollow core that develops in the charge at these high speeds. There is no longer a cascading region, as all the descending media are cataracting. As the mill speed approaches the critical speed, the charge assumes an increasingly circular path, forming a continuous annulus around the periphery of the mill. At the limit where the entire charge is centrifuging the CoC coincides with the centre of the mill. The angle of repose, κ, gradually increases from the minimum initial value, and tends towards 90°, which is the upper limit of the angle of repose. This maximum angle is only reached when the CoC coincides with the centre of the mill, so is not in fact defined.

The centre of mass (CoM) of the charge defines the equivalent point to which all the mass of the charge could be condensed and still exert the same lever arm about the centre of the mill. It should be noted that all investigations that have been reviewed define the CoM only for the *en masse* section of the charge; the material that is cascading or in flight is ignored. The total charge in a mill forms a system of particles that are acted upon by an external force, the mill. It is a fundamental law of mechanics that "the centre of mass of a system of particles moves like a single particle, whose mass is the total mass of the system, acted on by a force equal to the total external force acting on the system."[30] The interactions of the balls between each other

out, by Newton's third law, and the impacts of the balls on the shell of the mill and the lifting action of the shell sum up to the total external force applied to the system. The theorem takes into account that particles within the system may not be touching one another (i.e. be in flight) at all times.

The omission of part of the charge, by considering only the *en masse* charge, must introduce an error into the calculation of power, and the error increases as the speed of the mill is increased, because the charge is spread further across the mill. It is far more accurate, especially at high speeds, to utilise the actual CoM of the whole charge in any power calculations. The calculation of the CoM is rather complex, as the distribution of the charge around the entire mill at a given instant must be known. This precludes the use of simplifying equations for the average charge density, as it is essential to know the density at each point around the mill.

The location of each ball in a given layer of charge over a complete circuit around the mill, as shown in Figure 11, gives the distribution of the balls in that layer at an instant of time. This gives the location and the density distribution of the balls in that layer of the charge. The centre of mass (CoM) of the ball over a complete circuit around the mill is given by:

$$X_{CoM} = \frac{\sum_{i=1}^{N} x_i m_i}{\sum_{i=1}^{N} m_i} \qquad Y_{CoM} = \frac{\sum_{i=1}^{N} y_i m_i}{\sum_{i=1}^{N} m_i} \tag{3}$$

For N being the number of images of the ball for a complete circuit around the mill. For all the masses, m_i being the same, for any given ball, the mass can be taken out of the equation, leaving:

$$X_{CoM} = \frac{\sum_{i=1}^{N} x_i}{N} \equiv \bar{x} \quad , \quad Y_{CoM} = \frac{\sum_{i=1}^{N} y_i}{N} \equiv \bar{y} \tag{4}$$

Therefore the CoM is given by the simple averages of the x and y data over a whole layer of charge.

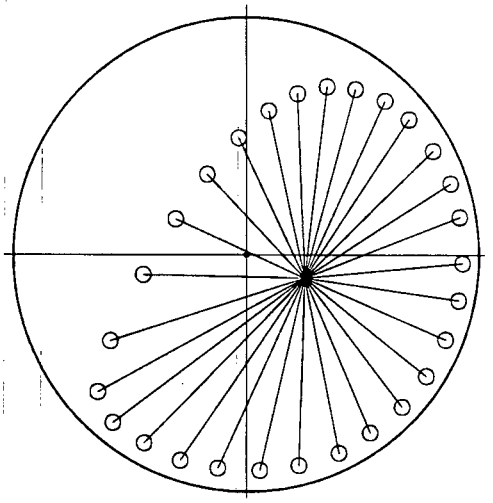

Figure 11. A single layer of balls in a slice of charge, showing the CoM

The CoM of the charge is not located at the same point as the CoC, except for a very thin layer of charge circulating at the CoC. In the case of the charge just circulating at a low speed, there is only one layer of balls cascading down the surface of the charge. The CoC will be located one layer of balls below the surface of the charge, but the CoM for the outermost layer of charge is located near the centre of the charge mass. This highlights another property of the CoM; unlike the CoC, the CoM is located at a different axis for each concentric layer of charge. To calculate the CoM of the entire charge, the CoM's must be summed over all layers of the charge. A comprehensive model of the motion throughout the bulk charge is required for this to be carried out.

4.2 BULK MOTION MODELLING

The theory that had been developed in the earlier work was extended to a limited extent. The objective was to model, in as simple a manner as possible, the motion in the bulk of the charge. The theories of White[3] and Davis[4] assumed that the ball rested in an isolated manner against the shell of the mill, and did not slip relative to the shell. They modelled the motion of the concentric layers in the same manner, by considering

the layer outside of the one being analyzed to be a smooth lining. Using this technique they could build up a complete image of the bulk charge.

Aside from the problem of assuming no slip, which has been analyzed in detail by Nates *et al*[29], it is incorrect to assume that the ball is isolated. Referring to Figure 12, in essence, if an isolated ball (1) reaches equilibrium at an angle γ_o, then the ball immediately below it (2) will not yet have reached the equilibrium angle, so the upper ball (1) must be resting on the lower ball (2). Thus for a smooth lining a ball can never be isolated while resting against the lining: the ball will always be resting on the bulk of the charge. For a charge consisting of balls all of the same size, a ball resting exactly on the top of another ball would be equivalent to it resting on a radial lifter of minimum height, as discussed in the theoretical derivations in Appendix I. The ball rests on the tip of a minimum height lifter, and falls free of the lifter as the point of equilibrium is reached.

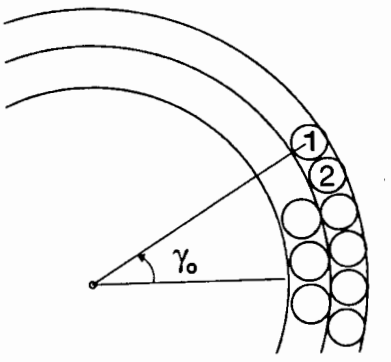

Figure 12. A ball always rests on the ball below it

To simplify the conditions in the charge so that the theory of an isolated ball can be applied, it must be assumed that only the three basic forces - gravitational, centrifugal, and normal reaction - that are used in the theory, act on the ball. These conditions need only apply in the upward-moving section of the balls trajectory, that is in the region where the ball moves out of the *en masse* media into the cascading region. Given that the charge consists of concentric layers of balls, then the inner of two adjacent layers has a lower critical speed than the outer layer (the critical speed is proportional to $\sqrt{R}$). A ball in the inner layer will therefore have a lower angle of equilibrium, γ_o, and fall away from the outer layer before the adjacent ball in the outer layer begins to move inwards. A ball in the inner layer therefore does not have the outer balls pushing downwards on it. So a ball approaching the top of the circular portion of its trajectory may well satisfy the conditions of an isolated ball resting on a 'lifter bar', where the balls immediately below it form the lifter.

It is unrealistic to assume the concentric layers of charge will all rotate with the angular velocity, Ω, of the mill. Vermeulen[22] and Morrell[27] have both shown that the angular velocity of the concentric layers decreases as the CoC is approached, becoming zero at the CoC. This slip can be accounted for by utilising the values measured in the experimental work. The actual angular velocities measured in the experimental work could be inserted for the angular velocity of each layer, thus taking full account of the slip in the charge.

Using the simplifications outlined above, and the theory for a ball on a lifter, a far more realistic estimation of the bulk charge motion should be obtained than those derived by White and Davis.

4.2.1 Possible drawbacks of the simplified theory

It is unlikely that a ball will rest directly on top of another ball; it will rather stack on top of at least two other balls. When a ball rests in the V between two balls, the net effect is still that of a radial lifter, but one that acts from part way up the side of the ball, rather than at the base of the ball. This is equivalent to considering the ball to be of a smaller radius, determined by how low it rests between the supporting balls. In the bulk of he charge a ball is more likely to stack between two layers, on top of three balls, than in a concentric row on top of only two balls. This three-dimensional stacking of the balls, illustrated in Figure 13 as a simplified end-view of the ball charge, results in a ball straddling two concentric rows of balls. Ball 1 would reach its point of equilibrium first, then ball 2 (because of its reduced radius). This leaves ball 3 effectively resting on a lifter with a very low face angle. In addition there is a normal force of reaction acting between ball

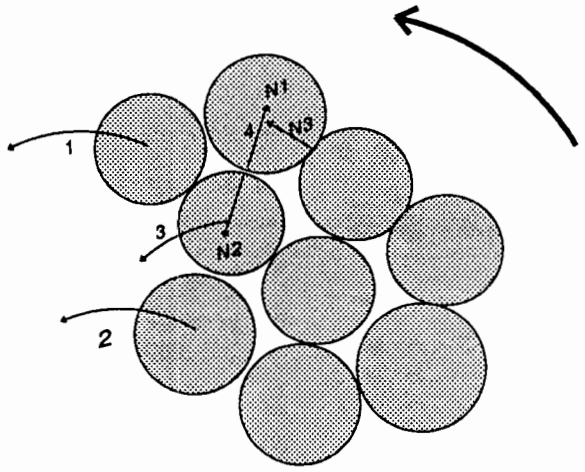

Figure 13. Simplified cross-sectional view of the stacking of balls

3 and ball 4, so there is some additional force acting on ball 3, other than the three considered in the theory.

The magnitude of these additional possible effects cannot be directly worked out, because of the complex range of interactions between all the balls in a mill, and the variability of the ball stacking. It was therefore felt that it would be informative to fit the simplified theory to the data, to ascertain whether this gives a reasonable estimate of charge motion in the bulk of the charge. If not, then an estimate of the magnitude of the additional forces could be obtained. Although this simplified model is not considered to be a realistic model of the action in the bulk charge, it was developed to ascertain whether it could yield some insights into the effect of changing the mill speed and liner configuration on the action within the charge.

CHAPTER 5
EXPERIMENTAL OBJECTIVES

The overall objective of the work was to analyze the actions within the grinding media and to correlate this with the milling that actually takes place. The emphasis was on how this action could be influenced by changing the design of the mill liners.

The overall objective was broken down into a number of more specific sub-objectives:

i) To view the motion of the grinding media within the bulk of the charge.

ii) To vary the mill liner and speed, and monitor how these affected the motion.

iii) To analyze the forces and interactions within the charge, in order to clarify the source of the grinding action.

iv) To attempt to correlate the observed action in the mill with the results of milling trials.

v) From these correlations to determine what type of charge motion/milling action is the most effective or efficient at reducing ore.

vi) To be able to develop a practical idea of how varying the design of the mill liner may help to optimise the performance of a mill.

vii) To correlate these results with the theoretical model of how lifter bars affect the motion of the outer grinding media.

These objectives presented a broad spectrum of work to be tackled. Therefore the work is divided into two distinct sections: experimental analysis of the charge motion, and milling trials.

5.1 CHARGE MOTION ANALYSIS

Here, the objectives were as follows. To be able to view, in some detail, the motion of a ball or balls in the bulk charge of the mill. To plot their trajectories in order to analyze the velocities, accelerations, impact forces, location of paths of motion, and their interactions with other balls. The findings of these interactions could then provide a means to develop a model of how and where the grinding physically takes place. Finally, to determine how these factors are affected as the mill speed and liner

configuration are varied, and in what way, and to what extent these can be used as a means of optimising the performance of a mill.

5.2 MILLING TRIALS

The primary objective of this part of the work was to investigate whether the liner profile affects the efficiency of the mill, where efficiency is defined in terms of the mill's ability to produce fines and handle the throughput of ore. The second objective was to try to correlate any findings with the findings of the charge motion analyses. It would then be known how a change in lining affects the milling action, and what influence this has on the rate of grinding.

Bearing in mind the diverse range of milling applications worldwide, and the variety of mills used, it was decided to concentrate on one particular type of milling. Autogenous grinding of run-of-mine (RoM) ores was chosen, as this accounts for about a third of all gold ore milling in South Africa, and is on the increase. It had been shown in work conducted on the mines[33] that a change in liner design could bring about a sevenfold improvement in liner life. This has sparked considerable interest on the mines, as the RoM mills have short liner lives and the cost of relining these large mills is very high.

Milling is a widely studied field, and this work was designed to look at only a particular aspect of it, that is the influence of liner design on the rate of production of fines. Although other observations of general interest may arise, these should be commented on, but not necessarily analyzed in detail, as they would be beyond the scope of this work, and could easily lead the work astray from the objectives of this study.

5.3 CROSS-CORRELATION

The final stage of the work was to establish a set of correlations between the different aspects of the study, so as to interrelate the design of the mill lining, the motion of the media, and the grinding action. It was not expected that such a broad goal could be fully attained, but rather that some insight would be achieved, and that this would also point to particular areas of study that may bear useful results.

CHAPTER 6
EXPERIMENTAL - CHARGE MOTION

The primary objective of viewing the motion of balls deep within the charge of a mill presented a substantial challenge in developing or finding a suitable experimental technique. A number of techniques were investigated, as outlined below, before acceptable methods were found. Before addressing the experimental methods, it is appropriate to detail the objectives of the work.

6.1 OBJECTIVES

The primary objective was to be able to trace the motion of a ball, or balls, within the bulk of the tumbling grinding media. To this end, it is of limited use viewing balls through a window at the end of a mill, as only a two-dimensional motion is observed, and the window has strong end-effects that lead to non-representative ball paths. As has been observed in the work of previous authors[5,6] these end effects can lead to erroneous conclusions, and misconstrued arguments. Therefore, whatever technique was used to trace the motion of the balls, it would have to penetrate the bulk of the charge.

Once the motion of the ball was traced, its position had to be located with sufficient clarity and precision to make possible an analysis of its velocity, acceleration and trajectory of motion. Thus it was desirable that the technique chosen should have a reasonably good resolution, say within a quarter of the diameter of the ball.

It was necessary to freeze the motion of the ball at many closely spaced consecutive intervals, so as to be able to calculate the velocity of the ball. This would necessitate rapid exposure times of the detection equipment, such as a fast shutter speed camera. Previously[1,2] the motion of rods had been filmed with a shutter speed of 1/300 second with a high speed cine´ camera, and despite the short exposure time per frame the images had been noticeably blurred when the rods were in flight. As the ball would circulate once around a small experimental mill in about a second, at least twenty separate locations of the ball would need to be detected each second, for any chance

of velocity calculations to be made. A consolation technique for detecting the velocity of the ball would be to measure the length of the blurred path in the image, and knowing the exposure time thus calculate the velocity. However, this tends to have limited accuracy and does not yield the instantaneous velocity and thus acceleration of the ball

A three-dimensional view of the motion of the ball would be preferable, so as to be able to link its radial path with that along the length of the mill. To achieve this it would be necessary to view the ball from both the side and front of the mill simultaneously.

It was also desired to view the rotation of a ball about its own axis, as this would help reveal how the grinding actually takes place. The ball would thus have to be able to be marked in a directional manner that could be detected by the tracking technique.

A further objective was to observe if there are any differences in motion between different size and mass balls, which could best be achieved by observing different balls simultaneously. Being able to track a few balls at once would also considerably reduce the observation time required and allow a comparison of the motion of balls in different parts of the mill at the same instant. This would provide information about the stability and regularity of the motion in the mill, and whether there are transient occurrences isolated to a part of the mill.

To be able to assess the effects of varying the operating parameters of the mill, it was necessary to be able vary the speed of the mill, and the configuration of the lining. It would also be desirable to be able to run it wet so as to assess the effect of a slurry on the motion of the balls.

With these objective in mind, clearly a rather specialised experimental rig, and tracking technique were required. The primary functions of the experimental technique would be to penetrate through the main body of the charge in a mill, while detecting the ball being tracked. It should also have a sufficiently good resolution to locate the ball with

sufficient accuracy to calculate velocity and acceleration vectors of the balls as they circulated in the mill.

6.2 THE SEARCH FOR AN EXPERIMENTAL TECHNIQUE

The first option considered to fill the requirements was radioactive tracing, as it has the penetrating power to pass through the media in a mill. However, it is difficult to obtain the desired resolution with radioactive emissions, as the radiation is even in all directions, and it is difficult to detect the actual position of the radiating particle. One possible technique would be to have a number of detectors arranged around the mill, and compare the directions and strengths of the emissions detected by each. With a suitably calibrated calculation routine one could then assess the location of the ball. There are obvious problems with the resolution of such a technique, and the sophisticated and rapid computer program required to operate such a system. A far better technique of locating the source of radioactive emissions would be to use a bank of collimators. These are in essence a set of long narrow pipes with a detector at the end of each: this only allows the detector to view what is directly in line with the pipe, as all other emissions are screened by the walls of the pipe. The collimators are set up in an array in the form of a grid, and so when a detector registers radioactive emissions the x-y co-ordinates of the ball can be established. This was considered to be a most suitable tracking technique and was pursued in depth. However, a commercially available collimator could not be found, and it would have been prohibitively expensive to build one, as the detectors and associated amplifiers are very costly. In fact it would have entailed a whole research programme in itself to develop one.

The possibility of telemetric detection was considered next. By the use of directional detectors one can, in theory, locate the source of emission by standard triangulation. This detection technique relies upon the strength of the signal to detect the direction of its source, and the highly non-uniform densities of charge surrounding the ball as it travels around the mill would drastically reduce the effectiveness of such a technique.

When heated an object has strong radiation in the infrared spectrum. By filming in the dark, and using an infrared-sensitive video camera, it may be possible to track a heated ball in the mill. The main drawbacks of this would be the strong attenuation of the radiation by the other balls in the mill, and the scattering of the radiation, which would most likely result in a weak and blurred image. Whatever its draw-backs, this technique offered an inviting possibility because of the simplicity of the technique and the availability of the equipment. However, better techniques were found so this was never tried out.

Another possible technique considered was X-ray filming. Whether any equipment existed that had a short enough exposure time to be of any use was not known. However, the decision was made to pursue this line in the hope that it may bear some fruit. As a start the medical X-ray equipment at the teaching hospital attached to the University of Cape Town was investigated. The initial objective was to find out the penetrative power of the X-rays, and ascertain what the shortest interval between exposures was, or whether a number of exposures could be taken on one film. With the very friendly, if bemused, assistance of the hospital staff the investigations eventually led to the ideal piece of equipment, a bi-planar angioscope. This is used in the cardiovascular theatre to detect the movement of heart valves, once a semi-opaque dye has been injected into the patient.

While investigating the equipment in the hospital another excellent piece of equipment was found, the gamma camera. This is a collimator, as had previously been sought, that detects radioactive emissions from a gamma ray source. It is used to track the passage of irradiated material though a persons cardiovascular or digestive system. This was selected as a secondary experimental technique, as discussed later in this chapter.

6.3 X-RAY FILMING

With the permission of the hospital to use the equipment obtained, the experimental rig was then purpose-built to suit the equipment. A detailed listing of all experimental equipment is given in Appendix II, so only a general description is given below.

6.3.1 X-ray equipment

The bi-planar angioscope uses high energy X-rays emitted in short pulses to stimulate a scintillating screen, similar to a television screen. The images are then detected by

(a)

(b)

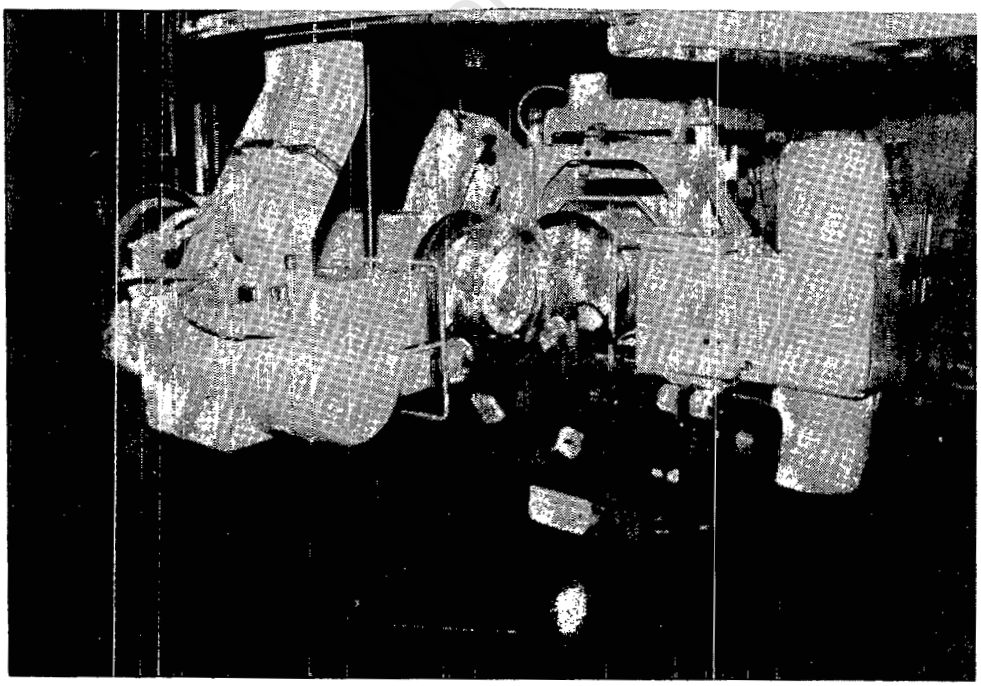

Figure 14. The bi-planar angioscope

a television camera and relayed to an external monitor. The image can be filmed simultaneously with a cine´ camera to provide a permanent record. The equipment can film at fifty frames per second, which was ideal for accurate tracking of the balls, and having a similar wave-length to visible light, the X-rays provide excellent resolution. An added advantage of the equipment is that it can film in two planes simultaneously. The arrangement of one of the fully-manoeuvrable arms is illustrated in Figure 14a. The arm has a semi-circular shaped holder, to which is attached the scintillator and camera at one end, and the X-ray emission tube at the other. Figure 14b illustrates both the cameras in the fully interlinked position, perpendicular to each other, with the mill in the centre. This gap within the U-mounting can be adjusted to vary the spacing of the tube and camera. The entire apparatus is remotely controlled and can provide very precise positioning. The maximum output of the X-ray tube is 150 kV, and the strength and exposure of the X-rays is automatically controlled by the angioscope.

6.3.2 Mill mounting frame

The mill was mounted above the drive train, and supported on the end flanges, as illustrated in Figure 15. This is the original mill construction which was later modified. The mill was rotated on four drive wheels that had side faces so as to prevent any longitudinal movement of the mill. Each pair of wheels was on a solid axle, and these were linked by a notched drivebelt so that all four wheels were driven. This ensured that there would not be any slip of the mill. The entire drivetrain was unlubricated so as to ensure that there was no oil or grease leakage in the operating theatre.

It had been found previously[1] that a DC motor controlled by a rheostat did not provide a constant speed under the variable loading of a mill, so an asynchronous electric motor was used to provide a very stable speed control. The motor was linked to a continuously variable gearbox so as to provide a full speed range from 0 to 120% of the critical speed of the mill, in both directions of rotation. It was most useful to be able to reverse the direction of rotation of the mill, as this meant that one lifter bar, with a different face angle on each side, could be used to provide two different conditions. This greatly reduced the time required during experimental work, by decreasing the number of changes of lifter bars required. A speed indicator was

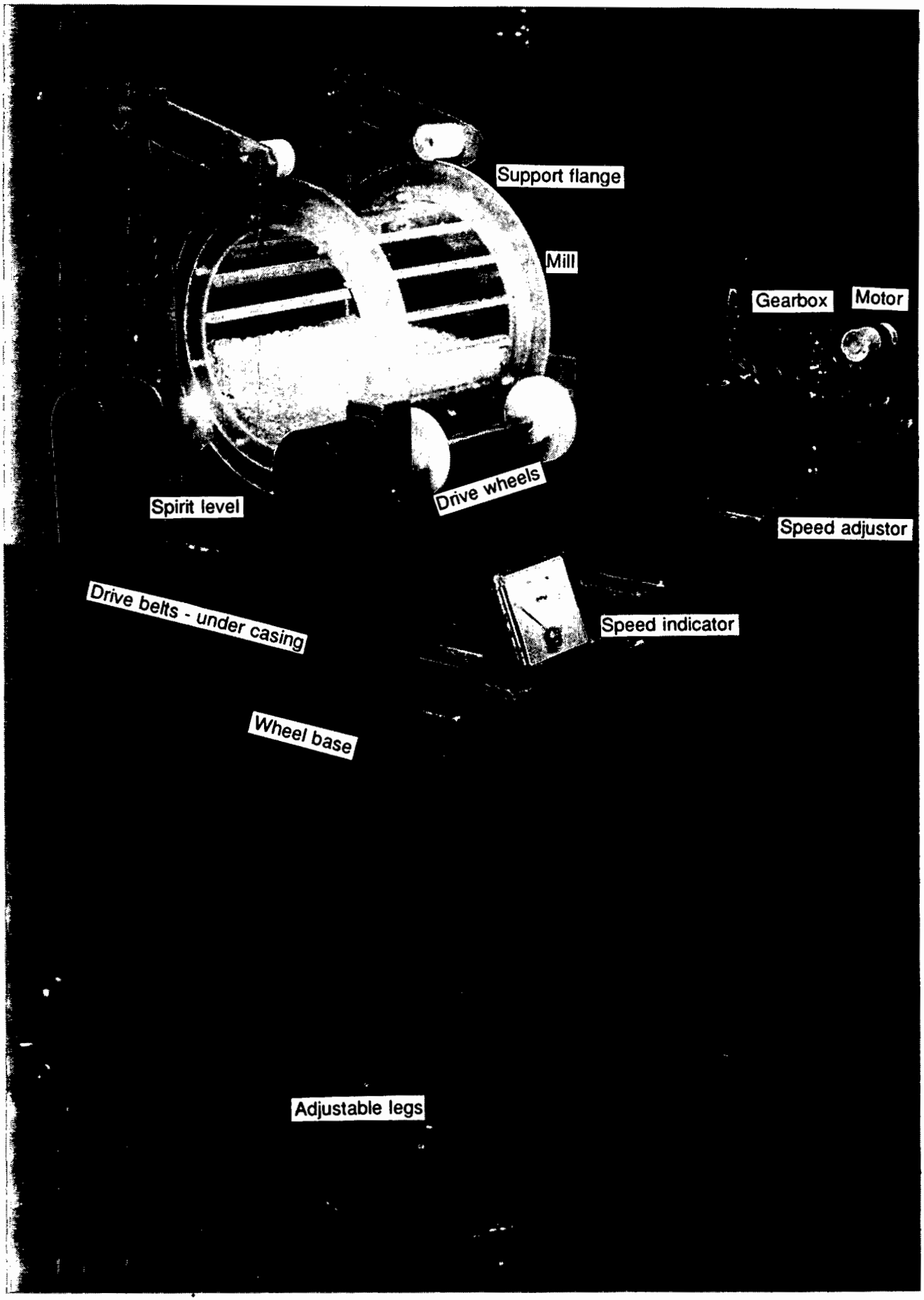

Figure 15. The original experimental rig

connected to the output shaft of the gearbox, and calibrated to the mill speed.
The frame of the rig was designed in two sectors. The top part, which included the motor and drivetrain, could be removed from the base so that the mill could be mounted on a table, or on the bed of the operating theatre, if necessary. This also facilitated transport of the apparatus. The base consisted of legs mounted on wheels, so as to make the mill manoeuvrable around the building. The wheels could be locked while the experimental work was in progress. The lengths of the legs could be adjusted so as to vertically align the mill with the X-ray equipment. A spirit level was mounted on the frame of the mill so the mill could be set horizontally. Initially rollers were mounted at the top of the mill, where they could press down, to prevent any jumping of the mill. These were subsequently found to be unnecessary so they were removed. The entire frame was neatly constructed and painted to give it a clinically clean appearance.

6.3.3 The mill shell

The mill was constructed entirely of perspex, which is very transparent to X-rays. The original mill is shown in Figure 16. The end flanges provided the drive to the mill, and raised it above the mounting rig. Once plastically welded to the mill, the flanges were carefully machined to ensure that they were absolutely circular. The end faces were both removable and recessed into the mill so as line up flush with the drive flanges: this ensured that none of the beads were hidden behind the width of the flange, when viewed from the side. When smeared with silicone vacuum gel the end faces were absolutely watertight.

The original internal mill dimensions were 250 mm diameter by 243 mm long. However, this was found to provide too much screening of the X-rays, so a smaller mill was constructed. The final mill had a diameter of 190.3 mm and was 97 mm long. This still provided a ball-to-mill size ratio of 1:32, and allowed for 20 layers of balls along the length of the mill, which was considered to be sufficient to allow for free movement of the balls.

A small ball bearing was recessed into the centre of the front face of the mill so as to provide a clear indication of the centre of the mill. This is invaluable when positioning the film image during analysis. A metal foil was mounted in the front of the mill, between the door and the flange, so as to provide a clear indication of the inner edge of the mill. This formed a flat annular ring 10 mm wide, with the inner edge having the same radius as the inside of the mill. A lead pointer was fixed to the flange to provide a marker for tracking the speed of the mill. Wire rods were mounted adjacent to one side of the mill, near either end. These were to provide a scale measure and locate the ends of the mill for the side view filming.

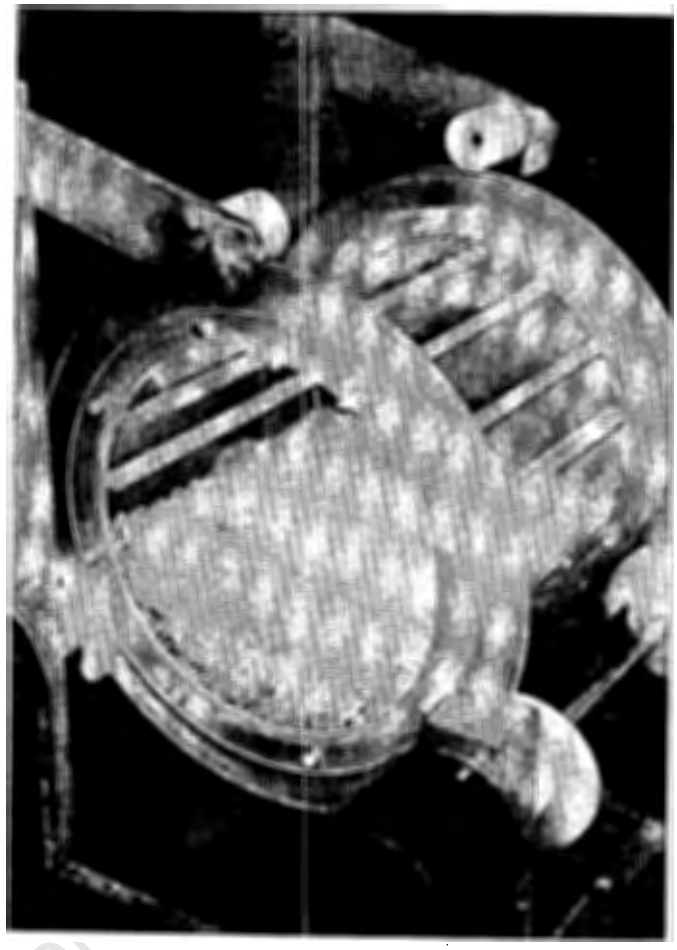

Figure 16. Close-up view of the original mill

6.3.4 Mill lining

One of the fundamental aspects of the work was to be able to vary the profile of the lining in the mill. The basic technique employed was to insert lifter bars of variable height and face angle, Figure 17. These were bolted in from the outside of the mill, using plastic bolts so as to retain the transparency of the mill (Figure 16). The lifters were machined out of perspex, to close tolerances. One end of each lifter had steel foil glued on so as to make the lifters visible in the films. There were 12 lifters mounted around the circumference of the mill. The detailed diagrams of the profiles of the lifter bars that were used are shown in Figure 160 of Appendix II. The heights of the lifters varied from 1.8 to 10 mm, and the face angles from 45° to 90° (rectangular).

Figure 17. The perspex lifter bars and the high-friction smooth lining

It was also desired to run the mill with a smooth lining. However, in a small experimental mill the charge pressure is too low to use a completely smooth lining, as the charge slips extensively. This problem was eventually overcome by gluing fine granules of plastic to the back of a self-adhesive plastic sheet. This provided a rough, high-friction surface that was transparent, and could be removed after use. It also covered the bolt holes.

6.3.5 Mill charge

Initially glass beads were selected as the media in the mill. Pure glass has a very low refractive index for X-rays so is transparent and shouldn't diffract the X-ray beams. The basic calculations used to establish this are given in Appendix III. A particular attraction of glass is that it has about the same density as rocks, so it represented an ideal experimental charge. Boiling beads of various sizes were used. However, much to our surprise, the mill charge was found to be totally opaque to the X-rays. The dimensions of the mill were reduced but this still didn't help. The chemical composition

of the balls was analyzed, and traces of heavy elements were found in them. Although these occur in minute quantities it appears that they present a barrier to the X-rays of the angioscope.

Finally 6 mm plastic beads were used, as no source of plastic balls could be found. Any burring of the beads was carefully cut off, so that each presented an evenly round ball. The X-rays penetrated excellently through the beads. The whole charge left only a shadowy outline of its profile. The initial concern that the bead would bounce around excessively was not at all justified, and in fact they had a fairly subdued action which was most suitable for the study.

The basic charge was 6.1 mm beads, weighing 0.0947 g each.
Four opaque balls were used for tracking in the mill. The range of balls was selected to provide a cross-section of different size and mass balls.

1. *Lead bead* This consisted of a normal bead with a small lead rod fitted down the centre. This provided an excellent method of tracking the rotation of the ball. Its mass was 0.2251 g.
2. *Steel ball* A standard 6.0 mm ball-bearing, weighing 0.8823 g
3. *Small steel ball* A smaller ball-bearing with a 3.2 mm diameter, and weighing 0.1297 g.
4. *Glass bead* One of the boiling beads that was originally to be used. This provided a fainter image than the other balls but was quite easy to track. It was smaller, 3.7 mm, and lighter than the beads, at 0.0699 g.

6.3.6 Procedure and precautions

As the filming equipment was available for only very limited periods, it was important to have an efficient experimental procedure planned. The appropriate set of lifter bars was bolted in and the mill filled to 45% of its internal volume with balls. It was decided to standardise on the volume of filling, so as to limit the number of variables in the experimental work, and also to be in line with the level of filling used as standard on the South African mills. The marked balls were then added. The circular metal ring, for marking the mill circumference, was placed onto the bolting face of the door, and

this was bolted into place. The lead pointer was fixed to the front of the mill flange. In the second batch of filming a plumbline was suspended next to the mill, to give a vertical reference line, and a lead number indicating the number of that run, was fastened onto the flange of the mill, so as to ensure that each run could be clearly identified. The mill was set horizontally, by use of the spirit level. The mill was then set at the speed for its initial run, and the apparatus was then ready to be wheeled into the theatre.

Because of the environment of the operating theatre, care had to be taken that everything was hygienically clean. The apparatus was carefully cleaned prior to use and the author had to dress in surgical vest, pants, and slippers, Figure 18. When filming was taking place a heavy lead overcoat was worn for personal protection.

The filming was carried out in two separate batches. Unfortunately only one of the cameras was working during the first batch of tests, so only the front view could be taken. After the first batch had been analyzed, a second batch was carried out to include the side view and complete a comprehensive set of experiments. The cameras could only interlink around the centre of the bed, so to be able to place the camera in the correct location the operating bed had to be removed. The bed is an integral part of the equipment, but could be unbolted from its support frame without too much difficulty.

Figure 18. Ready to head into the Cardiology theatre

It was possible to align the cameras automatically into perpendicular planes, and the mill was very carefully positioned parallel to the front-viewing camera. The mill was placed as close to the scintillator screen as possible. This reduced the degree of distortion of the image which arose from the divergence of the emitted X-rays. The further the object is from the source of radiation, and the closer it is to the receiver, the less the overall magnification of the image, and the less difference there is in the degree of magnification between the front and rear of the object. The mill was also placed as near as possible in line with the centre of the screen. This was to ensure equal magnification of the image about the centre of the mill, as the linear displacement of the image from its actual location increases as it moves further from the centre of projection. Thus if the mill was placed off-centre of the screen then the projected image would have been slightly oval. The cameras could only be aligned perpendicularly to one another in one location, with their paths crossing in the centre. So positioning the face of the mill close to the scintillator, entailed sacrificing its central alignment with the side-view camera, as can be seen upon inspection of Figure 14. It was considered that with the relatively short length of the mill, the resultant distortion would not be too great.

Each of the runs was for about four seconds, yielding 200 frames of film that could be analyzed. With the mill rotating at over one revolution per second, and the balls circulating at a higher rate than that, up to 8 complete revolutions of a ball could occur in that period. The films were developed at the hospital in the automatic developer dedicated to the X-raying equipment.

The detailed conditions of the runs are set out in Table I and Table II. The heights of the lifter bars were systematically varied from 1,8 through to 10 mm. Three different angles of lifter bars were used for the 6 mm lifters, 45°, 60°, and 90°. This was to provide a comprehensive picture of how the face angle of the lifter bar affected the motion of the charge. A smooth-profiled, high friction lining was used to simulate flat linings. The speed of the mill was varied from 68% through to 100% of the critical speed, which covers the range of operating conditions used on the mines. The critical

Table I The full set of test conditions used for X-ray filming, First batch

Run	Speed, % crit.		Lifter bar		Slurry
	Setting	Actual	Height mm	Angle, °	
1	68		3.12	90	
2	73	73.99	3.12	90	
3	82	82.71	3.12	90	
4	82	82.63	1.8	90	
5	73	73.48	1.8	90	
6	68	67.80	1.8	90	
7	92	97.25	1.8	90	
8	68	67.73	10	60	
8a	68	68.53	10	90	
9	73	73.09	10	90	
10	82	82.17	10	90	
11	82	82.07	10	60	
12	73	73.25	10	60	
13	68	68.10	6	60	
14	68	68.13	6	45	
15	73	72.84	6	45	
16	82	81.93	6	45	
17	82	82.10	6	90	
18	72	72.63	6	90	

speed was calculated as per eqn.(5), this is derived in Appendix III.

$$\%critical = \frac{rpm.\sqrt{D}}{42,3} \times 100 \qquad (5)$$

The only time the composition of the charge was varied was when a slurry was added. A slurry had to be made up that would be transparent to the X-rays. It was eventually decided to try a mixture of water and fine shavings of plastic. These shavings were

Table II The full set of experimental conditions for X-ray filming, Second batch

Run	Speed, % crit.		Lifter bar		Slurry
	Setting	Actual	Height mm	Angle, °	
19	92	91.81	3.12	90	
20	92	92.34	10	60	
21	92	92.05	10	90	
22	92	91.40	6	90	
23	68	68.23	6	90	
24	92	91.68	6	45	
25	92	91.81	6	60	
26	82	81.78	6	60	
27	73	72.83	6	60	
28	73	73.62	6	60	yes
29	82	81.97	6	60	yes
30	92	91.65	6	60	yes
31	92	91.57	6	90	yes
32	100	100.3	6	90	yes
33	73	73.35	6	90	yes
34	68	67.95	smooth		
35	99	99.22	smooth		
36	92	91.87	smooth		
37	82	81.89	smooth		
38	72	72.50	smooth		

similar in shape to small particles of sand. The slurry was not made up to any particular density, but rather mixed until it formed an even suspension, that felt of a reasonable consistency when stirred. This was at about 50% volumetric solids. This was not a realistic slurry, but rather a trial to observe its general effect on the charge motion. The amount of slurry added to the standard ball charge was sufficient to fill the interstices between the balls, representing about 45%, by volume, of the ball charge.

6.3.7 Experimental problem

A major drawback was that the speed of the mill could not be set accurately enough with the dial indicator. This was partially overcome by timing the mill over 30 revolutions so as to check the speed, and resetting if necessary, prior to each run. This was time consuming and it was difficult to set the speed accurately, as can be seen from the slight inconsistencies in the actual mill speeds. It is recommended that a number of reflective radial markers be spaced evenly around the flange of the mill and a photosensor used to detect the rotational speed. The speed can then be displayed on a digital readout for rapid and accurate speed setting.

6.3.8 Analysis of results

The objective of the analysis was to convert the raw data into x-y co-ordinates of the location of the beads in each frame of the film.

The results were in the form of reels of 35 mm film. This presented the problem of how to project them onto a screen for analysis, as a 35 mm projector could not be found. Finally an old slide projector was adapted to support the reels and feed the film, as shown in Figure 19. The films were manually wound from one reel to the other, passing through the carefully positioned frame holder. The image was projected onto a graphics tablet so that the coordinates could be automatically compiled.

A special holder was made for the film to feed through. This had to support the film in the vertical plane and, most importantly, locate it in the correct focal plane of the projector. The holder was designed with runners at the top and bottom to firmly hold the film in place, and with a wider clearance across the centre to ensure that the surface of the film did not get scratched. The film reel holders were mounted on the frame with a simple lock-nut system so that they could be set at the correct resistance to retain the film under slight tension as it was fed through. The horizontal position of the image was set by carefully positioning the film as it was reeled through, and the vertical position could be adjusted with the built-in adjuster screw mounted on the rear of the projector.

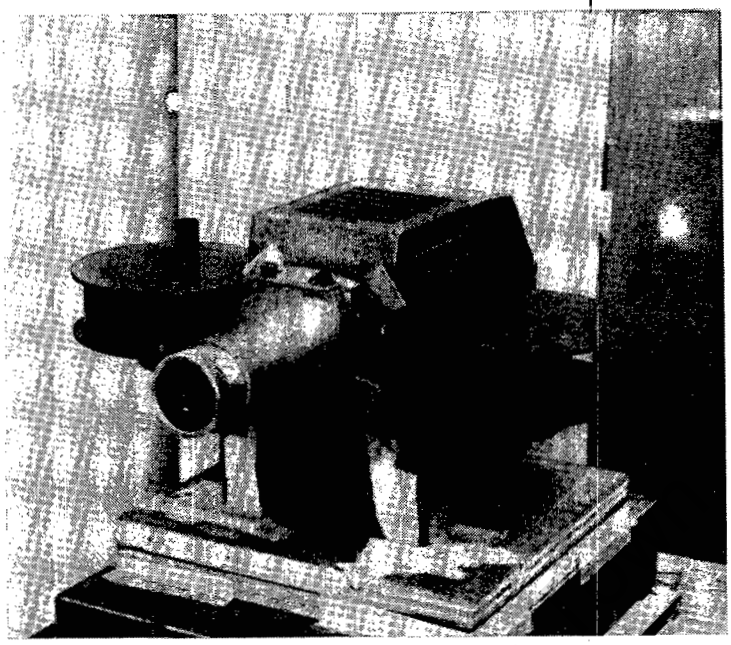

Figure 19. The projection equipment used for analysis of the X-ray films

The projection system was carefully aligned with the graphics tablet so that it was perpendicularly in line with the centre of the tablet. This was to prevent any distortion of the image arising from the skew projection of the film. A template of the mill was drawn onto the graphics tablet, and the projector set at the correct distance from the tablet for the image to coincide. This distance, and the focusing of the projector were kept constant throughout the analyses, so as to ensure that the size of the image did

not vary. It was not a simple matter to determine the size of the image, because of the differential magnification between the front and rear of the mill. This resulted in a blurred image of the overlap of the front and rear mill circumference delimiters. The image was set so that the front of the mill coincided with the template. As the rear of the mill had a greater magnification, this meant that the balls at the mill shell and at the rear of the mill, fell outside the demarcated mill template. It was hoped that for the runs that had been filmed from the side, that this could be compensated for. There was no way of overcoming this problem, being intrinsic to the experimental set up.

A dedicated computer program was written to record the data as the balls were tracked. A four-button mouse with a circular transparent viewer was used for locating the balls. The cross-hairs on the viewer had extra lines marked perpendicular to them to assist in accurately locating the centre of the ball. The functions of the buttons were to register the location of the ball; to delete any number of incorrect readings; to register a missing reading; and to complete the set of readings. The actual mill dimensions were fed into the program, and it automatically scaled the graphics tablet co-ordinates to real scale mm readings. The program allowed for a variable number of balls to be tracked, and saved the data to ASCII files for direct importation into analysis and plotting software.

A sheet of paper, with the mill template marked on it, was taped over the graphics tablet and the image of each ball was marked onto it. This formed a permanent picture of the locations of the balls in each frame, and could be used to check the recorded data points if there was any doubt about them. Each ball and the pointer on the front of the mill was marked with a different symbol, and after each circulation the colour was changed. The frame numbers were noted at each colour change so that the exact frame number of each point could be worked out. The marked points also helped to locate the mouse accurately over the image. The different balls had to be tracked in the same sequence for every frame, so when the image of a particular ball could not be seen it was registered as a missing reading. The film was projected frame-by-frame, and the image carefully aligned with the template for each set of data that was

recorded. Using the little ball that marked the centre of the mill, the mill image could be accurately aligned with the centre of the template.

6.4 GAMMA CAMERA FILMING

This was to be used to carry out extended filming of the motion of one bead, over periods of a few minutes. Although of a lower resolution than the X-ray filming, this would give a better statistical representation of the radial location and path of the ball.

6.4.1 Gamma camera

This is basically a honeycomb of collimators with detectors and amplifiers at the rear end, Figure 20. The most sensitive, highest resolution collimator was used. The resolution was finer than the diameter of the ball, so the best accuracy of tracking was obtained. A radioactive source is placed in the mill, and this is detected by the camera. The minimum exposure time of the camera is 0.1 s, so was not short enough to provide instantaneous ball positions. Exposure times of at most 0.01 s are required to freeze the image of a ball. Instead it was used to show a large number of almost full revolutions of the ball.

6.4.2 Experimental rig

The same apparatus was used as for the X-ray filming, except that the glass beads were used for this filming, as the gamma rays easily penetrated them. An equal volume of 4, 6, and 8 mm balls were used. A few hollow glass balls were purpose-made by a glass blower. These were left with a tiny hole to provide access to the centre. A cobalt 60 radioactive fluid was then injected into one of the balls, and fast-setting epoxy glue used to seal the hole. The strength of the radioactive source used was 13.6 mcurie. Only one ball could be used at a time, otherwise the image would become too blurred. A screw-in plug was fitted into the side of the mill, so that the ball could be added when ready. The radioactive tracer used has a short half-life, so it was

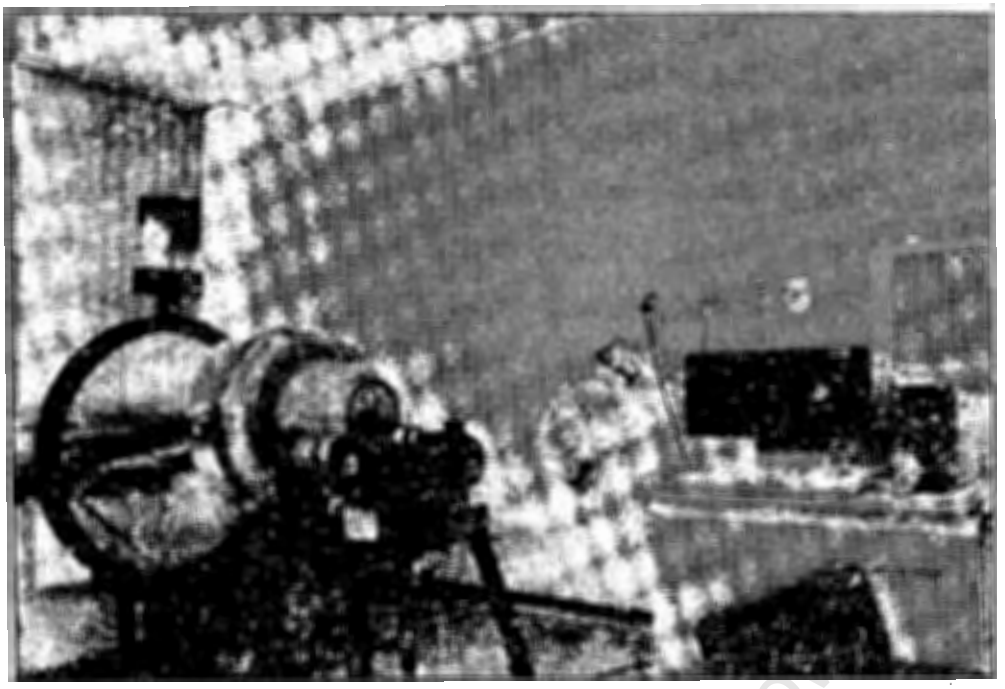

Figure 20. Gamma camera and control equipment

important to initiate the experiment as soon as possible once the marked ball was ready. A thin tube was filled with the radioactive fluid and wrapped around the edge of the front door of the mill, to provide a clear image of the mill.

The exposure time per image was varied between 0.6 and 0.5 s, depending upon the speed of the mill, so that the image formed slightly less than a complete circuit of the ball about the mill. The gamma camera equipment stored each frame on disk, up to a maximum of 500 frames. The frames could then be played back at any desired speed. The recording was played back at real-time speed, and the display monitor filmed with a video camera. Unfortunately the format of the playback was not compatible with standard video cameras, so it could not be directly recorded. However, the final resolution was still very good.

The details of the balls used and conditions of the runs are listed in Table III and Table IV. The marked ball had to be slightly larger than the other balls to enable it to hold sufficient radioactive fluid to be clearly visible.

6.4.3 Experimental problem

Table III Balls used in gamma camera filming

Ball type	Standard glass bead			Hollow ball
Size, mm	4	6	8	9.2
Mass, g	0.083	0.365	0.689	0.764 *

* When filled with fluid

Table IV The full conditions of the gamma camera filming

Run	Speed % crit	Lifter bar Height mm	Lifter bar angle °	Exposure time s	Run time s
1	72.8	6	90	0.5	355
2	82.4	6	90	0.5	261
3	64.2	6	90	0.6	300
4	64.2	1.8	90	0.6	300
5	72.8	1.8	90	0.6	300
6	82.1	1.8	90	0.5	250
7	82.1	3.12	90	0.5	250
8	72.7	3.12	90	0.6	300
9	63.4	3.12	90	0.6	300
10	73.7	6	60	0.6	300
11	81.9	6	60	0.6	300

The radioactive tracer used was for medical use, so it was not very strong, and this meant that only a larger ball could be used. It would have been informative to have used a smaller ball as well, so as to follow its radial segregation.

6.4.4 Analysis of results

The recorded runs were replayed on a television, and analyzed directly from the screen. A transparent template was placed over the image and the paths traced

directly on to it. From this the radius of rotation of the ball, the centre of circulation, and the angle of repose of the charge could be determined. Although a rather crude technique, it was quite adequate considering the resolution of the image. It is possible to display a video image on a dual-function computer screen, that allows for a crosshair to be located on the images, and their locations to be directly recorded by the computer. However, the cost of the hardware and software required was not justified for the amount and accuracy of the data.

The analysis template consisted of concentric circles marked at regular radial intervals within the circumference of the mill. The radius of rotation of the ball could then easily be located within each interval. The angle of repose of the charge could be directly measured with a protractor. Providing the path of the ball did not overlap itself in the time of the exposure, the rotational rate of the ball could be determined from the length of its path in the fixed interval of the exposure.

CHAPTER 7
RESULTS - CHARGE MOTION

As can be seen from the experimental work a wide range of results were gathered. These provided a novel, and often surprising, insight into the motion of individual balls within the mill charge. The results of the different types of experiments are treated separately.

7.1 X-RAY FILMS

In general the images of the marked balls could be seen very clearly, and accurately tracked from frame-to-frame. However they became faint when at the edge of the mill, and also moved out of the image where it was cut off. The cameras did not start filming until they were up to full speed, so all filmed frames were at the correct speed. The film that wound through while the camera built up speed was left unexposed. This meant that the frames could be used as an accurate clock, with 0,02 second intervals between them.

Prints were taken from the original films to illustrate the quality of the images. As a natural consequence of the photographic process these are a negative image of the films, so in the actual film images the balls are seen as white whereas they are black in the photographs. The complete set of runs are shown in Figure 162, in Appendix IV, and a selection are shown here to illustrate particular aspects.

7.1.1 Front view

A set of six consecutive runs are shown in Figure 21. The lead rod through the bead is clearly visible as a solid line, the steel ball is the large dot, and the glass bead is fainter than the small steel ball. The small dot in the centre is the ball permanently mounted on the front of the mill, this provided an excellent locator of the image coordinates. The marker can be seen at the one O'clock position. The line on the right is the plumbline, which, despite being supported independently of the mill, vibrated during the runs. The general outline of the charge can also be seen, giving an excellent picture of the profile of the bulk of the charge. The mill is rotating in the

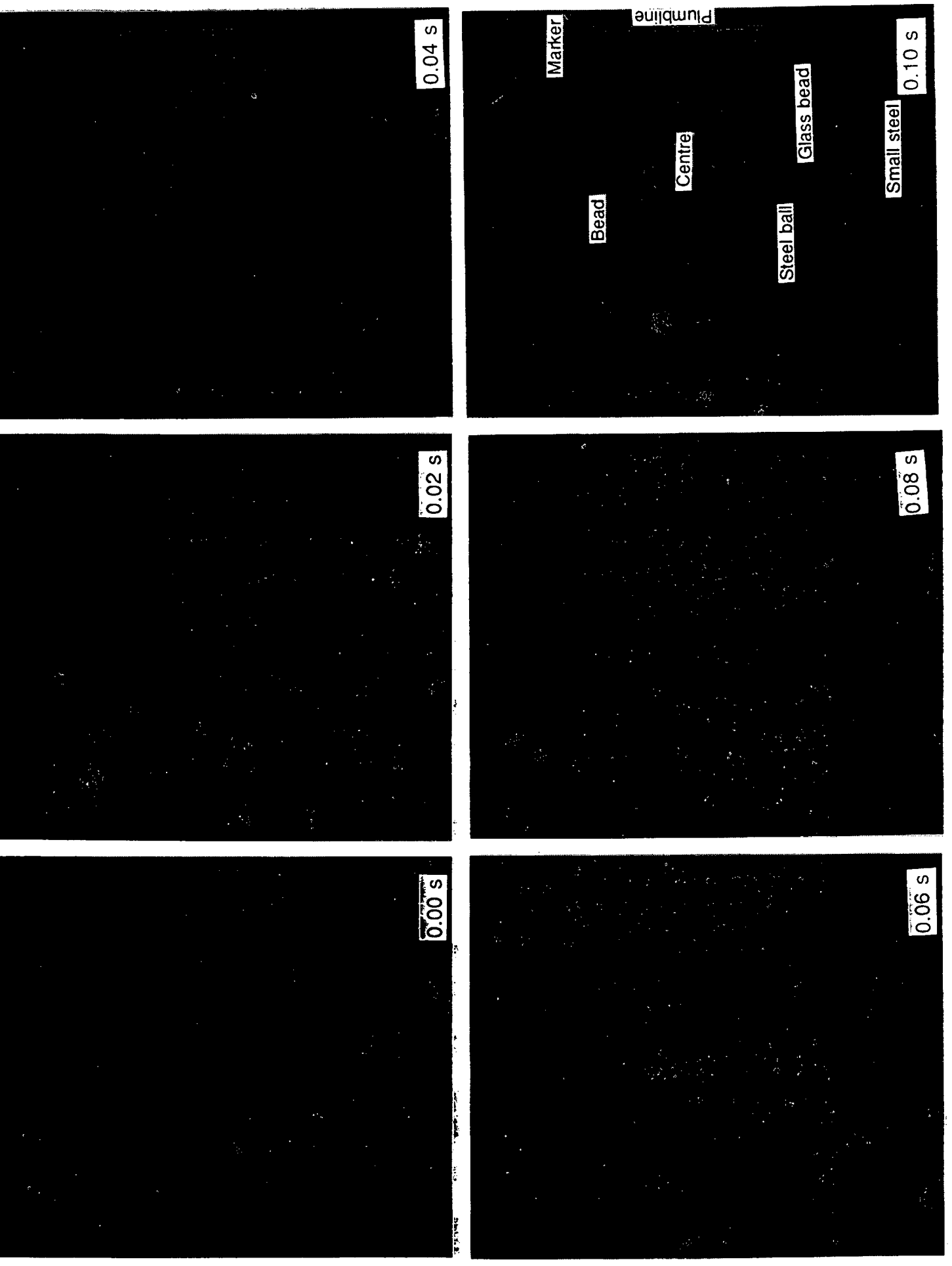

Figure 21. Six consecutive frames of the X-ray films of run 38

clockwise direction. The outline of the inner surface of the mill is quite distinct. It is a bit blurred due to the overlapping images from the front and rear marker rings. The balls on the very periphery at the rear of the mill are hidden behind the front marker ring.

Unfortunately a small section of the image fell outside the film frame. This was in fact within the reception area of the scintillator and was shown on the televised preview, so the 35 mm camera must have had a slightly narrower image area. This cut off area was a distinct drawback when analyzing the films, as it excluded the impact zone of

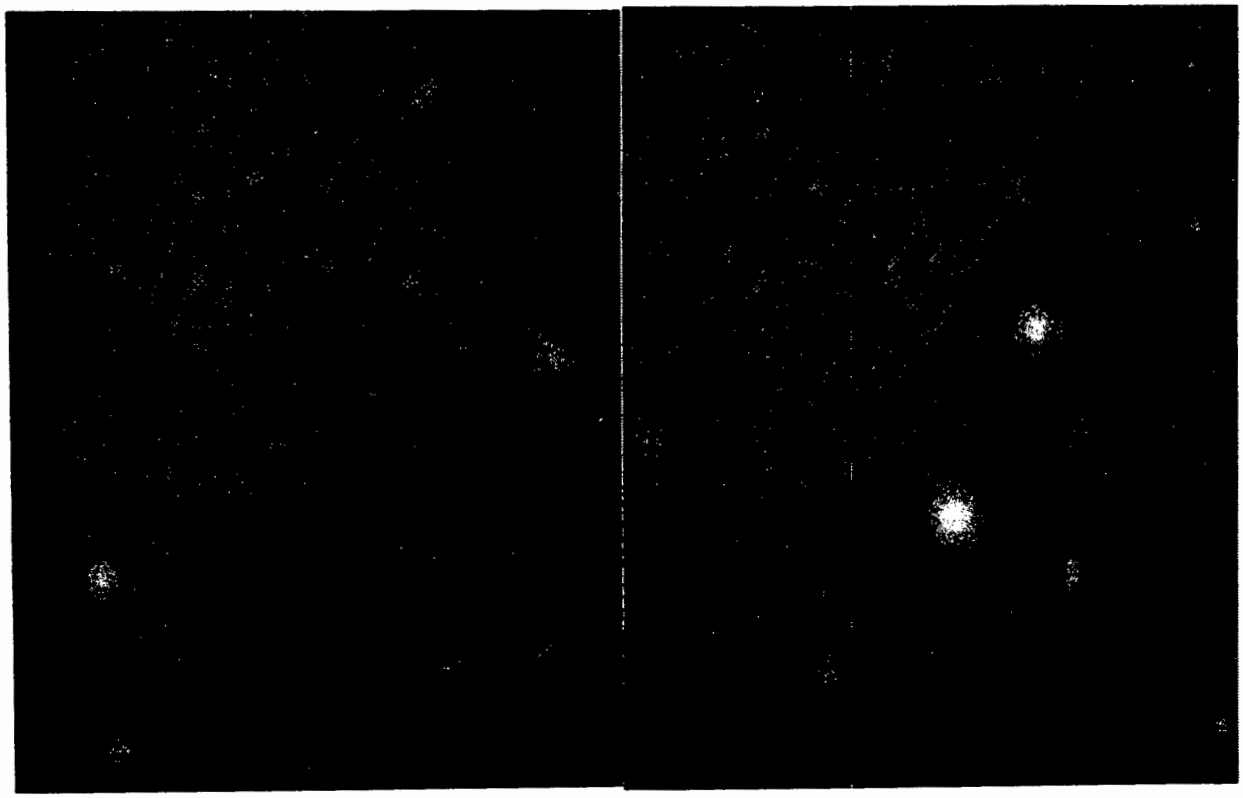

Figure 22. X-ray film of run 23; 6 mm, 90° lifters, running at 68% of critical speed

the outer balls, and hence a lot of useful data was lost. This was not always the case as the mill was run in the opposite direction for some of the runs, such as run 23 which is shown in Figure 22. Here the upward-moving balls are cut off at the edge. This photograph also shows the 6 mm lifter bars, and with the mill running in the ant-clockwise direction they were acting as 90° lifters. The 60° angle of the rear face was used when the mill was run clockwise. Distinct clusters of balls were projected by the

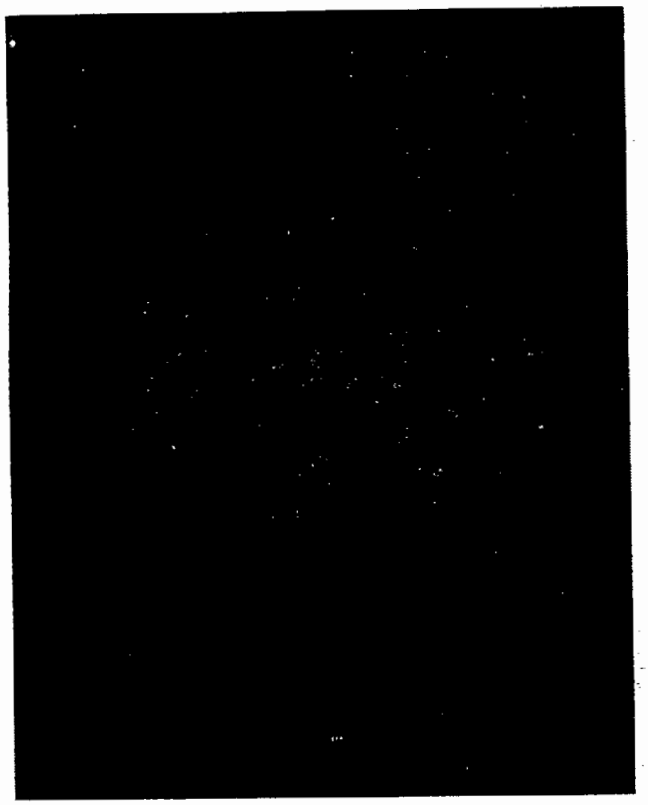

(a) Run 24 - 92% , 6mm , 45°

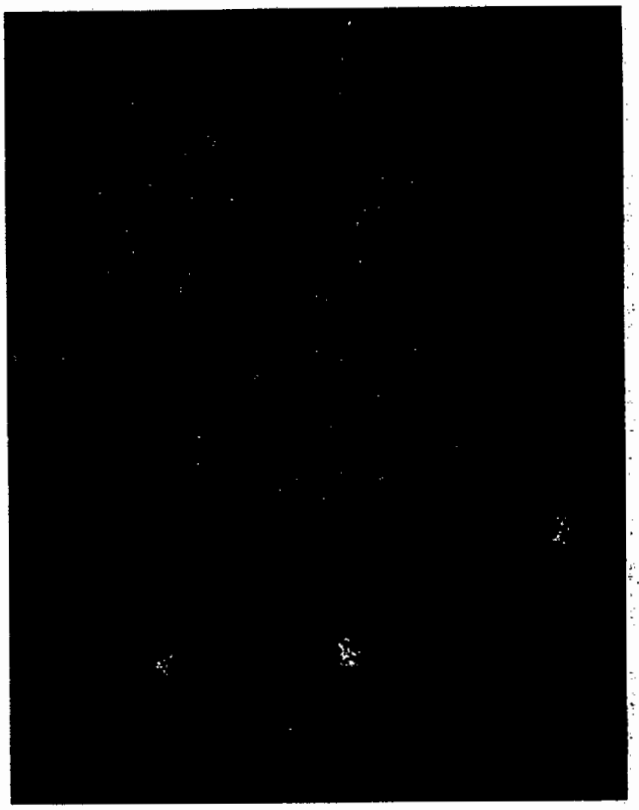

(b) Run 25 - 92% , 6mm, 60°

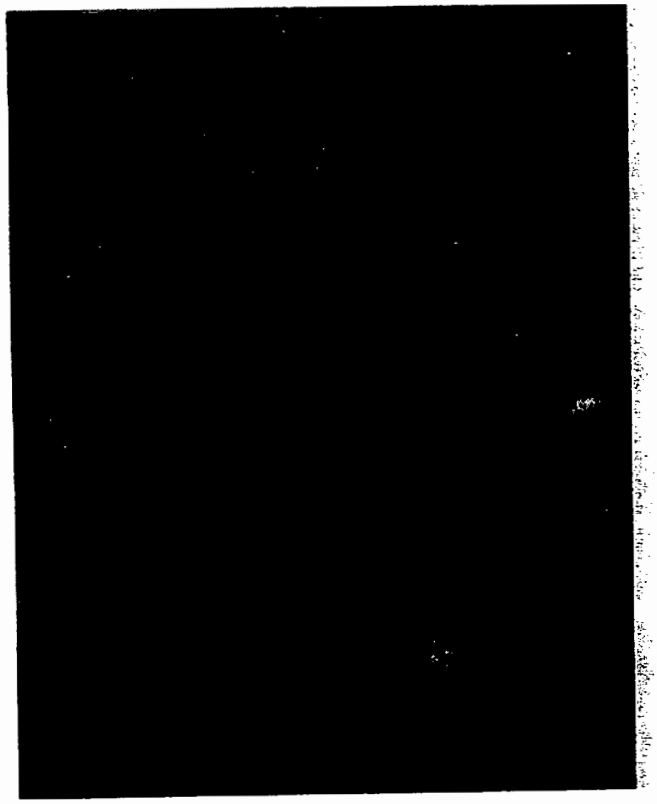

(c) Run 26 - 82% , 6 mm , 60°

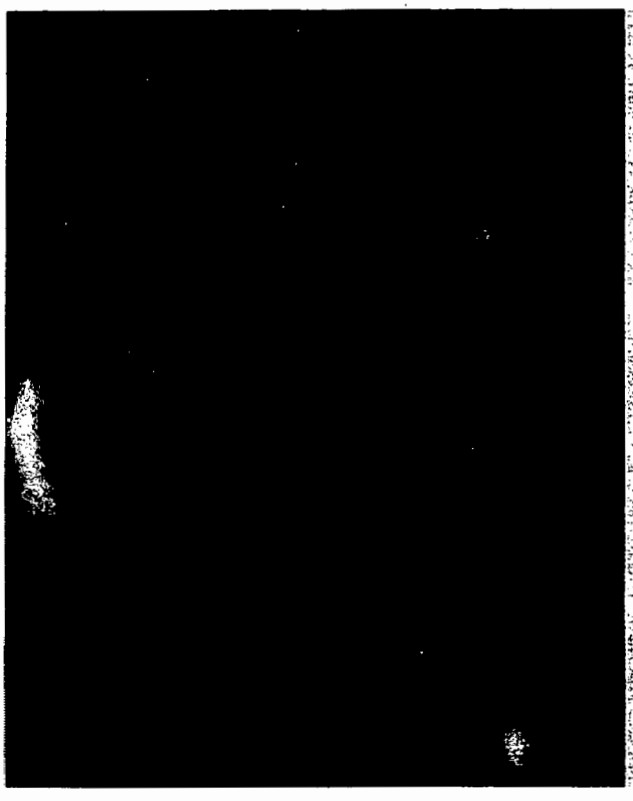

(d) Run 27 - 73% , 6 mm , 60°

Figure 23. X-ray films of four different runs

lifter bars clear of the bulk of the charge. These were groups packed between lifters, and that fell off in a close stream once they passed the point of equilibrium. Even at this low speed of 68% critical the outer balls were lifted to near the vertical and projected right across the mill onto the toe of the charge.

Figure 23 shows four different runs. Not all the balls are visible in the runs, it was often the case that one would be out of view in any given frame. These, along with the previous photographs, show how the charge profile varied widely with changing mill speed and liner configuration. A distinct difference can be seen in the change of lifter bar angle from 45° to 60°, from run 24 to 25 (note that the direction of rotation of the mill changes).

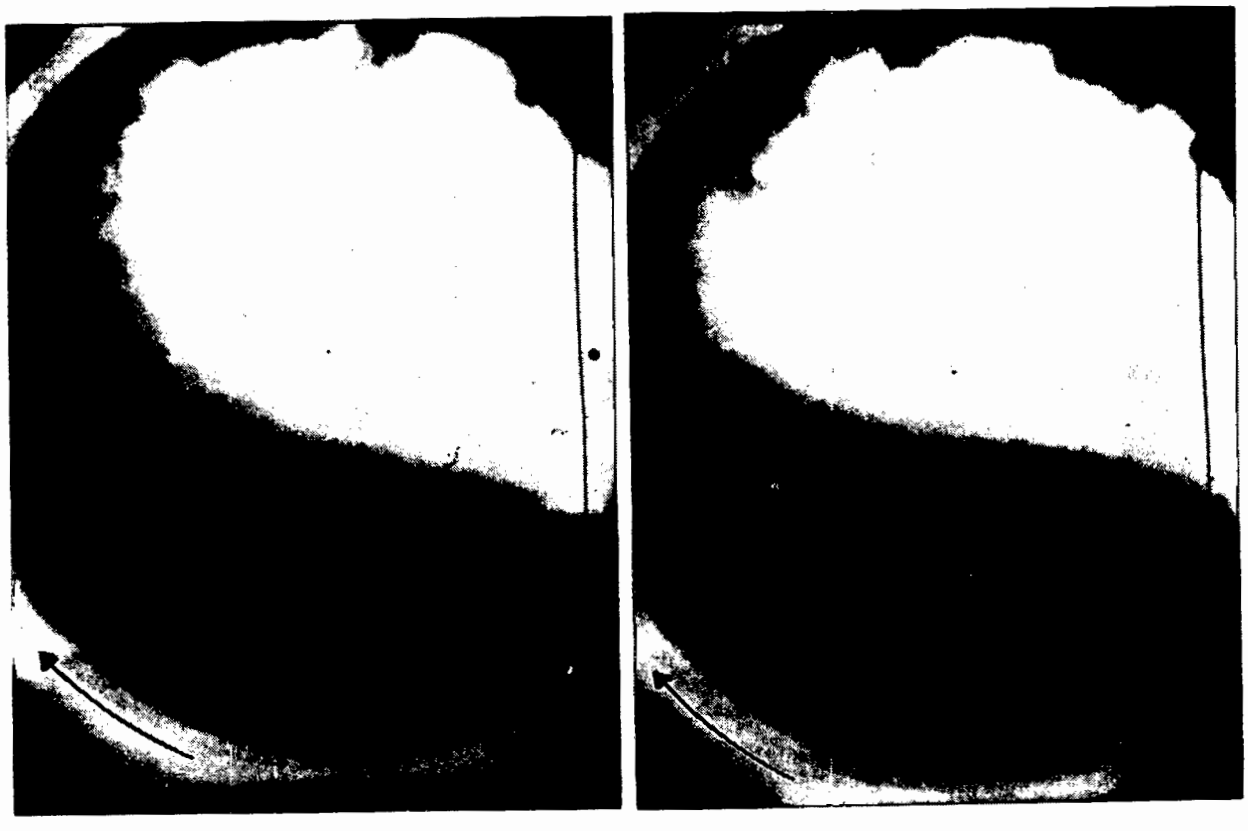

Figure 24. X-ray films of runs 32 and 33 with slurry in the mill

The runs with the slurry presented a rather different picture to the dry runs. Despite the plastic nature of the solids in the slurry, it still screened out the X-rays. As a consequence the motion of the balls within the bulk of the charge could not easily be

traced, as can be seen from Figure 24. However the balls can be seen quite distinctly in the cataracting region and along the surface of the cascading region.

7.1.2 Side view

These were rather disappointing, principally due to limitations in the experimental set-up. However, if access to the equipment had allowed time to experiment with the equipment it is felt that these limitations could, to a large extent, have been overcome, minimised, or proper allowance made for them. A series of six consecutive frames, and two more, 20 and 40 frames on, are shown in Figure 25 and Figure 26. The balls are very clear, and were easy to track. The left side of the mill, that was near the centre of the X-ray beam, has a sharp, straight image. The right side is curved because of the angle at which the rays passed through the face of the mill. The slightly oblique angle of the rays also accounts for the curved appearance of the image, as the marker ring is being viewed at a slight angle and not directly side-on. The mounting rollers for the mill are visible at the base, on either side.

Unfortunately the scaling markers are not visible in the image, which made it difficult to position the image and set the scale correctly. This precluded the possibility of carrying out accurate analyses. In the three to four second duration of the runs the balls drifted very little along the length of the mill. Some systematic longitudinal displacement was noted as the balls, in rotating about the mill, moved towards and away from the camera. Consequently, the lateral displacement of the images of the balls from their actual location varied in a predictable manner. The lateral movement of the steel ball after 0,50 and 0,90 seconds is real, as it is on the undistorted side of the image. The slow vertical movement of some of the balls occurs as they pass over the shoulder or under the base of the charge.

An added drawback of the sideview films is that they were not synchronised with the front view films. It had been indicated by the hospital staff that the cameras were synchronised, but clearly they were quite independent, with just their electric start buttons joined. This meant that a direct frame-by-frame correlation between the front and side views could not be obtained, to give a full x-y-z coordinate of the ball.

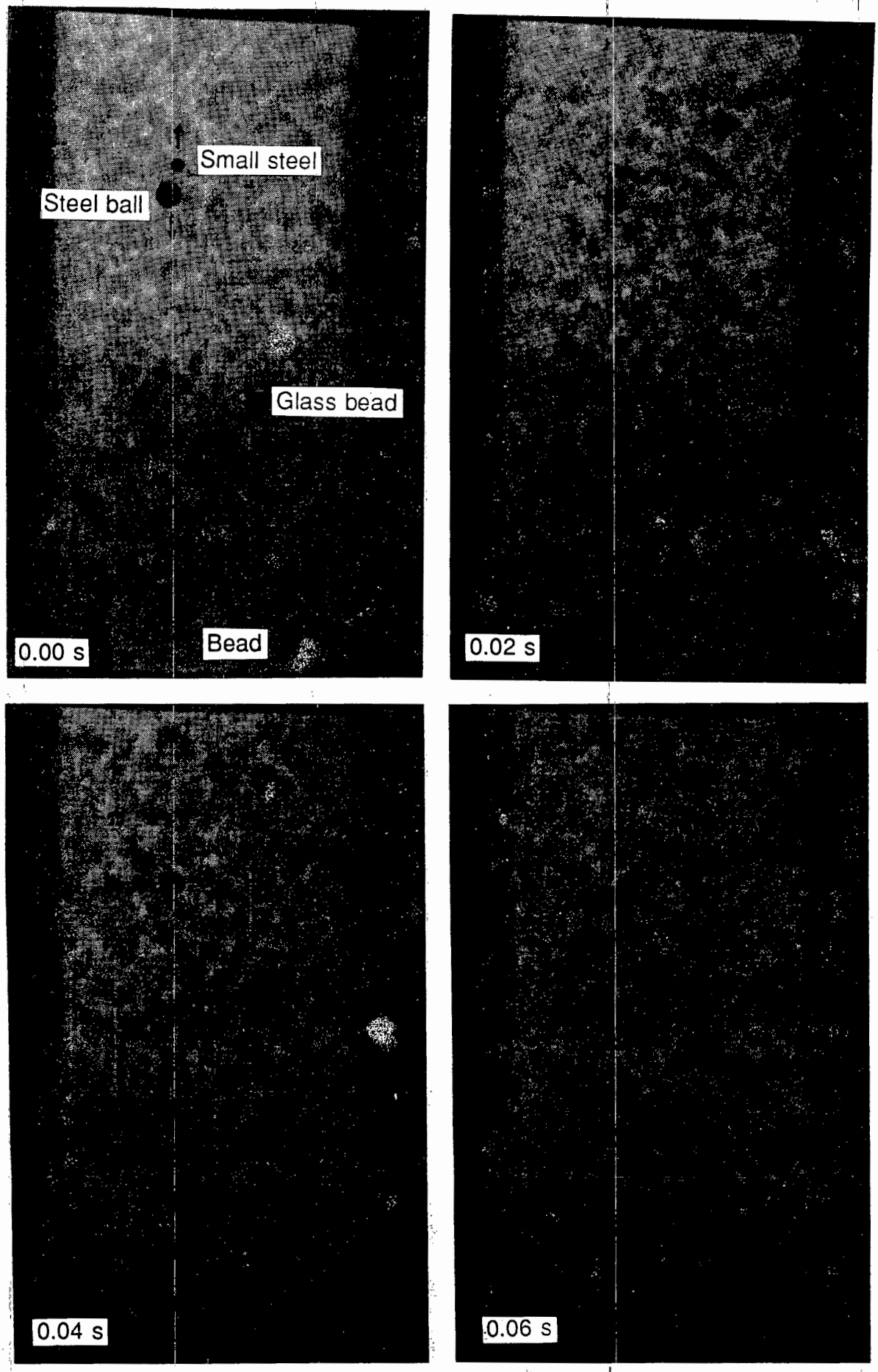

Figure 25. X-ray film of sideview, 4 consecutive frames, run 38

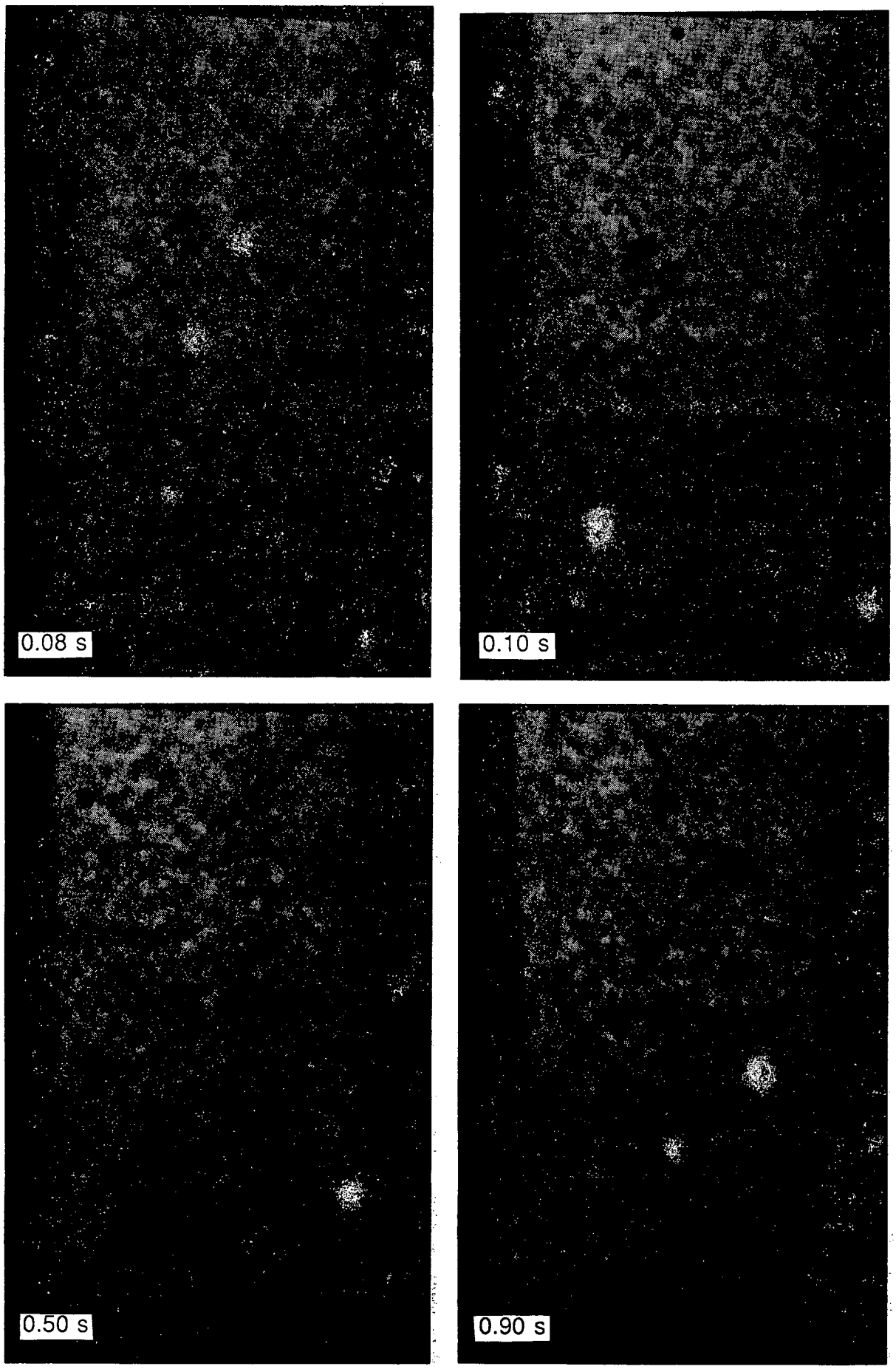

Figure 26. Run 38, two consecutive frames, then intervals of 20 frames

However, a general correlation could be found, indicating the approximate location of the ball along the mill as its rotary motion was tracked from the front.

7.1.3 Analysis

The data capture technique worked very well, and the images could be accurately tracked. However, the faintness of the images near the edge and their disappearance at times greatly hampered the tracking of their paths. Plots of all the runs are contained in the loose inserts at the rear of this thesis. They are numbered according to the runs, and labelled XRC0....XRC38 to indicate that they are plots made from the X-ray camera films. There is also a listing of a typical set of X-Y coordinates in table Table XXXIV of Appendix V. The coordinates are given in real scale mm, with the origin at the centre of the mill. As over 30 000 data points were measured these are not listed in whole.

7.1.3.1 *Front view*

The regions within the charge, that are referred to throughout this work are illustrated in Figure 10. They are also defined in the glossary.

Some of the points on the plotted images lie outside the radius of the mill, these are the balls on the outside of the charge, at the back of the mill, that had a higher magnification. All the data was standardised to an anti-clockwise rotation of the mill so as to simplify comparisons. This was done by simply changing the sign of the X coordinate. The blank spaces are missing data points, where the ball was not visible. Because of its peripheral position the marker was out of view for about a third of the frames. However, this was unimportant as it was only used to accurately check the speed of the mill. Where it was visible throughout a full circuit it was also used to check that the mill ran at a constant angular velocity. This was confirmed to be the case.

The bead is just shown as a point in the full plots of each run, but the central lead rod is shown in separate plots. The plots in Figure 163 to Figure 166 of Appendix IV, show how the bead rotates about its own axis. Each circuit around the mill is shown as a

different line type, and numbered sequentially, so that the path of the bead can be followed. Only the runs in which the path of the bead could be seen over a few circuits about the mill are shown. In the runs where the bead remained at the same radius, the images of each circuit about the mill are superimposed on top of each other, so the individual orientations of the bead cannot be seen.

7.1.3.2 *Initial observations*

Some interesting observations could be made prior to any numerical analysis taking place, and these can be observed directly from the plots of the runs.

• The paths of individual balls deep within the bulk of the charge are surprisingly smooth. It had been expected that the balls would, at least in the cascading and toe region, jump between layers of charge, and bounce around in the toe region. However, they follow remarkably regular paths. This implies fairly even pressure gradients, and consistent ball packing within the charge.

• The balls do not follow smooth paths in the very central region near the centre of circulation of the charge, as seen for the steel ball in run 1. They can move suddenly between layers and have irregular paths. This implies that the balls are not evenly packed in this region, but rather form a loosely packed, fluctuating zone.

• The balls have a tendency to spiral in and out of the charge. This does not take place by sudden and random jumping of the balls between layers, but rather in a smooth and consistent manner over a number of revolutions, the bead in runs 6 and 8a is a clear example. This action predominantly takes place in the inner half of the bulk of the charge

• It can also be seen that there tends to be a segregation of the different balls. The heaviest balls, the steel ball and marked bead, consistently remain near the centre of the charge. The lightest ball, glass bead, remains on the outside of the charge, as seen in run 14. However, this arrangement suddenly changes once the mill speeds up to 92% of critical speed, when the steel ball occupies the outermost trajectory, as shown by runs 24 and 35.

• The charge undoubtedly spreads out as the mill speeds up. The same quantity of charge occupies a far greater volume in the mill. This occurs in the cascading/cataracting region, not in the en-masse region which remains well packed,

this can be seen when comparing runs 34 and 36. The free surface, that divides the downward cascading material from that moving upwards in the en-masse region, remains a similar distance from the centre of the mill.

• The angle of repose of the charge increases as the mill is speeded up for each liner configuration, this is clearly shown for runs 6 and 4. The height and angle of the lifters don't have an obvious effect on the angle of repose. There is a noticeable difference in the angle of the cascading and cataracting trajectories, the cataracting path being steeper, as can be seen in run 5 when comparing the trajectory of the glass bead to that of the bead.

• In the slurry tests, runs 28 to 33, the balls cataract down quite independently of the bulk of the charge, and tend to land midway along the free surface, they then cascade very slowly down to the toe region. This is in sharp contrast to the vigorous motion observed in the dry runs. The angle of repose of the charge is also distinctly lower than the other runs. The slurry seems to subdue the entire motion of the charge.

• When the orientation of the bead is followed, it can be clearly observed that in all cases, except when in the very inner core, the bead doesn't rotate about its own axis while in the en-masse region of the bulk charge. The slight rotation observed is equal to that of the mill, ie. the orientation of the ball does not change relative to a point of observation within the mill (the frame of reference of the mill). Any rotation of the ball takes place as it falls off the shoulder of the charge, or as it lands on the toe. This can bee seen in the plots of the bead only, in Figure 163 to Figure 166 in Appendix IV.

7.1.3.3 *side view*

In only some of the runs were the balls tracked in every frame. In the others it was decided that little benefit was to be gained from detailed analysis, so the balls were only tracked every 10^{th} frame. Only the plots where all the points were tracked are shown, and the length of the mill is expanded so that the different balls can be seen more clearly. These plots are included as loose inserts with the front-view plots.

In general there was not as much longitudinal motion as had been expected from observing coloured balls in the mill. Thus it would appear that although the balls can

migrate up and down the full length of the mill, they do not do so in the short term, ie. in the space of a few revolutions. The apparent longitudinal drift, caused by the changing distance of the ball from the camera, is easily distinguished from the actual longitudinal movement. The ball repeatedly returns to the same axial, z, location as it reaches the same rotary position, and the path has a distinctly oval shape. Real movement can be observed from the location of the ball at a regular vertical position, say at the top or bottom of its trajectory.

It appears that there may be more longitudinal motion in the lower-speed mill than when running at high speeds, but there is too little data to draw a definite conclusion.

7.1.4 Error analysis

The major source of uncertainty in the results was the variable magnification between the front and rear of the mill, arising from the point source of the X-rays (Figure 27). Points A and B are at the same radius, and it is clear that their images fall on the screen at different radii. If the axial location of the ball, Z, is known this magnification factor can be compensated for to yield corrected x and y coordinates, x_c and y_c.

On the graphics tablet the image of the front of the mill was set at a diameter of 284 mm, and the maximum measured diameter was 315 mm. This is 1.11 times what the actual reading should be, so there is an 11% error. To correct for this the coordinates of a ball when at the very back of the mill should be corrected by a reduction factor of $^1/_{1.11} = 0.90$. For any intermediate point:

$$(x; y) = \left(\frac{z x 0.11}{L} + 1\right).(x_c; y_c)$$

for L =97 mm **(6)**

$$(x_c ; y_c) = \left(\frac{1}{z x 1.13 x 10^{-3} + 1}\right).(x ; y)$$

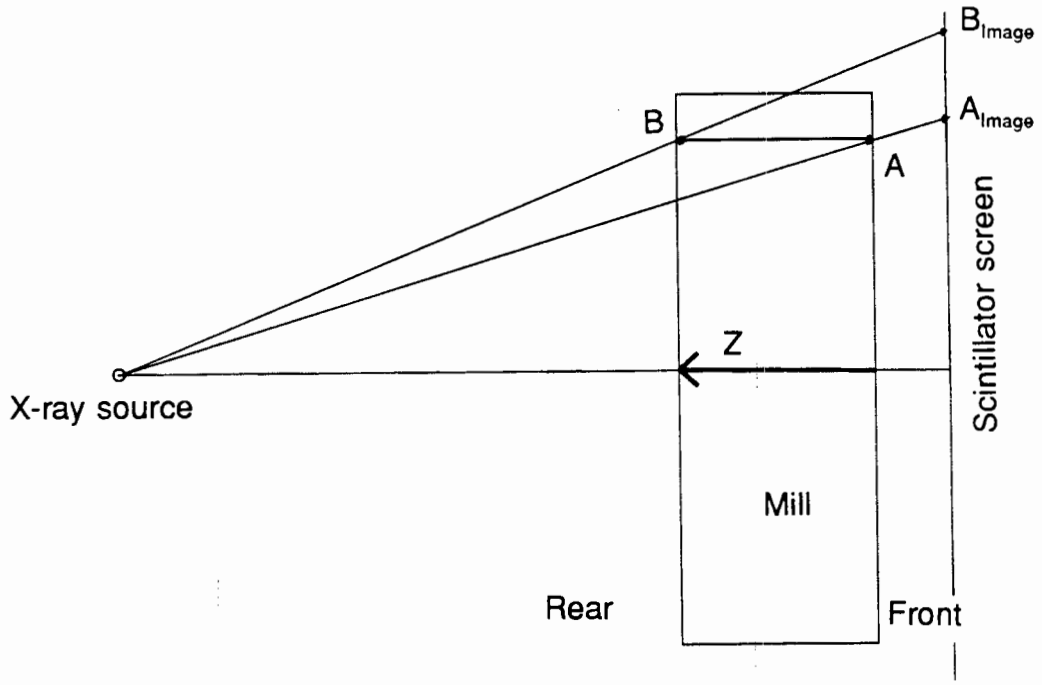

Figure 27. Variable magnification along the length of the mill, arising from the divergence of the X-ray beam.

The accuracy of the x,y coordinates is therefore dependent upon the accuracy of measurement of the z coordinate, which is taken from the side view of the mill. For runs 0 to 18 the side-view was not filmed, so the magnification uncertainty is 11%. The measurement of the ball location in the side-view films was rather approximate for the following reasons:

- The scale markers were not visible.
- The front of the mill was very blurred, so scaling the image from the length of the mill was approximate.
- The frames of the front- and side-views were not synchronised.
- There was a stronger magnification factor in the side-views, than in the front views, arising from the mill having a width of almost twice its length.

- The side-view magnification factor was not even across the mill, because the mill could not be placed centrally in the X-ray beam.

In view of these problems it was decided to exclude the z location correction factor, and accept that there could be an uncertainty of up to 11% in the location of the ball, depending upon its axial location in the mill.

The image could be aligned with the template to within 0,5 mm, and the balls could be located to within 0,5 mm, giving a maximum error of 1,0 mm. Over an image diameter of 284 mm, this represents an error of ±0,35%

The total error in the location of the image in the front view of the mill is not symmetric, as the magnification factor is only additive.

Net error range = -0.4% + 11.4%

This introduces a significant uncertainty into any modelling of the data. It was therefore realised that the data could not be used for rigorous modelling, but rather for trend analysis.

7.2 GAMMA CAMERA FILMING

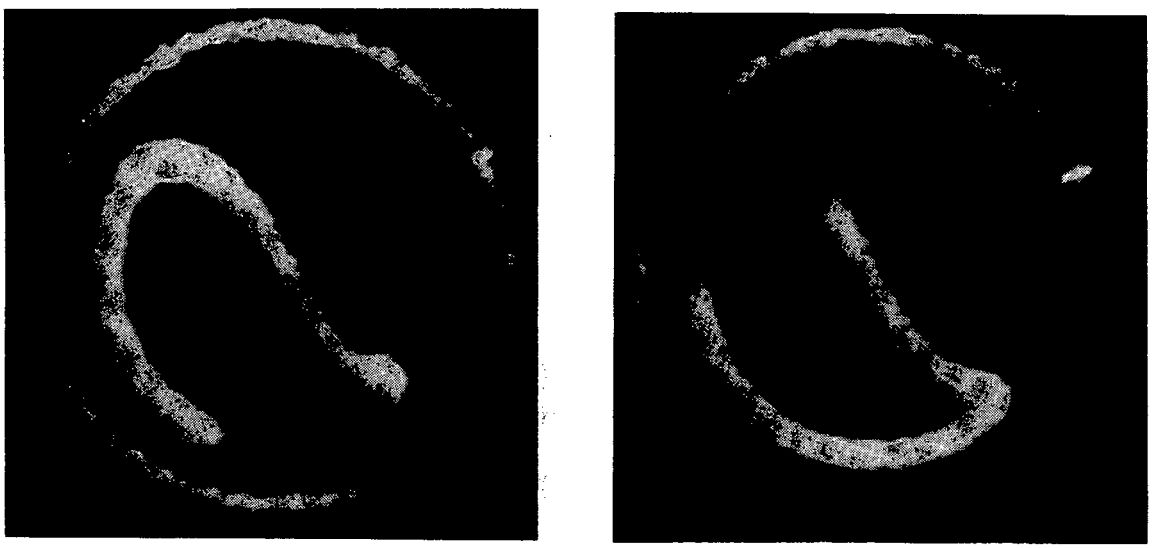

Figure 28. Gamma camera images of a radioactive ball, run 9

The radioactive ball left a very clear trace on the film, but was too blurred to carry out accurate measurements, as was expected. It provided very useful information on the long-term motion of the ball. Two images from run 9 are shown in Figure 28. The outline of the mill is shown by the circular track. The mill is rotating in the clockwise direction and the inner line represents a trace of the ball over 0.6 seconds. These are two quite separate frames, which, when viewed together, show the full path of the ball. The remainder of the gamma camera films are illustrated by the photographs in Figure 167, of Appendix IV.

As the radioactive ball was larger than the others, yet only slightly heavier than the bigger balls in the charge, it could be used to observe the effect of ball size upon radial segregation of the charge. At speeds from 73% critical down it spent most of the time in the outer layer of the charge. But when the mill was speeded up to over 80% of critical, this large ball spent most of the time in the inner third of the charge. At lower speeds the height of the lifters has no observable effect; however, at high speeds the higher lifters resulted in the ball spending even more time in the very central core region of the charge.

As the mill is speeded up the toe region becomes shorter and more rounded. The balls appear to be drawn in more rapidly to the rotary motion of the mill when the speed is faster. This implies that at lower speeds the toe region is looser and more active, and dissipates more energy through many small impacts and interactions. At high speeds there are fewer impacts but they will have a higher energy.

7.2.1 Error analysis

The gamma camera doesn't suffer from any magnification distortion factor, as the tracked image forms the point source of radiation, and this is received by parallel collimators. These images were only used to locate the ball within bands of radii within the mill, and as these bands were wider than the uncertainty in the location of the image, it is not necessary to carry out an error analysis for these measurements.

CHAPTER 8
ANALYSIS - CHARGE MOTION

8.1 CALCULATIONS

The charge motion was filmed at 50 frames per second, so each frame is separated by a fixed time interval of 0.02 s. The basis of the analysis was to divide the full set of data for each ball into separate sets, each representing a single circulation of the ball about the centre of the mill. The path was divided into a number of distinct zones, illustrated in Figure 29, which could each yield a particular set of information.

1. The circular path in the *en masse* region, where the ball is lifted up by the rotary motion of the mill - from A to B.

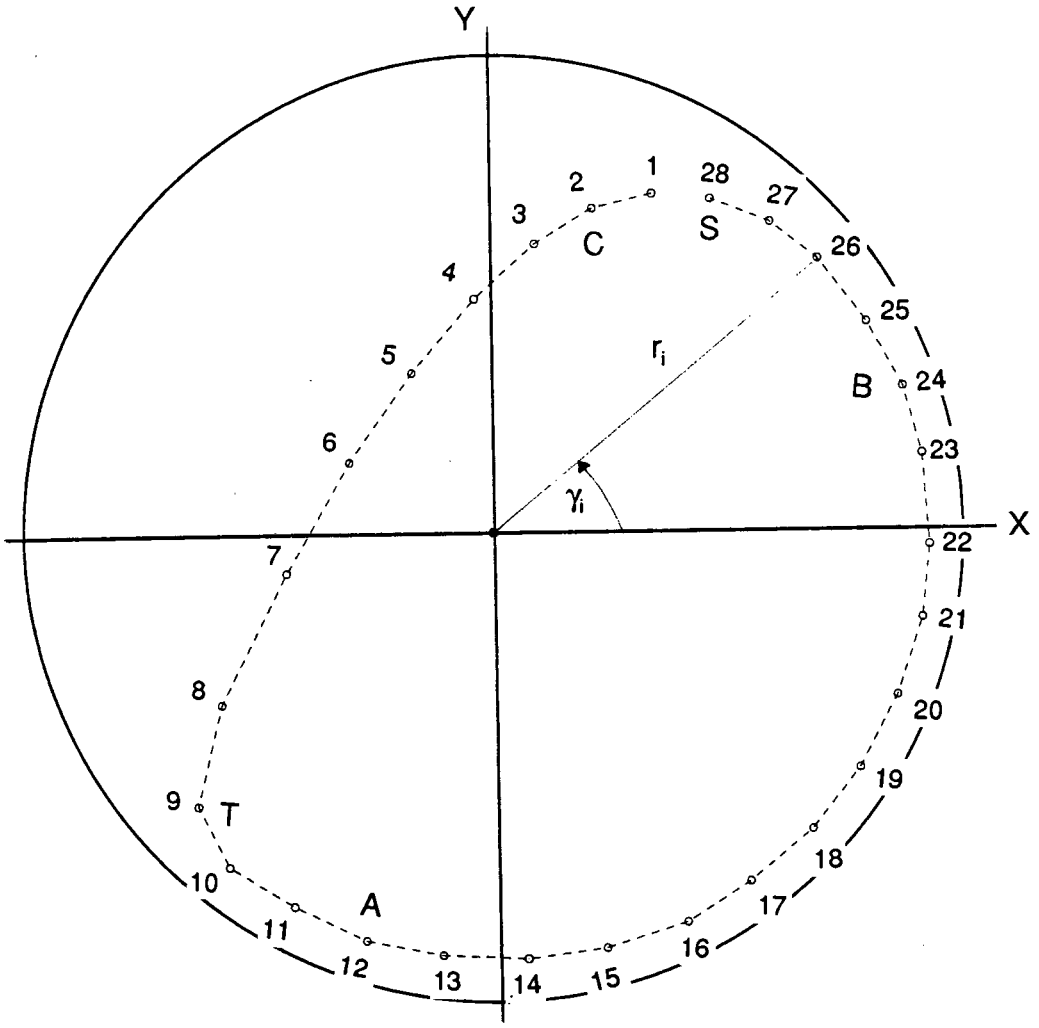

Figure 29. The path of a rotating ball, showing the various distinct zones

This zone is used to calculate the angular velocity of the ball, and its radial displacement from the centre of the mill. The angles are measured anti-clockwise from the horizontal.

$$\textit{Angular location:}\quad \gamma = \arccos\left(\frac{x_i}{r_i}\right) \quad \text{... for } y \geq 0$$

$$\gamma = 2.\pi - \arccos\left(\frac{x_i}{r_i}\right) \quad \text{... for } y < 0 \qquad (7)$$

$$\Omega = \left(\frac{\gamma_B - \gamma_A}{t_B - t_A}\right)$$

Average radius: r = average r_i from A to B

2. The shoulder zone - from B to C - where the ball falls away from the circular path, passes through the maximum height at S, and then begins to fall down towards the toe region.

3. Cascading/cataracting zone - from C to T - where the ball tumbles down the other descending balls (cascading) or falls freely (cataracting), until it impacts in the toe region.

The angle at which the ball cascades is given by the slope of this zone. The angle of incline of this zone is calculated over the range from C to frame 8.

For $\Delta x = x_8 - x_c$, $\Delta y = y_8 - y_c$, and Δr = distance from C to 8, then the angle of cascade is given by eqn.(7).

The value of the vertical acceleration of the ball indicates to what extent the ball is interacting with other balls: in free flight the value should be 9.8 $m.s^{-2}$. The acceleration, Acc, is calculated from C to frame 8, one frame before the impact point, T: For $\Delta y = y_{n+1} - y_n$, $v_y = \Delta y/0.02$

$$Acc = \frac{v_{y_{n+1}} - v_{y_n}}{0.02} \qquad (8)$$

The velocity of the ball just prior to impact is calculated as the average velocity over the last 4 frames before the impact point. There is an error introduced by taking the

average velocity over 0.08 s, but it is difficult to obtain an accurate measure of velocity over the period of a single frame. For an uncertainty in locating the point of ±1 mm, and a path length of 20 mm between two frames, a 10% error is introduced. This is reduced to 2.5% over a distance of 4 path lengths. As the results were to be used for comparative purposes the actual magnitudes of the measurements were not as important as maintaining the consistency between measurements for different mill configurations. So it was considered reasonable to introduce an approximately constant error into all the calculations by averaging over 4 frames.

$$V_{xI} = \frac{x_8 - x_4}{0.08} \qquad V_{yI} = \frac{y_8 - y_4}{0.08}$$

$$V_I = \frac{\sqrt{(x_8 - x_4)^2 + (y_8 - y_4)^2}}{0.08} = \sqrt{\frac{\Delta x_I^2 + \Delta y_I^2}{0.08}} \qquad (9)$$

4. The toe region - T to A - where the ball impacts on the charge and is drawn into the rotary motion of the mill. This is an active region of the charge, and where the interactive forces are greatest.

The velocity of the ball immediately after impact is calculated by eqn.(9) from frames 10 to 12, to yield the values of Δx_I and Δy_I. The direction of the ball's motion is changing and it is being drawn into the circular motion of the mill, so a longer time period cannot be used to calculate the velocity. The change in velocity of the ball from just prior to impact to just after impact is given by:

$$\Delta V_x = \frac{\Delta x_F}{\Delta t_F} - \frac{\Delta x_I}{\Delta t_I} \qquad \Delta V_y = \frac{\Delta y_F}{\Delta t_F} - \frac{\Delta y_I}{\Delta t_I} \qquad (10)$$

$$\Delta V = \sqrt{V_x^2 + V_y^2}$$

Knowing the change in velocity at impact, the force exerted on the ball during the impact can be calculated:

Force = mass x acceleration (m.acc)

$$F = m_{ball}\frac{\Delta V}{\Delta t} \qquad (11)$$

The impact force is the rate of change of momentum, so the impact time, Δt, is required to calculate the force.

Measurement of the impact time requires knowing when the impact started and ended. The best measure of this is the interval between the frames just prior to and after the impact, i.e. 0.04 s for this study. This is considerably longer than the impact time for a fully elastic collision between two rigid bodies. In fact Dunn and Martin[11] measured the impact force of a ball dropped on a steel plate, and obtained acceleration values for the ball of a few hundred-fold gravitational acceleration. From their graph of acceleration versus velocity at impact, it was calculated that the impact time was 1 ms when the ball was dropped onto a steel plate. When a single layer of ore particles was placed on the steel plate the acceleration dropped to a third of its initial value, indicating an impact time of 3 ms. Except when impacting directly on the shell, the ball impacts on a fluid bed of moving balls. There is some 'give' in this body that renders the impact inelastic. The impact time could easily rise to 10 ms when the ball impacts on a fluid bed of balls. To measure the impact time would require equipment capable of filming 1000 frames per second, which would preclude the use of X-ray filming. As the actual impact time could not be measured with the present equipment, the time interval of 0.04 s was used in all calculations. This gives an over-estimate of the actual time, but this is irrelevant when the relative impact forces between the different conditions are compared, as the constant correction factor cancels out. The actual loss in information is not knowing the variation of this impact time between individual impacts. For the purposes of this study the impact time is taken to be approximately constant for all impacts. Impacts of the ball directly against the mill shell will have a shorter impact time than those onto the charge body, so the calculated impact forces for these impacts will be low.

The energy transferred to the charge by the ball is calculated from the difference in the ball's energy immediately prior to and after the impact. The total energy of the ball

is the sum of its potential and kinetic energies. The change in potential energy is small over the period of the impact, (in the region of 1×10^{-7} J) as the ball falls only a small distance in this time. So the change in energy of the ball is calculated from the change in the ball's kinetic energy.

$$\Delta E_k = \frac{1}{2} m(v_I^2 - v_F^2) \qquad (12)$$

5. The complete circuit of the ball around the CoC is utilised in calculating the work done by the ball during each revolution of the ball. The net work per circuit is given by the sum of the work over each 0.02 s time interval between frames.

Work = force x displacement (d) ≡ mass x acc x d

displacement, $d = v_o t + \frac{1}{2}\, acc.t^2$,

for frame n, $d = d_n$; $v_o t = d_{n-1}$; $t = \Delta t$ (0.02 s)

$$Acc_{Net} = 2\frac{d_n - d_{n-1}}{0.02^2}\ (mm.s^{-2}) \quad = \frac{d_n - d_{n-1}}{0.2}\ (m.s^{-2}) \qquad (13)$$

However the net acceleration, acc_{Net} is made up of two components: gravitational acceleration, g ; and the acceleration applied by the charge mass, acc_m

so $acc_m = acc_{Net} - g$

$$Work_n = mass_{ball}\left[\left(\frac{d_n - d_{n-1}}{0.2}\right) - g\right] \qquad (14)$$

The CoM is given by the simple averages of the x and y data over a whole circuit of the mill, as derived in eqn.(4) of the chapter on extending the theory. If any data points are missing for a particular circuit then that circuit cannot be used.

8.2 PROCESSING

The x-y data from each run was imported into a 'master copy' of a Lotus spreadsheet that had been structured to analyze the data. Although the form of the calculations was automated, the data for each run had to be manually divided into single circuits of the ball about the CoC. The resultant data were then condensed into summaries

which were imported into a master summary spreadsheet for comparison of the different runs. The structure of these analyses is given in Appendix V.

It has been shown in the error analysis of the results that the balls could only be located with an accuracy of 11.4%, because of the magnification effects of the diverging X-ray beam. Consequently it was decided that the filmed charge motion would be analyzed in a qualitative manner, rather than attempting to mathematically model the data. The processed data are presented in the from of graphs, and these graphs make it apparent that the scatter in data may be as large as the differences that are being modelled. This scatter also arises from the intrinsic fluctuations in the motion of individual balls that must occur in a system consisting of such a large number of random interactions.

The line-joins shown on the graphs in this section have only been included to highlight the trends in the data. References to the charge trajectories apply to the set of 40 'XRC' plots included as loose inserts.

8.3 CHARGE TRAJECTORY PLOTS

The plots of the charge trajectories were analyzed directly to ascertain the angle of repose of the charge, and the location of the CoC. As illustrated in Figure 10, the equilibrium line was drawn onto the plot of each run, and the CoC marked on the plot. The dashed line joining the toe and shoulder illustrates that it is meaningless to define the angle of repose and the region of *en masse* charge by this line. The free surface was easily fitted to this plot, but cannot always be drawn in. At the high mill speeds the central portion of the ball paths were not available, so neither the free surface nor the CoC could be located, as can be seen for runs 20 to 22. The angle κ defines the angular location of the CoC. The tangent of the free surface at the CoC was found to be perpendicular to the radial line passing through the CoC, for all the plots. This agrees with the theory developed earlier in this work.

The radial location of the CoC varies with the speed of the mill, for a fixed charge filling, so this was measured for all the plots for which the CoC could be determined.

Table V Measured angles of repose and radii of the centre of circulation

Lifter		Mill speed													
		68%				73%				82%				Averages	
H, mm	Ang.°	run	r_{meas},mm	r_{act},mm	κ°	run	r_{meas},mm	r_{act},mm	κ°	run	r_{meas},mm	r_{act},mm	κ°	r	κ°
0	0	34	34	52.7	51.5	38	34	52.7	50.5	37	34	52.7	49.5	52.7	50.5
1.8	90	6	28	43.4	52	5	26	40.3	45.5	4	30	46.5	48	43.4	48.5
3.12	90	1	27.5	42.7	47	2	31	48.1	55	3	30	46.5	53	45.8	51.7
6	45	14	27	41.9	46	-				16	29.5	45.8	46	43.8	46.0
6	60	-				27	34	52.7	54	26	35	54.3	63	35.7	39.0
6	90	23	35	54.3	53.5	18	29	45.0	49	17	31	48.1	57	49.1	53.2
10	60	13	26.5	41.1	44	12	28	43.4	61	11	28	43.4	59.5	42.7	54.8
10	90	8a	28.5	44.2	42	9	26.5	41.1	55	10	28	43.4	58	42.9	51.7
Slurry															
		73%				92%				100%					
6	60	28	43	66.7	47.5	-								66.7	47.5
6	90	33	45	69.8	38.0	31	42.5	65.9	43	32	43	66.7	41	67.5	40.7

Table V gives the measured data for all the runs, and the overall averages. The uncertainty in measurement is estimated to be ±2 mm for the radius, and ±3° for the angle. Taking the uncertainty range into account, there is not a strong trend in the radius of the CoC with mill speed, over the speed range 68% to 82% of critical. Unfortunately data could not be obtained for the high speeds. What is revealed, however, is that the two batches of runs had different CoC's. The CoC for the second batch is at a larger radius than for the first batch. It would appear that some of the charge inadvertently went missing between the two batches of runs, leaving batch 2 with a lower charge level. This necessitates that data be compared relative to the CoC rather than the centre of the mill.

8.4 CENTRE OF MASS

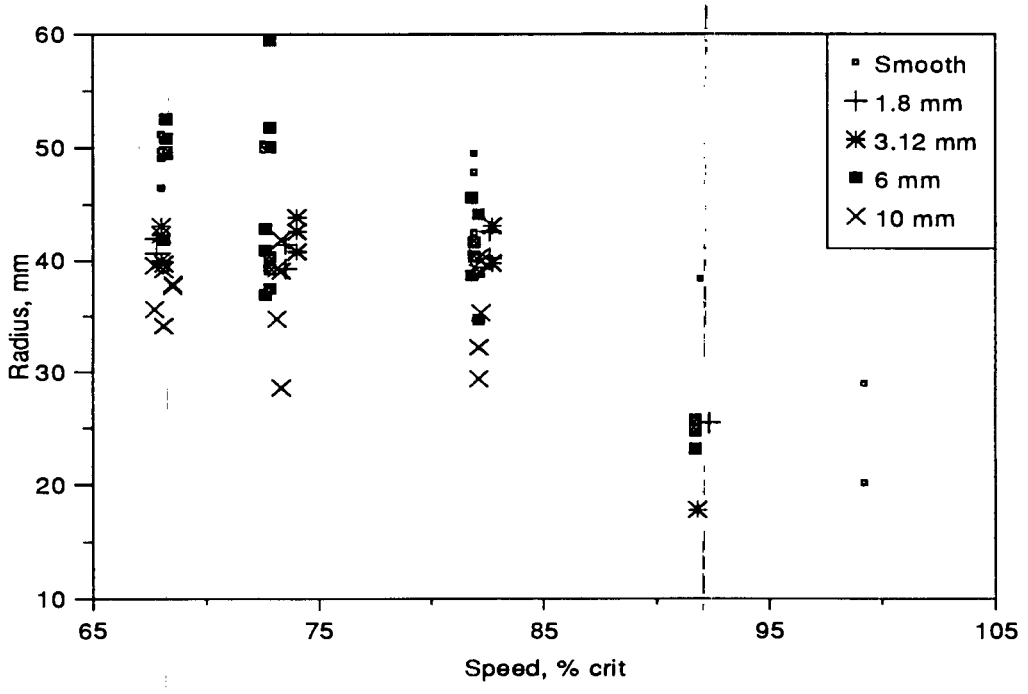

Figure 30. Radial location of the centre of mass of the charge

The CoM of the charge does not coincide with the CoC, as discussed in the theoretical section. The CoM was calculated from the average x and y coordinates of the ball over a complete circuit. If the ball could not be tracked over every frame for a circuit, then that circuit could not be used. The full data for the radius of the CoM as a function of the mill speed, and for the range of different lifters, are presented in

Figure 30. There is a definite decrease in the radial location as the mill speed increases from 68% critical. The spread of data for the 6 mm lifters, as clearly seen at 68% and 73% critical speeds, corresponds to the two separate batches, for the same reason as discussed for the CoC. The differences are about 10 mm, as for the CoC, so the readings for the second batch should be about 10 mm lower. However, there was no definite method of determining what the correction factor should be, so the data were left unchanged. The averages for each height of lifter are given in Figure 31. There is little change in the radial location as the speed increases from 68% to 82% of critical, but then the radius decreases rapidly, by over 15 mm as the speed is increased to 92% of critical. Taking into account that the values for the second batch should be reduced, and noting that all the smooth runs were in the second, and the data for 10 mm lifters from the first batch, the differences between radial locations for lifter heights are not as great as they appear. Even so, the runs with a smooth liner have a larger radius, and the runs with the 10 mm lifters a smaller radial location of the CoM. This is expected as the balls cataract more for the high lifters than for the smooth lining and, as discussed in the theory, this shifts the CoM towards the centre of the mill. The difference between the smooth lining and the lifters becomes most pronounced at the high speeds, where the difference in charge motion is most pronounced. At 100% critical speed the CoM for the mill with lifters would be near the centre of the mill, but for the smooth lining it is still well removed from the centre. The averages for the slurry runs have a much larger radial location of the CoM, as would be expected from viewing the charge trajectory plots.

The angle of repose of the CoM increases with speed, as shown in Figure 32. There does not appear to be any influence of lifter height on the angle, as shown by the averages in Figure 33. There is a fairly linear relationship of the overall average over the range from 68% to 100% of critical speed, with a gradient of 0.42 (degrees per % critical). When extrapolated back to Zero speed - i.e. with the mill stationary - the intercept is at 27°, not at the origin, as might be expected. When the mill is stationary, the charge will be at the base of the mill and the angle of repose of the CoM will be 0°. However, if the mill is slowly rotated the charge does not begin to cascade until it reaches an angle of about 30° (this was experimentally determined for the test mill).

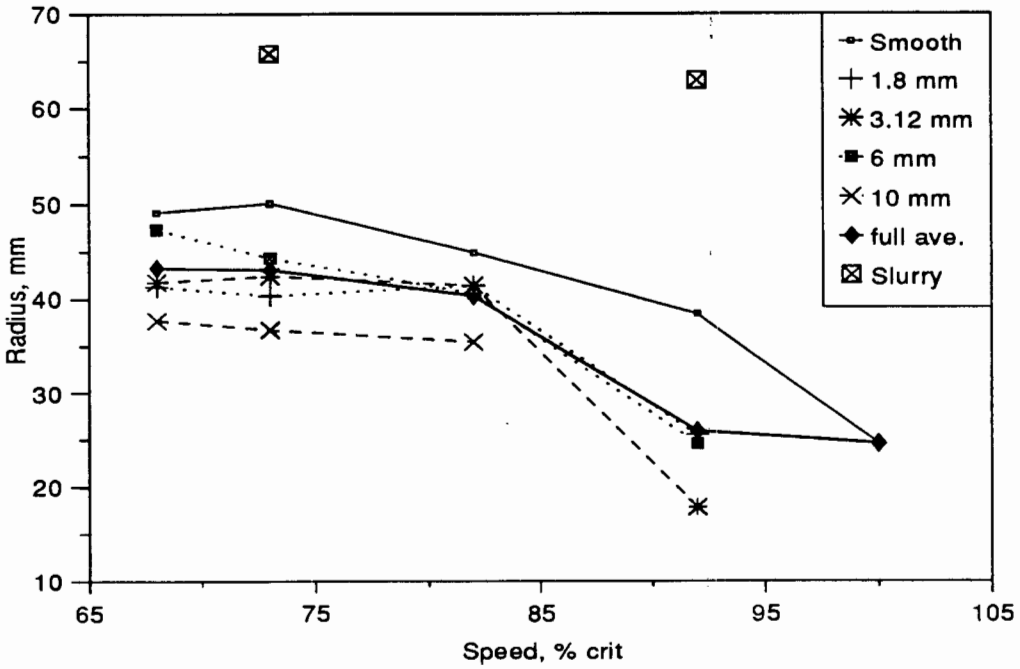

Figure 31. Average radius of the centre of mass of the charge

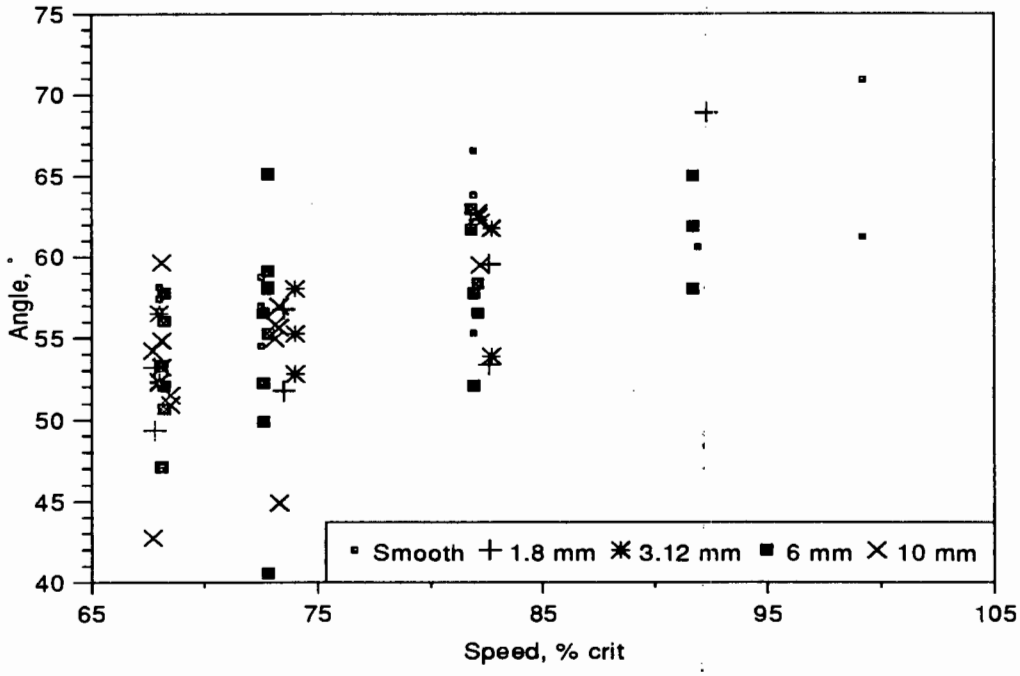

Figure 32. Angle of repose of the centre of mass of the charge

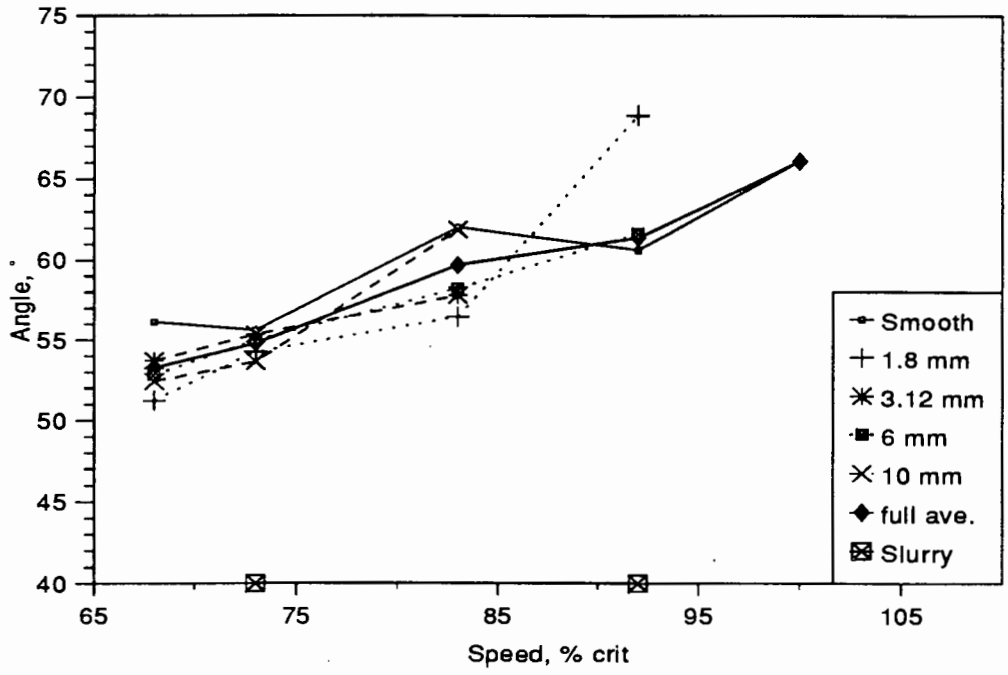

Figure 33. Average angle of repose of the centre of mass of the charge

So the charge can be left at a static angle of repose of 30°, which corresponds very well with the crude estimate of the intercept made from the plot of the angle of repose. The average angle of repose for the slurry is considerably lower than for the dry runs.

8.5 SLIP OF THE CHARGE

When the balls are in the *en masse* region and travelling upwards, driven by the mill shell and the balls surrounding them, they are not necessarily moving with the same angular velocity, Ω, as the mill. The ratio of the angular velocity of a ball to that of the mill indicates the degree of slip that is taking place. Expressing the angular velocity as a fraction of that of the mill also allows the relative slip between runs at different speeds to be compared. The measurement of the angular positions of the balls was not subject to the magnification error, as the X-ray beam was centred on the middle of the mill. The calculated radial velocities of the balls should be within an uncertainty range of 3%. So if there are any significant trends in the angular velocities as a function of the operating conditions, they should be evident from plots of the angular velocities.

The relative angular velocities of the balls for all conditions are shown in Figure 34 as a function of their radial locations. There are four distinct zones in the plot. There is a horizontal band at a relative angular velocity of one, that extends from the edge of the mill into a radius of about 65 mm. The angular velocities then decrease rapidly as the centre of the mill is approached. There are two distinct bands in this decreasing zone that tend towards different radial values for zero angular velocity. There is a fourth zone close to the mill shell where a wide scatter of angular velocities is evident.

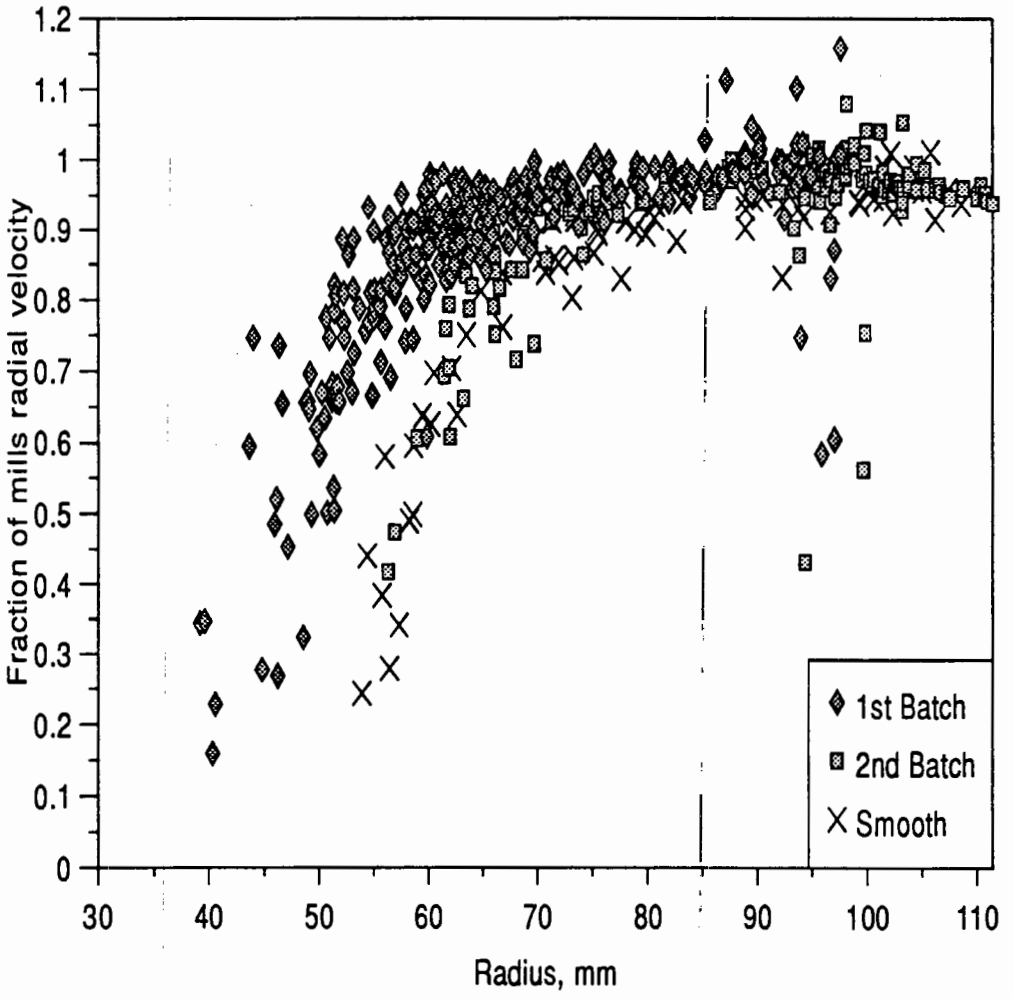

Figure 34. Fractional angular velocity of ball, as a function of radial location from the centre of the mill

At the centre of circulation (CoC) of the charge the angular velocity is zero, as this point does not move relative to the centre of the mill. So as the CoC is approached,

the angular velocity of the balls must tend to zero. When the line passing through the data points is extrapolated to zero angular velocity, it must intersect the x-axis at the CoC. The data in Figure 34 indicate that two separate CoC's exist. The data were divided into the two separate batches that were filmed, batch 1 consisting of runs 1 to 18 and batch 2 of runs 19 to 38. The data for the smooth liners belong to batch 2. The two descending zones in the graph separated unambiguously into the two separate batches. This indicated that there were different levels of charge in the two batches. The second batch had a larger radius of the CoC, so it must have had a lower mill filling. This was not intended, so some balls must have been inadvertently spilt or removed between the two batches of tests. The curves of the data were extrapolated to values of 44 mm for batch 1, and 53 mm for batch 2. It was noted that with the mill running at 68% critical speed, the CoC seemed to be at a smaller radius, about 39 mm. The values of the intercepts were validated by comparing them to the values measured from the plots of the charge trajectories, as discussed earlier. To facilitate direct comparison of the data from the different batches of tests, the results were plotted as a function of the distance from the CoC. This introduces a slight discrepancy at the edge of the charge, as the first batch extends over a greater radial distance than the second. The effect was considered to be small because the balls all had a very similar relative angular velocity, of unity, in that region.

The angular velocities as a function of the adjusted radius, i.e. the radius from the CoC, are shown in Figure 35. The data from the two batches coincide into one continuous trend. There are some points that fall below the zero radius. These are for the mill running at 68% critical speed, when the charge exhibits a CoC closer to the centre of the mill than for the other speeds. No distinct difference between the different mill speeds and between liner configurations is visible.

To ascertain whether the conditions in the mill did affect the angular velocities of the balls, the data were analyzed separately for each set of conditions. A selection of the plots is used to illustrate the trends. Figure 36 shows the relative velocities for all the different speeds with the smooth lining. There is a close correspondence between the data points for the different speeds. The different speeds cannot be compared over

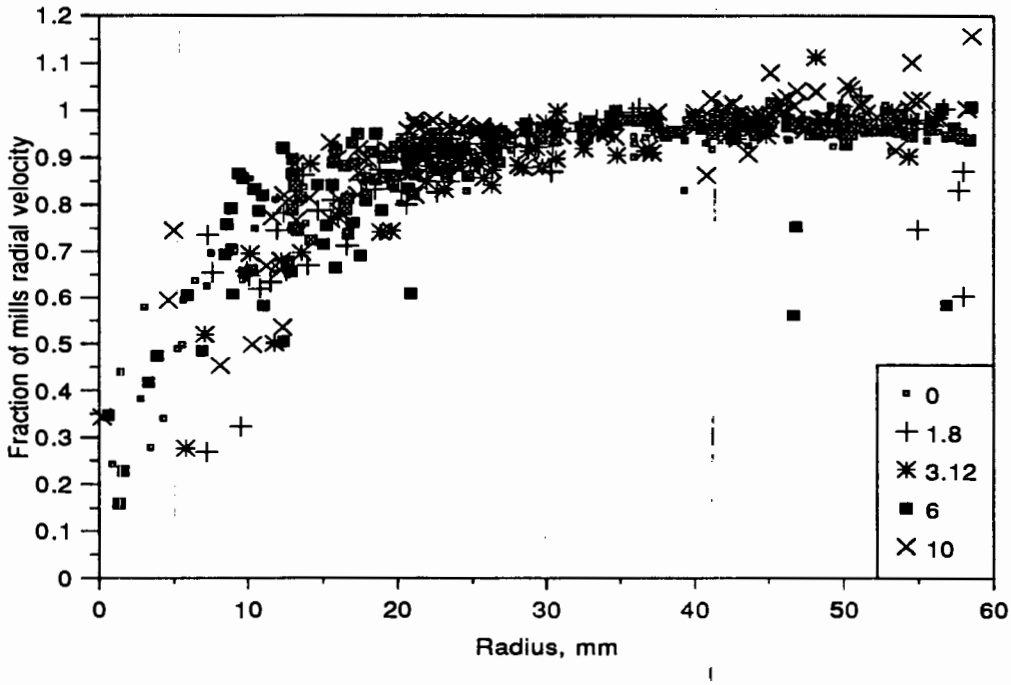

Figure 35. Fractional angular velocity of the balls for all conditions. Plotted as a function of radius from the centre of circulation (CoC).

the full range of radii, as the balls concentrate towards the edge of the mill at the higher speeds. The relative radial velocities over the full range of speeds for 6 mm lifters is given in Figure 37. The data again display a very close consistency between the different mill speeds. The few low points near the shell of the mill indicate that there may be intermittent slip of the charge one ball layer in from the shell.

The influence of lifter height on the angular velocities is analyzed by plotting the data for different heights of lifters at a fixed mill speed. Figure 38 shows that the height of the lifters does not seem to have a significant influence on the angular velocities. The 10 mm lifters do appear to produce slightly higher angular velocities, especially in the region from 10 to 20 mm radius. In Figure 39 the x-range of the graph is decreased, relative to the other graphs, as the data fall into a small radial range for the mill running at 92% critical speed. The 10 mm lifter seems to maintain a slightly higher angular velocity in the charge than do the lower lifters. There is also some evidence of this effect for the mill running at 68% critical speed.

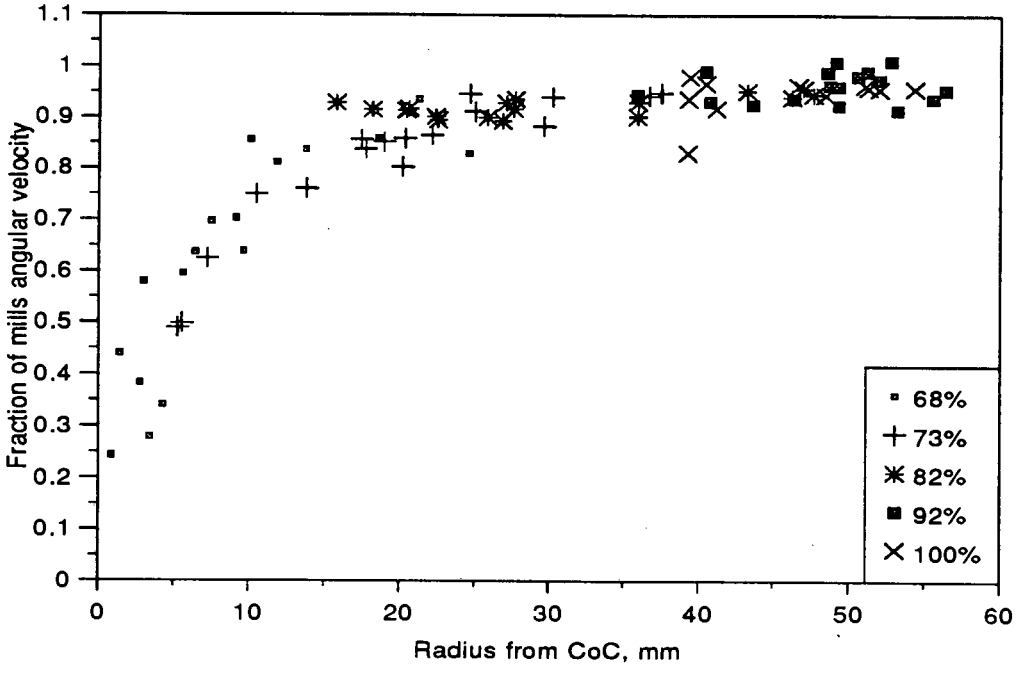

Figure 36. Fractional angular velocity of the balls for a smooth lining

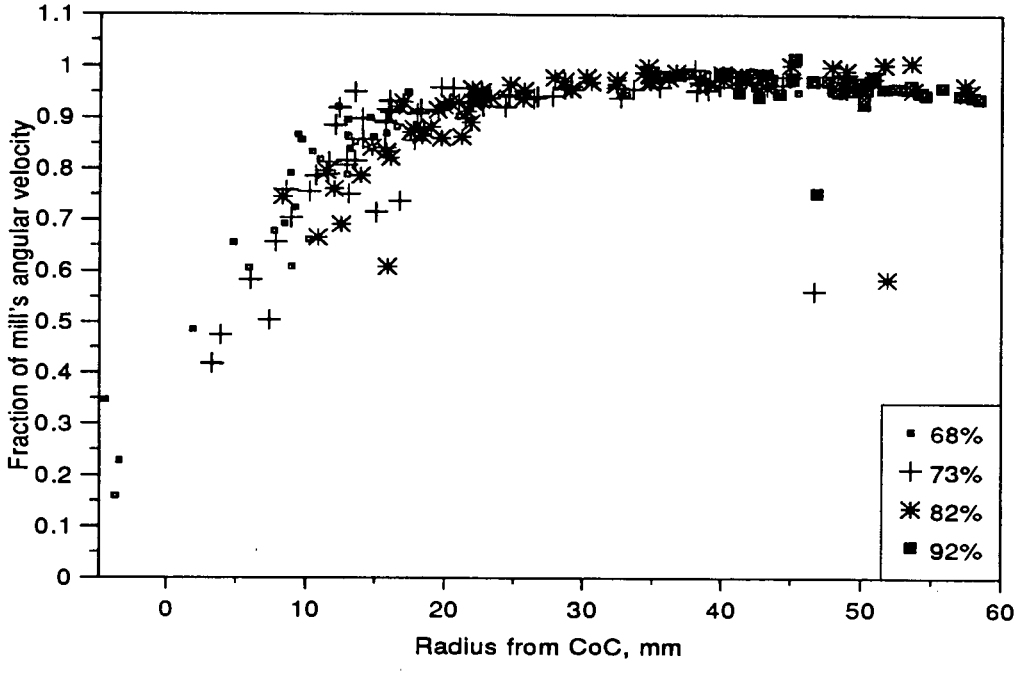

Figure 37. Fractional angular velocity of the balls for 6 mm lifters

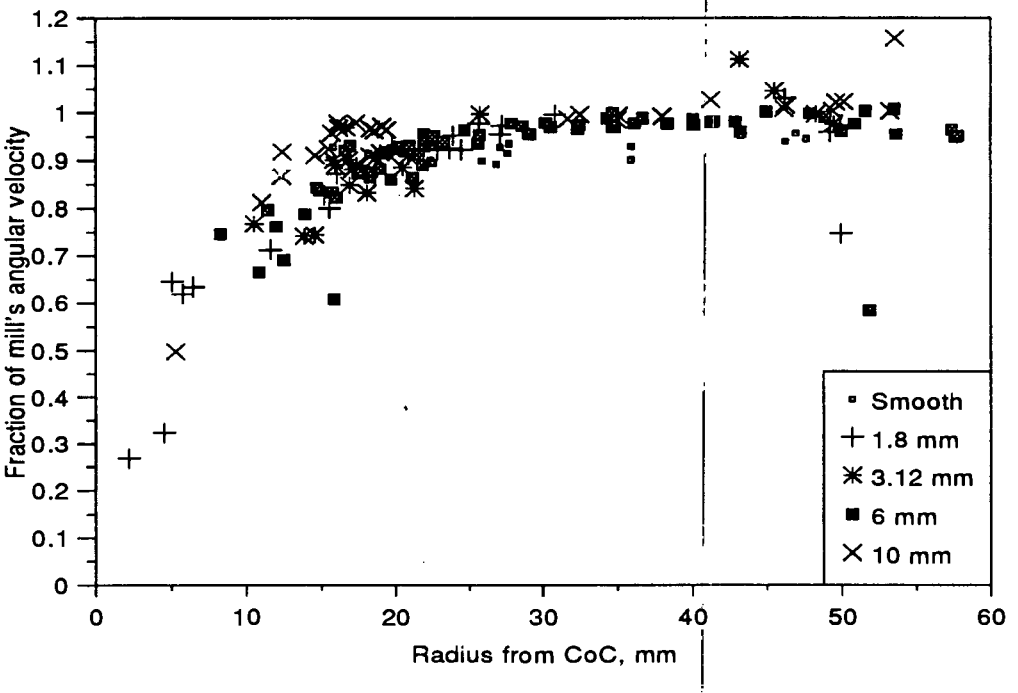

Figure 38. Fractional angular velocity of the balls for 82% critical speed

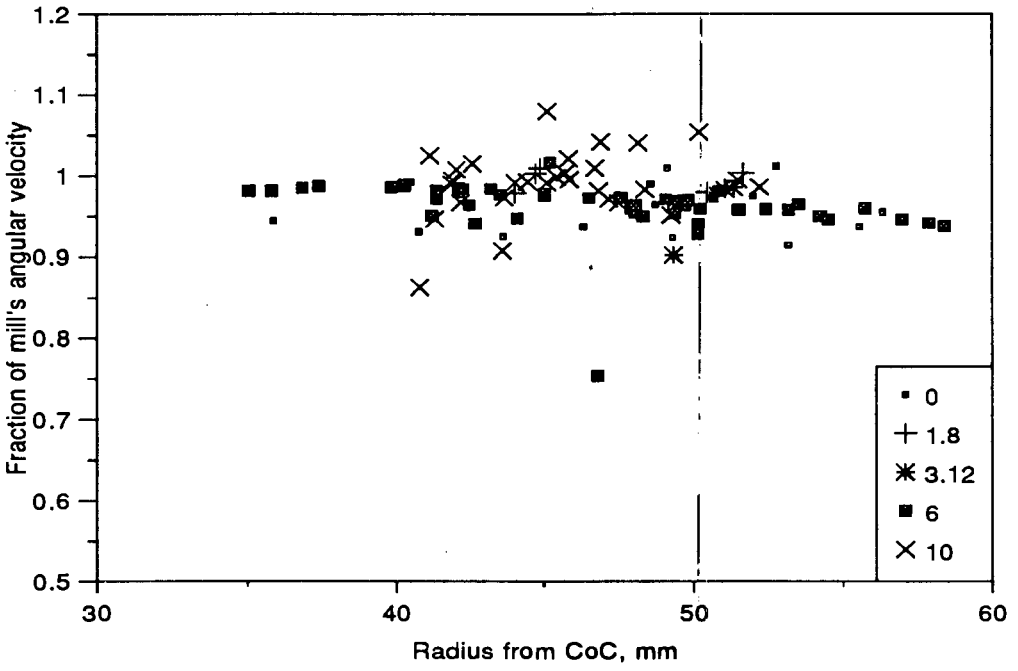

Figure 39. Fractional angular velocity of the balls for 92% critical speed

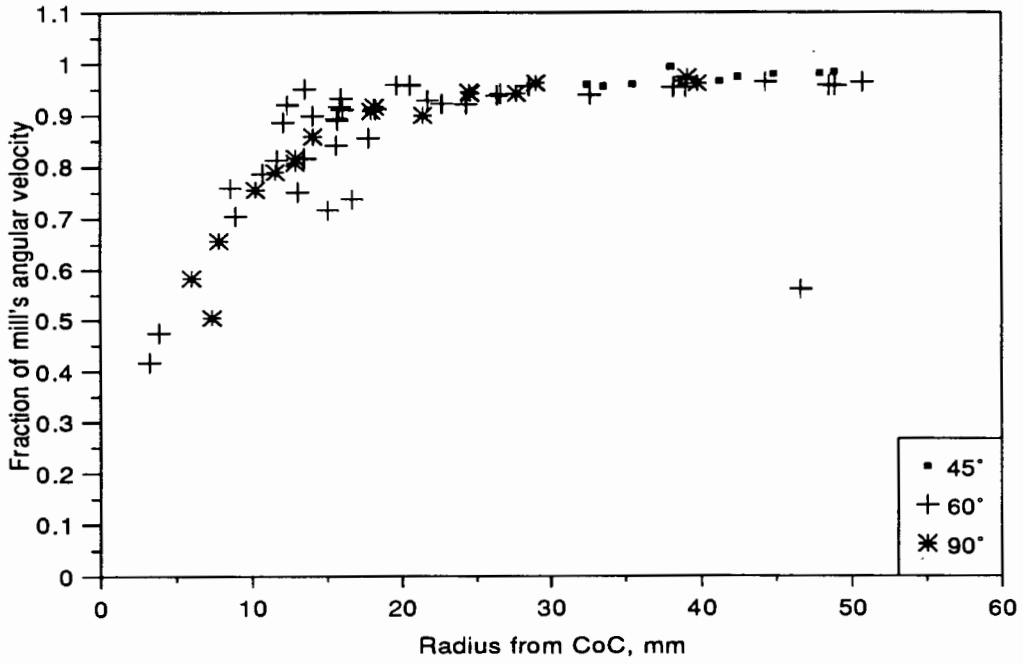

Figure 40. Fractional angular velocity of the balls for 73% critical speed, 6 mm lifters

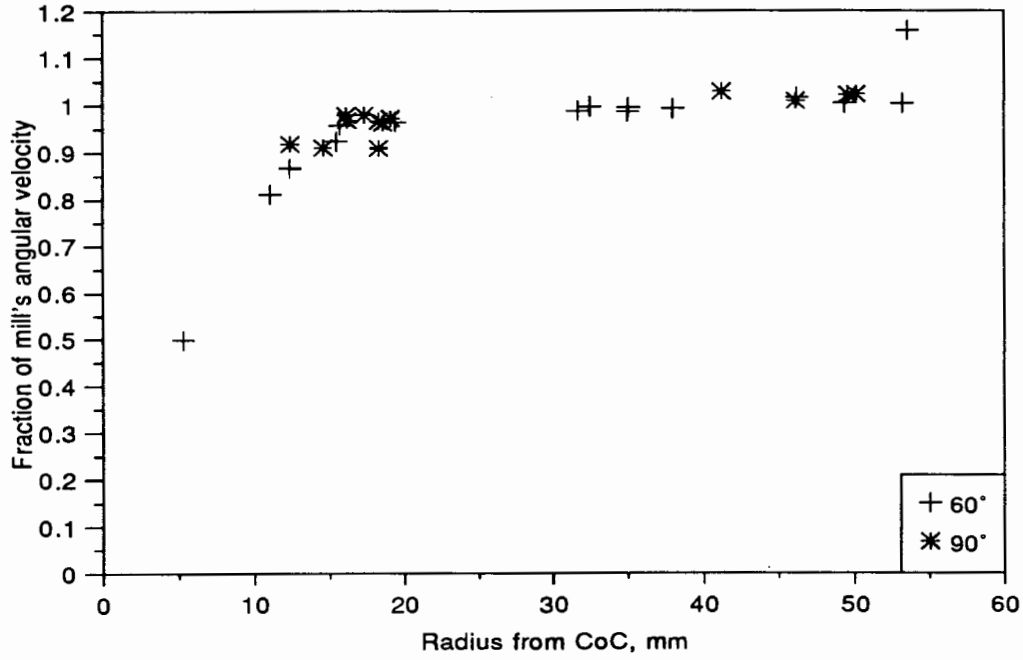

Figure 41. Fractional angular velocity of the balls for 82% critical speed, 10 mm lifters

The influence of the face angle of the lifter bars on the angular velocities of the balls, is illustrated in Figure 40 and Figure 41, for 6 mm lifters at 73% critical speed, and 10 mm lifters at 82% critical speed, respectively. There is no evidence of the face angle of the lifter having any influence on the slip within the charge.

As very little evidence had been found for the lifters having any influence on the degree of slip in the mill, all the data for the runs with slurry were plotted together. This is given in Figure 42 as a function of the radius from the centre of the mill. The addition of the slurry substantially changes the conditions in the mill, and the charge displays a very different action to that of the dry charge. The CoC is easily identified to be at 64 mm from the centre of the mill. The general trend is far more linear than for the dry runs, but with a very wide spread of angular velocities near the periphery of the mill, outside a radius of 85 mm. There is definite evidence of fluctuating slip in these outer regions, but the action in the inner regions is far more regular, with a fairly constant angular velocity.

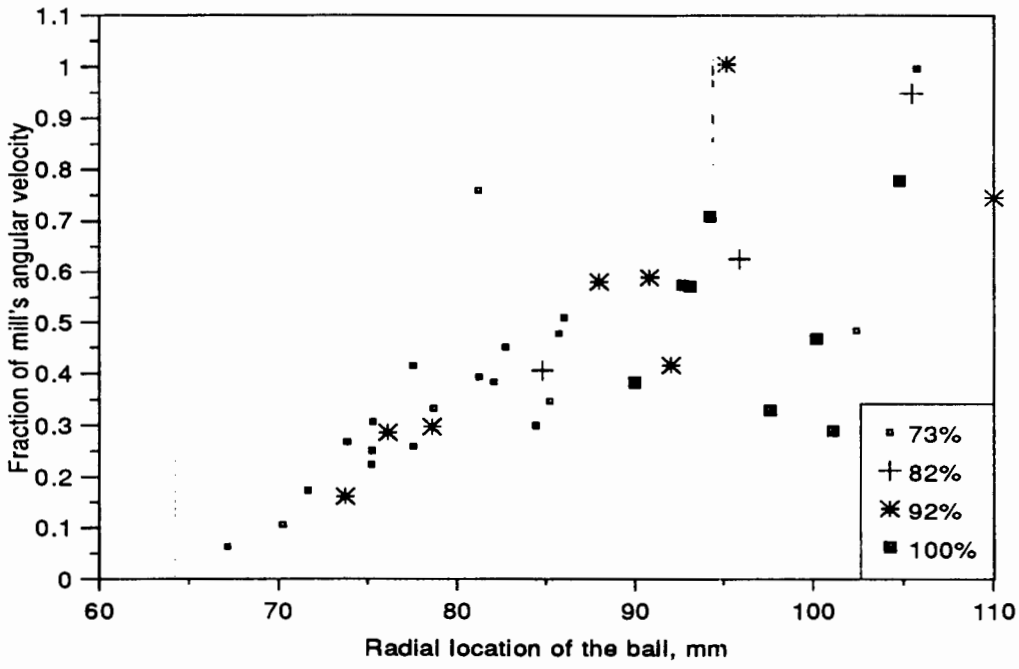

Figure 42. Fractional angular velocity of the balls for the mill loaded with a plastic slurry

8.6 RADIAL DISTRIBUTION

Viewing the plots of the charge trajectories makes it apparent that there is some segregation of the charge, which is dependent on the speed of the mill. The radial position of the ball is measured when the ball is in the *en masse* region of the charge, and is travelling in a circular path. Figure 43 shows the dependence of the balls' radial positions on the speed of the mill for each different type of ball that was tracked. The speeds are slightly off-set from the actual values so that the data for each type of ball is visible. The stepped line traces the average radial distribution of all the balls for each speed. The average radial position of the charge increases with speed, up to 92% critical speed, from where it levels off. With increasing speed the *en masse* region becomes narrower and longer as the shoulder moves upwards and the toe region further out, so the balls move closer to the mill shell. Figure 43 also shows that for each speed the different balls concentrate into restricted areas of the charge, the ranges of which are defined by the range of scatter for each set of points.

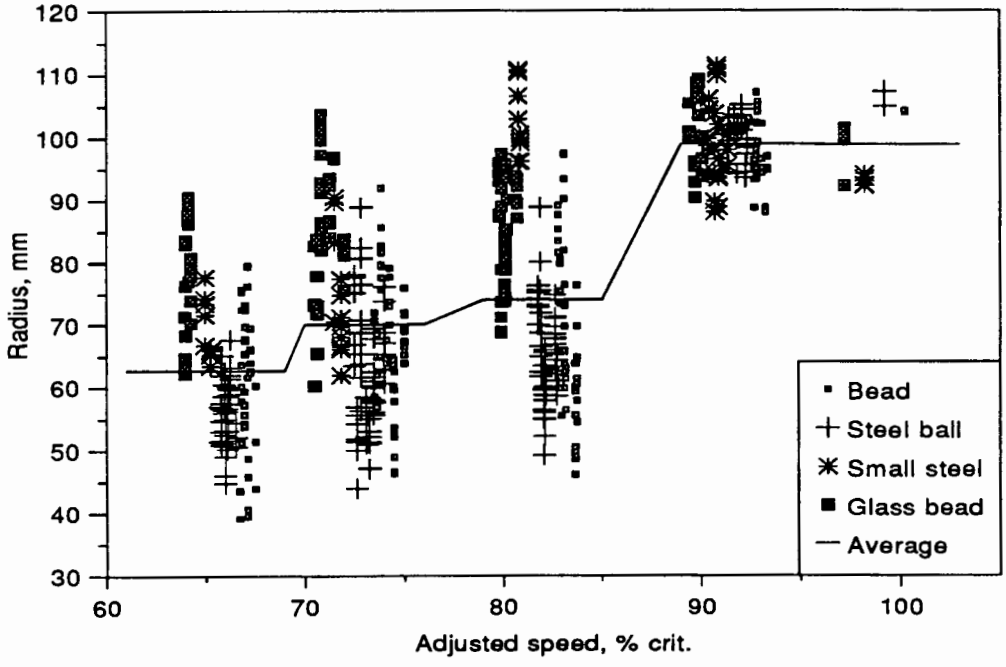

Figure 43. Radial distribution of the balls. The data range for each type of ball is offset from the actual mill speed to facilitate identification

To clarify the distributions of the separate balls, the average radial positions and accompanying standard errors were calculated, as given in Table VI. Twice the standard error indicates the 95% confidence interval of a data point lying in that range. Thus the average ± 2 x Std. err. gives the radial range where there is a 95% likelihood of finding a particular type of ball.

Table VI Average radial locations of the different balls

Average radial location, mm					
Speed	Bead	Steel ball	Small steel	Glass bead	Average
68%	60.4	56.0	69.0	77.3	62.7
73%	67.3	62.8	74.1	85.1	70.0
82%	68.5	65.5	103.4	86.5	74.0
92%	97.3	99.8	99.1	100.7	99.1
100%	104.2	106.2	93.1	98.3	98.9
2 x Standard Error ≡ 95% confidence interval					
68%	4.0	1.3	2.9	5.5	
73%	2.6	2.4	5.1	4.1	
82%	3.1	1.5	3.5	3.0	
92%	1.5	1.0	2.8	2.6	
100%	0.2	1.7	0.8	3.6	

Figure 44 illustrates the variation of the average radial distributions of each type of ball. There are significant variations in the relative radial positions of the different types of balls. At 82% critical speed and below, the heavier balls, the steel ball and the marked bead are concentrated towards the centre of the charge. At 92% critical speed all the balls are closely packed into a narrow region close to, or against, the mill shell. At 100% critical speed the balls again segregate, but the heavier balls now go to the outside of the charge. The small, lighter balls have the opposite trend. They are located around the middle of the charge at low speeds, and move to the inside of the charge body at high speeds. At 82% of the critical speed the small steel ball moves to the very periphery of the charge, before moving back inwards at higher speeds.

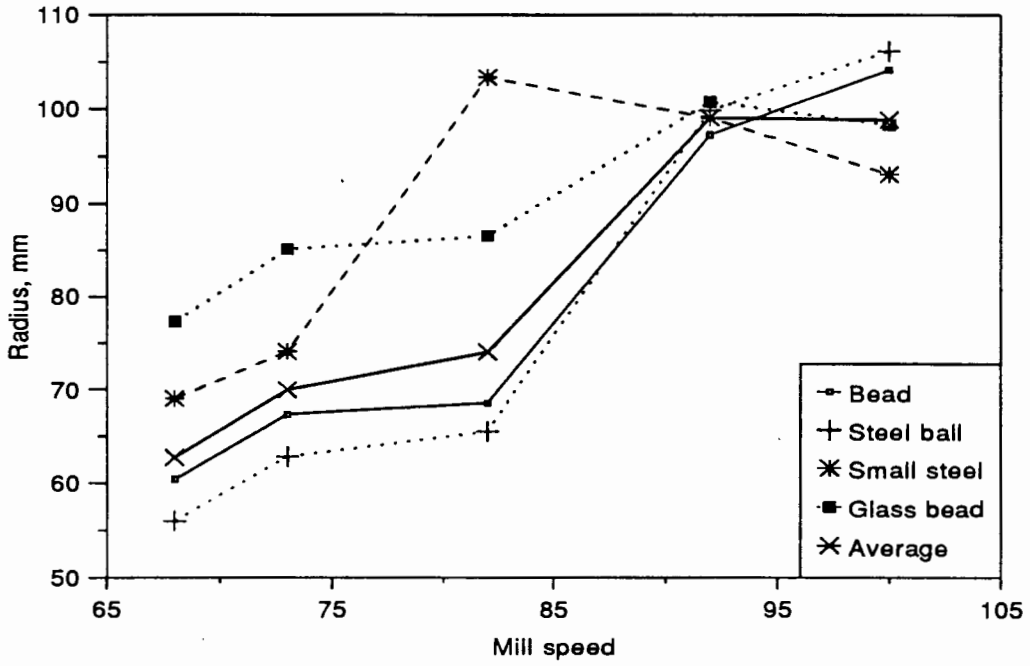

Figure 44. Average radial distribution of the balls

These effects are discussed in detail at a later stage.

8.7 INCLINE ANGLE OF THE CASCADING/CATARACTING REGION

The balls tumble down the cascading region in a fairly smooth and regular manner, as is apparent from the plots of the charge trajectories. The angle of inclination of this slope relative to the horizontal is plotted in Figure 45, for all conditions as a function of the radius of the ball path. There is a wide scatter in the angles, with the primary set of data covering a 15° band centred about 60°. For the high speeds, 92% and

100% critical, at the outer radii there is a 15 to 20° decrease in the angle of the incline. This correlates to the onset of a substantial degree of cataracting of the balls, where they are projected from the shoulder of the charge directly onto the mill shell. The outer layers of the charge are almost centrifuging as they impact on the shell at around 30 to 40° above the horizontal. It is clearly evident from the charge trajectories at these speeds (runs 19 to 22) that these balls follow a very shallow trajectory. The inclination angle of the cascading region is markedly lower for the runs with a slurry

in the mill. This can be seen from the slumped profile of the charge evident in runs 28 to 32.

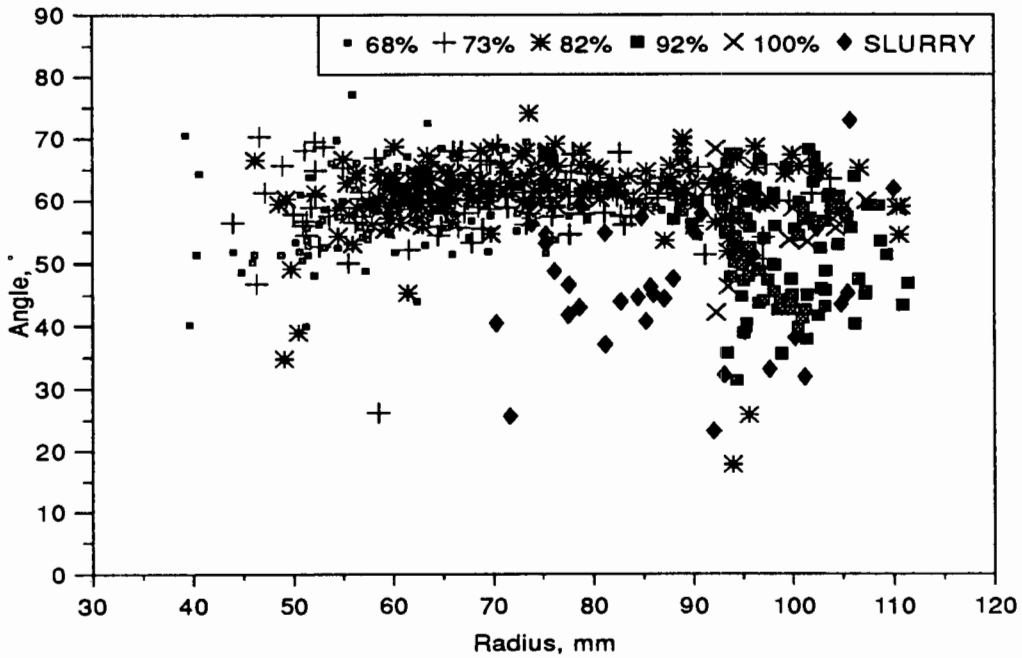

Figure 45. Angle of inclination, relative to the horizontal, of the cascading region for all speeds, as a function of the radial location of the balls.

The average angles of inclination of the cascading region are shown in Figure 46. This shows the average angle for each lifter height, at each speed of the mill. Up to 82% critical speed there is no significant difference between the different lifter bars. At 92% critical speed there is a definite drop in the angle for the 10 and 3.12 mm lifters, corresponding to the high cataracting paths discussed earlier. Surprisingly this is not as evident for the 6 mm lifters. This is because there are many inner paths used in the average figure, and the inner paths do not display this drop in angle. There are only a few data points for the 3.12 mm lifters at this speed, and these are at the very periphery of the mill. With no averaging effect of inner trajectories, the angle for the 3.12 mm lifters is much lower than it would be for a representative cross-section of the charge. The smooth lining produces a distinctly steeper cascading incline, about 7 to 10° steeper, than the lifter-bar linings. Careful comparison of the trajectories of the runs with smooth linings with those having lifter bars shows this up quite clearly, eg.

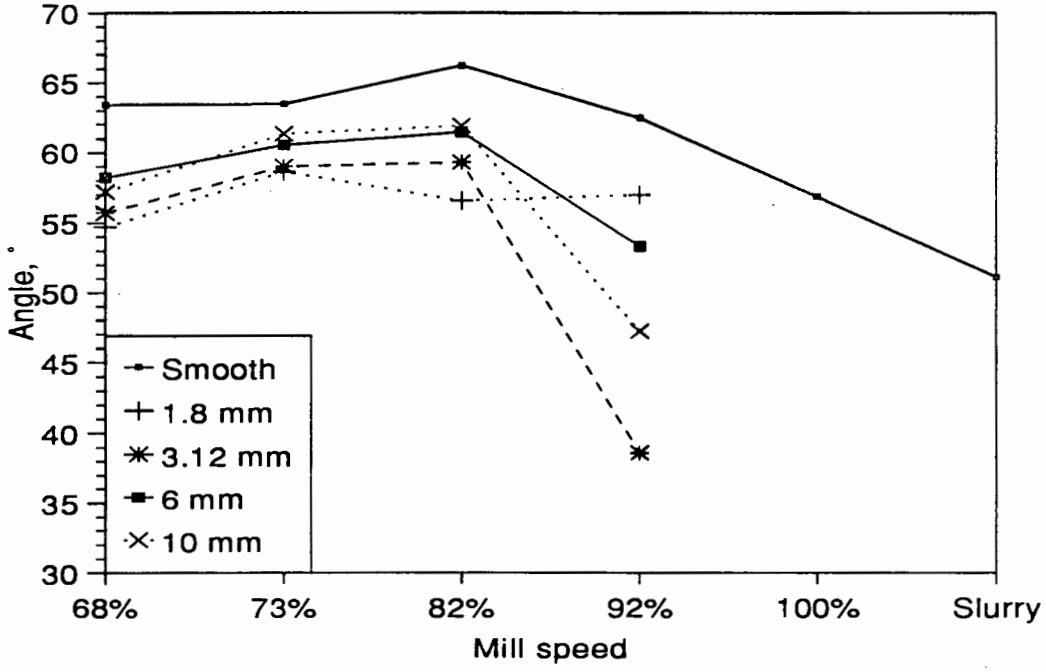

Figure 46. Average angle of inclination, relative to the horizontal, of the cascading region for different lifter heights, as a function of the mill speed.

runs 34 and 1.

8.8 ACCELERATION IN CASCADING REGION

When the balls are descending in the cascading and cataracting region, they are subject to gravitational acceleration, g. If the acceleration of a ball is less than g, then it must be interacting with other balls, and the interactive force must be equal to that required to reduce the acceleration from g to the measured value. The measured accelerations for all conditions are shown in Figure 47. The general trend is that at high radii, near the periphery of the mill, the acceleration is about 10 $m.s^{-2}$ ($g = 9.8\ m.s^{-2}$), and near the CoC the acceleration decreases to zero. This indicates that the balls on the outside of the mill are subject to free fall, and therefore are not interacting with the surrounding balls. There is an increasing interaction between balls as the centre of the charge is approached. These interactions start from around 30 mm from the CoC, indicating that the outer 20 mm, consisting of about 4 layers of balls, is free from interaction in the cascading/cataracting region. The higher the speed of the mill, the higher the acceleration values at a given radius are, showing that there

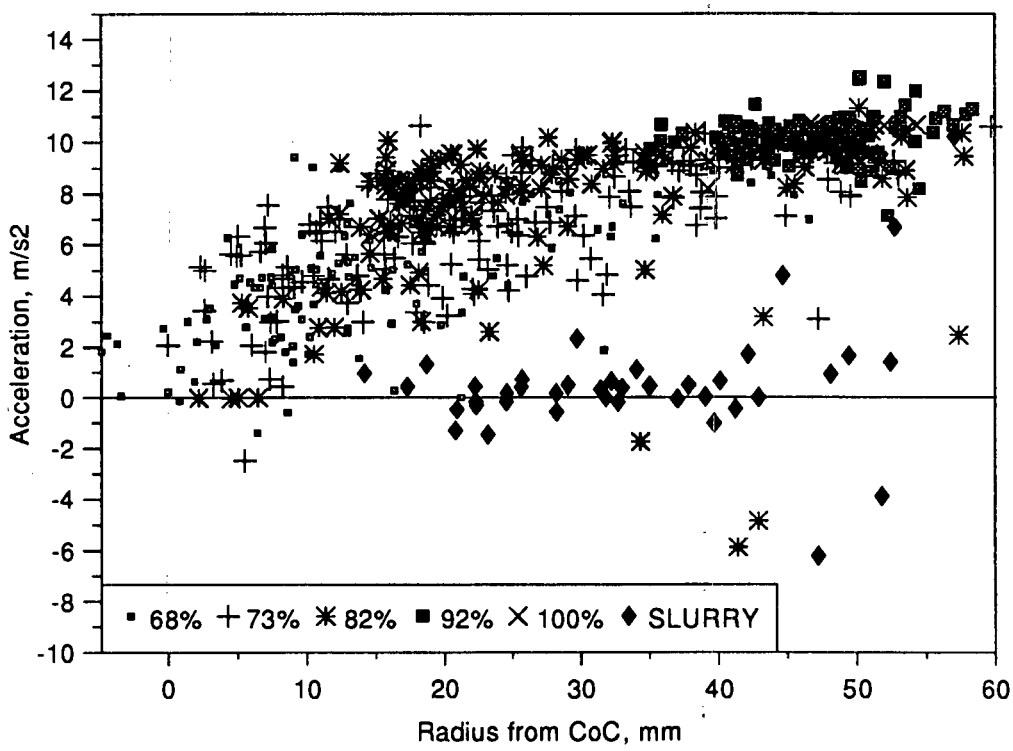

Figure 47. Average acceleration of the balls in the cascading/cataracting region. All conditions

is more cataracting at the higher speeds. This also shows that the charge is more dilute in the cascading region, as there is less interaction between the balls at the higher speeds.

There is a dramatic difference between the mill run dry and with a slurry. With a slurry the acceleration is close to zero, even close to the outside of the charge. Runs 28 to 31 show the low, slumped profile of the charge, and the short distance the ball travels between each frame, which accounts for the low values for the acceleration. The negative acceleration values arise when the ball slows down as it rolls down the cascading slope. It must be borne in mind that this was not a realistic slurry, just an attempt at roughly simulating the general effect of the addition of a slurry, so the results for the slurry are not of great importance. This is analysed further in the discussion.

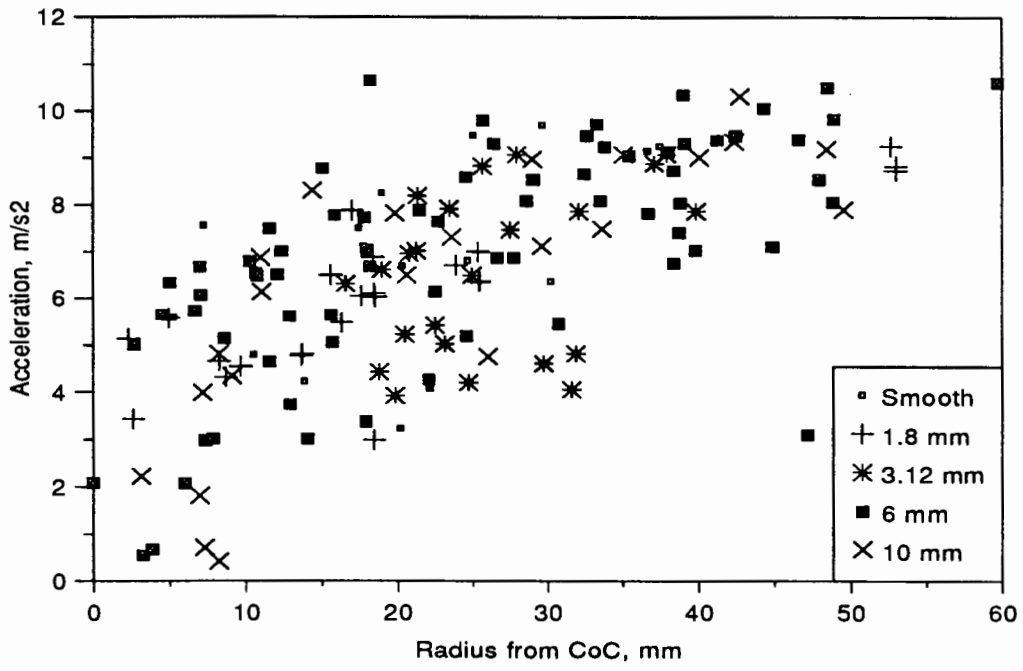

Figure 48. Average acceleration of the balls in the cascading/cataracting region 73% crit. speed

The plot of accelerations for 73% critical speed, Figure 48, shows a wide spread of acceleration values, between 10 and 40 mm from the CoC, of 4 to 9 $m.s^{-2}$. No difference between the different height lifters is apparent. There is a similar spread in acceleration values for 68% critical speed, but for 82% the majority of values are in a band only 1.5 $m.s^{-2}$ wide. The acceleration values for 92% and 100% critical speed are all around 10 $m.s^{-2}$, showing that the balls are all in free flight, i.e. in the cataracting region.

The influence of the face angle of the lifters is shown, for the mill running at 82% critical speed, in Figure 49. There is no definite influence of lifter face angle. The three negative and three low values of acceleration correspond with the action of the glass bead in run 26. The bead bounces off the charge before reaching the bottom of its trajectory, giving up a large portion of its kinetic energy in the process. The calculated acceleration includes this section, so it gives an unrealistic value. These low values are therefore not taken into account. For the other mill speeds there is also no

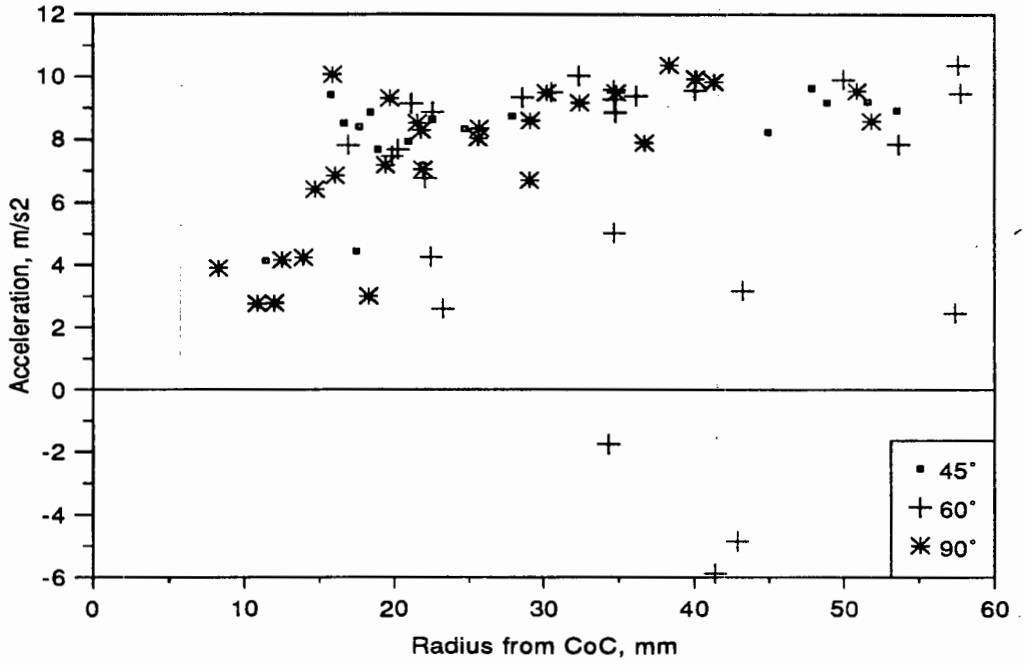

Figure 49. Average acceleration of the balls in the cascading/cataracting region 82% crit. speed, 6 mm lifters

influence of the lifter face angle on the acceleration values.

8.9 IMPACT ENERGY

The impact energy is a measure of the amount of work done by the ball on the charge, as it impacts. The calculated energy is normalised to that for the standard bead in the charge, so that the values for all the different balls can be compared. The values are expressed as a function of the displacement of the ball from the centre of the mill. The values of the energies of impact for all the different mill speeds are presented in Figure 50. The main body of points lie in a linear band that extends from 0 near the CoC to 0.06 mJ at the edge of the mill. There are many low impact energies for balls near the periphery of the mill, especially at 92% critical speed. This arises from the ball striking the shell and bouncing off with little transfer of energy, in a nearly elastic collision. As can be seen from the negative values, the shell can actually transfer energy to the ball, because the shell is travelling in a similar direction to the ball.

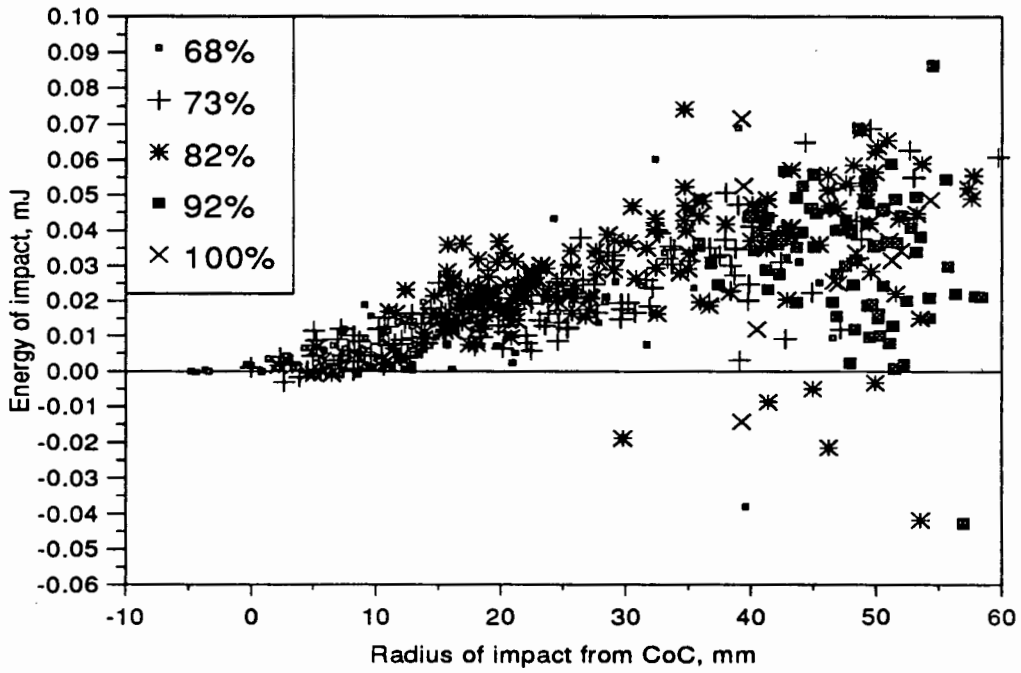

Figure 50. Impact energy of ball relative to radius from CoC, all speeds

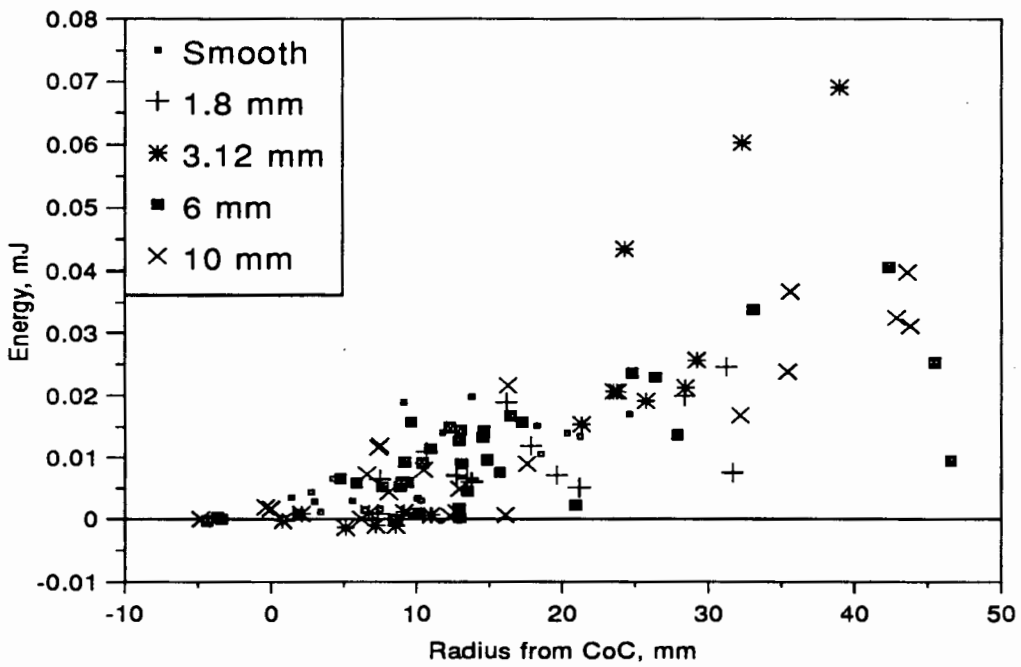

Figure 51. Impact energy of ball, for 68% crit. speed

In Figure 51 the impact energies for different heights of lifters as a function of the radius of impact are given, for the mill running at 68% critical speed. There is no distinct difference between the different lifters. The line passing through the centre of the data points has a maximum value of about 0.035 mJ at the edge of the mill, which is lower than the average for the full set of conditions. This indicates that the impact energies are lower for the lower speed. There are three impact energies that lie well clear of the rest of the values, and they lie on a straight line passing through the CoC. This implies that they are subject to a different set of conditions as compared to the bulk of the charge. They are quite possibly balls that have cataracted free of the rest

of the charge, and therefore had a higher acceleration than the rest of the balls. The plots for 73% and 82% critical speed are very similar to that for 68%, except that there is no sign of a region of higher impact energies. The plot at 92% critical speed, Figure 52, is quite different. The data are only available in a limited range, from 35 mm radius to the edge of the mill. The impact energy is approximately independent of the radius of impact, but actually drops off right at the shell. These low energy impacts would be for the balls that impact very high up on the shell of the mill, as in runs 21 and 22, so there is a very small difference in speed between the balls and the shell. Similarly to the plot for 68% critical speed, there are a few points that lie well above the rest. These points correspond to the 6 mm 45° lifters, and to the smooth lining, runs 24 and 36 respectively, where the balls have a good height of fall before impacting at the toe. There would be many more points in this region, but the images unfortunately fell beyond the edge of the film, so the data could not be gathered.

Plotting the impact energy as a function of the average acceleration in the cascading/cataracting region, Figure 53 shows that there is a strong correlation between the two. This is expected, as a high acceleration results in a higher velocity at impact. For a high acceleration, close to free fall, the energy of the ball is reserved for a high-energy impact. If the ball interacts with the charge as it descends, then the ball's energy is dissipated before striking the toe region, resulting in a low-energy impact.

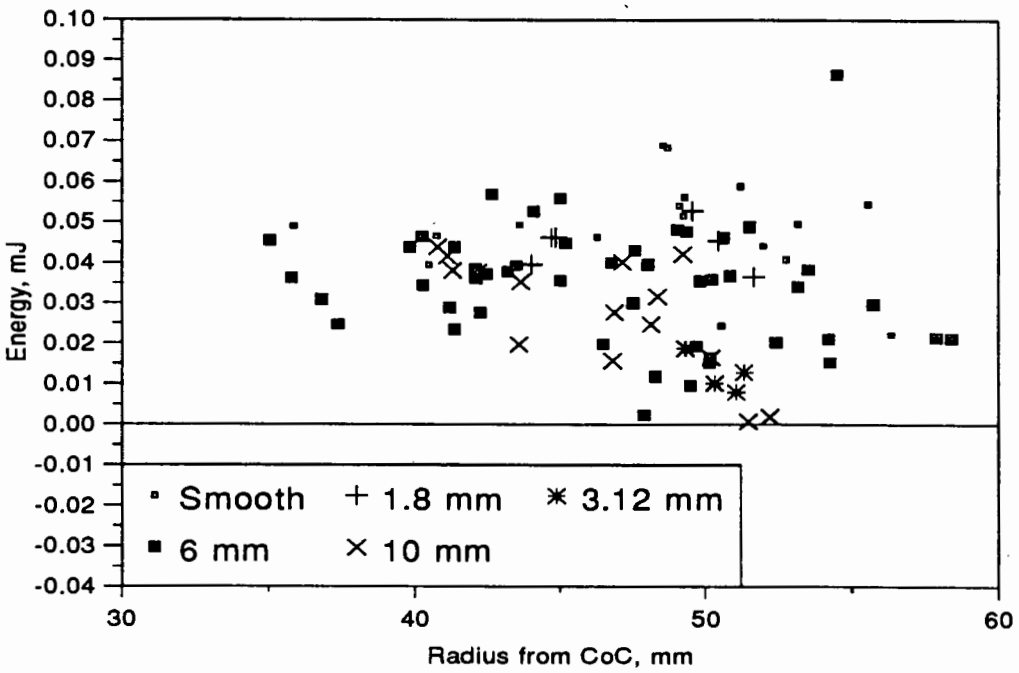

Figure 52. Impact energy of ball, for 92% crit. speed

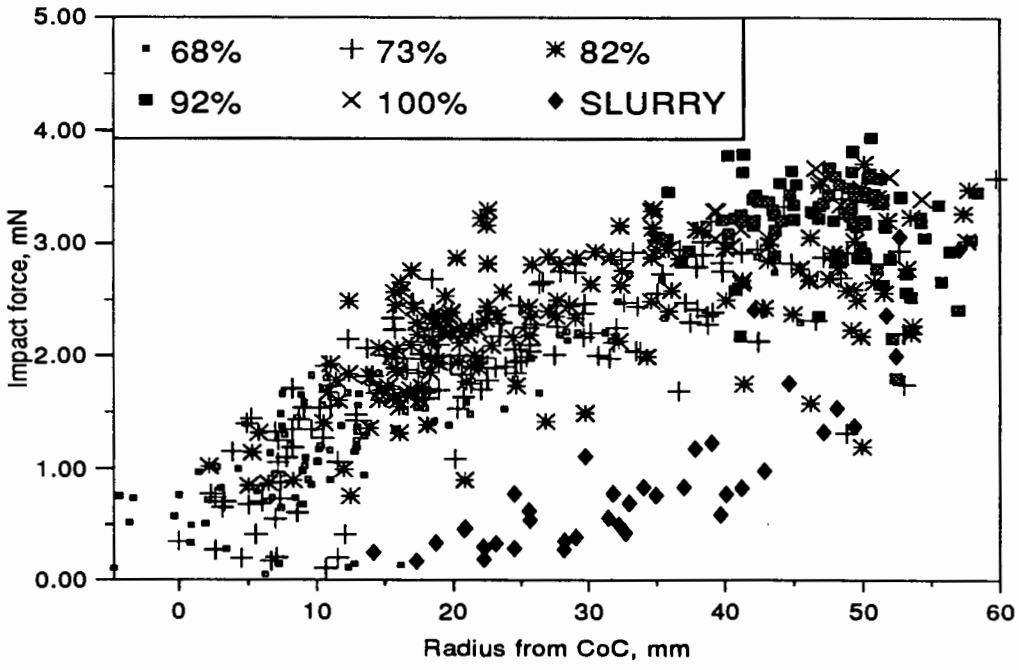

Figure 54. Impact force of the balls on the toe of the charge, all conditions

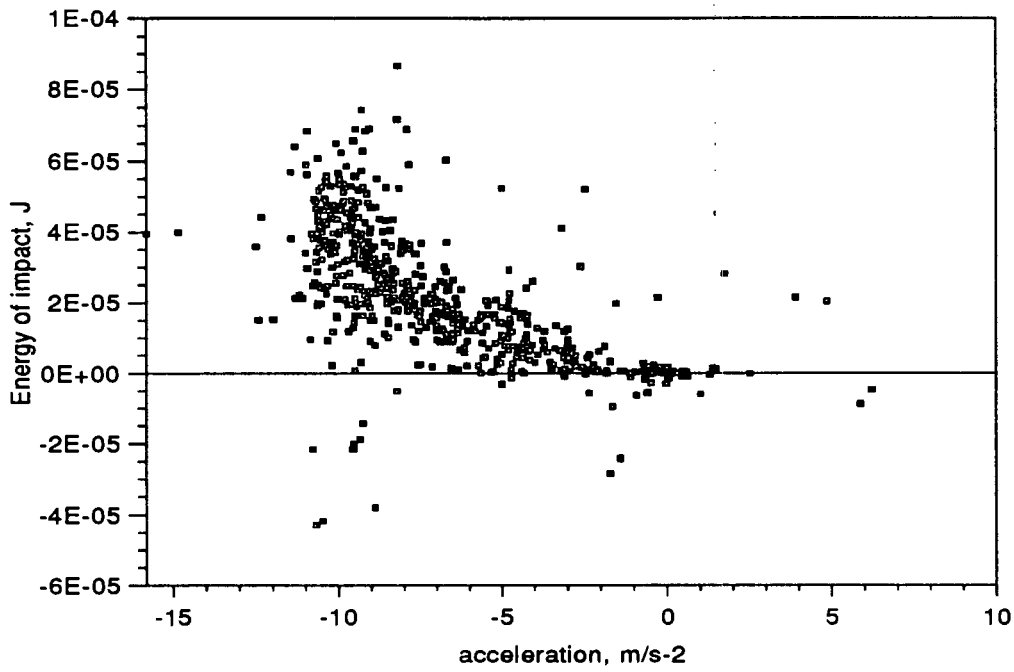

Figure 53. Energy of impact as a function of the average acceleration of the ball in the cascading/cataracting region

8.10 IMPACT FORCE

The impact force is measured where the ball impacts on the toe of the charge, and gives a measure of the greatest force acting on particles in a mill. Figure 54 shows the impact forces, given in milliNewtons, for all mill speeds, as a function of the radius from the CoC. The impact force decreases from about 3 mN at the periphery of the mill to zero at the centre of the charge. There is no apparent influence of mill speed on the impact force, except for the mill running at 92% critical speed. These higher forces arise from the balls impacting directly on the mill shell, rather than on the toe of the charge. The impact forces for the slurry runs are considerably less than for the dry runs, with a few high values at the periphery of the mill. These low values arise from the balls landing on the charge mid-way along the cascading zone, (see runs 28 to 31) rather than at the toe, so the values measured at the toe are for the balls that have been tumbling slowly down the cascading region.

There appears to be no influence of the heights of the lifters, as shown in Figure 55 for the mill running at 73% critical speed. There is also no evidence for the lifter height playing any role at the other speeds. There is a slight influence of lifter face angle, as

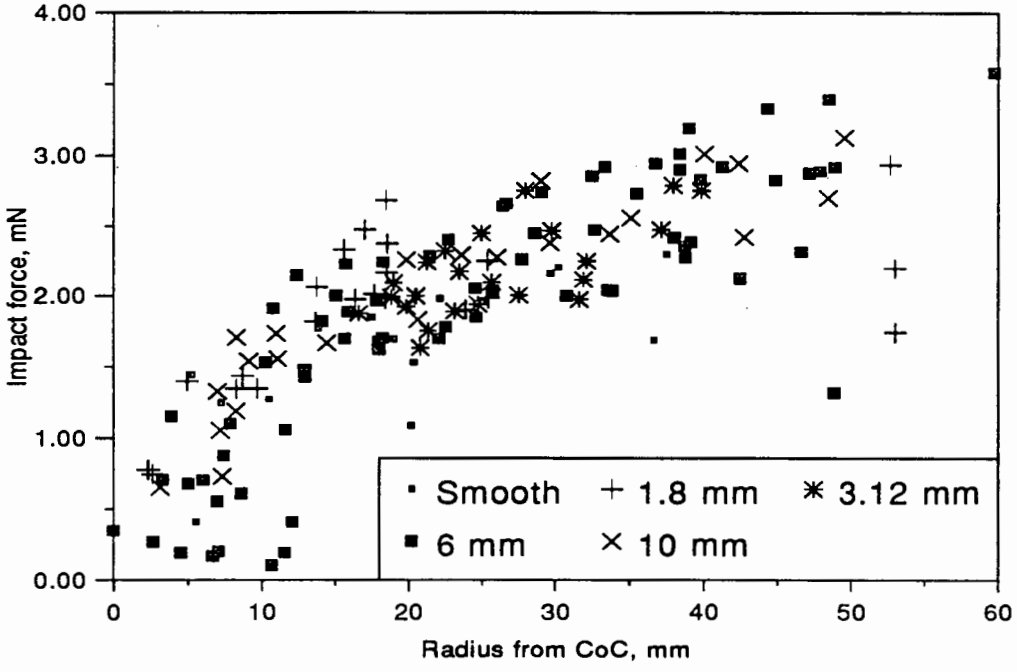

Figure 55. Impact force as the ball lands in the toe region, 73% crit. speed

shown in Figure 56, for 73% critical speed. The 60° lifters yield higher maximum impact forces than the other angle lifters. This is also the case for the mill running at 82% critical speed. For the mill operating at 92% critical speed the 45° lifter yields the highest impact forces, as illustrated in the discussion, Figure 115.

8.11 WORK PER REVOLUTION

Work done on a ball can increase its potential energy, linear kinetic energy, rotational kinetic energy, and temperature. Once the charge has reached an equilibrium temperature, no more work goes into increasing the temperature of the ball, so this factor can be ignored. As shown in the results (Figure 163 to Figure 166 of Appendix IV), the ball rotates approximately once about its own axis for each revolution around the mill, so in the frame of reference of the mill the ball does not have a rotational kinetic energy component. The potential energy imparted to the ball as it is lifted up is all lost on the descent, so the sum of the work imparted in changing the potential energy over a complete circuit is zero, providing the ball remains in the same layer of charge. If a ball does swop layers, the change in potential energy will cancel out when the ball returns to that layer, so on average the net change in potential energy per

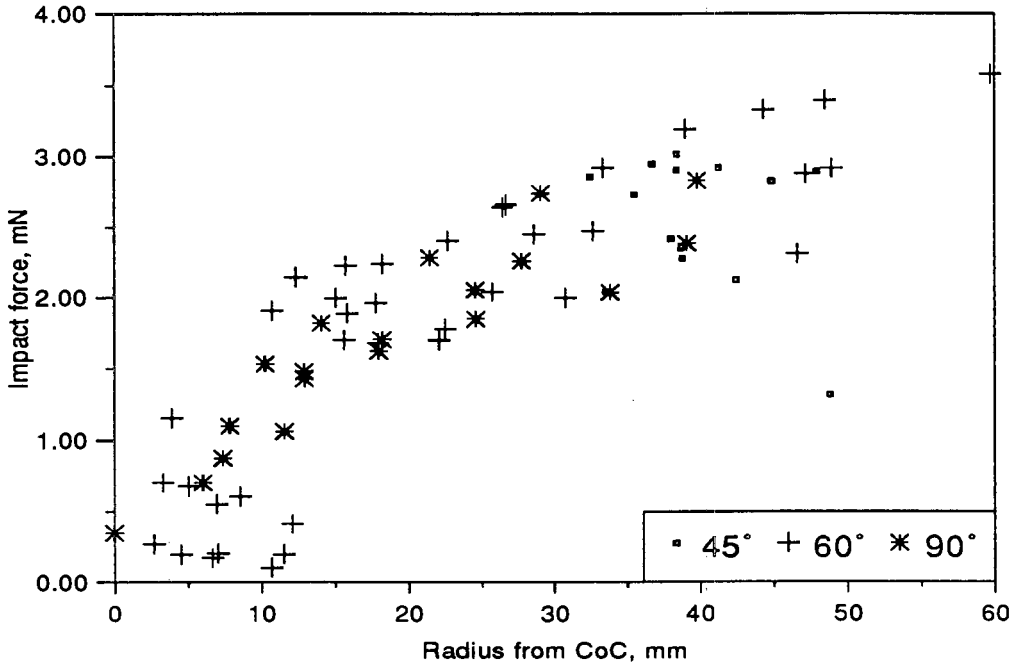

Figure 56. Impact force of the ball as it lands in the toe region, 73% crit. speed, 6 mm lifters

circuit about the mill is zero. As the ball tumbles down the charge in the cascading region and impacts on the toe region, it does work on the charge. The potential energy gained when the ball is lifted up is transferred to kinetic energy as the ball descends. As there is little change in the ball's linear kinetic energy while it is in the circular path and being lifted up through the *en masse* region, the net kinetic work per revolution done by the ball reflects the work done in the cascading and toe regions.

The work done by the ball per circuit about the mill, as given by eqn. (14), for all conditions, is given in Figure 58. Some points lie beyond the mill radius of 95 mm because of the 14% magnification error. It is observed that for most of the circuits of a ball, less than 0.1 mJ of work is done by the ball per revolution. For the mill running at 82% critical speed the ball does noticeably more work than for the other speeds. When the work is plotted separately for each speed, there is a distinct peak in the work done at a radius from the CoC that varies with the speed. The radial location of this zone of peak work increases from 10, to 15, to 20, to 47 mm as the speed is increased up to 92% of the critical. For the mill running at 68% critical speed,

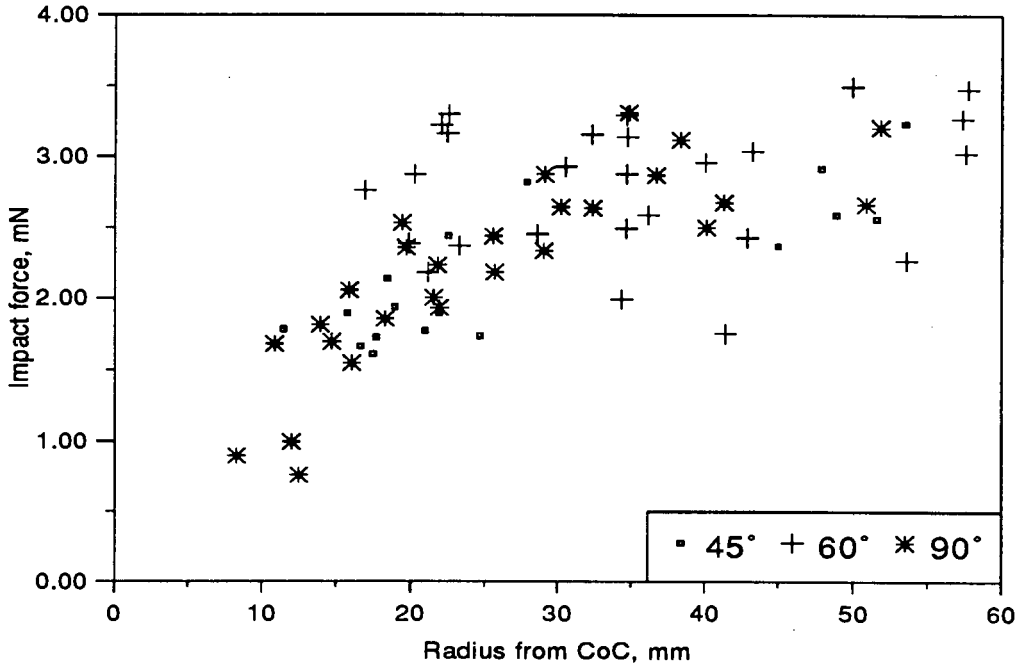

Figure 57. Impact force of the ball as it lands on the toe, 82% crit. speed, 6 mm lifters

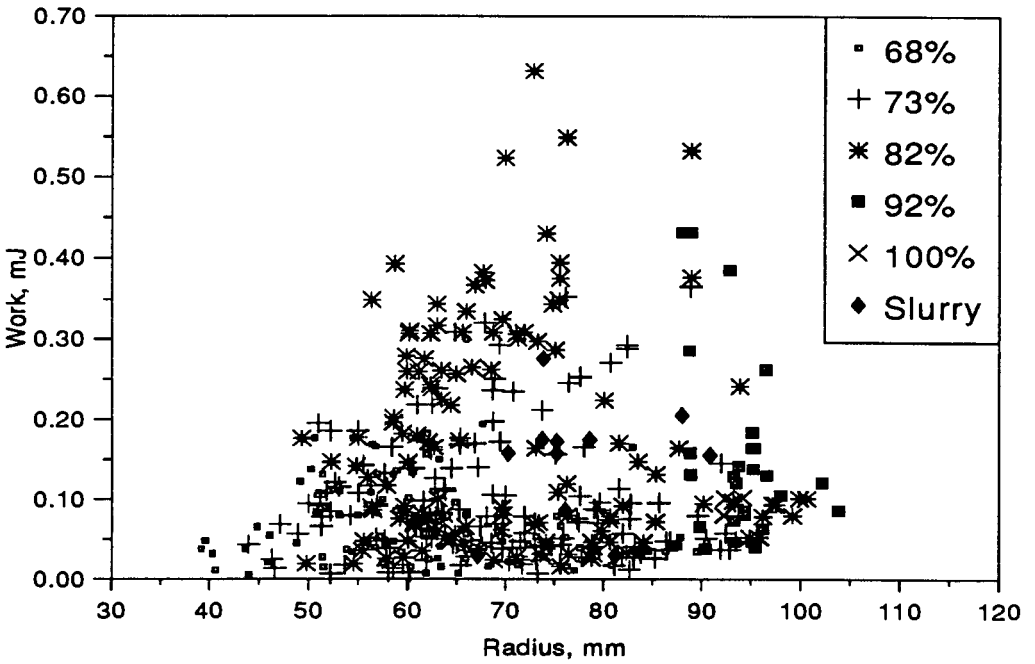

Figure 58. Work per revolution of ball, for all conditions

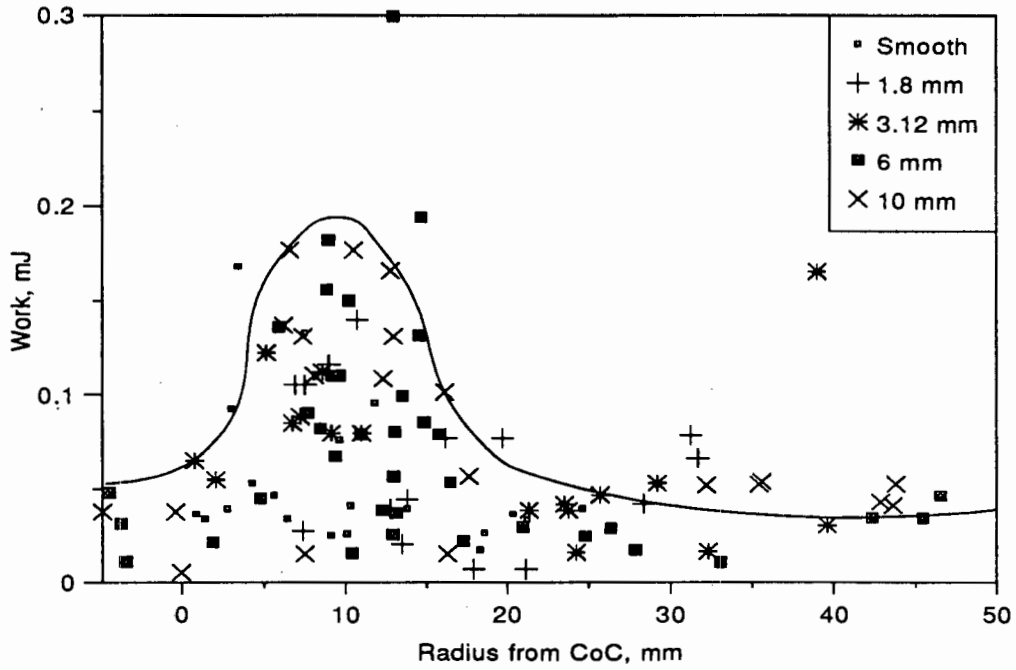

Figure 59. Work per revolution of ball, for 68% crit. speed

Figure 59, the peak amount of work per revolution takes place at around 10 to 15 mm from the centre of circulation, as illustrated by the trend curve superimposed on the data. The 6 and 10 mm lifters produce the majority of the work. Figure 60 shows the situation for 82% of critical speed, the peak is 20 mm from the CoC. At this speed the 6 mm lifters produce the peak amount of work.

Figure 61 shows the influence of the face angle of the 6 mm lifters on the work done by the ball in the mill running at 68% critical speed. The 90° lifters produce more work than the 45° lifters. The 60° lifters produce the most work at 73% critical speed, as shown in the peak of Figure 62. There is a secondary set of points for 45° lifters, quite removed from the main body of work values. These occur near the periphery of the mill, and appear to arise from the 45° lifters dropping the balls onto the face of the cascading portion of the charge, as can be seen for the glass bead in run 15. For 82% critical speed the peak values also occur for the 60° lifters. For both 73% and 82% critical speeds, the 10 mm lifters yield a lower peak work value than the 6 mm lifters. The peak is displaced nearer the centre of the mill, and the 90° lifters become more dominant in the peak work zone, as seen in Figure 63 and Figure 64. For the mill

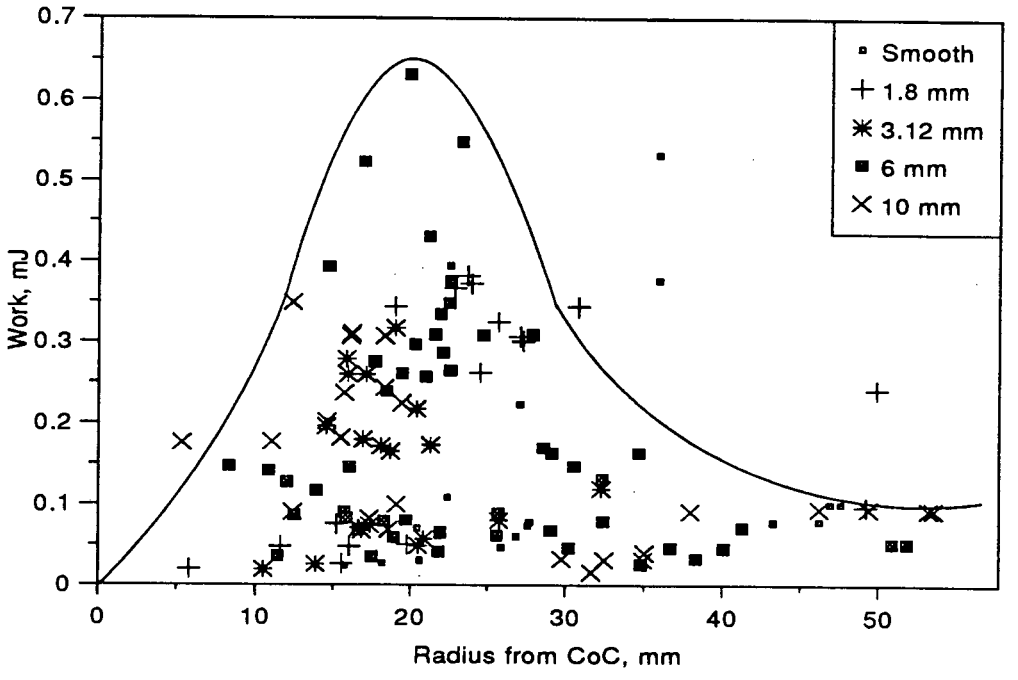

Figure 60. Work per revolution of ball, for 82% crit. speed

running at 92% critical speed, Figure 65, the low 1.8 mm, and the 6 mm, 45° lifters are responsible for the most work.

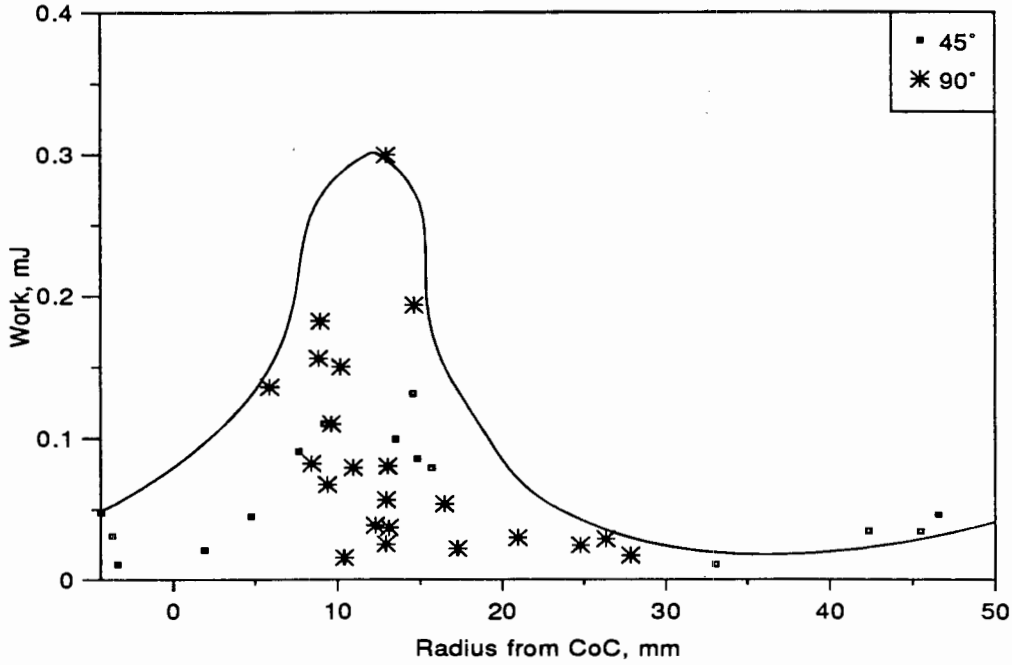

Figure 61. Work per revolution of ball, for 68% crit. speed, 6 mm lifters

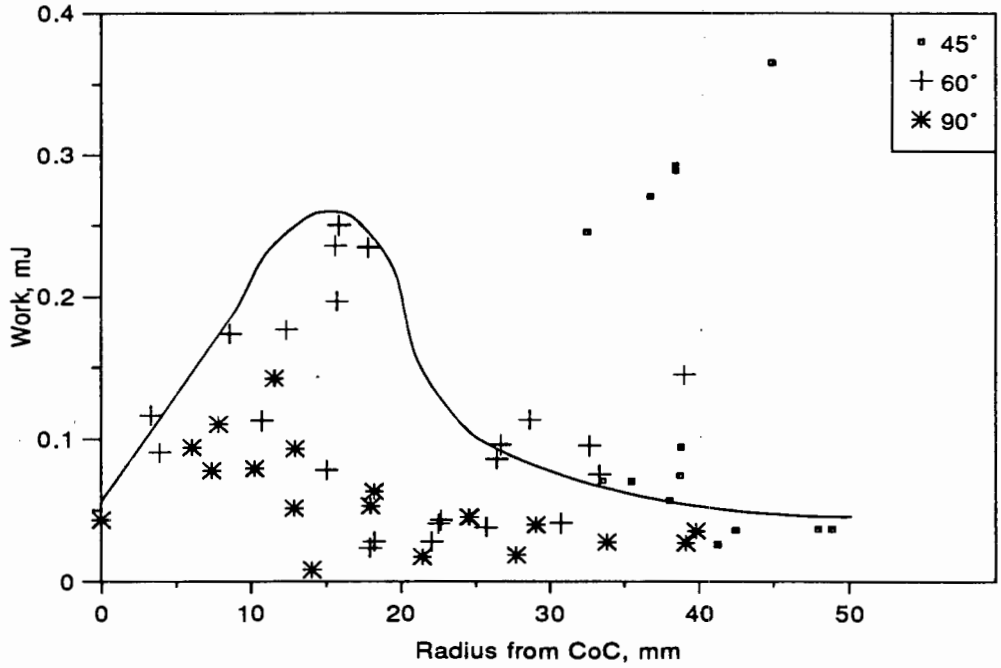

Figure 62. Work per revolution of ball, for 73% crit. speed, 6 mm lifters

8.12 GAMMA CAMERA FILMING

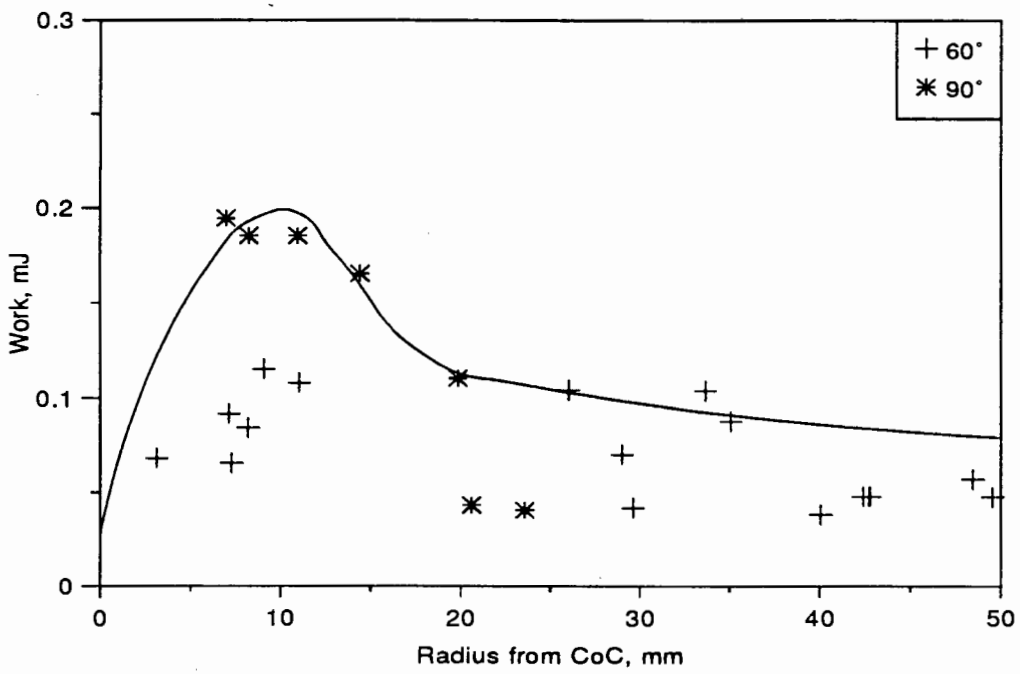

Figure 63. Work per revolution of ball, for 73% crit. speed, 10 mm lifters

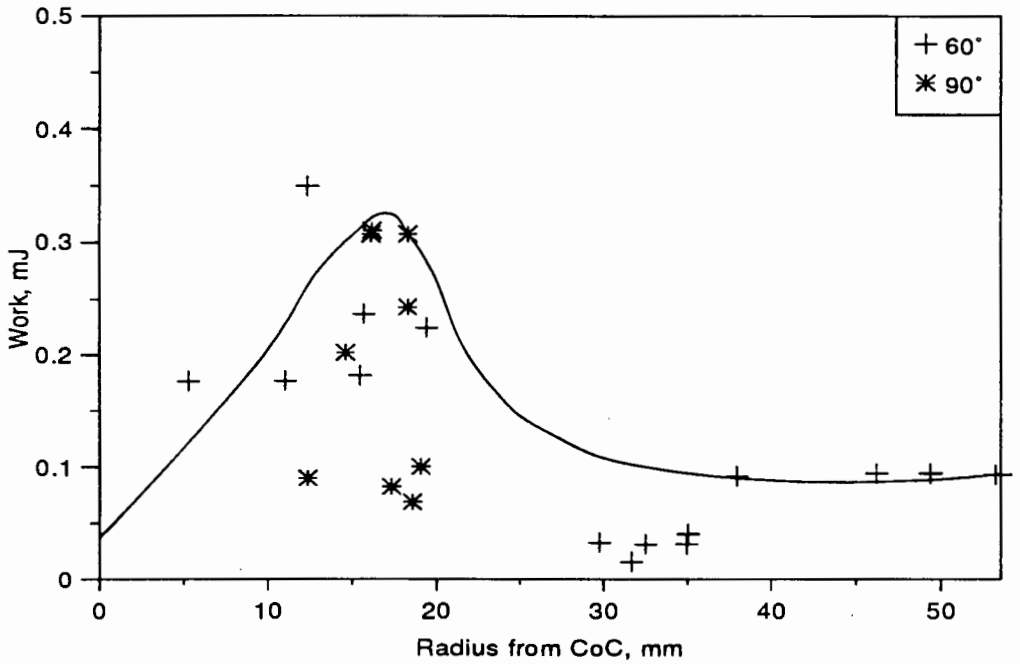

Figure 64. Work per revolution of ball, for 82% crit. speed, 10 mm lifters

Detailed information on the motion of the balls was extracted from the X-ray films. The results of the gamma camera filming were not sufficiently precise to carry out a

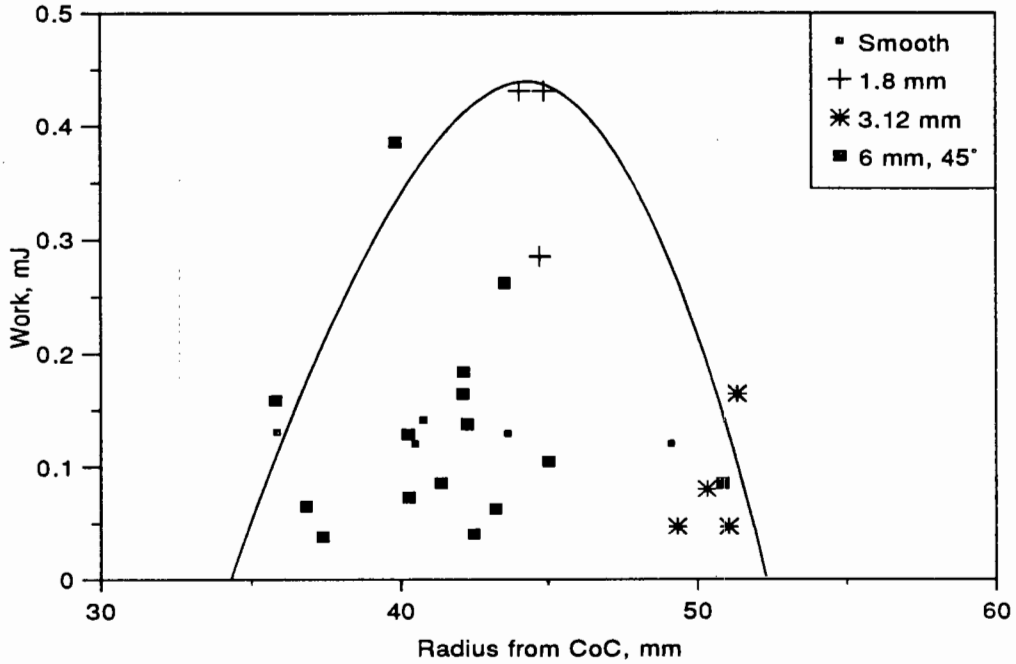

Figure 65. Work per revolution of ball, for 92% crit. speed

rigorous analysis of the charge motion, so they were only used to study the radial distribution of the ball, and the location of the centre of circulation (CoC).

8.12.1 Radial segregation

A summary of the radial distributions are presented in Table VII. The percentage distribution is the percentage of circuits of the ball about the mill that fell within the given radial interval. The radial interval is expressed as the average radius of the interval. The width of each interval is approximately 12 mm, so the radial range within which the ball was located is the given radius ±6 mm. The smallest radius, 43 mm, coincides with the CoC of the charge, so for this radius the range is 43+6 mm. As the radius of the ball is 4.6 mm, there is a very low likelihood of the ball being in that region, unless it is at the CoC. The next radial range, 55 mm, thus represents the central region of the charge. The 90 mm radius represents the ball against the mill lining. As the intervals are 11.7 mm apart, and the ball diameter is 9.2 mm, each interval represents approximately the width of the ball path.

Table VII The radial distribution of the large ball

			Radial location, mm				
	Lifter bar		90	78	66	55	43
Run	Speed %	Height mm	Percentage distribution				
0*	74	6	0.0	15.3	54.0	20.6	10.1
1	73	6	7.3	75.5	11.6	5.6	0.0
2	82	6	0.0	3.7	10.1	85.8	0.4
3	64	6	1.0	87.0	12.0	0.0	0.0
4	64	1.8	3.9	90.4	5.7	0.0	0.0
5	73	1.8	25.0	60.5	12.9	1.6	0.0
6	82	1.8	0.0	0.0	2.2	97.8	0.0
7	82	3.12	0.0	3.9	7.4	88.7	0.0
8	73	3.12	9.2	71.5	14.7	4.6	0.0
9	64	3.12	48.9	49.7	1.4	0.0	0.0

* For this run the ball was the same size as the median ball size of the charge, i.e. 6 mm

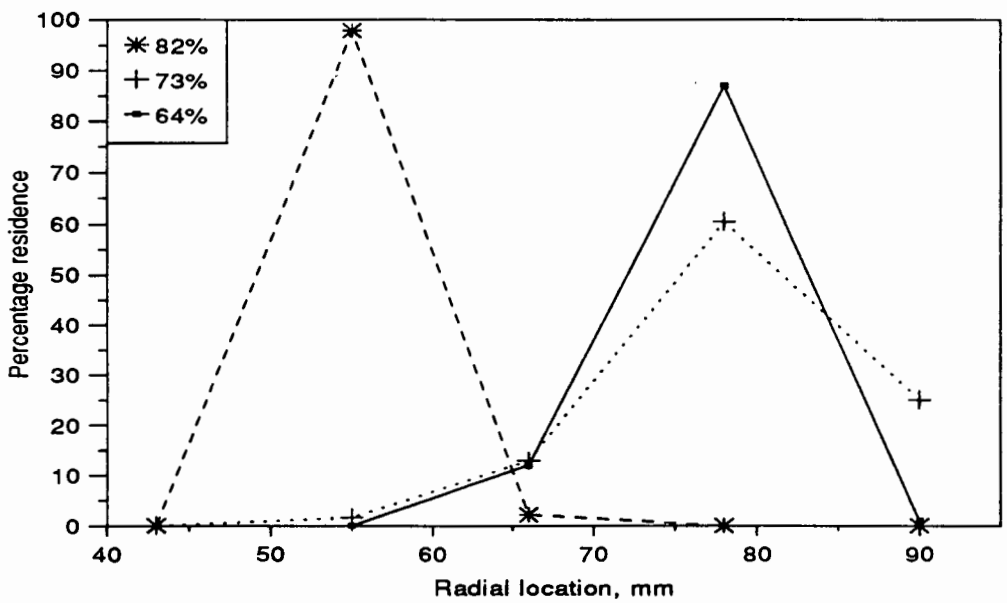

Figure 66. Radial distribution of the large ball, 1.8 mm lifters

Figure 66 to Figure 68 show the dependence of the radial distribution of the ball on mill speed, for each height of the lifters. The data points are linked by lines so as to

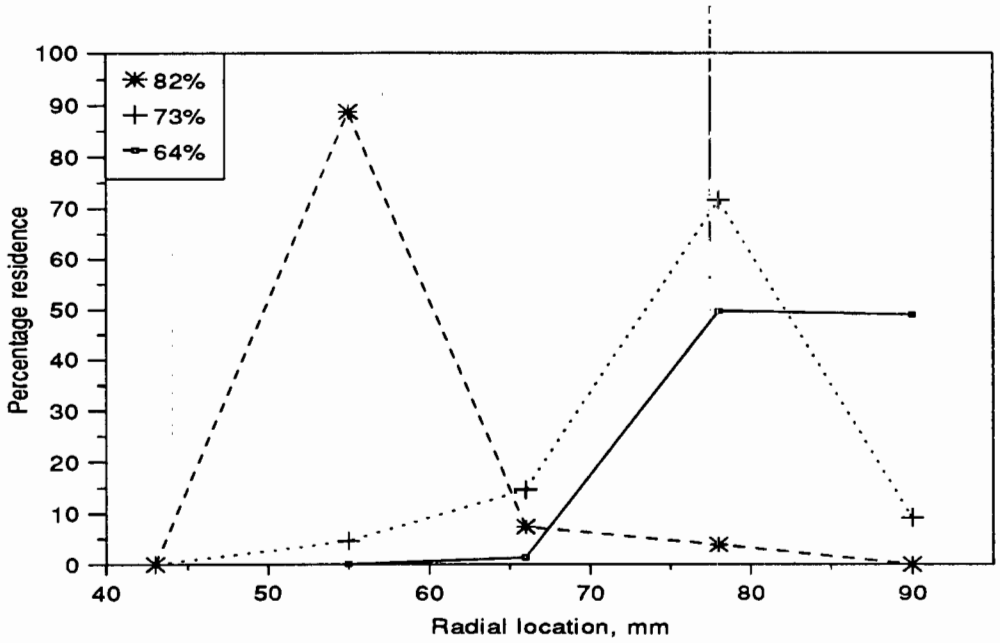

Figure 67. Radial distribution of the large ball, 3.12 mm lifters

emphasise the distributions. It is immediately apparent that the radial distribution of the large ball is well defined for a given set of conditions, as shown by the percentage distribution peaks mostly ranging from 70% upwards. For all the lifter heights the ball is at the centre when the mill is running at 82% of critical speed, and near the outside for the lower speeds. The 6 mm ball, in Figure 68, shows quite a different distribution; the ball had a far more even radial distribution, spending 50% of the time in the middle regions of the charge, and showing a bias towards the centre of the charge. This is fully in accordance with the other observations, for at that speed of 74% of critical the large balls are concentrated at the outside of the mill, as shown in Figure 70. It would therefore be expected that the small balls would be near the centre of the mill, and the medium-sized balls in the middle regions of the charge. The bulk ball charge consisted of 4, 6, and 8 mm balls, so the size of this tracked ball coincides with the mid-sized balls. As each of the size intervals of balls makes up a third of the ball charge, it is expected that they will have a range of radial distributions.

Figure 69 to Figure 71 show the dependence of the radial distribution on the height of the lifters, for each mill speed. The distribution is undoubtedly independent of the height of the lifters, as shown by the correspondence of the distribution peaks for each

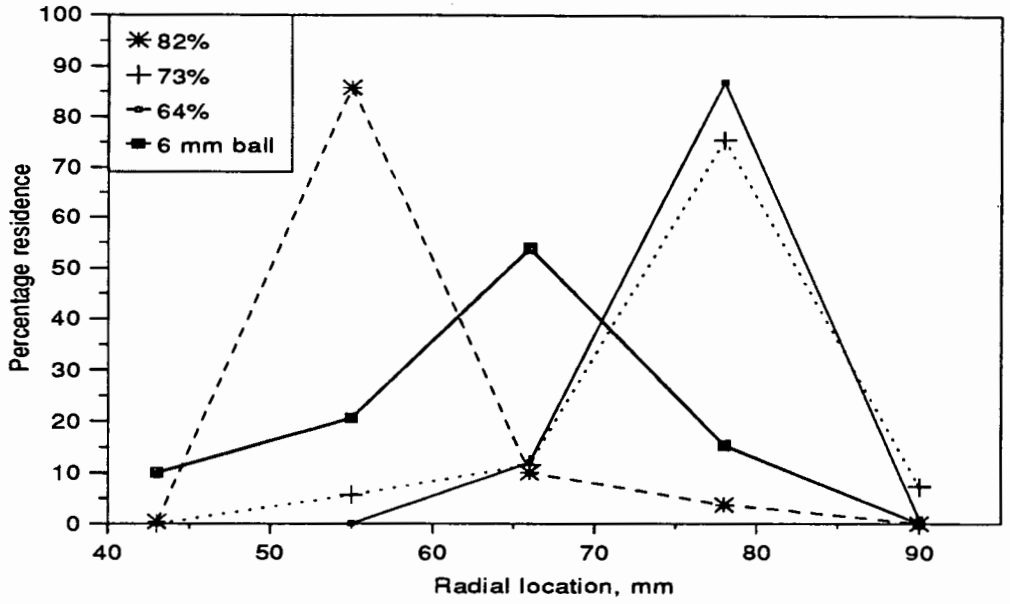

Figure 68. Radial distribution of the large ball, 6 mm lifters

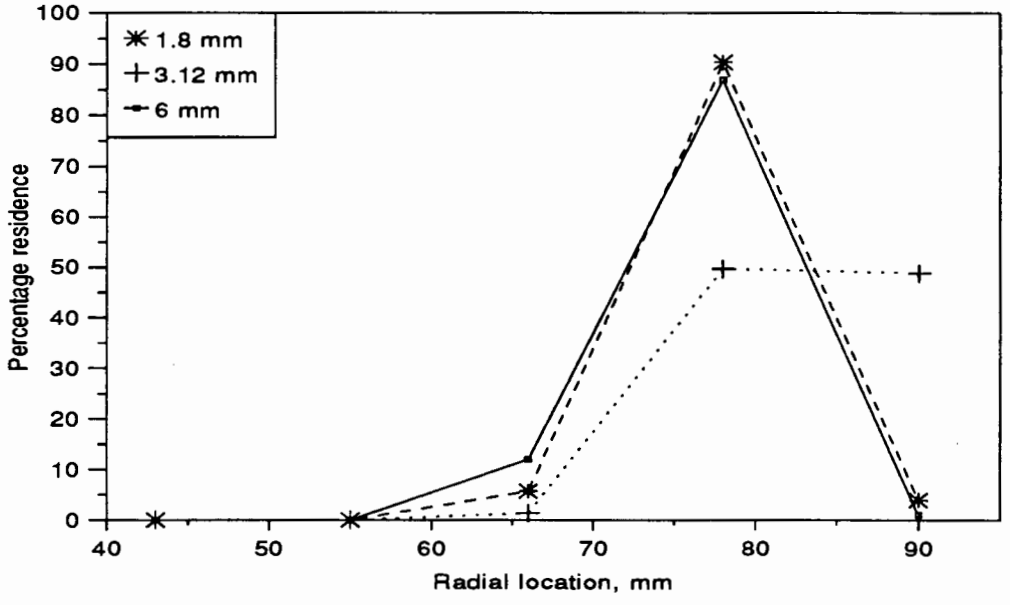

Figure 69. Radial distribution of the large ball, 64% crit. speed

height of lifter. The only discrepancy is for the 3.12 mm lifter at 64% of the critical speed, which shows an equal distribution of the ball between the outer two layers. Upon inspecting the original plots of the data, the ball was observed to lie on the border between the two radial zones. It would therefore be more accurate to describe the ball's location as being at 84 mm. For the other two lifter heights the ball was

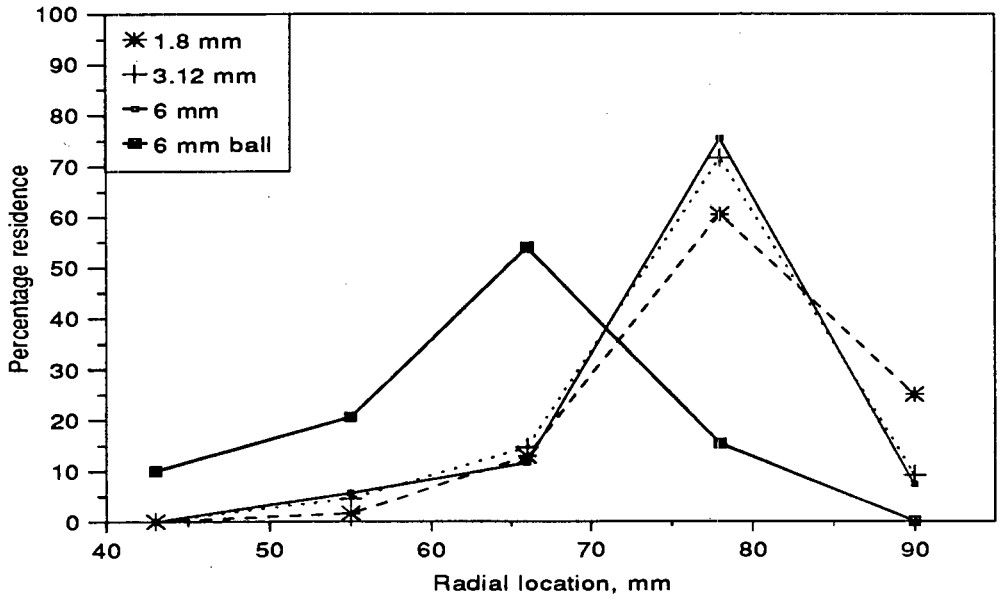

Figure 70. Radial distribution of the large ball, 73% crit. speed

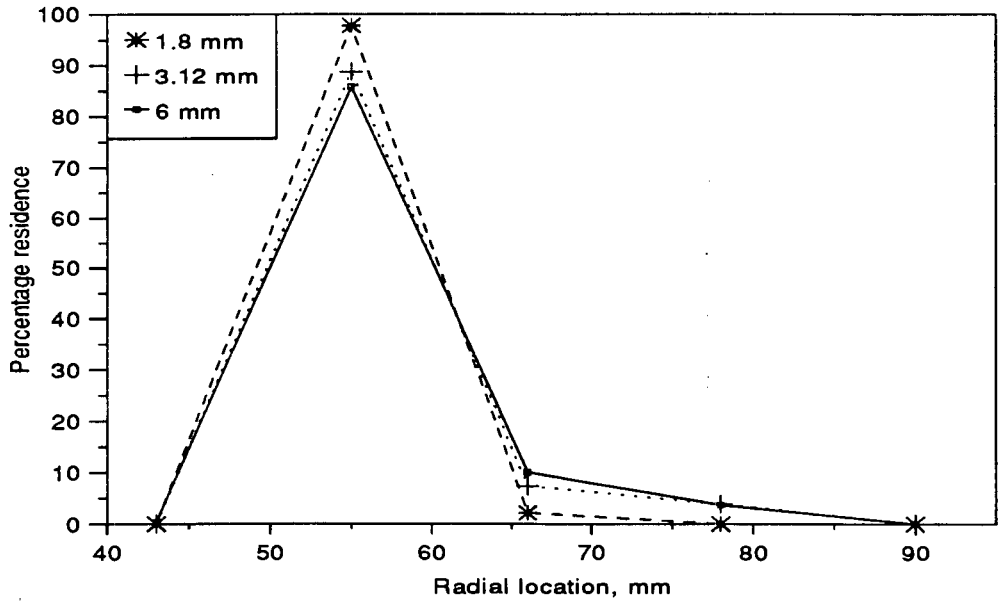

Figure 71. Radial distribution of the large ball, 82% crit. speed

located near the outside of the 72 to 84 mm zone. The actual difference in radial locations is thus small, as would have been shown if it had been possible to use

smaller radial intervals[a]. The distributions for 73% of critical speed are not quite as decisive as for the other speeds, with the peak value lying at about 70%, as compared to 90% for the other speeds. This indicates that 73% is nearing the speed at which the transition from outer to inner segregation of the large balls take place.

Table VIII Average radial distributions of the large ball, for each speed

	Radial location, mm				
	90	78	66	55	43
Speed	Average percentage residence				
64%	18.0	75.7	6.4	0.0	0.0
73%	13.8	69.2	13.1	4.0	0.0
82%	0.0	2.5	6.5	90.8	0.1
2 x Standard error					
64%	25.2	21.2	5.0	0.0	0.0
73%	9.1	7.3	1.4	2.0	0.0
82%	0.0	2.1	3.7	5.9	0.2

The consistency of the data for each height of lifter bar allows a summary of the distributions to be presented, by averaging the data over all lifter heights. Table VIII shows the average distributions, and the associated standard errors. The standard errors are low, except for the mill running at 64% critical speed. These correspond with the 3.12 mm lifter, the case of which has already been discussed. Figure 72 illustrates the average radial distributions. It can be conclusively stated that at 82% of the critical speed the large ball resides near the centre of the charge, and at speeds below 73% of critical the large ball resides near the periphery of the charge. Between these two ranges there must be a 'neutral' speed at which there is no radial segregation of the ball. This transition is beginning to take place at 73% critical speed, and is fully

[a]. As is discussed in the results section, the width of the observed image was used as the width of the radial zones.

accomplished by 82% critical, so the 'neutral' speed is likely to be around 77% of the critical speed.

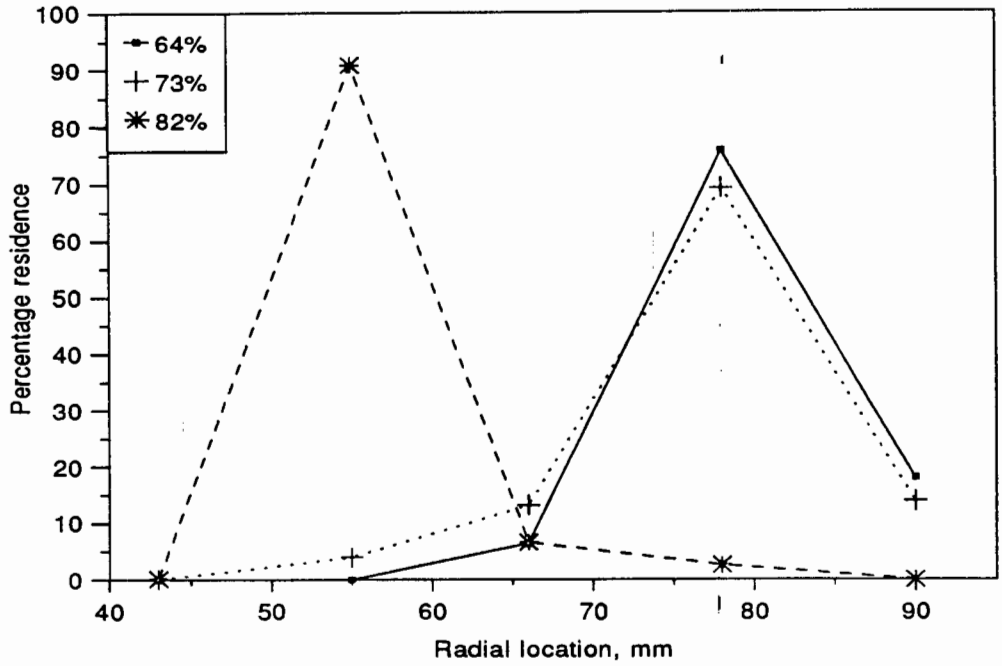

Figure 72. Average radial distribution of the large ball

8.12.2 Position of the charge

The position of the charge is defined by the position of the CoC, as discussed in more detail under the section on the extension of the theory. The displacement of the CoC from the centre of the mill is shown in Figure 73. There is very little variation in the radial position with either lifter height or mill speed. There does seem to be a slight increase in the radius of the CoC at 82% of critical speed. However the experimental error range is ±2 mm, so no firm conclusions can be draw from this trend. Within the experimental speed range of 64% to 82% of critical, the mill speed and the lifter height do not have a measurable influence on the radial position of the CoC.

The angle of repose of the charge is defined as the angle subtended at the centre of the mill by the CoC and base of the mill. The dependence of the angle of repose on the mill speed and the lifter height is shown in Figure 74. At each speed there is a degree of scatter which does not seem to be a consistent function of the height of the lifters. The experimental error in the measurement of the angle was about ±3°. This

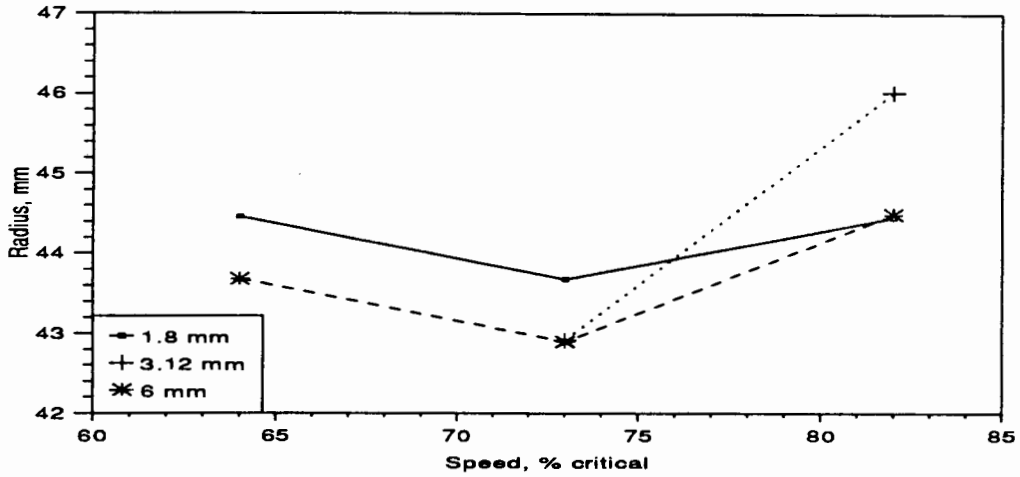

Figure 73. Radius of location of the centre of circulation

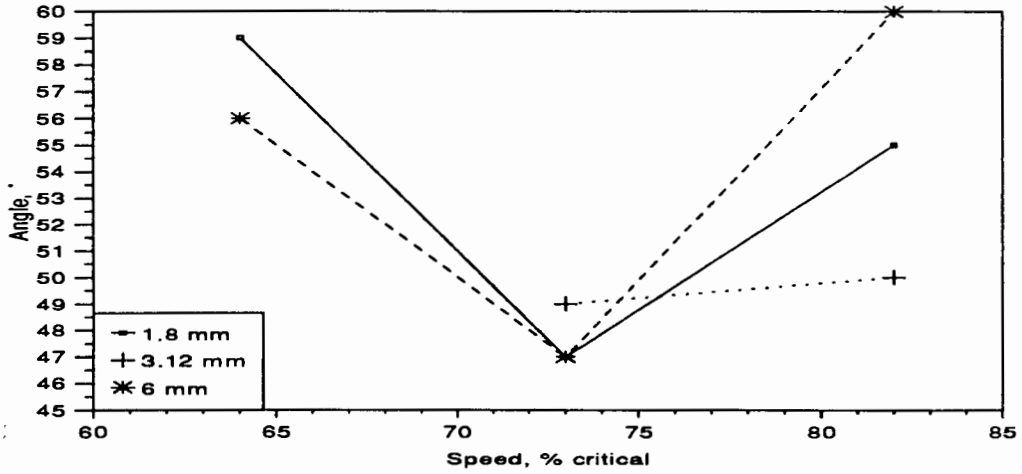

Figure 74. Angle of the centre of circulation

was partially due to the thickness of the ball path, which made it difficult to determine the exact CoC. The other contributory factor was that the location of the CoC seemed to fluctuate over a range of a few degrees. Taking the uncertainty in the measurement into account, there does appear to be a relationship between the mill speed and the angle of repose. The angle drops as the speed is increased from 64% to 73% of the critical, and then rises again as the speed is further increased. This is a surprising observation, as it would be expected that if there is any trend, the CoC would move upwards with increasing mill speed. Because of the uncertainty in the measurements, no firm conclusions can be drawn from these results.

CHAPTER 9
EXPERIMENTAL - MILLING TRIALS

The objective of part of the present work was to develop a technique which could be economically used to assess the influence of liner design on the metallurgical performance of a mill. This could then be used to investigate whether the liner profile affects the efficiency of the mill, in terms of production of fines and throughput of ore. An attempt was made to correlate the results with the findings of the work on charge motion. That is, knowing how a change in lining affects the milling action, what influence does this have on the actual grinding.

9.1 ASSESSING POTENTIAL TECHNIQUES

The ideal would have been to carry out trials on full-scale production mills, to produce directly applicable results. However, there are numerous drawbacks to working in a production environment, such as:

- Production comes first (quite understandably), so any experimental work loses out if a choice has to be made. This means that months of painstaking work can be lost when conditions are suddenly changed, liners removed, or such like.
- There are large fluctuations around the milling circuit, with numerous variables coming into play. These include changes in ore composition; wearing of spigots in hydrocyclones; wear of flow splitters; change of ball addition to satisfy tonnage requirements; liner renewal; to mention some of the major factors.
- Inaccuracies in the measurement of flow rates; feed masses (on weighbelts); percentage of fines in the flows (from grab samples); and even final product size. This is exacerbated by the drift of set points of the measuring apparatus, which requires regular checking.
- The difficulty of maintaining an accurate log of the relevant data, for which one has to rely on the plant personnel.
- The duration of each test condition can be anything from a year upwards, and a number of different liners would have to be tested. Aside from the slow accumulation of results, there can be long-term changes in the operating conditions on the mine,

such as changes in the ore-body, increased tonnages being treated, and different plant operation strategies.

• The cost of the work can be very high, as the mine would have to purchase a full new lining for each test condition, and often invest in extra monitoring equipment.

• In practical test work an attempt is made to monitor the effect of what could be a relatively small variation (say 5%) superimposed upon all these fluctuations and uncertainties. At the end of the experimental programme the results can be inconclusive, after a lot of time and effort has been directed into the work.

The problems listed above had been encountered in other testwork carried out on the mines[31,32,33,34], so it was considered advisable to look to pilot plant work.

An option that was considered was to use a large pilot plant for full circuit testing. This would involve installing a number of different liners, and optimising the mill throughput for each. Unfortunately, the available circuit had a fixed-speed mill whose rpm was too slow to simulate the conditions found on the South African RoM mills, and it is essential that the liner design is selected to suit the mill speed.

It has been established over the years that to simulate the conditions found in autogenous mills one needs to use a pilot mill with a minimum diameter of about 1.8 m [35]. Thus for the objectives of the work to be met a small pilot plant mill could not be used.

Fortunately a large batch mill had been built for wear testing work[36]. When this was designed it was hoped that liner test work could also be carried out on it, so the construction allowed for variable liners. It was consequently decided to make use of this mill for the testwork, and assess the rate of production of fines for a range of liners.

9.2 EXPERIMENTAL DESIGN

The angles of the lifter bars were decided upon after carrying out calculations of the projected impact point of the outer rocks, using the computer program developed

previously[1]. They were designed to drop the balls within the angular range of 60° to 70° , as measured from the bottom of the mill. The 90° lifter was tried out to see how a badly designed lifter would affect the milling efficiency. It has been determined[1,2] that the height of the lifter bar, once higher than the radius of the ball or rock, has little effect upon the impact point of the charge on the toe or mill shell. However, in work carried out by Meaders and MacPherson[8], they had found that the spacing-to-height ratio of the lifters is important. They recommended a ratio in the range of 4 to 4.5 for a mill running at 77% of critical speed. They also found that the ratio of mill diameter to lifter height was important, and that it varied according to the speed of the mill. The Skega mill lining company also recommends that the height and spacing of the lifter bars be varied with the speed of the mill. Their simple formula[37] is based on a large body of practical data. Bearing these recommendations in mind, two different heights of lifter bars were used, to assess the influence of spacing-to-height ratio of the lifters on the grind.

Figure 75. A typical grid lining in a gold mine mill

It was desired to simulate the structure of the grid linings found on about half the gold mine mills in South Africa[38]. The grid liners pack with balls or rocks and present a

rough, corrugated surface to the charge (Figure 75). However, to try and maintain a similar internal mill diameter throughout the tests with different liners, a low-profile lining was required. This was solved by selecting a thick woven mesh. In the South African minerals processing industry the majority of the grid linings do not have lifter bars mounted on them, and have either a flat profile or low wave pattern[38], so it was of interest to investigate the performance of a flat-profiled grid of this nature relative to a smooth lining or a liner equipped with lifter bars.

Two mill speeds were chosen; 80% and 90% of critical. This coincides with the speed range that RoM mills are commonly operated at on South African mines[38]. Five liner configurations were tested for each speed. The complete set of liner configurations are given in Table IX. The majority of the tests were repeated three times, so as to check for reproducibility, and to obtain statistically significant data.

Table IX Full set of conditions for the milling trials

Test	Run no's	Speed, % crit	Liner height,mm	angle, °
1	1, 2, 3	90	smooth	
2	4, 5, 6	80	smooth	
3	7, 8, 9	80	70	70
4	10, 11, 12	90	70	50
5	13, 14	90	70	90
6	15, 16, 17	90	grids	
7	18, 19	80	grids	
8	20, 21, 22	90	40	50
9	23, 24, 25	80	40	70

The aim of the batch tests was to assess the rate at which the final product was produced. On the gold mines the desired fineness of grind is 80% of material smaller than 75µm in the final product. So the desired fines for this test were defined as

-75μm material. To be able to determine the rate of production of fines the total mass of fines in the mill had to be measured at a number of time intervals. The most obvious technique, and often used on small experimental mill tests, is to dump the entire charge of the mill, and size the lot. But for a 1 100 kg charge of rock and slurry to be sized 9 times for each test would be totally impractical.

Only the quantity of fines in the mill is of interest, so only the fines fraction needs to be obtained for a measurement to be made. All the fine material passes into the slurry, so it was realised that if one knew what the total volume of the slurry in the mill was, at a given time, and could measure the mass of fines in it, then the total mass of fines would be known. The mass of fines in the slurry could be assessed by taking a representative sample of the slurry, and measuring the percentage of fines in the sample. It was further realised that knowing what was originally in the mill, then by measuring the density of the slurry the total mass of material in the slurry could be calculated. So it is possible to assess the total mass of fines in the mill from a sample of the slurry. The mathematical derivation of this is given below.

In a standard procedure the following sequence is followed:

the slurry sample is weighed,

the solids are filtered out,

the solids are oven dried to remove all moisture,

they are then weighed,

finally, the dried sample is dry screened to obtain a size distribution.

From this the following information is available:

m_{sample}	mass of sample
m_{sands}	mass of sands in the sample
γ	fraction of fines in the sands

The sands are any particles fine enough to pass out in suspension through a sampling valve (see below).

The mass of fines in the sample is $m_{fines} = \gamma . m_{sands}$

The ratio of fines to water is $\frac{m_{fines}}{v_{water}}$ where $v_{water} \equiv m_{water} = m_{sample} - m_{sands}$

Where the relationship of 1 mℓ ≡ 1 g is used for water.

So for the total volume of water in the mill being V_{water} the total mass of fines in the mill is given by

$$M_{fines} = \frac{\gamma . m_{sands}}{(m_{sample} - m_{sands})} . V_{water} \qquad (15)$$

The density of the slurry is not required for this calculation. If the volume and mass of the sample are determined, then the density is available, and from that the total mass of sands in the mill can be calculated. This measurement technique is not as accurate as weighing the dried sands, but it serves as a useful check.

The volume of slurry can be divided into the volumetric fractions of sands and water

$$V_{slurry} = V_{sands} + V_{water}$$

now: $V_{sands} = \frac{m_{sands}}{2,7}$ (g) / (g/mℓ)

Again using the relationship that mass and volume of water are numerically equivalent if expressed in g and mℓ. Once the mass of sands in the slurry are calculated then eqn. (15) can be used. The units are correct in the derived equation, as there is a hidden density of 1 g/mℓ.

$$\rho = \frac{m_{slurry}}{V_{slurry}} = \frac{m_{slurry}}{\left(\frac{m_{sands}}{2,7} + m_{water}\right)}$$

substituting $m_{water} = m_{slurry} - m_{sands}$ (16)

$$\rho = \frac{m_{slurry}}{m_{slurry} - \frac{1,7}{2,7} m_{sands}}$$

$$m_{sands} = \frac{2,7}{1,7} m_{slurry}\left(1 - \frac{1}{\rho}\right)$$

With this technique of calculating the total mass of fines in the mill, an accurate

sampling technique had to be sought. The major problem with sampling a slurry is that the material begins to settle out very rapidly once it is no longer agitated. The particles settle at different rates which are dependent upon the sizes of the particles. Thus if the mill was stopped and then a sample extracted by whatever means, it undoubtedly would not be representative of the slurry in the mill.

A dynamic sampling technique was developed to overcome the problem of retaining the slurry in an agitated state. A valve was fitted to the door of the mill, against the periphery of the mill. The concept was that the valve could be partially opened and a sample collected from it, while the mill rotated. A plastic bag was tied to the valve, and the mill run. The mill was then stopped, the valve quickly opened, and the mill turned at full speed for a few more revolutions. The bag was then removed and the process repeated. Table X shows the total mass and volume of the sample, and the derived

Table X Results of reproducibility trials carried out on the sampling technique

Time hrs.	Mass g	Volume mℓ	Density g/mℓ	Mass solids, g	Fraction solids	% variation
834.68	1284.9	945	1.360		0.4220	±0.43
834.69	1264.3	930	1.360		0.4218	
834.70	1093.2	803	1.361		0.4236	
835.68	1496.9			738.7	0.4935	±0.07
835.69	1275.9			628.8	0.4928	
934.16	592.3	382	1.551	334.2	0.5642	±0.89
934.18	1082.5	705	1.536	600.0	0.5542	

The time given is that shown by the mill clock, in decimal hours.

fraction of solids. For the run at 835 hours, the dried mass of the sample was used to calculate the density, and this yielded the best set of results. Excellent reproducibility of both the slurry density and percentage fines in the sample were obtained. The percentage variation in the calculated fraction of solids in samples taken over a short time period, ranged from 0.07 to 0.89%.

It was reasoned that in a dynamic, agitated system of this nature, if a reproducible sample is obtained then it is very unlikely to be subject to a systematic bias. So this sampling technique was adopted for the experimental work.

9.3 APPARATUS

(a)

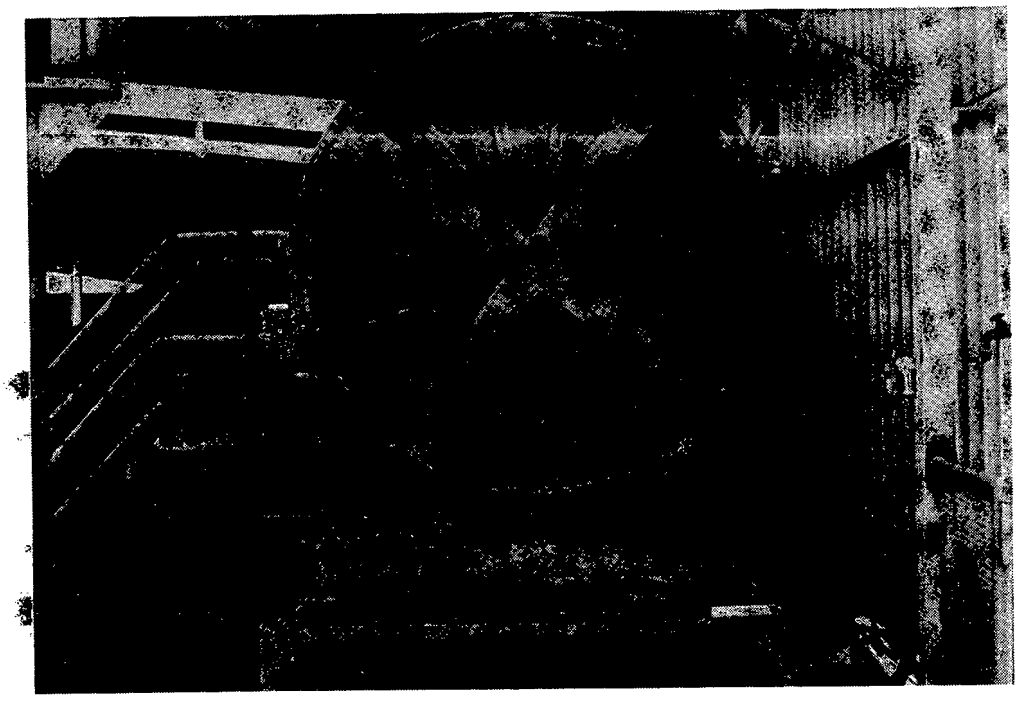

(b)

Figure 76. The 1.8 m batch mill used for the milling trials

9.3.1 The mill

A batch mill with an internal diameter of 1.8 m, and a length 0.5 m was used, as illustrated in Figure 76. It is mounted on a central shaft, and the full front door of the mill is removable, as can be seen in Figure 76(a). It is driven by a fixed speed asynchronous motor, through a continuously variable speed gearbox, and finally by a chain drive to the mounting shaft. The mill has fifteen sets of liner-mounting bolt holes. The inner sides of the end faces of the mill were designed to be smooth, so as to exert the minimum effect on the charge motion. If any form of end-liners were installed then the lifting effect that the ends of the mill imparted to the charge could overshadow the influence of the shell lining on the charge motion. As the influence of lifters in long mills was the especial interest of the work, it was important to minimise the influence of the end faces.

The mill power is monitored via a set of torque transducers mounted on the drive shaft. These consist of strain gauges that measure the twist in the shaft as it drives the mill. This is accepted to be one of the most accurate of the standard torque measuring techniques, as it is direct, and no drive-train or power losses have to be accounted for. The signals are transferred to the pick-up point via sliprings mounted on the shaft. The data is filtered to cut out noise from the signal and then recorded directly on a computer logging system. The power supply to the mill is linked to a clock, that records the total actual running time of the mill, to 0.01 hr, ie 36 s intervals. These time intervals are smaller than the time between measurable differences in mill product, so this is sufficiently accurate for this work.

The mill door has a rubber gasket that seals against the flange of the mill, and the door has bolts around its full circumference so that it can be firmly bolted on, and thus prevent any leaking. The door has a recessed cross in it for the support spider of the mill to slot into, so as to present a smooth face to the charge. There is a hatch in the door through which the ore can be loaded. There is a 60 mm gate valve mounted in line with the inner edge of the mill, for adding water, taking samples, and draining the slurry.

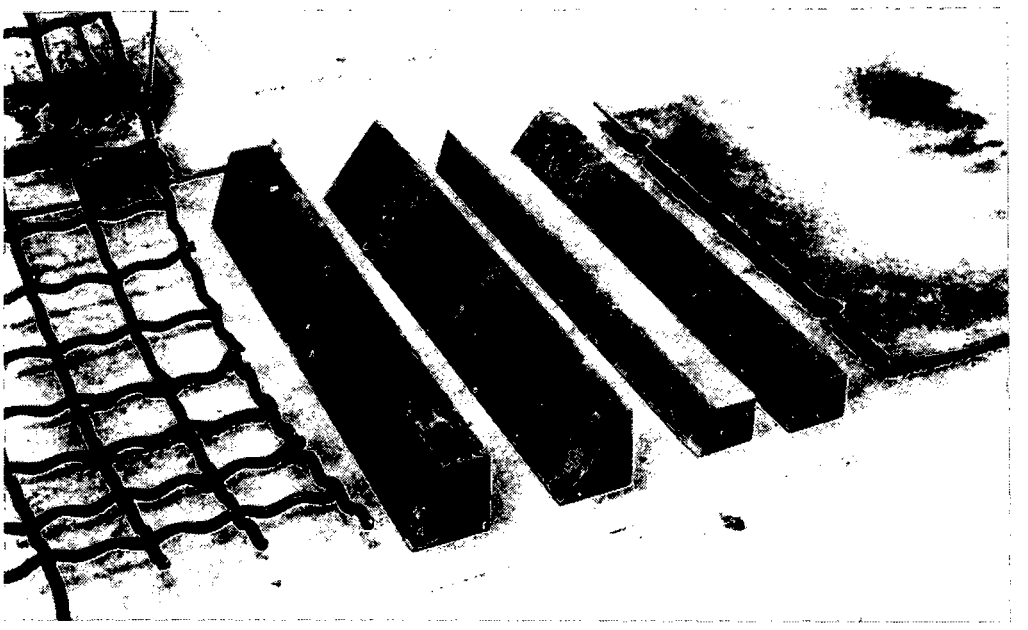

Figure 77. The liners used in the practical trials

9.3.2 Test liners

A range of liners was constructed to vary the liner profile from smooth through to high lifter bars (Figure 77). The liners were constructed of mild steel as they only had to last for a short set of tests.

Smooth lining Flat 5 mm plates were fastened into the mill with round-headed carriage bolts.

Grid lining A steel mesh with a 65 mm spacing and 10 mm mesh, and maximum thickness of 20 mm was tack welded into the mill.

Lifter bars These were bolted directly onto the shell from the outside of the mill. All fifteen sets of mounting holes were used for lifters, as this is similar to the bolt spacing found on the South African mills.

The grid, and the 40 mm, 50° lifter are shown installed in the mill in Figure 78.

9.4 PROCEDURE AND PRECAUTIONS

The success of the experiment was dependent upon careful loading of the mill, and consistent sampling of the mill product. It was established from initial test work that the required degree of accuracy and reproducibility could be achieved. The following procedure was established and stuck to rigorously, so as to maintain consistency

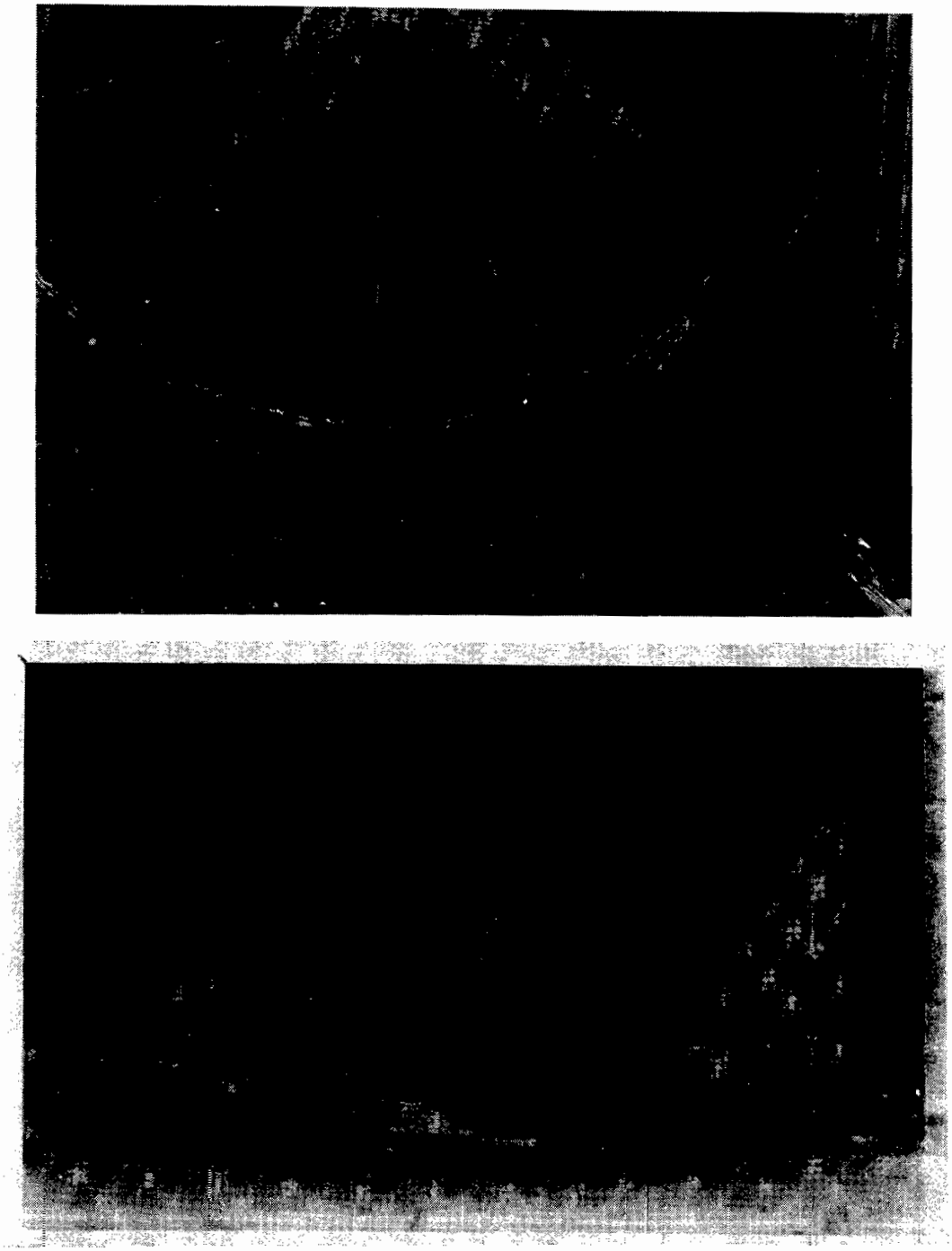

Figure 78. The grid and a lifter bar installed in the mill

between experiments.

9.4.1 Ore sorting

It was essential the ore used throughout the tests had a consistent mineralogy, and therefore constant grinding characteristics. This was achieved by collecting several truckloads of ore from a single waste dump (Libanon gold mine, Harvey Watt shaft)

Table XI Size distribution of the ore received

Size interval mm	No. drums	Total mass kg
+12 -25	50	15 000
+25 -50	22	6 871
+50 -75	11	3 367
+75 -150	31	8 750

over a short period, of a few days. The ore was dried and sorted through a rotary trommel (screen) into 5 size fractions (one of which was the fine material, that was discarded). The largest rocks were sorted into 5 mass intervals, to be added as topsize rocks. The mass of rocks in each size interval were weighed (Table XI), and from this the final ratio in which they should be blended was calculated.

For the first set of tests the mass of rocks were selected to provide a 45% filling of the mill. This was 800 kg, which was divided up as shown in Table XII, with the total mass reflecting the mass required for 28 runs. For each run the same blended mixture was

Table XII Size distribution of ore used for each run

Size, mm	Mass, kg	Total mass, kg
+12 -25	147.0	4 116
+25 -50	236.0	6 680
+50 -75	112.0	3 136
+75 -150	280.0	7 840
2 Large rocks	25.0	700
TOTALS	800.0	22 400

used, using a scale accurate to 0.2 kg to weigh out the size fractions. The two large rocks consisted of a 10 kg and a 15 kg rock, it was attempted to maintain this split by careful selection of the rocks.

9.4.2 Liner installation

For each of the liner configurations used it was imperative that the mill shell be watertight. Some silicone sealant was squeezed into the bolt holes, and then carriage bolts were used to seal the holes for the smooth liner. These were also used to block the holes beneath the grid (mesh) liner. Gaps between the smooth liner plates and the mill shell were also sealed with silicone sealant to prevent the ingress of the fines, and subsequent loss from the samples. When the lifter bars were installed, the base of the lifter was packed with silicone sealant to prevent slurry accumulating beneath the lifters, and leaking from the bolt holes.

9.4.3 Mill loading

Any remaining fine material was washed out of the interior of the mill prior to loading. The 800 kg of ore was tipped in through the chute (Figure 79), that was mounted on

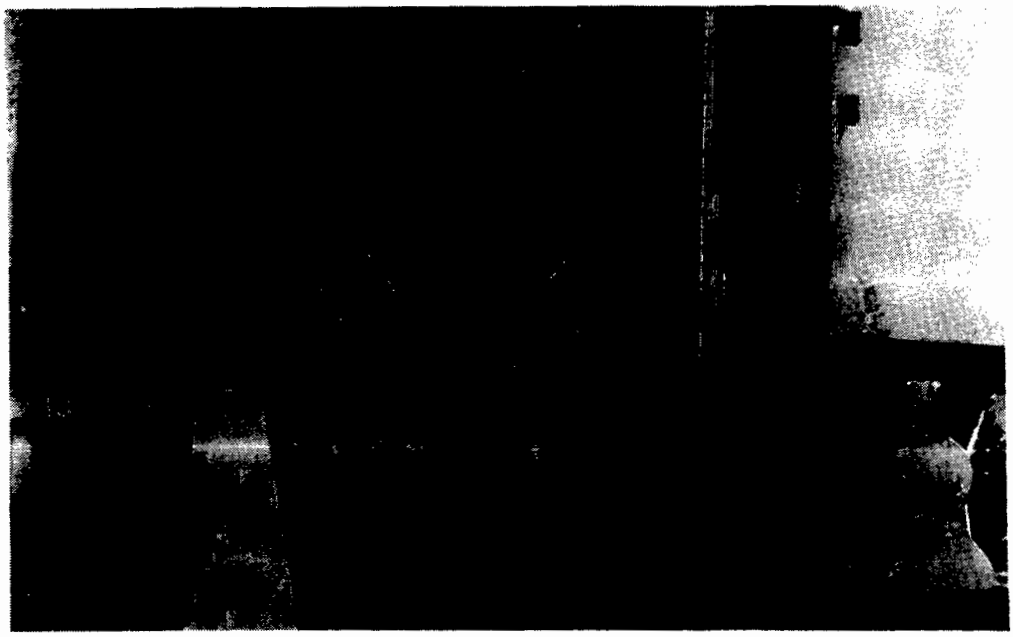

Figure 79. The mill being loaded with ore

the hatch, ensuring that none was spilled. The quantity of water added was 300 ℓ, this was sufficient to fill the rock voidage, and allowed a maximum possible density of 72% solids by mass, when all the rock was ground to a slurry. The quantity of water added had to be accurately measured as calculation of the percentage of fines in the mill from a sample was dependent on the amount of water in the charge. The water measurement was carried out by weighing the water and decanting directly from the container. A hanging drum with an inlet port and outlet tap was constructed for this (Figure 80). The drum was suspended from the hanging scale, filled with water and then drained into the mill, via an attached hose. The mass of water added to the mill could then be directly calculated from the difference between the initial and final mass of the drum. It was ensured that the feeder hose was drained, and free of the mill when the mass was recorded. The mill was then checked for watertightness as leaks obviously affected the quantity of slurry in the mill.

9.4.4 Mill operation

The mill speed was set prior to loading the mill and then checked for every run once the mill was fully loaded, at the start of the run. Any minor adjustment that may have been necessary was made during the first few minutes of the run. The easiest check was to time the mill over 30 revolutions, and repeat the measurement at least once. The mill was run at two speeds for each liner configuration, 80% and 90% of critical speed.

Figure 80. Weighing the water as it was added to the mill

These were set according to the following:

80% crit.	≡	25,6 rpm	≡	70,4 s for 30 revs.
90% crit.	≡	28,8 rpm	≡	62,5 s for 30 revs.

The start time of each run, the time as each sample was taken, and the finish of a run were recorded from the mill clock. The duration of each run was 4 hours, actual running time. Readings of the torque of the mill on the digital display were recorded at half hourly intervals, as a back-up to the automatically logged data. The readings on the digital display naturally fluctuated, so the maximum and minimum readings observed over a few seconds were recorded.

At the end of each run the mill was drained and washed out, and all +12 mm rock (later +5 mm) was washed off, dried, and weighed. It was then labelled according to the run number and stored, for a measurement of the size distribution to be carried out afterwards.

9.4.5 Sampling

The accuracy of the sampling was pivotal to this work, and also the most prone to error, so extreme care was taken with all sampling. Samples of the slurry were taken at half hourly intervals, the first commencing one minute after the mill had been started. So 9 samples were taken for each run. The sample was collected in a tough plastic bag, with a wall thickness of about 200µm. The bag was firmly tied around the neck of the discharge valve on the door of the mill. This was done in advance, so as to reduce the mill stoppage time prior to taking a sample.

Some skill was required in stopping the mill at the right point, so that the valve was above the slurry level and still accessible to being opened. This was practised in advance by the person carrying out this operation. The 60 mm valve was opened by ¾ of a turn, as indicated by a marker on the handle. This procedure was carried out as quickly as possible, so as to limit the solids settling out of the slurry. The mill was then turned for 3 full revolutions, during which period the sampling bag filled with slurry (Figure 81), and stopped with the valve above the slurry level. The bag was untied

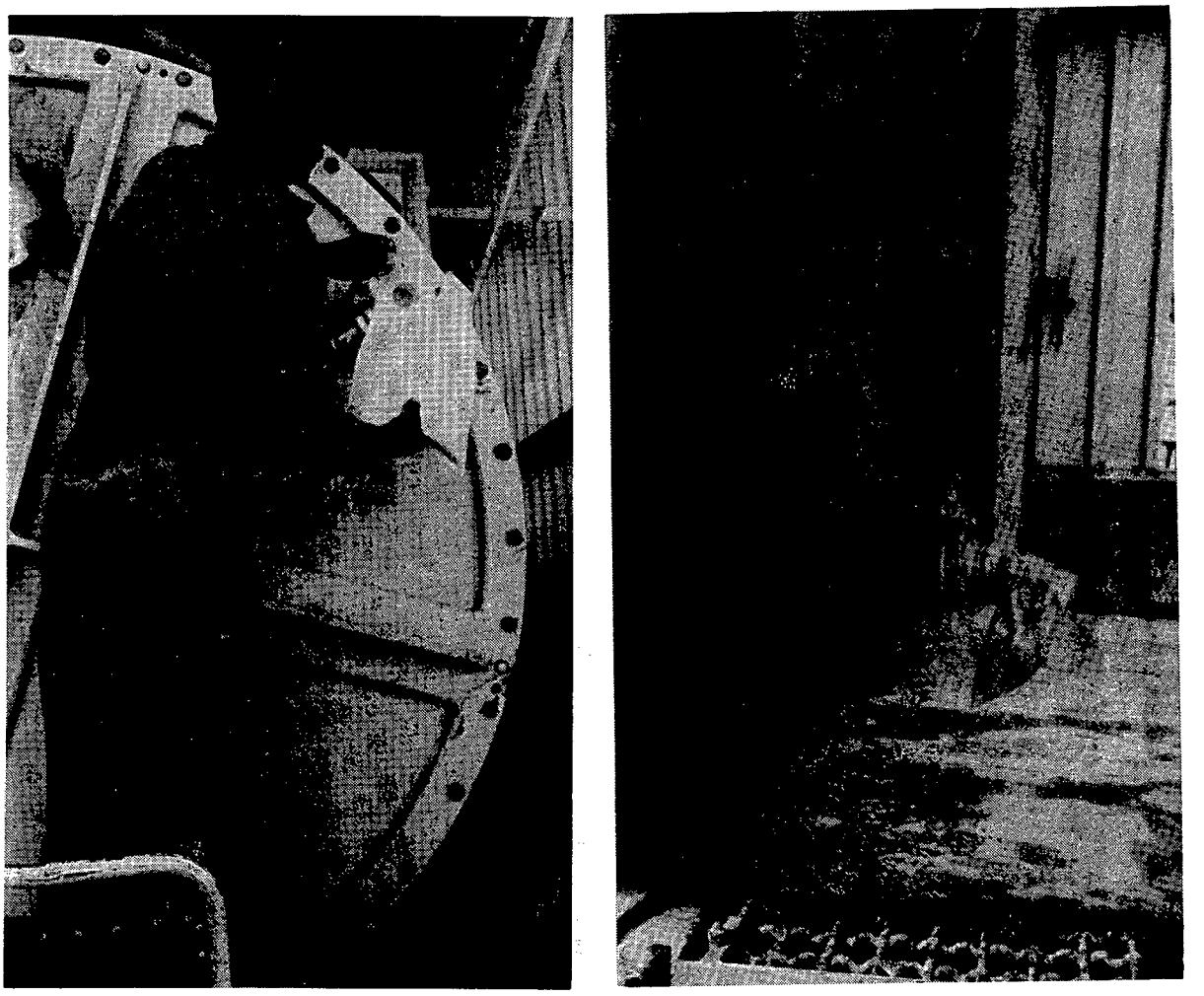

Figure 81. Sampling the slurry

from the valve, and the slurry that had settled in the neck was scraped out by finger. This was carried out in a standard manner, so as to obtain consistency of sampling. The valve was then washed out, by spraying it with a wash bottle and wiping with a cloth. The valve was then closed and a fresh bag tied on, ready for the next sample. If there was any doubt about the quality of a sample then the mill was run for at least another half minute prior to taking the next sample, so as to ensure that the charge was fully mixed. The milling time was recorded at each sample. The filling and removal of the sample bag is illustrated in Figure 81.

The sample was decanted into a 1ℓ measuring cylinder, for volume measurement. The cylinder was initially weighed. During the tests the scale was tared with it on, to simplify weighing of the sample. The sample was thoroughly shaken, so as to remix the slurry, and poured into the measuring cylinder. To prevent spillage the neck of the

bag was inserted into the cylinder quickly so that the slurry remained well mixed. It had to be ensured that the entire contents of the bag was emptied into the cylinder. In general the slurry 'beaded' into droplets and flowed out smoothly, providing a new bag was used, but when there was a high percentage of fines in the slurry it then tended to stick to the bags and it was difficult to totally empty the bag. The volume of slurry was measured and the cylinder weighed. This yielded the percentage solids in the slurry. It was then decanted into a clean plastic bag, any slurry sticking in the cylinder was washed into the bag using a wash bottle. The bag was labelled according to run and sample number and sealed with a strip-element heat sealer, so as to prevent any spillage.

Because of the problems experienced with transferring the sample to the measuring cylinder, this step was abandoned for the last five runs. This measurement acted as a check on the slurry density calculated from the mass of dried solids in the sample. As no problems had been encountered it was deemed to be unnecessary to continue with the checking procedure. Instead the sample bag was weighed prior to being fastened on the valve, and then sealed as soon as it was removed from the mill. The full bag was then weighed, and the mass of slurry calculated.

The sample was then taken for size analysis. It was filtered wet and oven dried to remove all moisture, and then the mass of solids was determined. The majority of the samples were then wet screened on a 75μm sieve, as only the percentage of minus 75μm material was required. It was then oven dried again, and dry screened at 75μm, using an automatic sieve shaker. From this the quantity of fines could be determined. A full standard size analysis was carried out on the 2 hour and the final sample from each run.

9.5 PROBLEMS

Problems were experienced with the data-logging computer, which eventually had to be repaired. This resulted in a loss of some torque data, some partially and some totally. Fortunately manual readings had been taken as a back-up.

During ore sizing with the rotary trommel screen the material that passed through the final screen size was collected in two drums placed alongside each other below the screen. The smaller rocks fall through the screen sooner than the larger rocks, so the first drum accumulated a slightly finer size distribution than the second drum, in the 50-75 mm size range. This difference in sizes was only detected in retrospect, so some of the runs were conducted with a larger size distribution, in that range, than the other runs. This was reflected in the results.

During the runs that had the highest rate of production of fines there was a low pressure in the mill for the first 2 hours. So as the valve was opened there was a strong suction through any gaps between the neck of the valve and the bag. The sample would be an almost dry slurry. It was obvious when this occurred, as signalled by loud hissing sounds and the sample being sucked back into the mill as it flowed out. To overcome this the mill was stopped a minute prior to the sample being taken and the valve opened to allow air to flow in. The mill was then restarted and the sample taken in the normal manner. This surprising effect could only be due to a reduction in volume of the contents of the mill, which more than overcame the expansion of the air from heating. It is possible that the very fine material is sufficiently small to move into the interstices between the water molecules without appreciably affecting the volume of the water[b]. Thus finely ground rock could disappear from the total rock volume. The reverse can also occur, with the water being absorbed into the micro-porosity of the rocks. These effects would both leave a smaller net charge volume.

The major down-fall of the experiment, as conducted, was only detected at the end of the trials. This was that the volume of slurry became far too large for the volume of rocks, as the test progressed. Allowance had not been made for the considerable reduction in the volume of rocks, as the total volume of the slurry increased during the test. This lead to an unrealistic volumetric filling of the mill with slurry, and inefficient

[b] This is a property of water, arising from its polar molecular structure resulting in 'gaps' between the molecules. An everyday example is immersing cotton wool into a full glass of water, without any of the water spilling.

milling (which becomes apparent in the results). Consequently a second set of tests were conducted, in which the volumetric filling and the slurry density were carefully controlled.

9.6 SECOND SET OF TESTS

The objective of these tests was to establish that the batch-milling technique could be used to provide a comparison of liner performance under realistic milling conditions.

For a given rock size-distribution in a mill, there is a definite voidage between the rocks. Ideally this voidage should be completely filled with slurry, yet not over-filled as this leads to padding of the grinding media and reduced milling efficiency. The ratio of slurry to total charge volume will be termed the fractional slurry filling.

The fractional slurry filling and the slurry density both vary with time in batch milling. There is a unique time-dependent relationship between the fractional slurry filling and the slurry density, for given initial quantities of rock and water. It is desirable to have both quantities at ideal values simultaneously. The required initial quantities, for given desired conditions, can be calculated as follows.

For: V_R = Initial volume of rock
V_w = Volume of water
V_f = Volume of fines in the slurry
ρ_R = Density of the ore
S = Desired slurry density
F = Fractional slurry filling just sufficient to fill the voids
P = Percentage filling of the mill with charge

$$S = \frac{M_f + M_w}{V_f + V_w} = \frac{V_f \cdot \rho_R + V_w}{V_f + V_w}$$

$$V_f + V_w = \frac{V_f \cdot \rho_R + V_w}{S} \qquad (17)$$

This can also be expressed as a function of the volume of fines:

$$V_f \cdot \left(1 - \frac{\rho_R}{S}\right) = \frac{V_w}{S} - V_w$$

$$\rightarrow \quad V_f = \frac{V_w - S.V_w}{S - \rho_R} \qquad (18)$$

Once the volume of the slurry completely fills the voidage, i.e. F is at the desired value, the following applies:

$$V_w + V_R = V_{charge} = V_{mill} \cdot P \qquad (19)$$

$$F = \frac{V_f + V_w}{V_w + V_R}$$

$$\rightarrow \quad V_f + V_w = F.(V_w + V_R) \qquad (20)$$

Substituting Eqns. (17) and (19) yields:

$$\frac{V_f \cdot \rho_R + V_w}{S} = F.V_{mill}.P$$

$$\rightarrow \quad V_f \cdot \rho_R + V_w = S.F.P.V_{mill} \qquad (21)$$

Substituting eqn (18) yields:

$$\left(\frac{V_w - S.V_w}{S - \rho_R}\right).\rho_R + V_w = S.F.P.V_{mill}$$

$$\rightarrow \quad \frac{V_w.\rho_R - S.V_w.\rho_R + S.V_w - \rho_R.V_w}{S - \rho_R} = S.F.P.V_{mill}$$

$$\Rightarrow \quad V_w.\left(\frac{-S.\rho_R + S}{S - \rho_R}\right) = S.F.P.V_{mill} \qquad (22)$$

$$\rightarrow \quad \frac{V_w.S.(1 - \rho_R)}{S - \rho_R} = S.F.P.V_{mill}$$

$$\rightarrow \quad V_w = \left(\frac{S - \rho_R}{1 - \rho_R}\right).F.P.V_{mill}$$

Substituting for the mass of rock in eqn (19) yields:

$$M_R = \rho_R.(P.V_{mill} - V_w) \qquad (23)$$

9.6.1 Selection of test criteria

Utilising the equations that had been developed the required mass of rock and volume of water could be calculated. The voidage in the rock charge was measured at 0.46, the density of the quartzite used was 2.72, and the slurry density was taken as that found on the RoM mills, at about 1.70. The volume of the mill is 1219 ℓ, and the percentage filling generally used to give optimum power draw on the RoM mills is around 43%, giving a charge volume of 521 ℓ. This yielded a water volume of 140 ℓ, and charge mass of 1010 kg, which was rounded out to 1 ton.

The rock was charged in the same ratios of sizes as previously, and the two large rocks were increased in mass to 13 and 19 kg. The same test procedure was used as previously, except that the run time was reduced to 90 minutes, as the required ideal conditions were reached within 60 minutes.

The set of tests at 90% of critical speed were repeated, except for the smooth lining, which had originally been included for the sake of interest. The grid at 80% critical speed was also tested for comparison with the higher speed. The tests were only

carried out once for each condition, as the reproducibility of the results had been adequately demonstrated in the first set of tests. The results of these tests are analyzed separately from the first tests.

CHAPTER 10
MILLING RESULTS

10.1 FIRST SET OF TESTS

The results obtained, are given in Table XXX of Appendix IV. A summary of the important data is given in Table XIII, Table XIV, and Table XV. A few of the unsatisfactory samples were discarded. The mass of fines is the mass of material smaller than 75µm, and is calculated from the fines fraction in the sample. The torque values are the averages of the readings taken from the digital display.

Figure 82. Pebbles discharged from the mill

A typical set of remaining pebbles is shown in Figure 82 as it discharged from the mill. The rocks were well-rounded, and there was very little rock in the size fraction between the slurry fraction and 10 mm stones. There was little evidence of freshly broken rock, implying that the majority of size reduction took place by surface abrasion. There was a wide range in the mass, and distribution of the remaining rocks, within each milling condition, as can be seen from Table XXXI in Appendix IV. The two large rocks from each run were easily located and were individually weighed, Table XXVIII.

Figure 83 shows the intrinsic scatter in the torque data. A major source of this scatter was the asymmetric weighting of the mill, arising from the heavy hatch on one side of the door. However, the readings are very evenly scattered about the average, giving a good measure of the average torque at any time. The data taken from the digital readings is also shown on the plot. This demonstrates the excellent correlation between the two sets of data. Most noticeable about the torque is that it drops off rapidly with milling time. This is a function of the mill being run in batch mode, and is related to the changing composition of the charge with time.

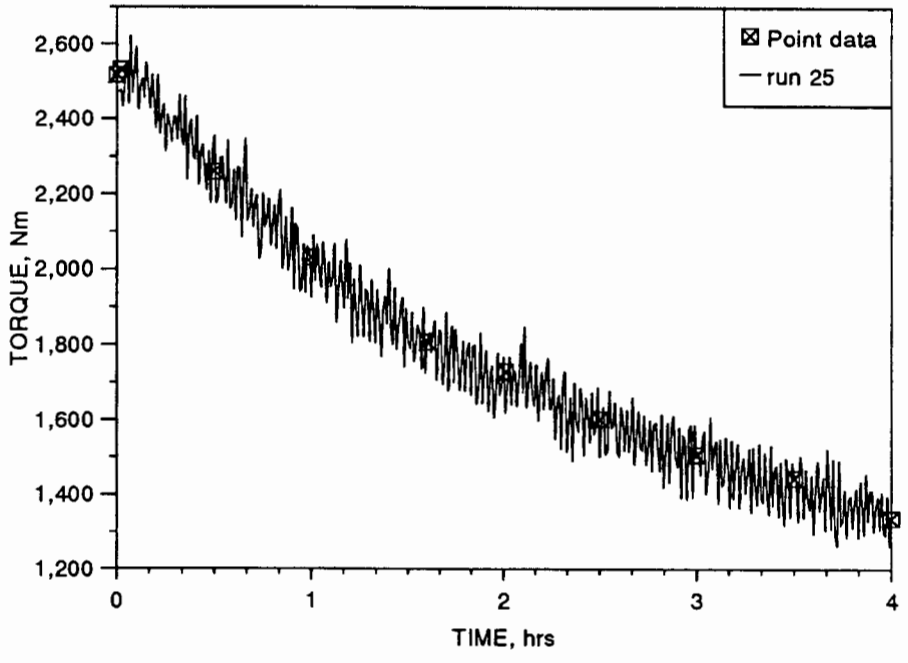

Figure 83. A full set of continuous and point torque data for the grids at 80% crit. speed

Table XIII Summary of data from the milling trials, runs 1 - 12

	Time	-75 µm	Mass fines	Torque		Time	% -75 µm	Mass fines	Torque
run 1	Test 1	Smooth, 90% crit. speed			run 7	Test 3	70mm, 70° Lifter, 80% crit.		
1	2.0	49.0	26.4	2443	1	1.5	46.7	7.2	2461
2	30.0	52.4	80.0	1947	2	37.2	56.7	65.6	2048
3	60.6	55.2	141.4	1440	3	60.0	58.3	98.8	1908
4	90.0	66.1	186.5	1177	4	92.1	65.5	135.2	1720
5	120.0	68.1	226.2	1010	5	122.7	64.8	174.6	1610
6	151.5	69.8	258.8	882	6	153.0	67.1	192.8	1547
7	181.8	70.8	286.9	798	7	182.4	67.9	232.0	1487
8	211.8	71.7	310.9	757	8	206.7	69.2	254.4	1439
9	240.3	71.0		707	9	239.1	71.3	241.6	
run 2					run 8				
0	0.0				0	0.0			2394
1	1.8	49.7	16.3	2454	1	1.8	44.4	8.7	
2	31.8	56.4	87.8	1990	2	30.6	51.7	52.9	2118
3	60.6	63.6	149.8		3	61.8	57.9	112.7	1868
4	90.6	69.9	216.8	1297	4	91.2	61.1	149.0	1723
5	120.3	70.5	242.9	1140	5	120.0	63.5	159.1	1621
6	150.3	73.7	275.1		6	150.3	65.5	198.8	1542
7	180.3	73.7	299.6	862	7	179.7	66.1		1456
8	210.6	75.0	312.1	759	8	213.5	67.3		1382
9	242.7	75.3	327.2		9	240.3	67.5	253.3	
	run 3			2541		run 9			
1	1.2	60.0	6.3	2510	1	2.4	31.1	8.6	2371
2	29.4	68.5	68.7	2218	2	28.2	40.5	54.3	2140
3	62.1	77.7	150.4	1797	3	58.2	46.5	101.9	1839
4	91.5	81.0	189.9	1497	4	88.2	50.2	132.8	1725
5	121.8	83.2	243.1	1334	5	120.6	54.2	168.2	1648
6	151.8	85.6	271.0	1145	6	148.8	57.7	201.2	1535
7	181.8	85.7			7	178.8	58.8	217.6	1458
8	212.4	87.6	330.9	834	8	208.2	60.1	248.4	1384
9	241.8	87.7	348.9		9	240.3	61.5	260.7	
run 4	Test 2	Smooth, 80% crit. speed			run 10	Test 4	70mm, 50deg Lifters, 90% crit.		
0	0.0				0	0.0			
1	2.4	52.2	11.7	2395	1	1.8	46.9	6.6	2209
2	30.0	61.9	58.7	2148	2	29.1	54.7	51.8	2116
3	60.0	73.2	134.1	1870	3	58.2	62.7	107.0	1939
4	89.7	80.5	176.4	1542	4	90.3	57.2	154.3	1785
5	119.7	84.0	217.0	1355	5	120.3	63.4	190.0	1692
6	152.4	87.5	248.9	1245	6	154.2	62.7	233.1	1596
7	187.2	88.9	277.8	1125	7	187.2	60.9	255.3	1501
8	211.2	89.4	297.7	1068	8	216.0	61.4	286.1	1444
9	240.0	88.8	321.6	997	9	246.0	61.3	299.0	
run 5					run 11				
0	0.0				0	0.0			2136
1	1.8	55.1	6.1	2485	1	1.2	51.9	8.7	2140
2	31.8	73.5	73.8	2094	2	30.0	55.3	55.0	2035
3	60.6	60.0	151.0	1743	3	60.0	61.2	110.5	1835
4	97.2	82.1	184.0	1412	4	87.6	55.4	143.4	1714
5	119.7	83.5	202.5	1275	5	115.2	60.4	174.8	1616
6	157.2	84.5	220.0	1108	6	141.6	62.9	205.2	1549
7	181.2	84.5	259.5	1028	7	179.4	62.6	254.4	1472
8	211.8	82.8	287.2	874	8	151.8			1415
9	240.0	85.2	298.6		9	243.0	62.6	267.2	
run 6					run 12				
0	0.0				0	0.0			2193
1	1.8	59.3	14.8		1	4.8	53.8	13.2	
2	31.2	55.7	67.3	1864	2	30.9	60.6	65.2	2124
3	60.0	60.3	119.5	1498	3	61.2	66.5	113.3	
4	90.0	63.7	167.3	1235	4	90.6	71.2	154.8	1825
5	120.0	67.0	197.0	1119	5	120.0	71.7	191.5	1752
6	150.3	65.0	237.5	981	6	150.0	75.1	224.4	1673
7	183.3	68.1			7	180.0	75.8	249.6	1592
8	207.0	73.2	282.3	725	8	210.3	77.3	283.0	1551
9	240.0	71.5	312.6		9	240.3	77.6	277.1	1513

Table XIV Summary of data from milling trials, runs 13 - 22

	Time min.	% -75 µm	Mass fines kg	Torque Nm		Time min.	% -75 µm	Mass fines kg	Torque Nm
run 13	**Test 5**	**70mm, 90deg Lifters, 90% crit.**			run 18	**Test 7**	**Grid liners, 80% crit. speed**		
0	0.0				0	0.0			
1	1.8	52.5	6.8	2060	1	1.8	49.7	8.6	2435
2	30.0	60.9	53.7	1925	2	30.3	62.9	70.9	2186
3	60.0	67.1	99.8	1769	3	61.2	69.3	129.9	1844
4	91.2	71.5	149.2	1638	4	90.0	72.9	185.9	1608
5	122.4	73.8	179.4	1529	5	120.0	81.9	230.4	1459
6	149.4	75.4	206.9	1436	6	150.3	78.7	266.5	1308
7	180.0	77.4	237.0	1411	7	180.0	79.9	286.3	1208
8	210.3	77.6	252.5	1325	8	210.6	81.2	312.7	1110
9	240.0	78.6	285.1	1292	9	240.6	81.4		
run 14					run 19				
0	0.0			2083	0	0.0			2523
1	1.2	55.9	6.5	2039	1	2.7	50.9	10.0	2503
2	30.0	49.7	50.5	1897	2	30.3	70.1	65.2	2275
3	60.6	50.8	102.8	1599	3	61.8	78.5	134.0	1977
4	91.8	54.0	152.7	1497	4	90.3	83.0	178.3	1782
5	123.9	54.5	178.8	1410	5	122.7	85.2	218.8	1581
6	150.6	55.7	195.4	1347	6	150.0	89.0	242.2	1484
7	180.0	57.8	221.9	1265	7	180.6	89.2	275.0	1399
8	210.6	57.5	245.9	1240	8	209.7	90.6	311.1	1304
9	240.0	58.7	270.9	1208	9	240.0	91.1		1241
run 15	**Test 6**	**Grid liners, 90% crit. speed**			run 20	**Test 8**	**40mm, 50 deg Lifters, 90% crit.**		
0	0.0			2306	0	0.0			
1	1.8	50.9	8.5	2287	1	1.5	38.8	5.2	1886
2	29.7	59.4	66.3	2185	2	30.0	58.8	63.8	2204
3	59.7	65.0	132.9	1880	3	60.3	65.2	113.7	1978
4	89.7	68.3	175.8	1635	4	92.1	71.0	171.0	1844
5	119.7	69.9	212.6	1448	5	120.0	73.0	210.3	1764
6	149.4	71.9	273.0	1279	6	150.0	76.0	244.9	1665
7	179.7	73.6	292.6	1170	7	180.9	77.3	275.8	
8	209.7	74.3	310.0	1076	8	209.7	77.6	308.9	1479
9	239.7	73.7	339.1	988	9	240.0	77.5	325.0	1406
run 16					run 21				
0	0.0			2324	0	0.0			2312
1	1.8	54.2	8.6	2271	1	2.1	47.9	7.7	2294
2	31.8	61.2	66.1	2156	2	33.0	54.8	70.5	2105
3	62.4	69.7	128.5		3	61.8	59.4	127.0	1944
4	90.6	74.8	195.4	1702	4	89.7	61.4	172.5	1714
5	120.0	75.8	223.5	1528	5	119.7	63.4	203.6	1578
6	150.0	79.6	284.3	1364	6	150.0	65.5	247.8	1469
7	182.4	81.0	292.7	1266	7	180.0	65.9	267.7	1360
8	210.6	83.3	334.2	1172	8	210.0	65.8	273.2	1303
9	240.0	81.5	355.9	1140	9	240.0	66.2	306.8	1217
run 17					run 22				
0	0.0			2286	0	0.0			2274
1	2.4	42.7	10.8	2280	1	1.2	51.1	5.8	2278
2	30.0	55.7	68.9	2127	2	30.0	47.4		2161
3	60.0	62.4	144.5	1801	3	61.8	58.9	125.5	1908
4	90.9	68.3	197.2	1535	4	90.0	60.5	170.4	1657
5	120.0	78.1	240.9	1348	5	120.0	62.1	175.1	1514
6	150.0	72.1	283.0	1242	6	150.0	64.0	250.4	1403
7	180.0	74.2	314.1	1137	7	180.0	64.3	259.5	1272
8	210.0	75.2	335.3	1064	8	210.0	65.3	306.0	1201
9	240.3	82.7	385.8	988	9	240.0	65.0	301.0	1177

Table XV Summary of data from the milling trials, runs 23 - 25

	Time min.	% -75 µm	Mass fines kg	Torque Nm
run 23	Test 9	40mm, 70 deg Lifters, 80% crit.		
0	0.0			2487
1	1.2	53.0	6.5	2488
2	30.0	64.4	61.7	2240
3	60.6	70.2	126.6	2031
4	90.0	72.1	165.5	1826
5	120.0	75.1	204.3	1720
6	150.0	77.5	243.2	1600
7	180.6	77.8	269.3	1515
8	210.0	78.2	296.5	1410
9	240.6	79.7	322.9	1343
run 24				
0	0.0			2513
1	1.8	49.7	7.8	2468
2	30.0	56.3	64.1	2143
3	60.0	59.4	121.3	1867
4	90.0	61.9	165.0	1689
5	120.0	62.4	208.7	1473
6	150.0	64.0	241.7	1377
7	180.0	63.9	266.6	1272
8	211.2	65.5	296.5	1178
9	240.0	65.8		1098
run 25				
0	0.0			2518
1	1.2	51.3	7.9	2532
2	30.0	65.6	67.0	2260
3	60.0	72.1	119.8	2032
4	96.0	76.0	180.5	1808
5	120.6	76.9	215.8	1730
6	150.0	79.1	246.9	1603
7	180.0	79.7	279.5	1507
8	210.0	80.8	306.4	1445
9	240.0	81.1	330.3	1337

The full size distribution of the solids in the slurry samples taken from the mill were determined for the 2 hour and final sample. The full set of sizings are presented in Table XXXIII of Appendix IV. Plots of the cumulative size distributions of the sands fraction taken from the slurry are given in Figure 168 to Figure 176 in appendix IV. Only the final sizings are shown, as the distributions of the mid-run samples were almost identical to those of the final samples.

10.2 ERROR ANALYSIS

An initial source of error was the accuracy of the sorting of the ore into different size intervals. With the ore being sorted through a rotating trommel screen, there was no bias between different drums of each size interval. A source of error that was only perceived at the end of the tests was that the topsize material was not evenly graded, some of the drums contained a slightly larger size. This introduced an error in the feed ore, and a change in the rate of production of fines. However, it was not noted which runs had these slightly larger rocks, so all the data were used, in preference to risking incorrect data selection. This error introduces some scatter into the data, which need not have arisen. In many of the sets of data, the data from one run is different to the other two, which are generally very close. It is concluded that this arises from one of the runs in a set having a slightly different topsize to the others.

The accuracy of measurement, and resultant uncertainties for each measurement in the experiments, are given in Table XVI. The mass of rocks is not used directly in any calculation, so the effect of this cannot be quantified, but would be very small. The other measured values are used in eqn. (15) to determine the total mass of fines in the mill. Errors within a multiplication or division step are cumulative and for addition or subtraction the largest error is taken. Using this the total effect of the uncertainties in the measurements can be determined.

$$M_{fines} = \gamma . m_{sands} / (m_{sample} - m_{sands}) \times V_{water}$$

Error in $M_{fines} = (0.20 + 0.03) + (0.03) + 0.13 = 0.39\%$

The errors arising from spillage, sample remaining in the packet, losses when filtering, and the like, can generally be taken as equal to the measurement uncertainties, which gives a total error of ±0.8%. This is low, and well within the degree of reproducibility of a sampling procedure, such as was used in this experiment.

As repeat runs were done of each experiment, the scatter in the data points provides the best measure of the error bars that should be used when comparing the different tests. This scatter is indicated by the residuals that are derived from the curves fitted

to the data. It is appropriate to use these because the fitted curves are used for comparison purposes, rather than the data. The standard deviation of the residuals falls within the range of 4 to 11 kg, with an average of about 8 kg. Taken over an average total mass of around 200 kg, the error bars should be 4%. This is presented in the results analysis section, and the standard deviations of the individual curves are used.

Table XVI Uncertainties in the measurements

	Ore kg	Water kg	Slurry sample g	Dry sample g	Size frac. g
Accuracy	1	0.4	0.1	0.1	0.1
Total measured	800	300	1000	300	50
Uncertainty, ± %	0.13	0.13	0.01	0.03	0.20

The averages of the half-hourly torque measurements were surprisingly reproducible. The standard deviations of the averages for each test ranged from 120 to 20 Nm, with an average of 80 Nm, representing a scatter of ±5% for an average value of 1600 Nm. The scatter between the minimum and maximum values in the computer logged torques was 200 Nm initially and 100 Nm at the end of the run. These represent errors of ±100 Nm over 2500 Nm and ±50 Nm over 1000 Nm respectively, which is an error of ±5%.

10.3 SECOND SET OF TESTS

Table XVII Full size analysis of the samples

Size, µm	Run 1	Run 2	Run 3	Run 4	Run 5
300	5.5	15.2	3.2	5.0	3.1
212	3.0	8.4	3.0	5.3	2.9
150	7.7	11.6	8.3	10.0	8.0
106	8.8	8.1	9.5	9.6	9.1
75	10.0	7.6	10.5	11.0	10.1
53	11.1	7.8	11.6	8.4	11.1
38	6.6	4.9	7.0	6.4	6.7
<38	47.1	36.4	46.9	44.2	48.9

The results are given in Table XIX and Table XVII. The slurry density and fractional charge filling are included in the results.

Table XVIII Summary of the data from milling trials, Test two.

Time min.	% -75µm	Mass fines kg	density g/cm3	Fractional slurry filling	Mass rocks kg
Run 1		40 mm, 50° Lifters			
1.8	50.42	19.7	1.16	0.30	960.9
30.6	64.89	146.1	1.63	0.44	774.8
40.8	63.29	167.3	1.70	0.47	735.6
51.0	68.92	185.6	1.71	0.47	730.7
61.2	71.67	210.0	1.74	0.49	707.0
72.0	73.16	222.9	1.76	0.50	695.3
102.9	74.10	266.5	1.83	0.54	640.3
Run 2		70 mm, 90° Lifters			
1.8	63.43	9.8	1.07	0.29	984.5
10.2	49.07	41.7	1.31	0.34	915.0
20.4	52.84	76.3	1.47	0.38	855.6
30.6	59.84	111.7	1.56	0.41	813.3
40.2	58.64	143.2	1.67	0.45	755.8
50.7	63.19	171.3	1.71	0.47	729.0
61.2	63.06	192.3	1.76	0.50	695.0
71.4	63.75	206.1	1.78	0.51	676.6
81.6	66.65	229.5	1.81	0.53	655.6
90.0	67.65	240.8	1.82	0.53	644.1

Table XIX Summary of the data from milling trials, Test two.

Time min.	% -75µm	Mass fines kg	density g/cm3	Fractional slurry filling	Mass rocks kg
run 3		Grid			
2.4	55.08	14.9	1.11	0.30	972.9
10.2	43.57	47.4	1.38	0.36	891.1
22.2	55.08	94.1	1.53	0.40	829.2
30.6	65.45	142.0	1.62	0.43	783.0
40.8	64.52	161.1	1.68	0.46	750.4
52.2	67.93	186.1	1.71	0.47	726.0
61.2	71.16	212.0	1.75	0.49	702.1
71.4	72.32	218.6	1.76	0.50	697.7
81.6	74.85	246.9	1.79	0.52	670.2
89.4	76.24	262.9	1.81	0.53	655.2
Run 4		70 mm, 50° Lifters			
1.8	52.66	7.1	1.06	0.29	986.6
10.2	40.80	28.9	1.27	0.33	929.2
20.1	49.22	66.7	1.45	0.37	864.5
30.3	58.99	112.4	1.57	0.41	809.4
40.5	55.64	128.9	1.65	0.44	768.4
51.6	58.42	152.0	1.69	0.46	739.8
60.6	61.30	169.0	1.72	0.48	724.3
71.4	62.38	189.8	1.76	0.50	695.7
81.0	59.38	188.3	1.78	0.51	682.9
91.8	64.01	217.5	1.80	0.52	660.1
Run 5		Grid, 80% crit.			
2.4	56.6	11.4	1.09	0.29	979.8
10.2	49.3	43.7	1.35	0.35	901.4
20.4	52.0	88.2	1.53	0.40	830.5
30.6	66.8	137.6	1.60	0.43	793.9
40.8	65.7	161.8	1.67	0.45	753.8
51.0	71.0	189.4	1.70	0.47	733.2
63.0	75.1	204.6	1.71	0.47	727.5
71.4	76.5	221.5	7.74	0.59	710.2
81.6	72.5	238.8	1.76	0.50	691.8
90.0	78.4	248.1	1.77	0.51	683.6

CHAPTER 11
ANALYSIS OF MILLING RESULTS

The first set of tests are analyzed in full, followed by the second set.

11.1 RATE OF PRODUCTION OF FINES

To assess the rate of production of fines, the slope of the curve of mass of fines as a function of time had to be obtained. The best technique to achieve this was to fit a curve to the data, and then differentiate the function of the curve. Before this could be carried out, a physically reasonable basis for fitting of curves to the data had to be determined.

It has been found in previous investigations[1] that the mass of grinding media in a mill decays as an exponential function of the form:

$$M_R(t) = M_{Ro}\, e^{-\frac{t}{\theta}} \qquad (24)$$

Where M_R is the mass of rocks (for fully autogenous grinding)
M_{Ro} is the mass of rocks at time zero
t = time , and θ is a time constant

The charge is made up of a fixed mass of rocks and water. The mass of water remains constant throughout the milling process, so it can be excluded from the mass balance. For M_s being the mass of sands in the slurry:

$$\begin{aligned} M_s(t) &= M_{Ro} - M_R(t) \\ &= M_{Ro} - M_{Ro} e^{-\frac{t}{\theta}} \\ M_s(t) &= M_{Ro}\left(1 - e^{-\frac{t}{\theta}}\right) \end{aligned} \qquad (25)$$

The mass of fines, M_f, is some fraction of the total mass of sands and is dependent upon the %-75μm in the slurry. Thus the mass of fines will not tend to M_{Ro} but to some

fraction thereof, which can be called $M_{f\infty}$, the maximum mass of fines that can be produced as time tends to infinity. Eqn.(25) becomes:

$$M_f(t) = M_{f\infty}\left(1 - e^{-\frac{t}{\theta}}\right) \tag{26}$$

Upon differentiating the expression, the rate of production of fines at any time is obtained:

$$\frac{dM_f}{dt} = \frac{M_{f\infty}}{\theta} e^{-\frac{t}{\theta}} \tag{27}$$

The form of expression (26) forces it to pass through the origin. If the ore used in the experiments was absolutely clean, then M_{fo} would have been zero. But there were always a few kilograms of fines in the ore, as shown by the values of M_f after 2 minutes of milling time. To accommodate this a third parameter had to be added, which equalled the mass of fines in the charge at t = 0. The value of $M_{f(1.5 - 2\ min)}$ was calculated from the first sample. To obtain a figure for M_{fo} for each set of test runs, the two-parameter curve (26) was fitted to the data, the resultant function differentiated, and the slope at t = 0 calculated. The masses of fines at the first sample (at about 2 min) were then used to calculate the initial mass of fines:

$$M_{fo} = M_f(t_1) - \text{slope}(t=0) \times t_1$$

Where t_1 = time of first sample

Eqn (26) is then modified to the form:

$$M_f(t) = M_{fo} + M_{f\infty}\left(1 - e^{-\frac{t}{\theta}}\right) \tag{28}$$

The differential (27) remains the same.

The data from all runs within a test were grouped together and a curve fitted to the full set. The Statgraphics program was used for all data fitting. The calculated intercept, the fitted parameters, standard errors, r^2, and the average of the residuals are given for each of the 9 tests, in Table XX.

Table XX The curve fits for mass of fines as a function of time.

Test No.	M_{fo} kg	$M_{f\infty}$, kg			θ, min			Ratio sum sqrd.	r^2	Resid ave.
		est.	std err.	ratio	est.	std. err.	ratio			
1	11.4	409.2	16.1	25.5	152.4	10.6	14.3	7635	0.993	-0.33
2	5.9	397.4	20.2	19.7	168.9	14.8	11.4	5405	0.990	0.05
3	4.5	367.8	18.3	20.1	199.5	15.4	12.9	8582	0.994	0.07
4	3.9	402.3	20.1	20.0	194.2	15.6	12.5	7385	0.993	-0.39
5	3.7	397.5	22.8	17.5	212.2	18.9	11.2	7695	0.995	-0.11
6	4.2	515.8	34.0	15.2	207.9	21.5	9.7	5401	0.990	-0.41
7	3.5	441.8	24.0	18.4	178.0	15.4	11.6	7475	0.996	-0.25
8	2.4	432.6	25.2	17.2	188.4	18.0	10.5	5571	0.990	-0.07
9	4.1	470.2	12.8	36.7	210.8	8.8	23.8	34691	0.998	-0.04

In Table XX the following definitions apply:

Ratio gives the ratios of the standard error to the estimated value; the higher this value the better the fit

Ratio sum sqrd. is the ratio of the mean square to the sum of the squares

The residuals are the difference between the actual values and the fitted values, so they give a measure of the scatter of the points about the fitted curve, and whether there is a systematic bias. The closer the average to zero, the better the fit.

Plots of the fitted curves and all the data points are shown for each set of data, from Figure 84 to Figure 92 . It can be seen that the fitted curves are in general in excellent agreement with the data points, well within the range of experimental scatter. Plots of the residuals and the observed versus fitted points are shown in Figure 177 to Figure 194 in Appendix V. The residuals are symmetrically scattered about the zero, which indicates that there is no systematic bias in the data. The observed versus fitted data lies close to the 45° line, which also indicates a good fit.

The final test has the best set of data, with a very small scatter of points. This indicated that the simplified sampling procedure was preferable, and that with some practice at standardising the sampling procedure, excellent results and reproducibility could be achieved. Because of the closeness of the fits, the fitted curves can be used with confidence to compare the data.

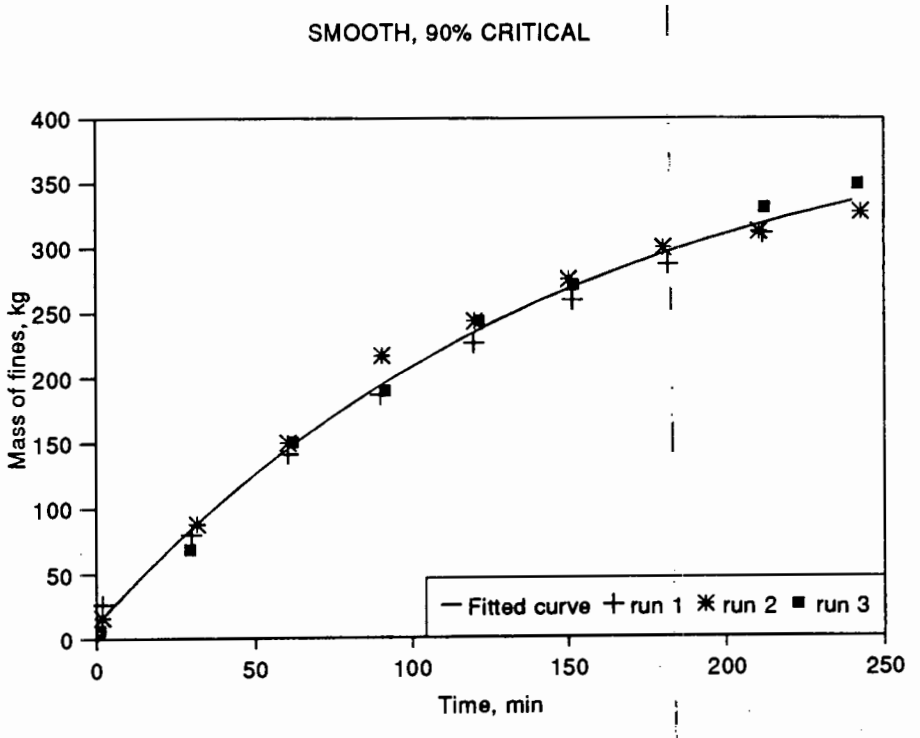

Figure 84. Mass of -75µm material in the mill, Test 1

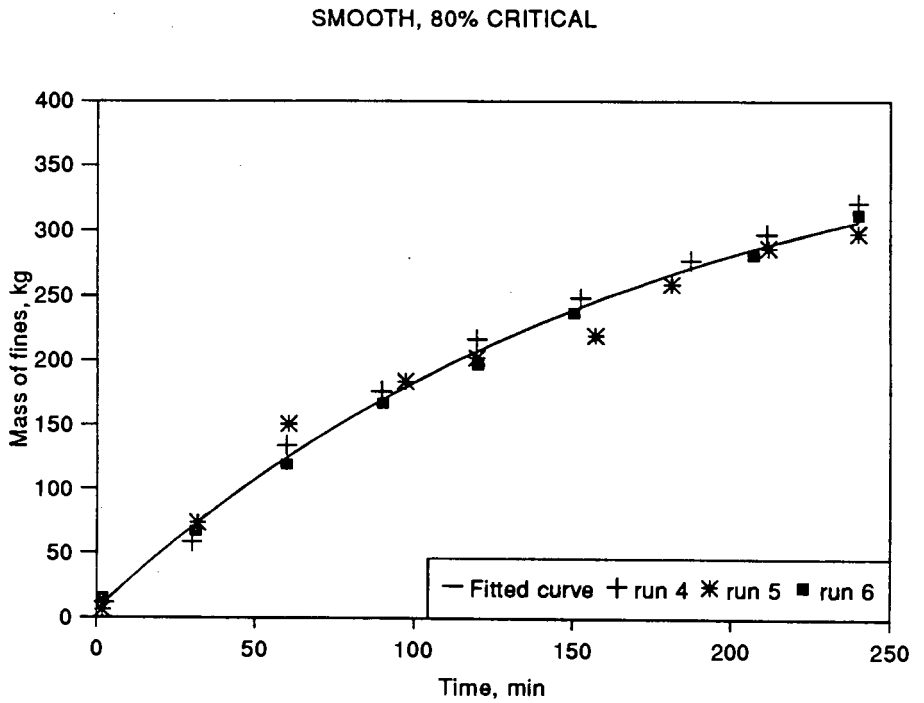

Figure 85. Mass of -75µm material in the mill, Test 2

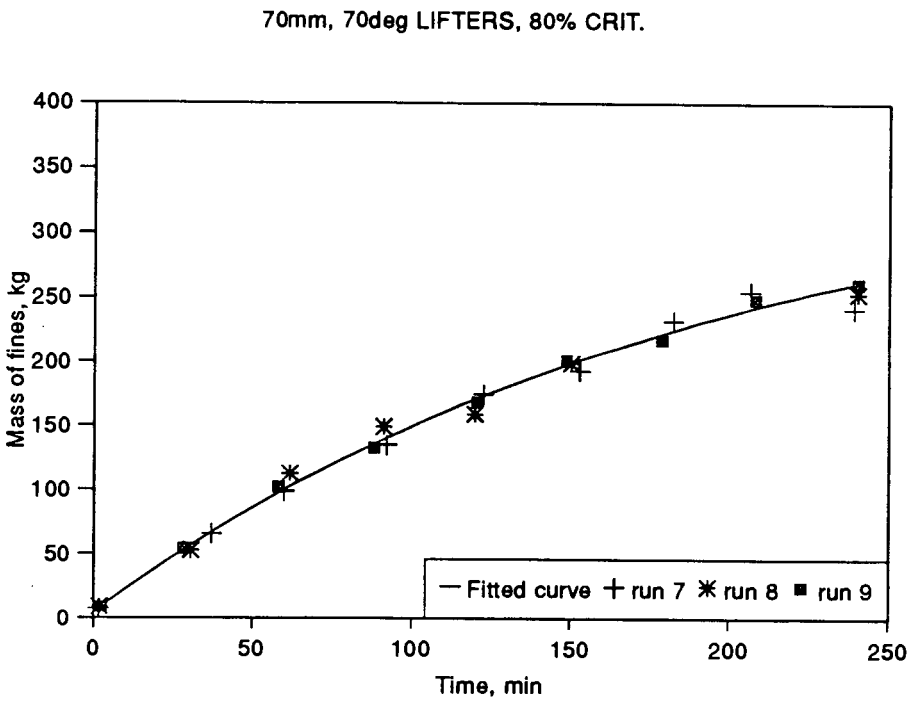

Figure 86. Mass of -75µm material in the mill, Test 3

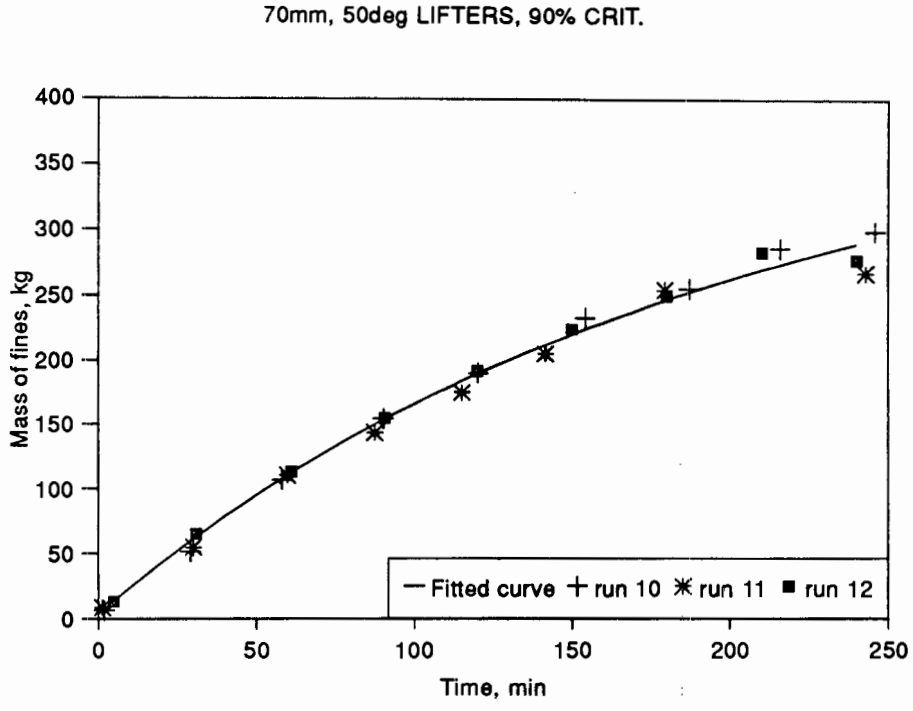

Figure 87. Mass of -75μm material in the mill, Test 4

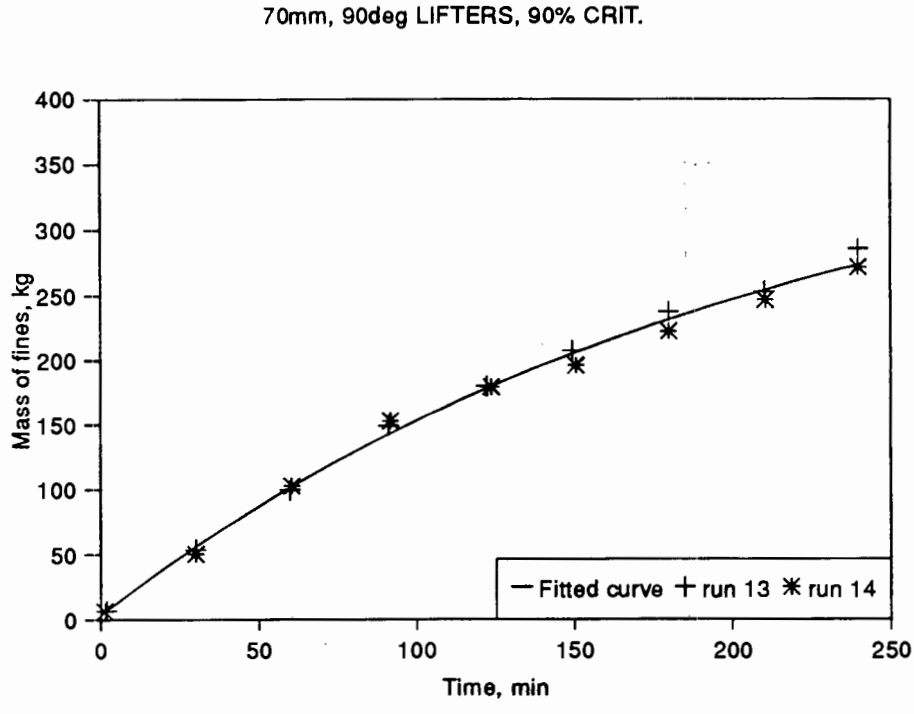

Figure 88. Mass of -75μm material in the mill, Test 5

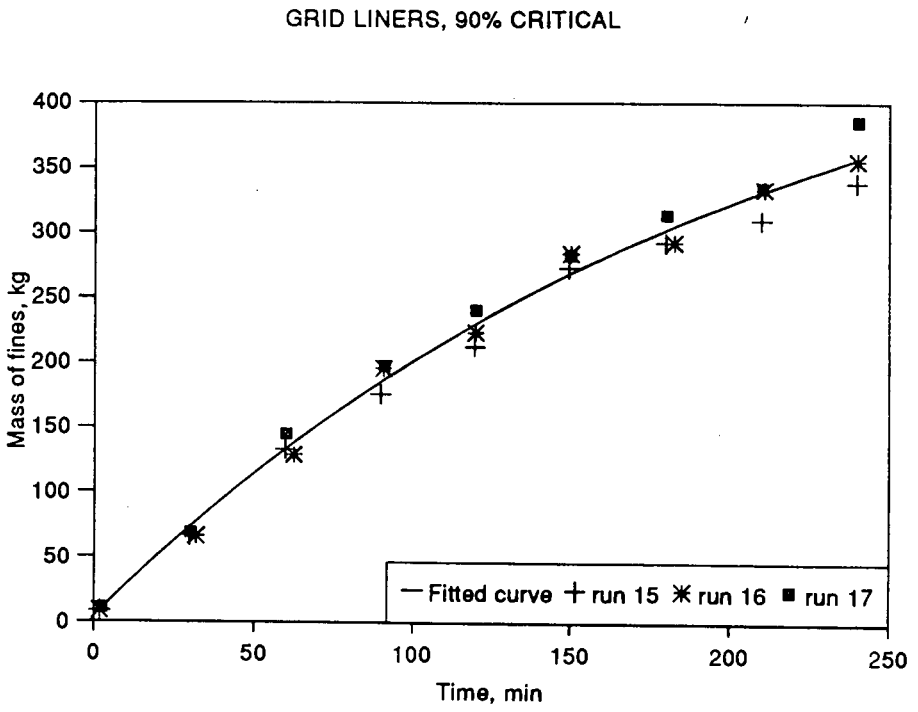

Figure 89. Mass of -75µm material in the mill, Test 6

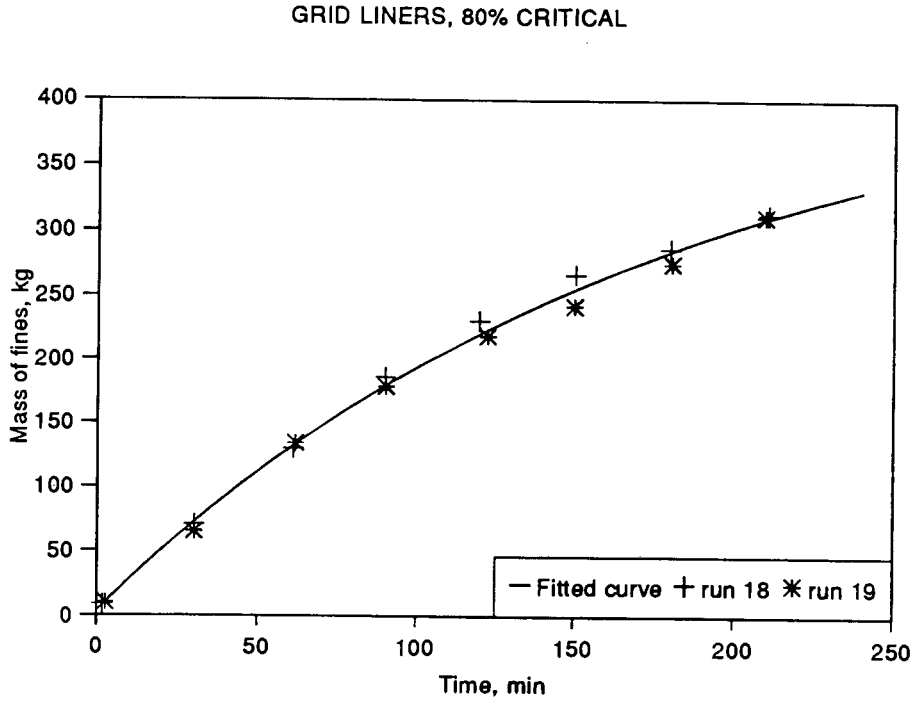

Figure 90. Mass of -75µm material in the mill, Test 7

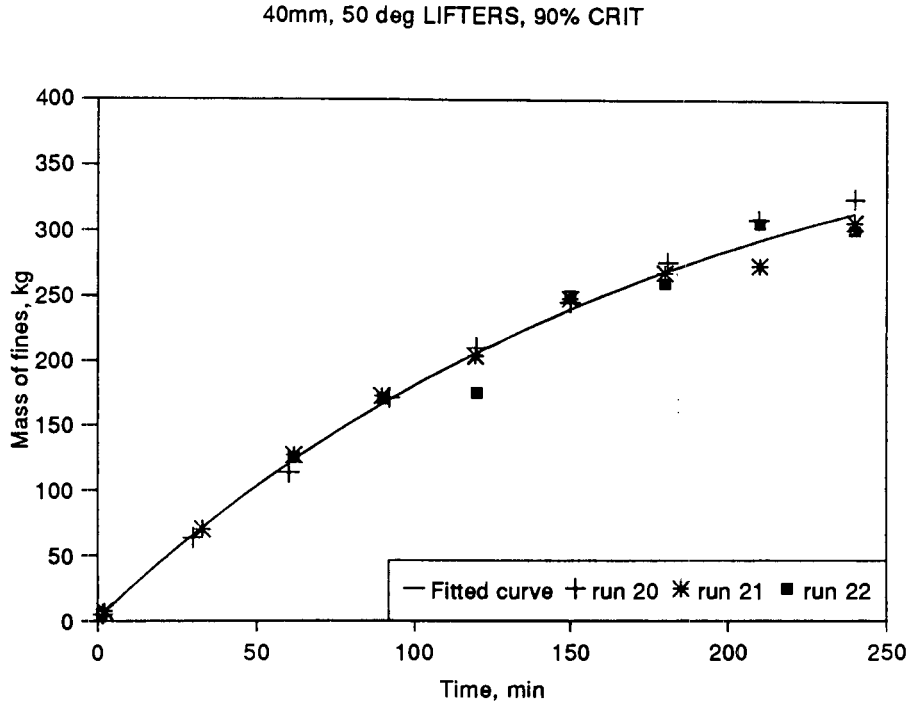

Figure 91. Mass of -75µm material in the mill, Test 8

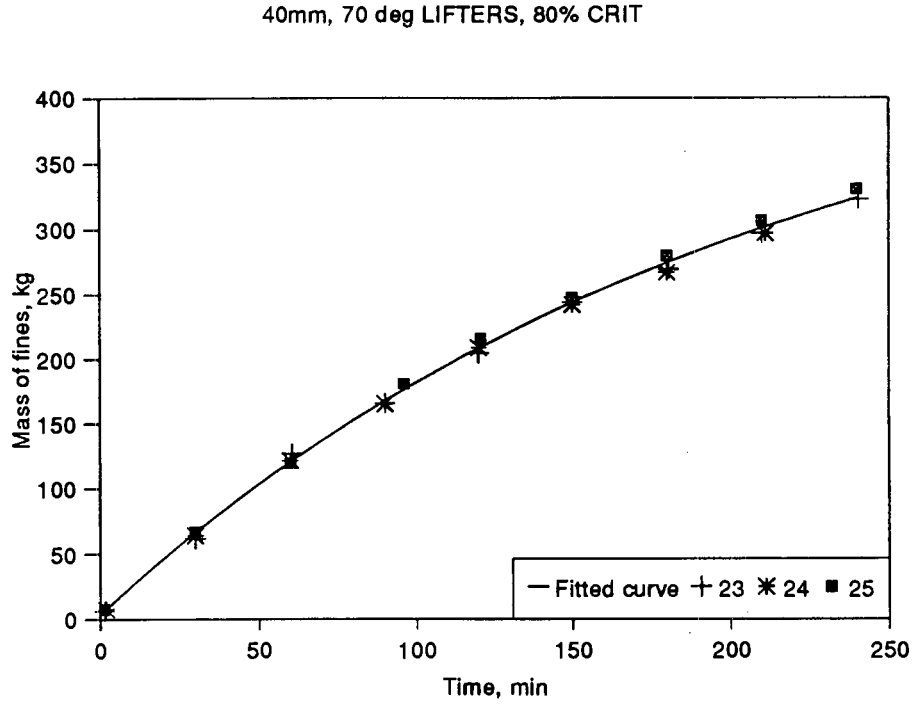

Figure 92. Mass of -75µm material in the mill, Test 9

11.2 POWER DRAW AND ENERGY USAGE

It is obviously preferable to use the continuously logged torque readings, but because of the problems with the computer logging system, only about half the runs had a full set of these data. It therefore had to be ascertained whether the half-hourly readings were sufficiently accurate to be used for comparison of the runs.

From the appearance of the curves and the findings of researchers that the production of material in a mill is directly related to the power draw[25], it was decided that an exponential function may fit the torque data. Accordingly the following function was fitted to the data:

$$T = T_{\infty} + (T_o - T_{\infty})\, e^{\left(-\frac{t}{\tau}\right)} \qquad (29)$$

Where: T_{∞} is the value of the torque to which the mill tends to as the charge becomes fully ground down.

T_o is the torque at $t = 0$

$T_o - T_{\infty} \equiv \Delta T$ is a parameter giving the range of the torque from its initial to final value.

τ is the time constant of the decay of the torque. This will have a different value to the time constant for the rate of production of fines, so it is accordingly given a different symbol.

It was found that this equation gave an excellent description of the decay in the torque, as can be seen from the fits for the continuous data (Table XXI). The parameter values for both the continuous and point data are given separately for each set of fitted data. The fit for runs 23 and 25 is given as 9a. The values for run 24 are distinctly different, and are responsible for the substantial standard error values of run 9. The fit to 9a illustrates the excellence of the fit to the point data taken from the digital display.

Plots of the fitted curves for both the continuous (fitted cont.) and point data (fitted points), the averaged continuous data (ave. cont), and the point data are given in Figure 93 to Figure 101, for each test.

Table XXI Parameter values of the equation fitted to the torque readings

Test No.	T_∞, Nm		$T_o - T_\infty$, Nm		τ, min		Ratio sum sqrd	r^2	Ave. resid
	Est.	Std. err.	Est.	Std. err.	Est.	Std. err.			
1	508	135	2013	127	105	17	1386	0.97	0.27
2	765	130	1731	120	95	19	1049	0.94	0.08
3	1297	29	1122	27	94	6	34803	0.99	0.04
4	1262	147	941	137	146	43	5373	0.93	0.09
5	1106	93	974	86	124	26	4525	0.96	-0.07
6	513	176	1819	167	186	31	6002	0.98	0.15
7	944	143	1582	132	123	24	2690	0.97	0.02
8	764	283	1562	266	202	62	3265	0.95	0.20
9	1005	144	1501	135	140	27	3932	0.96	0.12
9a	1063	38	1447	35	150	8	77250	0.998	0.07
Continuous data									
2	871.5	8.6	1669.0	9.0	79.9	1.3	10^4	0.999	-0.006
4	1244.2	21.9	1012.3	18.0	116.7	6.1	10^4	0.993	0.029
7	961.0	13.9	1611	11.4	115.1	2.4	10^4	0.999	-0.007
8	918.6	38.6	1432.4	33.3	166.1	8.6	10^4	0.996	0.075
9	1060.4	16.2	1461.5	13.3	126.5	3.2	10^4	0.999	0.004

9a is the fit for runs 23 and 25, as 24 was quite different.

Not only do the fitted curves match the continuous data very well, but they are also almost indiscernible from the curves derived from the point data. This is most important as it shows that the point data can be used for comparison of the different runs. The only exception was for test 4, where the continuous data were only for run 11. However, the point data for run 11 match the fitted continuous curve excellently.

The following tests have one run noticeably different to the other two:

Test	1	2	8	9
Run	3	6	20	24

The difference in the torques for these runs is concluded to arise from the difference in the feed ore of the topsize material.

As a consequence of the excellent correlation between the continuous and point data over the experimental range, the point data were used for all comparisons, so as to maintain a conformity of comparison.

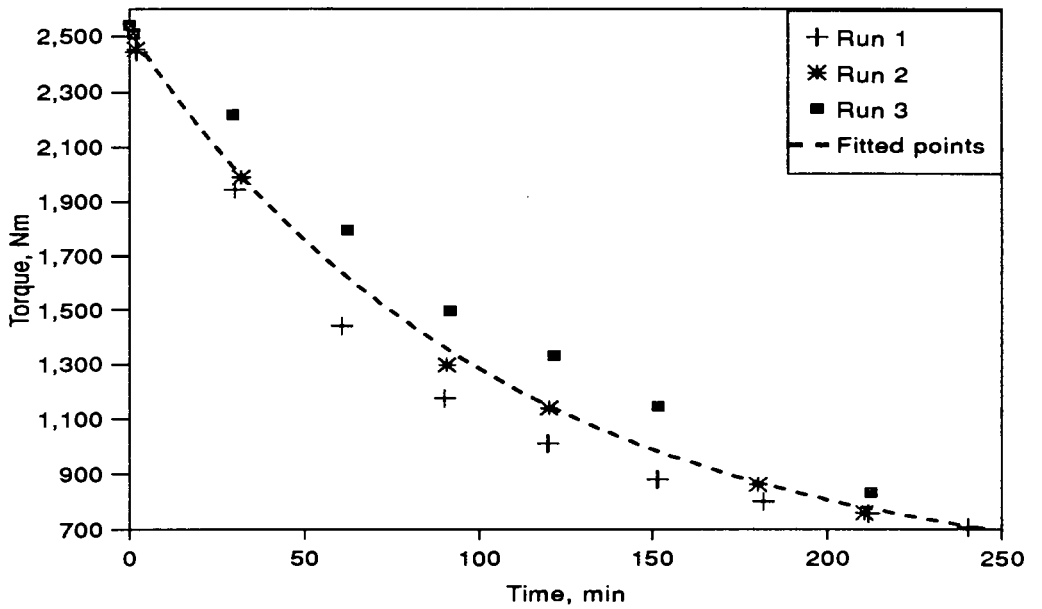

Figure 93. Full set of torque readings, test 1, 90% crit., smooth lining

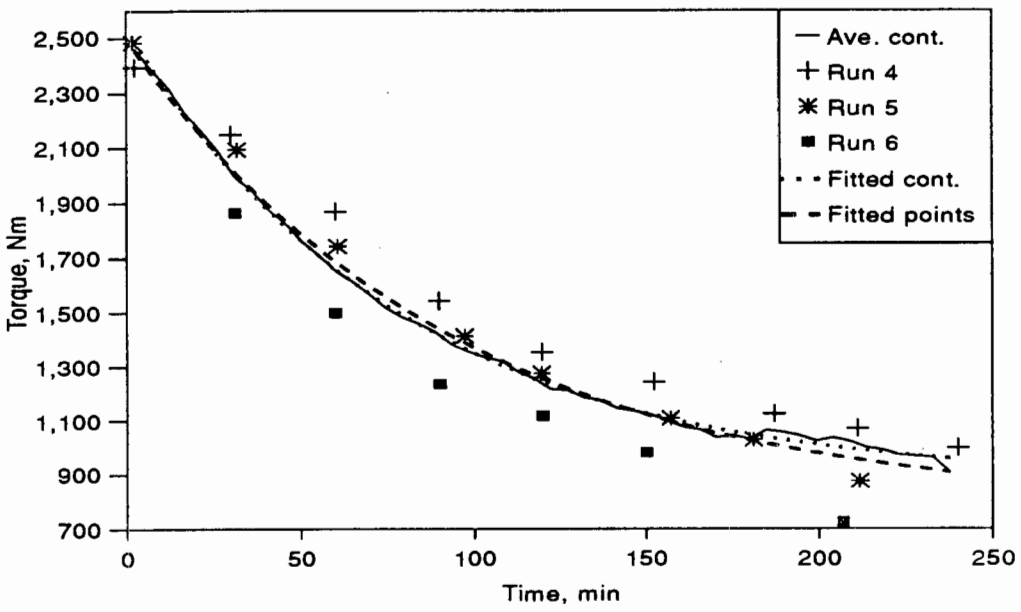

Figure 94. Full set of torque readings, test 2, 80% crit., smooth lining

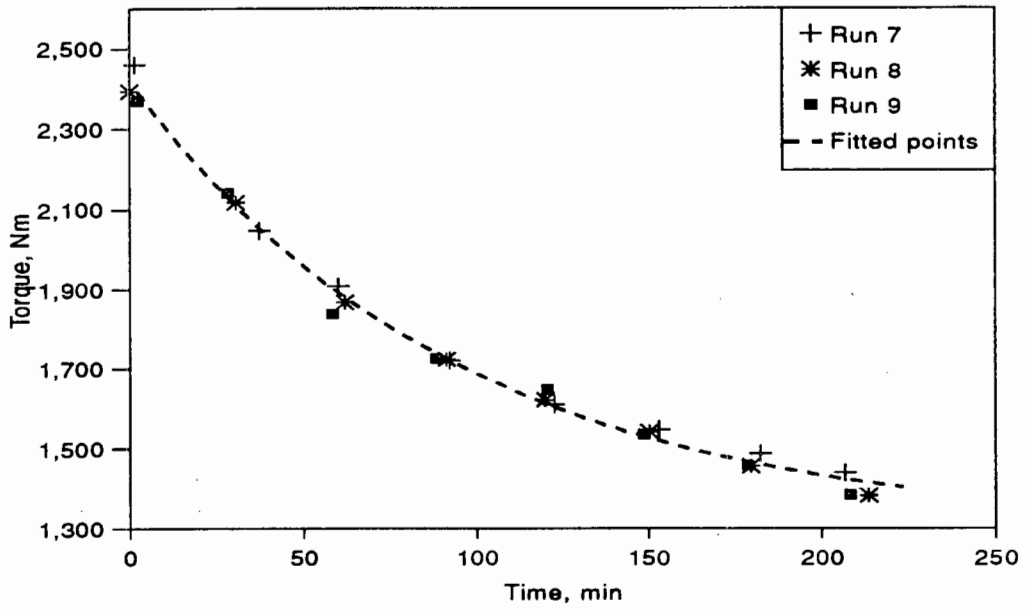

Figure 95. Full set of torque readings, test 3, 80% crit. 70 mm, 70° lifters

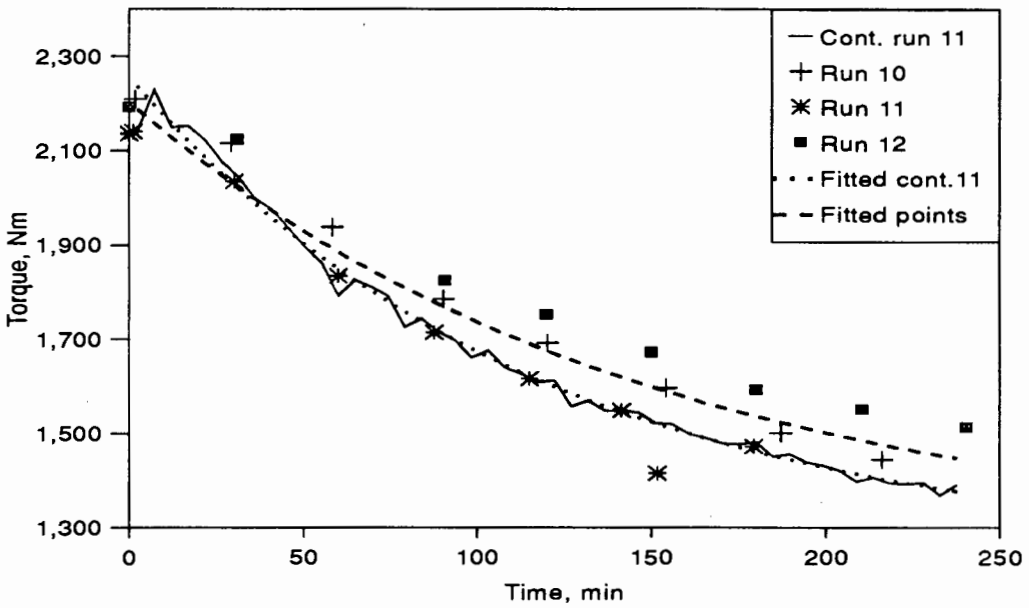

Figure 96. Full set of torque readings, test 4, 90% crit. 70 mm, 50° lifters

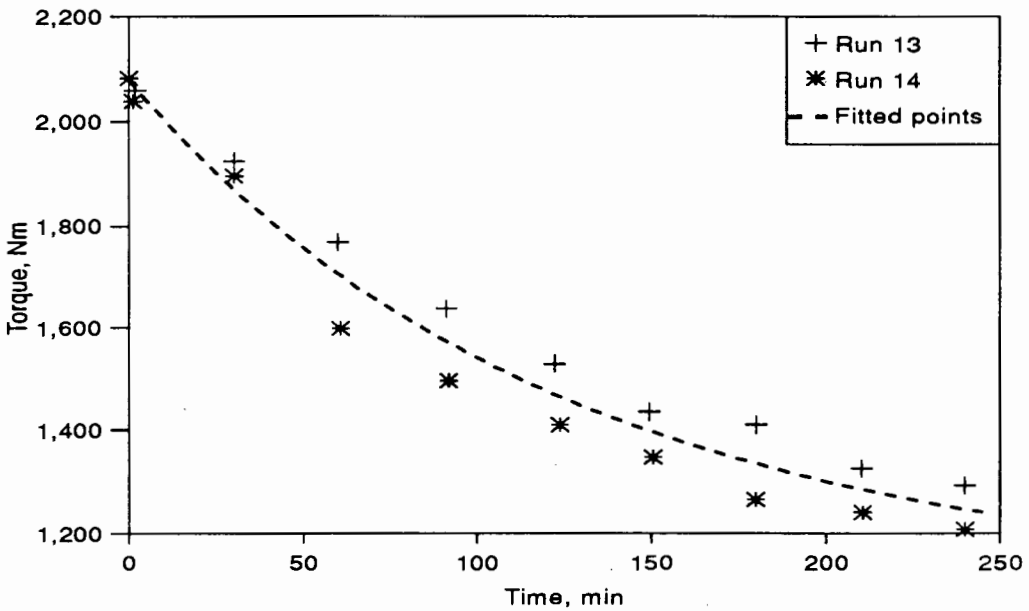

Figure 97. Full set of torque readings, test 5, 90% crit. 70 mm, 90° lifters

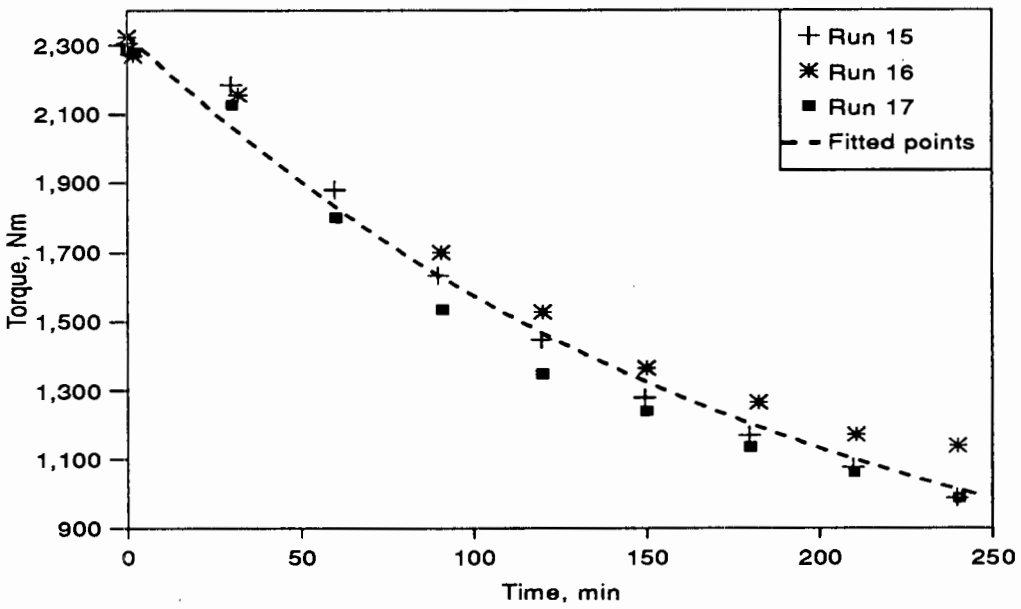

Figure 98. Full set of torque readings, test 6, 90% crit. grid lining

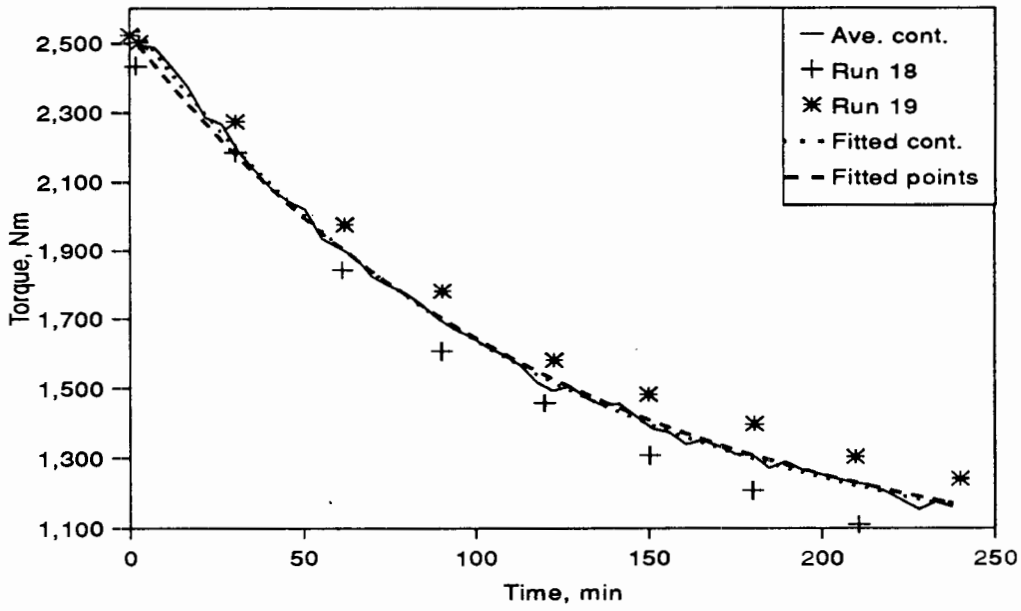

Figure 99. Full set of torque readings, test 7, 80% crit. grid lining

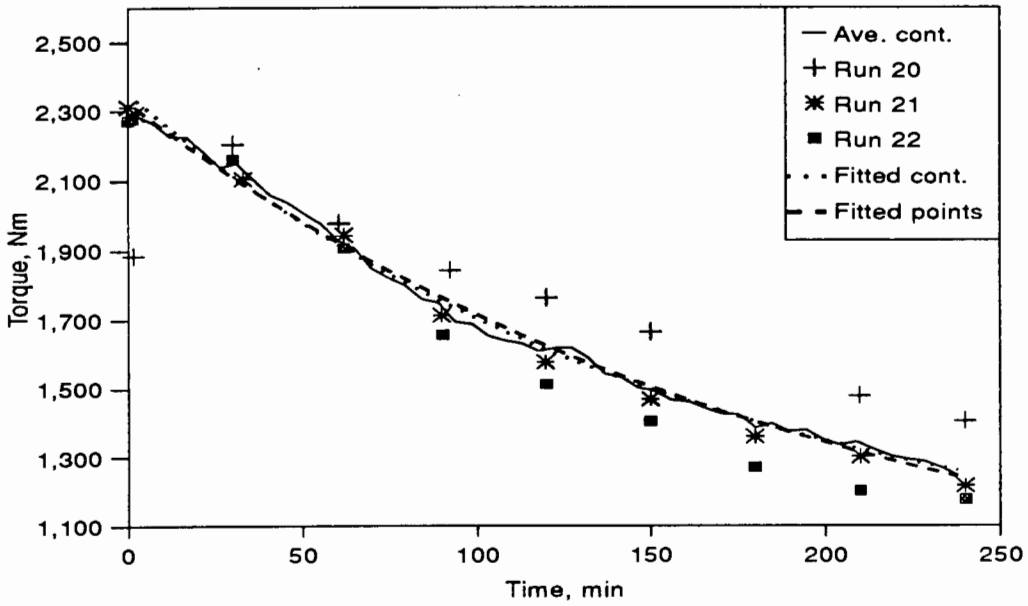

Figure 100. Full set of torque readings, test 8, 90% crit. 40 mm, 50° lifters

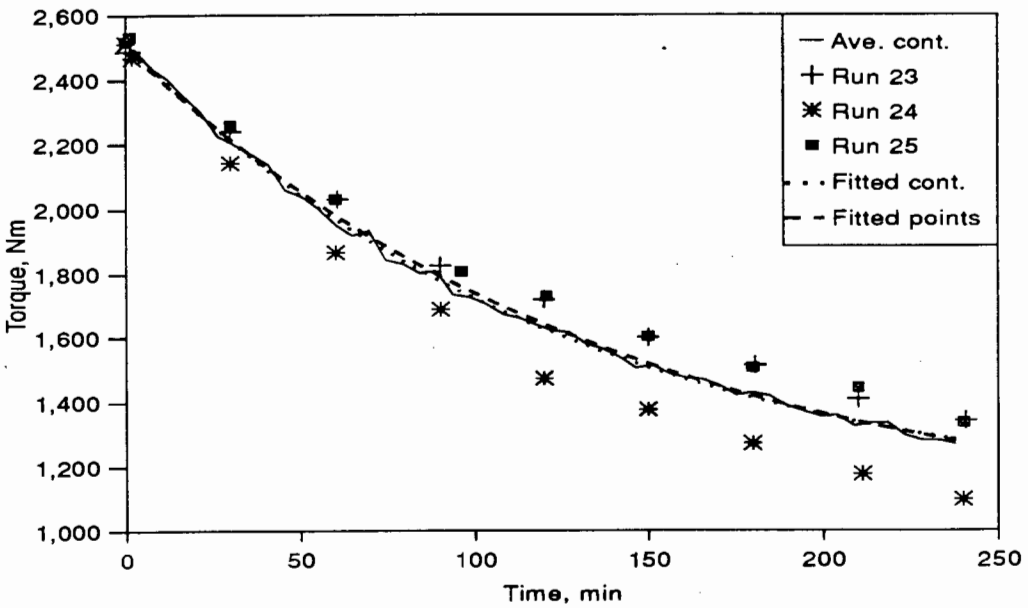

Figure 101. Full set of torque readings, test 9, 80% crit. 40 mm, 70° lifters

11.3 SIZE DISTRIBUTION

The size distributions are not analyzed in detail as they do not form part of the main thrust of this work. The averaged mid-run and final distributions are given in Figure 102 to Figure 105. The mid-run and final distributions are almost indistinguishable. At 90% critical speed the smooth and grid linings give very similar distributions, which are about 10% finer than those for the lifters. At 80% critical speed there is a far greater spread of distributions, but following the same trend as at 90% critical speed. The grid gives by far the finest grind, with a noticeably high percentage of the finest material. For the type of milling desired, the smooth liners were possibly producing too high a percentage of very fine material.

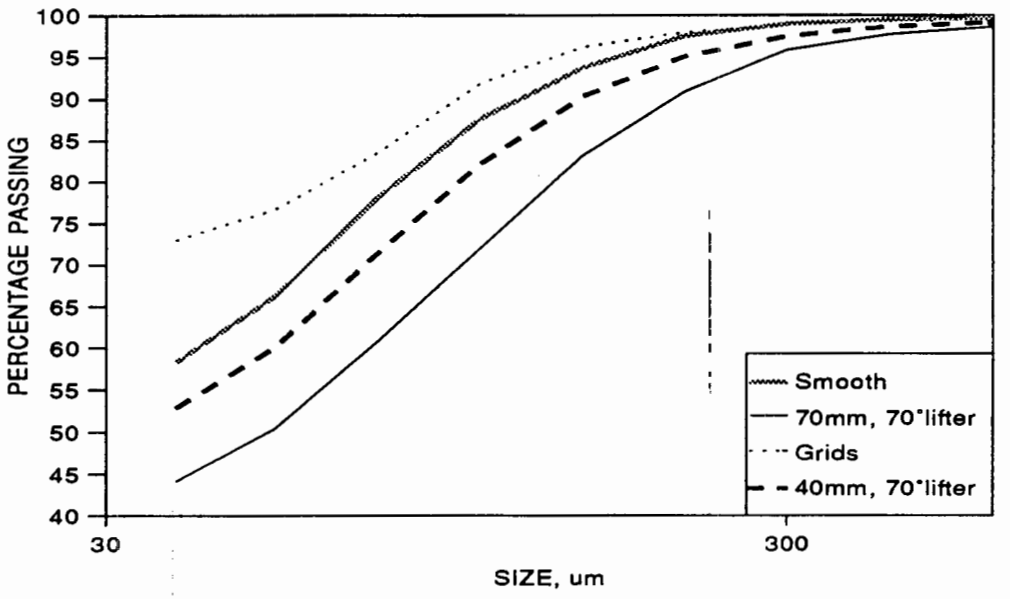

Figure 102. Mid-run cumulative size distributions of the sands, 80% crit. speed

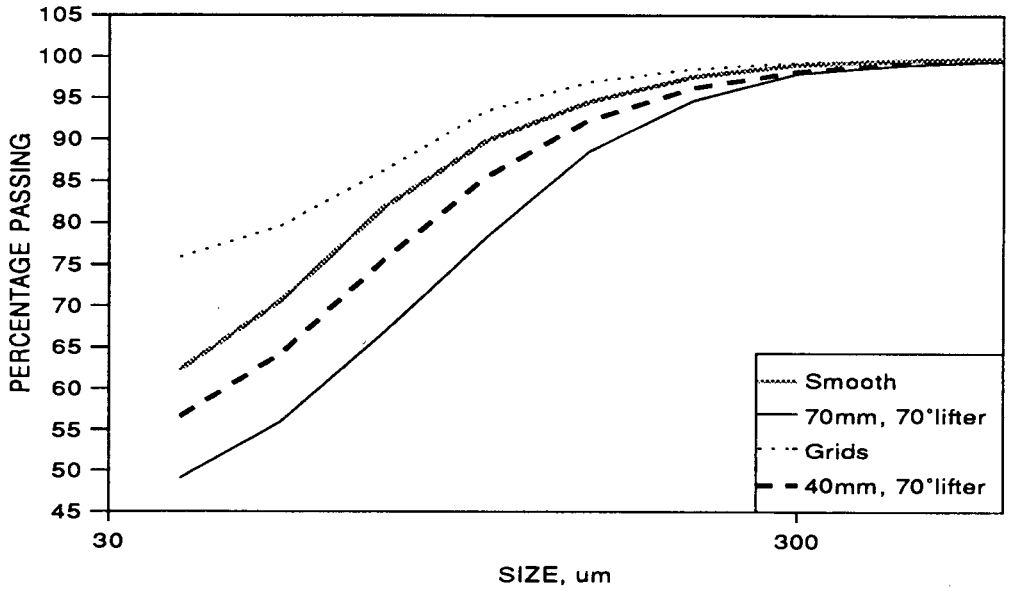

Figure 103. Final cumulative size distributions of the sands, 80% crit. speed

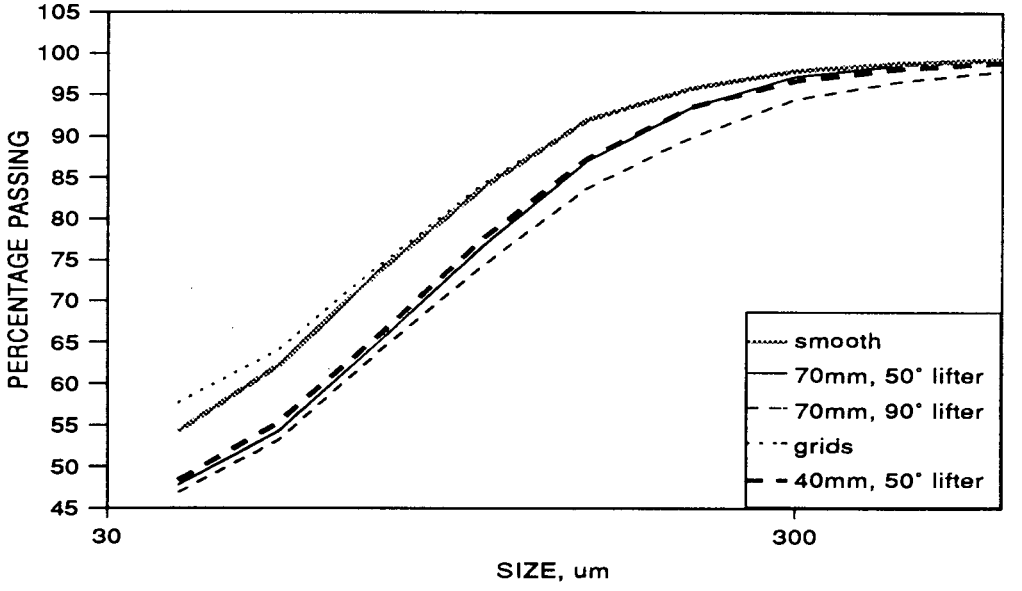

Figure 104. Mid-run cumulative size distributions of the sands, 90% crit. speed

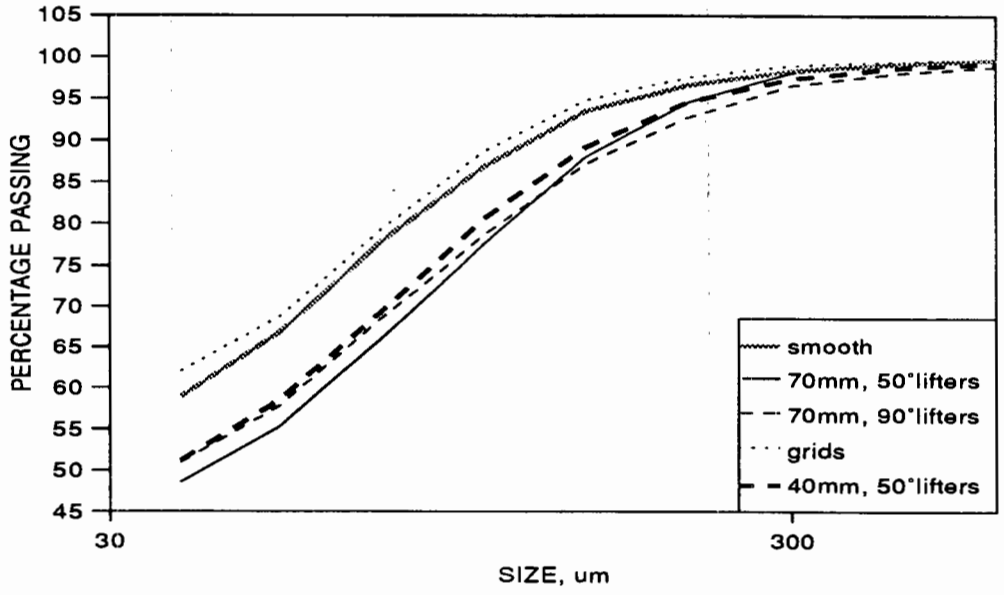

Figure 105. Final cumulative size distributions of the sands, 90% crit. speed

11.4 SECOND SET OF TESTS

The analyses are carried out in an analogous manner to the first set of tests. Additional analyses of the fractional slurry filling, the slurry density, and of the mass of rocks are given here. The filling and density data curves had the same exponential form as the rate of production of fines, and would be expected to behave the same, so similar exponential curves were fitted to the data.

The curve fits for the mass of fines as a function of time are given in Table XXII. The torque drawn by the mill lies in three distinct regimes, as seen in Figure 106. There is an initial region of rapidly increasing torque, until about 20 minutes. This is followed by an exponentially decaying region, as for the first set of tests. From about 70 to 80 minutes the torque begins to again increase. Only the torque in the 'normal operation' region has been analyzed (Table XXIII), utilizing the same equations as for the first set of tests. The torque curves, Figure 107, are only shown for the 'normal' region of operation where they apply.

Table XXII The curve fits for mass of fines as a function of time, set 2.

Test No.	M_{fo} kg	$M_{f\infty}$, kg			θ, min			Ratio sum sqrd.	r^2	Resid ave.
		est.	std err.	ratio	est.	std. err.	ratio			
1	11.8	296.5	13.5	22.0	55.1	4.8	11.6	$4.5x10^3$	0.996	0.04
2	3.0	367.9	17.6	20.8	86.0	6.2	13.8	$1.3x10^4$	0.999	-0.40
3	4.9	350.7	26.9	13.0	70.0	8.8	7.9	$3.2x10^3$	0.994	-0.40
4	2.4	295.1	31.1	9.5	73.4	12.5	5.9	$1.7x10^3$	0.990	-1.00
5	1.5	313.5	14.6	21.5	58.1	4.9	11.8	$5.4x10^3$	0.996	-0.81

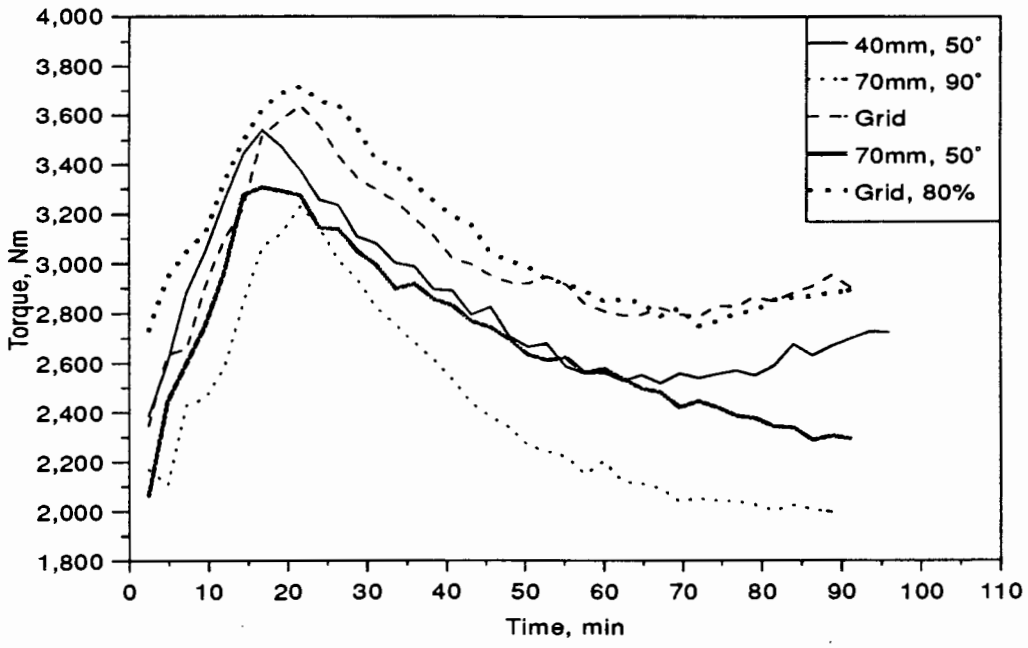

Figure 106. Torque drawn by the mill, 2.4 min. averages, second set of tests

11.4.1 Fractional slurry filling

The fractional slurry filling gives the fraction of total charge, by volume, that is slurry. As it is important to ensure that the comparison of data takes place during a period when the load is not under- or over-filled with slurry, this factor is modelled. The exponential curve, eqn.(30), fitted very well, as shown in Table XXIV.

$$F = F_o + (F_\infty - F_o).\left(1 - e^{-\frac{t}{\tau}}\right) \qquad (30)$$

Table XXIII Parameter values of the equation fitted to the torque readings,set 2.

Test No.	T_∞, Nm		$T_0 - T_\infty$, Nm		τ, min		Ratio sum sqrd	r^2	Ave. resid
	Est.	Std. err.	Est.	Std. err.	Est.	Std. err.			
1	2154	104	2125	72	36.0	5.8	7.9×10^4	0.957	0.12
2	1829	47	3247	142	25.6	1.9	8.5×10^4	0.983	0.01
3	2704	34	2821	304	19.2	2.0	8.3×10^4	0.946	0.00
4	2156	102	1845	52	38.3	6.6	9.9×10^4	0.957	0.07
5	2537	64	2654	135	28.2	3.1	9.9×10^4	0.969	0.14

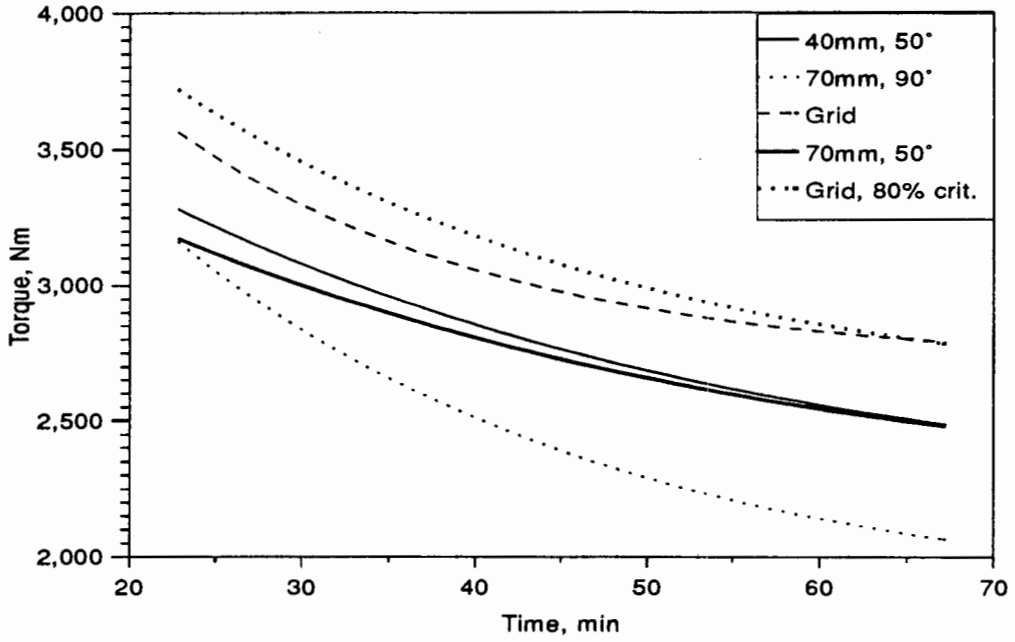

Figure 107. Fitted torque values for the second set of tests, in the exponentially decaying region

Table XXIV Parameter values of the equation fitted to the fractional slurry filling

Test No.	F_o		F_∞ - Fo		ξ, min		Ratio sum sqrd	r^2	Ave. resid
	Est.	Std. err.	Est.	Std. err.	Est.	Std. err.			
1	0.295	0.011	0.248	0.017	37.9	6.4	$5.0x10^{3}$	0.988	$3.1x10^{-7}$
2	0.278	0.004	0.308	0.008	50.1	3.4	$4.7x10^{4}$	0.998	$2.4x10^{-6}$
3	0.285	0.007	0.255	0.008	36.5	3.7	$1.7x10^{4}$	0.995	$1.1x10^{-6}$
4	0.274	0.003	0.281	0.006	45.3	2.8	$5.0x10^{4}$	0.998	$1.9x10^{-6}$
5	0.275	0.006	0.234	0.006	28.8	2.3	$2.1x10^{4}$	0.995	$4.3x10^{-7}$

11.4.2 Slurry density

The slurry density plays a large part in the milling dynamics, so it should also be monitored to ensure that the mill is under 'normal' conditions when comparisons are made of the milling efficiency. The curve fits are given in Table XXV

$$\rho = \rho_o + (\rho_\infty - \rho_o).\left(1 - e^{-\frac{t}{\lambda}}\right) \qquad (31)$$

Table XXV Parameter values of the equation fitted to the slurry density data

Test No.	$\rho_{o,\ g/cm3}$		ρ_∞ - ρ_o, $g.cm^3$		λ, min		Ratio sum sqrd	r^2	Ave. resid
	Est.	Std. err.	Est.	Std. err.	Est.	Std. err.			
1	1.11	0.03	0.70	0.03	23.5	3.0	$1.1x10^{4}$	0.992	$8.1x10^{-6}$
2	1.03	0.02	0.82	0.02	28.9	1.6	$3.7x10^{4}$	0.997	$6.2x10^{-7}$
3	1.06	0.03	0.74	0.03	21.1	2.0	$1.6x10^{4}$	0.991	$-1.4x10^{-5}$
4	1.01	0.01	0.80	0.01	25.7	1.1	$7.6x10^{4}$	0.999	$5.7x10^{-6}$
5	1.01	0.02	0.75	0.02	18.0	1.3	$2.3x10^{4}$	0.994	$5.1x10^{-5}$

11.4.3 Mass of rocks

The mass of rocks is given by the initial mass of rocks less all the material that has passed into the slurry.

$$M = M_{\infty} + (M_0 - M_{\infty}).e^{-\frac{t}{\xi}} \quad (32)$$

The time constant for the Mass of rocks is the same as that for the fractional filling, as the mass of fines in the slurry is a direct function of the mass of rocks that have been ground down. This was confirmed by fitting the curves independently, and obtaining the same time constants, as given in Table XXVI.

Table XXVI Parameter values of the equation fitted to the mass of rocks

Test No.	M_{∞}, kg		$M_0 - M_{\infty}$, kg		ξ, min		Ratio sum sqrd	r^2	Ave. resid
	Est.	Std. err.	Est.	Std. err.	Est.	Std. err.			
1	630	22	343	23.2	38.0	6.4	7.0×10^{3}	0.988	8.8×10^{-3}
2	573	13	425	11	50.2	3.4	7.5×10^{4}	0.998	2.5×10^{-3}
3	635	13	353	12	36.5	3.7	2.7×10^{4}	0.995	1.2×10^{-3}
4	615	10	389	9	45.3	2.8	8.5×10^{4}	0.998	3.7×10^{-3}
5	678	8	324	9	28.8	2.3	3.6×10^{4}	0.995	1.3×10^{-4}

11.4.4 Size distribution

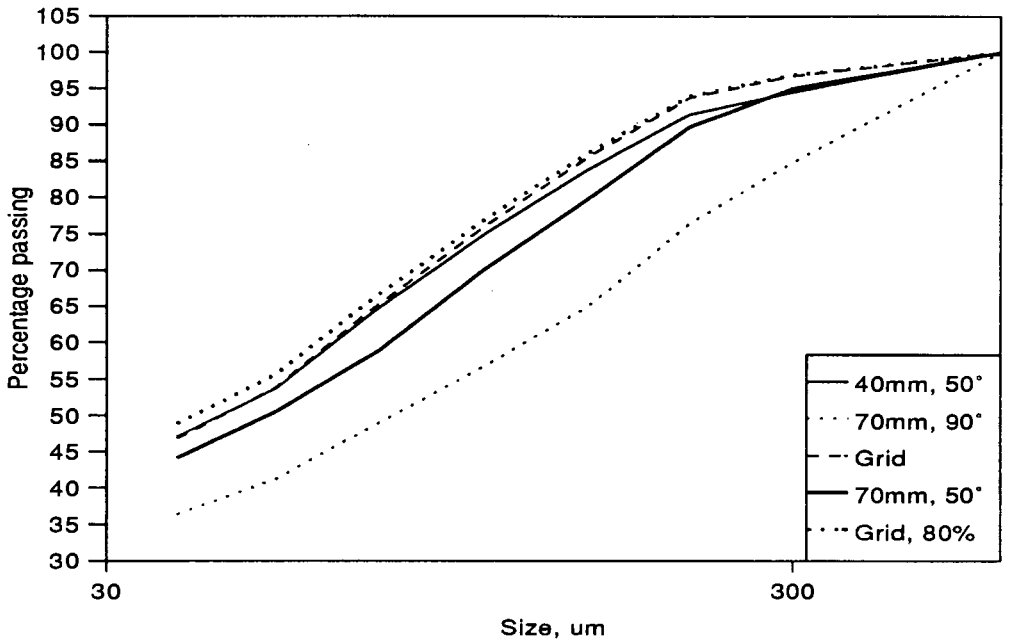

Figure 108. Cumulative size distribution for the second set of tests

The full size distribution of the solids in the slurry was measured once during each test, Figure 108. These demonstrate the same trends as in the first set of tests, Figure 104, with the grid producing the finest grind and the high lifters the coarsest grind.

CHAPTER 12
TESTING THE SIMPLE THEORY

The simple theory, based on the theory for a ball on a lifter, and extended into the bulk of the charge, is tested here by fitting it to experimental data. Run 17 was chosen for comparison because of the wide spread of trajectories across the mill. Comparison of the slip of concentric layers within the charge showed the slip to be independent of the mill speed and liner configuration. The figure of the average slip for all the conditions was used to determine the slip in each layer of the charge. Table XXVII gives the measured slip for each layer and its calculated angular velocity. The radius is the effective liner radius within which a given layer moves. In the model mill 17 layers of 6 mm balls had a measured thickness of 85 mm, giving a layer thickness of 5 mm. Thus there is 5 mm between each concentric layer of charge. The height and face angle of a radial lifter of minimum height varies as the radius from the centre of the mill decreases with each concentric layer of charge. The calculated values of these are given as 'equivalent lifter' in the Table XXVII, as they are required for the calculation of charge trajectories. Layer 1 rests against the mill shell and the lifter that is mounted in the mill. The mill parameters are: 79.61 rpm ≡ 82.1 % critical speed; 6 mm, 90° lifters.

The kinetic coefficient of friction between the ball and lifter was measured by sliding a group of balls, glued together to form a flat slab, down an inclined plane. The coefficient of friction can be calculated from the time taken by the balls to slide a fixed distance down the plane. The plane was vibrated by a mechanical vibrator over a range of frequencies, from 100 Hz to 15 kHz, to simulate the natural vibration of the mill. The frequency of vibration of the lifters in the mill was measured by attaching an accelerometer to a lifter, and running the mill. A rather weak signal was obtained, in the region of a few kHz. Using a range of frequencies of vibration around this value for the sliding friction tests, a value for the kinetic coefficient of friction of between 0.03 and 0.08 was obtained. The particulars of the experimental technique are not reported here, as they were described in detail in the earlier work[1,2].

Table XXVII Parameters used in the calculation of the simplified theoretical trajectories

Layer	Effective Radius mm	% slip	Ang. Vel. layer		Equiv. lifter	
			Ω_b	% crit.	h, mm	Ang.°
1	95	0	79.6	82.0	6.00	90.0
2	90	2	78.0	78.3	3.05	88.0
3	85	2	78.0	76.1	3.05	87.9
4	80	3	77.2	73.0	3.06	87.8
5	75	5	75.6	69.3	3.06	87.6
6	70	8	73.2	64.8	3.07	87.4
7	65	13	69.3	59.0	3.07	87.2
8	60	20	63.7	52.2	3.08	87.0
9	55	35	51.8	40.6	3.09	86.7
10	50	60	31.8	23.8	3.10	86.3

The trajectories as predicted by the simple theory are plotted in Figure 109, with a selection of the experimentally measured trajectories superimposed on them. The theoretical paths are shown by the individual balls, and the measured paths by solid lines. The concentric circles demarcate the layers of charge. The predicted trajectories are clearly different from the measured ones. The actual trajectories have a far more rounded shoulder, and a shallower angle of incline of the cascading ball charge. Even more marked is the non-correlation of the CoC's of the charges. The theoretical charge has an angle of repose 30° higher than the actual charge.

The theory was then applied to the ball stacking between two balls, as discussed in the extension of the theory. For this condition the angle of an equivalent lifter was calculated to be about 60°, and the height ranged from 1.6 to 1.7 mm, as the layer at the centre of the mill was approached. The same conditions of slip were used as for the first set of calculations. The predicted trajectories are shown in Figure 110. These are so different to the measured trajectories that the actual data do not need to be shown for direct comparison. For the theory the shoulder region has a considerably

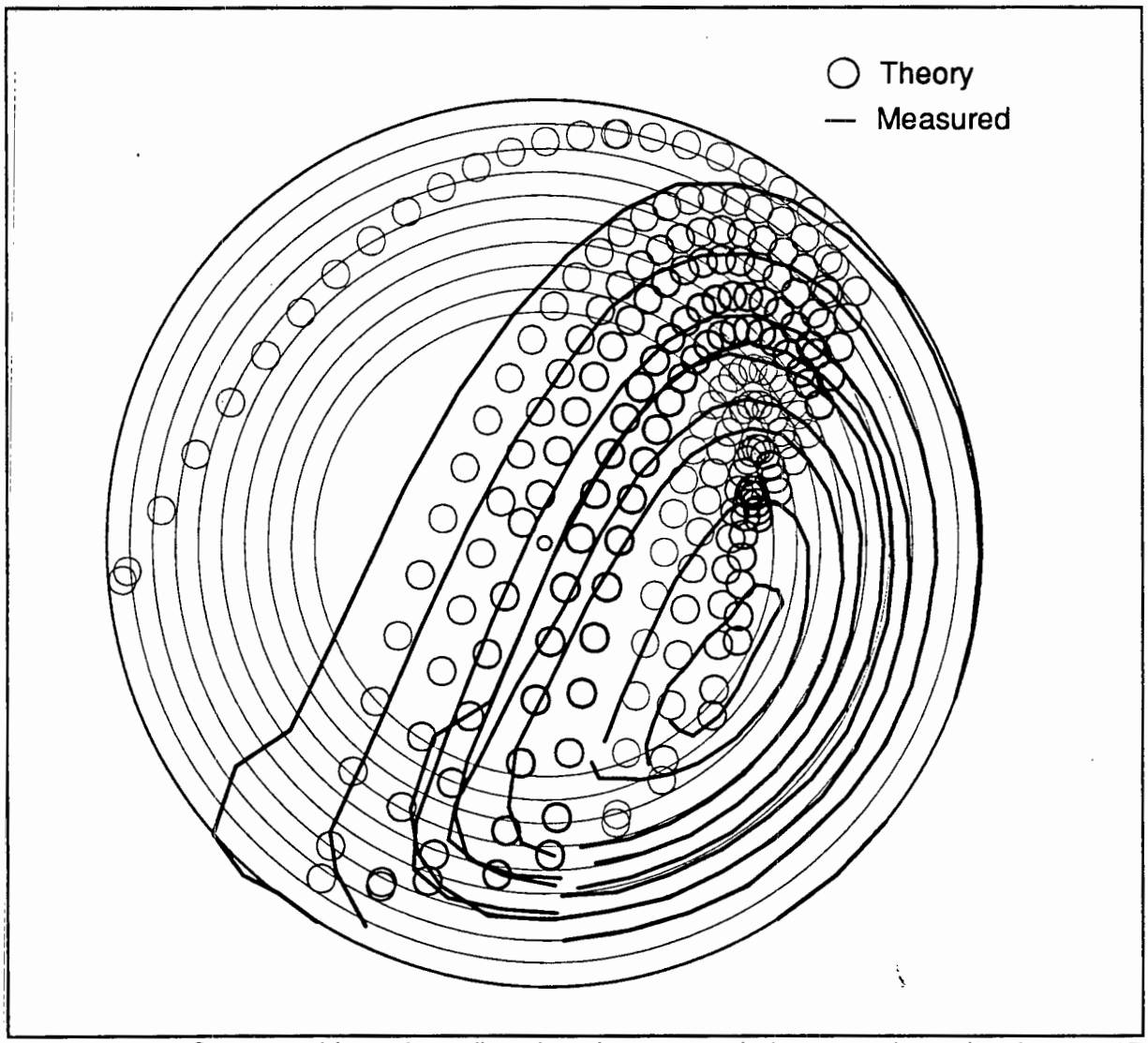

Figure 109. Superposition of predicted and measured charge trajectories for run 17

sharper angle than the observed trajectories, with the balls dropping very steeply, and the CoC is 10° higher than the actual value. The CoC actually lies nearer the centre of the mill than the descending trajectories of layers 1 to 5. This is clearly not possible, so the balls of each layer would in fact have to roll over the shoulder of the inner layer. Even if the ball is assumed to stack between two layers of balls, this still does not bring the CoC down to the same level as for the actual charge, and the trajectories are far different to those observed.

Observation of the charge motion gives strong evidence that the balls do in fact slide over the inner layer. The rounded shoulder of the charge shows that the balls move further across than they would be thrown, even by the equivalent 87° to 88° lifter used

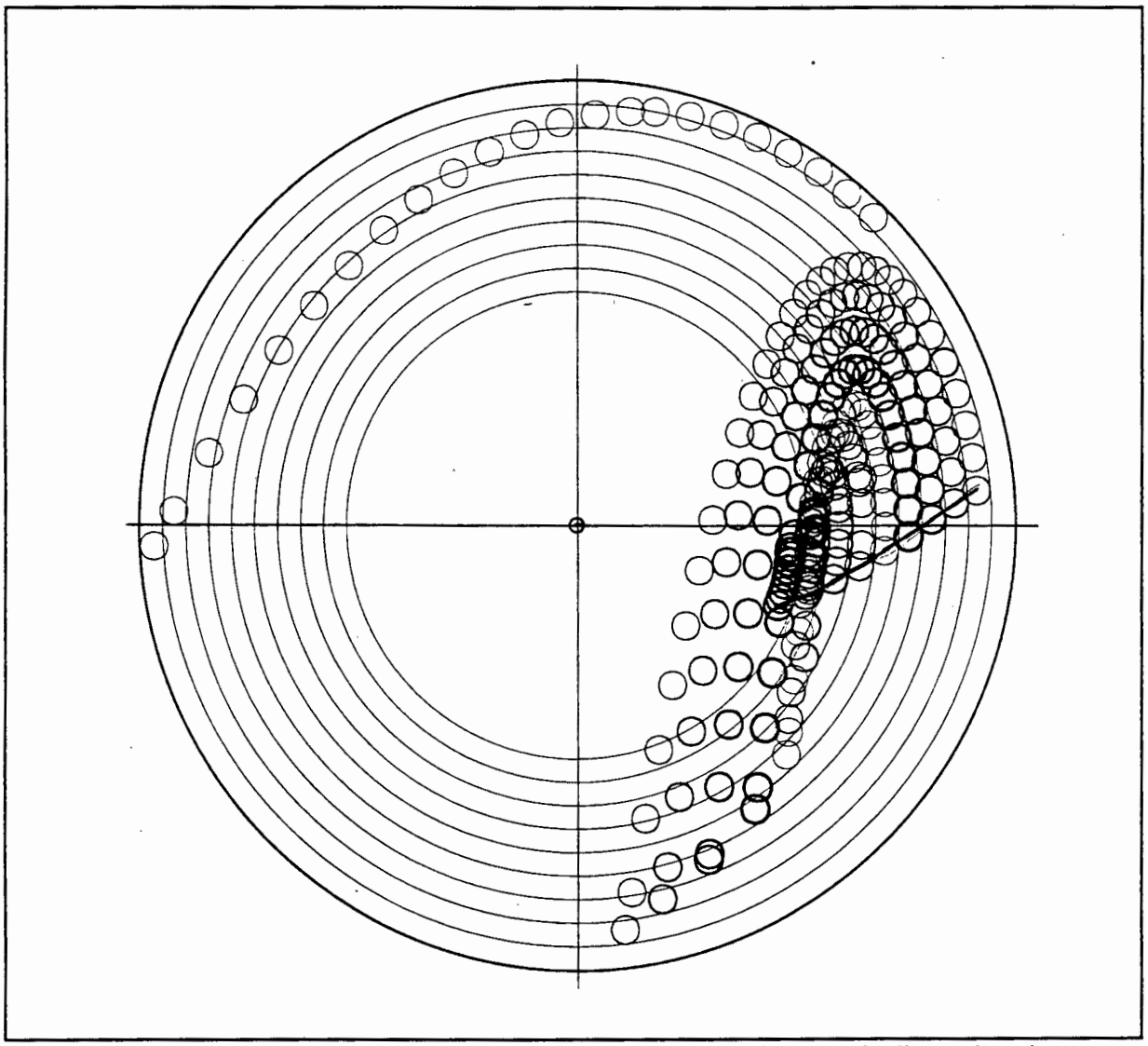

Figure 110. Predicted charge trajectories for run 17, for the ball resting between layers of balls

in Figure 109. The lower angle of incline of the cascading region as compared to the free-flight cataracting region, the interaction of the balls in the cascading region, and the far lower CoC than that predicted by the theory, show that a simplified theory that treats the balls as isolated from the surrounding layers gives an incorrect description of the charge motion. The simplified theory used for the predictions was an improvement on other theories that don't consider the ball to be resting on the balls below it. This shows conclusively that there is interaction of the balls between the layers, and that any theory that considers the balls to be isolated is incorrect.

In the theoretical plots, the first point in the trajectory for each layer is the point of equilibrium, i.e. the point at which the forces acting on the ball are in equilibrium, and the ball begins to move off the lifter. The line joining these points passes through the CoC of the charge, showing that the CoC is defined by the point of equilibrium of the innermost layer of charge.

CHAPTER 13
DISCUSSION

The charge motion and milling experiments are discussed separately for the sake of clarity. Supporting evidence for the arguments presented here is given in the analysis of the results, so is it not repeated in this section.

13.1 CHARGE MOTION

The motion of the media in a mill involves a complex array of interactions between a large number of particles. To analyze the motion, and obtain useful information from it, entails deciding what aspects may be useful, developing a technique to extract the information from the mill, and assessing which of the useful aspects can feasibly be analyzed from the information that is obtained. As with all experimental studies, the conclusions that are drawn are limited by the scope and accuracy of the data that are obtained from the experiments. It is important that cognisance is taken of these limitations so that the range of applicability and degree of certainty of the conclusions can be assessed. To this end, the degree of uncertainty and the errors in the experimental work have been discussed within the relevant sections. In the discussion the overall impact of the experimental limitations is taken into account, and the results assessed accordingly.

The motion of particles can be scaled-up without any distortion of the results. The motion occurring in a large production mill will be the same as that in a small model mill, providing the conditions are not changed. The first factor is to scale everything in proportion, for instance to a twentieth of the size, in the model mill. The second is to retain the same type of materials in the mill, so that factors such as the coefficient of friction and slurry viscosity are kept constant. The influence of the factors that cannot be retained at the values found in production mills, need to be assessed, and preferably built into any models. For instance, if the coefficient of friction cannot be held at a realistic value then if it is included in a model as a variable, and the value is determined independently of the tests, then the correct value can be inserted into the modelling equations.

The surface properties of the media could not be maintained, and the mill could not be run with a realistic slurry in the types of experiments that were conducted. The primary effect of these factors is to change the coefficient of friction between the grinding media in the mill. The slurry does not form a pool in the mill through which the balls flow, but rather a thin layer between the balls, so it introduces an 'effective' coefficient of friction between the balls. In the theory that was developed for the projection of a ball from a lifter bar, the only variable is the coefficient of friction between the ball and the lifter. When this is measured for the actual conditions in a mill, then the theory can be applied to production mills with confidence. For the bulk charge motion, no mathematical models were developed, so there is no technique for taking into account the friction between the balls. Although the friction changes the absolute values of factors such as the position of the shoulder, it does not affect the trends in the results, such as the effect of increasing lifter height. So although the experimental observations cannot be used to predict the absolute values of the interactions, the influence of milling variables such as speed and liner design can be assessed. In addition, the form of the charge motion and the relative scale of the interactions can be applied to production mills.

Charge interaction is used to refer to the relative movement between neighbouring balls that can result in size reduction of the ore. Balls moving closer together can slowly crush ore particles, balls sliding or rolling across each other can nip particles between them, and balls landing on a surface can crush particles.

13.1.1 Addition of a slurry

For some of the runs an artificial slurry was added to the charge, to obtain some indication of the effect of a slurry on the charge motion. The charge was found to slump considerably, as can be seen from the charge trajectories of runs 28 to 33. This degree of slumping is undoubtedly unrealistic, and was concluded to arise from the lubricating effect of the water and from the balls having a lower density than water. Liddell and Moys showed that addition of glycerine to a charge caused slumping[21]; this could be overcome by the addition of sand. The effect of the glycerine is to lower the coefficient of friction in the charge. So it appears that the ground plastic that was used

in the slurry for this work did not act as a friction enhancer, which was its intended purpose.

The density of the balls was 0.94 $g.cm^{-3}$, so they could in fact float. This was not expected to happen, as the water was only sufficient to fill the interstices between the balls. However, it appears that the water separated out from the balls to form a peripheral layer that the balls floated on. The balls near the core of the charge exhibited far more normal behaviour, so most probably had a thin layer of water and plastic grindings on them. Because of the abnormal behaviour of the slurry runs, they are not discussed in any detail. Reference is only made to them where it is felt that the slurry results may expand the understanding of the observed effects.

13.1.2 Position and shape of the charge

The form of the charge changes extensively as the speed of the mill is increased. The general structure of the charge body is described according to Figure 10. The photographs of the X-ray films (Appendix IV) provide excellent images of the general charge structure, with the intensity of the image reflecting the charge density at any point in the mill. As the mill speeds up the charge spreads out across the mill, reducing the average density of the charge body. The ratio of cascading to *en masse* charge, and the rate at which the charge circulates around the mill both increase with mill speed. This indicates that there is more interaction in the grinding media in the charge, so the grinding rate should increase with mill speed. However, when the speed is increased above 90% of the critical, a large portion of the charge begins to impact directly on the lining, and the core of the charge spreads out, so that there is no longer a cascading region. The interaction rate drops to about once or twice for each ball per revolution around the mill, and eventually the charge centrifuges and the charge interaction ceases altogether. So there must be a turning point in the plot of rate of production of final product versus speed of the mill. The location and magnitude of the maximum production rate will depend on the liner configuration and ore composition.

All of the media circulates around a central core, the centre of circulation (CoC) of the charge. This CoC uniquely defines the location of the charge. The charge body has a natural static angle of repose, which defines a minimum angle of repose for the charge. This is dependent upon the bulk charge friction, which is a function of media shape and surface roughness, and of the slurry viscosity. For the experimental conditions this minimum angle of repose was 30°. The low coefficient of friction between the plastic balls, in the range from 0.03 to 0.08, indicates that this natural minimum angle of repose will be greater for a real charge body. Rough measurements of the incline angle of the charge in production mills that are turning very slowly (while turning on a barring gear during relining), indicate a minimum angle of repose of 40 to 45°. The CoC is narrow in the radial direction, but elongated in the circumferential plane, often extending over a range of about 10°. This made it difficult to locate the angular position of the CoC, a problem which is reflected in the wide scatter of the experimental data. No trend in the angle of repose could be detected with changes in mill speed or liner profile. The radius of the CoC could be more closely determined, and over the range from 64% to 82% critical speed no significant variation could be detected from direct measurements. Unfortunately the charge is too dilute above 90% critical speed to locate the CoC, so the range of measurement was restricted to below a speed of 82% of the critical.

The plot of angular velocity of the ball as a function of radius from the centre of the mill should intersect the x-axis at the radius of the CoC of the charge, as the charge has zero angular velocity there. The plot of relative tangential velocity as a function of radius, Figure 112, shows this effect. Four distinct intercepts are apparent, the slurry runs at 66 mm, batch 2 at 53 mm, batch 1 at 44 mm, and the 68% of critical at 39 mm. The slumped form of the slurry profile gave rise to the high radius of the CoC for these runs. The difference in the radii between the two batches shows the strong influence of charge filling on the CoC. The layers of charge circulating close to the CoC represent a small percentage of the total charge, so a small change in the charge volume can change the location of the CoC by a significant amount. The radial locations indicated by the intercepts correlate with those from the direct measurements. What is indicated by the intercepts is that the mill running at 68%

critical speed does have a slightly smaller radius of location than at the higher speeds.

It is predicted that the radial location of the charge will start one ball layer below the charge surface, and then gradually move closer to the periphery of the mill as the mill speed increases. Beyond a certain speed the CoC will begin to move back in towards the middle of the mill, until at centrifuging it is located at the centre of the mill. This prediction could not be verified by the experiments. However, there is an indication that at 68% critical speed the radius of the CoC is smaller than at the higher speeds. Over the range of 64% to 82% critical speed there is little effect of either mill speed or liner profile on the location of the CoC. A factor that is significant is the mill filling: the radius of the CoC decreases markedly as the filling is increased.

The centre of mass (CoM) of the charge is independent of the CoC, and coincides with the average location of the ball, calculated over a whole revolution about the mill. As theoretically predicted, the radius of the CoM decreases with increasing mill speed, tending towards the centre as the charge centrifuges. Within the speed range from 68% to 82% critical speed the radius of the CoM coincides closely with the CoC, but above 82% the CoM rapidly moves towards the centre of the mill, as centrifuging of the charge becomes more dominant. The angular location of the CoM varies approximately linearly with mill speed. A linear fit to the average data yields a relationship of:

$$Angle(^{o}) = K = 27 + 0.42\,x speed(\%\,crit.) \qquad (33)$$

The intercept agrees well with the measured minimum angle of repose of 30°. There is a large scatter in the data from which this equation is derived, so it does not provide proof of a linear relationship between mill speed and angular location of the CoM, but rather indicates the trend. The angle of the CoM is 69° when the mill is running at 100% of the critical speed. Although the outer layer of charge is almost centrifuging at this speed the inner layers are far from centrifuging, so the CoM is not yet located at the centre of the mill.

The power drawn by the mill is commonly calculated by the simple torque-arm method. The mass of the charge is considered to be at the centre of the charge, and the torque is given by: $T = Mg.R.\sin K$

Where M is the total mass of the charge, R the radial location and K the angle of repose of the centre of the charge.

The major problem with this simple model is defining the location of the centre of the charge. A common interpretation is to join the toe and shoulder of the charge with a chord, and then calculate the centre of mass of a solid body of that shape. This simplification is reasonable at low speeds, but above 70% critical speed the charge becomes spread out, and the shape very different from a solid segment. The power calculations using this simplification do not predict a peak power draw, as discussed by Liddell and Moys[21]. A far more realistic technique for interpreting the shape of the charge was used by Vermeulen[19]. He considered all the charge to be in the *en masse* region defined by the free surface of the charge, the BHF surface. But this also failed to produce correct predictions of the power draw. Attempts have also been made to account for added lift and stickiness arising from the pulp[25]. However, all these proposed techniques consider the entire body of the charge to be located within the *en masse* region of the charge. This is an invalid assumption, and the error introduced thereby increases dramatically as the degree of cataracting increases at higher speeds. If the actual location of the CoM of the entire charge is used, this must surely yield a more accurate prediction of the power draw. The linear function of K obtained in the experimental work, combined with the decreasing value of the radius of the CoM, predicts a peak in the torque of the mill at about 85% critical speed. Thereafter the torque drops rapidly with the rapidly decreasing radius of the CoM. Figure 111 gives the curve for torque as a function of mill speed, which is derived from the approximate function for the angle of repose of the CoM, eqn.(33), and the average radius of the CoM, Figure 31. The initial radius of the CoM, when at rest, is 45.8 mm. This is derived by integrating the torque arm over the charge mass. The form of the derived curve is the same as that measured by Liddell and Moys[21] for a charge filling of 40% and with a sand slurry in the mill. The power draw is proportional to the mill speed, so the power peak curve will be a steeper function than the torque peak.

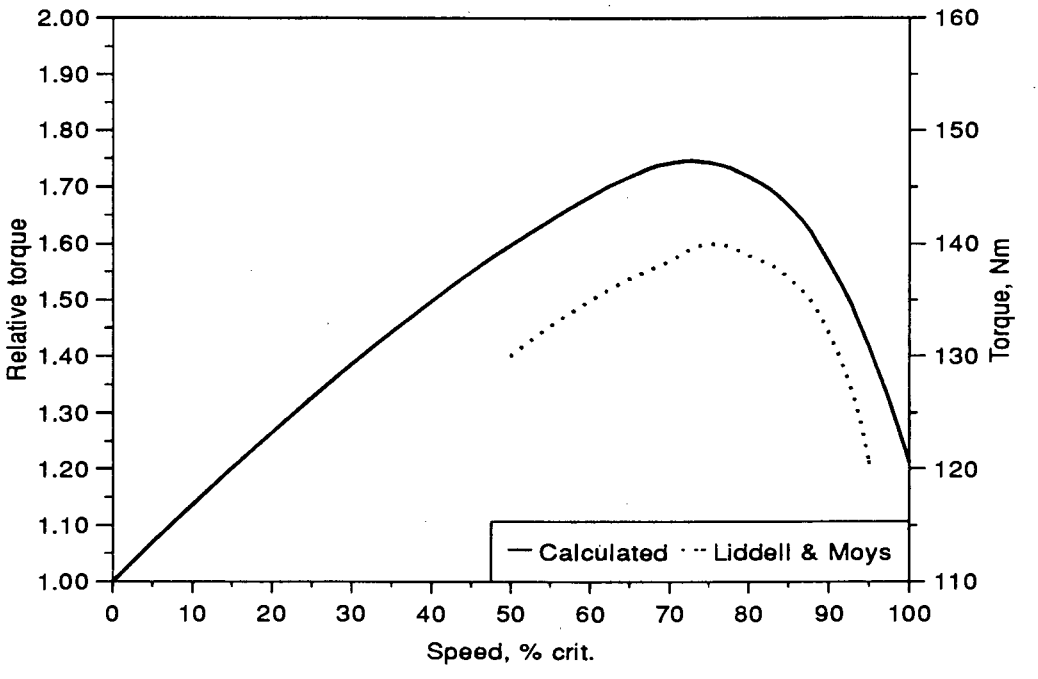

Figure 111. Curve of torque as a function of power, as predicted by use of the CoM of the charge

13.1.3 Slip of the charge

There can be slip of the charge against the liner, and slip between layers within the charge. The relative angular velocities of the balls, as a function of the radius from the CoC, reveals the degree of slip. Multiplying the angular velocity by the radial displacement of the ball yields the tangential ball velocity. The steeper slope of this graph assists in locating the radius of the CoC. Morrell[27] has reported that such a plot yields a straight line passing through the CoC, but this graph is only linear beyond a radius of about 70 mm. Near the CoC the velocities drop off sharply. The run with a slurry behaves quite differently. Near the CoC there is a linear relationship between the tangential velocity of the balls, and the radius. But beyond a radius of 85 mm there is a wide scatter in the ball velocities, indicating surging and fluctuating slip of the charge. However, as discussed earlier, the slurry formed an unrealistic set of conditions in the mill. It is therefore possible that a real charge would have a linear relationship between the tangential velocity and the radius, as reported by Morrell. It

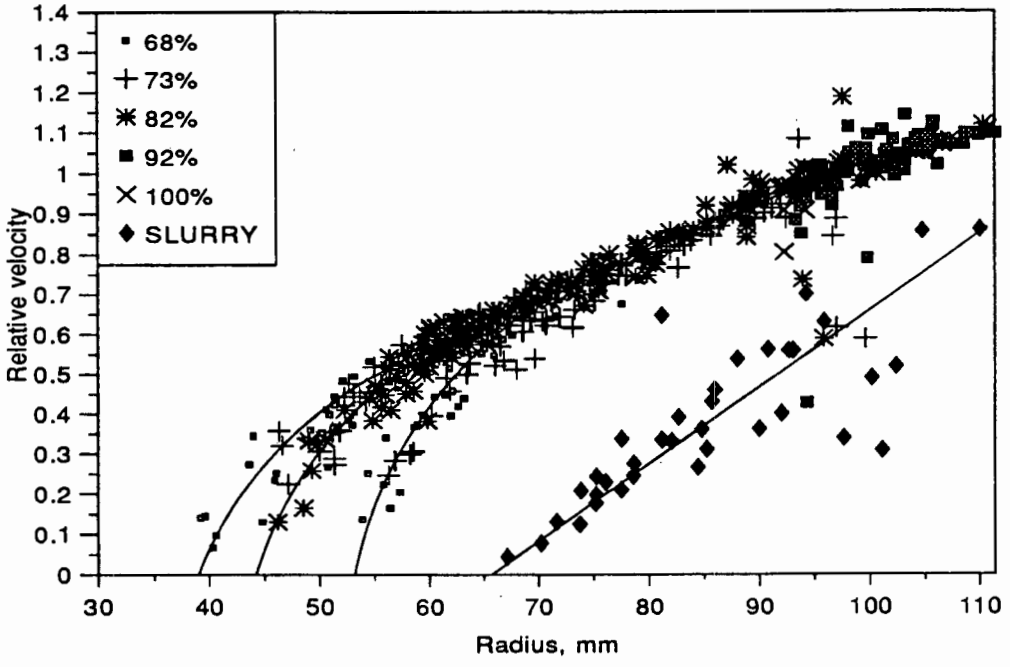

Figure 112. Relative tangential velocities of the balls, as a function of radius from the centre of the mill

must be borne in mind that Morrell's observations were made on the charge against the window of the mill, so they would have been subject to the end-window effects.

No influence of lifter height or face angle could be found on the degree of slip in the charge. Even the smooth lining had the same effect as the lifter bar linings, except possibly at 68% critical speed, where there seemed to be a bit more slip near the centre of the mill for the smooth lining, as shown in Figure 113. It also appears that the 10 mm lifters result in slightly less slip near the centre of the mill. But these observations are not conclusive.

The amount of slip between the liner and the charge has a direct influence on the transfer of energy to the charge. All the lifter linings and the smooth lining were effective at preventing slip on the lining over the tested speed range. It should be noted that the smooth lining has a flat profile, but a rough, high-friction surface. Fahrenwald and Lee[7] found that the introduction of a slurry reduces the coefficient of

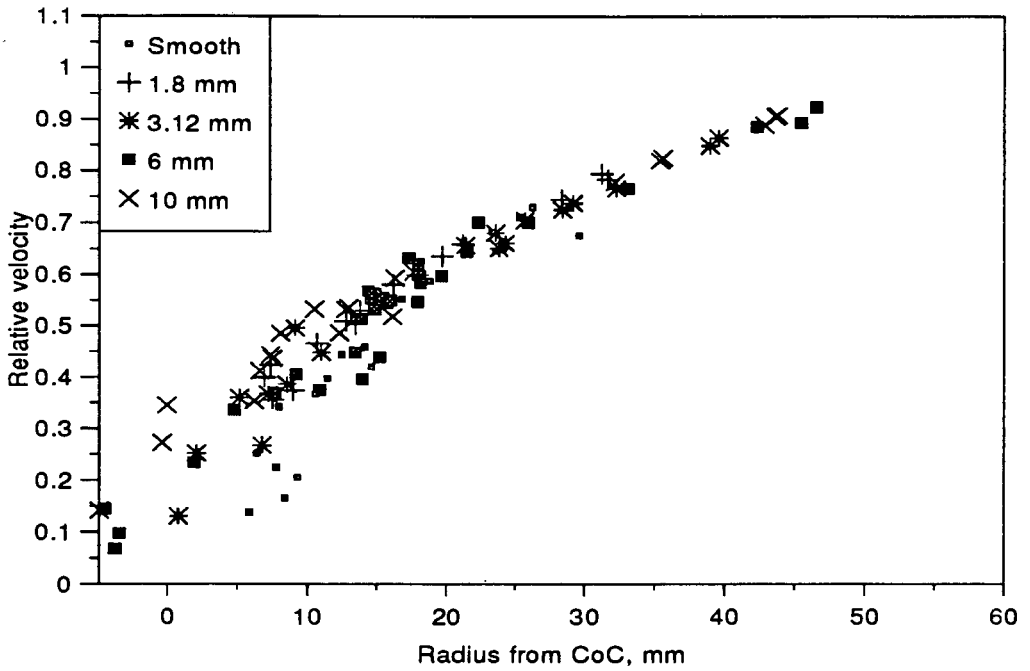

Figure 113. Relative tangential velocity of the balls for 68% critical speed

friction between metal surfaces, and would thus promote slipping of the charge. Circumferential grooving of flat grid liners has been observed during the course of this work on gold mine ball mills, indicating that there can be slip of the charge in production mills with flat linings, showing that a smooth lining is not necessarily adequate for the efficient transfer of energy to the charge.

Vermeulen[22] found that if there was slip between the liner and the charge, then the motion throughout the charge was quite different to that of a keyed-in charge. The curve of angular velocity as a function of radius (Figure 35) is of the same form as that found by Vermeulen for the mill fitted with lifter bars (Figure 4). The amount of slip within the charge is almost independent of the design of the lining, once the charge is keyed in to the rotary motion of the mill.

13.1.4 Angle of incline of the cascading region

The angle of incline of the cascading region is different to that of the cataracting region. The balls in the cascading region tumble down over the inner layers of balls.

The incline angle of the cascading region is independent of the speed of the mill and the liner configuration. At high speeds the average incline angle of the descending balls is substantially decreased, but this shallower angle does not apply to the balls that are cascading, only to the cataracting portion that is impacting high up on the mill shell. The angle of incline appears to be determined by the natural angle of incline of the charge. The angle of repose of the charge was also found to be independent of mill speed over the range of speeds investigated. The average angle of repose varied between 50 and 55°, and that of the cascading region between 55 and 60°. When the tumbling action of the balls at the CoC is considered, Figure 114, the angle at which the balls tumble down is found to be steeper than the tangent to the CoC. Thus it appears that the angle of incline of the cascading region is determined by the angle of repose of the charge. This explains why models of charge motion that do not consider the interaction between the layers of balls yield incorrect predictions of the form of the cascading region.

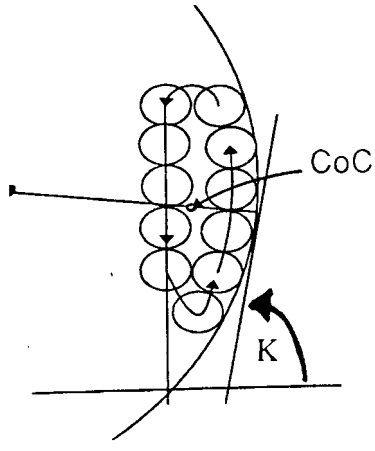

Figure 114. Cascading angle of balls at the CoC

13.1.5 Acceleration in the cascading region

Interaction between balls in the cascading region reduces the acceleration of the balls from free fall, g, to some value, Acc. The difference between these values gives a measure of the force of interaction between the balls. As would be expected, the balls in the cataracting region had an acceleration of g. The outer layers of the cascading region are also almost in free-fall; from about halfway into the charge there is extensive interaction between the balls; and the acceleration drops off to close to zero at the CoC. There is a very wide scatter in the values of the acceleration, but this is to be expected for the random, multi-body interactions that occur in the cascading region of the mill. The lower the acceleration of the balls, the higher the interactive forces, and the greater the likelihood of grinding taking place in the region.

13.1.6 Impacting in the toe region

After a ball has descended in the cataracting or cascading region, it impacts on the toe of the charge, or possibly directly on the mill liner. This impacting accounts for the highest energy interactions in the mill, and is responsible for the crushing or fracturing of the larger ore particles (3 - 300 mm). The highest energy impacts occur when the ball is projected into free-flight from the shoulder of the charge, and cataracts directly onto the toe of the charge. If the ball tumbles down the cascading region, interacting with other balls *en route*, then it will have a far lower impact energy when striking the toe region. Thus it will be less effective at carrying out the crushing of larger ore particles.

The impact energy gives a measure of the amount of work done during the impact, and the impact force reflects the peak stress applied by the impacting ball. The tougher and the larger particles require a certain minimum stress to fracture them, and this is determined by the impact force. If the impact force is not sufficiently large, then these particles are not fractured; instead they have to be gradually abraded away, which is an inefficient form of size reduction.

As would be expected, the impact energy and the impact force increase as the radius of impact increases, as this allows a greater height of fall of the ball, and in the outer layers of charge the ball has less interaction with other balls as it falls to the toe. The impact energy is approximately proportional to the radius of impact. However, a considerable proportion of impacts at the periphery of the mill have a low impact energy, Figure 50. This occurs for impacts directly onto the shell, where the shell is travelling in a similar direction to the ball, so the energy transfer is low. This occurs primarily for the high speeds, where cataracting onto the shell is more likely than at lower speeds. Impacts on the shell are counter-productive, as they wear out the mill lining and do no work on the mill charge, except possibly for breaking the large grinding media in an autogenous mill. During the course of this work a lining has been inspected in which the rear face of the lifter was heavily peened and more worn than the leading face, as a result of direct impacts by balls

The impact force has a sub-linear relationship with the radius of impact, Figure 55, unlike the impact energy, which has a linear relationship. This is expected, as the impact force is proportional to the change in velocity, ΔV, and the impact energy is proportional to ΔV^2. This also explains why there is not as significant a reduction of the impact forces (Figure 54) as there is in the impact energies, near the mill periphery. The impact force depends primarily on the distance the ball falls, hence the strong correlation of impact force to radius of impact.

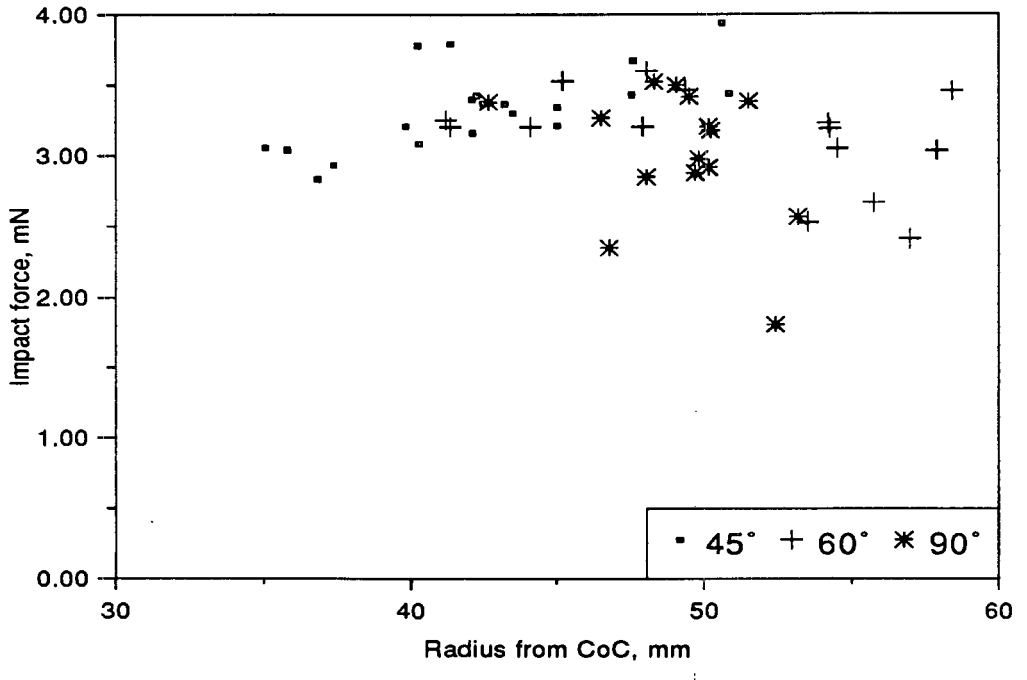

Figure 115. Impact force of the ball as it lands in the toe region, 92% crit. speed, 6 mm lifters

There is no definite trend reflecting the influence of mill speed or lifter height on the impact energies, or impact forces. However, for the higher speeds there is a greater proportion of impacts at the outer radii, hence there is a greater frequency of high impact forces than for the slower speeds. Figure 115 shows the variation of impact force with radius from the CoC, for the mill running at 92% critical speed, with different angle lifters, all 6 mm high. The lowest radius of impact is at 35 mm from the CoC, and the impact forces range from 2.5 to 4 mN, which is in contrast to the range of impact forces for the lower speeds (Figure 54). This illustrates the effect of the large proportion of high impact forces. The 45° lifters produce the highest impact forces,

almost 4 mN, and the impacts closest to the CoC. At this speed of 92% of critical the 45° lifters drop the balls onto the toe of the charge, which gives the balls the greatest height of fall, and hence the highest impact forces. As mentioned earlier, it is far more desirable for the balls to land on the toe than on the mill shell, so the 45° lifters also result in more effective impacts. The same effect was observed for the mill running at 73% and 82% critical speed, but for 60° lifters. This is in accordance with the predictions of the charge trajectory theory, that a lower angle lifter bar is required at higher speeds, if an acceptable point of impact is to be maintained. The influence of lifter angle on the point of impact of the outer balls, and on the maximum impact force, indicates the importance of installing lifters of the correct face angle for the operating speed of the mill.

13.1.7 Work done by the ball

The work done by the ball is a measure of the amount of energy transferred by the ball to the charge as it tumbles down the cascading region and into the toe region. This includes the energy transferred during the impact at the toe region, as discussed earlier. The impact energies range up to 0.07 mJ, and although a large portion of the values for the work done by the ball are below 0.1 mJ, the work values range up to 0.6 mJ. So although the single impacts at the toe may account for the majority of the work done by the ball in some instances, in the main more work is done by the ball in the cascading region; or just after impact in the toe region, as the ball is drawn into the rotary motion of the mill.

There is a peak in the amount of work done by the ball, which occurs at a definite radius from the CoC. The maximum value, and the radius at which it occurs are summarised in Figure 116. In general the radius at which the maximum work values occur increases with mill speed. Up to 82% critical speed the maximum work values occur close to the CoC, mainly in the range of 10 to 20 mm from the CoC. This shows that the majority of energy is dissipated near the core zone of the cascading region, where the balls were shown to have the most irregular motion. This also corresponds to the region where the acceleration gradient across the layers of balls is the steepest. As can be seen in Figure 47, the rapid decrease in accelerations, from 8 to 2 $m.s^{-2}$

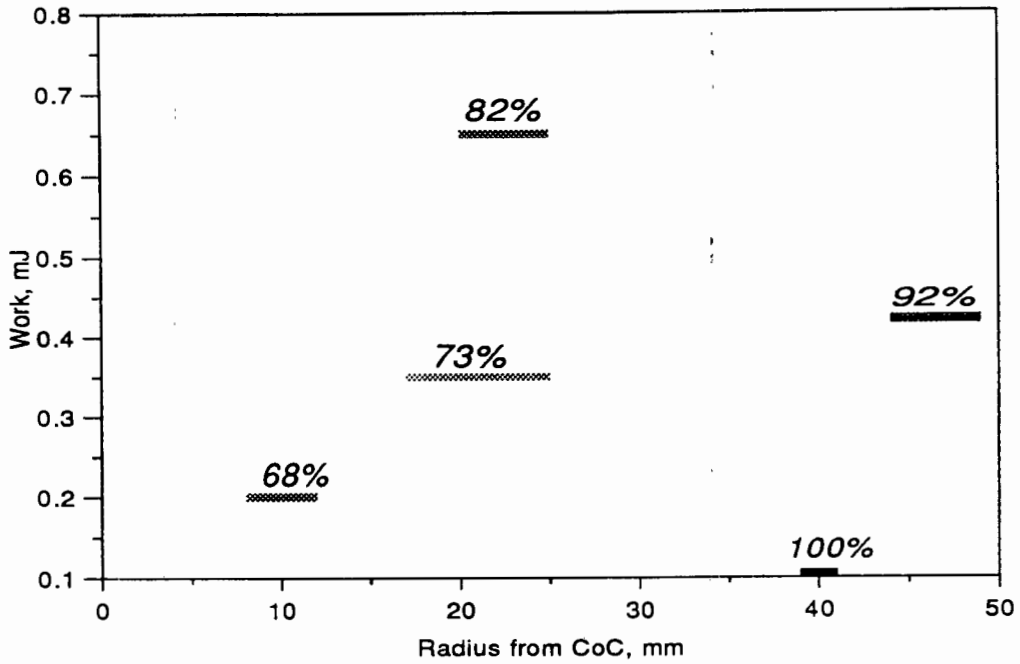

Figure 116. The maximum values of the work per revolution, and the radii at which they occur, for different mill speeds.

occurs from 25 to 5 mm from the CoC. So this region has the most active interaction between the layers of charge, and would be expected to account for a large portion of the grinding. The charge pressure is also greater here than in the outer cascading regions, where it may actually be too low to initiate grinding of the particles. In the outer cascading regions there is little interaction of the balls, so little work is done. The total amount of work done is made up of many interactions, and as the maximum energy of impact at the toe region is about a tenth of the total work done, and this value must be considerably greater than the energy of individual impacts in the cascading region, it follows that the work done by the ball takes place over 20 or more interactions. The maximum value of the work done peaks at 82% critical speed, which implies that in the neighbourhood of this speed the most work is done on the charge per revolution. The average values of work per revolution of the ball are shown in Figure 117. The total amount of work done on the charge is dependent upon the rate of revolution of the charge. The degree of slip of the charge was found to be independent of the mill speed or liner configuration, so the rate of revolution of the charge is proportional to the speed of the mill. The mill running at 92% of critical

speed rotates 0.12 more per unit time than at 82% critical speed. If the rate of revolution of the mill is taken as unity for 82% critical speed, and the 0.12 increase for the mill running at 92% critical speed is introduced, the same work rate for the two speeds is obtained. The other speeds, 68%, 73%, and 100% of critical, have considerably lower work rates.

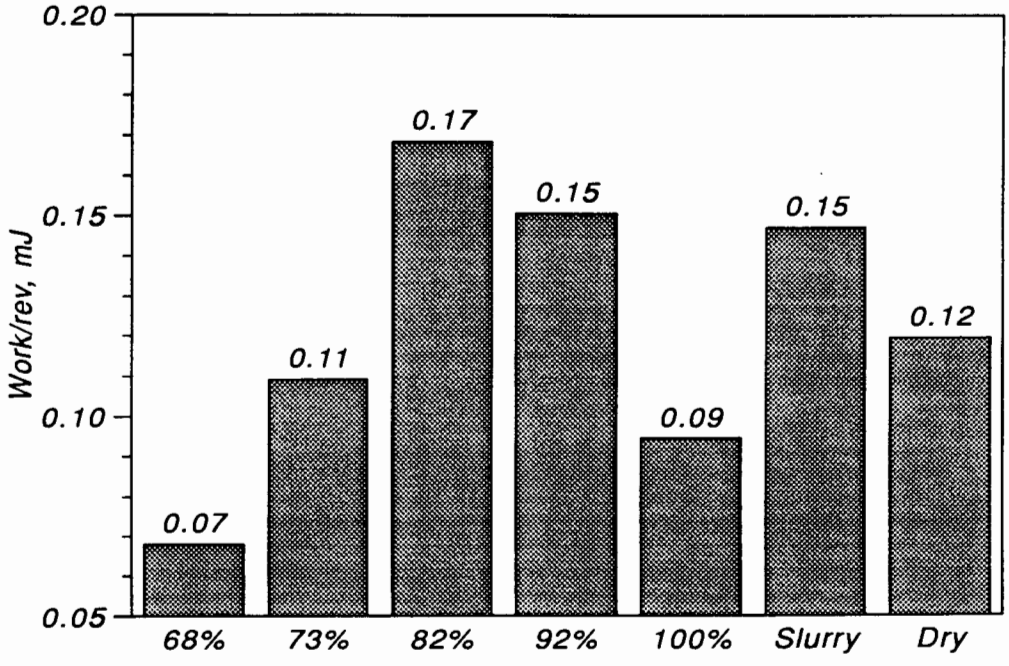

Figure 117. Average work per revolution of a ball, for all conditions

The face angles of the lifers have a distinct influence on the work done per revolution. At 68% critical speed the 90° lifters account for the maximum work. As the speed rises to 73% and 82% of critical, the 60° lifters yield the maximum work, and at 92% critical speed the 45° lifters account for the maximum work. These face angles correspond with those found to result in the highest impact forces, so there is a consistency in the favourable face angle of the lifters.

13.1.8 Radial segregation of the balls

There is a definite correlation between the size and mass of a ball, and its radial location in the mill. The radial location is taken as the ball's location when in the *en masse* region. A large ball, with a similar mass to the balls in the bulk charge (as used in the gamma camera filming), segregates very distinctly. At 64% critical speed such

a ball was found to have a more than 90% probability of being in the range of 78 to 90 mm from the centre of the mill (which has a 95 mm radius). At 73% critical speed it had a 70% probability of being in the range of 72 to 84 mm. It also had a 13% probability of being located in the 12 mm wide bands on either side of this. So its radial location was slightly closer to the centre of the charge, and also less well defined than at 64% critical speed. At 82% critical speed the ball had a 95% probability of being within a 12 mm band centred about 55 mm.

At 64% critical speed, the ball is firmly located at the periphery of the charge. As the speed increases to 73% of critical, the ball moves in slightly and has a slightly wider radial distribution, and at 82% critical speed it is firmly located near the centre of the charge. So in the range of about 75% to 78% of critical speed there is a 'neutral' speed, at which there is no radial segregation by ball size.

The average radial location of the charge shown in Figure 44 does not reflect the middle of the charge, as it is the average of the data collected from 'abnormal' balls, i.e. not from balls that constitute the average ball in the charge. The location of the *en masse* charge lies in the radial range from the CoC to the periphery of the mill. For speeds up to 82% of critical, the radial location of the CoC did not vary much and was at about 45 mm. So the middle of the charge lies at about 75 mm, and the quarter-way marker is at 60 mm, from the centre of the mill. The volume of charge contained within each quarter segment of charge increases substantially as the radius increases, approximately proportional to r^2. Using the average radius within each segment, the following ratios of charge volume are obtained for each successive quarter-segment: 12%, 19%, 29%, 40%. So for a ball residing in the inner quarter-segment, it is actually restricted to 12% of the charge volume.

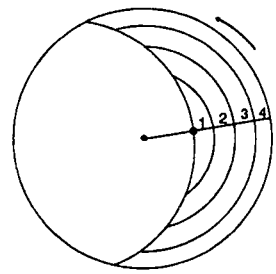

Figure 118. Division of the charge into quarter-segments

The mass of the balls induces a distinct radial segregation of the charge. Heavy balls, of the same size as the balls in the bulk of the charge, reside near the centre of the charge at speeds below 82% of critical, and the heaviest ball is nearest the centre. At 92% critical speed all the balls are evenly distributed throughout the charge, and at 100% critical speed the heavy balls are located at the very periphery of the charge.

This effect can be observed in the influence on the product size distribution of the addition of balls to a mill. When balls are added to a high-speed mill the large rocks are ground more rapidly, and the distribution below 12 mm coarsens, as was observed by Jackson[40] on mills running at 91% of critical speed. However, when balls are added to a slower mill, the larger rocks are not reduced and the minus 25 mm material becomes finer[41], as was observed on a 6 m diameter mill running at 77% of critical speed. These observations imply that at high speeds the balls are near the periphery of the mill, and promote impact crushing, and at lower speeds the balls are near the centre of the charge, and carry out attrition grinding.

The small, light ball (glass bead) resides in the third quarter, just outside the middle of the charge, at 82% critical speed and below. At higher speeds it resides in the middle of the charge. The location of the ball reflects the resolution of two conflicting forces. As a small ball it is inclined to move to the inside, but as a light ball it should move to the outside of the charge, at low speeds. As the speed increases the two tendencies swop direction, so the ball remains near the middle of the charge.

The small, heavy ball (small steel ball) resides just within the middle of the charge at low speeds, but at 82% critical speed it is firmly located at the very periphery of the charge. This again reflects a balance between the opposing trends of size and mass segregation. The transition in the size segregation occurs in the speed range from 73% to 82% critical speed, resulting in the small ball having a tendency to move to the outside of the charge, and the transition in mass segregation occurs between 82% and 92% critical speed; this also drives the ball to the outside of the charge. So at 82% critical speed the small heavy ball has an overwhelming tendency to be located at the very periphery of the mill.

There were insufficient data available to carry out a quantitative analysis of the influence of lifter height and face angle on the segregation of the charge. However, a qualitative analysis revealed that the design of the lining does appear to influence the segregation of the charge. At slow speeds the heavier balls are concentrated progressively closer to the CoC as the lifter angle is increased from 45 to 90°. This effect is stronger for the higher lifters. Increasing the height of the lifters seems to accentuate the charge segregation. It also seems that when the mill is run close to the 'neutral' speed, where transition to the opposite trend occurs, an increase in the lifter height can change the radial segregation altogether. These observations are not substantiated, but indicate that liner design could be used to manipulate the radial segregation of the charge.

The essence of this segregation is that at low speeds the large particles segregate to the outside of the charge, and the small particles consequently move to the inside of the charge. At high speeds the trend reverses. The 'neutral' speed, at which there is no segregation by size, is around 76±2% of critical speed. Segregation by the mass of the balls seems to occur quite independently. The heavy balls segregate to the inside at low speeds, and to the outside at high speeds, and light particles consequently have the opposite trend. The 'neutral' speed at which there is no mass segregation occurs around 92±4% critical speed.

The phenomenon of charge segregation has been observed by other workers[5,6,7,24] in the field of milling, and has been extensively studied in the field of mixing different components[42]. All these observations were through the end windows of mills (except for some mechanical segmenting of the charge at very low speeds carried out by Nityanand *et al* [42]). The present work confirms for the first time that the effects discovered occur throughout the charge, at speeds used for milling ores. The influence of liner geometry has also not been observed previously.

The explanation of Nityanand *et al* [42] applies to very slow rotation of the mill, below a few per cent of critical speed, and to size segregation only. The basis is that the voidage between balls is greater in the cascading region than in the *en masse* region,

so small particles can percolate through the cascading region towards the centre of the charge. This percolation effect seems unlikely to occur to a significant degree at the higher speeds used in milling. Although higher mill speeds were not investigated in detail, a general explanation of the reverse segregation occurring at high speeds was given. It was concluded that this arises from the smaller particles having a higher critical speed for a given speed of rotation of the mill, because of their greater displacement from the centre of the mill. This higher critical speed induces them to move to the outside of the mill. The explanations of Rogovin and Herbst[24] were based primarily on the end effects of the mill. In a short mill with substantial end lifters, the end effects are strong and result in longitudinal as well as radial segregation. With the greater length-to-diameter ratio of the mill and the smooth end windows used in the present work, the end effects were not dominant in producing the charge segregation.

It is proposed that the larger the ratio of ball size or mass to that of the average balls, the stronger the segregating forces, and the more definite the radial location of a ball. This is seen for the steel ball, which is heavier than the marked bead, being closer to the centre at slow speeds and closer to the periphery at high speeds, than the bead. The large bead used in the gamma camera filming had a substantially larger diameter (9.2 mm) than the average ball size (6 mm), and segregated very strongly.

The mass and size effects have different 'neutral' speeds. The 'neutral' speeds should not change with changing ratios of ball size or mass to the average ball. Although the strength of the segregating forces decreases with the reducing ratios, the forces remain in the same direction. The importance of changing the ratios, is found when both the mass and size ratios change simultaneously, for instance with larger rocks in an autogenous mill. The effects of increasing size and mass operate in opposing directions of segregation, so the relative ratios will determine the radial location of the rock.

A fundamental law of nature is that any body will strive to be in the lowest possible energy state that it can achieve. This is likely to be responsible, to a large degree, for the charge segregation. To achieve the lowest energy state of the charge as a whole,

the heaviest balls must segregate to the centre of the mill, where the amount of work done in lifting them per revolution is at a minimum. At a given radius the centre of mass of the large balls is closer to the centre of the mill than the small balls. So it is energetically favourable for the larger balls to be located near the periphery of the mill, as the centre of mass does not have to be moved quite as far as for the small balls, for each revolution of the mill. These conditions apply at lower speeds. When the speed of the mill is increased a second factor comes into play. This factor is thought to be the centrifugal force acting on the ball.

The centrifugal force is = $m\Omega^2 r$
where m = mass of ball, Ω = angular velocity of the ball, r = radial location of the ball

At higher speeds the Ω^2 factor begins to dominate the energy factor, as the mill begins to act as a centrifuge, and the heavier balls move to the outside. This only occurs at speeds above 90% of critical, when the centrifugal force becomes very high. The centrifugal force is also stronger for small particles, as they have a larger radial displacement at a given radius, so the small particles move to the outside at high speeds.

A factor in considering this explanation of charge segregation, is that the density of the media is intrinsic to the mass of the ball or rock. Low density media would have the opposite segregation trend to high density media.

To firmly establish the reason for the charge segregation and to model the relative influences of the opposing forces would require a thorough body of research to be carried out. This would have to include varying the size, mass, and density of the balls over a full range of mill speeds. The radial distribution of the media is an important factor in optimising the efficiency of a mill. If the large or heavy media, responsible for carrying out the impact crushing of ore, is located at the centre of the mill charge, then it will be ineffectual. The same argument applies to small media located at the periphery of the mill. If the balance of the forces responsible for the radial segregation of the charge can be modelled, and therefore predicted, then the composition of the

media and the milling parameters can be designed to optimise the location of the media.

13.1.9 Rotation of the ball

A bead was marked for tracking by inserting a lead rod down the centre. This also allowed the rotation of the ball about its centre to be followed with ease, as the ball was carried up by the rotary motion of the mill and then tumbled down the cascading region. Figure 119

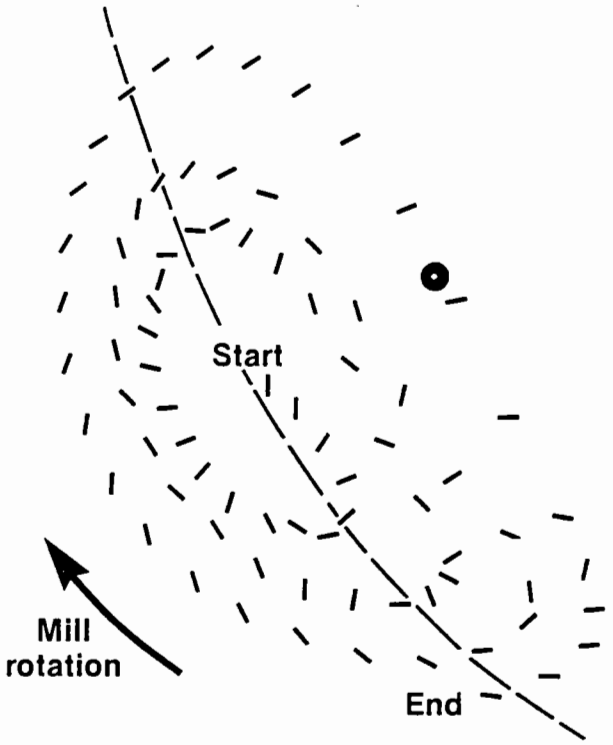

Figure 119. Rotational motion of a ball in the mill

illustrates the typical motion of the ball as it travels around the mill. The ball does not rotate about its own axis in the *en masse* region, and there is very little rotation in the cascading region. The only regions of rotation are the shoulder, as the ball rolls off the top of the charge, and the toe when the ball impacts and bounces. In general the ball rotates approximately once about its own axis for each revolution about the mill, so relative to the rotating charge mass, the ball barely rotates. The non-rotation of the ball in the *en masse* region is readily explained by the illustration in Figure 120. The frictional force between the mill shell and the balls in the outermost layer induces them to rotate in a clockwise direction. This rotation must in turn induce an anti-clockwise rotation of the second layer of balls. However, the balls within a layer cannot all rotate in the same

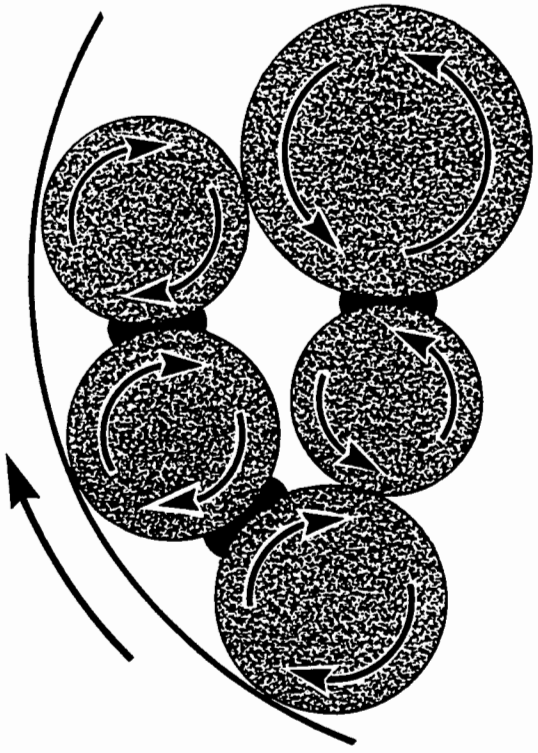

Figure 120. The locking together of balls in the charge

direction, as their contacting surfaces would then be moving in opposite directions, as indicated at the darkened contact zones. This force is at least equal to, and opposes, the propagating force at the mill shell interface. Thus any rotary motion is effectively prevented in the *en masse* region of the charge. In the cascading region the same type of situation holds. Although the balls within a layer spread out as they begin to descend in the cascading region, they are still trapped between the layers on either side of them. The balls must in fact slide down the cascading region. Only in the cataracting region are the balls actually free to rotate, and even so very little rotation of these balls is observed.

This non-rotation of the balls indicates that grinding does not take place by rotary nipping of the ore particles. Instead the particles must be caught in a shearing force between the balls.

13.1.10 Longitudinal motion of the balls

The side view of the mill did not yield very accurate data on the longitudinal location of the balls, because of the distortion introduced by the magnification factor, and the fact that the mill could not be centrally located around the X-ray beam. However, the general longitudinal motion of the balls could be easily observed. Most notable was that there was not a substantial degree of longitudinal motion in the 3 second duration of the run. The coloured balls in the charge, when their positions are observed, are seen to migrate along the length of the mill; this shows that longitudinal mixing does take place. Figure 121 shows an exceptionally active ball. The ball starts near the middle of the mill, then moves rapidly to the front of the mill in about a fifth of a second, and then spirals outwards back towards the middle of the mill.

13.1.11 Charge mixing

The charge displays a tendency to spiral in and out from the CoC, as illustrated in Figure 122. This type of spiralling action was noted in over 30% of the trajectories that were tracked, and was predominant in the inner half of the charge. The spiralling was not noted in the mill running at above 90% critical speed, but occurred in over 40% of the trajectories at speeds below 90% of critical. This action takes the form of a

smooth, continuous spiral: the ball does not suddenly jump or shift randomly between layers. As a ball cannot act independently of the balls surrounding it, this implies that all the balls in that region are also spiralling in or out. For this to occur there must be a flow of balls into the centre of a region that is spiralling outwards, and away from the centre of a region that is spiralling inwards. This action must in turn set up a longitudinal flow of balls within the mill, as sketched in Figure 123. This was not observed to occur in a continuous steady-state manner, but rather in brief spurts, lasting four to six revolutions of the ball, that is about 3 seconds. This is similar to the transient whirlpools and eddies in a river. Attempts were made to try and test this dual-spiral hypothesis by correlating the spiralling action with the longitudinal motion of the ball seen in the side views of the mill. However, in the brief 3 second duration of each run, there was generally very little longitudinal motion of the ball. For a full double spiral action to be observed, the side view would have to last for about 6 seconds. The strongest evidence in support of the hypothesis is the side view given in Figure 121. The ball starts in the middle of the mill and moves rapidly to the front along a path at a radius of about 20 mm. It then spirals back out to a radius of over 60 mm, while moving back to the middle of the mill. The run stops at that point, so it does not provide conclusive evidence of the proposed double-spiral action. This means that the hypothesis has not as yet been verified.

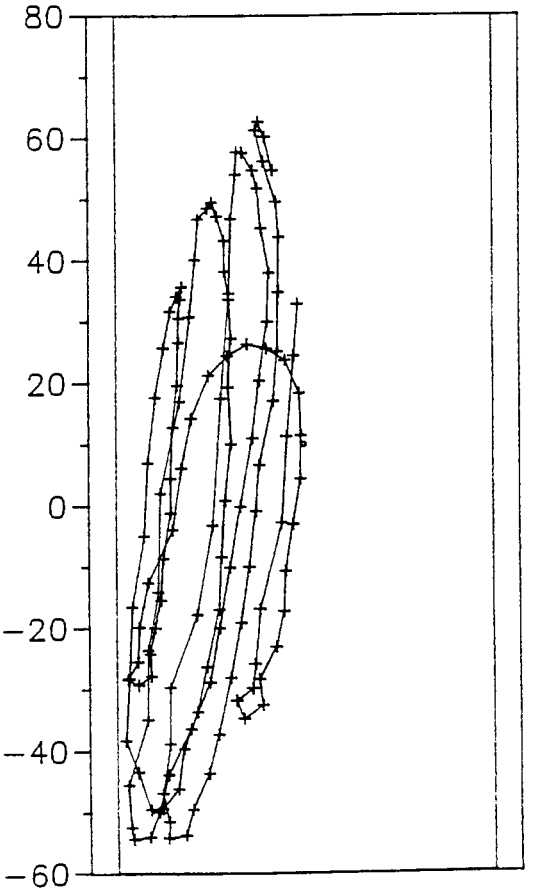

Figure 121. A sideview of the mill, showing the longitudinal and spiralling motion of the ball

The smooth action of the balls in the bulk of the charge does not occur at the CoC, where the paths are irregular and frequently cross over themselves, as shown in the enlarged view of the CoC in Figure 124.

The observed motion of the balls indicates that good natural mixing of the charge takes place in a rotary mill, even when run in batch mode. The exception to this is the radial segregation of a ball or media that is substantially different in size or mass to the average media in the mill.

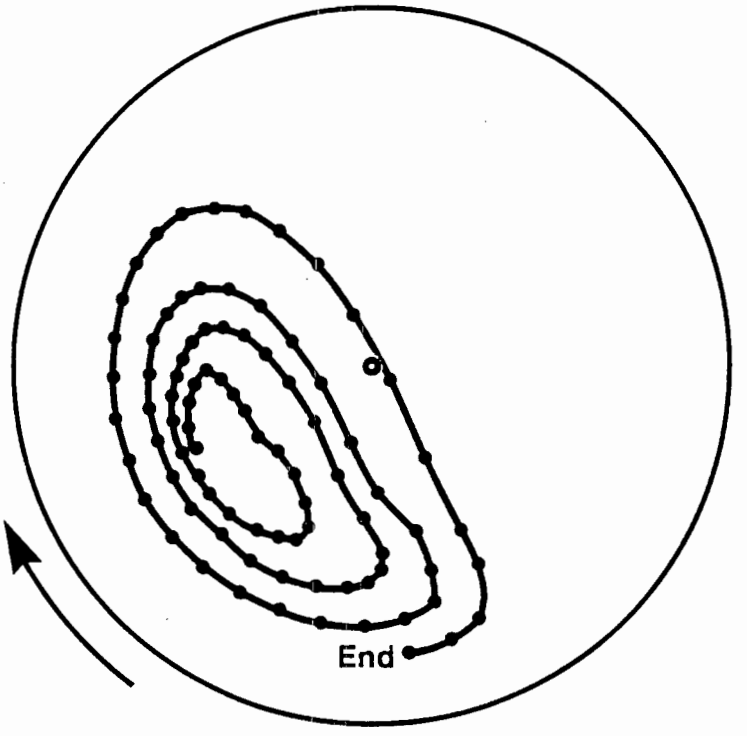

Figure 122. Spiralling action of a ball, over two revolutions of the mill

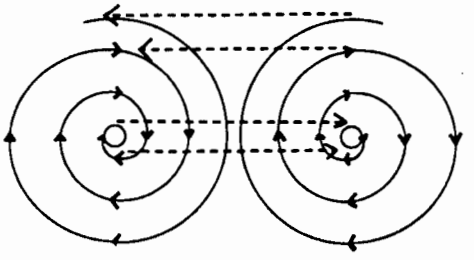

Figure 123. The proposed double spiralling effect in mills

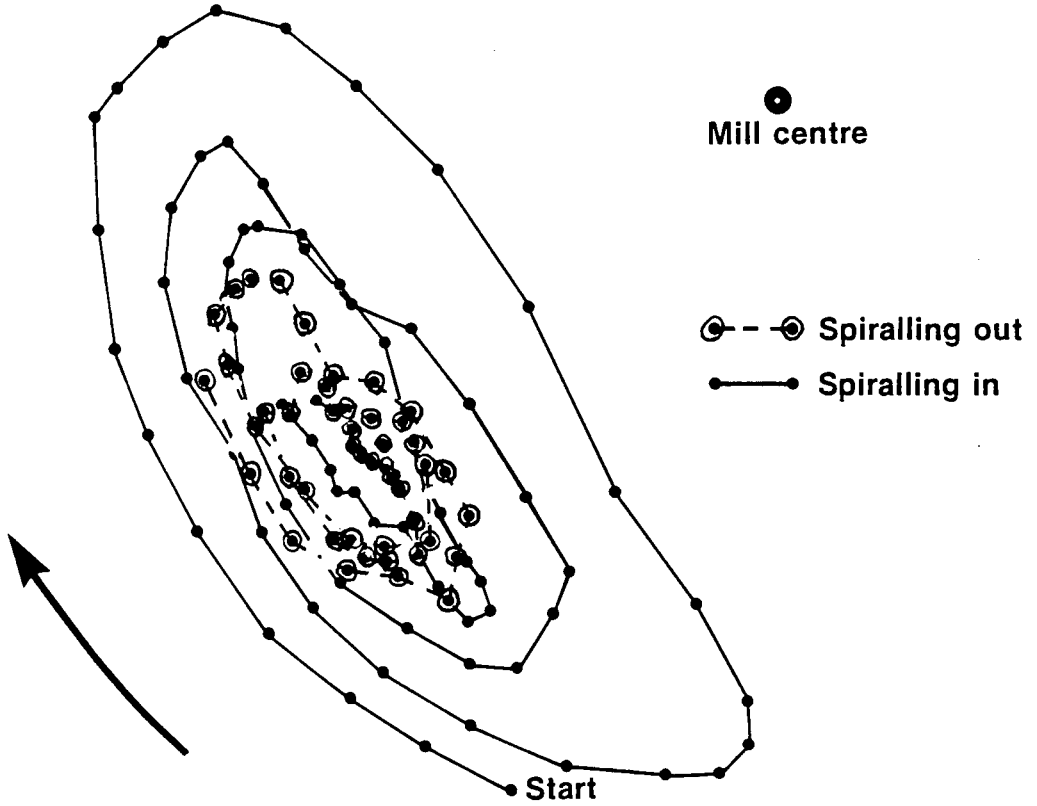

Figure 124. Inward and outward spiralling of a ball, and the uneven charge motion near the CoC

13.2 MILLING TRIALS

The results for the two different sets of tests are discussed separately. It must be borne in mind that the first set of tests were conducted with a high slurry filling, so the results are not necessarily applicable to production mills. The second set of tests were conducted under ideal conditions for standard RoM mills in South Africa. During the discussion of the second set of tests, the results are compared to the first set, to yield a comparison under conditions of different slurry filling and slurry density.

13.3 THE FIRST SET OF TESTS

13.3.1 Production of fines

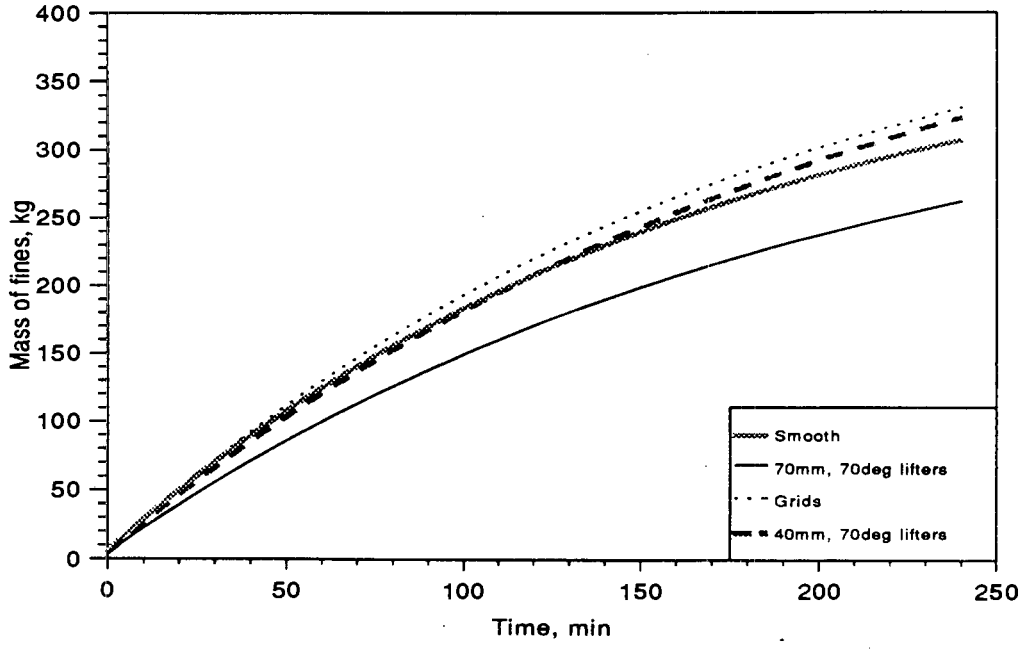

Figure 125. Mass of fines with time, 80% crit. speed

These trials yielded distinctly discernable differences between the production of fines for different liner configurations, and at the two different mill speeds.

Figure 125 and Figure 127 are plots of the total mass of fines in the mill as a function of milling time, for each different liner configuration. Considering the change in liner configuration at 80% critical speed, Figure 125, there is a clear difference in the mass

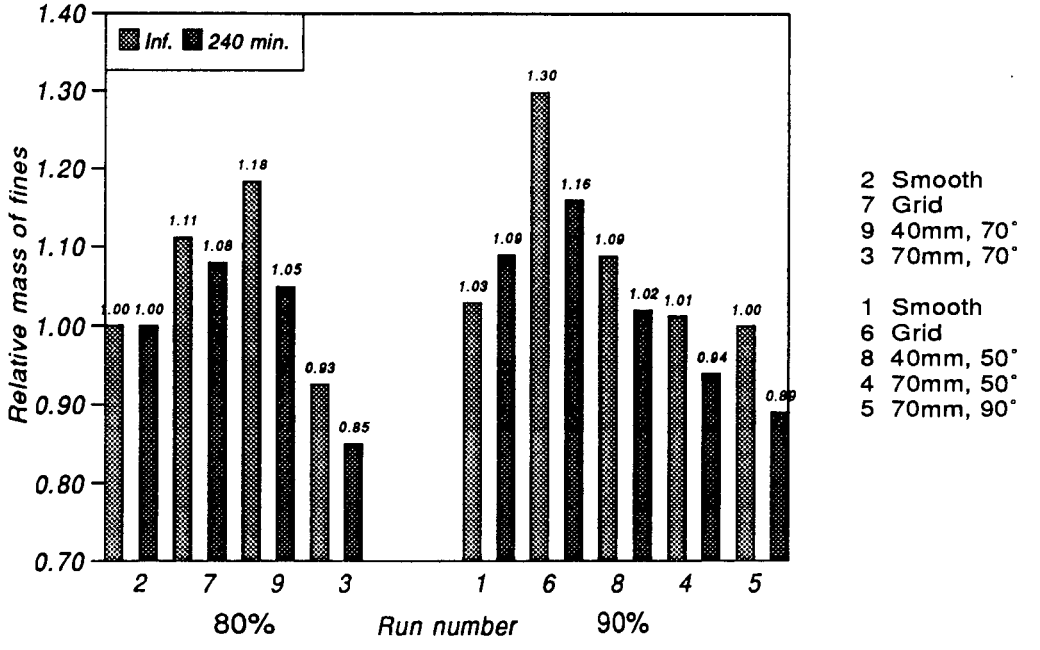

Figure 126. Comparison of the relative values of $M_{f\,240}$ and $M_{f\infty}$

of fines produced with the different liners in the mill. The grids produce the most fines, closely followed by the 40 mm lifters. The smooth liner has a slightly lower performance, and the higher, 70 mm, lifters have by far the worst performance.

A measure of these differences is given by the $M_{f\,240}$ and $M_{f\infty}$ values shown in Figure 126. The mass of fines relative to the mass produced by the smooth liner at 80% critical speed is used to compare the performance of the different liners. The mass of fines produced after 240 minutes is the best data for comparison, the mass at infinity shows how the mass of fines produced changes after a longer milling time than that used in the experiments. For the mill running at 80% critical speed, the 40 mm lifters will actually produce the most fines as the test progresses. There is a surprisingly large, 22%, drop in the total fines produced when the height of the lifter is increased from 40 to 70 mm. So clearly this apparently small change has a dramatic effect on the milling action.

Looking at the effects of liner changes at 90% of critical speed, Figure 127, a wide spread in the mass of fines produced can again be seen, although the ranking of liners is slightly altered as shown by the $M_{f\,240}$ and $M_{f\infty}$ values in Figure 126. After 2 hours

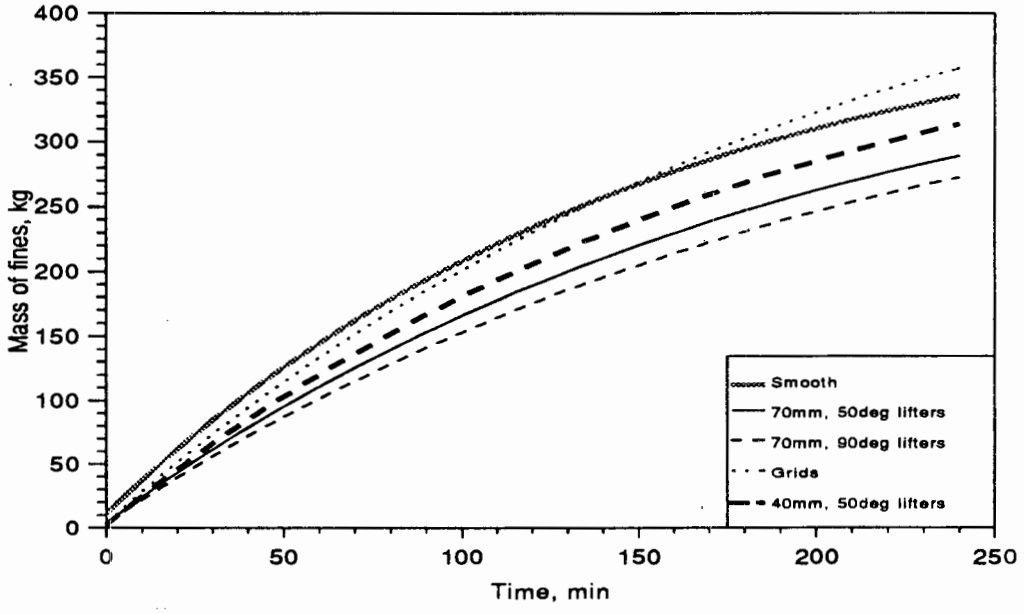

Figure 127. Mass of fines with time, 90% crit. speed

the grid lining begins to produce more than the smooth lining, and eventually far outperforms the other linings, with a 30% higher production of fines than the worst lining. The performance of the smooth lining drops off dramatically with time, and eventually the 40 mm lifters outperform it. There is a small drop-off in performance when the angle of the lifters is changed from 50° to 90°, and an 8% improvement when the height is reduced to 40 mm.

The rate of production of fines drops off exponentially with time, and the differences between the different liners converge as the rates drop off, as seen in Figure 128 and Figure 129. For both speeds the smooth liners have a much steeper rate curve than the other liners. This would primarily be a function of the coefficient of friction between the charge and the lining. Initially the coarse nature of the rock charge would result in a high coefficient of friction, and a reasonable keying-in and lifting action of the charge, with a favourable milling action. But as the rocks rounded out and a slurry was produced, the coefficient of friction would lower[5], and the charge would slip more. This resultant loss of efficiency would account for the more rapid drop-off in the rate function for the smooth lining as compared with the other linings that could key-in the

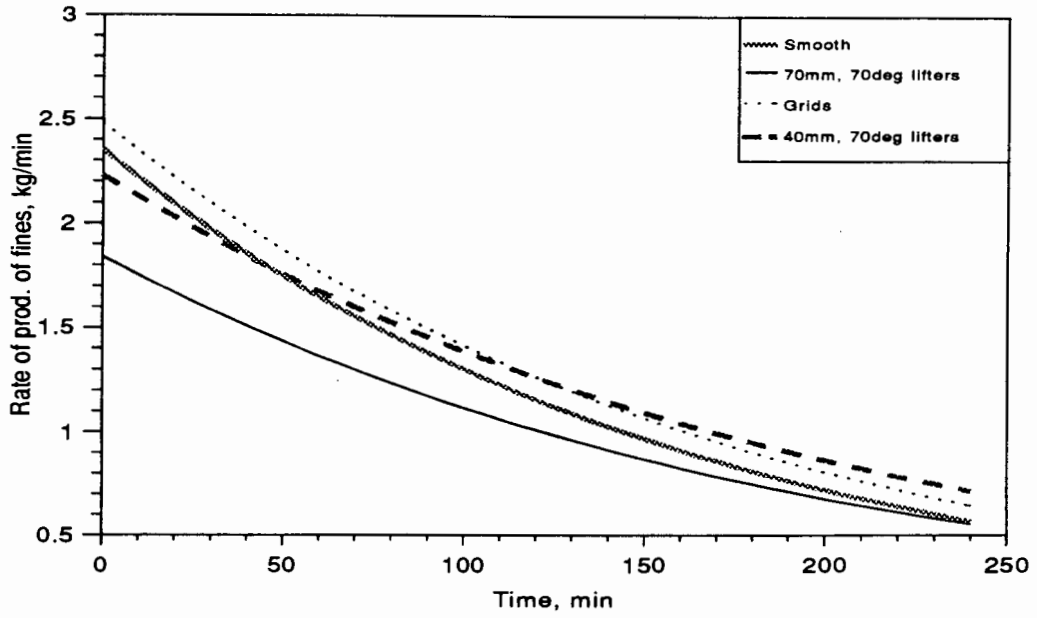

Figure 128. Rate of production of fines with time, 80% crit speed

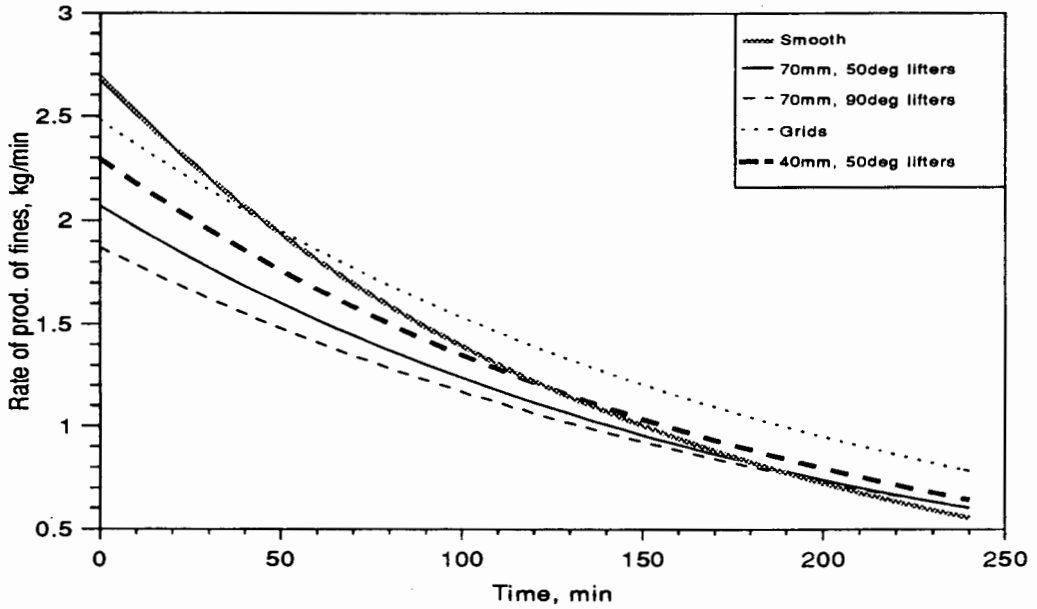

Figure 129. Rate of production of fines with time, 90% crit. speed

charge regardless of its frictional characteristics. As the equilibrium condition of a continuous throughput mill is similar to that of the batch mill near the end of its run, this indicates that a smooth lining would not be favourable. At the slower speed, the grid lining has a similar slope to the smooth lining. So despite the relatively rough

nature of the grid, once it was packed with small pebbles, as can be seen from Figure 130, it appears that the charge still experienced extensive slip. This was not the case at 90% critical, so the higher centrifugal force was sufficient to key-in the charge. The rate function is a function of time, that tends to zero as time tends to infinity. This presents the problem of when to compare the rate functions for the different conditions. The conditions in the mill at the end of the run most closely resemble those found in a continuous throughput mill, with a slurry solids density of over 50% by mass, so 4 hours was chosen as the comparison time. The histogram of Figure 131 shows the comparative rates of production of fines at 4 hours. There is a 25% difference between the smooth lining and 40 mm lifter for 80% critical, and a 39% difference between the smooth and grid linings at 90% critical. This factor indicates the possible expected difference in performance for continuous throughput mills.

Figure 130. A view inside the mill, showing the packing of the grid with pebbles

Comparing the influence of the height of the lifters at different speeds, the most favourable height of lifter for 80% critical is not necessarily the best for 90% critical speed. The change in performance as the lifter height is changed should not be only attributed to the change in the ratio of mill diameter to height of the lifter (DH ratio), but also to the change in the ratio of lifter spacing to height of the lifter (SH ratio). The experimental setup yielded the ratios as given in Table XXVIII. An SH ratio of 4.5 was

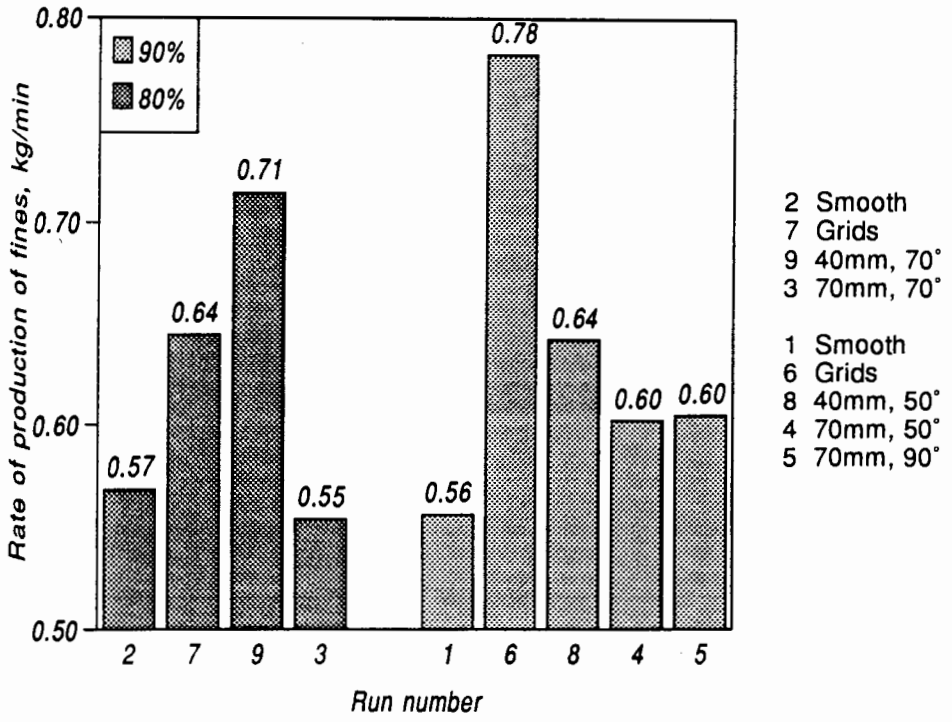

Figure 131. Relative rate of production of fines at 4 hrs.

unfavourable at both speeds, whereas a ratio of 7.9 was most favourable for 80% of critical speed, but only a marginal improvement for 90% critical speed. The Skega formula[37] predicts an SH ratio of 5 for 80% critical, and 10 for 90% critical. But the performance cannot possibly peak at a ratio of 5, when it improves by 22% with the ratio changing from 4.5 to 7.9, for the 80% speed. A firm conclusion cannot be drawn for the 90% speed, but with only an 8% difference in performance between ratios of 4.5 and 7.9, and noting the improvements for the 80% speed, the implication is that a far greater ratio than 10 would be required to optimise the mill performance. So these results indicate that the formula is not applicable at these high speeds (it was established from data of lower speed mills). To properly assess this would, naturally, require a more comprehensive range of spacings and heights to be tested.

Meaders and MacPherson reported[8] that at 77% speed, the DH ratio should be 17.6, and the SH ratio 4.0 to 4.5. But using these ratios requires that there be only 11 rows of lifter bars in a mill (this is independent of mill size). In a 5 m diameter mill this would

Table XXVIII Height and spacing ratios for the lifter bars

Height	DH ratio	SH ratio *
70 mm	25.7	4.5
40 mm	45.0	7.9

* The spacing is that between the lifters, so it = $\pi D/15$ - 60 mm.

give lifter spacings of 1.3 m, which would result in very high liner wear-rates. So to achieve reasonable SH ratios much higher DH ratios were used in the experiments. The mill performed very well with a DH ratio of 45, at 80% speed, which indicates that a ratio of 17.6 is not necessarily optimum. Taking into account that both the DH and SH ratios were greatly increased from the favourable ratios reported by Meaders and MacPherson for only a 3% increase in speed, the implication is that for a given speed, the DH ratio can be varied provided that the SH ratio is varied simultaneously. Because only the height of the lifters were changed, and this changes both the DH and SH ratios, firm conclusions could not be drawn on whether one or the other was optimised. However, it can be stated that the mill performance did improve as the DH and SH ratios increased.

13.3.2 Rock size distribution

The size distribution of the discharge pebbles gives a measure of the overall grinding taking place in the mill. The degree of reduction of the largest rocks in the mill indicates the degree of impact grinding, and how suitable the mill is for carrying out reduction of autogenous ore. Figure 132 shows how the degree of reduction of the two large rocks varied with liner profile, and mill speed. For the mill running at 80% critical speed, the reduction of the rocks is considerably less than at 90% critical speed, for smooth to low lifters. Then there is a sudden jump in the degree of reduction for the higher lifter, indicating that impact grinding took place. The faster mill has a levelling-off in the degree of reduction with the higher lifter, and then a drop-off once the lifter angle is increased from 50° to 90°.

These effects can be explained by the changing impact conditions in the mill, as predicted by the charge trajectories theory. If the rocks are considered to be spherical,

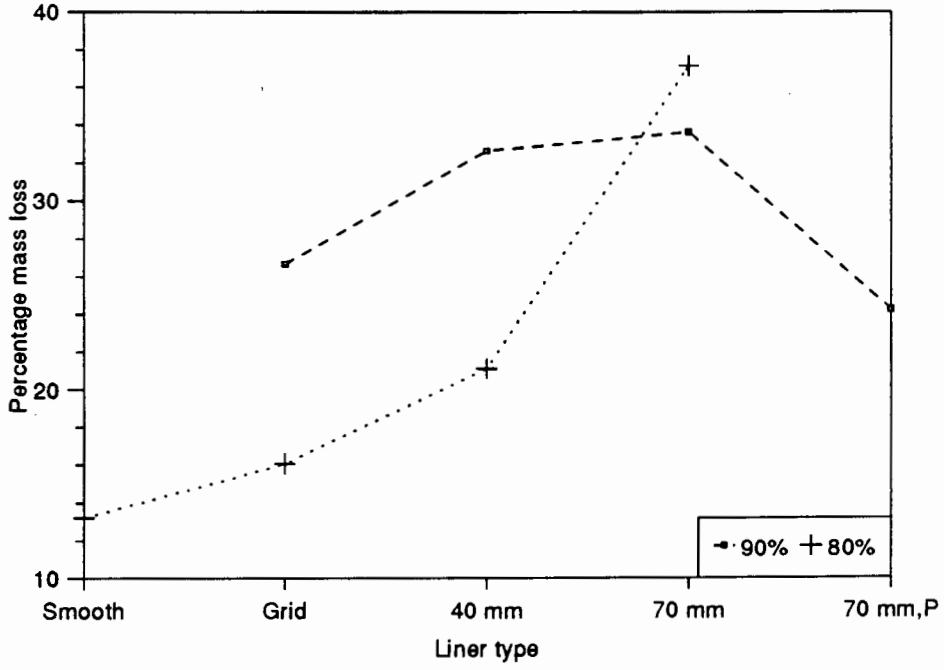

Figure 132. Average percentage mass-loss of the large rocks, for each type of liner

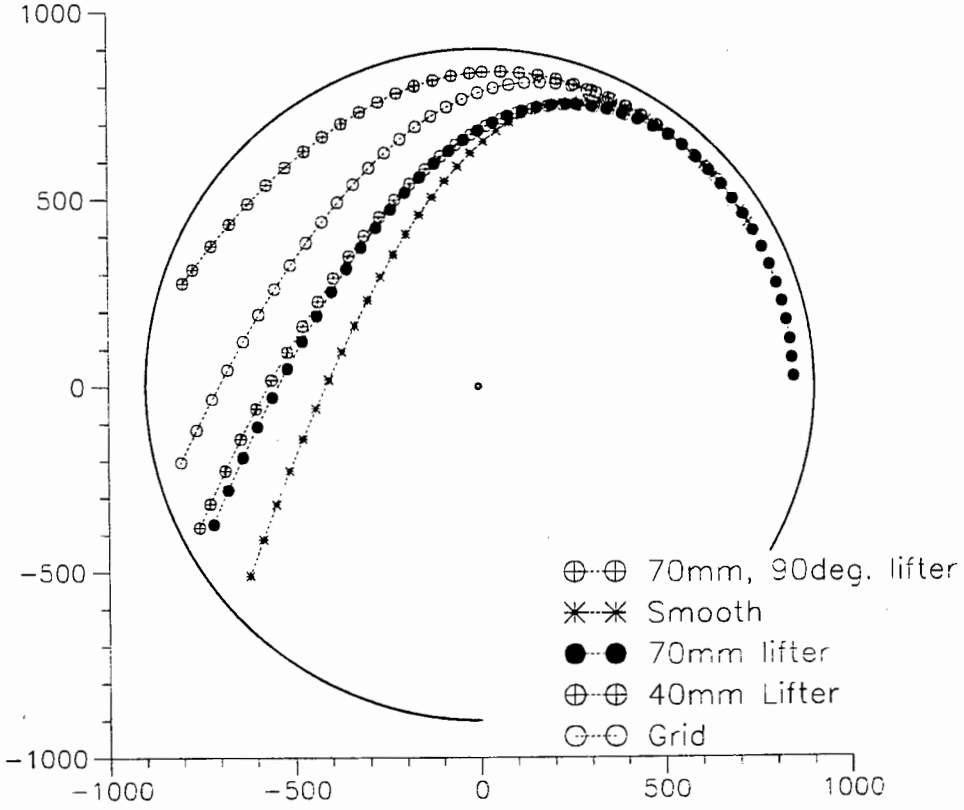

Figure 134. Theoretically calculated trajectories of large rocks, 90% crit. speed

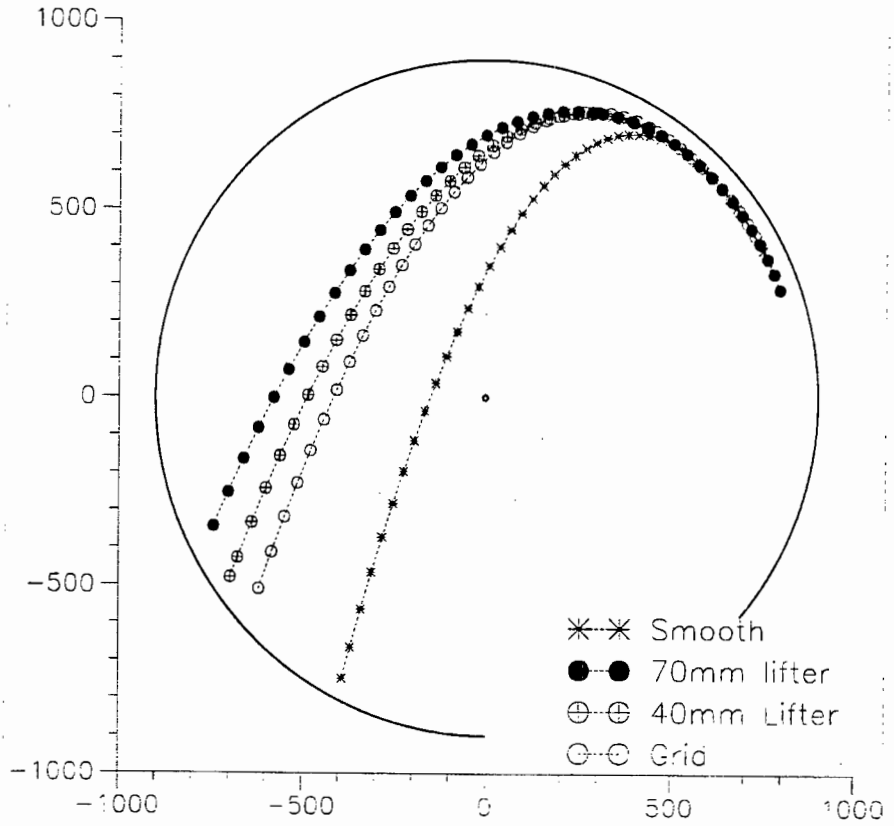

Figure 133. Theoretically calculated trajectories of the large rocks in the mill, for the different liners, at 80% critical speed

then their radii would be 110 and 96 mm for the 15 and 10 kg rocks respectively. However, they were actually somewhat oval in shape, and they reduced in size during the test, so it was estimated that their actual radii, on the narrow cross section, was in the range of 67 to 76 mm. The precise value of the radius has little effect on the predicted trajectories, provided it is definitely greater or less than the height of the lifter bar. The calculated trajectories are shown in Figure 133 and Figure 134. The impact point, at 80% critical speed, is higher for the 70 mm lifter than for the other liners. It is not much higher than for the 40 mm lifter, but this must be sufficient to carry the rock clear of the toe of the charge, and thus allow it to impact directly onto the liner. Direct impacts onto steel greatly accelerate the wear rate of rocks. The trajectory for the smooth lining is basically only cascading, as the rock is not projected much above the bulk charge. For the mill running at 90% critical speed the impact point moves up so high for the 70 mm, 90° lifter, that the rock has a low impact velocity. It has a very small height of drop onto the liner and is travelling at a similar velocity to the liner when it does impact. The 40 and 70 mm lifters have very similar impact points, hence

the similar wear rate of the rocks. The wear rate for rocks with the grid lining is somewhat anomalous relative to their impact points. It is possible that with the smooth liner profile there was more slip on the lining than used in the calculations, so the trajectory is lower than that predicted.

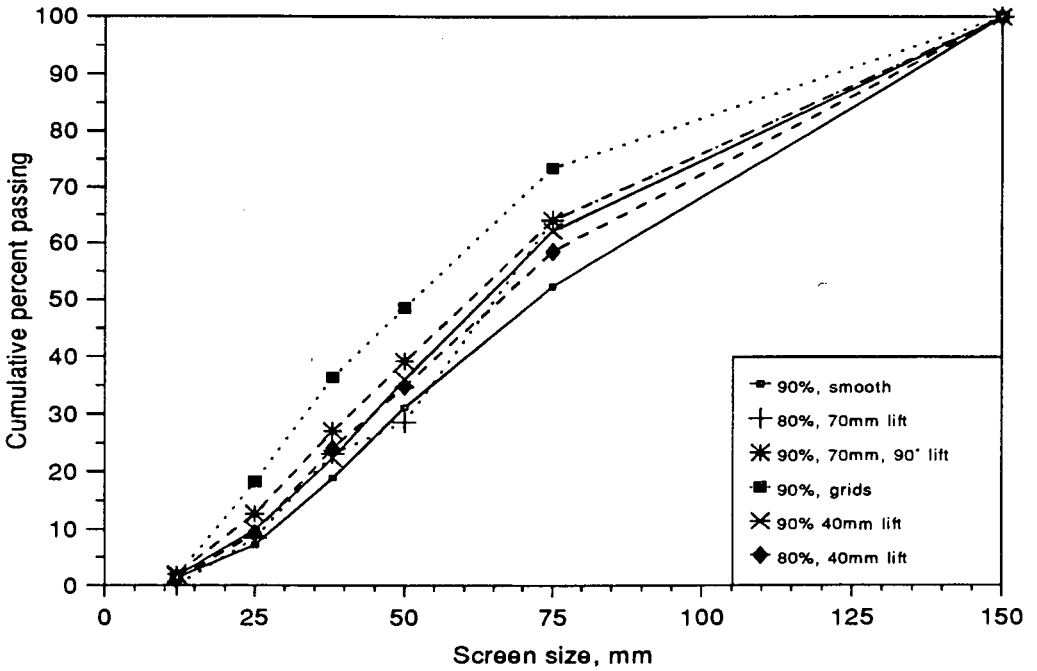

Figure 135. Cumulative rock size distribution

The full discharge pebble sizing displayed considerable scatter, of around ±10 percentage points. This error range must be taken into account when interpreting the

plots of cumulative size distribution given in Figure 135. The smooth lining, at 90% critical speed, gave the coarsest pebble grading, indicating that it was not very efficient at reducing the larger rocks. This is consistent with the concept of little impact grinding taking place under these conditions. The grids at 90% crit speed have the finest size

distribution, so they appear to have done the most coarse size reduction. It is of interest to note that this liner configuration also results in the finest size distribution in the sands fraction, and the highest rate of production of fines, with the lowest energy consumption at the end of the run (see Figure 142 below). Because of the error range,

nothing firm can be stated about the size distributions arising from the other liner configurations.

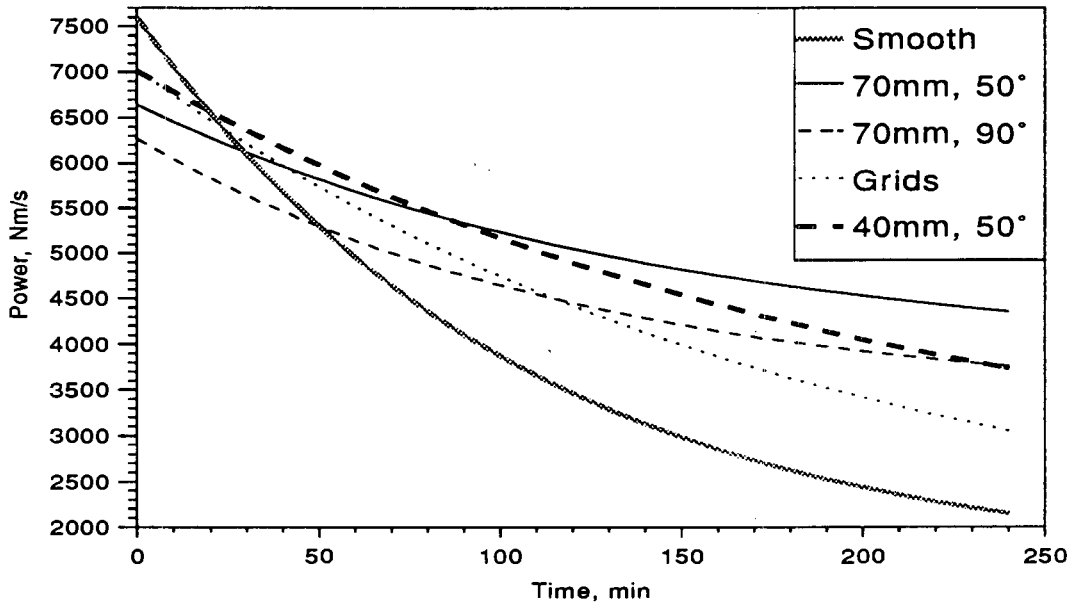

Figure 136. Power draw of the mill with time, 90% crit. speed

13.3.3 Power draw

The power draw of the mill dropped off considerably as the tests progressed (Figure 136 and Figure 137). The slope of these curves differs substantially between the different liner configurations. Most notable is the difference between the liners with lifters, and those without (smooth and grids). The smooth lining starts with a high power draft, that drops off rapidly with milling time, down to about a third of its initial value, after 4 hours. The lifter bar powers start lower, but drop to only around 70% of their initial value. This difference between the liners would be strongly related to the degree of slip in the mill. As the charge slips more and more on the smooth lining, so less energy is transferred into the charge, and hence the mill draws progressively less power. This is related to the correspondingly lower rate of production of fines, as discussed in the previous section.

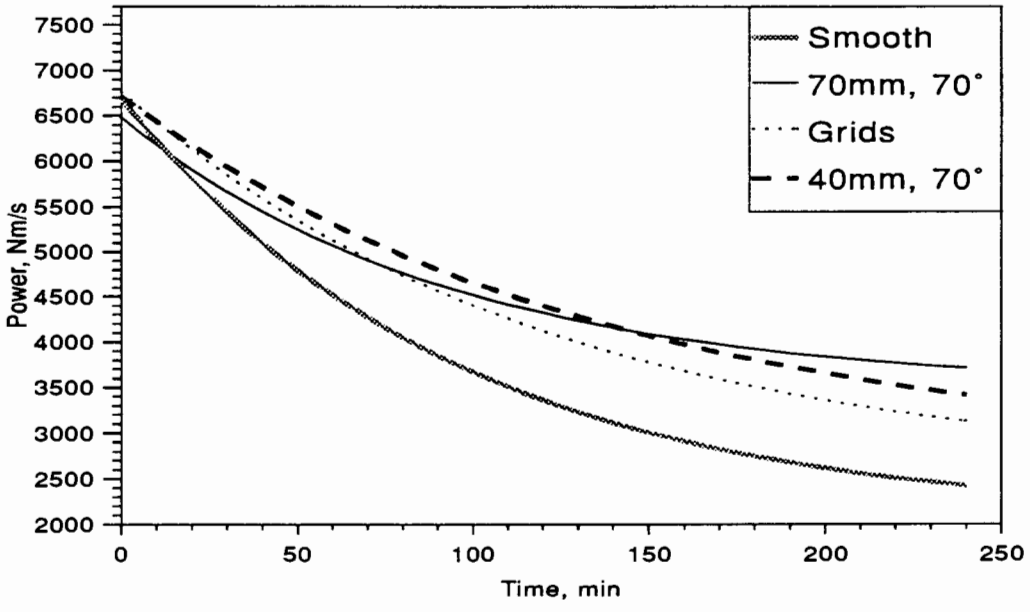

Figure 137. Power draw of the mill with time, 80% crit. speed

It was considered likely that the rate of production of fines would be related to the drop in power, so the two are plotted against each other in Figure 138 and Figure 139. Although not linear, there is a definite and smooth trend, which is slightly sub-linear. This indicates that the rate of production of fines and the power draw of the mill are strongly related, but that there is another factor involved as well. This difference is exemplified by the different time constants for the rate and power functions, for each set of conditions. Fuerstenau *et al*[25] have shown that the slurry viscosity in a batch mill varies exponentially with time, as given in eqn. 25. The exponential reduction in power draw of the mill implies that there may be a link between the power draw and the slurry viscosity. The origins of the graphs are not shown as the curves do not pass through the origin. This arises because the mill still has a power draw, which can be termed the 'hold-up power draw', when the charge is fully ground down to a slurry.

It is well established that the power draw of a mill is strongly dependent upon the mill loading. However, in this work the total load did not vary from the original 1 100 kg of rock and water, yet the power draw dropped dramatically during the course of the test. Therefore the power draw must be dependent upon the composition of the charge.

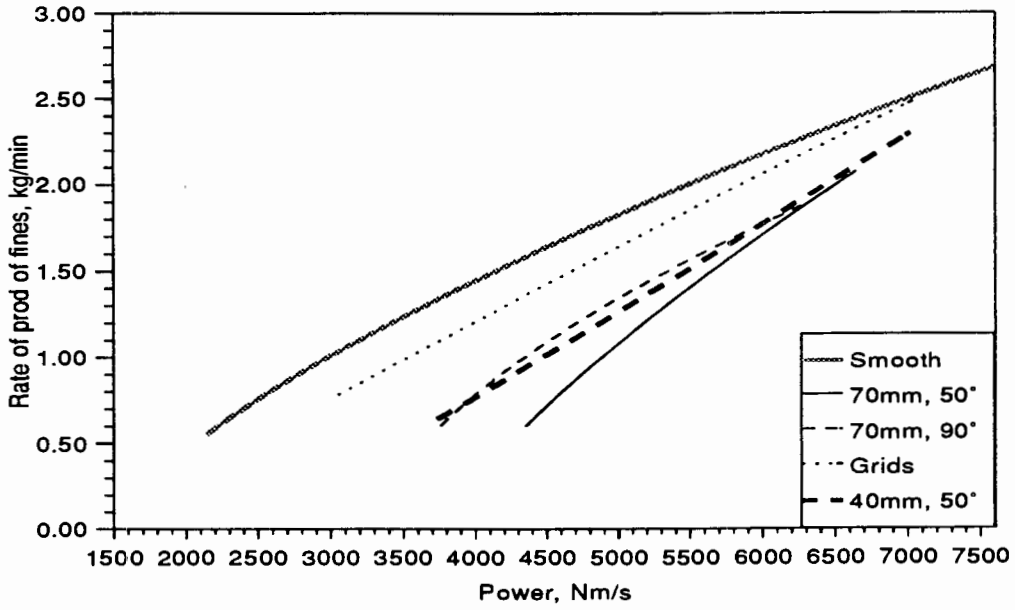

Figure 138. Rate of production of fines as a function of the power draw of the mill, 90% crit. speed

With this in mind, it was decided to plot the power draw as a function of the mass of rocks remaining in the mill, these are given for each speed and liner configuration in Figure 140 and Figure 141. The plots are largely linear, although not completely so. The slopes of the curves are dependent upon the liner configuration, with the smooth lining having a decidedly different slope to that for the other liners. It can be concluded that the power draw of a mill is strongly dependent upon the mass of grinding media in the mill, as opposed to the total charge mass. However, the power is also dependent upon the liner design, and composition of the charge.

The grinding energy can be derived from the slope of the curve of power versus rate of production of fines, as given by the Power(t) / Rate of production(t). The power was converted from Nm/s to Kw so as to give the final figures in units that are used in production. Figure 142 and Figure 143 show how the energy consumption varies with time for the different liner configurations. The gross energy consumption is far greater than in production mills, which have a figure of around 32 kW.hr/t fines[38]. This could be due to the over-grinding inherent in the batch milling process, and the production

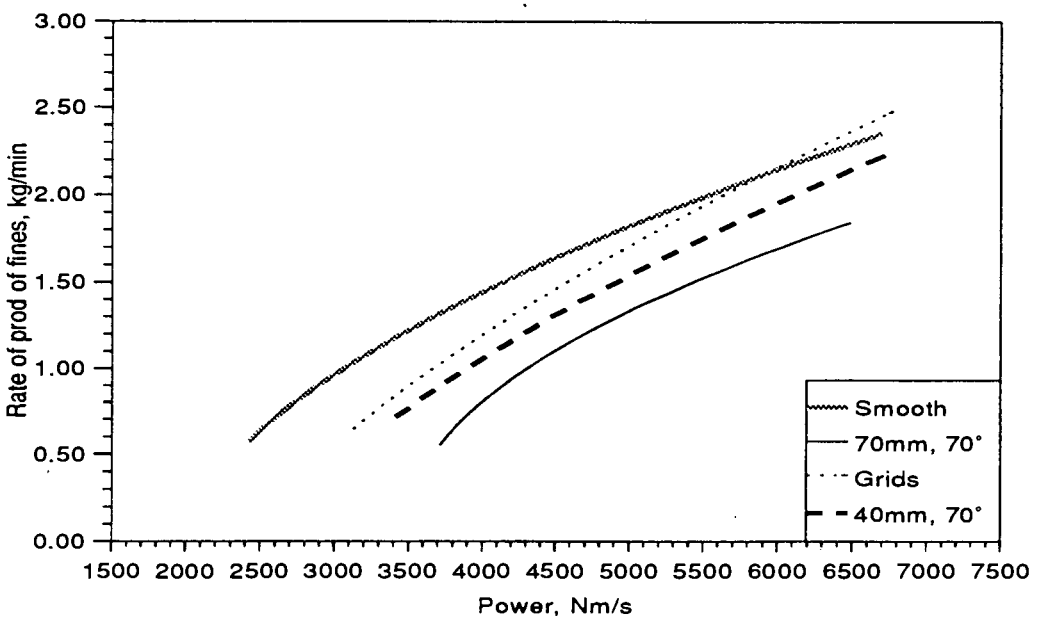

Figure 139. Rate of production of fines as a function of the power draw of the mill, 80% crit. speed

of a very fine product is very energy intensive for quartzitic ores. Another contributory factor to the low efficiency of the batch mill is that the charge composition is not optimal, as the test starts with almost no slurry, only water. As fines are produced the volume of the slurry becomes too great for the available interstices between the rocks. This results in padding of the rocks by the slurry, which leads to a low grinding efficiency.

It is of interest to note that the relationship for the smooth liner is quite different to the others. As the run progresses, and the power draw drops, so it has an increasingly greater efficiency, when compared to the other liners. It has a minimum at about 80 min, and then an increasing energy usage, especially at 80% of critical speed.

The high lifters require far more energy to produce fines, especially at the lower speed. Surprisingly, the 90° lifters require less energy than the 50° lifters, at 90% critical speed. It is predicted by the charge motion theory that the rocks will impact on the shell at these high speeds with a rectangular lifter, while the sloping lifter is

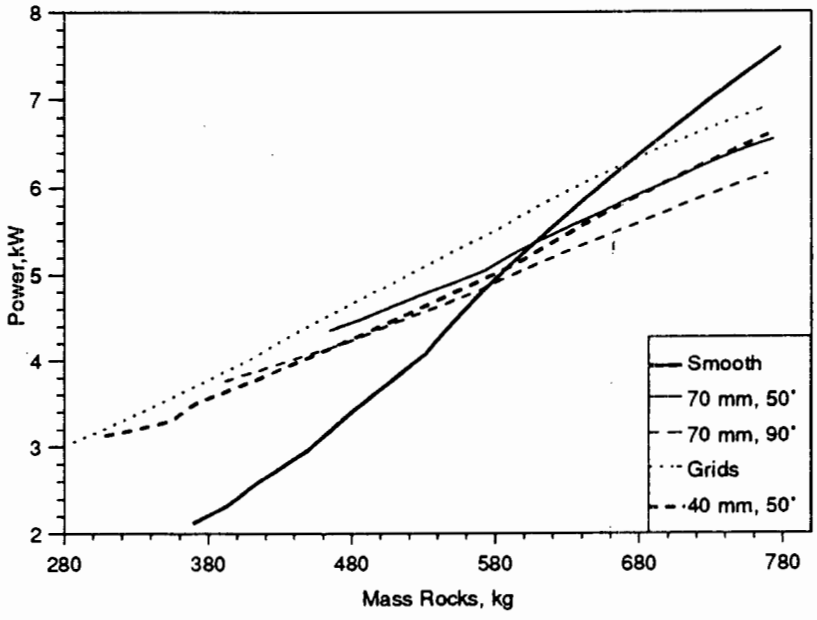

Figure 140. Power draw as a function of the mass of rocks remaining in the mill, 90% crit. speed

designed to drop the rocks on the toe of the charge. It is concluded that with the outer rocks almost centrifuging, and landing on the shell, they return a substantial portion of their energy to the mill, and thus lower the gross power draw of the mill. This is substantiated by the fact that it has a lower power draw than the sloping lifter. This

lowering of the power draw is greater than the lowered rate of production of fines, thus giving it a higher efficiency. The 40 mm lifters at 80% critical speed have by far the best energy efficiency of the lifter bar linings, indicating the correctness of its design. It is also a fairly linear function of time, indicating a good grinding action over a widely varying range of slurry and charge conditions.

The energy efficiency of the grid lining changes quite dramatically between 80% and 90% of critical speed. At 90% the slope is almost linear (Figure 144), indicating fairly consistent grinding kinetics, whereas it climbs steeply for 80% speed, similar to the smooth lining, indicating that the charge was suffering from increasing slip on the lining, with a concomitant loss of power efficiency.

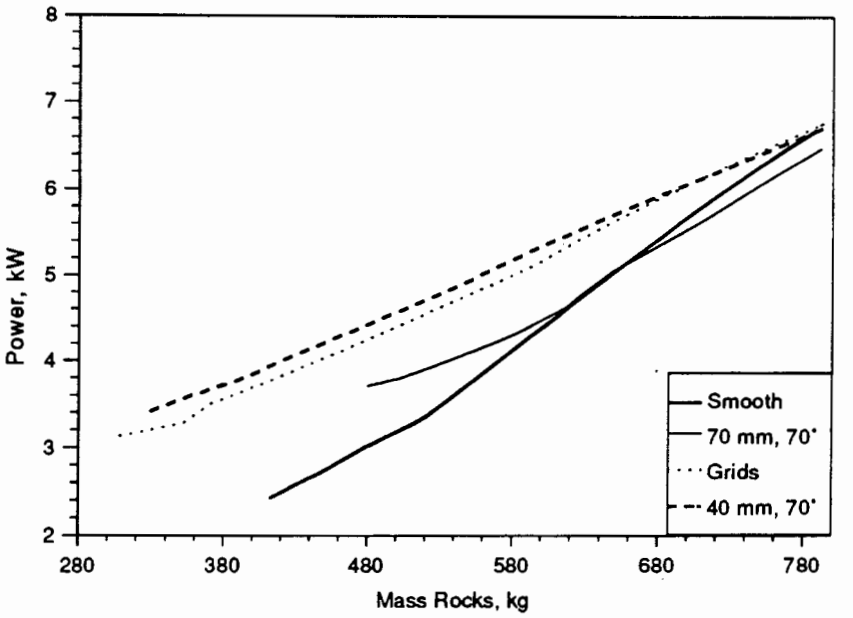

Figure 141. Power draw as a function of the mass of rocks remaining in the mill, 80% crit. speed

The lowest energy usage of the smooth lining at 80 min indicates that it requires a reasonable slurry density to perform well. The mill operator has to be aware that when changing the lining configuration of a mill, the grinding action will change, and therefore the operating conditions of the mill must be changed accordingly, to re-optimise the milling efficiency.

There is a consistent relationship between the torque drawn by the mill and the fineness of grind, within each set of tests: the higher the torque drawn by the mill, the finer the product size distribution. This is shown by run 1 in test 1, run 6 in test 2, run 12 in test 4, and most obviously in tests 5 and 7. Thus for a given set of milling conditions, the fineness of grind is directly related to the power draw of the mill. However, this does not hold over different milling conditions, such as changing the

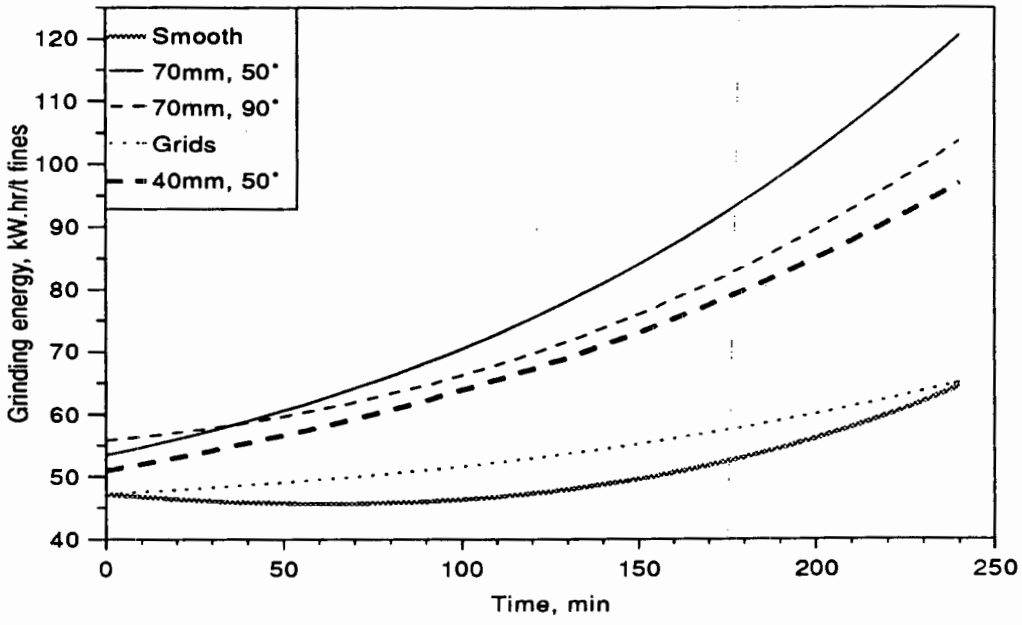

Figure 142. Energy consumption for the production of the fines, 90% crit. speed

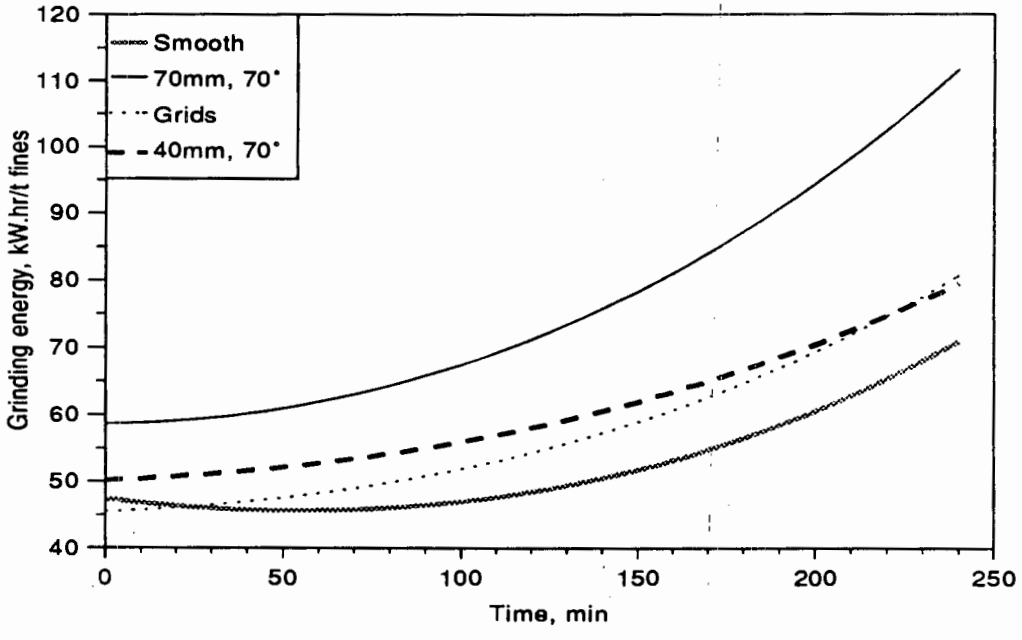

Figure 143. Energy consumption for the production of the fines, 80% crit. speed

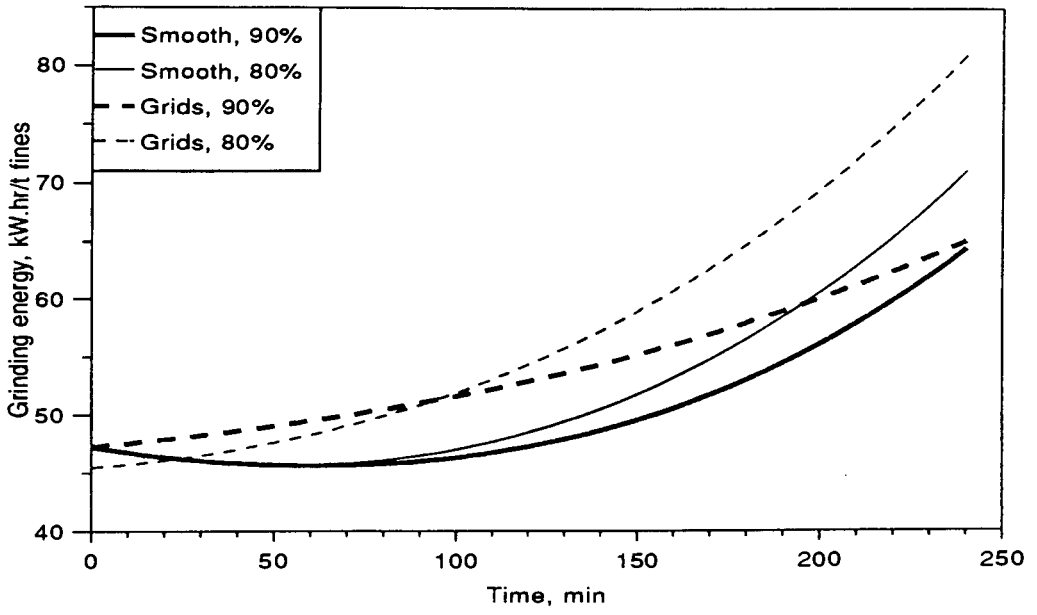

Figure 144. Energy consumption for the production of the fines, smooth and grid lining

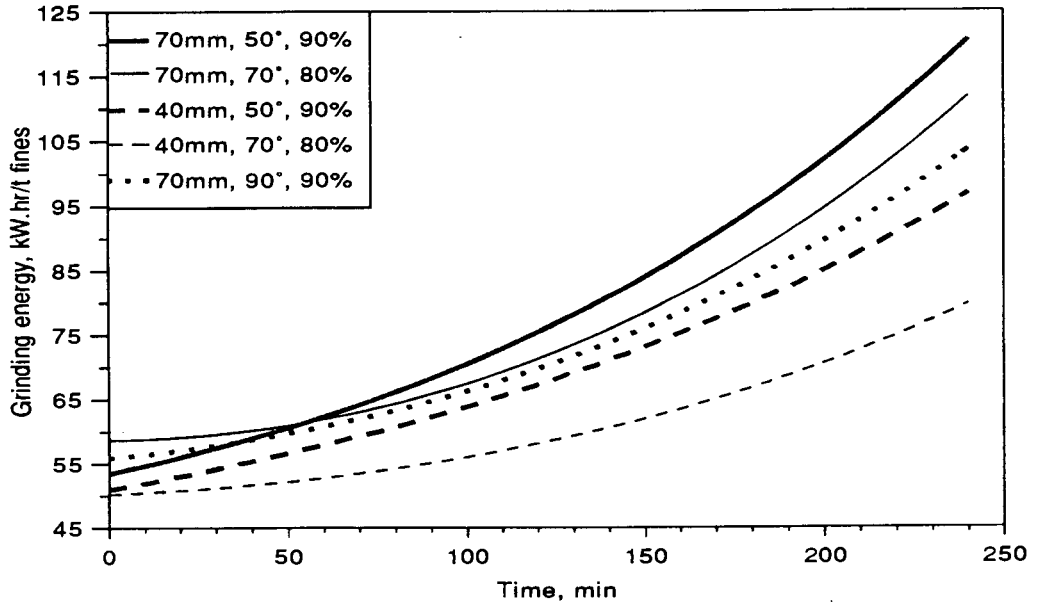

Figure 145. Energy consumption for the production of the fines, with lifter bars

lining of the mill. It was found that the linings that had the lowest power draws, had the finest grind, and that the highest power draw gave the coarsest grind. This is reflected in the widely varying energy consumption per ton of fines produced, between the different liner configurations (Figure 142 to Figure 145). This clearly indicates a change in the milling dynamics when the liner configuration is changed. This finding is in contradiction to that of Fuerstenau and Abouzeid[18], who claimed that the energy required to produce a product was invariant with lifter size.

In most cases there is a trade-off of milling capacity (in terms of rate of production of fines), and milling efficiency (in terms of kW.hrs/t of fines produced). However, this is not the case for the grid at 90% of critical speed, as it has a similar energy consumption to the smooth lining, and in fact will be lower after 4 hours, yet it also has the highest rate of production of all the liners. Furthermore it has the highest degree of reduction of the coarser rocks, and quite a high reduction of the very large rocks. This indicates that with correct liner design one should be able to minimise energy consumption while maximising milling rate.

13.4 THE SECOND SET OF TESTS

These tests were conducted under the normal operating conditions of South African RoM mills. As shown in the experimental section of the milling trials, the conditions for loading the mill to achieve a given set of operating conditions was derived. Because this is a batch milling process these conditions only apply for a short period of time. It is at this ideal point that the performance of the mills is compared, this is not necessarily at the same milling time for each experiment. The objective of the second set of tests was to establish that the experiments could be conducted under normal conditions, and to compare the results with those obtained under the abnormal milling conditions of the first set of tests. A full set of trials were conducted at 90% of the critical speed, and one test for the grids at 80% critical speed.

13.4.1 Production of fines

There were distinctly discernable differences between the production of fines for the different liner configurations. Figure 146 gives a plot of the total mass of fines in the

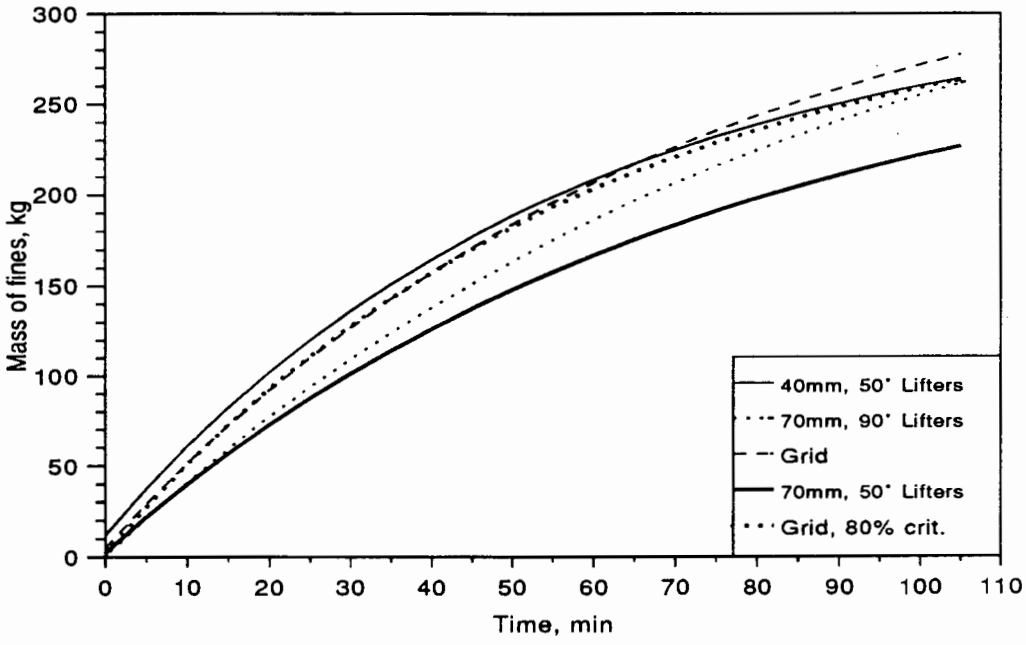

Figure 146. Mass of fines in the mill

mill as a function of milling time. The form of these curves is similar to those given in Figure 127, but the rankings are changed slightly. In both cases the grid produces the most fines, followed by the 40 mm lifters. The 70 mm lifters have a lower production, but the order is swopped, with the 90° lifters outperforming the 50° lifters. As before the mill running at 90% critical speed produces more fines than at 80% critical speed, as shown by the run at the lower speed, for the grid lining.

13.4.2 Slurry conditions

The fractional slurry filling (volumetric fraction of the total charge that is slurry) increases with time, as the fine material that passes into suspension is produced. The data points and fitted curves are illustrated in Figure 147. The ideal fractional slurry filling, for maximum power draw and milling rate, is in the range 45 to 50%, which provides complete filling of the voids between the rocks, but not over-filling. The mill charge is in this range from 40 to 75 minutes, providing an adequately long period in which the performance of the different liner configurations can be compared.

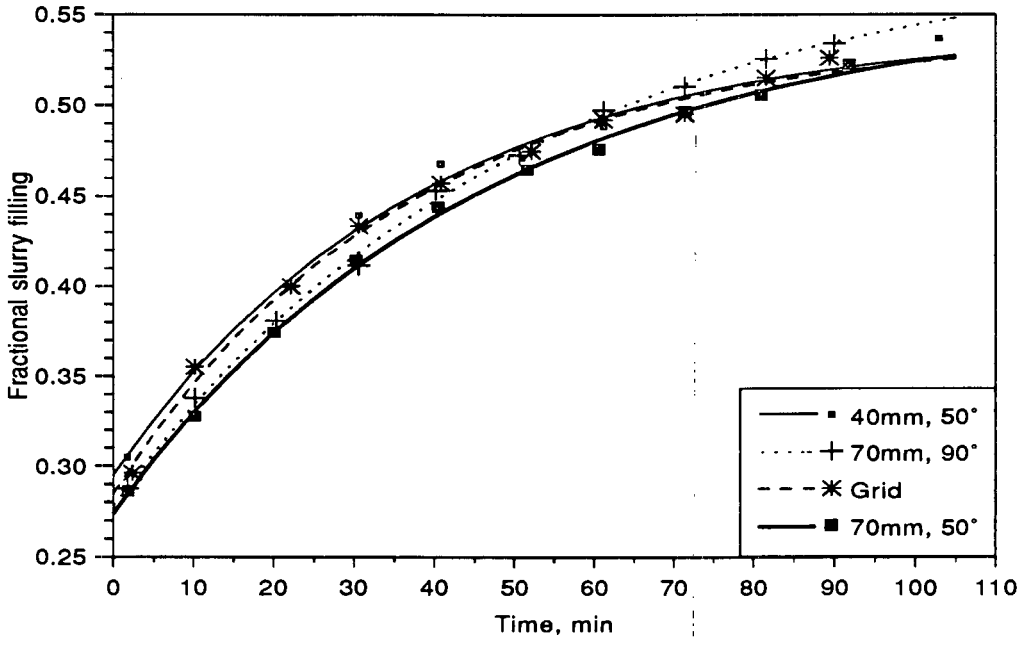

Figure 147. Fractional slurry filling with milling time

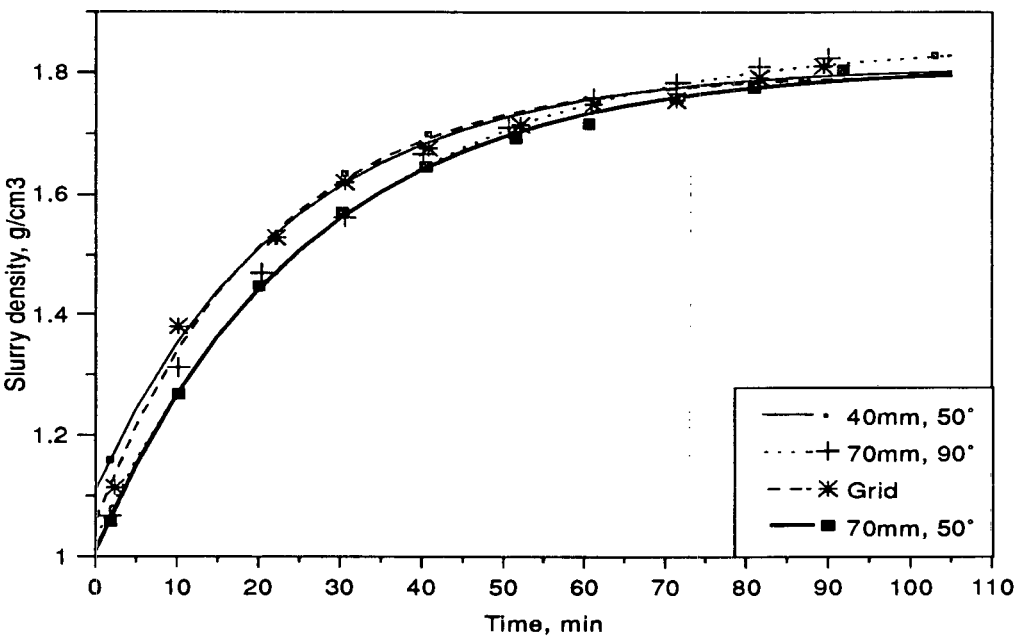

Figure 148. Change of slurry density with milling time

The slurry density (Figure 148) is in the desirable range, of 1.70 to 1.75 g.cm^{-3}, for the same period of 40 to 75 minutes. This is not by coincidence as the charge loading conditions were specifically chosen to produce this set of conditions. The conditions can be readily manipulated by varying the initial conditions, and these can be calculated by eqn's. (22) and (23) given in the experimental section.

13.4.3 Rate of production of fines

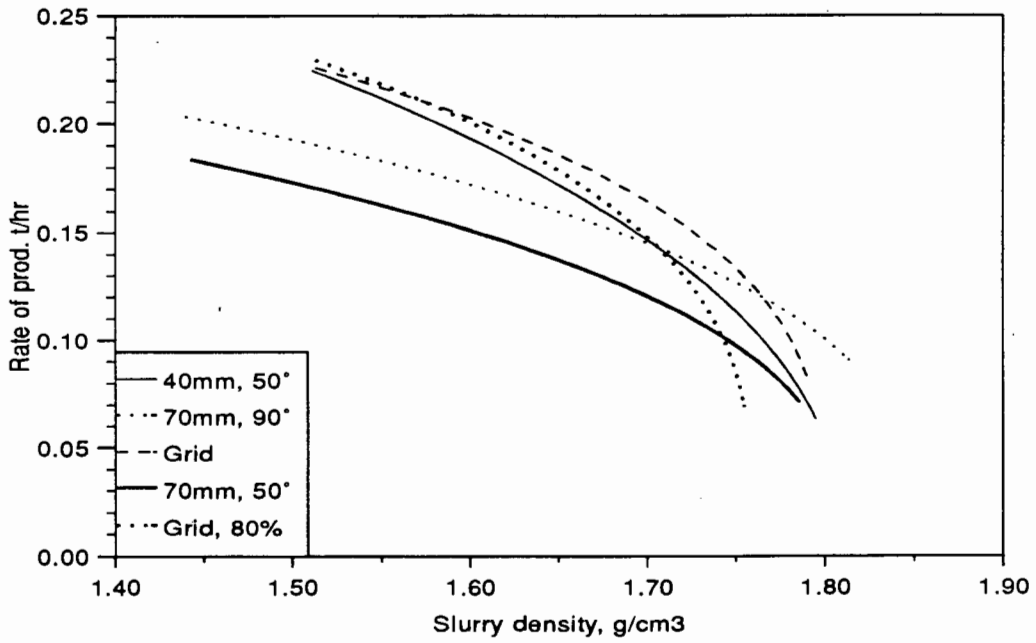

Figure 149. Rate of production of fines as a function of the slurry density

This is the primary criterion for the comparison of the different liners. Rather than comparing at a given time, as was done for the first set of results, these are compared when the mill charge is at the same conditions. The slurry density is used as the comparison base, as the mill performance is sensitive to the slurry viscosity, which is dependent on the slurry density, for a given ore. Because the mill was loaded in the same manner for each test, the fractional slurry filling and the mass of rocks in the mill are identical for a given slurry density. The rate of production of fines as a function of the slurry density is shown in Figure 149. The figure is slightly deceptive as it shows that the rate of production drops with increasing slurry density. However, the rate of

production, as reflected by the power draw, is a strong function of the mass of rocks in the mill, as shown for the first set of tests, Figure 140, and again for the second set of tests, Figure 151. The slurry density and the mass of rocks are inter-dependent, so their separate influences on the rate of production could not be directly deduced from this set of experiments. A range of tests, with the same liners but changing the charge loading would need to be conducted to isolate the influence of rock mass and slurry density on milling rate. However, it is known that for a continuous throughput mill the power draw and rate of production increase with increasing slurry density up to a critical density and thereafter drop off. This turning point can be deduced from Figure 149 by observing the departure from linearity of each curve. The curves have a fairly linear region initially which then suddenly drops sharply as the slurry density is increased further. This varies for each liner configuration, but is principally at around a density of 1.70. The two liners with 70 mm lifters have the turning point at a distinctly higher slurry density, closer to 1.75. This would imply that the mill can be run at a higher slurry density with high lifters than with a low-profile liner. This finding is in contrast to that of the first set of tests, where it appeared that the high lifters required a lower slurry density.

Table XXIX Rate of production of fines at two slurry densities

Test No.	1	2	3	4	5
Slurry density = 1.70 g.cm^{-3}					
Time, min.	44	49	46	42	51
Rate of prod., t/hr	0.145	0.145	0.147	0.165	0.120
Slurry density = 1.75 g.cm^{-3}					
Time, min.	58	61	78	57	67
Rate of prod., t/hr	0.113	0.126	0.085	0.133	0.097

The performance of the liners are compared at two slurry densities, 1.70 and 1.75, which reflect the range of optimal milling conditions for the mills under consideration, Table XXIX and Figure 150. The different times at which the liners are at the same conditions are shown in the table. At the lower slurry density the grid performs the best, with a 37% improvement over the 70 mm 50° lifter which performs the worst. The other liners have a very similar performance, which is 12% poorer than the grid liner. As for the first set of tests (Figure 131) the higher speed mill has a higher rate of production, with a 14% difference as compared to a 21% difference for the first set.

At the higher slurry density there is a change in the spread of the rankings. The performance of the grid liner at 80% critical speed drops off considerably at the higher density, to lag that at 90% critical speed by 36%. This indicates that for the lower speed the mill should be run at a lower slurry density. The low lifter has a 15%, and the 70 mm 90° lifter a 5% lower rate of production than the grid lining. The change in the relative performance of the liners with changing slurry density reflects the importance of comparing the liners at the correct slurry density, and indicates how the slurry density should be changed for different liner configurations.

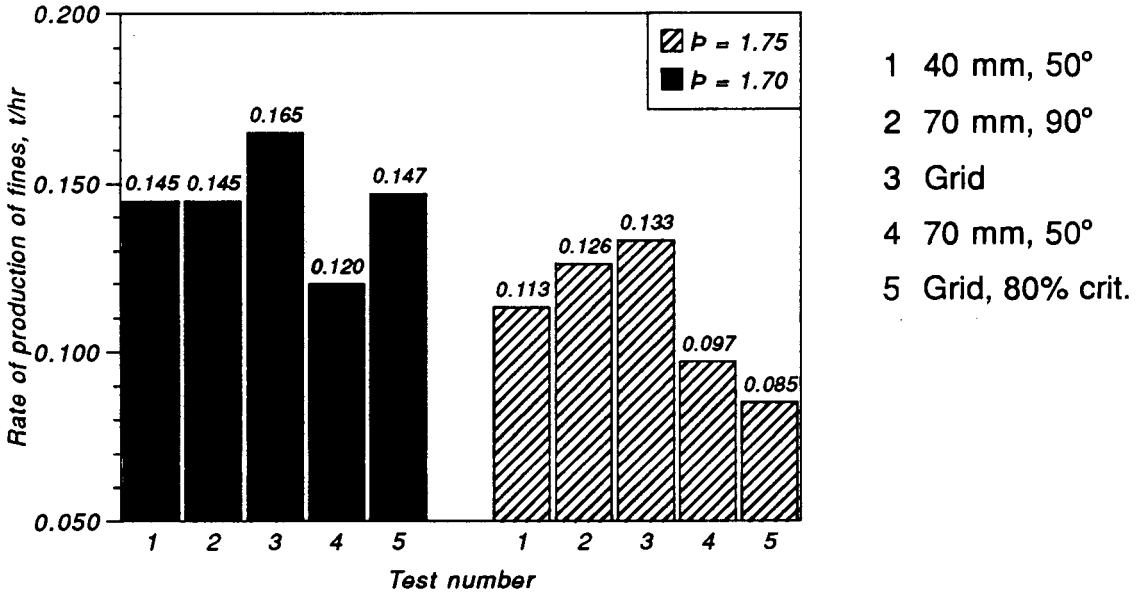

Figure 150. Comparison of the rate of production of fines at two slurry densities

13.4.4 Power draw and energy consumption

The initial increase in torque drawn by the mill (Figure 106) arises to a large extent from the reduction in the volume of the charge. Initially, for the loadings used, the slurry does not fill the voidage so the gross charge density is lower than the maximum obtainable. As the slurry volume increases the charge becomes more compact and has a radial location closer to the periphery of the mill, thus increasing the torque arm. It is also likely that for the initial slurry being almost plain water, it is not lifted effectively by the charge and partially forms a pool at the toe of the charge. This effectively lowers the angle of the centre of mass of the charge, and thus reduces the torque arm. Once the voids are more effectively filled and the slurry more viscous these effects fall away and the torque begins to drop as the mass of rocks decreases. The increase in torque towards the end of the run most likely arises from the increasing slurry density, such that the viscosity becomes high enough to cause the entire charge to be lifted higher up, and thus increase the torque arm.

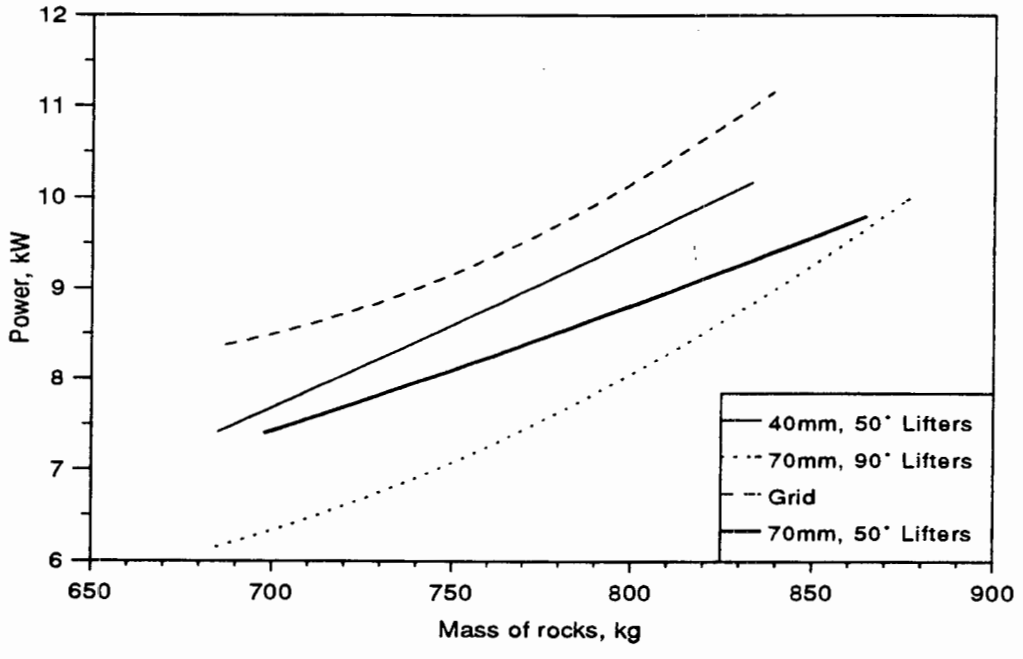

Figure 151. Power consumption as a function of the mass of rocks in the mill

As with the first set of tests the power consumption is a strong function of the mass of rocks in the mill, Figure 151.

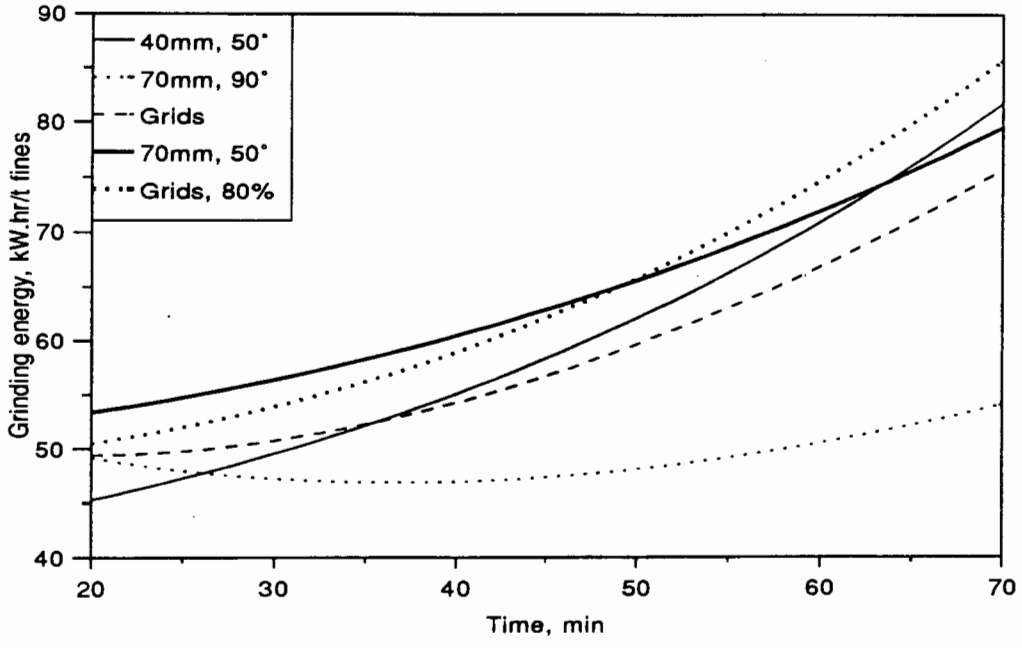

Figure 152. Energy consumption for the production of fines, set 2

The grinding energy varies with time, Figure 152, as it did for the first set of tests, Figure 142. However, the 70 mm 90° lifter now has the lowest energy consumption, as was the case previously with the grid and smooth liners. This would imply that the milling conditions have changed from favouring attrition grinding to favouring impact grinding. The degree of impact grinding taking place for the 70 mm 90° lifter is reflected in the far coarser size distribution of the slurry, Figure 108.

The grinding energy is still considerably higher than that found in production mills, despite the fractional slurry filling being correct. When screening the rock into size fractions for blending the <12 mm material was screened out and discarded. This was to reduce the quantity of fine material in the mill so that the slurry density did not rise too rapidly as the test progressed. It was anticipated that the breakage of the >12 mm material would produce material in the size interval of 1 to 12 mm. However, this was not the case and at the end of the test there was found to be a dearth of material in this size range, instead most of the material was abraded directly down to less than 1 mm. The lack of material in this size range would decrease the efficiency of the

milling process, by reducing the crushing-grinding component. In addition the mill is coping with a far greater size reduction to be carried out. These effects are likely to be of a significant magnitude as the <12 mm material constitutes 30 to 40% of the run-of-mine feed rock.

The shortage of material in the <12 mm range may also explain the anomalous performance of the 70 mm 90° lifter. As this lifter promotes impact grinding it would favour the direct reduction of the larger material, that would otherwise have to be abraded away. It is expected that this advantage would fall away once the feed size distribution is normalised. The rapid reduction of the larger material by impact breakage is not favourable in the long-term as it destroys the grinding media that mills the finer material, so a continuous throughput mill would suffer from a build-up of critical size material. The direct impacting on the mill liner also increases the rate of liner wear.

CHAPTER 14
CONCLUSIONS

14.1 GENERAL CONCLUSIONS

Novel techniques were developed for investigating the motion of balls deep within the charge of a model grinding mill. The experiments provided many original observations that have enhanced the understanding of charge motion in rotary mills. The techniques have been developed to the point where further work in this field should be able to provide more quantitative modelling of the milling action, and improve the models of torque.

It is felt that a viable technique for comparing the performance of different liners in a realistically large mill has been developed. Although the batch mill presents problems with regard to maintaining the correct slurry density and fractional slurry filling, these problems can be overcome. A general solution to the loading of the mill has been developed, which will ensure that all conditions are optimal simultaneously. It has been demonstrated that these remain in the correct range for a sufficiently long period of time for realistic comparisons to be made between different liners. This test provides a cheap and effective method for comparing the metallurgical milling performance of different liners, which would otherwise have to be tested in full-scale RoM mills, at considerable expense and with some doubt as to the reliability of the results, arising from fluctuating operating conditions.

A wide range of conclusions were drawn from the results. These are presented in point form for clarity and conciseness.

14.1.1 Motion of the balls

1) The composition of the charge, the types of media and the slurry viscosity, have a substantial influence on the motion of the media and the resultant milling action.

2) All of the media in a mill rotate about an axis - the centre of circulation (CoC) of the charge. This CoC uniquely defines the location of the charge.

3) The angular velocity of the media drops off from about the angular velocity of the mill at the periphery of the mill to zero at the CoC.

4) The amount of slip within the charge is almost independent of the design of the lining, once the outer layer of charge is keyed into the rotary motion of the mill.

5) In the cascading region, the outer half of the charge is in free-fall, and there is little interaction between the balls. The inner half of the charge undergoes extensive interaction between the balls, indicating that extensive grinding may take place in this region.

6) There is very little rotation of the balls about their own axes. The majority of rotation takes place in the shoulder and toe regions, and the ball slides, rather than rolls, over other balls in the *en masse* and cascading regions. This implies that grinding does not take place by rotary nipping of the ore between the balls.

7) The balls were observed to spiral in and out of the charge in a smooth manner. This implies that the surrounding balls also undergo a spiralling motion. From this it is deduced that there is a double spiralling action: an inward and an outward spiral linked by the axial flow of balls. This occurs in short spurts of a few revolutions, and should promote good mixing of the charge.

14.1.2 Charge location

1) The radial location of the CoC is sensitive to the volume of the charge, decreasing rapidly with increased filling, when the filling approaches 50%.

2) The angular location of the CoC defines the angle of repose of the charge. It increases with mill speed from a static angle of repose determined by the composition of the charge body, towards the horizontal as the charge centrifuges.

3) Over a speed range of 64 to 82% of critical speed, the location of the CoC varies little with the speed.

4) The centre of mass (CoM) of a layer of charge is determined by the average location of the ball during a complete circuit about the mill. Each concentric layer of charge has a slightly different CoM. The net CoM of the charge is determined from the sum of the CoM's over all layers of the charge.

5) There is an approximately linear relationship between the angle of repose of the CoM and the mill speed, starting at the point determined by the natural angle of repose of the charge, when the mill is just rotating, and tending towards the horizontal (90°) when the whole of the charge centrifuges. The angle is well below 90° at 100% of critical speed, since only the outer layer of charge is centrifuging at that speed. The location of the CoM of the charge is independent of the CoC, but the two nearly coincide over the speed range from 68 to 82% of critical speed.

6) The true CoM of the entire charge, as opposed to the CoM of the *en masse* charge, should be used to calculate the torque of the mill when the torque-arm method is used. Use of the true CoM yields a torque curve of the correct form, when compared with experimental data.

7) The angle of incline of the cascading region depends on the angle of repose of the charge, which is independent of the liner configuration, and varies very little with mill speed over the range of speeds from 64 to 82% of critical speed.

14.1.3 Charge interaction

1) The highest-energy impacts occur when the grinding media are projected from the shoulder of the charge directly onto the toe. For a given ball size, the impact force depends primarily on the height of fall; it is therefore greatest in the outer regions of the charge and increases with mill diameter. Impacts onto the mill shell should be avoided, because they waste milling energy and result in rapid wear of the liner and media.

2) Although the impact force does not increase with mill speed, a greater proportion of high-energy impacts occur, resulting in a greater proportion of impact grinding at increased speeds.

3) The height of the lifter bars does not influence the impact force, but the angle does. The maximum impact force can be obtained by designing the lifter to drop the media onto the toe of the charge. Lower-angle lifters are required for higher speeds.

4) The maximum work is carried out in the cascading region near the CoC of the charge, in the inner half of the charge. This corresponds with the region of maximum interaction between the balls. It is likely that this region of the charge is responsible for a large portion of the grinding work.

5) A mill running at speeds of between 82 and 92% of critical speed has the highest work rate, with speeds outside that range resulting in lower work rates.

6) The face angles of the lifters have a distinct influence on the amount of work done, and the favourable angles correspond with those that cause maximum impact energy. The optimal angle is a strong function of the mill speed.

14.1.4 Charge segregation

1) Radial segregation of the balls occurs within the charge, even in a mill with smooth end faces. At low speeds, the larger elements separate to the periphery of the mill, and at high speeds they are concentrated near the centre of the charge. The 'neutral' speed, at which there is no segregation by size, is in the range of 75 to 78% of critical speed. The heavy balls reside near the centre at most speeds, and near the periphery of the charge at high speeds. The 'neutral' speed for segregation by ball mass is around 92% of critical speed. These segregation tendencies oppose each other, because the size and mass of a ball are intimately related, and the final location of a ball depends on the balance of these forces. In the speed range of about 80 to 90% of critical speed, small, heavy balls are strongly segregated to the periphery of the mill. This is directly applicable to steel balls in a semi-autogenous mill.

2) The radial segregation of balls is thought to arise primarily from energy considerations, with the mill charge attempting to assume the lowest available energy state. Counter-segregation at high speeds is thought to arise from the centrifuging effect of the mill.

3) It appears that the liners can be designed so as to have some influence on the radial segregation of the balls.

14.1.5 Milling rate

1) The rate of production of fines and the energy efficiency of a mill are both affected by the liner configuration.

2) In batch autogenous milling, changes in the liner design can cause variations of up to 30% in the mass of fines produced in a fixed period.

3) The rate of production of fines is sensitive to the height of the lifter bars.

4) The rate of production of fines can vary by over 30% between the best and worst linings.

14.1.6 Liner design

1) The optimal liner profile varies with mill speed. A lower lifter, with a lower face angle, is required for higher mill speeds.

2) The performance of the mill is strongly influenced by the spacing-to-height (SH) ratio of the lifters. The Skega formula[37] for determining the SH ratio does not appear to hold for high mill speeds (above 85% of critical speed). The diameter-to-height (DH) and SH ratios recommended by Meaders and MacPherson[8] are not invariant. The height of the lifter can be substantially reduced, provided that the SH ratio is increased. A DH ratio of 45 with a SH ratio of 7.9 was found to yield an excellent mill performance at 80% of critical speed.

14.1.7 Mill efficiency

1) The power draw of the autogenous batch mill varies considerably with milling time. There is an initial run-in period as the volume of slurry increases to fill the voids. The power then drops to values as low as one-third of the highest value. This phenomenon is well modelled by an exponential decay. The changing composition of the charge body with time must account for this dramatic reduction; the ratio of slurry to rocks increases substantially as the test progresses. The power draw is predominantly dependent on the mass of rocks (grinding media), as opposed to the total mass of the charge.

2) The energy consumption, expressed in terms of kW.hr/t fines, increases with milling time, indicating a reduction in the milling efficiency of the batch mill. This will also be a function of the changing charge body. The energy consumption varies widely with different liner types, showing that a change in liner profile affects the reduction efficiency of the mill.

3) The optimal milling efficiency for different liners is achieved at different slurry densities. For a mill running in the range of normal fractional slurry filling and slurry density a lifter-bar lining requires a higher slurry density than a mill with a smooth-profile lining.

4) For a given set of milling conditions, the fineness of grind is directly related to the power draw of the mill. However, this invariance does not hold over different milling conditions.

14.2 CONCLUSIONS OF PARTICULAR PRACTICAL IMPORTANCE

1) With the correct liner design, it should be possible to minimize the energy consumption of the mill while maximizing the milling rate.

2) The lining must have a sufficiently high profile to key in the outer layer of charge to the rotary motion of the mill. However, a profile that is too high leads to a reduction in the milling efficiency.

3) The shape (profile) of the lining does influence the grinding action and milling efficiency, however, in the light of point (2), it is dubious whether intricate designs have any advantage over simple profiles of the same general face angle.

4) The profile of a lining can be 'tuned' to optimize the impact point of the cataracting media, and it is important that the media impact on the toe of the charge rather than directly on the mill shell.

5) The milling efficiency is very sensitive to the ratio of the SH of the lifters. This ratio depends on the DH ratio, and on the speed of the mill.

6) The torque and the power draw of a mill depend on the physical characteristics of the charge such as slurry viscosity, internal friction, and charge density which determine the location of the true CoM of the charge. The torque drawn by the charge determines the amount of energy available for grinding. The grinding rate is determined by the power draw of the mill, not *vice versa*.

7) Simple models that assume that there is no interaction between neighbouring balls cannot predict the action of the charge in a mill, because there is a significant interaction of particles in a mill, even in the shoulder region of the charge.

14.3 RECOMMENDATIONS FOR FUTURE WORK

The present study has highlighted a number of areas that would greatly benefit from further experimental work.

14.3.1 Charge segregation

This phenomenon is of particular practical importance, because the radial location of the media can have a profound influence on the milling efficiency. If all the large or heavy grinding media are concentrated at the centre of the charge, then they are not carrying out impact grinding, and the small media are not in the region of the most interactions where they can promote abrasion of the ore. To establish firmly the cause of the segregation would require a range of experiments with balls differing in size and mass to the bulk media, and using mills of different sizes. The gamma-camera tracking of a radioactive ball is a most suitable method, since the ball can be tracked over many revolutions of the mill, and the output lends itself to automatic data assimilation.

14.3.2 Influence of the slurry

The slurry that was used in the analysis of the charge motion was too unrealistic to yield representative results. It would be most beneficial to compare the motion in a realistic type of slurry to that in a mill running dry, since it is likely that the addition of slurry will influence the magnitude of the effects that have been observed. A fluid of lower density than water and slightly denser plastic beads would be required, so as to establish a realistic ratio of densities between the balls and the slurry.

14.3.3 X-ray filming technique

A number of improvements could be made to the arrangement of the X-ray filming experiment, if adequate access to a biplanar angioscope could be obtained. It is important to ensure that the entire image falls within the image area of the 35 mm camera, since this is slightly smaller than the TV image area. Alternatively, if a video machine and display with the correct format (high resolution 1249 line) could be obtained, then the images could be transferred directly onto videotape. This would facilitate a more automated data-acquisition technique, and enable longer sets of filming to be conducted for each run. If a clear image of the side view of the mill could be obtained, the results would be greatly enhanced. If the longitudinal location of the ball could be pinpointed, the magnification error could be compensated for, and the ball's location could be determined to within an accuracy of 1%. This would make the

quantitative analysis of the data possible, as well as the derivation of models of the bulk charge motion from the observed interactions.

The following suggestions should help to pinpoint the longitudinal location with sufficient accuracy:

Very clear markers should be placed at the front and back of the mill, and a scaled marker placed parallel to the length of the mill.

The scaling can be assessed by filming a stationary coordinate box placed in the location of the mill. The transparent box has balls fitted into it at fixed coordinates, say three along each edge. An analysis of the distorted image, relative to the real-space coordinates, will yield the magnification factor across and along the mill.

The mill can be placed in the centre of the image of the transverse camera. However, this will reduce the size of the mill that will fit into the image screen of the front view, as the mill won't be up against the image screen.

It must be ensured that the full image of the side view is visible on the film. Ready access to the x-ray equipment will be required to enable the experiment to be optimally set-up. However, if this access can be gained, then it will be possible to greatly enhance the quality of the results.

14.3.4 Power draw

If an experimental rig were designed in which the power draw could be accurately monitored, the power draw could be directly correlated to the location of the charge and that of the true CoM of the charge. This would be invaluable in establishing universally applicable power equations.

14.3.5 Influence of liner design on milling rate

A viable technique has been developed to determine the rate of production of fines for different liner configurations in a realistically large autogenous pilot mill. The optimal charging of the mill, with a full size distribution of media, needs to be further developed. Tests under a range of charge fillings and slurry densities could be conducted to investigate the dependence of grinding rate and power draw on the mass of rocks and the slurry density. A comprehensive programme can then be designed

to optimize the milling rate for various mill speeds and ore types. In particular, the influence of lifter height and spacing could be established, since these have a substantial influence on the milling rate. An automatic sampling device could be attached to the mill, in which the valve is operated remotely - thus eliminating the need to stop the mill in order to open the valve. This would also avoid the operator error inherent in manual sample collection.

REFERENCES

1. POWELL, M.S. The effect of liner design upon charge motion in a rotary mill. Masters dissertation, University of Cape Town, Sep. 1988

2. POWELL, M.S. The effect of liner design on the motion of the outer grinding elements in a rotary mill. *Int. J. Min. Proces.*, vol. 31. 1991. pp. 163-193.

3. WHITE, H.A. The theory of the tube mill. *The journal of the Chem., Metall. and Min. soc. of S.A.* May 1905. pp. 290-305.

4. DAVIS, E.W. Fine crushing in ball mills. *AIME Trans., vol. 61. 1919. pp. 250-296.*

5. HAULTAIN, H.E.T., and DYER, F.C. Ball paths in tube mills. *CIM Trans.*, vol. 25. 1922. pp. 276-291.

6. GOW, A.M., CAMPBELL, A.B., and COGHILL, W.H. A laboratory investigation of ball milling. *AIME Trans.*, Milling methods. 1930. pp. 51-81.

7. FAHRENWALD, A.W., and LEE, H.E. Ball mill studies. *AIME Tech. publ. no. 375.* 1931.

8. MEADERS, R.C., and MacPHERSON, A.R. Technical design of autogenous mills. *Mining Eng.*, vol. 16. 1964. pp. 81-83.

9. MARECHAL, B. Contribution to a study of dry quasi-autogenous milling. Third part: Internal mechanics of the aerofall mill. *Mintek translation*, TR-1199. (Contribution a l'etude de la fragmentation quasi-autogene en voie seche. Presented at the faculty of sciences, Nancy, 17th May, 1968.)

10. ROSE, M.E., and SULLIVAN, R.M.E. A treatise on the internal mechanics of ball, tube and rod mills. *Constable,* London. 1958

11. DUNN, D.J. and MARTIN, R.G. Measurement of impact forces in ball mills. *Mining Eng.* Apr. 1978. pp. 384-388.

12. ROGERS, R.S.C., SHOJI, K., HUKKI, A.M., and LINN, R.J. The effect of liner design on the performance of a continuous wet ball mill. *Proc. of XIV Int. Min. Proces. cong.*, 17-23 Oct. 1982. CIM, Toronto, Canada.

13. McIVOR, R.E. Effects of speed and liner configuration on ball mill performance. *Mining Eng.*, Jun. 1983. pp. 617-622.

14. VERMEULEN, L.A., and HOWAT, D.D. Fluctuations in the slip of the grinding charge in rotary mills with smooth liners. *Int. J. Min. Proces.*, vol. 16. 1986. pp. 153-188.

15. VERMEULEN, L.A. The lifting action of lifter bars in rotary mills. *J. S.A. Inst. Min. Metall.*, vol. 85, no. 2. 1985. pp. 51-63.

16. VERMEULEN, L.A., OHLSON DE FINE, M.J., and SCHAKOWSKI, F. Physical information from the inside of a rotary mill. *J. S.A. Inst. Min. Metall.*, vol. 84, no. 8. 1984. pp. 247-253.

17. ROLF, L., and VONGLUEKIET, T. Measurement of energy distributions in ball mills. *Ger. Chem. Eng.*, vol. 7. 1984. pp. 287-292.

18. FUERSTENAU, D.W., and ABOUZEID, A.-Z.M. Scale up of lifters in ball mills. *Int. J. Min. Proces.*, vol. 15. 1985. pp. 183-192.

19. VERMEULEN, L.A. Estimation of milling parameters by use of a conductivity bolt. *Mintek TM.*, no. 19048, Mintek, Randburg. July 1985.

20. BARTH, W. Power consumption in tube mills. *Forschung in Ingenieurweren*, vol. 1. 1930. pp. 321-328.

21. LIDDELL, K.S., and MOYS, M.H. The effects of mill speed and filling on the behaviour of the load in a rotary grinding mill. *J. S.A. Inst. Min. Metall.*, vol. 88, no. 2. Feb. 1988. pp. 49-57.

22. VERMEULEN, L.A., and HOWAT, D.D. Effects of lifter bars on the motion of *en masse* grinding media in milling. *Int. J. Min. Proces.*, vol. 24. 1988. pp. 143-159.

23. YASHIMA, S., HASHIMOTO, H., KANDA, Y., and SANO, S. Measurement of kinetic energy of grinding media in a tumbling ball mill. *Proc. XVI Int. Min. Proces. cong.*, ed. E. Forssberg. Elsevier Science Publ. Amsterdam. 1988. pp. 299-309.

24. ROGOVIN, Z., and HERBST, J.A. Charge motion in a semi-autogenous grinding mill. *Min. Metall. Proces.*, Feb. 1989. pp. 18-23.

25. FUERSTENAU, D.W., KAPUR, P.C., and VELAMAKANNI, B. A multi-torque model for the effects of dispersants and slurry viscosity on ball milling. *Int. J. Min. Proces.*, vol. 28. 1990. pp. 81-98.

26. MISHRA, B.K., RAJAMANI, R.K., and PARISEAU, W.G. Simulation of ball charge motion in ball mills. *Soc. Min. Metall. and Exploration, inc.*, Prep. 90-137. Mar. 1990. pp. 1-5.

27. MORRELL S. Prediction of grinding-mill power. *Trans. Inst. Min. Metall. (Sect. C: Mineral Process. Extr.)* vol. 101. Jan.-Apr. 1992. pp. C25-C32.

28. MOYS, M.H., and SKORUPA, J. Measurement of the forces exerted by the load on a liner in a ball mill, as a function of liner profile, load volume and mill speed. *Prep. Comminution R&D: current status*, First ICRA symposium, Univ. Witwatersrand, Johannesburg, 29 Oct. 1991. paper 7.

29. NATES, M.B., NURICK, G.N., and REDDY, B.D. The slip of a single particle on the inside of a rotating cylinder. Part 1 - theoretical analysis, and part 2 - experimental investigation. *Int. J. min. proces.*, to be published 1993.

30. SYMON, K. R. Mechanics, second edition. *Addison-Wesley publ. co., inc.* London, 1960. p. 158.

31. POWELL, M.S. The materials selection and design of rotary mill liners. *Prep. Antiwear '88*, Sept. 1988. The Royal Society, London. pp. 14.1-14.9.

32. POWELL, M.S. Improving the design of the liners of rotary mills. *Int. deep min. conf.*, vol. 1. Innovations in metallurgical plant. Ed. G.A. Brown, and P. Smith. The SAIMM symposium series S10. 1990. pp. 57-70.

33. POWELL, M.S. The design of rotary-mill liners, and their backing materials. *J. S.A. Inst. Min. Metall.*, vol. 91, no. 2. Feb. 1991. pp. 63-75

34. POWELL, M.S., and CORNELIUS, F.S. Composite rubber-metal liners in rotary grinding mills. *Prep. 11th Nat. Conf. S.A. sect. of PRI*, Johannesburg, S.A. 17-18 Oct. 1991. paper 6.

35. BARRATT, D.J., and ALLAN, M.J. Testing for autogenous and semiautogenous grinding: A designers point of view. *Min. and Metall. Proces.*, May 1986. pp. 65-74.

36. POWELL, M.S., and CORNELIUS, F.S. A test for the realistic simulation of coarse abrasive wear. *Prep. Tribology '92*, SAIT, Pretoria. 15-17 Sep. 1992.

37. MOLLER, T.K., and BROUGH, R. Optimizing the performance of a rubber-lined mill. *Mining Eng.*, Aug. 1989. pp. 849-853.

38. POWELL, M.S. A survey of the milling and mill-lining practice of South african gold mines. Randburg, Mintek, *Mintek Report* M350. 21 June 1988. 25 pp.

39. VERMEULEN, L.A. and HOWAT, D.D. Semi-empirical models of the wear rate and consumption of grinding media and the rate of production of fine material in open circuit milling. *Prep. 7th European sym. on comminution.* Ljubljana, June 12-14, 1990, pp. 875-892

40. JACKSON, O. A. E. Autogenous and composite load milling practice at the South African gold mines of Union Corporation, limited. *VII Int. Mineral Process. congress.* March 1965. pp. 557-572.

41. DAVIES, A. *Priv. comm.* Amandelbult sect., Rustenburg Platinum Mines. March 1993.

42. NITYANAND, N, MANLEY, B., and HENEIN, H. An analysis of radial segregation for different sized spherical solids in rotary cylinders. Metall. Trans. B, vol. 17B, June 1986. pp. 247-257

43. VERMEULEN, L.A. Personal communication, 1989

44. SEARS, F.W., ZEMANSKY, M.W., and YOUNG, H.D. University Physics, 5th ed. Addison Wesley, New York, 1977. p. 648.

APPENDIX I
THEORY

This theory was developed in the earlier set of work[1,2], but has been expanded and modified, so a condensed form of the full derivations are presented here for completeness.

The theory derives the effect that lifter bars of varying face angle and height have upon the outer layer of charge within a rotary mill. The simplest case of an isolated ball keyed-in to the motion of the mill is considered. Although lifter bars are considered, this also covers any profiled liner, as any wave pattern on a lining is, in essence, a lifter.

A ball resting on a lifter bar, and against the shell of a rotating mill, reaches a point of equilibrium where the sum of the forces acting on it is zero. Here, the net forces on the ball, parallel to, $F_{\parallel}$, and radially perpendicular to, $F_{\perp}$, the motion of the ball, are zero. The ball will then start to roll or slip down the face of the lifter bar.

I.1 POINT OF EQUILIBRIUM

With reference to Figure 153 and Figure 154 ,the forces acting on the ball are as follows:

gravitational force, acting vertically downwards (mg),
centrifugal force directed radially outwards towards the mill shell ($m\Omega^2 r$),
normal force of the lifter bar (N), and
frictional force between the ball and lifter bar, which is parallel to the face, and directed towards the mill shell f.

For this analysis, the forces are resolved into components that are parallel and perpendicular to the leading face of the lifter bar, and in the plane of rotation of the mill. A list of all the terms that are used is given in the Nomenclature, and is also shown in Figure 153 and Figure 154.

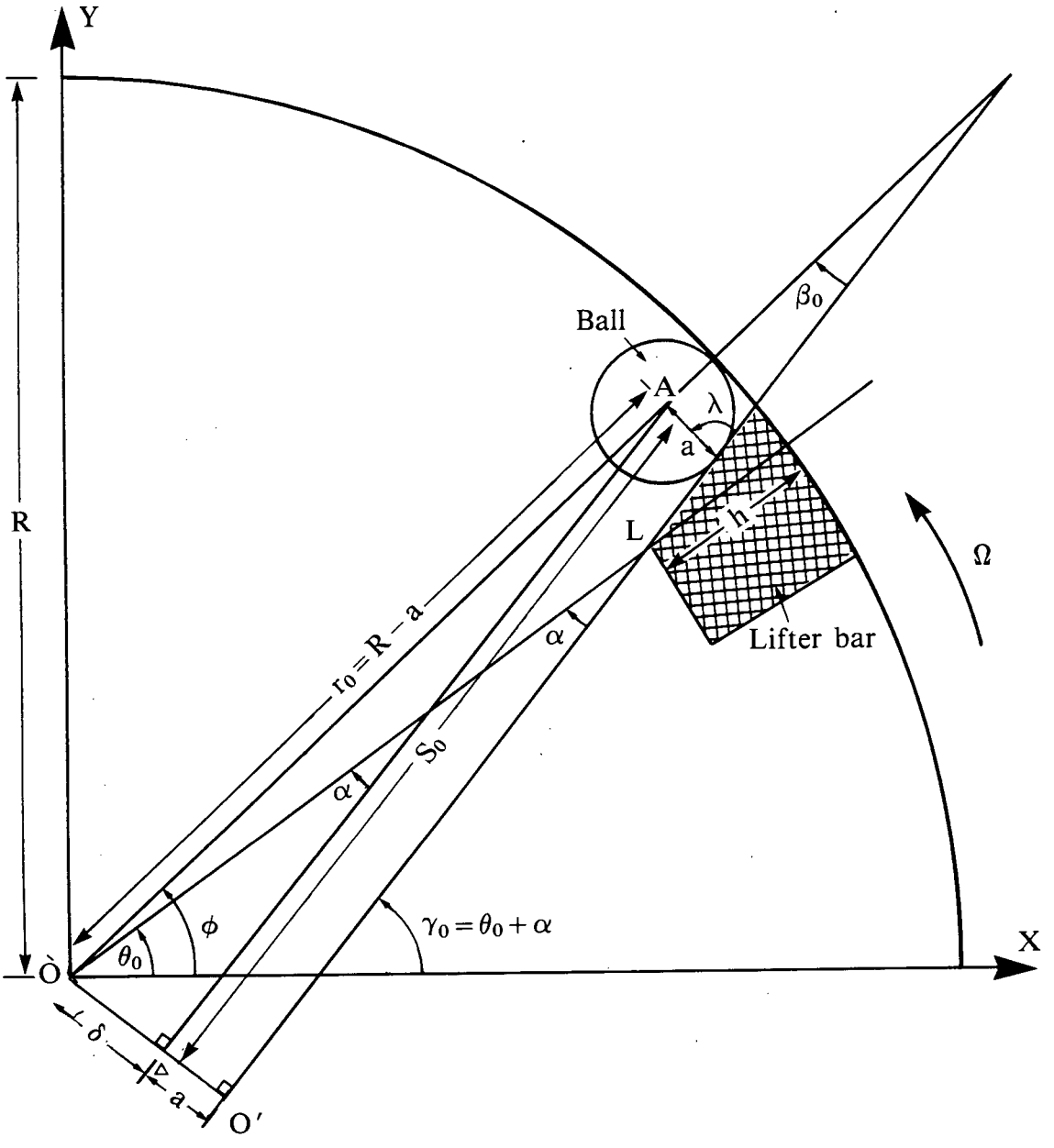

Figure 153. Ball on a lifter bar in a rotary mill

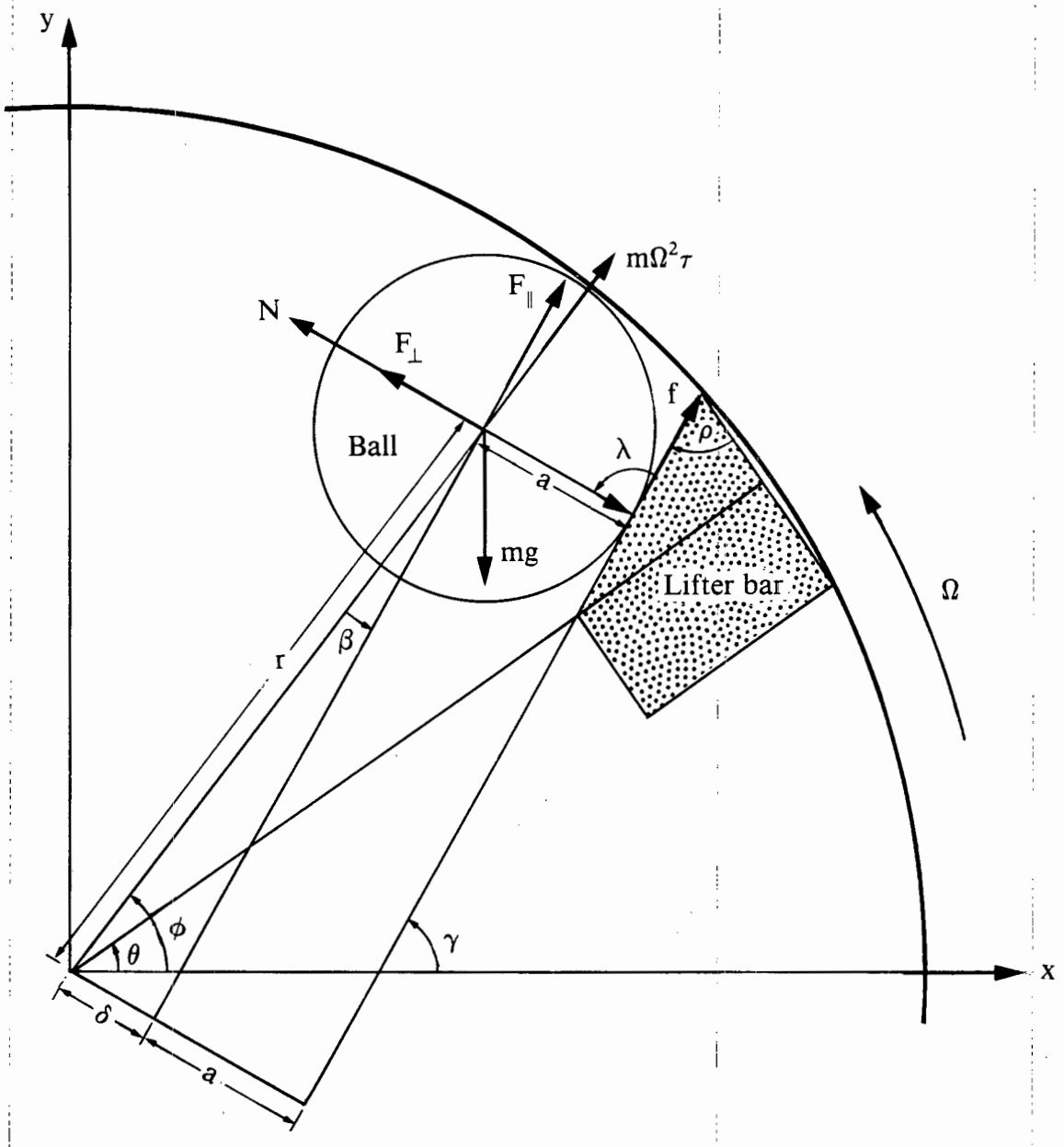

Figure 154. Forces acting on a ball on a lifter bar

At the point of equilibrium the forces ‖ to the face of the lifter bar are:

$$m\Omega^2 r_o.\cos\beta_o + \mu_s N - mg.\sin\gamma_o = 0 \tag{34}$$

and forces ⊥ to the face of the lifter bar are:

$$N - mg.\cos\gamma_o - m\Omega^2 r_o.\sin\beta_o = 0 \tag{35}$$

Substituting for N into equation (1), and dividing by m, gives:

$$\begin{aligned} &\Omega^2 r_o(\cos\beta_o + \mu_s.\sin\beta_o) + g(\mu_s.\cos\gamma_o - \sin\gamma_o) = 0 \\ \rightarrow\ &\sin\gamma_o - \mu_s.\cos\gamma_o = \frac{1}{g}.\Omega^2 r_o(\cos\beta_o + \mu_s.\sin\beta_o) \end{aligned} \tag{36}$$

Substituting $\tan\kappa$ for μ_s, where $\kappa \equiv$ friction angle,
and multiplying by $\cos\kappa$ yields:

$$\begin{aligned} \sin\gamma_o.\cos\kappa - \cos\gamma_o.\sin\kappa &= \frac{\Omega^2.r_o}{g}(\cos\beta_o.\cos\kappa + \sin\beta_o.\sin\kappa) \\ \sin(\gamma_o - \kappa) &= \frac{\Omega^2.r_o}{g}.\cos(\beta_o - \kappa) \\ \gamma_o &= \kappa + \arcsin\left(\frac{\Omega^2.r_o}{g}.\cos(\beta_o - \kappa)\right) \end{aligned} \tag{37}$$

For s̈ , which is the unit vector parallel to the face of the lifter bar and which is directed outwards, it can be seen from Figure 143 that, at the point of equilibrium:

$$s_o = r_o.\cos\beta_o \tag{38}$$

$$\beta_o = \arcsin\left(\frac{\delta}{r_o}\right) \tag{39}$$

where $\delta = (R - h).\sin\alpha - a \equiv$ constant.

By use of equations (27), (28), and (29) the location of the ball at the point of equilibrium can be determined fully.

It should be noted that the directions of some of the the forces change as the face angle of the lifter bar changes.

radial lifter: $\alpha = 0 \Rightarrow \delta = 0 \Rightarrow \beta_o = 0$

lower face angle: $\alpha > 0 \Rightarrow \delta > 0 \Rightarrow \beta_o > 0$

higher face angle (eg. 90°): $\alpha < 0 \Rightarrow \delta < 0 \Rightarrow \beta_o < 0$

I.2 BALL MOVING ALONG LIFTER

Between the point of equilibrium and the tip of the lifter bar the ball rolls and slides down the face of the bar. It is not projected into free flight from the point of equilibrium because while N is finite, the ball must interact with the lifter bar. It can happen that the face of the lifter bar is almost vertical, i.e. $\gamma \approx 90°$ while the ball is still in contact with the bar. In this case, the ball will fall away from the lifter bar once the normal force N is zero. From eqn. (25):

$$\begin{aligned} m\Omega^2 r.\sin\beta + mg.\cos\gamma &= 0 \\ g.\cos\gamma + \Omega^2\delta &= 0 \end{aligned} \qquad (40)$$

All calculations must be checked continuously for this condition, as the following derivations apply where N is positive and the ball remains in contact with the face of the lifter bar until it reaches the tip of the bar.

I.2.1 Pure rolling

If the static coefficient of friction is greater than zero, the ball will initially undergo pure rolling due to the torque applied by f (Figure 144), where:

$$f \leq \mu_s$$

If the forces that act on a sphere as it rolls down a slope that is subjected to a constant angular velocity are considered, the following equations can be derived, using Figure 145.

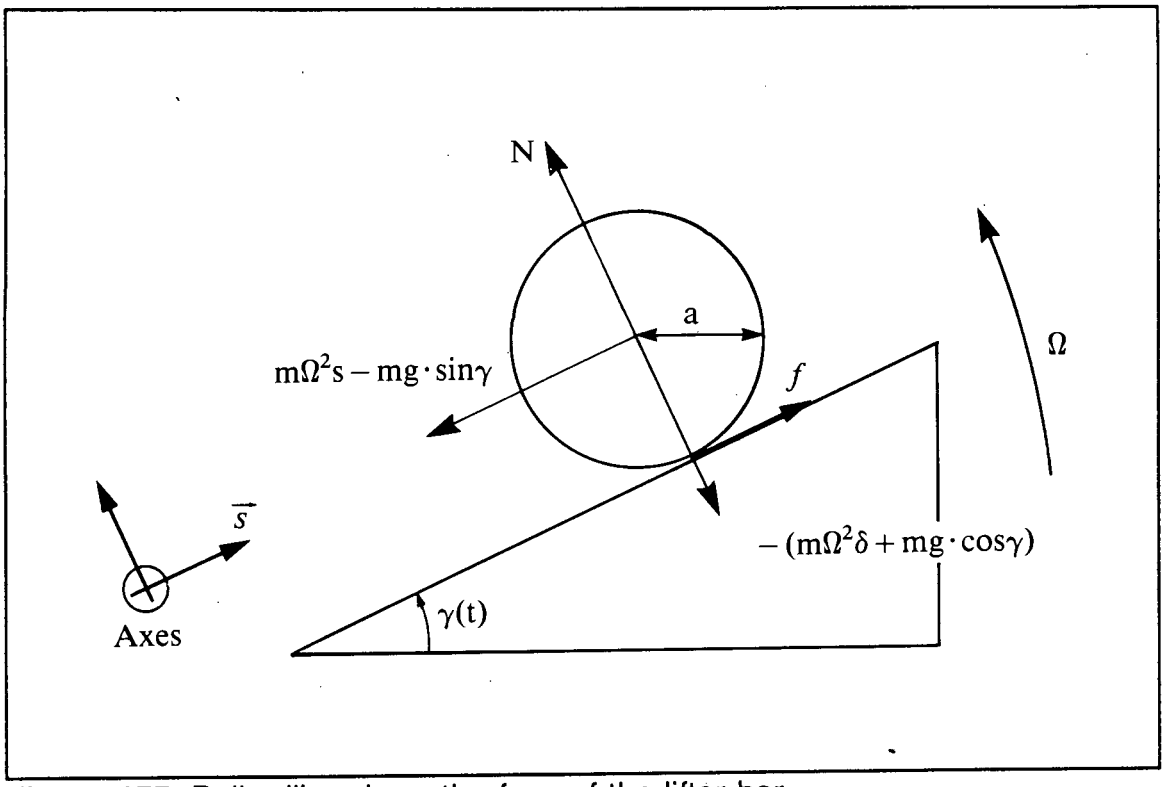

Figure 155. Ball rolling down the face of the lifter bar

normal to incline:

$$N - mg.\cos\gamma - m\Omega^2\delta = 0 \tag{41}$$

in plane of incline:

$$m\Omega^2 s - mg.\sin\gamma + f = m\ddot{s} \tag{42}$$

torque about centre of mass (cm)

$$\Gamma_{cm} = I_{cm}\alpha \tag{43}$$

where $\gamma = \gamma_o + \Omega.t$

The only force that acts at a distance from the centre of mass is f, so:

$$f.a = I_{cm}.\alpha$$

For a sphere,

$$I_{cm} = \frac{2}{5}ma^2 \tag{44}$$

This moment of inertia about the centre of mass is the only factor that differentiates between the motion of a ball and a rod when rolling down a plane. For a rod, I_{cm} = ½ma^2, which is the only factor that needs to be changed in order for the calculations to be applied to rods. While the ball doesn't slip, the angular acceleration is directly related to the linear acceleration by:

$$\alpha = -\left(\frac{\ddot{s}}{a}\right) \tag{45}$$

where s̈ is negative for a positive α, as a result of the orientation of the axes. Hence:

$$f = -\frac{2m\ddot{s}}{5} \tag{46}$$

The substitution of this into equation (12) yields:

$$\ddot{s} - \frac{5}{7}\Omega^2 s = -g.\sin\gamma \tag{47}$$

The solution of this linear, non-homogenous second order differential equation, which is consistent with the boundary conditions of: $s(o) = s_o$, which is known, and $\dot{s}_{t=0}$ = 0 (as the ball has not yet started rolling) is:

$$s(t) = \left(s_o - \frac{5g}{12\Omega^2}.\sin\gamma_o\right).\cosh\sqrt{\frac{5}{7}}.\Omega t - \frac{\sqrt{35}g}{12\Omega^2}.\cos\gamma_o.\sinh\sqrt{\frac{5}{7}}.\Omega t + \frac{5g}{12\Omega^2}.\sin\gamma \tag{48}$$

$$\dot{s} = \sqrt{\frac{5}{7}}\Omega\left(s_o - \frac{5g}{12\Omega^2}.\sin\gamma_o\right).\sinh\sqrt{\frac{5}{7}}.\Omega t - \frac{5g}{12\Omega}\left(\cos\gamma_o.\cosh\sqrt{\frac{5}{7}}.\Omega t - \cos\gamma\right) \tag{49}$$

These equations describe the position and velocity of the ball for pure rolling down the face of a lifter bar.

I.2.2 Maximum angle for pure rolling

There is a limit on the force f given by $\mu_s N$, so, for a given static coefficient of friction (μ_s) and mill parameters, there is a maximum angle (γ_m) up to which pure rolling will occur. Beyond this angle, the linear acceleration is too high for eqn. (35) to hold, and the surface of the sphere must begin to slip across the face of the lifter bar. The theoretical maximum angle for pure rolling can be calculated from the equations that express the forces on the rolling sphere, and that give its acceleration. The substitution of eqn. (37) into eqn. (32) yields:

$$f = \frac{2m}{7}(g.\sin\gamma - \Omega^2 s) \tag{50}$$

$f \leq \mu_s N$, so from eqns. (31) and (40)

$$\sin\gamma_m - \frac{7}{2}\mu_s.\cos\gamma_m \leq \frac{\Omega^2}{g}\left(\frac{7}{2}\delta\mu_s + s\right) \tag{51}$$

However, s = s(t), so this can only be solved numerically. The solution of eqn. (41) when $s = s_L$ yields γ_m(min), which is the minimum possible value of γ_m at the limit. Eqn. (38) can then also be numerically solved for $s = s_L$. However, if $\gamma_L > \gamma_m$(min), then there must be a transition from pure rolling to rolling and sliding.

I.2.3 Transition from pure rolling to combined rolling and sliding

The simultaneous solving of the eqns. (41) and (38) for γ_m and s(t) yields the limit for pure rolling. The resulting equation:

$$\frac{7}{12}.\sin\gamma_m - \frac{7}{2}\mu_s.\cos\gamma_m \leq \frac{7\Omega^2}{2g}\delta\mu_s + \left(\frac{s_o}{g}\Omega^2 - \frac{5}{12}\sin\gamma_o\right)\cosh\sqrt{\frac{5}{7}}\Omega t_l - \frac{5\sqrt{3}}{12}.\cos\gamma_o.\sinh\sqrt{\frac{5}{7}}\Omega t_l \tag{52}$$

can be solved by increasing t until the inequality is satisfied for $t = t_l$, where t_l is the time at which the transition from rolling to sliding takes place. By use of eqns. (38) and (39), the location and velocity of the ball can be calculated at this transition point.

I.2.4 Combined rolling and sliding

Once the ball begins to slide, its motion is retarded by the force arising from the kinetic coefficient of friction. A combination of rolling and sliding yields a linear motion that is equivalent to pure sliding under friction. As there is a torque about the centre of mass, there must still be an angular acceleration of the ball about its centre of mass, but under sliding conditions this is not dependent upon the linear motion. Some of the gravitational energy that would otherwise be lost due to friction, in the case of a flat-bottomed block, is instead converted to rotational motion of the ball about its centre. From eqn. (33) it is derived that:

$$f\,a = \frac{2}{5} m a^2 \alpha \tag{53}$$

Now:

$$f = \mu_k N = \mu_k (mg.\cos\gamma + m\Omega^2 \delta)$$

$$\text{so:} \qquad \alpha = \frac{5\mu_k}{2a}(g.\cos\gamma + \Omega^2 \delta) \tag{54}$$

which yields the angular acceleration of the ball once it starts sliding.

I.2.5 Sliding

When pure sliding down the face of the lifter bar is considered, and (with reference to Figure 144) the forces are resolved parallel and perpendicular to the face of the lifter bar, we have the following:

$\parallel$ to the face of the lifter bar:

$$m\Omega^2 r.\cos\beta + \mu_k N - mg.\sin\gamma = m\ddot{s} \tag{55}$$

$\perp$ to the face of the lifter bar:

$$N - mg.\cos\gamma - m\Omega^2 r.\sin\beta = 0 \tag{56}$$

The linear acceleration is found by the substitution for N into eqn. (45) and the expression of this in terms of s and δ :

From this transition point, it is easiest to start with a new time, which can be designated by τ. The boundary conditions at $\tau = 0$ are given as:

$$\ddot{s} - \Omega^2 s = g(\mu_k.\cos\gamma - \sin\gamma) + \Omega^2\mu_k\delta \qquad (57)$$

$s(o) = s_l$ and $\dot{s}_{\tau=o} = \dot{s}_l$

The solution of this differential equation that is consistent with these boundary conditions is:

$$\begin{aligned} s(\tau) = &\left[s_l + \mu_k\delta + \frac{g}{2\Omega^2}(\mu_k.\cos\gamma_l - \sin\gamma_l)\right]\cosh\Omega\tau \\ &+ \left[\frac{\dot{s}_l}{\Omega} - \frac{g}{2\Omega^2}(\mu_k.\sin\gamma_l + \cos\gamma_l)\right]\sinh\Omega\tau \\ &- \frac{g}{2\Omega^2}[\mu_k.\cos(\gamma_l + \Omega\tau) - \sin(\gamma_l + \Omega\tau)] - \mu_k\delta \end{aligned} \qquad (58)$$

$$\begin{aligned} \dot{s} = &\Omega\left[s_l + \mu_k\delta + \frac{g}{2\Omega^2}(\mu_k.\cos\gamma_l - \sin\gamma_l)\right]\sinh\Omega\tau \\ &+ \left[\dot{s}_l - \frac{g}{2\Omega}(\mu_k.\sin\gamma_l + \cos\gamma_l)\right]\cosh\Omega\tau \\ &- \frac{g}{2\Omega}[-\mu_k.\sin(\gamma_l + \Omega\tau) - \cos(\gamma_l + \Omega\tau)] \end{aligned} \qquad (59)$$

Equation (48) is solved numerically for $s(\tau) = s_L$, and yields τ, which in turn yields the velocity and position, γ, for the ball at the tip of the lifter bar. τ is zero at the transition point between rolling and sliding, so that the total time moving along the lifter bar is:

$$t_L = t_l + \tau.$$

I.3 LIFTER BAR LOWER THAN H_{crit}

For a lifter bar lower than the radius of the ball, the ball rests on the tip of the lifter, is lifted to the point of equilibrium, and then projected directly into flight. The critical height of the lifter, to be equal to or lower than the height of the ball radius, is dependent upon the face angle of the lifter. When the lifter is lower than the critical height $\lambda > 90°$, and when the lifter is higher then $\lambda = 90°$, so the calculation of λ indicates whether or not the ball is resting on the tip of the lifter. From Figure 146 it can be seen that:

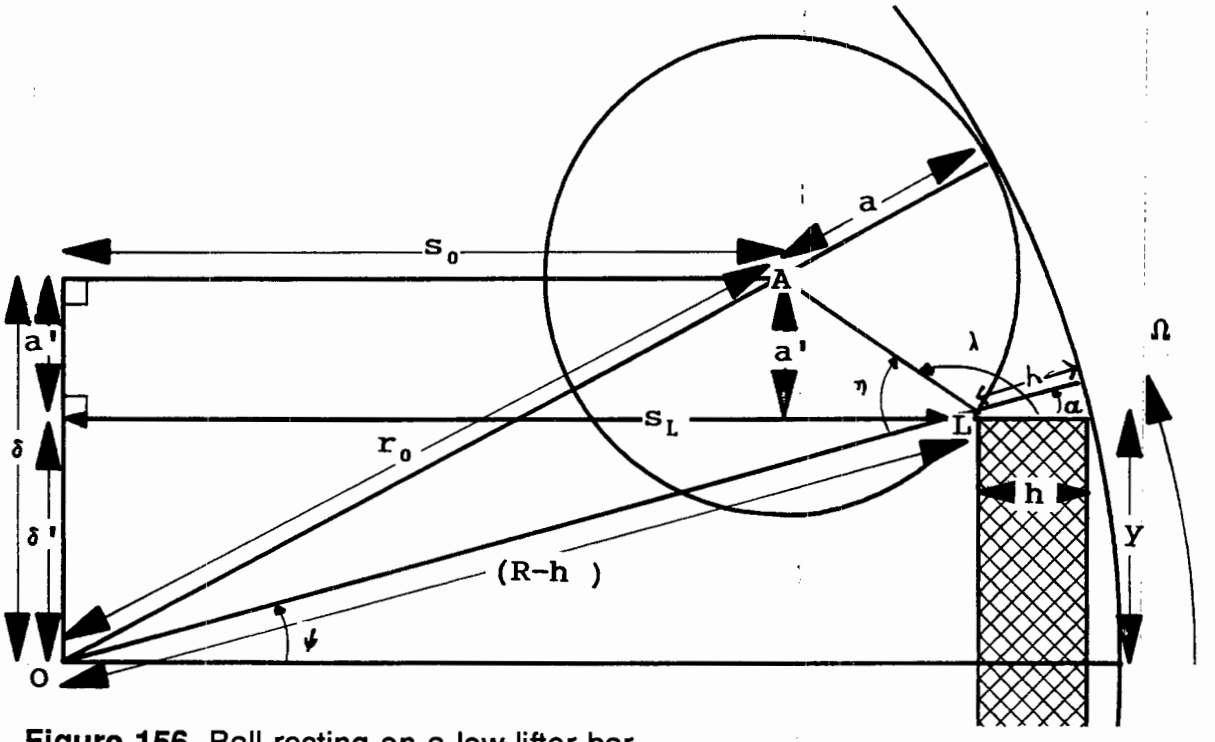

Figure 156. Ball resting on a low lifter bar

$$\eta = \arccos\left(\frac{a^2 + (R-h)^2 - r_o^2}{2a(R-h)}\right) \qquad (60)$$

$$\lambda = 180^o - \eta - \alpha \qquad (\alpha < 0 \text{ for } \perp \text{ lifter})$$

The forces acting on the ball when it rests on the tip of a low lifter are illustrated in Figure 147, and given by:

$$F_l = -mg.\sin\gamma - N.\cos(180° - \lambda) + m\Omega^2 r_o.\cos\beta_o + \mu_s N.\sin(180° - \lambda) \qquad (61)$$

These simplify to eqns (24) and (25) when $\lambda = 90°$ (λ cannot be less than 90°).

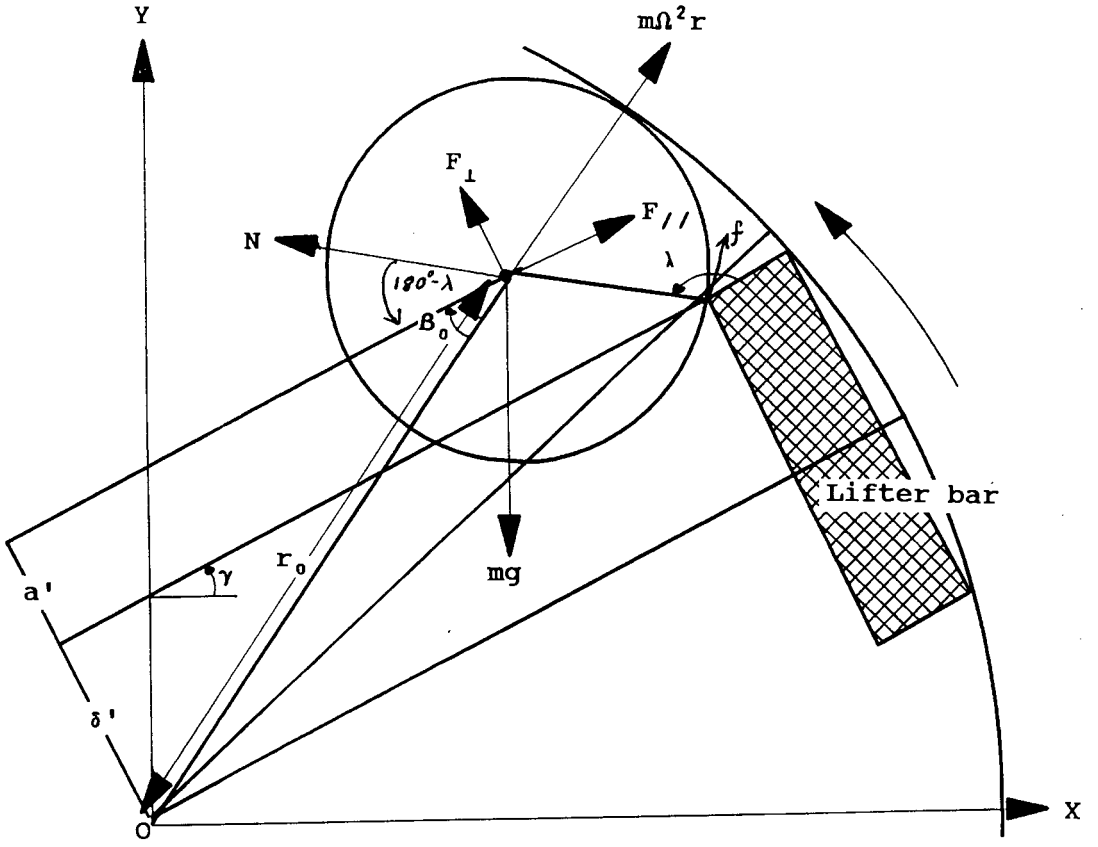

Figure 157. Forces acting on a ball resting on a low lifter

At equilibrium $F_\perp$ and $F_{//} = 0$, so from eqn. (52) we get

$$N.\sin(180° - \lambda) + N\mu_s.\cos(180° - \lambda) = mg.\cos\gamma_o + m\Omega^2 r_o.\sin\beta_o$$

$$\rightarrow \quad N = \frac{mg\cos\gamma_o + m\Omega^2 r_o.\sin\beta_o}{\sin(180° - \lambda) + \mu_s.\cos(180° - \lambda)} \tag{63}$$

Substituting eqn.(53) into eqn. (51) gives

$$- mg\sin\gamma_o - \frac{\cos(180° - \lambda)(mg.\cos\gamma_o + m\Omega^2 r_o.\sin\beta_o)}{\sin(180° - \lambda) + \mu_s.\cos(180° - \lambda)} \tag{64}$$

$$+ m\Omega^2 r_o.\cos\beta_o + \mu_s.\sin(180° - \lambda)\left(\frac{mg.\cos\gamma_o + m\omega^2 r_o.\sin\beta_o}{\sin(180° - \lambda) + \mu_s.\cos(180° - \lambda)}\right) = 0$$

Now :

$$\frac{\cos(180°-\lambda)}{\sin(180°-\lambda)+\mu_s.\cos(180°-\lambda)} = \frac{1}{\tan(180°-\lambda)+\mu_s} = \frac{1}{-\tan\lambda+\mu_s} = \frac{-1}{\tan\lambda-\mu_s} \quad (65)$$

And :

$$\frac{\mu_s.\sin(180°-\lambda)}{\sin(180°-\lambda)+\mu_s.\cos(180°-\lambda)} = \frac{\mu_s}{1+\frac{\mu_s}{\tan(180°-\lambda)}} = \frac{\mu_s}{1-\frac{\mu_s}{\tan\lambda}} = \frac{\mu_s.\tan\lambda}{\tan\lambda-\mu_s} \quad (66)$$

Substituting equations (55) and (56) into eqn. (54) and dividing by m gives.

$$-g\sin\gamma_o + \frac{(g.\cos\gamma_o + \Omega^2 r_o.\sin\beta_o)}{\tan\lambda-\mu_s} + \Omega^2 r_o.\cos\beta_o + \frac{\mu_s.\tan\lambda(g.\cos\gamma_o + \Omega^2 r_o.\sin\beta_o)}{\tan\lambda-\mu_s} = 0 \quad (67)$$

$$g\sin\gamma_o - \frac{g.\cos\gamma_o}{\tan\lambda-\mu_s} - \frac{\mu_s\tan\lambda.g.\cos\gamma_o}{\tan\lambda-\mu_s} = \frac{\Omega^2 r_o\sin\beta_o}{\tan\lambda-\mu_s} + \Omega^2 r_o\cos\beta_o + \frac{\mu_s\tan\lambda.\Omega^2 r_o\sin\beta_o}{\tan\lambda-\mu_s}$$

$$g\left[\sin\gamma_o - \frac{(\mu_s.\tan\lambda+1)\cos\gamma_o}{\tan\lambda-\mu_s}\right] = \Omega^2\left[\frac{(\mu_s.\tan\lambda+1)r_o.\sin\beta_o}{\tan\lambda-\mu_s} + r_o.\cos\beta_o\right]$$

$$\sin\gamma_o(\tan\lambda-\mu_s) - (\mu_s.\tan\lambda+1)\cos\gamma_o = \frac{\Omega^2 r_o}{g}[(\mu_s.\tan\lambda+1)\sin\beta_o + \cos\beta_o(\tan\lambda-\mu_s)] \quad (68)$$

using $\mu_s = \tan\kappa = \dfrac{\sin\kappa}{\cos\kappa}$ *substituting* $\tan\lambda = \dfrac{\sin\lambda}{\cos\lambda}$

$$\left(\frac{\sin\lambda}{\cos\lambda} - \frac{\sin\kappa}{\cos\kappa}\right)\sin\gamma_o - \left(1 + \frac{\sin\kappa.\sin\lambda}{\cos\kappa.\cos\lambda}\right)\cos\gamma_o =$$

$$\frac{\Omega^2 r_o}{g}\left[\cos\beta_o\left(\frac{\sin\lambda}{\cos\lambda} - \frac{\sin\kappa}{\cos\kappa}\right) + \sin\beta_o\left(1 + \frac{\sin\kappa.\sin\lambda}{\cos\kappa.\cos\lambda}\right)\right] \tag{69}$$

multiplying by $\cos\kappa.\cos\lambda$

$$(\sin\lambda.\cos\kappa - \cos\lambda.\sin\kappa) - (\cos\kappa.\cos\lambda + \sin\kappa.\sin\lambda)\cos\gamma_o =$$

$$\frac{\Omega^2 r_o}{g}[\cos\beta_o(\sin\lambda.\cos\kappa - \cos\lambda.\sin\kappa) + \sin\beta_o(\cos\kappa.\cos\lambda + \sin\kappa.\sin\lambda \tag{70}$$

$$\sin(\lambda - \kappa).\sin\gamma_o - \cos(\lambda - \kappa).\cos\gamma_o = \frac{\Omega^2 r_o}{g}[\sin(\lambda - \kappa).\cos\beta_o + \cos(\lambda - \kappa).\sin\beta_o]$$

$$\cos(\lambda - \kappa + \gamma_o) = \frac{\Omega^2 r_o}{g}\sin(\lambda - \kappa + \beta_o)$$

$$\rightarrow \quad \gamma_o = \kappa - \lambda + \arccos\left(\frac{\Omega^2 r_o}{g}.\sin(\lambda - \kappa + \beta_o)\right) \tag{71}$$

The ball is already at the tip of the bar, and is therefore projected directly into flight from the point of equilibrium. When the ball is at the tip of the lifter bar, the distance

s_L and the angle β_L are given by the condition that s_L = LO' (Figure 143), Therefore, from ∠ OLO':

$$s_L = (R - h).\cos\alpha \tag{72}$$

$$\beta_L = acrtan\left(\frac{\delta}{s_L}\right) \tag{73}$$

I.4 FREE-FLIGHT TRAJECTORY

At the tip of the lifter bar the ball is immediately projected into free-flight, as there is no further significant interaction with the tip of the bar as a result of the radial velocity

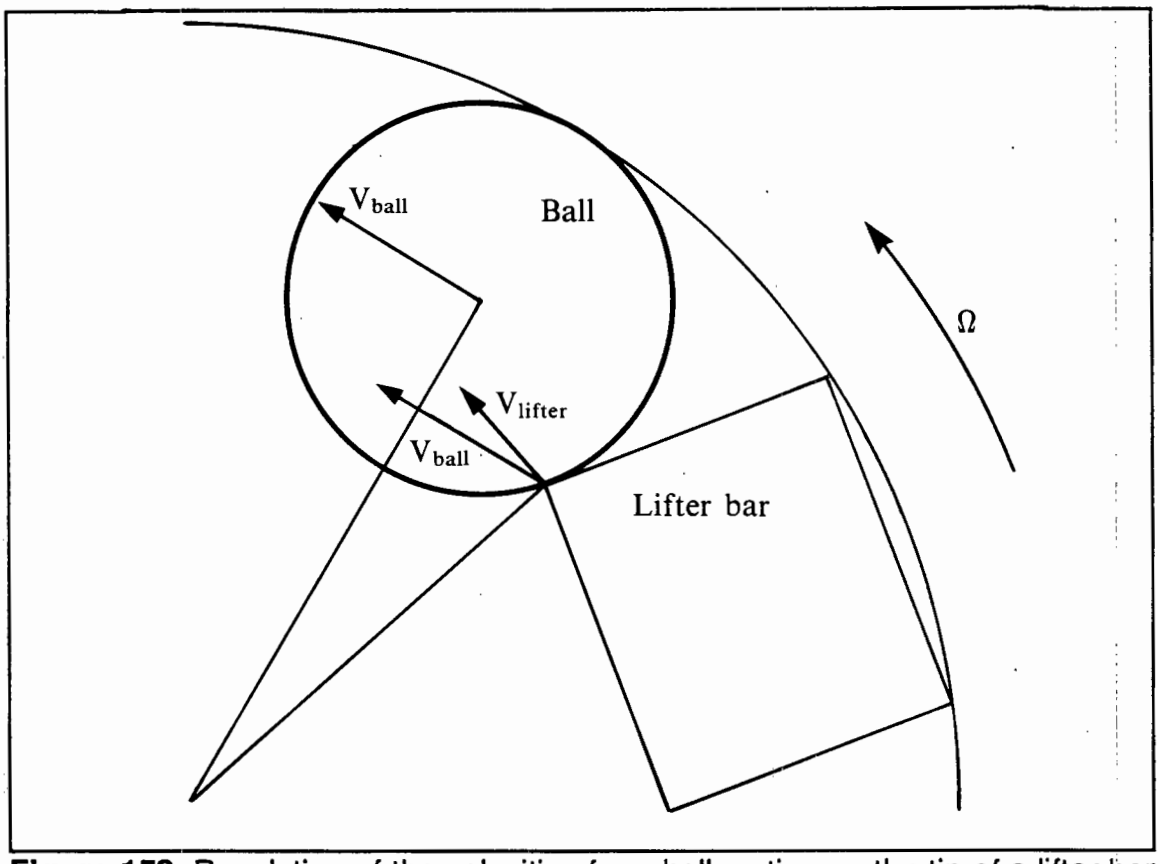

Figure 158. Resolution of the velocities for a ball resting on the tip of a lifter bar

of the ball, and the curve of its surface. Figure 148 illustrates clearly the reason why the ball escapes[1]. As the ball is a rigid object, all its parts travel with the same velocity as the centre of the ball, which causes a difference in velocity between the point of the ball that is in contact with the tip of the lifter bar and the tip itself. It can be seen that even if the ball does not have a radial velocity, i.e. for a lifter bar with a height that is the same as or less than a ball radius, there is a velocity difference between the ball and the tip of the lifter, and this has a radial component which allows the ball to escape from the lifter bar without interaction at the tip. If the lifter bar is worn or rounded at the tip, then the point at which the rounding begins is effectively the tip. The curvature of the surface of the lifter bar results in a decreasing face angle, and the lower the face angle of the lifter bar, the less the lift of the ball. Therefore, as soon as the ball, moving along the lifter bar, encounters a lower face angle, it must fall free of the bar. For a lifter bar that curves from the base, the ball must be projected into free flight from the point of equilibrium, and will not move along the bar at all.

The free flight trajectory is illustated in Figure 149. At the tip of the lifter bar, the following is known: s_L , $\dot{s}_L$, θ_L , β_L , γ_L. The radial coordinates of the ball are:

$$(r_L ; \phi_L) = \left(\frac{s_L}{\cos\beta_L} ; \gamma_L - \beta_L \right) \tag{74}$$

So that the free-flight trajectory can be determined, it is convenient to change the frame of reference to Cartesian coordinates, with the origin at the centre of the mill:

$$(x_L ; y_L) = (r_L.\cos\phi_L ; r_L.\sin\phi_L) \tag{75}$$

$\dot{s}_L$ is the velocity of the ball along the face of the lifter bar, to which the velocity due to the rotation of the mill must be added. This velocity component is tangential, and equals Ωr_L.

$$(v_{xL} ; v_{yL}) = (\dot{s}_L.\cos\gamma_L - \Omega r_L.\sin\phi_L ; \dot{s}_L.\sin\gamma_L + \Omega r_L.\cos\phi_L) \tag{76}$$

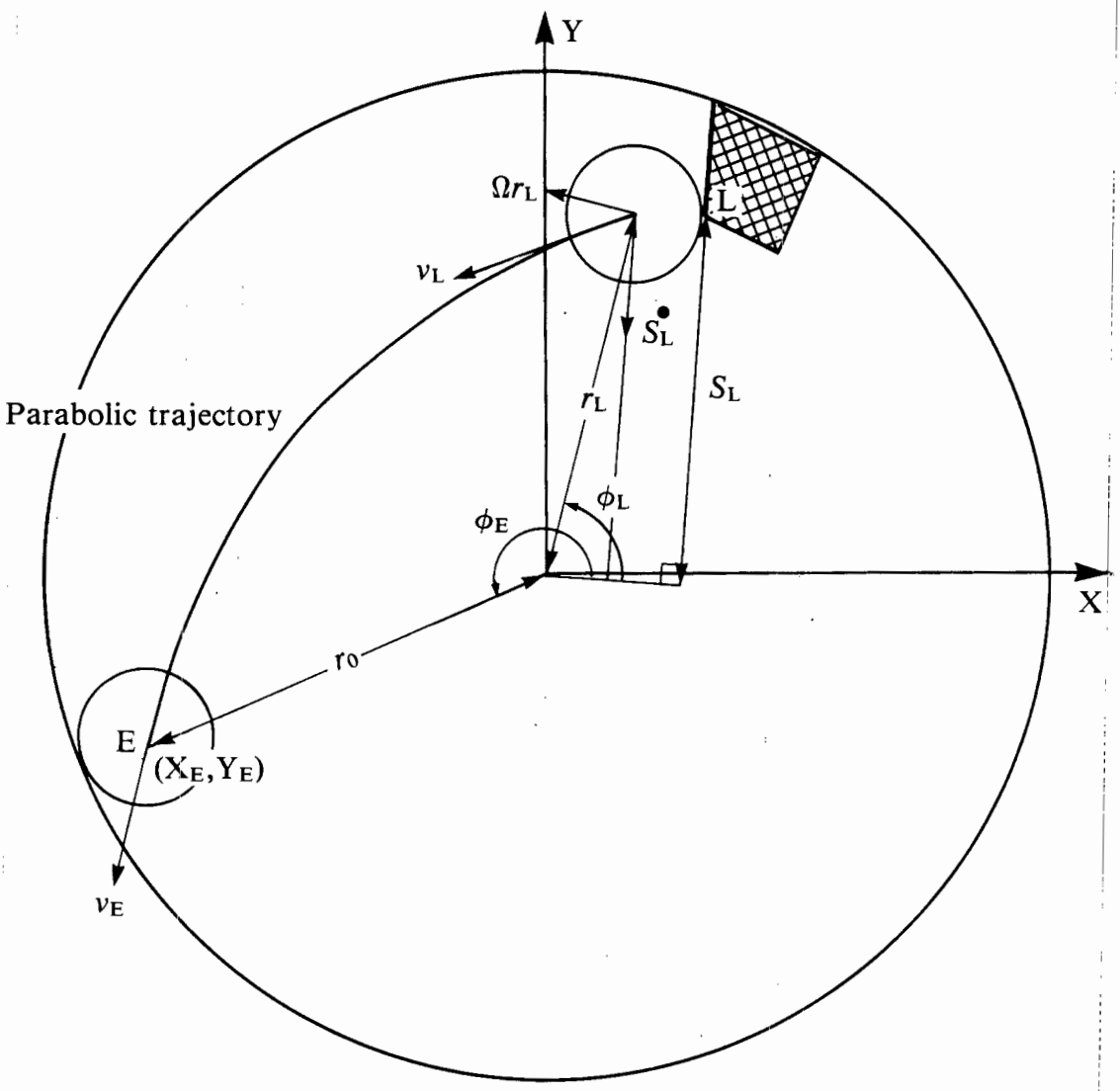

Figure 159. Parabolic trajectory of the ball from its point of departure from the lifter bar

The net velocity is:

$$V_L = \sqrt{V_{xL}^2 + V_{yL}^2} \tag{77}$$

The angle of projection to the horizontal is:

$$\sigma_L = actan\left(\frac{V_{yL}}{V_{xL}}\right) \tag{78}$$

Once in free flight the ball follows a parabolic path, which is given by:

$$x = x_L + v_{xL}t \tag{79}$$

$$y = y_L + v_{yL}t - \frac{1}{2}gt^2 \tag{80}$$

The point at which the ball strikes the shell of the mill, assuming that no interaction with the charge mass occurs en route, is satisfied by the condition:

$$x_E^2 + y_E^2 = r_o^2 \tag{81}$$

The velocity components are given by:

$$(v_{xE} ; v_{yE}) = (v_{xL} ; v_{yL} - gt) \tag{82}$$

so the velocity of impact with the mill shell is:

$$v_E = \sqrt{v_{yE}^2 + v_{xE}^2} \tag{83}$$

at an angle σ_E to the horizontal:

$$\sigma_E = \arctan\left(\frac{v_{yE}}{v_{xE}}\right) \tag{84}$$

The full path of the ball in flight, and its conditions of impact with the shell, have thus been derived. This completes the theoretical analysis of the motion of an isolated ball in a rotary mill with flat-faced lifter bars of any face angle and of any height.

1. VERMEULEN, L.A. Personal communication, 1989

APPENDIX II

DETAILED LISTING OF EXPERIMENTAL APPARATUS

II.1 X-RAY FILMING

X-ray equipment - Biplanar angioscope

Siemens biplane Angiskop
100 Kw X-ray tubes
Videomed high resolution TV channels, 1249 lines
Arritechno 35 mm cameras, 25 to 150 frames/s
Agfa Scopex IC3B, 35 mm film

Mill mounting frame

Painted mild steel structure
Motor - 0.5 Hp, asynchronous
Gearbox - Tavernelle, Var-spe, hydraulic, continuously variable speed, 0 - 1400 rpm
Speed indicator - Var-spe, dial indicator
Height to centre of mill - 1 to 1.2 m
Drive Wheels - Polyethylene,
- 80.5 mm diameter of loading surface
- 100 mm diameter support flange

Spirit level
Plumbline

Mill

Constructed entirely of perspex
Internal diameter 190.3 mm
Internal Length 97.0 mm
Diameter of flanges 360 mm
Thickness of flanges 11 mm
Centre locator, 1 mm ball bearing mounted in centre of door

Circumference demarcator, 0.5 mm flat metal foil ring, 190.3 mm internal diameter and 236 mm external diameter

Lifter bar mountings: two holes in each of 12 equally spaced rows along the length of the mill.

Numbering the runs, two sets of numbers (0 - 9) made of lead

Tube of silicone vacuum grease

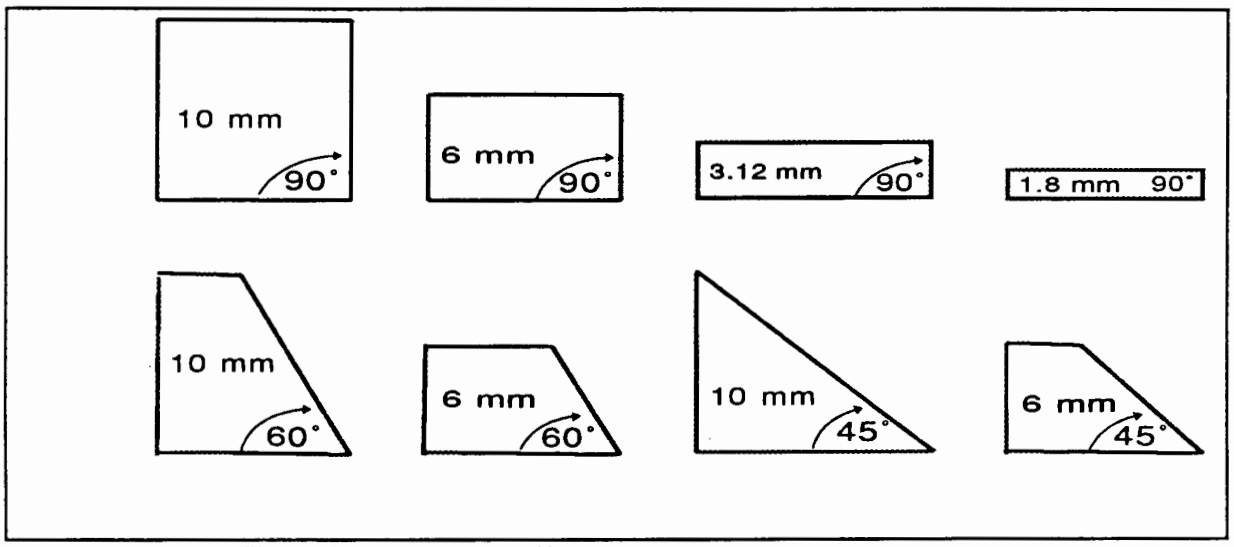

Figure 160. Profiles of the perspex lifter bars

Mill lining

Six sets of 12 lifter bars, made of perspex, and with 2 bolt holes tapped in the base of each, as per ?

Marker on end of each lifter bar, 0.5 mm metal foil

Two sets of 24 plastic screws for mounting the lifter bars, one set shorter to mount the low lifters

Transparent plastic sheets, with adhesive on one side, and plastic shavings glued to the other side

Mill charge

6.1 mm, 0.0947 g plastic beads, sufficient to fill the mill to 45% of capacity

Marked bead - lead strip glued down the centre of the bead, bead a different colour to the bulk charge for easy locating. mass of 0.2251 g

6 mm ball bearing, 0.8823 g

3.2 mm ball bearing, 0.1297 g

Glass boiling bead, 3.7 mm diameter, 0.0699 g

Slurry mixture - plastic shavings, powder, mixed to about 50% by volume with water

II.2 ANALYSIS OF X-RAY FILMS

Summagraphics MM101 graphics tablet

Four-button mouse, with transparent viewfinder

Hilyte 35 mm slide projector

Two 35 mm high, 132 mm diameter reels for winding the film onto

Rack for mounting the film reels on, with precision machined frame for feeding the film through, and holding it in the correct focal plane

Computer with Parallel communications port

II.3 GAMMA CAMERA FILMING

The mill and support frame the same as for X-ray filming.

Mill charge

Glass boiling beads, equal quantities of 4, 6, and 8 mm diameter

Hollow glass ball, 9.2 mm diameter

Needle and syringe for filling the ball with radioactive fluid

Quick-setting epoxy glue for sealing the ball

Radioactive tracer

Cobalt 60 radioactive fluid, Strength, at least 13.6 mcurie

Marking the mill circumference - thin plastic tubing, 600 mm long

Recording Equipment

Standard 8 mm portable video camera
Tripod
8 mm video film

II.4 MILLING TRIALS

Mill

1.8 m internal diameter, by 0.5 m long
Centrally mounted on a 100 mm diameter steel shaft
Motor - Asynchronous, 18.5 Kw, 14330 rpm
Gearbox - Stüfends, hydraulic, continuously variable, 120 - 1450 rpm, torque 800 Nm
15 rows of liner mounting bolt-holes
Clock, activated by mill power draw, accurate to 0.01 hr

Liners

Smooth 5 mm plates, bolted to the inside of the mill with round-head carriage bolts
Woven Steel mesh, 65 mm spacing, 10 mm wire meshing, 20 mm maximum thickness of mesh structure
Lifter bars, 5 sets of 15 of each type, as per Figure 161
Silicone sealant to seal bolt-holes

Mill charge

Wiwatersrand quartzite, topsize 200 mm
Ore sorting - rotary trommel screen, 0.5 m internal diameter
screen sizes: 12, 25, 50, 75 mm

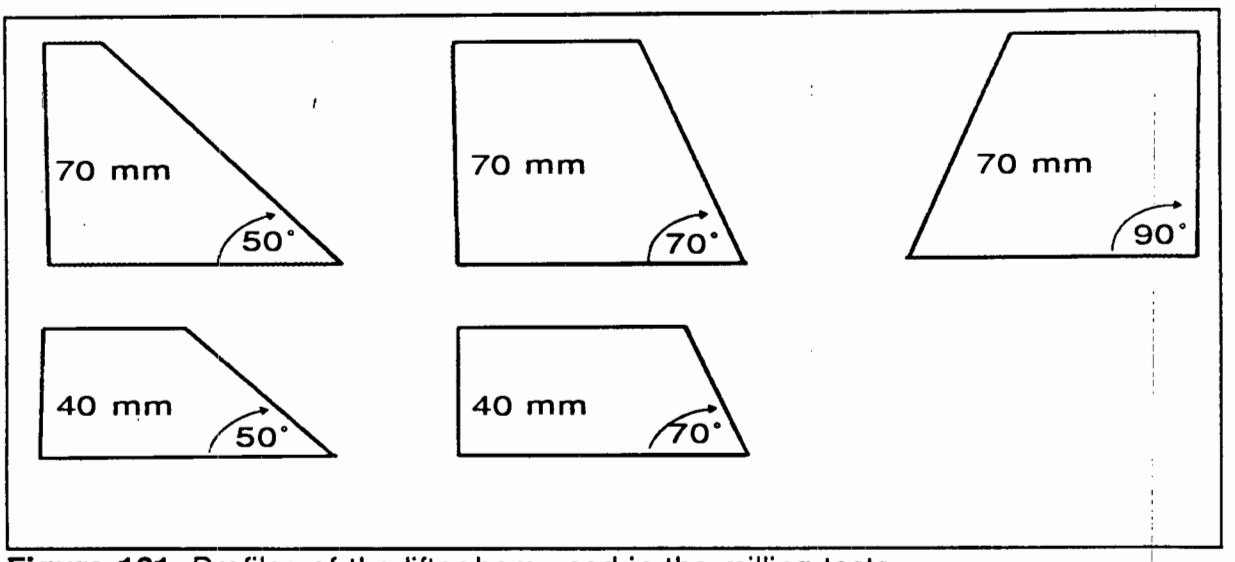

Figure 161. Profiles of the lifter bars used in the milling tests

Water measurement - 100ℓ steel drum, with fitted valve and inlet port, and mounted in a steel brace from which to suspend it

Masskot hanging scale, 0 - 600 kg ±0.2 kg

Forklift truck, with hydraulic drum-grabbing arms

Slurry sampling

250 by 400 mm plastic bags, with nominal wall thickness of 200 µm

Plastic 1ℓ measuring cylinder

Top pan balance, 0 - 1200 g, ±0.001 g

Wash bottles, 500 mℓ

Heated element strip sealer, for sealing the sampling bags

Sample sizing

Standard set of Tyler mesh screens: 38, 53, 75, 106, 150, 212, 300, 425, 600 µm

Automatic screen shaker

Low-pressure filter screens

Drying ovens

APPENDIX III
DERIVATIONS OF MINOR EQUATIONS

III.1 PERCENTAGE CRITICAL SPEED

The critical speed of a mill is that speed at which a particle against the shell will just centrifuge, provided there is no slip. This provides a useful basis for comparing different sized mills. At the top of the mill the following force balance exists:

$$m.\Omega^2.R = m.g$$

where Ω is the radial velocity of the mill

R is the internal mill radius, and D the diameter, in meters

m is the mass of the particle

g is the gravitational acceleration, 9.8 m/s^2

rpm is the rotational speed in revolutions per minute

$$\Omega_{crit} = \sqrt{\frac{g}{R}} = \sqrt{\frac{2g}{D}} \qquad (85)$$

Now:

$$rpm = \Omega \frac{60}{2\pi}$$

$$\Omega = \frac{rpm.\pi}{30} \qquad (86)$$

$$\%\ crit = \frac{\Omega}{\Omega_{crit}} 100$$

$$= rpm\sqrt{D}\left(\frac{\pi}{30\sqrt{2g}}\right)100 \qquad (87)$$

$$\%\ crit = \frac{rpm\sqrt{D}}{42.3} 100$$

III.2 ABSORPTION OF X-RAYS

The intensity of the incoming and outgoing radiation passing through a body is related by Lambert's law [1] :

$$I = I_o e^{-\mu x} \tag{88}$$

Where:

$$\mu = \rho\, 12.3 \left(\frac{Z}{E}\right)^{2.83} \qquad (cm^{-1}) \tag{89}$$

I = final intensity
I_o = initial intensity
Z = atomic number
E = energy of the emission
μ = absorption coefficient
ρ = density of the material

Glass is made up of silica, which has an atomic mass of 14. The density of glass is 2.2 g.cm^{-3}, and making allowance for a packing density of 0.8 of the balls, the bulk density of a charge of glass balls is 1.76. The strength of the emitted x-ray beam is 100 kW.

$$\Rightarrow \quad \mu = 0.0830$$

The length of the mill is 9.7 cm

$$\Rightarrow \quad I = I_o\, 0.47$$

This would be sufficient to allow a clear image of the mill contents.

What wasn't realised at the time of designing the apparatus, was that the asymmetric loading of the mill with balls (half packed, half empty) resulted in the x-ray equipment reducing its output so that the average intensity received by the detectors was at an acceptable level. This reduced output was about 70 kW. When the calculations are carried out for that strength of emission, the final intensity is found to be:

$$I = I_o\, 0.12$$

In addition to silica, traces of the following elements were found in the glass beads

Small beads	K, Ca, Ti, Na
Large beads	Pb, K

It seems that the quantity of these elements, along with the reduced strength of emission of the x-rays, was sufficient to reduce the output intensity to almost zero.

APPENDIX IV
DETAILED RESULTS

IV.1 X-RAY FILMS

Prints taken from the X-ray films are shown for every run. The direction of rotation of the mill is not constant, so is shown for each run. Run 0, has only 2 balls, runs 1 to 18 have 3 balls, and runs 19 to 38 have 4 balls, that are tracked. The balls are dark against the light background of the rest of the mill charge. The title of each photograph gives the percentage of the critical speed, the lifter height and lifter face angle.

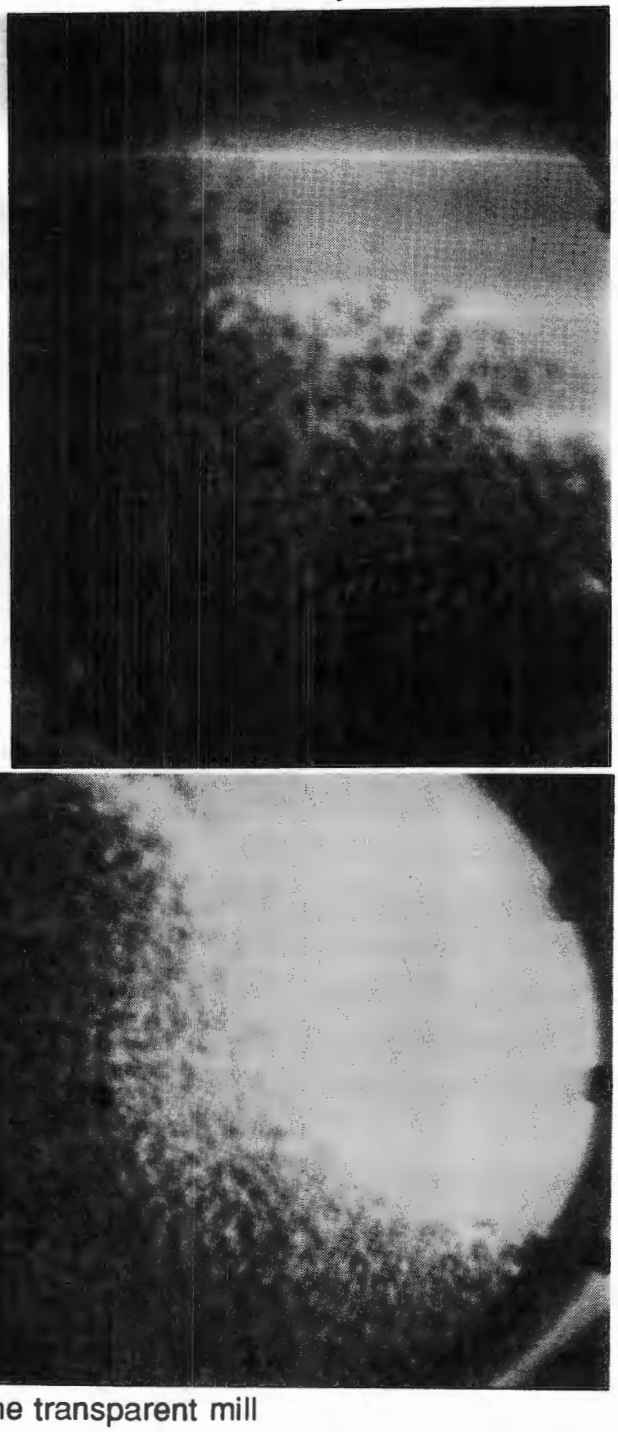

Run 0
73% , 6 mm , 60°

Run 1
68%, 3.12 mm, 90°

Figure 162. X-ray images of the balls in the transparent mill

Run 2

73%, 3.12 mm, 90°

Run 3

82%, 3.12 mm, 90°

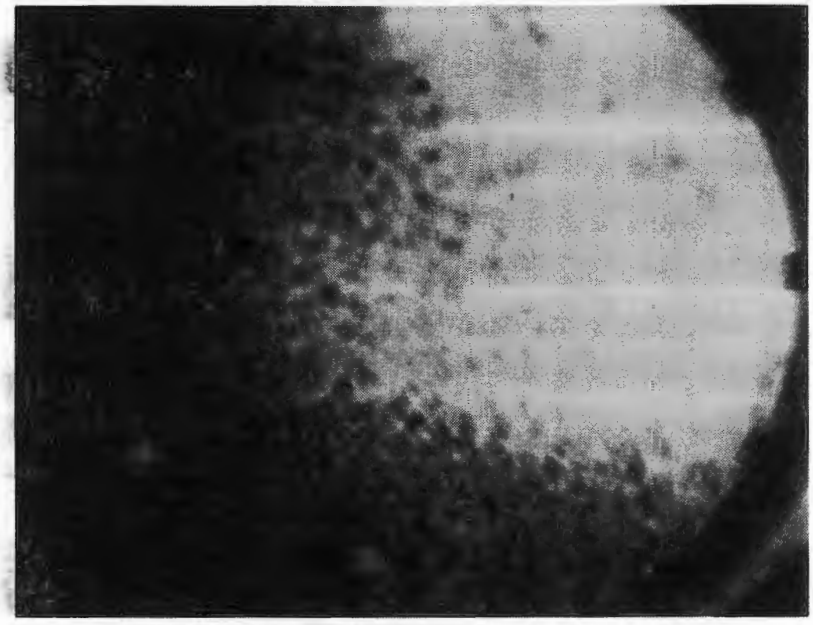

Run 4

82% , 1.8 mm , 90°

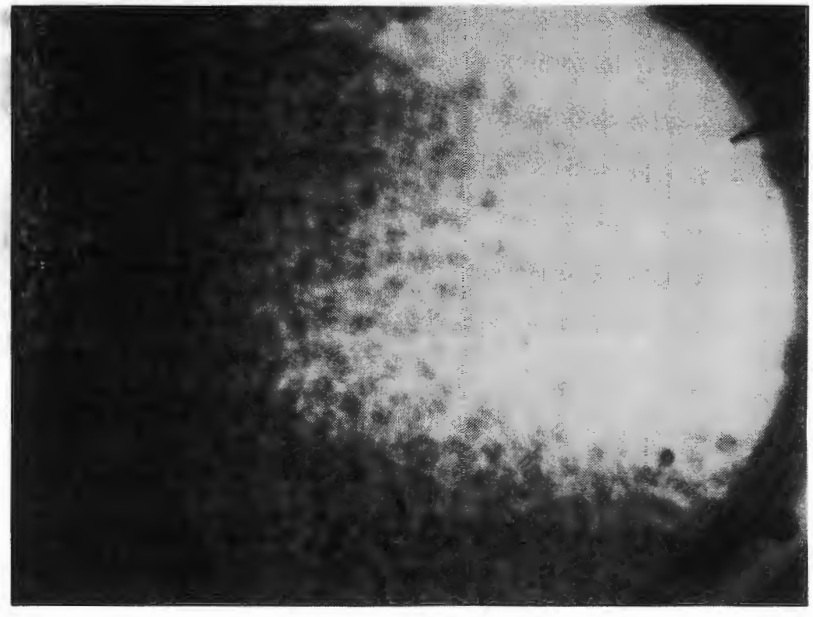

Run 5

73% , 1.8 mm , 90°

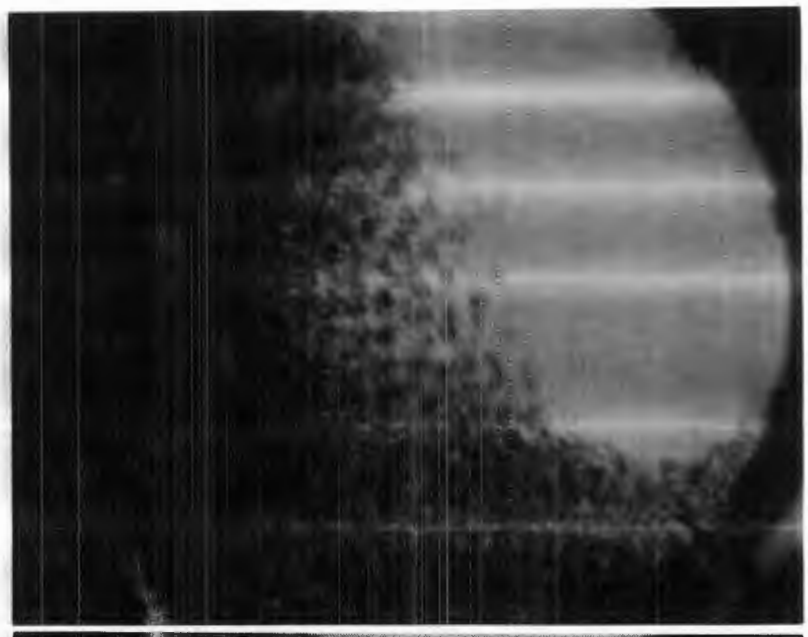

Run 6

68% , 1.8 mm , 90°

Run 7

92% , 1.8 mm , 90°

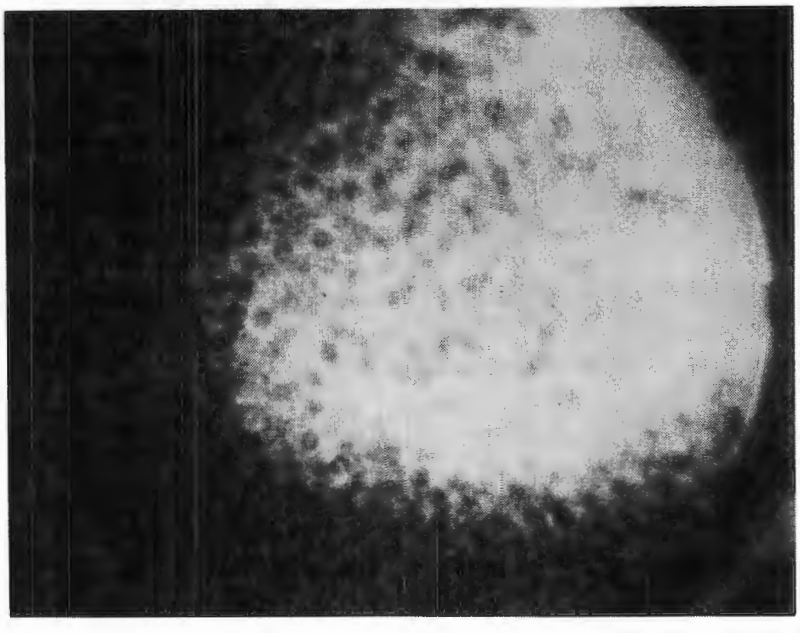

Run 8

68% , 10 mm , 60°

Run 8a

68% , 10 mm , 90°

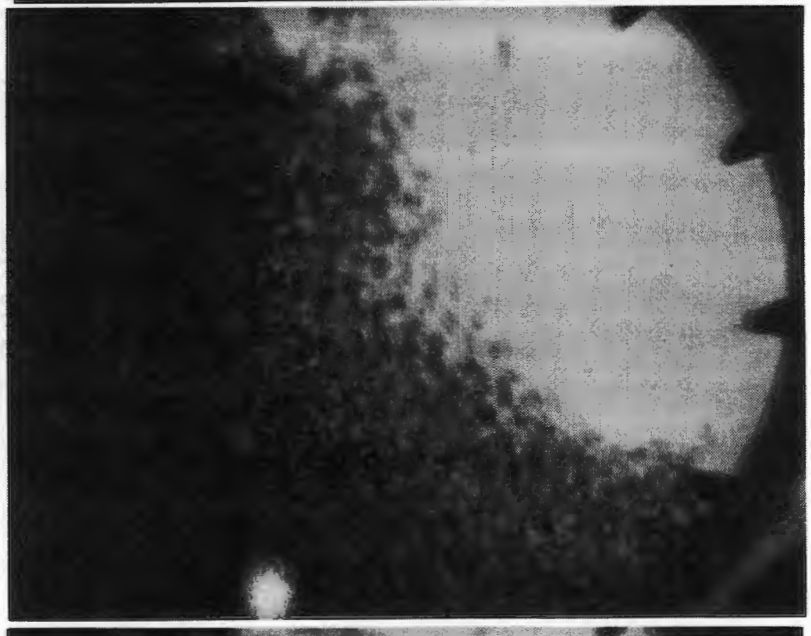

Run 9

73% , 10 mm , 90°

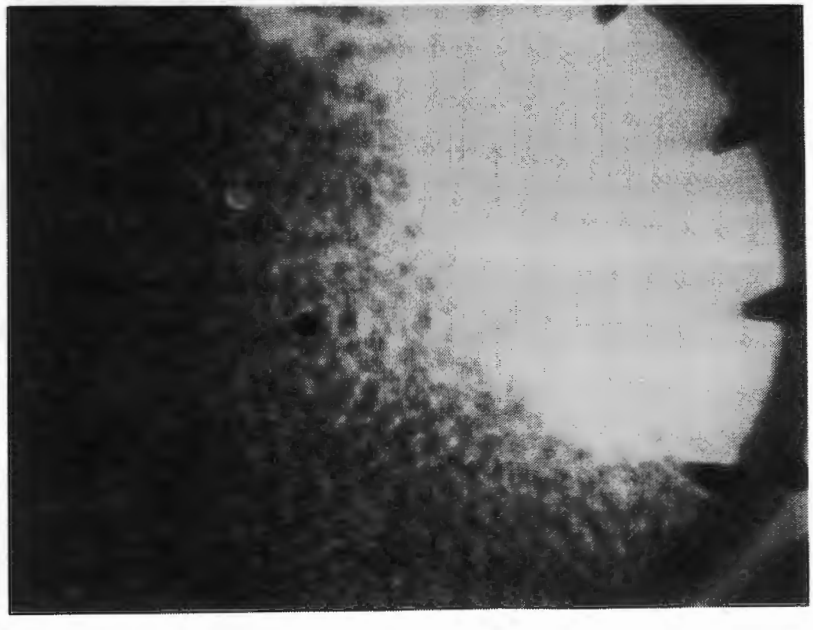

Run 10

82% , 10 mm , 90°

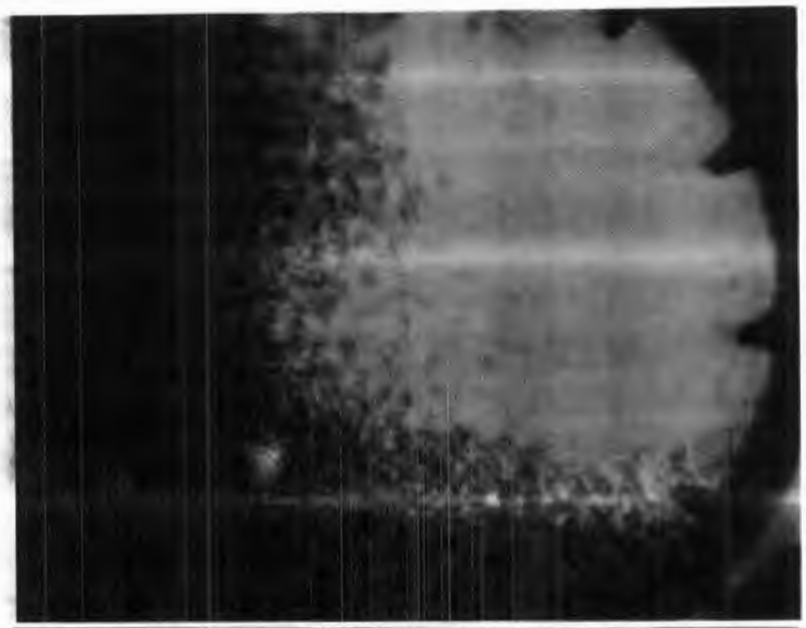

Run 11

82% , 10 mm , 60°

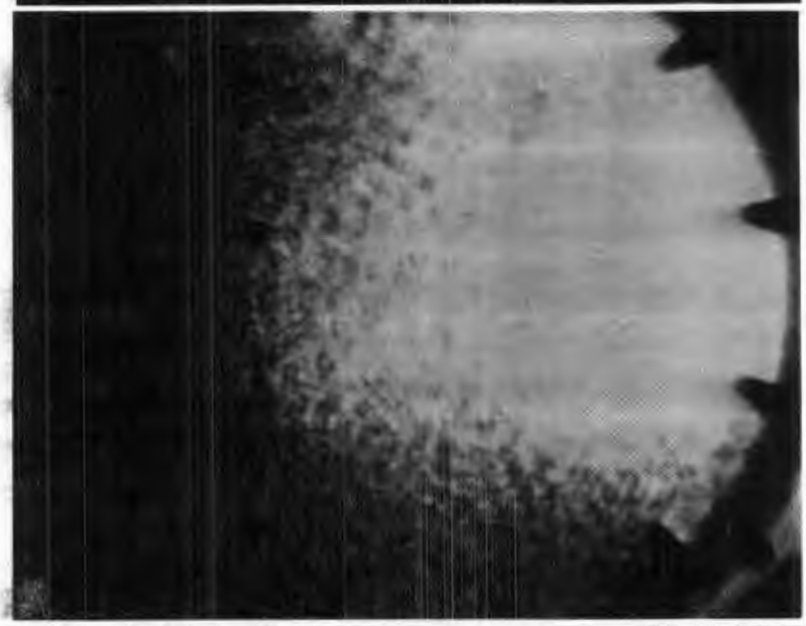

Run 12

73% , 10 mm , 60°

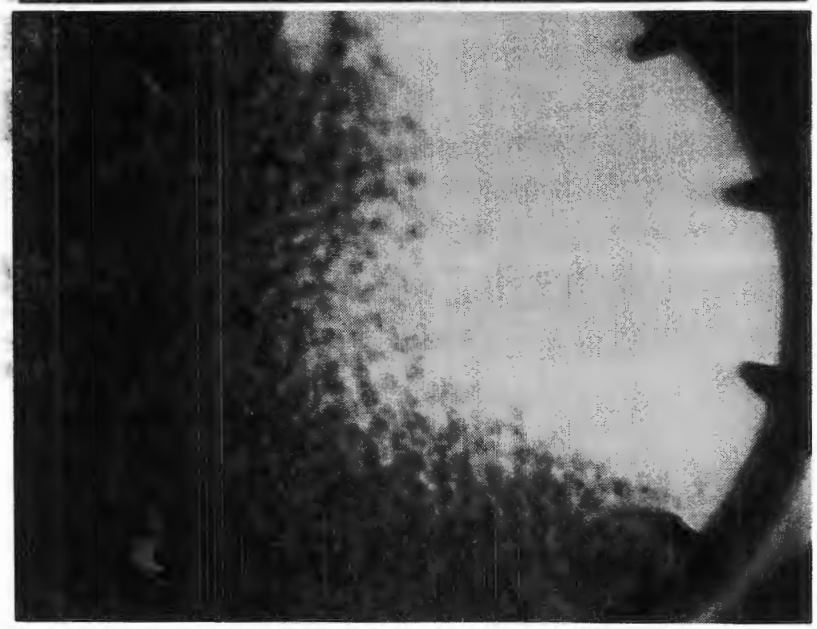

Run 13

68% , 10 mm , 60°

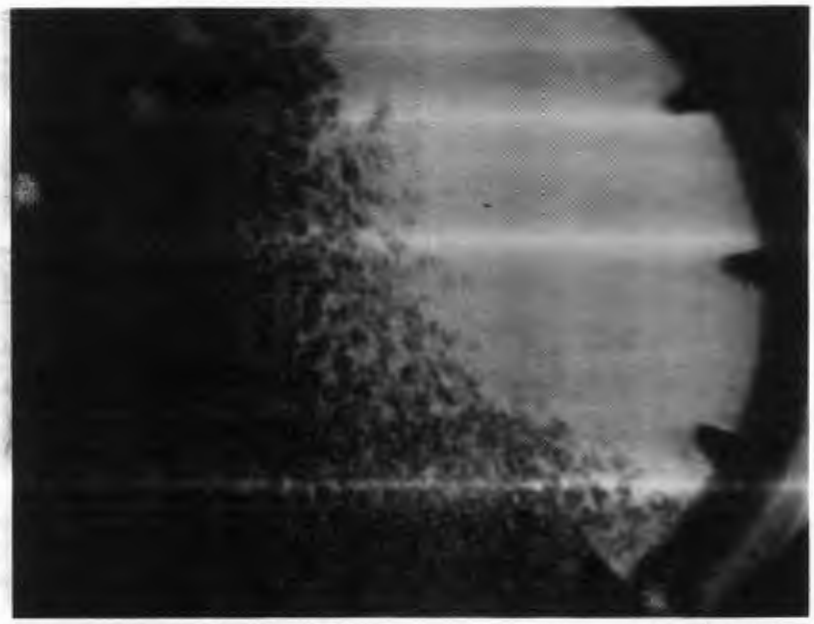

Run 14

68% , 6 mm , 45°

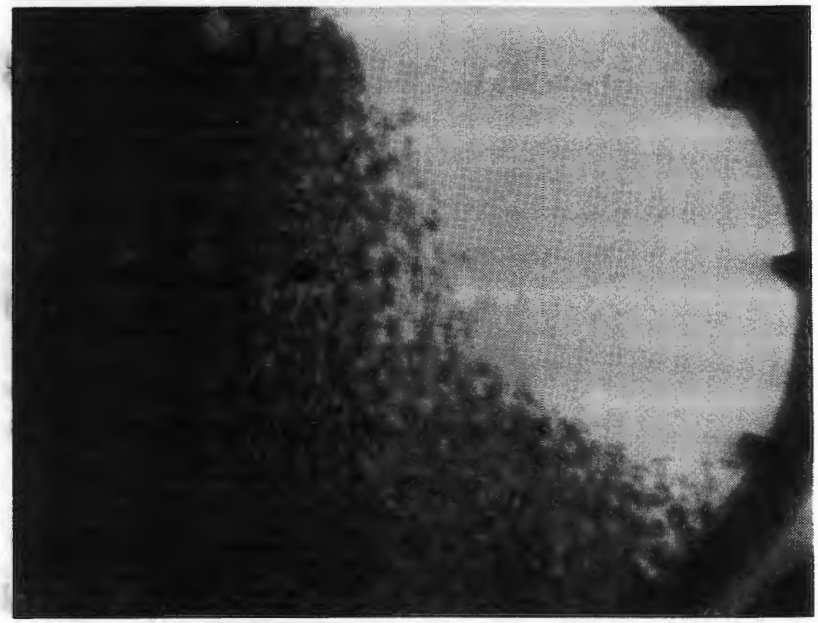

Run 15

73% , 6 mm , 45°

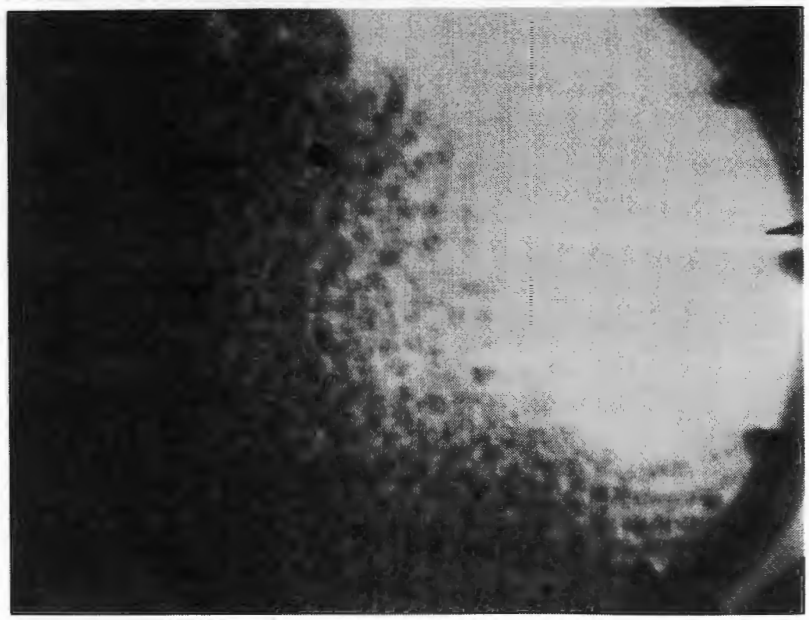

Run 16

82% , 6 mm , 45°

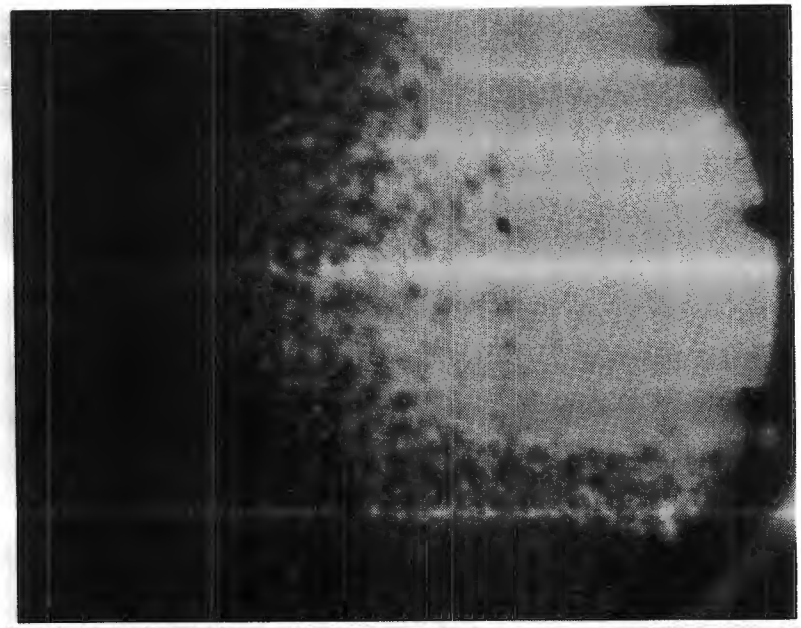

Run 17

82% , 6 mm , 90°

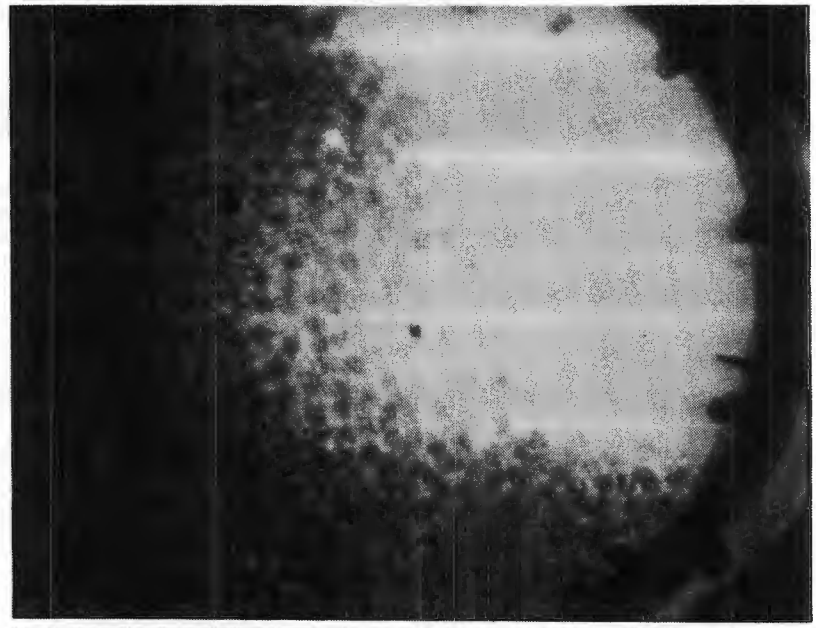

Run 18

73% , 6 mm , 90°

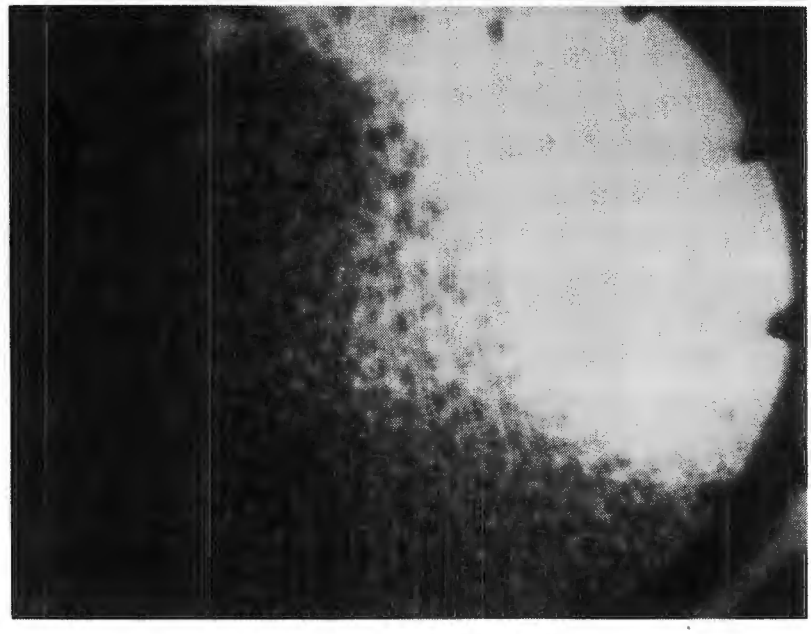

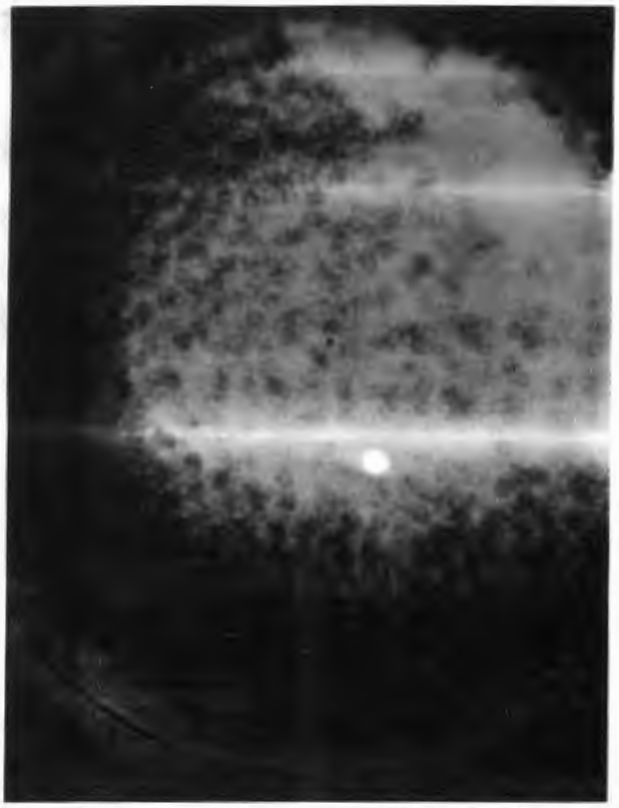

Run 19 - 92% , 3.12 mm , 90°

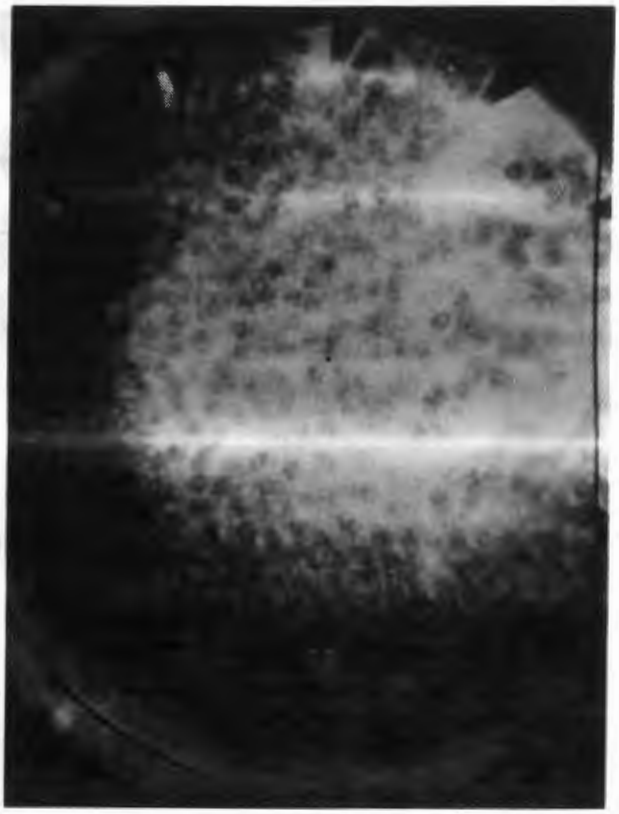

Run 20 - 92% , 10 mm , 60°

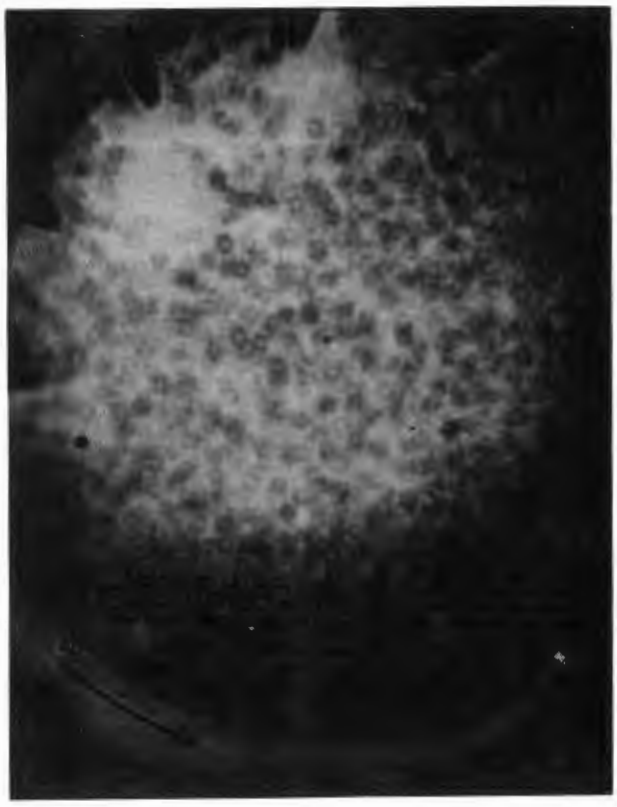

Run 21 - 92% , 10 mm , 90°

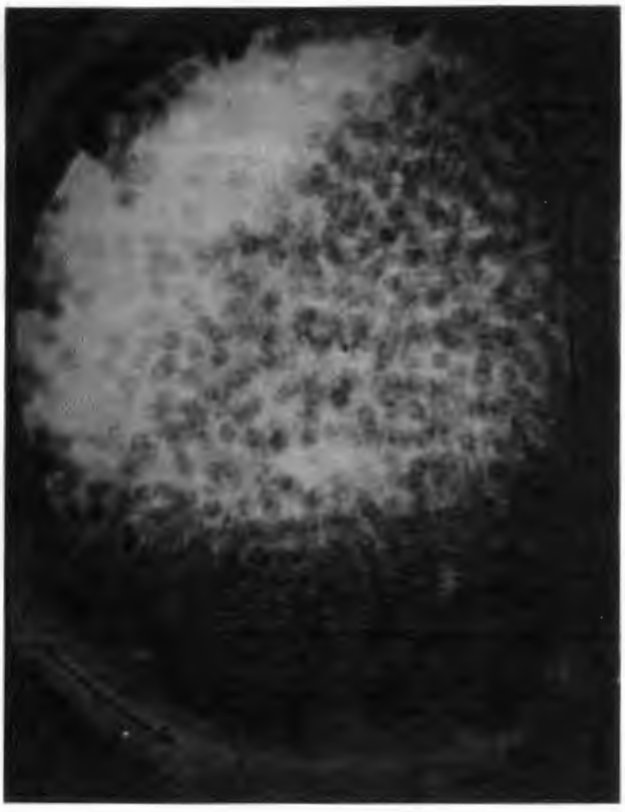

Run 22 - 92% , 6 mm , 90°

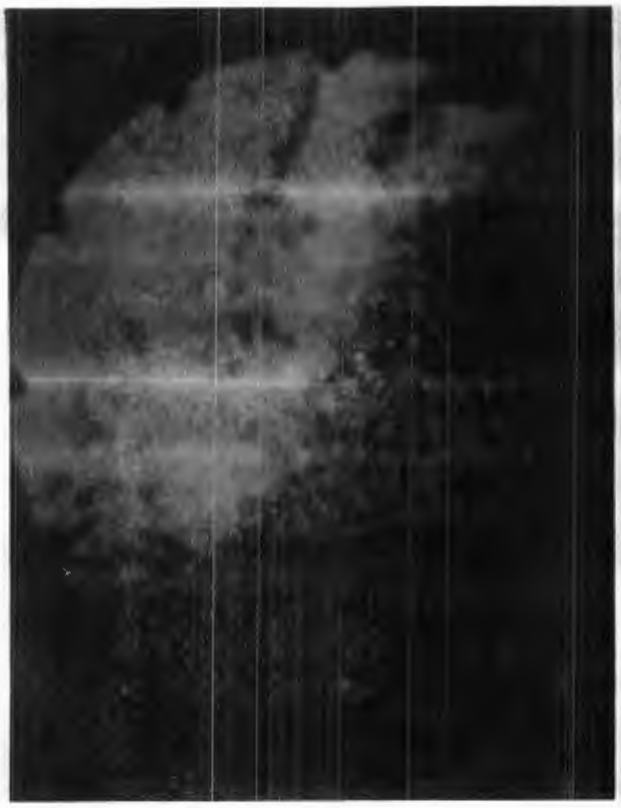

Run 23 - 68% , 6 mm , 90°

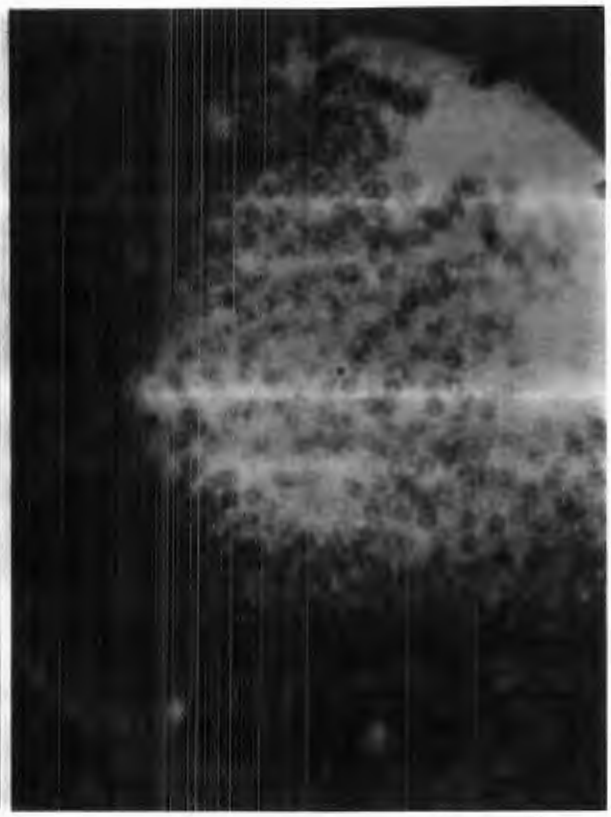

Run 24 - 92% , 6 mm , 45°

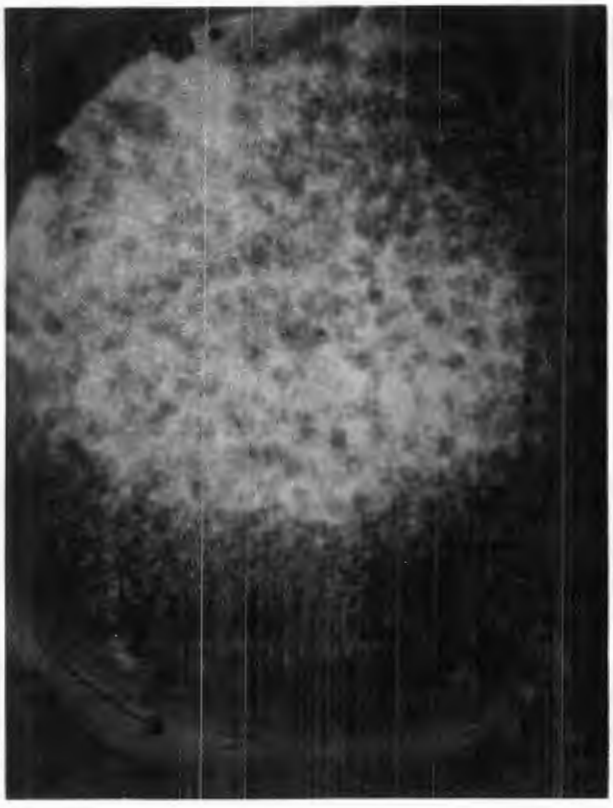

Run 25 - 92% , 6 mm , 60°

Run 26 - 82% , 6 mm , 60°

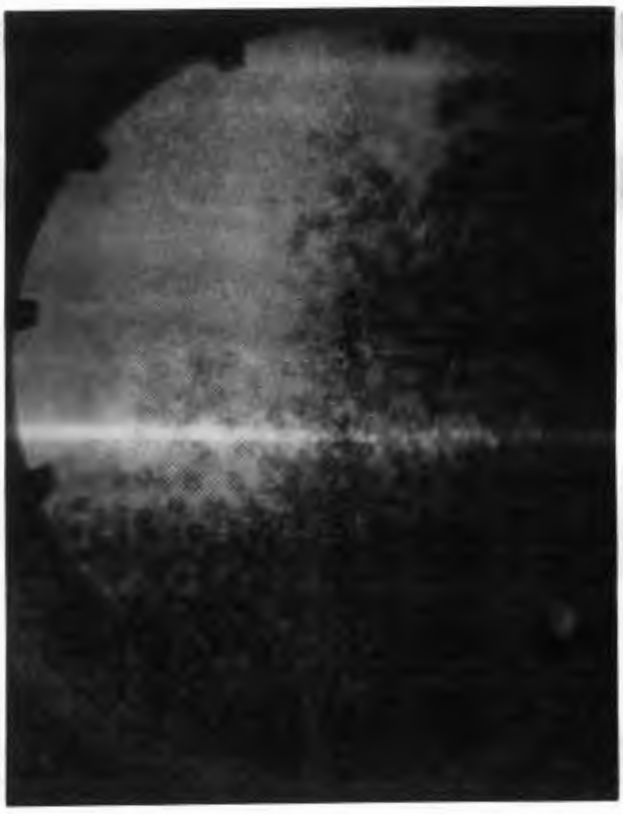

Run 27 - 73% , 6 mm , 60°

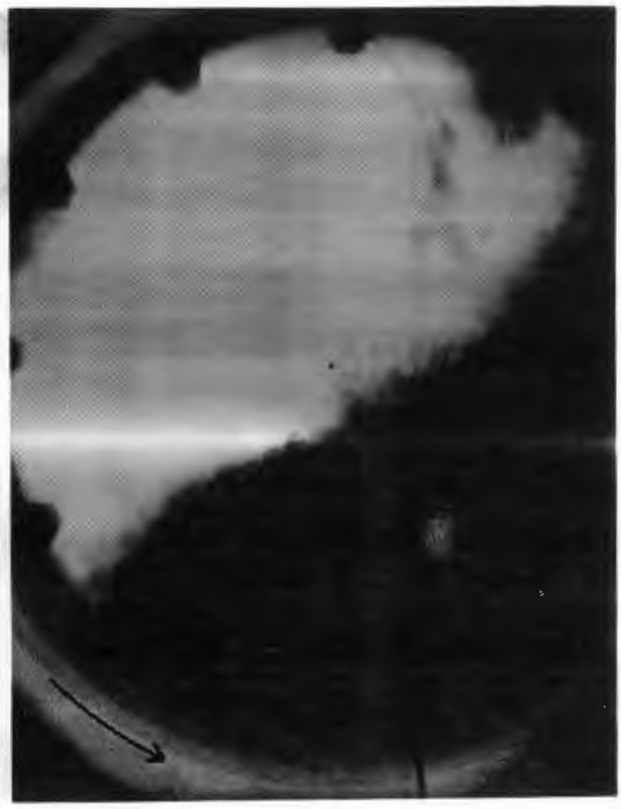

Run 28 - 73% , 6 mm , 60° , slurry

Run 29 - 82% , 6 mm , 60° , slurry

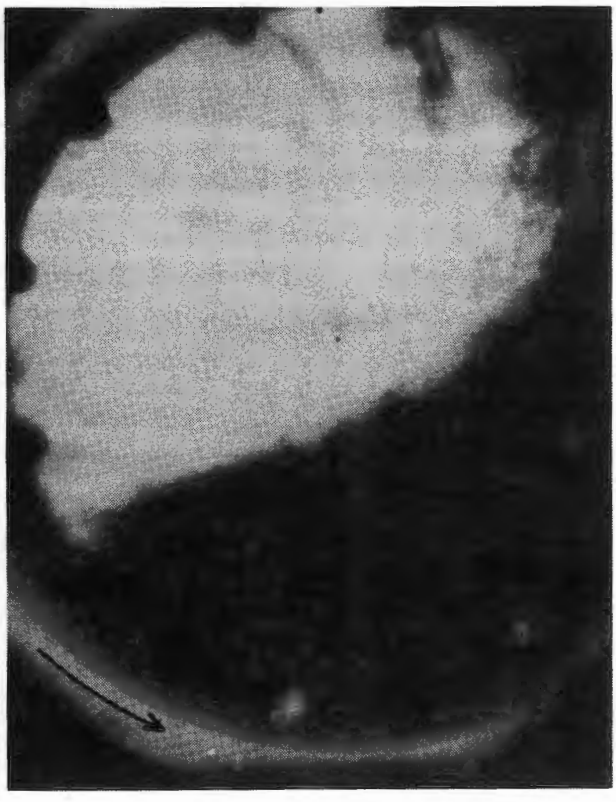

Run 30 - 92% , 6 mm , 60° , slurry

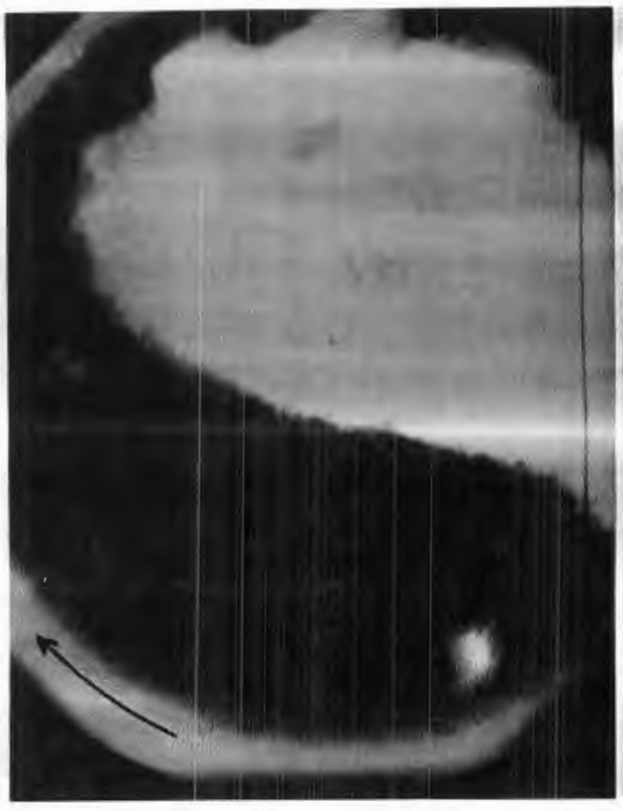

Run 31 - 92% , 6 mm , 90° , slurry

Run 32 - 100% , 6 mm , 90°

Run 33 - 73% , 6 mm , 90° , slurry

Run 34 - 68% , smooth

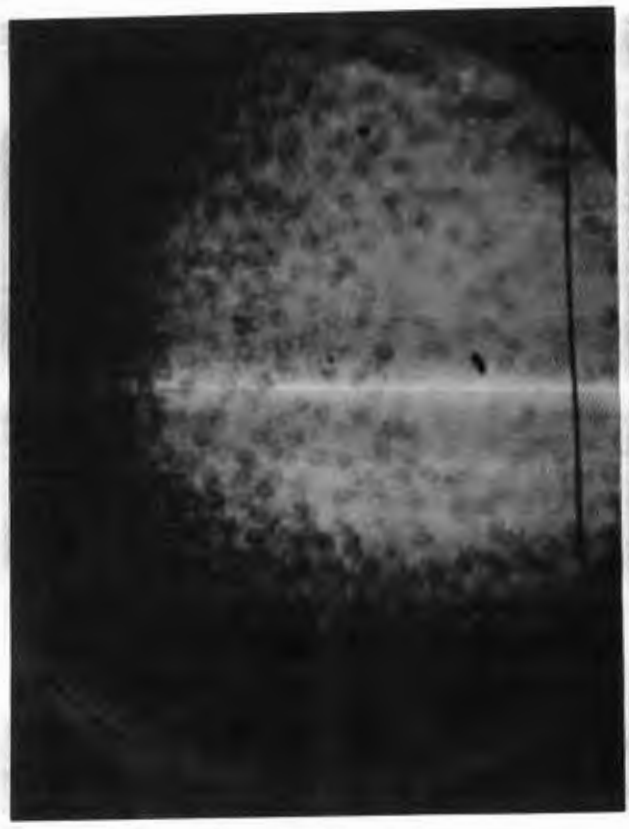

Run 35 - 100% , smooth

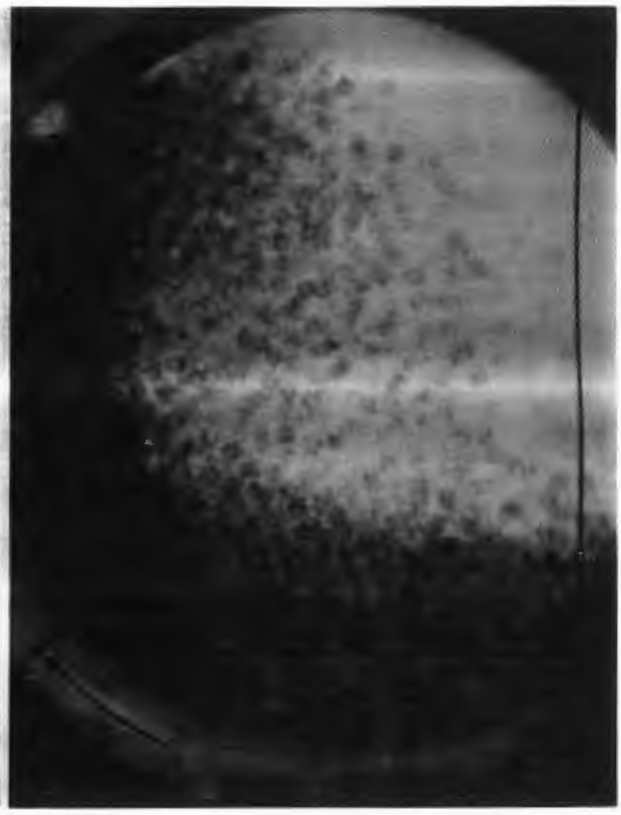

Run 36 - 92% , smooth

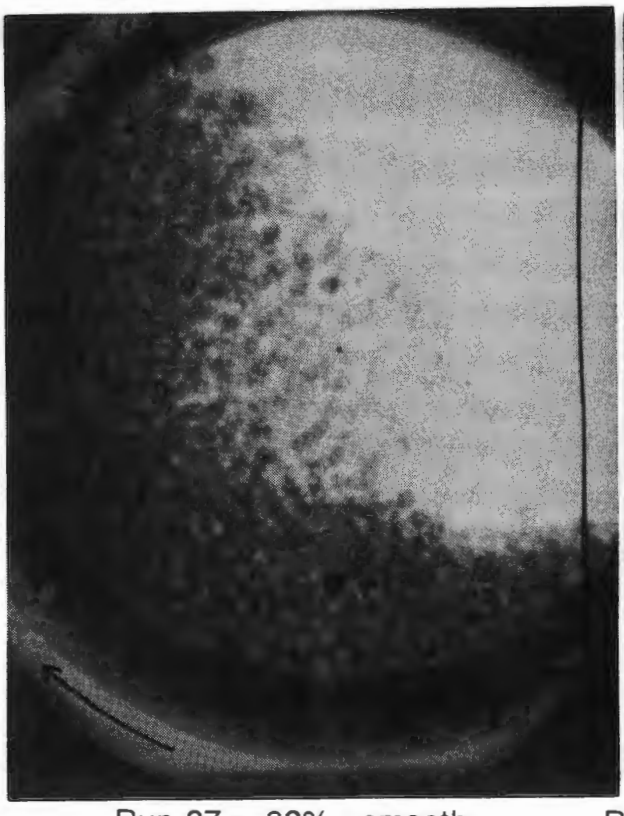

Run 37 - 82% , smooth

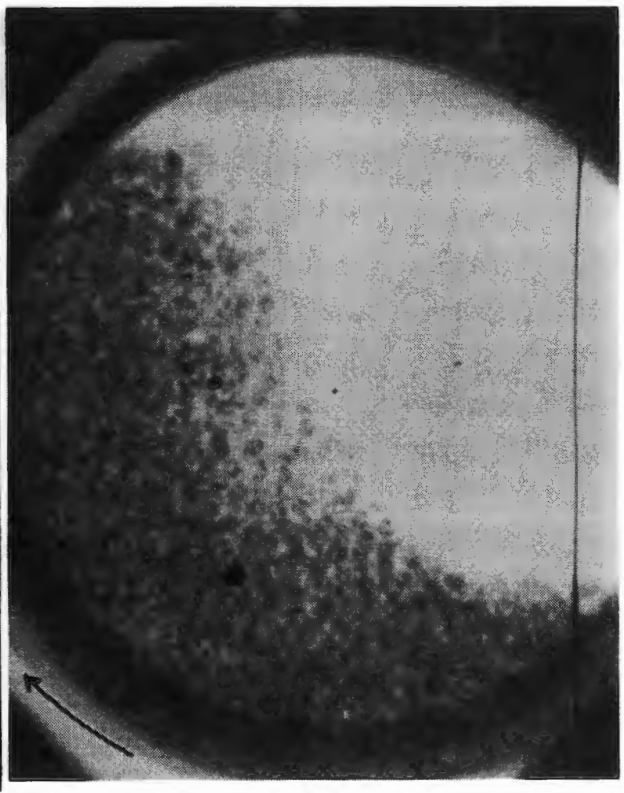

Run 38 - 73% , smooth

IV.1.1 Rotation of the bead

A selection of plots showing the rotation of the bead about its own axis are given. The numbers 1 to 6 in the legend refer to separate circuits of the ball. The orientation of the ball is shown by the line representing the lead rod that was mounted in the bead. A single line-type should be followed within one circuit to ascertain the degree of rotation of the ball. The scale of the plots is enlarged to show just the bead path, and the centre of the mill is shown by the bold dot.

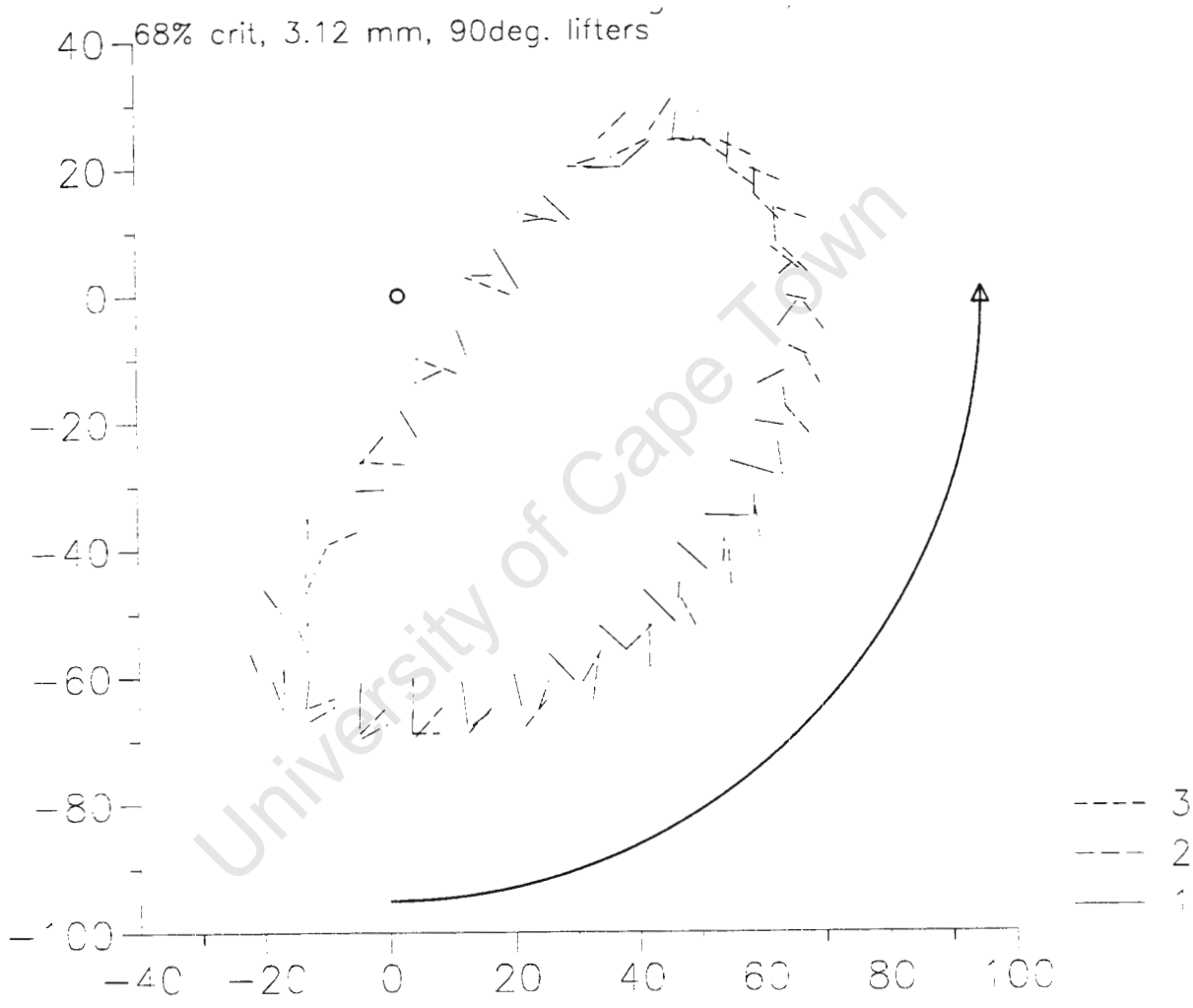

Figure 163. Orientation of the bead, run 1

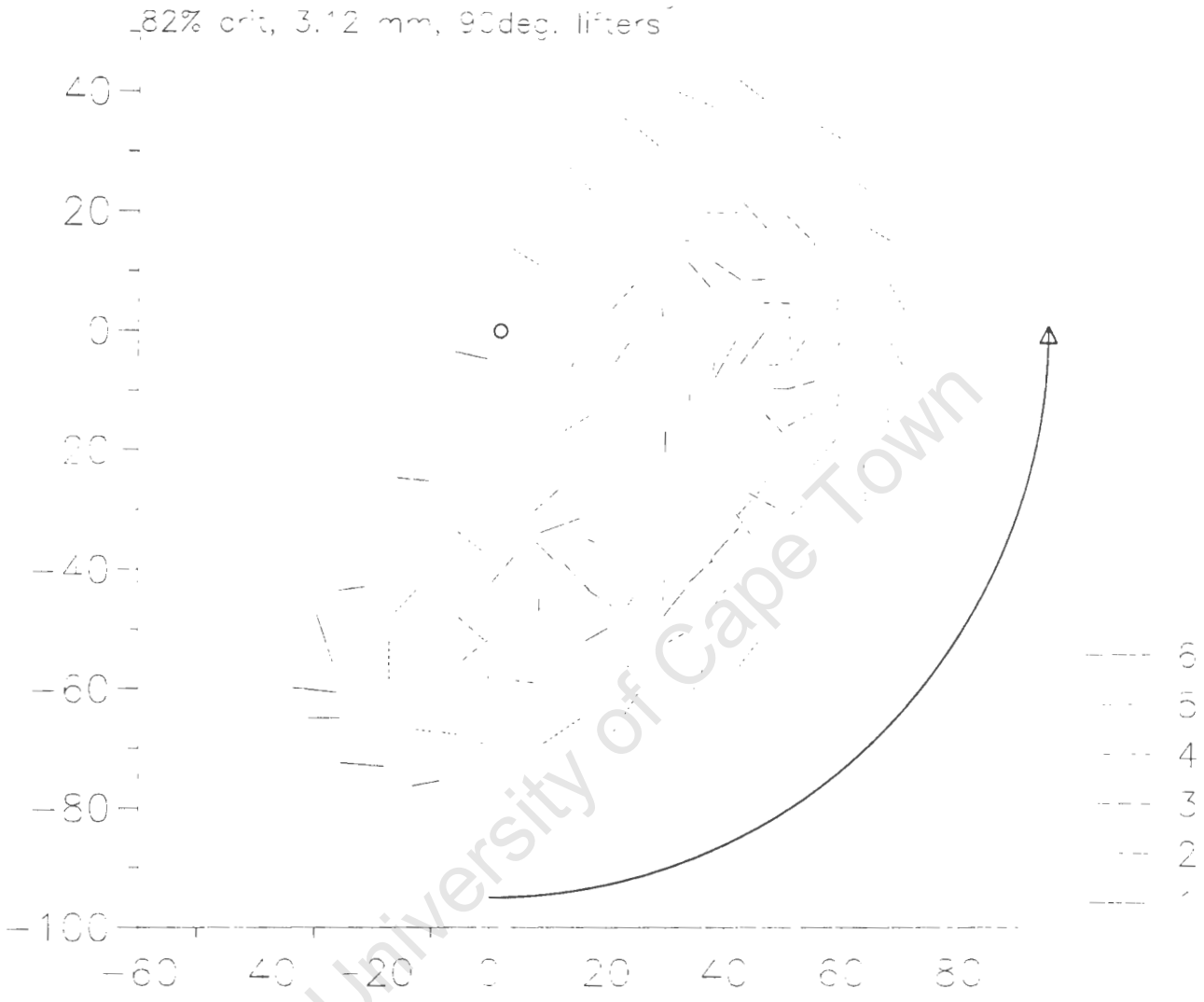

Figure 164. Orientation of the bead, run 3

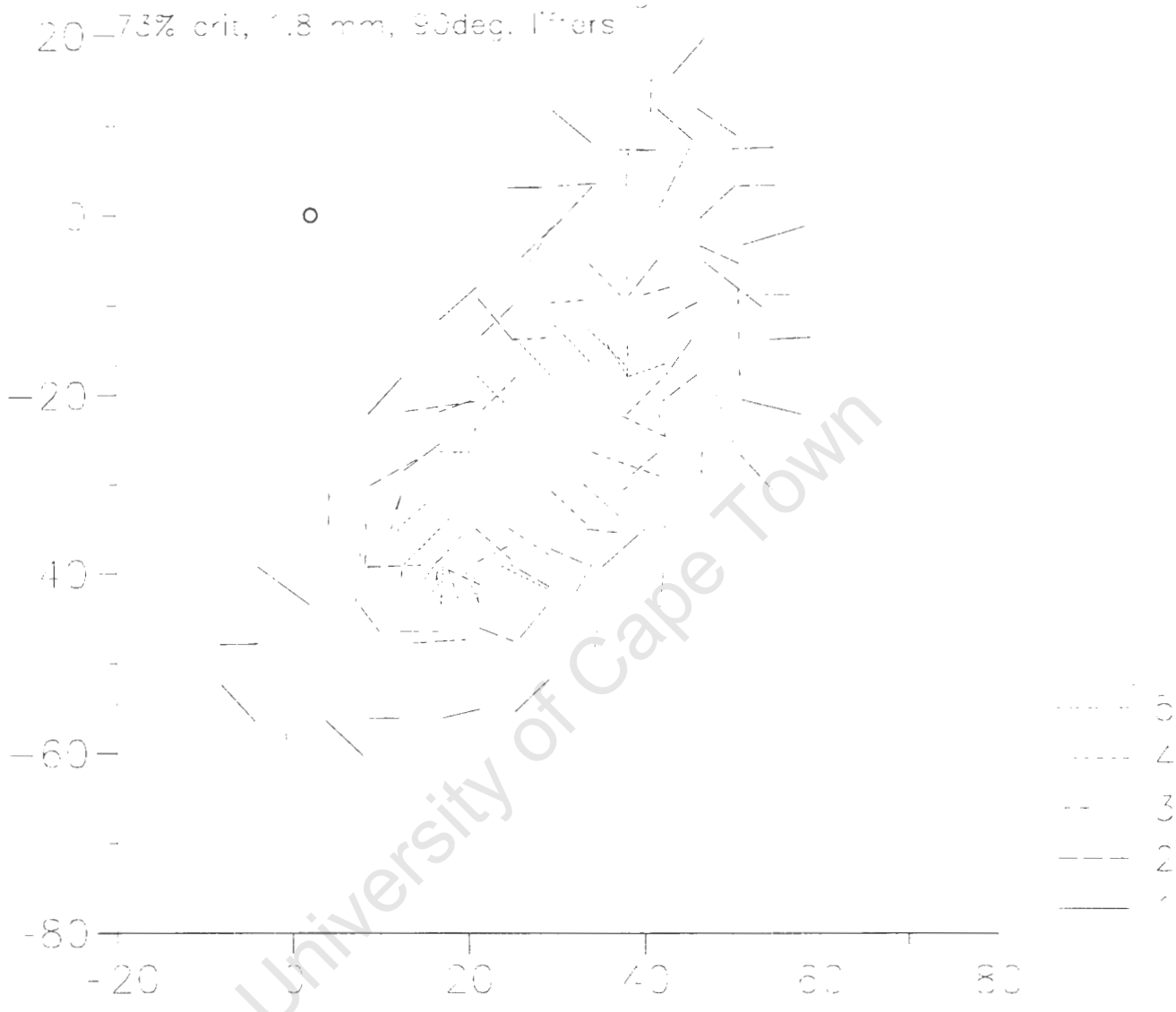

Figure 165. Orientation of the bead, run 5

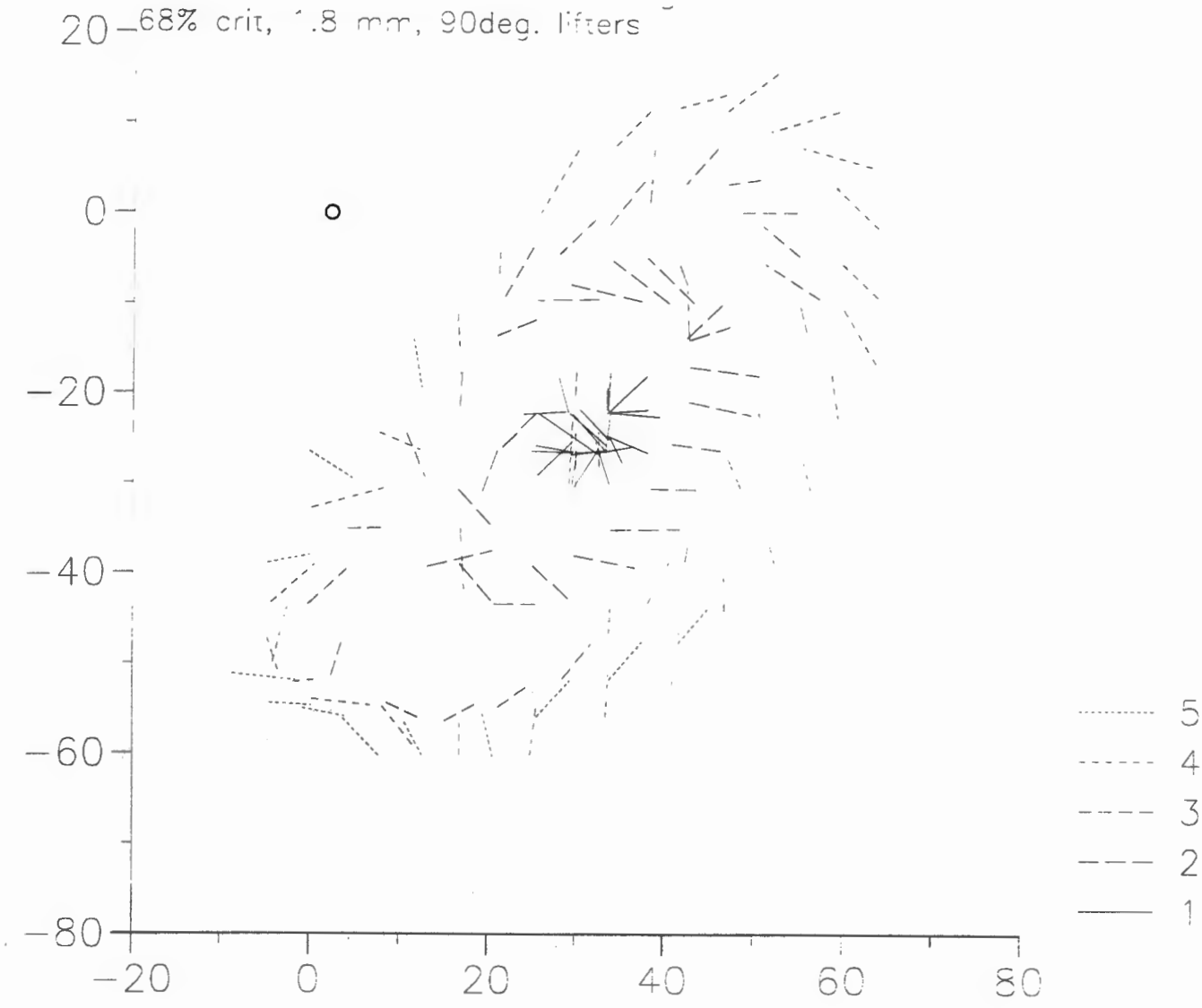

Figure 166. Orientation of the bead, run 6

IV.2 GAMMA CAMERA FILMS

Photographs of the tracks left by the radioactive ball are shown for runs 0 to 8, run 9 is shown in the results section. The circle represents the outside of the mill. The track of the ball is over 0.5 to 0.6 seconds, and the mill is rotating clockwise for all the runs.

Run 0 - 74% , 6 mm , 60°

Run 1 - 73% , 6 mm , 90°

Run 2 - 82% , 6 mm , 90°

Run 3 - 64% , 6 mm , 90°

Figure 167. Photographs of the track of the radioactive ball, taken from the gamma camera film

Run 4 - 64% , 1.8 mm , 90°

Run 5 - 73% , 1.8 mm , 90°

Run 6 - 82% , 1.8 mm , 90°

Run 7 - 82% , 3.12 mm , 90°

Run 8 - 73% , 3.12 mm , 90°

IV.3 MILLING TRIALS

The measured data from all the runs are presented in Table XXX. The time for 30 revolutions was used to check the mill speed, where a number of readings were taken the average was used. The mill time is the time on the mill's built-in clock, in hours and decimal fractions thereof. From run 21 onwards the volume of the sample was not measured, as detailed in the experimental section. Two different scales were used to weigh the samples, the more accurate scale could only register up to 1200g, so heavier samples had to be weighed on a scale accurate to 0.1 g. The torque readings are from the digital torque meter, the maximum and minimum values are given. The mass of the analyzed sample was that of the dried solids, prior to screening.

The discharge rocks from a number of the runs were screened into 6 size intervals, the summary of these sizings is given in Table XXXI. The final column gives the percentage of the total mass of the size intervals relative to the original mass of rock discharged from the mill. Drum 1 had lost some rock, and drum 5 gained some rock, so the rock size distributions from these two runs could not be used in any analyses.

The initial and final masses, and the resultant mass-losses, of the two large rocks used in each run, are given in Table XXXII.

Table XXXIII gives the full size distributions of the solids for both the 2 hour and final sample, for each run. The averages and standard deviations for each test are also given. The plots of the size distributions from the final sample of each run are given in Figure 168 to Figure 176.

IV.3 MILLING TRIALS

The measured data from all the runs are presented in Table XXX. The time for 30 revolutions was used to check the mill speed, where a number of readings were taken the average was used. The mill time is the time on the mill's built-in clock, in hours and decimal fractions thereof. From run 21 onwards the volume of the sample was not measured, as detailed in the experimental section. Two different scales were used to weigh the samples, the more accurate scale could only register up to 1200g, so heavier samples had to be weighed on a scale accurate to 0.1 g. The torque readings are from the digital torque meter, the maximum and minimum values are given. The mass of the analyzed sample was that of the dried solids, prior to screening.

The discharge rocks from a number of the runs were screened into 6 size intervals, the summary of these sizings is given in Table XXXI. The final column gives the percentage of the total mass of the size intervals relative to the original mass of rock discharged from the mill. Drum 1 had lost some rock, and drum 5 gained some rock, so the rock size distributions from these two runs could not be used in any analyses.

The initial and final masses, and the resultant mass-losses, of the two large rocks used in each run, are given in Table XXXII.

Table XXXIII gives the full size distributions of the solids for both the 2 hour and final sample, for each run. The averages and standard deviations for each test are also given. The plots of the size distributions from the final sample of each run are given in Figure 168 to Figure 176.

Table XXX The measured data from all the milling experiments

	Speed	Mill time	Sample			Torque,Nm		Analysed sample	
	% crit.	hrs	No.	Vol,ml	Mass,g	-	+	Mass,g	%-75um
Run 1	89.70	934.840							
Time for 30 rev.		934.873	1	405	447.105	2345	2540	68.1	49.0
1	63.91	935.340	2	413	537.331	1857	2036	181.2	52.4
2	62.84	935.850	3	292	417.069	1334	1545	192.1	55.2
3	62.83	936.340	4	864	1246.5	1084	1269	604.2	66.1
4	62.12	936.840	5	661	990.26	904	1115	520.3	68.1
5	62.07	937.365	6	1060	1642.9	807	957	908.1	69.8
		937.870	7	991	1554.8	725	871	893.4	70.8
		938.370	8	812	1291.2	692	822	763.2	71.7
		938.845	9	851	1314.5	625	788	736.1	71.0
Run 2	89.95	938.950							
Time for 30 rev.		938.980	1	562	596.49	2382	2526	58.7	49.7
1	62.58	939.480	2	495	641.953	1916	2064	219.3	56.4
2		939.960	3	368	516.766			227.3	63.6
3		940.460	4	716	1050.8	1188	1406	534.2	69.9
4		940.955	5	350	549.204	1024	1255	293.6	70.5
5		941.455	6	640	978.8			542.7	73.7
		941.955	7	533	842.515	764	959	484.8	73.7
		942.460	8	440	706.818	631	886	410.7	75.0
		942.995	9	505	814.74			482.0	75.3
Run 3	89.95	943.030				2416	2665		
Time for 30 rev.		943.050	1	518	531.562	2408	2611	18.0	60.0
1	62.58	943.520	2	419	498.952	2119	2317	125.0	68.5
2		944.065	3	706	946.104	1675	1918	371.1	77.7
3		944.555	4	519	714.893	1401	1593	313.6	81.0
4		945.060	5	589	850.95	1254	1413	419.9	83.2
5		945.560	6	629	930.904	1073	1217	478.0	85.6
		946.060	7	680	1029.183			500.6	85.7
		946.570	8	706	1079.6	762	905	601.7	87.6
		947.060	9	700	1085.8			619.0	87.7
Run 4	79.96	947.090							
Time for 30 rev.		947.130	1	620	650.963	2274	2515	45.3	52.2
1	70.37	947.590	2	263	313.072	2084	2212	75.2	61.9
2	70.43	947.965	3a	317	417.797	1778	1961	139.2	73.2
3		948.090	3	690	888.082			323.0	78.2
4		948.585	4	603	815.243	1431	1652	344.1	80.5
5		949.085	5	708	992.118	1242	1467	459.0	84.0
		949.630	6	670	960.679	1144	1345	467.6	87.5
		950.210	7	1008	1577.2	1043	1206	804.7	88.9
		950.610	8	865	1295.4	996	1140	681.5	89.4
		951.090	9	840	1302.2	888	1105	712.2	88.8
Run 5	79.96	951.140							
Time for 30 rev.		951.170	1	720	750.144	2390	2579	26.6	55.1
1		951.670	2	738	873.504	2006	2182	219.1	73.5
2		952.150	3	195	279.279	1632	1853	127.4	60.0
3		952.760	4	820	1188.1	1311	1513	508.1	82.1
4		953.135	5	502	703.957	1173	1376	314.7	83.5
5		953.760	6	608	899.014	1007	1209	417.7	84.5
		954.160	7	549	811.176	942	1113	410.3	84.5
		954.670	8	620	938.64	795	952	503.3	82.8
		955.140	9	560	854.7			460.5	85.2

	Speed	Mill time	Sample			Torque,Nm		Analysed sample	
	% crit.	hrs	No.	Vol,ml	Mass,g	-	+	Mass,g	%-75um
Run 6	79.96	955.150							
Time for 30 rev.		955.180	1	560	586.837			45.0	59.3
1		955.670	2	365	457.116	1797	1931	131.3	55.7
2		956.150	3	300	412.05	1414	1582	163.9	60.3
3		956.650	4	505	719.048	1163	1307	335.6	63.7
4		957.150	5	580	845.417	1031	1207	418.5	67.0
5		957.655	6	400	623.396	872	1090	342.3	65.0
		958.205	7	768	1349.8			567.1	68.1
		958.600	8	335	534.418	643	806	300.6	73.2
		959.150	9	845	1348.3			799.6	71.5
Run 7	79.98	959.575							
Time for 30 rev.		959.600	1	1110	1137.7	2397	2524	55.4	46.7
1	70.40	960.195	2	712	852.629	1982	2113	237.4	56.7
2	70.35	960.575	3	331	432.814	1861	1955	156.2	58.3
3	70.40	961.110	4	529	707.127	1662	1778	288.2	65.5
4		961.620	5	490	696.412	1584	1636	329.5	64.8
5		962.125	6	616	885.728	1473	1620	433.3	67.1
		962.615	7	511	768.111	1440	1534	409.0	67.9
		963.020	8	430	668.676	1373	1504	368.2	69.2
		963.560	9	415	639.745			339.3	71.3
Run 8	80.10	963.570				2331	2457		
Time for 30 rev.		963.600	1	511	522.679			32.1	44.4
1	70.21	964.080	2	647	763.974	2035	2200	194.3	51.7
2	70.26	964.600	3	494	651.935	1825	1911	256.6	57.9
3	70.36	965.090	4	360	505.388	1652	1793	226.6	61.1
4		965.570	5	400	565.598	1540	1702	257.4	63.5
5		966.075	6	481	694.842	1463	1620	349.4	65.5
		966.565	7 ?	644	1151.3	1371	1540	496.6	66.1
		967.128	8 ?	706	1272.4	1315	1449	592.1	67.3
		967.575	9	576	873.4			485.4	67.5
Run 9	80.10	967.590							
Time for 30 rev.		967.630	1	580	608.996	2267	2474	51.4	31.1
1		968.060	2	420	521.368	2082	2197	161.0	40.5
2		968.560	3	500	680.516	1765	1913	287.2	46.5
3		969.060	4	376	542.526	1638	1811	254.2	50.2
4		969.600	5	470	701.074	1554	1741	356.5	54.2
5		970.070	6	836	1278.7	1497	1572	687.3	57.7
		970.570	7	590	908.13	1366	1550	501.5	58.8
		971.060	8	640	1006.9	1317	1450	583.4	60.1
		971.595	9	707	1101.5			645.0	61.5
Run 10	90.11	971.860							
Time for 30 rev.		971.890	1	745	761.989	2093	2325	33.9	46.9
1		972.345	2	680	801.51	2024	2208	192.4	54.7
2	62.59	972.830	3	690	894.945	1837	2041	324.5	62.7
3	62.35	973.365	4	650	937.637	1715	1855	444.0	57.2
4		973.865	5	840	1233	1623	1760	616.1	63.4
5		974.320	6 a	1285	1945.6	1522	1670	1064.0	62.7
		974.430	6	550	857.757			483.7	60.1
		974.980	7	803	1258.6	1412	1590	733.6	60.9
		975.460	8	846	1356.9	1362	1525	825.5	61.4
		975.960	9	947	1537.4			951.9	61.3

	Speed	Mill time	Sample			Torque,Nm		Analysed sample	
	% crit.	hrs	No.	Vol,ml	Mass,g	-	+	Mass,g	%-75um
Run 11	90.21	975.870				2025	2247		
Time for 30 rev.		975.890	1	630	646.14	2060	2220	34.1	51.9
1	62.40	976.370	2	600	712.081	1977	2093	177.2	55.3
2		976.870	3	665	869.195	1734	1936	326.5	61.2
3		977.330	4	555	783.675	1626	1802	363.0	55.4
4		977.790	5	560	808.204	1562	1670	396.8	60.4
5		978.230	6	610	910.665	1462	1635	474.4	62.9
		978.860	7	730	1198.8	1392	1552	689.7	62.6
		978.400	8	645	1013.2	1327	1502		
		979.920	9	995	1588			932.5	62.6
Run 12	90.09	979.960				2117	2268		
Time for 30 rev.		979.978	1 ?	1071	1078.8			34.8	59.6
1	62.52	980.040	1 a	988	1007.3			76.0	53.8
2	62.45	980.475	2	1080	1275.7	2041	2207	336.7	60.6
3		980.980	3	868	1108.3			401.4	66.5
4		981.470	4	934	1254.6	1761	1889	527.1	71.2
5		981.960	5	1017	1428.9	1656	1848	673.0	71.7
		982.460	6	631	913.113	1586	1759	455.6	75.1
		982.960	7	568	838.121	1514	1670	438.6	75.8
		983.465	8	866	1309.3	1467	1635	719.6	77.3
		983.965	9	944	1444.8	1435	1590	785.2	77.6
Run 13	90.33	983.970							
Time for 30 rev.		984.000	1	1016	1023.8	1963	2156	42.3	52.5
1	62.30	984.470	2	972	1112.8	1854	1996	252.7	60.9
2	62.30	984.970	3	580	719.688	1712	1825	238.5	67.1
3	62.34	985.490	4	600	799.481	1575	1701	328.0	71.5
4		986.010	5	778	1063.6	1451	1607	476.1	73.8
5		986.460	6	420	588.705	1369	1503	281.2	75.4
		986.970	7	632	911.7	1343	1478	460.5	77.4
		987.475	8	508	761.092	1261	1389	396.0	77.6
		987.970	9	966	1457.7	1216	1368	797.8	78.6
Run 14	90.27	987.980				1987	2178		
Time for 30 rev.		988.000	1	988	979.912	1962	2116	36.5	55.9
1	62.39	988.480	2	599	699.664	1803	1990	177.0	49.7
2	62.33	988.990	3	716	946.43	1541	1656	381.3	50.8
3		989.510	4	776	1105.8	1437	1556	536.6	54.0
4		990.045	5	674	990.8	1328	1491	517.5	54.5
5		990.490	6	687	1036	1287	1406	558.5	55.7
		990.980	7	716	1106.9	1192	1338	621.3	57.8
		991.490	8	748	1181.1	1187	1293	694.1	57.5
		991.980	9	769	1224	1140	1275	741.8	58.7
Run 15	90.25	991.985				2264	2348		
Time for 30 rev.		992.015	1	1105	1028.8	2171	2402	54.4	50.9
1	62.49	992.480	2	700	829.968	2067	2303	225.1	59.4
2	62.40	992.980	3	609	806.084	1774	1986	326.7	65.0
3	62.23	993.480	4	578	803.659	1516	1753	371.1	68.3
4		993.980	5	748	1079.267	1332	1564	543.4	69.9
5		994.475	6	818	1248.348	1164	1394	697.4	71.9
		994.980	7	604	930.687	1070	1269	530.4	73.6
		995.480	8	939	1483.721	976	1176	863.1	74.3
		995.980	9 ?	789	938.052	876	1100	567.8	73.7

	Speed	Mill time	Sample			Torque,Nm		Analysed sample	
	% crit.	hrs	No.	Vol,ml	Mass,g	-	+	Mass,g	%-75um
Run 16	90.32	995.980				2232	2416		
Time for 30 rev.		996.010	1	881	894.259	2155	2386	45.0	54.2
1	62.28	996.510	2	550	650.751	2055	2257	172.2	61.2
2	62.36	997.020	3	488	635.543			241.9	69.7
3		997.490	4	941	1316.483	1609	1794	612.8	74.8
4		997.980	5	772	1109.168	1448	1608	549.8	75.8
5		998.480	6	539	809.731	1250	1478	440.1	79.6
		999.020	7	665	997.757	1157	1374	545.2	81.0
		999.490	8	772	1189.896	1076	1267	680.8	83.3
		999.980	9	775	1218.523	1025	1254	722.3	81.5
Run 17	90.31	999.980				2144	2427		
Time for 30 rev.		1000.020	1	730	753.01	2115	2445	58.3	42.7
1	62.43	1000.480	2	561	677.97	2002	2252	197.9	55.7
2	62.23	1000.980	3	598	816.186	1688	1914	355.6	62.4
3		1001.495	4	829	1186.751	1421	1649	582.0	68.3
4		1001.980	5	561	817.01	1215	1480	414.2	78.1
5		1002.480	6	628	966.439	1116	1367	547.8	72.1
		1002.980	7	728 ?	1217.727	1040	1233	712.7	74.2
		1003.480	8	601	953.461	946	1181	570.0	75.2
		1003.985	9	651	1049.44	876	1100	638.7	82.7
Run 18	79.98	4.100							
Time for 30 rev.		4.130	1	693	706.376	2324	2546	38.4	49.7
1	70.36	4.605	2	831	989.229	2050	2321	270.1	62.9
2	70.40	5.120	3	525	685.713	1716	1971	263.7	69.3
3		5.600	4	543	756.776	1491	1724	347.7	72.9
4		6.100	5	474	686.004	1337	1580	332.0	81.9
5		6.605	6		1116.8	1166	1449	592.2	78.7
		7.100	7	516	778.993	1072	1343	424.0	79.9
		7.610	8	678	1032.6	1001	1219	580.4	81.2
		8.110	9a	452	686.192			376.4	81.4
			9	562	874.263			488.4	75.9
Run 19	79.90	8.165				2414	2632		
Time for 30 rev.		8.210	1	750	765.186	2390	2616	47.2	50.9
1	70.45	8.670	2	665	771.236	2143	2406	182.6	70.1
2	70.45	9.195	3	563	725.501	1868	2086	263.1	78.5
3		9.670	4	676	910.306	1677	1886	379.8	83.0
4		10.210	5	730	1019.263	1484	1678	470.1	85.2
5		10.665	6	418	593.53	1353	1614	282.3	89.0
		11.175	7	702	1024.244	1270	1527	519.1	89.2
		11.660	8	716	1063	1184	1424	567.3	90.6
		12.165	9	619	966.3	1117	1365	570.0	91.1
Run 20	90.10	12.230							
Time for 30 rev.		12.255	1	800	806.658	1703	2068	34.8	38.8
1	62.51	12.730	2	1145	1351.4	2087	2321	358.9	58.8
2	62.46	13.235	3	694	892.938	1875	2081	328.2	65.2
3	62.46	13.765	4	940	1288.9	1734	1954	574.0	71.0
4		14.230	5	651	936.296	1660	1867	458.7	73.0
5		14.730	6	792	1162.4	1532	1797	602.0	76.0
		15.245	7	845	1273.9			692.0	77.3
		15.725	8	506	780.545	1389	1568	445.1	77.6
		16.230	9	710	1113	1284	1527	648.8	77.5

	Speed	Mill time	Sample			Torque,Nm		Analysed sample	
	% crit.	hrs	No.	Vol,ml	Mass,g	-	+	Mass,g	%-75um
Run 21	90.15	16.240				2218	2406		
Time for 30 rev.		16.275	1	1409	1427.631	2160	2428	72.4	47.9
1	62.44	16.790	2	-	1301.9	2004	2206	390.7	54.8
2		17.270	3	-	1119.957	1850	2038	466.0	59.4
3		17.735	4	-	892.157	1601	1826	431.5	61.4
4		18.235	5	-	968.15	1467	1689	500.6	63.4
5		18.740	6	-	1261.2	1327	1611	703.4	65.5
		19.240	7	-	556.472	1242	1478	320.1	65.9
		19.740	8	-	1174.4	1176	1429	681.8	65.8
		20.240	9	-	1034.698	1107	1327	628.1	66.2
Run 22	90.00	20.240				2150	2397		
Time for 30 rev.		20.260	1	-	1484.8	2137	2419	54.3	51.1
1		20.740	2	-	684.157	2075	2246	145.9	47.4
2		21.270	3	-	1054.363	1733	2083	437.8	58.9
3		21.740	4	-	778.136	1539	1774	376.8	60.5
4		22.240	5	-	1086.66	1388	1639	526.5	62.1
5		22.740	6	-	791.113	1271	1535	447.8	64.0
		23.240	7	-	1377.8	1154	1390	790.3	64.3
		23.740	8	-	961.685	1086	1316	586.3	65.3
		24.240	9	-	879.296	1051	1302	533.6	65.0
Run 23	79.16	24.350				2411	2563		
Time for 30 rev.		24.370	1		1542.1	2358	2618	61.0	53.0
1	71.11	24.850	2		1288.6	2140	2340	311.8	64.4
2		25.360	3		1419.9	1928	2134	533.2	70.2
3		25.850	4		946.509	1716	1935	410.3	72.1
4		26.350	5		1027.717	1612	1828	488.7	75.1
5		26.850	6		1158.3	1483	1717	592.2	77.5
		27.360	7		909.016	1413	1616	487.0	77.8
		27.850	8		1434	1318	1502	800.6	78.2
		28.360	9		1376.6	1246	1439	790.9	79.7
Run 24	79.92	28.380				2403	2623		
Time for 30 rev.		28.410	1		1291.6	2367	2569	64.5	49.7
1		28.880	2		992.828	2047	2239	273.2	56.3
2	70.43	29.380	3		909.959	1733	2001	368.5	59.4
3		29.880	4		717.729	1550	1827	337.7	61.9
4		30.380	5		1260.1	1342	1604	664.3	62.4
5		30.880	6		988.714	1277	1477	551.0	64.0
		31.380	7		769.826	1196	1348	447.8	63.9
		31.900	8		996.139	1080	1275	599.1	65.5
		32.380	9		866.258	1004	1191	516.7	65.8
Run 25	80.06	32.250				2410	2625		
Time for 30 rev.		32.270	1		1059.953	2458	2605	52.0	51.3
1	70.31	32.750	2		1424.6	2169	2350	361.7	65.6
2		33.250	3		987.558	1946	2118	352.0	72.1
3		33.850	4		1417.7	1717	1898	626.4	76.0
4		34.260	5		1294.7	1646	1814	625.8	76.9
5		34.750	6		809.176	1489	1717	412.6	79.1
		35.250	7		1319	1403	1611	710.9	79.7
		35.750	8		1489.4	1322	1567	831.6	80.8
		36.250	9		1689.7	1245	1428	973.0	81.1

Table XXXI Size fraction of the rocks discharged from the mill after each run

SIZE FRACTION (mm)	+75 -150		+50 -75		+38 -50		+25 -38		+12 -25		-12		Total mass of fractions	Original weighed mass	% sorted rel. to original
MASS (kg)															
DRUM No.		%		%		%		%		%		%	(kg)	(kg)	
1	182.0	52.5	55.0	15.9	43.9	12.7	29.0	8.4	21.8	6.3	14.8	4.3	346.5	417	83%
2	100.0	33.7	93.5	31.5	36.0	12.1	47.5	16.0	20.0	6.7	0.0	0.0	297.0	300.5	99%
3	223.5	53.2	78.0	18.6	50.5	12.0	48.3	11.5	19.6	4.7	0.0	0.0	419.9	471	89%
4														396	
5	147.5	29.3	133.5	26.5	56.6	11.2	39.8	7.9	89.0	17.7	37.5	7.4	503.9	403	125%
6														304	
7	131.0	35.8	130.0	35.6	20.0	5.5	54.0	14.8	30.3	8.3	0.2	0.1	365.5	365	100%
8														340	
9														337.5	
10														298.5	
11														309	
12	79.8	20.9	127.2	33.4	62.0	16.3	72.0	18.9	39.2	10.3	1.0	0.3	381.2	382	100%
13	52.8	12.7	126.8	30.6	57.5	13.9	86.2	20.8	89.6	21.6	2.0	0.5	414.9	416.4	100%
14	144.5	44.1	58.0	17.7	34.0	10.4	49.0	14.9	33.5	10.2	8.8	2.7	327.8	337	97%
15	113.0	36.8	78.0	25.4	38.2	12.5	48.2	15.7	23.4	7.6	6.0	2.0	306.8	326.2	94%
16	113.8	32.2	95.3	27.0	43.6	12.4	55.2	15.6	37.0	10.5	8.0	2.3	352.9	362.2	97%
17	143.0	44.8	83.0	26.0	52.0	16.3	19.1	6.0	19.1	6.0	2.9	0.9	319.1	306	104%
18														357.6	
19														401.8	
20	99.5	26.4	125.0	33.2	41.5	11.0	65.5	17.4	38.0	10.1	6.7	1.8	376.2	359.2	105%
21	148.0	49.5	61.0	20.4	29.0	9.7	40.0	13.4	17.0	5.7	4.0	1.3	299.0	285	105%
22	152.0	52.4	43.6	15.0	33.0	11.4	38.2	13.2	23.4	8.1	0.0	0.0	290.2	289.8	100%
23	124.7	31.8	107.7	27.4	48.2	12.3	59.2	15.1	44.7	11.4	8.0	2.0	392.5	378.4	104%
24	179.5	57.1	37.0	11.8	38.5	12.2	36.5	11.6	20.0	6.4	2.9	0.9	314.4	296.4	106%
25	72.4	21.1	117.4	34.2	40.6	11.8	55.4	16.1	47.4	13.8	10.0	2.9	343.2	373.8	92%

Table XXXII Masses of the two large rocks

RUN	ROCK 1 INIT.	FINAL	LOSS	% LOSS	ROCK 2 INIT.	FINAL	LOSS	% LOSS	BOTH ROCKS INIT.	FINAL	LOSS	% LOSS	AVE.	Liner
1		No readings				No readings								90%
2														smooth
3														
4	12.025	9.456	2.569	21.36	14.738	13.574	1.164	7.90	26.763	23.030	3.733	13.95	13.2	80%
5	12.466	10.908	1.558	12.50	11.397	9.551	1.846	16.20	23.863	20.459	3.404	14.26		smooth
6	16.410	14.957	1.453	8.85	10.154	8.579	1.575	15.51	26.564	23.536	3.028	11.40		
7	13.366	9.736	3.630	27.16	11.226	5.280	5.946	52.97	24.592	15.016	9.576	38.94	37.2	80%
8	16.030	13.778	2.252	14.05	8.937	3.739	5.198	58.16	24.967	17.517	7.450	29.84		70 mm
9	14.960	10.789	4.171	27.88	11.437	4.341	7.096	62.04	26.397	15.130	11.267	42.68		lifters
10	14.357	9.032	5.325	37.09	11.380	7.897	3.483	30.61	25.737	16.929	8.808	34.22	33.6	90%
11	14.448	10.199	4.249	29.41	10.661	8.409	2.252	21.12	25.109	18.608	6.501	25.89		70 mm
12	13.268	7.543	5.725	43.15	11.403	7.061	4.342	38.08	24.671	14.604	10.067	40.80		lifters
13	13.632	10.286	3.346	24.55	11.562	9.175	2.387	20.65	25.194	19.461	5.733	22.76	24.3	90%
14	15.652	12.521	3.131	20.00	9.567	6.174	3.393	35.47	25.219	18.695	6.524	25.87		90deg
15	14.782	13.190	1.592	10.77	10.452	7.930	2.522	24.13	25.234	21.120	4.114	16.30	26.7	90%
16	15.597	6.730	8.867	56.85	9.644	4.605	5.039	52.25	25.241	11.335	13.906	55.09		grid
17	12.919	8.288	4.631	35.85	12.072	7.439	4.633	38.38	24.991	15.727	9.264	37.07		
18	15.202	13.009	2.193	14.43	9.872	7.532	2.340	23.70	25.074	20.541	4.533	18.08	16.1	80%
19	15.032	13.235	1.797	11.95	10.001	8.275	1.726	17.26	25.033	21.510	3.523	14.07		grid
20	15.539	8.530	7.009	45.11	9.529	7.818	1.711	17.96	25.068	16.348	8.720	34.79	32.7	90%
21	15.131	8.598	6.533	43.18	9.921	8.426	1.495	15.07	25.052	17.024	8.028	32.05		40 mm
22	15.101	10.442	4.659	30.85	9.896	6.774	3.122	31.55	24.997	17.216	7.781	31.13		lifter
23	15.252	11.992	3.260	21.37	9.728	7.898	1.830	18.81	24.980	19.890	5.090	20.38	21.1	80%
24	15.242	12.580	2.662	17.46	9.760	8.061	1.699	17.41	25.002	20.641	4.361	17.44		40 mm
25	14.726	10.560	4.166	28.29	10.438	8.165	2.273	21.78	25.164	18.725	6.439	25.59		lifter

Table XXXIII Full size analysis of the samples taken from the mill, for each run

	um	SMOOTH, 90%						SMOOTH, 80%					
RUN		1	2	3	AVE.	STD DEV	Cum.ave	4	5	6	AVE	STD DEV	Cum.ave.
sample	600	0.7	0.9	0.3	0.6	0.2	100.0	0.2	0.3	0.4	0.3	0.1	100.0
1	425	0.9	0.5	0.2	0.5	0.3	99.4	0.2	0.2	0.3	0.2	0.0	99.7
	300	1.5	0.9	0.3	0.9	0.5	98.9	0.3	0.4	0.8	0.5	0.2	99.5
	212	3.1	2.3	1.1	2.2	0.8	98.0	0.7	0.9	2.7	1.4	0.9	99.0
	150	4.9	4.4	2.1	3.8	1.2	95.8	2.2	1.9	7.3	3.8	2.5	97.5
	106	9.7	9.5	4.9	8.0	2.2	92.0	4.6	4.5	9.0	6.0	2.1	93.7
	75	11.1	11.0	8.0	10.0	1.4	84.0	7.8	8.3	12.5	9.5	2.1	87.7
	53	10.3	12.6	12.3	11.7	1.0	73.9	12.3	11.5	12.0	11.9	0.3	78.2
	38	8.1	7.1	8.6	7.9	0.6	62.2	8.2	8.6	7.0	7.9	0.7	66.2
	<38	49.7	50.8	62.3	54.3	5.7	54.3	63.5	63.4	48.0	58.3	7.3	58.3
TOTAL		100.0	100.0	100.1	100.0			100.0	100.0	100.0	100.0		
sample	600	0.6	0.3	0.2	0.4	0.2	100.0	0.2	0.1	0.3	0.2	0.1	100.0
2	425	1.1	0.3	0.1	0.5	0.4	99.6	0.1	0.3	0.3	0.2	0.1	99.8
	300	1.5	0.6	0.3	0.8	0.5	99.1	0.3	0.5	0.8	0.5	0.2	99.6
	212	2.6	1.8	0.7	1.7	0.8	98.3	0.6	1.2	2.5	1.4	0.8	99.0
	150	4.1	3.5	1.9	3.2	0.9	96.6	1.7	1.7	5.8	3.1	1.9	97.6
	106	8.4	8.2	3.3	6.6	2.4	93.5	2.9	3.7	7.5	4.7	2.0	94.5
	75	10.7	10.0	5.8	8.8	2.2	86.8	5.4	7.3	11.3	8.0	2.5	89.8
	53	10.2	12.4	10.8	11.1	0.9	78.0	10.6	11.3	11.8	11.2	0.5	81.8
	38	8.2	7.5	8.4	8.0	0.4	66.9	8.6	9.1	7.3	8.3	0.8	70.6
	<38	52.6	55.4	68.5	58.8	6.9	58.8	69.6	64.8	52.4	62.3	7.2	62.3
TOTAL		100.0	100.0	100.0	100.0			100.0	100.0	100.0	100.0		

	um	GRID LINER, 90%						GRID LINER, 80%						70mm, 90deg. LIFTERS, 90%				
RUN		15	16	17	AVE	STD DEV	Cum.ave	18	19	AVE	STD DEV	Cum.ave	13	14	AVE	STD DEV	Cum.ave
sample	600	0.9	0.7	0.5	0.7	0.2	100.0	0.2	0.7	0.5	0.2	100.0	0.9	3.2	2.1	1.1	100.0
1	425	0.5	0.4	0.4	0.4	0.0	99.3	0.2	0.3	0.3	0.1	99.6	0.5	2.1	1.3	0.8	98.0
	300	0.9	0.7	0.7	0.8	0.1	98.9	0.4	0.4	0.4	0.0	99.3	0.8	3.5	2.2	1.4	96.7
	212	2.7	1.9	1.8	2.1	0.4	98.1	1.1	0.8	1.0	0.2	98.9	2.0	7.1	4.6	2.6	94.5
	150	4.8	3.4	3.6	3.9	0.6	96.0	2.1	1.4	1.8	0.4	98.0	3.6	8.8	6.2	2.6	90.0
	106	9.1	7.1	6.6	7.6	1.1	92.0	5.0	3.6	4.3	0.7	96.2	7.6	11.0	9.3	1.7	83.8
	75	11.2	10.0	8.3	9.8	1.2	84.4	9.1	7.6	8.4	0.8	91.9	10.8	9.8	10.3	0.5	74.5
	53	11.5	11.7	8.3	10.5	1.6	74.6	11.5	2.2	6.9	4.6	83.6	12.0	9.9	11.0	1.0	64.2
	38	6.7	7.7	4.8	6.4	1.2	64.1	7.3	0.1	3.7	3.6	76.7	7.2	5.5	6.4	0.8	53.2
	<38	51.7	56.4	65.0	57.7	5.5	57.7	63.1	82.9	73.0	9.9	73.0	54.6	39.1	46.9	7.8	46.9
TOTAL		100.0	100.0	100.0	100.0			100.0	100.0	100.0			100.0	100.0	100.0		
sample	600	0.5	0.3	0.2	0.3	0.1	100.0	0.3	0.2	0.3	0.1	100.0	0.7	1.7	1.2	0.5	100.0
2	425	0.3	0.2	0.2	0.2	0.0	99.7	0.2	0.1	0.2	0.0	99.8	0.3	1.2	0.8	0.4	98.8
	300	0.7	0.4	0.3	0.5	0.2	99.4	0.5	0.1	0.3	0.2	99.6	0.6	2.4	1.5	0.9	98.1
	212	1.9	1.1	1.2	1.4	0.4	99.0	1.1	0.4	0.8	0.3	99.3	1.5	6.1	3.8	2.3	96.6
	150	3.8	2.3	2.3	2.8	0.7	97.6	2.3	0.9	1.6	0.7	98.6	2.6	8.6	5.6	3.0	92.8
	106	7.9	5.1	5.3	6.1	1.3	94.8	5.0	2.1	3.6	1.4	97.0	5.9	11.1	8.5	2.6	87.2
	75	10.9	9.1	7.8	9.3	1.3	88.7	9.2	5.1	7.1	2.0	93.4	9.8	10.2	10.0	0.2	78.7
	53	11.4	11.9	8.5	10.6	1.5	79.4	11.4	1.9	6.7	4.8	86.3	11.8	9.9	10.9	0.9	68.7
	38	7.4	7.9	5.0	6.8	1.3	68.8	7.4	0.0	3.7	3.7	79.6	7.8	5.9	6.9	0.9	57.8
	<38	55.2	61.7	69.2	62.0	5.7	62.0	62.6	89.2	75.9	13.3	75.9	59.0	42.9	51.0	8.0	51.0
TOTAL		100.0	100.0	100.0	100.0			100.0	100.0	100.0			100.0	100.0	100.0		

	um	40mm, 50deg. LIFTERS, 90%						40mm, 70deg. LIFTERS, 80%					
RUN		20	21	22	AVE	STD DEV	Cum.ave	23	24	25	AVE	STD DEV	Cum.ave.
sample	600	0.7	1.0	1.3	1.0	0.2	99.9	0.7	1.2	0.5	0.8	0.3	100.0
1	425	0.5	0.8	0.9	0.7	0.2	98.9	0.5	0.7	0.3	0.5	0.2	99.2
	300	0.8	1.6	2.0	1.5	0.5	98.2	0.9	1.9	0.7	1.2	0.5	98.7
	212	1.8	3.6	4.1	3.2	1.0	96.7	1.8	4.0	1.5	2.4	1.1	97.5
	150	3.9	7.4	7.3	6.2	1.6	93.6	3.5	7.7	3.2	4.8	2.1	95.1
	106	7.7	10.5	10.6	9.6	1.3	87.4	7.1	10.4	6.5	8.0	1.7	90.3
	75	11.6	11.6	11.7	11.6	0.0	77.8	10.6	11.5	10.3	10.8	0.5	82.3
	53	11.8	10.5	10.1	10.8	0.7	66.1	12.0	10.6	11.7	11.4	0.6	71.5
	38	7.8	6.7	6.5	7.0	0.6	55.3	7.2	6.3	8.0	7.2	0.7	60.0
	<38	53.3	46.2	45.5	48.3	3.5	48.3	55.9	45.5	57.2	52.9	5.2	52.9
TOTAL		99.9	99.9	100.0	99.9			100.2	99.8	99.9	100.0		
sample	600	0.4	1.0	0.9	0.8	0.3	100.0	0.3	0.7	0.3	0.4	0.2	100.0
2	425	0.3	0.7	0.8	0.6	0.2	99.3	0.3	0.7	0.3	0.4	0.2	99.6
	300	0.7	1.4	1.7	1.3	0.4	98.7	0.7	1.6	0.5	0.9	0.5	99.2
	212	1.4	3.2	3.7	2.8	1.0	97.4	1.3	3.5	1.2	2.0	1.1	98.2
	150	3.1	6.4	6.9	5.5	1.7	94.6	2.6	6.7	2.5	3.9	2.0	96.2
	106	6.2	9.7	9.9	8.6	1.7	89.2	5.5	9.8	5.1	6.8	2.1	92.3
	75	10.4	11.5	11.3	11.1	0.5	80.6	9.7	11.1	9.1	10.0	0.8	85.5
	53	11.8	10.6	10.5	11.0	0.6	69.5	11.6	10.7	11.7	11.3	0.4	75.5
	38	8.4	7.0	6.7	7.4	0.7	58.5	7.8	6.7	8.3	7.6	0.7	64.2
	<38	57.4	48.6	47.5	51.2	4.4	51.2	60.3	48.4	61.1	56.6	5.8	56.6
		100.1	100.1	99.9	100.0			100.1	99.9	100.1	100.0		

	um	70mm, 50deg. LIFTERS, 90%						70mm, 70deg LIFTERS, 80%					
RUN		10	11	12	AVE	STD DEV	Cum.ave	7	8	9	AVE	STD DEV	Cum.ave.
sample	600	0.6	0.9	0.7	0.7	0.1	100.0	1.3	1.7	1.1	1.4	0.2	100.0
1	425	0.6	0.8	0.5	0.6	0.1	99.3	0.9	0.9	0.9	0.9	0.0	98.6
	300	1.5	1.7	0.9	1.4	0.3	98.6	1.7	1.5	2.4	1.9	0.4	97.7
	212	4.0	5.1	2.2	3.8	1.2	97.3	3.9	4.0	7.1	5.0	1.5	95.9
	150	7.1	8.2	4.0	6.4	1.8	93.5	6.2	6.6	10.3	7.7	1.8	90.9
	106	11.0	11.5	8.2	10.2	1.5	87.1	10.1	10.5	12.6	11.1	1.1	83.2
	75	11.8	11.4	11.3	11.5	0.2	76.8	11.1	11.3	11.4	11.3	0.1	72.1
	53	10.9	10.5	11.8	11.1	0.5	65.3	10.9	10.9	9.4	10.4	0.7	60.8
	38	6.4	5.9	7.2	6.5	0.5	54.3	7.1	6.4	5.4	6.3	0.7	50.4
	<38	46.1	44.0	53.2	47.8	3.9	47.8	46.8	46.2	39.4	44.1	3.4	44.1
TOTAL		100.0	100.0	100.0	100.0			100.0	100.0	100.0	100.0		
sample	600	0.7	0.1	0.3	0.4	0.2	100.0	0.3	0.8	0.5	0.5	0.2	100.0
2	425	0.8	0.2	0.3	0.4	0.3	99.6	0.3	0.6	0.5	0.5	0.1	99.5
	300	1.8	0.9	0.5	1.1	0.5	99.2	0.7	1.1	1.3	1.0	0.2	99.0
	212	4.8	4.3	1.5	3.5	1.5	98.1	2.3	3.0	4.5	3.3	0.9	98.0
	150	7.8	9.1	2.9	6.6	2.7	94.6	4.7	5.5	8.2	6.1	1.5	94.7
	106	11.4	13.3	6.5	10.4	2.9	88.0	9.1	10.0	11.9	10.3	1.2	88.6
	75	11.4	12.5	10.4	11.4	0.9	77.6	11.3	11.5	11.6	11.5	0.1	78.2
	53	10.2	10.3	12.1	10.9	0.9	66.2	11.4	11.1	10.0	10.8	0.6	66.8
	38	6.2	6.1	8.0	6.8	0.9	55.3	7.5	6.9	6.2	6.9	0.5	55.9
	<38	44.9	43.2	57.5	48.5	6.4	48.5	52.4	49.5	45.3	49.1	2.9	49.1
TOTAL		100.0	100.0	100.0	100.0			100.0	100.0	100.0	100.0		

IV.3.1 Plots of cumulative size distributions

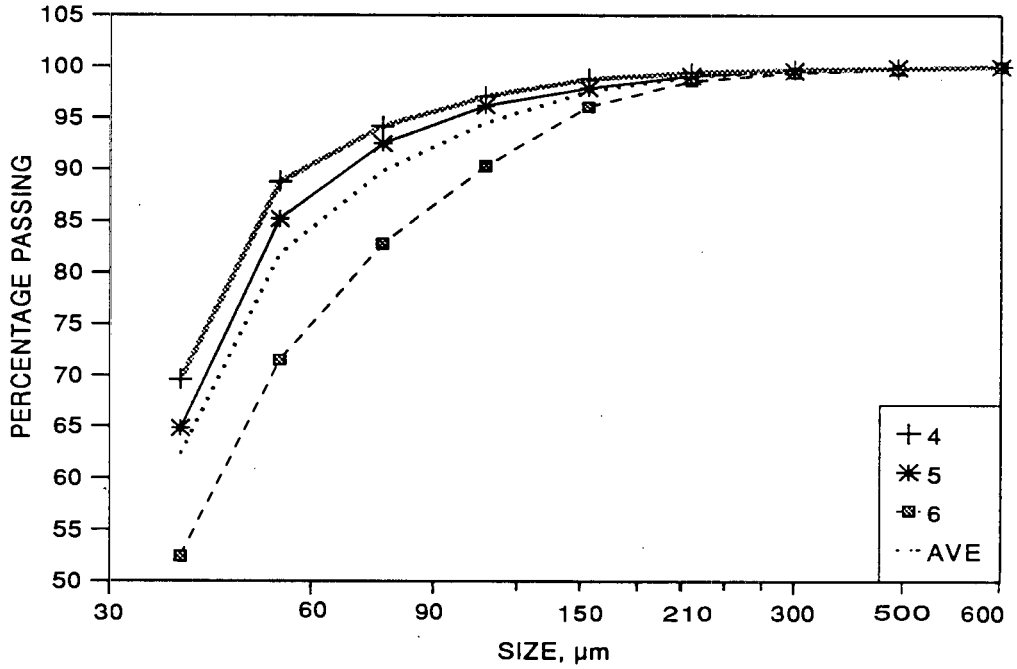

Figure 168. Cumulative size distribution for test 2, 80% crit. speed, smooth lining

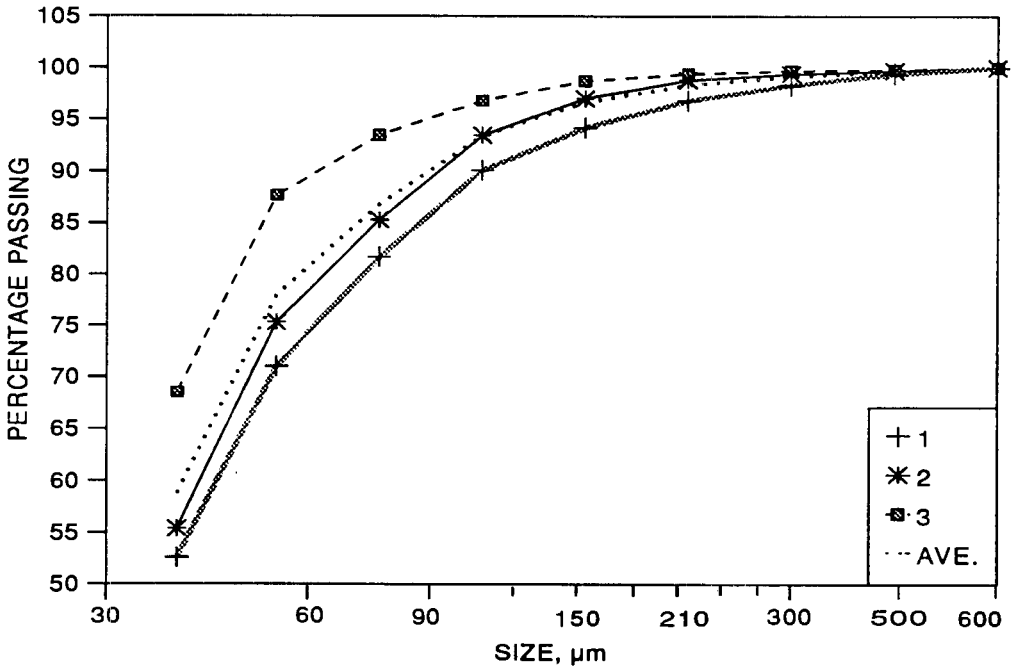

Figure 169. Cumulative size distribution for test 1, 90% crit. speed, smooth lining

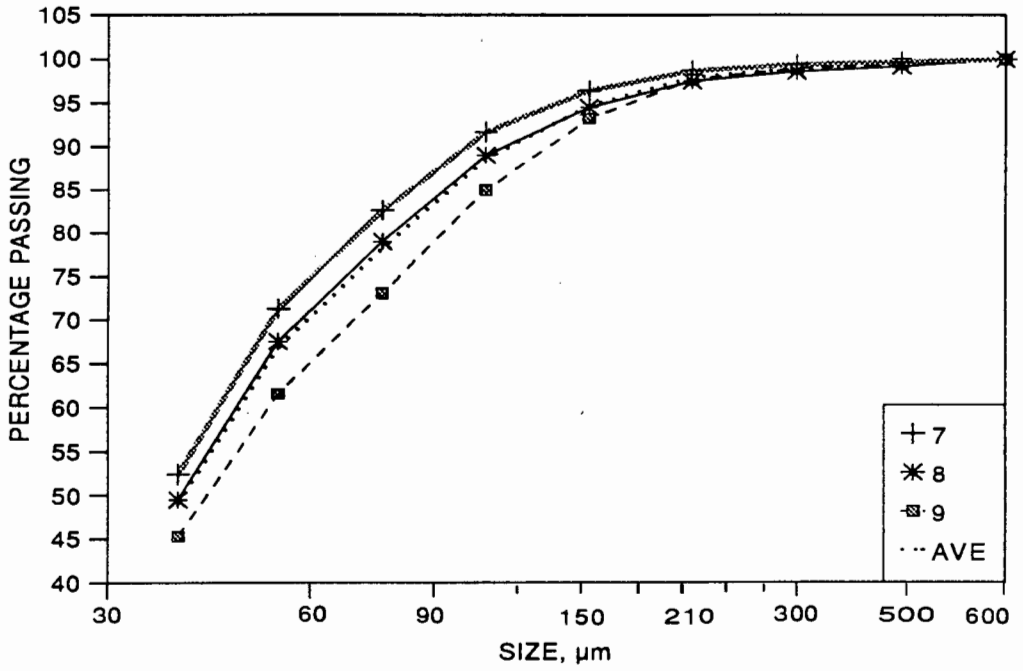

Figure 170. Cumulative size distribution for test 3, 80% crit. speed, 70 mm, 70° lifters

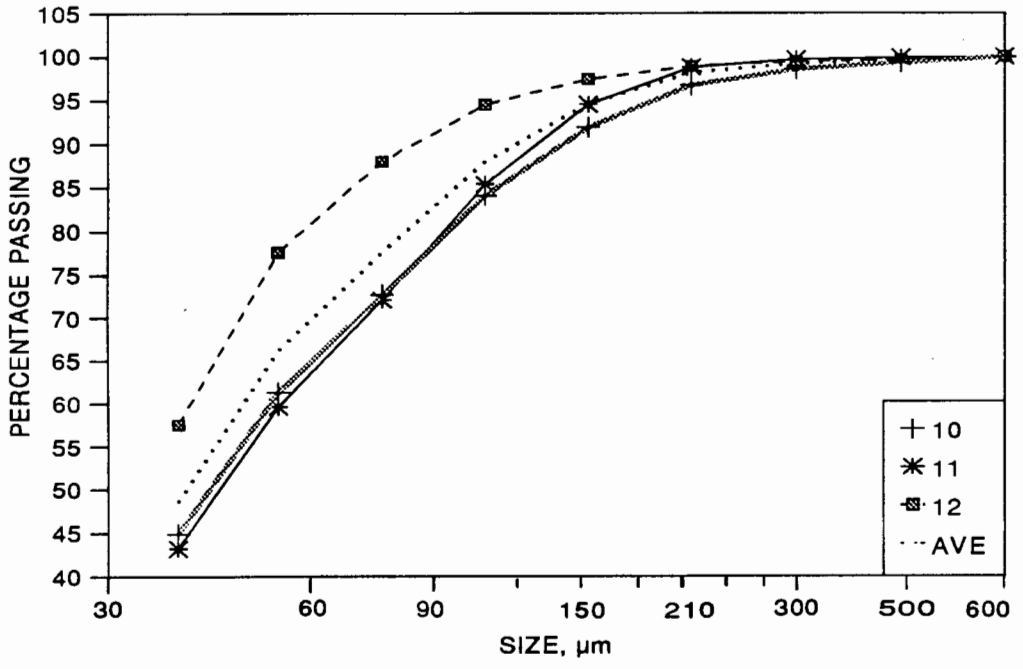

Figure 171. Cumulative size distribution for test 4, 90% crit. speed, 70 mm, 50° lifters

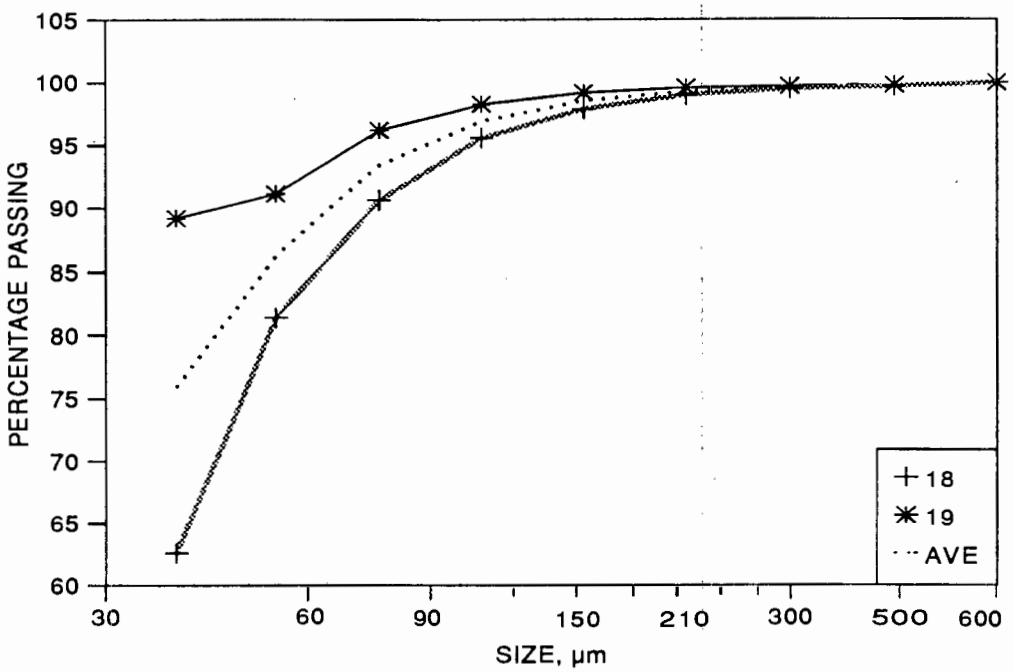

Figure 172. Cumulative size distribution for test 7, 80% crit. speed, grid lining

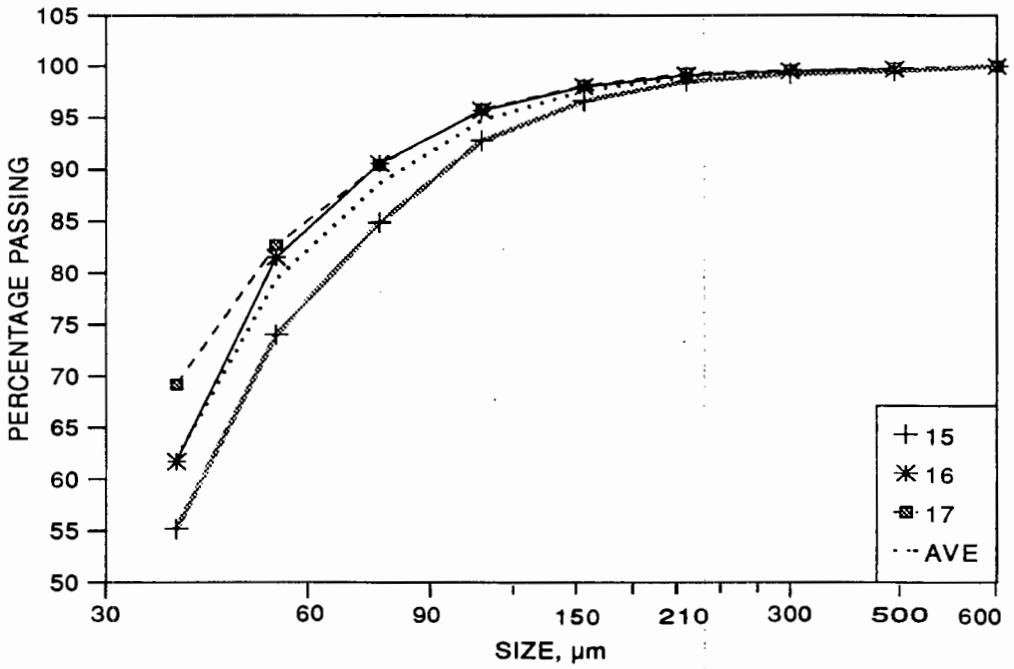

Figure 173. Cumulative size distribution for test 6, 90% crit. speed, grid lining

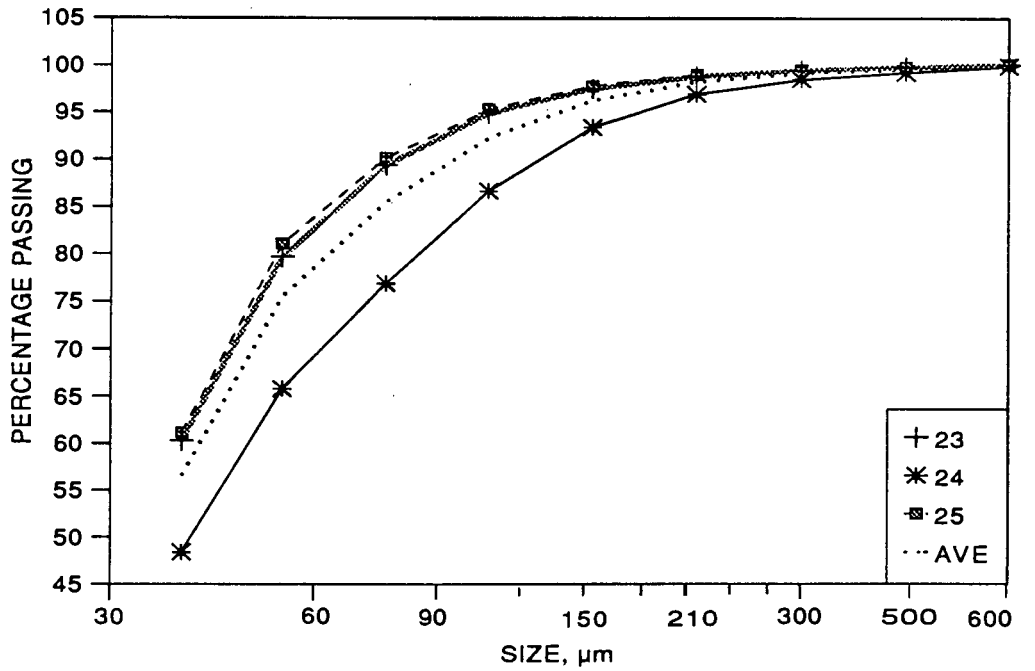

Figure 174. Cumulative size distribution for test 9, 80% crit. speed, 40 mm, 70° lifters

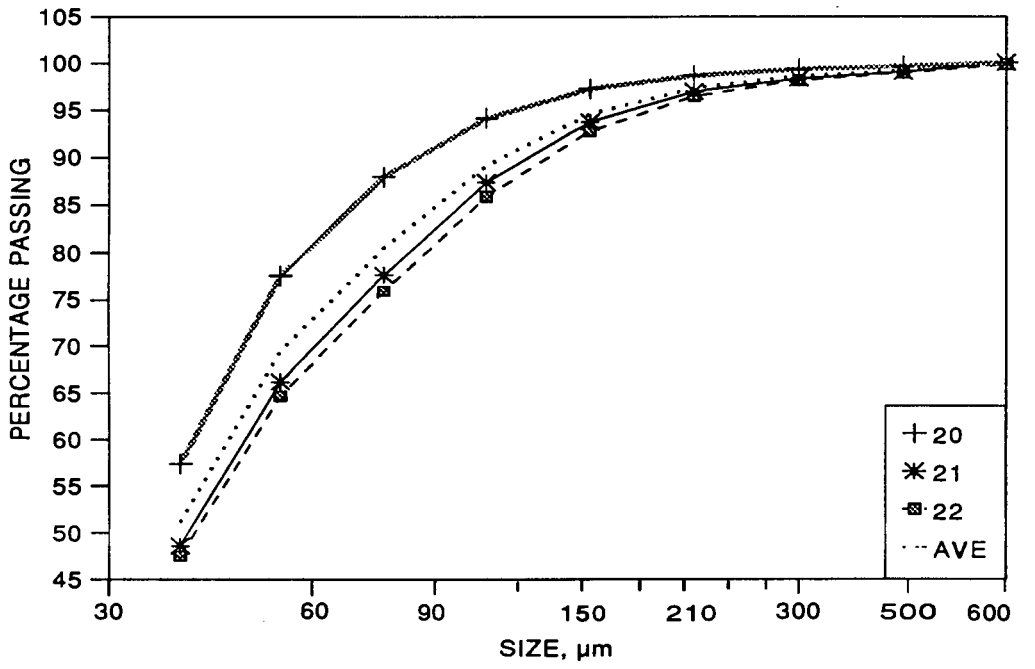

Figure 175. Cumulative size distribution for test 8, 90% crit. speed, 40 mm, 50° lifters

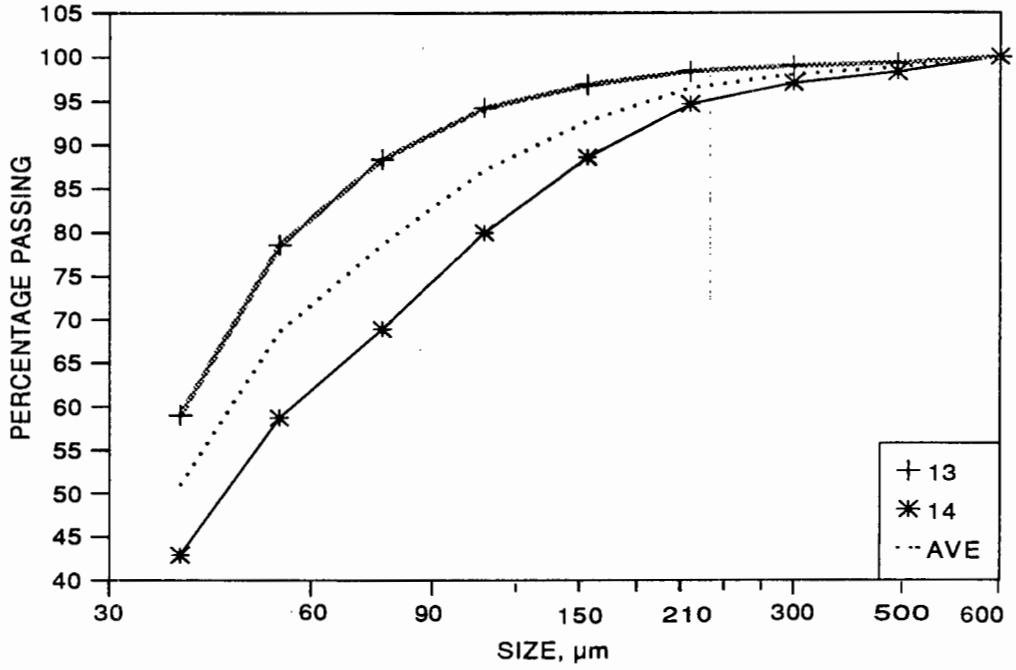

Figure 176. Cumulative size distribution for test 5, 90% crit. speed, 70 mm, 90° lifters

APPENDIX V
RESULTS OF ANALYSES

The graphs and tables of analyzed data are presented here.

V.1 CHARGE MOTION

The locations of the balls, in x-y coordinates, were used to calculate a range of properties of the ball path. An example of run 27 is used here to illustrate the full set of data (Table XXXIV), and of the analyses carried out on the spreadsheets.

The calculations used in the analyses, are given in the analysis section. Table XXVI shows the x-y data for the first 38 frames of run 27, and the data calculated from it. The location of the ball is converted into polar coordinates, with the radius in mm, and the angle in radians and degrees. Column 8 gives the distance moved between two frames. The work and accelerating forces are calculated according to the equations derived in the analysis section. The work/rev. is the sum of the work done by the ball over a full circuit around the mill. The ball impacts at frame 33, and the initial conditions are calculated from frame 28 to 32. The final conditions are calculated from frame 34 to 36. The accelerations are calculated from the ΔX and ΔY data. The bottom row of calculated data, from F to Work/rev, was abstracted into a summary spreadsheet, an example of which is given in the following table.

The full set of data extracted from run 27 is shown in the summarised data of Table XXVII. Table XXVIII shows the instantaneous acceleration of each ball in the 7 frames prior to impact. This acceleration indicates whether the ball is in free-flight or interacting with other balls.

Table XXXIV The full set of x-y data for run 27

No.	BEAD		STEEL BALL		SMALL STEEL		GLASS BALL		MARKER	
	X	Y	X	Y	X	Y	X	Y	X	Y
1	28.3	10.0	68.7	-17.0	47.0	19.3	70.4	-37.0		
2	19.5	-3.3	68.5	-8.4	38.6	13.1	74.6	-26.8		
3	11.0	-21.0	67.9	-0.5	30.7	2.5	76.9	-16.9		
4	0.4	-39.0	66.0	5.6	22.4	-11.9	78.0	-6.0		
5	-8.5	-52.3	62.8	10.6	14.3	-30.9	76.5	4.5		
6	-12.4	-62.1	59.4	13.9	7.6	-42.0	73.4	13.9		
7	-10.7	-71.6	55.6	15.2	5.7	-58.6	69.1	22.0		
8	-5.1	-76.1	49.8	13.4	10.9	-64.4	62.7	27.6		
9	3.6	-78.1	44.2	8.4	15.8	-66.9	56.4	29.3		
10	14.0	-78.6	37.5	-0.4	23.6	-66.7	49.5	26.8		
11	24.4	-76.0	31.5	-13.0	32.6	-63.5	41.6	21.2		
12	35.0	-71.7	24.7	-28.4	40.9	-58.7	33.4	12.3	-52.2	96.7
13	44.7	-65.6	18.7	-42.1	48.6	-52.5	25.6	-0.7	-65.1	87.3
14	53.3	-59.0	14.6	-54.3	54.8	-45.5	18.0	-17.7	-77.9	77.5
15	61.2	-50.6	14.7	-61.5	60.5	-37.5	8.1	-32.2	-88.5	64.7
16	67.4	-41.5	17.3	-63.3	64.1	-28.8	-1.1	-42.3	-53.3	94.6
17	72.1	-31.5	22.9	-62.7	66.0	-20.3	-13.4	-52.6	-67.2	85.5
18	75.3	-21.3	28.6	-61.8	66.7	-12.4	-21.3	-66.8	-80.5	76.1
19	76.8	-10.5	36.6	-58.7	67.0	-6.3	-24.6	-79.9	-91.2	63.4
20	75.8	-0.4	44.7	-53.3	64.3	1.3	-17.7	-87.3		
21	74.4	9.0	51.3	-46.3	59.5	6.9	-6.3	-90.1		
22	70.4	16.2	57.6	-38.7	54.6	8.4	6.4	-90.6		
23	65.4	21.1	62.0	-30.0	50.1	5.4	19.3	-88.9		
24	59.9	23.7	65.1	-21.3	45.8	0.5	31.9	-85.5		
25	54.2	24.8	66.7	-12.7	41.0	-4.5	43.6	-80.2		
26	47.9	23.7	66.9	-3.9	34.8	-12.6	54.2	-73.2		
27	41.4	18.4	65.9	3.4	28.9	-24.6	64.5	-64.5	-90.3	-61.0
28	34.5	9.2	63.3	8.3	25.5	-36.2	72.5	-55.0	-82.7	-75.5
29	27.3	-3.2	60.8	11.3	24.7	-44.7	79.7	-44.7	-71.6	-88.1
30	19.3	-18.0	57.1	13.8	22.4	-52.7			-56.6	-96.0
31	10.4	-35.3	52.3	13.6	26.5	-53.2			-39.8	-98.2
32	0.9	-50.0	47.5	11.0	32.3	-55.1			-23.5	-98.4
33	-3.6	-61.0	41.8	5.0	38.1	-52.5				
34	-0.8	-68.2	37.0	-4.3	42.5	-49.2				
35	6.1	-71.4	31.5	-17.3	45.6	-47.4	82.9	25.6		
36	13.2	-71.3	24.6	-33.4	52.0	-43.0	77.5	34.8	37.1	-97.6
37	22.0	-71.9	19.4	-45.4	57.1	-35.7	71.7	42.6	54.3	-97.6
38	32.0	-68.3	16.3	-56.1	59.8	-27.7	65.3	47.8	66.9	-87.8
39	41.1	-63.7	18.2	-62.6	61.9	-19.3	58.3	51.3		
40	49.3	-57.6	22.3	-63.9	61.9	-11.2	48.9	50.7		
41	57.0	-50.4	28.9	-62.8	61.4	-4.5	39.1	46.4		
42	62.9	-42.0	36.9	-60.2	60.4	0.6	28.3	38.0		
43	68.1	-32.7	44.7	-55.6	59.3	3.5	18.0	25.3		
44	72.1	-23.2	52.0	-50.8	58.5	3.4	7.6	8.4		
45	74.2	-13.4	58.1	-42.7	54.3	4.4	-2.0	-12.5		
46	74.5	-4.0	62.5	-34.7	49.4	1.1	-12.3	-37.9		
47	73.5	5.1	65.8	-26.8	43.9	-2.7	-28.7	-55.4		
48	71.2	12.7	67.3	-17.8	38.7	-10.6	-40.6	-64.9		
49	66.6	18.9	66.7	-10.1	32.8	-19.4	-44.7	-75.5		
50	61.6	23.3	65.1	-3.1	28.6	-28.8	-38.8	-88.9		
51	55.8	24.8	63.1	2.6	24.6	-38.8	-26.7	-96.8		
52	48.5	24.1	59.9	6.7	20.4	-43.9	-11.9	-99.5		
53	40.5	19.9	56.2	9.2	19.0	-51.2	2.8	-100.7		
54	33.0	11.3	51.5	9.4	21.6	-54.5	15.8	-100.5		
55	24.5	0.2	46.7	6.9	27.2	-54.0	30.0	-97.5		
56	16.1	-15.2	41.3	0.2	32.0	-50.5	43.5	-92.5		
57	7.2	-33.9	36.1	-9.9	38.3	-46.3	54.2	-85.9		
58	-4.8	-51.0	29.9	-22.6	44.2	-41.4	68.3	-76.1	-48.1	97.1
59	-8.1	-61.5	23.2	-36.7	49.6	-35.7			-62.9	90.4
60	-9.4	-69.4	17.5	-48.7	54.6	-32.1			-75.8	80.6
61	-5.5	-75.8	15.0	-58.2	57.8	-26.0			-87.0	68.6
62	2.5	-78.3	15.0	-62.9	59.0	-22.1			-95.1	54.6
63	12.7	-77.8	19.9	-63.5	59.5	-18.5				
64	23.3	-75.9	27.2	-62.0	61.0	-13.5				
65	33.9	-72.0	33.9	-59.1	61.2	-6.3				

No.	BEAD		STEEL BALL		SMALL STEEL		GLASS BALL		MARKER	
	X	Y	X	Y	X	Y	X	Y	X	Y
66	44.1	-66.8	40.9	-55.7	59.5	-0.8				
67	52.9	-59.7	47.8	-50.5	57.6	1.4				
68	60.8	-52.2	53.9	-43.2	55.6	0.1				
69	66.9	-42.8	58.9	-36.0	51.3	-0.3			-93.5	-55.2
70	72.4	-32.8	62.7	-27.7	45.3	-3.6	68.6	66.4	-86.9	-70.1
71	76.2	-22.3	65.5	-19.3	40.1	-11.0	58.2	70.3	-77.1	-83.5
72	78.3	-12.3	66.2	-11.2	34.9	-15.0	46.6	71.2	-64.5	-94.1
73	79.0	-2.1	65.9	-4.5	30.6	-23.7	35.7	67.6	-46.8	-98.5
74	77.9	8.5	64.2	0.8	26.7	-36.4	24.3	59.5	-29.3	-98.7
75	74.2	17.7	61.3	5.1	24.5	-47.6	13.2	47.3		
76	69.4	25.7	56.7	7.5	19.9	-55.5	2.1	31.4		
77	62.2	30.8	52.8	7.0	21.2	-59.8	-9.0	11.2		
78	54.4	32.1	48.1	3.2	27.1	-60.5	-19.6	-12.9		
79	46.0	29.7	43.3	-3.7	35.1	-57.3	-30.7	-41.9	46.1	-98.6
80	37.8	24.2	37.6	-12.9	41.7	-51.8	-46.4	-65.4	62.2	-93.2
81	28.5	14.4	31.2	-25.1	48.8	-46.0	-55.4	-75.5	74.7	-82.8
82	20.1	1.3	23.7	-36.2	54.4	-38.7	-49.9	-86.2		
83	11.0	-16.2	17.0	-48.7	58.6	-31.7	-37.9	-94.6		
84	1.9	-37.2	15.2	-55.8	61.4	-24.9	-24.1	-100.6		
85	-5.6	-56.3	15.4	-59.2	63.0	-18.7				
86	-10.2	-67.5	18.8	-63.8	62.6	-11.9				
87	-5.9	-72.3	25.0	-64.2	61.4	-7.8				
88	2.4	-76.5	33.0	-60.3	60.5	-4.1				
89	9.4	-76.9	41.1	-55.1	60.7	-2.0				
90	18.5	-76.5	48.3	-49.3	61.4	-1.2	60.4	-84.6		
91	28.9	-73.5	54.3	-42.3	59.2	-0.6	71.9	-75.4		
92	39.1	-68.9	59.3	-35.2	57.2	3.5				
93	48.3	-63.1	62.8	-29.0	53.8	5.7				
94	56.8	-55.3	66.0	-21.0	50.1	5.1				
95	63.9	-46.8	66.3	-12.9	44.8	2.1				
96	70.0	-37.9	65.9	-6.2	37.5	-4.2				
97	74.6	-28.5	64.4	-0.6	30.7	-15.1				
98	77.7	-17.8	61.4	3.7	23.7	-28.1				
99	79.2	-7.9	57.3	6.3	16.0	-39.6				
100	79.2	2.1	52.8	6.1	10.2	-52.5				
101	77.2	11.9	48.0	2.5	8.4	-62.9			-56.3	93.0
102	73.8	21.3	42.7	-3.9	10.6	-66.6			-70.2	84.9
103	68.3	27.9	36.5	-12.4	15.5	-70.7	62.6	64.0	-82.6	73.3
104	62.6	31.8	29.1	-23.4	24.2	-70.7	52.5	64.7	-93.3	60.3
105	56.6	32.4	22.7	-36.4	34.0	-66.7	41.0	61.9		
106	48.8	31.6	17.7	-46.7	43.1	-61.5	29.1	56.0		
107	40.8	27.5	15.9	-53.2	50.7	-55.2	18.1	45.8		
108	32.6	19.9	17.0	-57.8	57.7	-47.2	6.6	31.2		
109	24.6	8.4	22.5	-58.4	63.8	-38.8	-4.5	12.7		
110	15.7	-7.6	27.0	-56.1	68.0	-29.8	-15.3	-10.3		
111	6.7	-26.4	31.4	-55.7	70.8	-20.6	-26.1	-37.1		
112	-1.7	-46.6	36.8	-52.2	72.8	-11.5	-36.2	-63.5	-90.0	-64.4
113	-9.3	-59.8	42.2	-48.1	73.1	-3.1	-43.5	-76.2	-80.5	-77.7
114	-9.0	-71.9	48.0	-43.2	71.1	4.7	-37.9	-84.2	-69.3	-90.0
115	-3.1	-76.6	52.7	-37.0	69.2	11.5	-29.7	-90.4	-55.1	-98.1
116	5.5	-78.5	56.4	-30.2	65.9	16.2	-17.5	-93.8		
117	16.1	-78.7	58.7	-24.1	61.7	17.8	-3.8	-96.2		
118	26.6	-76.5	60.0	-17.7	54.3	19.2	10.1	-96.4		
119	37.4	-72.2	59.8	-11.9	46.3	17.2	23.6	-94.0		
120	47.7	-66.9	58.4	-7.6	37.8	12.2	37.1	-89.7		
121	56.2	-59.3	56.2	-4.8	30.8	1.7	49.0	-84.9		
122	64.3	-50.8	54.1	-4.6	24.0	-11.8	59.6	-76.8	56.9	-96.9
123	70.9	-41.5	51.2	-6.4	17.3	-29.5	70.5	-67.5	70.5	-88.3
124	75.4	-30.6	48.8	-9.9	14.8	-42.5	79.9	-55.9		
125	78.7	-19.7	45.7	-17.1	7.1	-51.1				
126	80.2	-8.6	42.9	-24.3	4.8	-58.8				
127	80.1	2.2	40.1	-28.9	6.4	-62.7				
128	78.2	12.0	37.3	-33.7	11.8	-65.5				
129	73.5	20.6	34.8	-36.8	17.8	-63.7				
130	69.3	27.8	33.2	-39.0	21.2	-64.1				
131	61.8	32.4	32.7	-41.9	24.3	-65.2				
132	53.5	33.9	33.0	-43.5	31.2	-63.0				
133	44.6	30.9	33.5	-44.4	39.4	-58.6	70.9	50.7		

No.	BEAD		STEEL BALL		SMALL STEEL		GLASS BALL		MARKER	
	X	Y	X	Y	X	Y	X	Y	X	Y
134	36.0	24.3	36.0	-41.9	46.6	-52.3	61.5	56.4		
135	27.2	13.1	38.9	-39.9	53.3	-45.5	51.7	58.7		
136	18.3	-1.7	41.1	-38.1	58.6	-37.7	41.1	56.4		
137	9.9	-20.8	44.1	-36.1	62.8	-29.3	30.8	50.3		
138	-0.4	-42.0	45.4	-33.3	65.5	-20.6	20.3	39.3		
139	-9.4	-57.7	47.7	-31.9	66.2	-13.0	10.0	24.9		
140	-13.4	-65.6	49.5	-26.5	66.3	-8.6	-0.1	5.7		
141	-12.1	-76.2	50.4	-20.4	66.9	-4.4	-10.1	-17.0		
142	-7.3	-81.1	49.3	-16.2	65.6	3.4	-19.3	-41.9		
143	1.6	-84.7	47.6	-15.5	62.0	10.1	-35.7	-53.9	-51.1	96.0
144	12.6	-84.8	45.7	-18.6	57.6	14.6	-49.4	-64.3	-66.0	89.8
145	24.2	-82.5	44.4	-23.4	51.6	15.1	-49.0	-72.2	-78.0	78.7
146	36.0	-78.4	42.5	-27.3	45.4	11.7	-45.5	-79.7	-89.1	66.2
147	45.9	-72.5	39.1	-30.5	37.8	4.2	-40.6	-88.0	-96.8	51.6
148	55.4	-65.5	36.3	-35.3	30.9	-7.6				
149	64.2	-57.0	34.7	-39.8	22.1	-22.6				
150	71.1	-47.2	34.5	-42.0	12.0	-39.7				
151	76.4	-37.4	35.6	-43.2	7.9	-49.4				
152	80.9	-26.1	37.6	-42.1	6.2	-57.3				
153	82.7	-14.4	42.4	-38.2	7.3	-58.7				
154	83.3	-3.1	46.2	-34.6	11.0	-62.9			-92.6	-58.4
155	82.6	8.8	48.8	-31.3	16.3	-61.7			-85.4	-72.4
156	81.3	17.3	49.8	-27.1	22.8	-60.9	31.7	-97.2	-74.9	-85.1
157	76.5	26.3	51.8	-24.2	30.1	-58.3			-61.4	-95.7
158	70.8	32.6	52.8	-19.9	36.9	-54.6			-43.7	-98.4
159	65.2	38.0	53.1	-15.8	43.3	-51.8				
160	57.9	40.1	52.4	-14.0	49.5	-51.6				
161	48.4	40.8	50.2	-12.6	56.4	-45.9				
162	37.4	38.3	47.8	-12.1	61.6	-37.9				
163	27.1	31.0	44.8	-15.7	65.3	-29.5				
164	16.4	19.9	41.1	-21.9	68.6	-20.5			50.0	-98.7
165	6.2	4.3	37.0	-29.6	70.0	-10.9			64.9	-92.6
166	-3.8	-15.4	33.8	-38.6	70.8	-1.7			76.9	-81.0
167	-14.1	-39.6	34.3	-44.1	69.3	6.7				
168	-24.9	-62.0	35.5	-46.8	67.3	13.5	62.3	65.1		
169	-28.7	-75.4	37.2	-48.7	64.3	17.5	52.4	65.4		
170	-21.9	-84.4	39.8	-48.1	59.5	22.7	41.3	62.4		
171	-12.1	-88.4	45.1	-44.3	53.4	24.8	31.1	56.0		
172	-0.5	-91.6	50.1	-39.1	46.0	23.6	20.2	45.9		
173	11.3	-91.6	54.2	-33.9	37.6	18.5	9.7	31.2		
174	24.2	-88.6	57.9	-26.6	29.3	8.9	-1.9	13.2		
175	36.7	-84.7	60.2	-19.7	21.2	-4.8	-13.2	-8.7		
176	47.9	-78.1	61.4	-11.8	13.1	-21.0	-24.0	-35.2		
177	58.8	-70.9	61.5	-3.8	3.9	-41.6	-37.6	-54.5		
178	67.9	-62.5	60.5	2.4	-4.8	-58.9	-45.7	-71.7		
179	75.6	-52.2	57.9	7.2	-6.6	-68.2	-44.4	-80.7		
180	82.0	-40.6	54.3	10.5	-2.6	-75.1	-36.6	-92.1		
181			50.1	10.3	6.1	-76.6	-26.5	-97.1		
182			45.8	7.1	16.3	-75.3	-11.8	-100.8		
183			41.1	0.5	26.8	-72.2				
184			35.5	-7.6	36.1	-68.3				
185			29.2	-19.1	45.1	-63.0				
186	81.6	31.4	22.8	-33.3	53.4	-56.0			-59.2	93.0
187	74.5	39.7	16.6	-44.9	60.6	-48.3			-73.2	84.0
188	66.0	45.5	15.3	-53.4	66.4	-39.3	68.4	-76.1	-85.2	72.1
189	57.5	49.1	17.9	-59.6	70.8	-30.0			-94.7	58.2
190	48.4	49.1	23.9	-61.2	74.5	-20.3				
191	38.7	45.2	32.1	-57.6	75.7	-10.0				
192	28.6	36.6	39.8	-52.6	75.2	-1.6				
193	18.8	23.8	46.8	-46.3	74.3	5.9				
194	9.1	6.5	52.8	-39.4	72.4	13.9				
195	-0.2	-14.3	57.6	-31.8	70.5	21.7				
196	-10.2	-38.6	60.5	-24.1	66.5	28.2			-95.6	-51.4
197	-19.2	-53.7	62.2	-16.7	61.1	30.9			-88.3	-66.2
198	-23.5	-70.1	61.5	-9.4	54.8	31.5			-78.6	-79.9
199	-18.2	-74.8	58.8	-3.6	46.7	29.1	72.9	60.8	-67.5	-92.2

Table XXVI Abstract of the analysis table used, run 27

	MASSES bead 2.25 10^{-4} kg 0.2251 g			steel ball 8.82 10^{-4} kg 0.8823 g			small steel 1.297 $^{-4}$ kg 0.1297 g		glass bead 6.99 $^{-5}$ kg 0.0699 g															
			XRC27	6 mm, 60 deg lifters, 73.0% crit.																				
	X	BEAD Y	time s	radius mm	ang rad	ang deg	dist mm	Work mJ	Acc Force m/s2	Work/ rev mJ														
1	28.3	10	0.00	30	0.34	19.5																		
2	19.5	-3.31	0.02	19.8	6.11	350	16																	
3	11	-21	0.04	23.7	5.19	298	19.7	0.08	28.3															
4	0.368	-39	0.06	39	4.72	271	20.9	0.03	16															
5	-8.46	-52.3	0.08	53	4.55	261	16	0	-15															
6	-12.4	-62.1	0.10	63.3	4.51	259	10.5	0	-17															
7	-10.7	-71.6	0.12	72.4	4.56	262	9.66	0	5.54															
8	-5.08	-76.1	0.14	76.3	4.65	266	7.18	0	-2.6															
9	3.646	-78.1	0.16	78.2	4.76	273	8.95	0.02	18.6															
10	14.05	-78.6	0.18	79.8	4.89	280	10.4	0.02	17.1															
11	24.35	-76	0.20	79.8	5.02	288	10.6	0	10.9															
12	35.02	-71.7	0.22	79.8	5.17	296	11.5	0.01	14.1															
13	44.65	-65.6	0.24	79.3	5.31	304	11.4	0	9.44															
14	53.32	-59	0.26	79.5	5.45	312	10.9	0	7.16															
15	61.21	-50.6	0.28	79.4	5.59	320	11.5	0	12.9															
16	67.43	-41.5	0.30	79.2	5.73	328	11	0	7.55															
17	72.11	-31.5	0.32	78.7	5.87	336	11	0	9.62															
18	75.32	-21.3	0.34	78.3	6.01	344	10.7	0	8.37															
19	76.8	-10.5	0.36	77.5	6.15	352	10.9	0	10.8															
20	75.76	-0.43	0.38	75.8	6.28	360	10.1	0	5.56															
21	74.39	9.031	0.40	74.9	0.12	6.92	9.56	0	7.18															
22	70.44	16.19	0.42	72.3	0.23	12.9	8.17	0	2.85															
23	65.39	21.07	0.44	68.7	0.31	17.9	7.03	0	4.06		Δ X	Δ Y	Vy	ΔVy	ACC									
24	59.91	23.75	0.46	64.4	0.38	21.6	6.1	0	5.19		-5.75	1.0703	53.52											
25	54.15	24.82	0.48	59.6	0.43	24.6	5.85	0	8.54		-6.25	-1.07	-53.5	-107	-5.4		ave. acc. in cascading region							
26	47.9	23.75	0.50	53.5	0.46	26.4	6.35	0	12.3		-6.49	-5.352	-268	-214	-11	-8								
27	41.41	18.4	0.52	45.3	0.42	24	8.41	0.02	20.1		-6.96	-9.232	-462	-194	-9.7	-8.6								
28	34.45	9.165	0.54	35.6	0.26	14.9	11.6	0.04	25.5		-7.12	-12.34	-617	-156	-7.8	-8.4								
29	27.33	-3.18	0.56	27.5	6.17	353	14.3	0.04	23.3		-7.99	-14.85	-743	-125	-6.3	-8								
30	19.33	-18	0.58	26.4	5.53	317	16.9	0.05	22.9		-8.93	-17.29	-865	-122	-6.1	-7.7								
31	10.4	-35.3	0.60	36.8	5	286	19.5	0.06	22.8		-9.5	-14.68	-734	130	6.52	-5.6								
32	0.903	-50	0.62	50	4.73	271	17.5	0	0		-33.5	-59.17	0.08	68	850	4.2	240	0						
33	-3.61	-61	0.64	61.1	4.65	267	11.9	0	-18															
34	-0.84	-68.2	0.66	68.2	4.7	269	7.68	0	-11					standard analysis										
35	6.121	-71.4	0.68	71.7	4.8	275	7.69	0	9.87	0.04														
36	13.21	-71.3	0.70	72.5	4.9	280	7.09	0	6.81		14.05	-3.144	0.04	14.4	360	6.06	347	0		ANG		Work		
37	22.04	-71.9	0.72	75.2	5.01	287	8.85	0.02	18.6		F	E	P	AP	Vx	Vy	R	Ω	% Ω	REP	ACC	/REV		
38	31.98	-68.3	0.74	75.4	5.15	295	10.5	0.02	18.3		5.715	6.7e-05	0.229	40.6	771	661	75.7	65.1	0.92	240	-7.65	0.043		

Table XXVII Summarised data abstracted from run 27

Impact Force $Nx10^{-3}$	Impact energy mJ	ΔP $Nsx10^{-}$	Angle β °	ΔVx $m.s^{-1}$	ΔVy $m.s^{-1}$	Radius mm	Ω_b rad.s^{-}	Frac. Ω_{mill}	Angle °	Ave. Acc $m.s^{-2}$	Work /rev mJ
Bead											
5.71	0.0668	0.23	40.64	770.6	661.4	75.68	65.12	0.92	240.4	-7.65	0.04
6.32	0.0620	0.25	39.87	862.5	720.4	79.64	66.47	0.94	242.1	-6.88	0.10
6.28	0.0902	0.25	43.50	809.9	768.4	79.39	66.22	0.94	244.3	-9.31	0.09
5.82	0.0806	0.23	40.00	792.7	665.2	81.59	67.58	0.96	242.7	-8.10	0.11
5.88	0.0934	0.24	40.08	799.8	673.1	85.64	66.34	0.94	242.7	-9.48	0.10
7.59	0.1123	0.30	38.84	1050	845.8	91.98	67.40	0.95	243.3	-10.34	0.15
	rpm	ave. R	ball vel	Wk/rev	ave.X	ave.Y					
Sum.	66.52	82.32	573.47	0.10	38.7	-45.2					
Steel ball											
17.60	0.2023	0.70	48.99	523.5	602.0	68.84	64.67	0.92	243.2	-7.78	0.25
18.33	0.1785	0.73	48.88	546.5	625.9	70.77	60.47	0.86	246.1	-7.73	0.23
20.76	0.1317	0.83	49.20	615.0	712.4	68.70	62.85	0.89	246.5	-5.06	0.20
15.84	0.1553	0.63	37.69	568.2	439.0	68.61	59.41	0.84	239.7	-5.64	0.24
17.78	0.1411	0.71	45.69	563.2	577.0	63.71	55.56	0.79	239.6	-6.48	0.11
6.56	0.0183	0.26	48.53	196.9	222.8	56.27	29.47	0.42	236.5	-0.54	0.12
10.74	-0.0166	0.43	49.70	314.8	371.2	56.86	33.45	0.47	241.4	-0.67	0.09
5.66	0.0236	0.23	21.92	237.9	95.7	61.57	53.57	0.76	232.1	-5.14	0.17
20.00	0.1267	0.80	43.13	661.9	620.0	65.34	64.92	0.92	241.6	-7.01	0.18
Sum.	53.82	64.52	363.63	0.18	43.9	-27.4					
Small steel ball											
3.07	0.0338	0.12	41.85	705.3	631.7	71.21	64.37	0.91	240.6	-10.65	0.03
2.33	0.0137	0.09	46.56	493.4	520.9	66.06	53.04	0.75	247.9	-4.26	0.03
2.30	0.0096	0.09	46.58	487.1	514.7	61.91	49.75	0.70	241.3	-3.38	0.02
2.44	0.0080	0.10	44.01	540.6	522.2	66.50	57.66	0.82	247.0	-6.15	0.04
2.74	0.0229	0.11	36.27	681.5	500.0	74.73	65.60	0.93	240.5	-5.45	0.04
2.80	0.0287	0.11	47.53	582.0	635.9	69.69	52.08	0.74	245.8	-9.80	0.04
2.74	0.0345	0.11	44.80	599.6	595.3	68.03	50.56	0.72	240.9	-8.78	0.08
4.00	0.0440	0.16	43.17	899.8	844.1	77.31	65.05	0.92	243.3	-9.72	0.08
Sum.	57.26	69.43	416.33	0.05	42.6	-26.4					
Glass bead											
2.12	0.0087	0.08	25.96	1092.5	531.8	91.16	67.32	0.95	231.3	-3.09	
2.51	0.0238	0.10	27.09	1276.9	653.0	101.51	67.66	0.96	236.7	-10.50	
2.64	0.0449	0.11	34.21	1251.0	850.4	103.73	68.08	0.96	243.4	-10.62	
2.46	0.0479	0.10	42.17	1042.3	944.0	97.31	68.13	0.96	245.7	-10.06	
1.71	0.0382	0.07	37.08	779.3	589.1	99.62	39.67	0.56	239.9	-9.39	
2.15	0.0395	0.09	32.45	1039.4	661.0	101.9	67.57	0.96	241.1	-9.83	
	rpm	ave. R	ball vel.	work/ rev	ave.X	Ave.Y					
Sum.	62.17	98.67	642.37								
Mill speed, rpm 70.62											

Table XXVIII Acceleration of the ball in the seven frames prior to impact, run 27

Radius mm	BEAD										Average
	75.68	79.64	79.39	81.59	85.64	91.98					49.39
Frame	Instantaneous Acceleration, $mm.s^{-2}$										
7	-5.35	-9.1	-9.37	-3.68	-11.21	-7.86					-7.76
6	-10.70	-10.87	-7.78	-8.28	-9.03	-12.12					-9.80
5	-9.70	-6.27	-10.70	-8.70	-11.62	-9.37					-9.39
4	-7.78	-10.70	-8.36	-9.87	-8.78	-11.29					-9.46
3	-6.27	-8.36	-10.87	-11.12	-10.87	-10.45					-9.66
2	-6.10	4.01	-8.78	-6.94	-5.35	-10.95					-5.69
1	6.52	16.72	4.93	-3.60	13.80	4.26					7.11

Radius mm	STEEL BALL										Average
	68.84	70.77	68.70	68.61	63.71	56.27	56.86	61.57	65.34		64.52
Frame	Instantaneous Acceleration, $mm.s^{-2}$										
7	-4.85	-6.61	-6.44	-7.19	-6.69	-4.26					-6.01
6	-7.78	-5.94	-10.62	-8.28	-8.61	-9.37	-4.01		-7.61		-7.78
5	-8.11	-8.53	-8.61	-8.03	-7.19	0.08	2.17		-8.28		-5.81
4	-9.45	-8.36	-6.52	-5.44	-5.02	6.44	1.84		-3.85		-3.79
3	-9.70	-9.20	-3.26	-7.44	-6.36	-0.50	-4.10		-8.70		-6.16
2	-6.77	-7.78	5.10	2.51	-5.02	4.35	0.75	-6.52	-6.61		-2.22
1	4.26	10.37	6.19	-3.51	6.77	2.17	5.85	-3.76	6.69		3.89

Radius mm	SMALL STEEL BALL										
	71.21	66.06	61.91	66.50	74.73	69.69	68.03	77.31			55.54
frame	Instantaneous Acceleration, $mm.s^{-2}$										
7											
6		-4.60	-1.34	-7.11	-6.10	-7.36	-9.78	-9.95			-6.61
5		-0.17	-10.20	-10.37	-8.36	-13.80	-10.03	-11.04			-9.14
4	-11.04	-7.94	-2.01	8.36	-11.29	-7.78	-11.04	-10.45			-6.65
3	-9.45	-9.70	-1.67	-11.62	-5.27	-10.29	-8.03	-6.02			-7.76
2	-11.46	1.09	-1.67	-10.03	3.76	11.79	-5.02	-11.12			-2.83
1	19.82	7.61	12.54	3.93	-3.68	10.95	18.48	8.19			9.73

Radius mm	GLASS BEAD										AVE
	91.16	101.51	103.73	97.31	99.62	101.90					59.52
frame	Instantaneous Acceleration, $mm.s^{-2}$										
7	-8.61	-10.03	-11.46	-8.11	-9.28	-8.53					-9.34
6	-9.95	-10.87	-10.03	-10.70	-12.29	-9.28					-10.52
5	-10.12	-10.45	-9.20	-10.70	-8.53	-11.54					-10.09
4	6.19	-10.20	-10.87	-10.03	-11.96	-8.03					-7.48
3	11.04	-10.95	-9.78	-11.12	-8.61	-9.95					-6.56
2	-0.59	19.73	-12.38	-9.70	-5.69	-11.62					-3.37
1	-9.62	19.73	14.05	1.17	32.36	18.15					12.64

V.2.1 Mass of fines - residuals and comparison

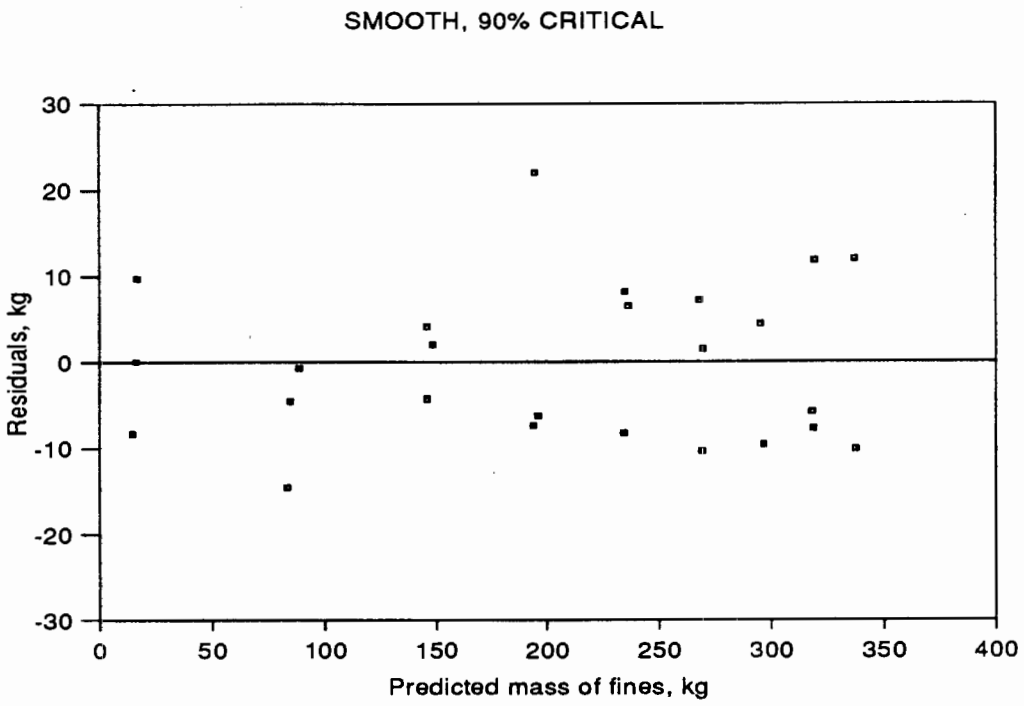

Figure 177. Residuals of test 1

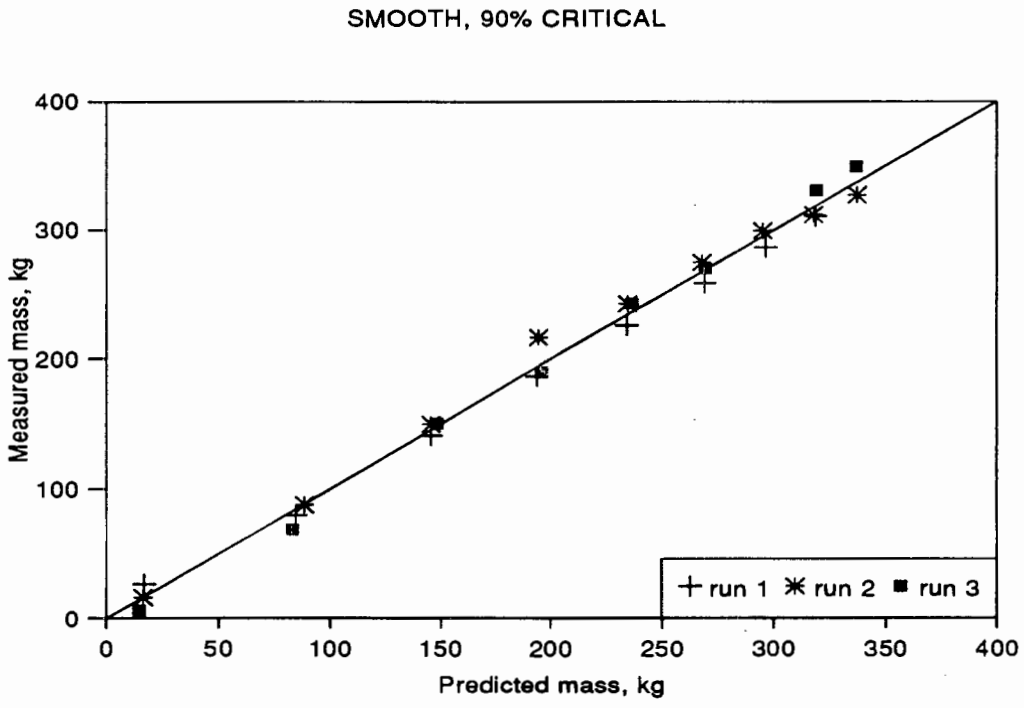

Figure 178. Comparison of experimental and predicted data, test 1

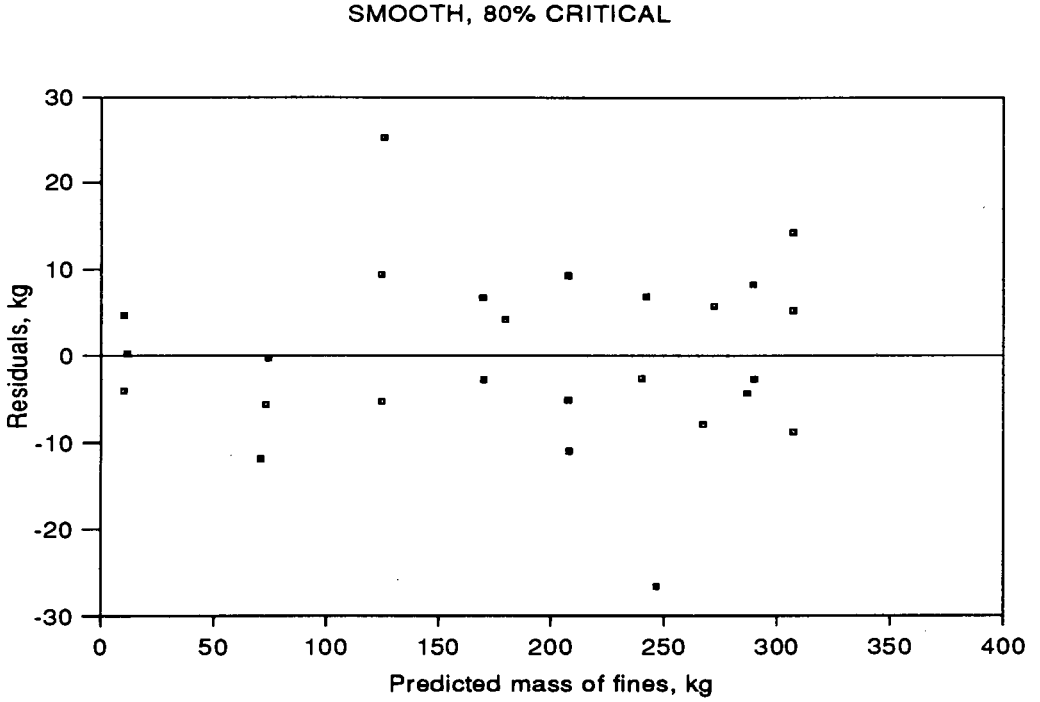

Figure 179. Residuals of test 2

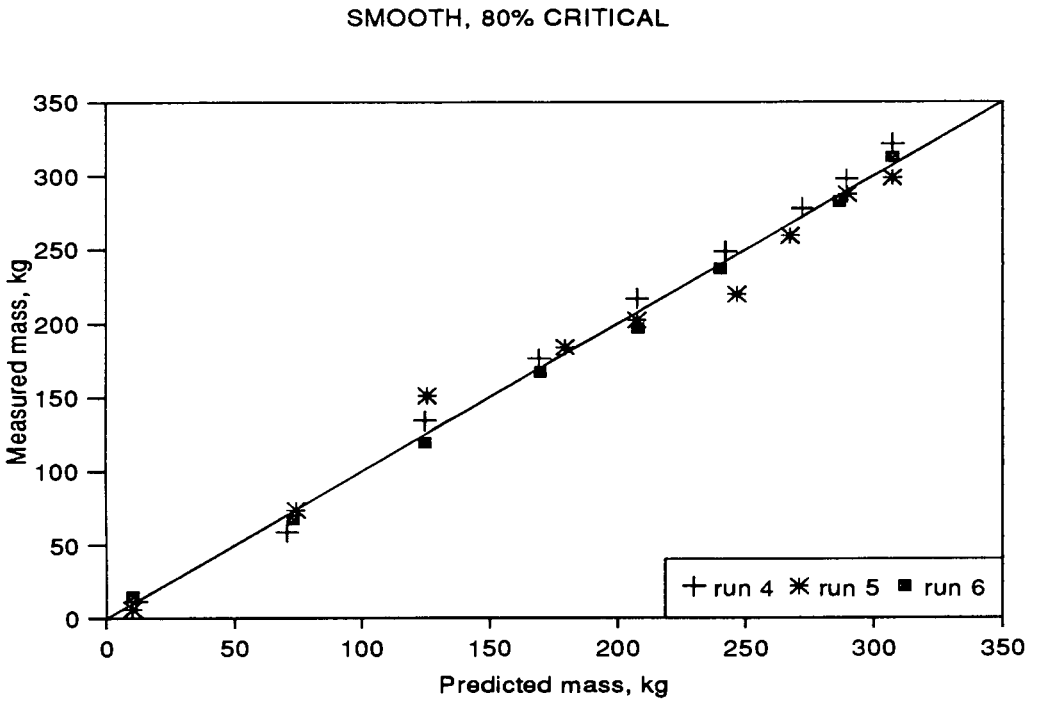

Figure 180. Comparison of experimental and predicted data, test 2

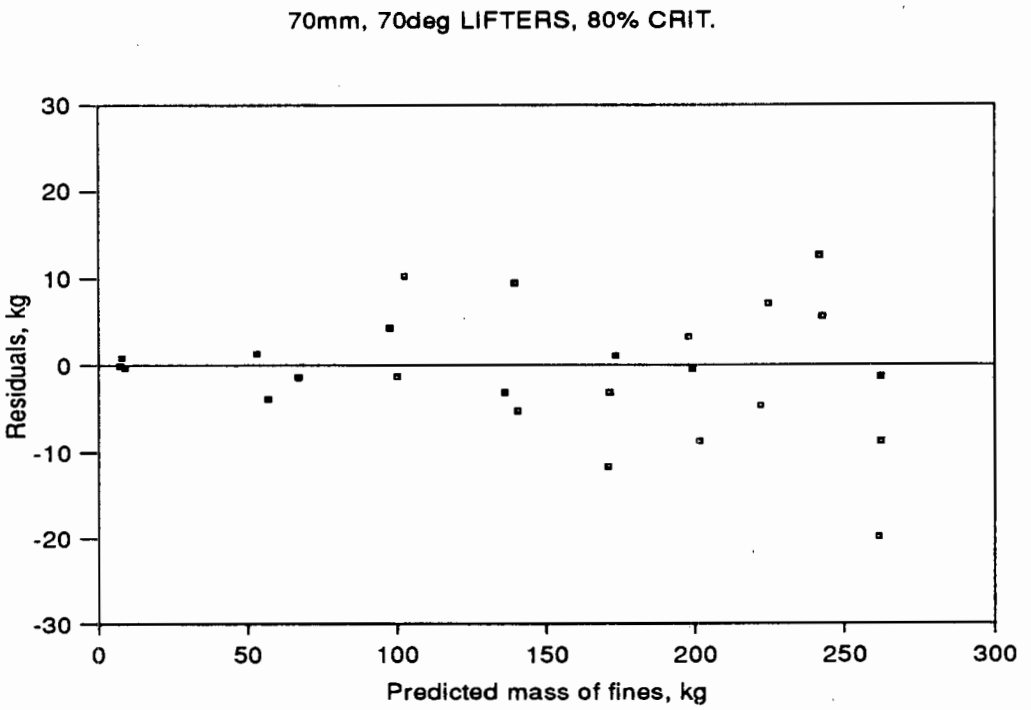

Figure 181. Residuals of test 3

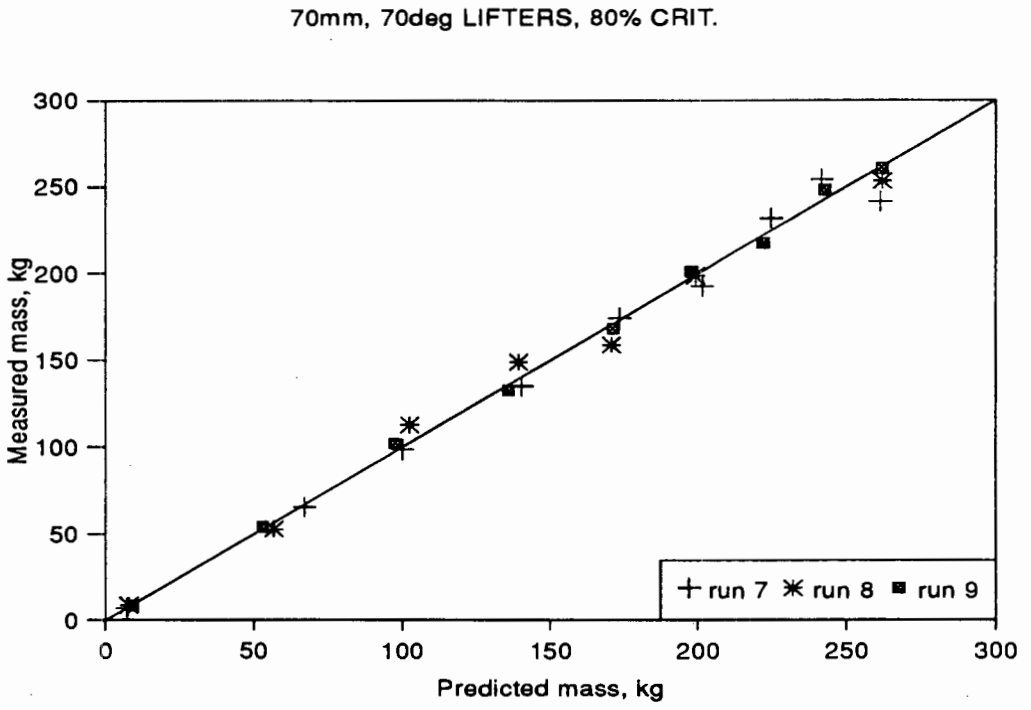

Figure 182. Comparison of experimental and predicted data, test 3

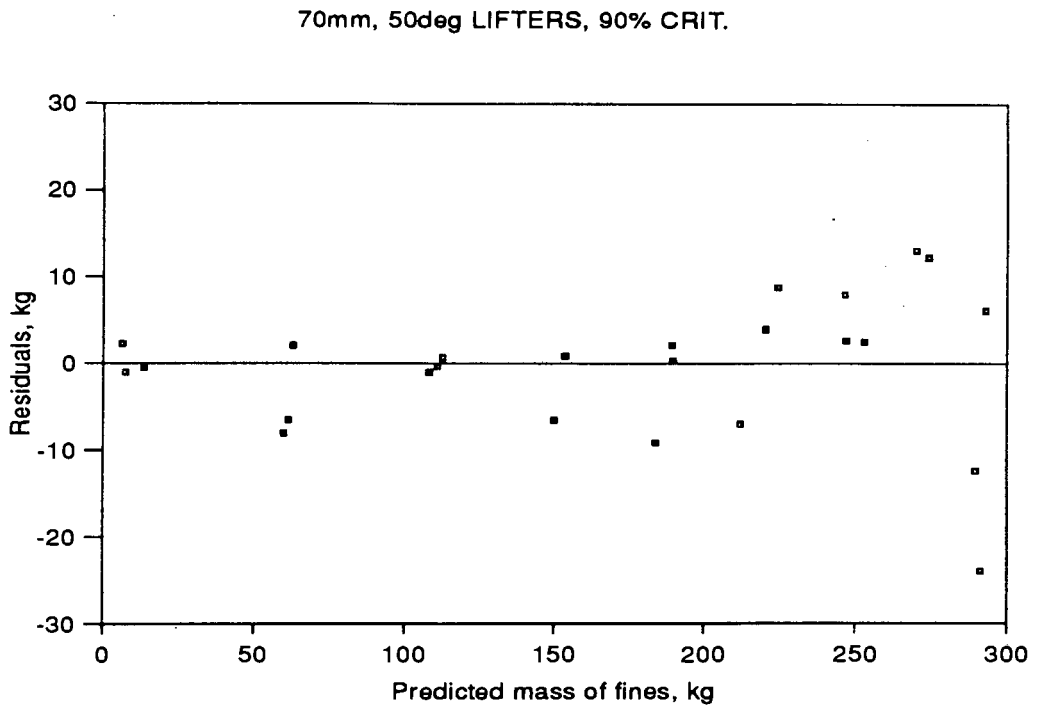

Figure 183. Residuals of test 4

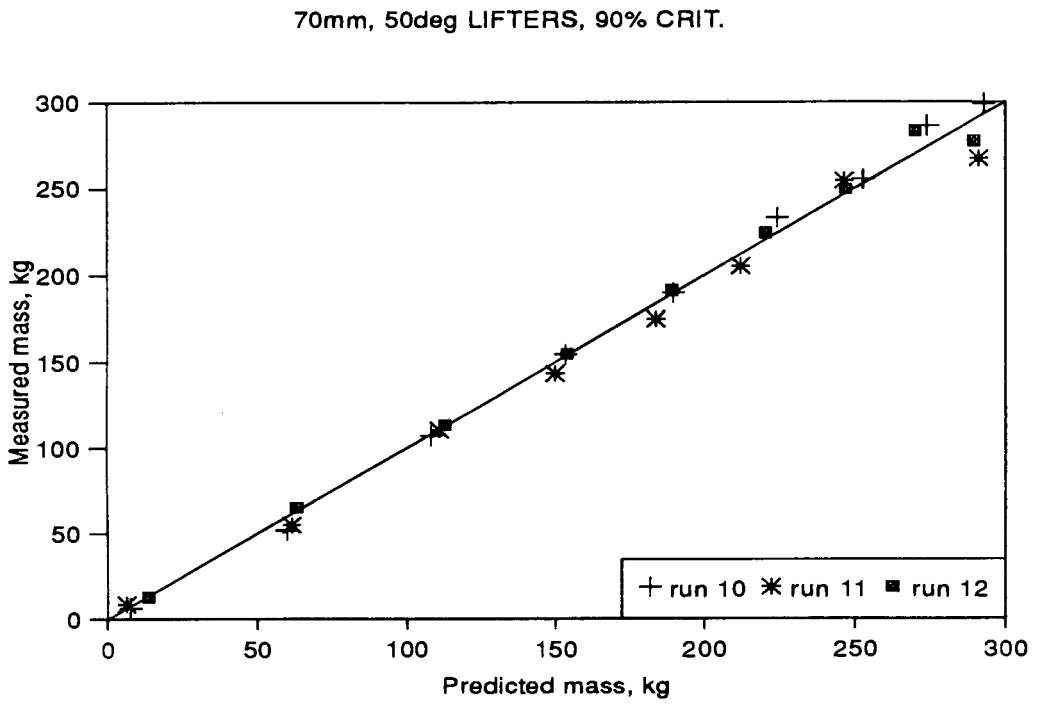

Figure 184. Comparison of experimental and predicted data, test 4

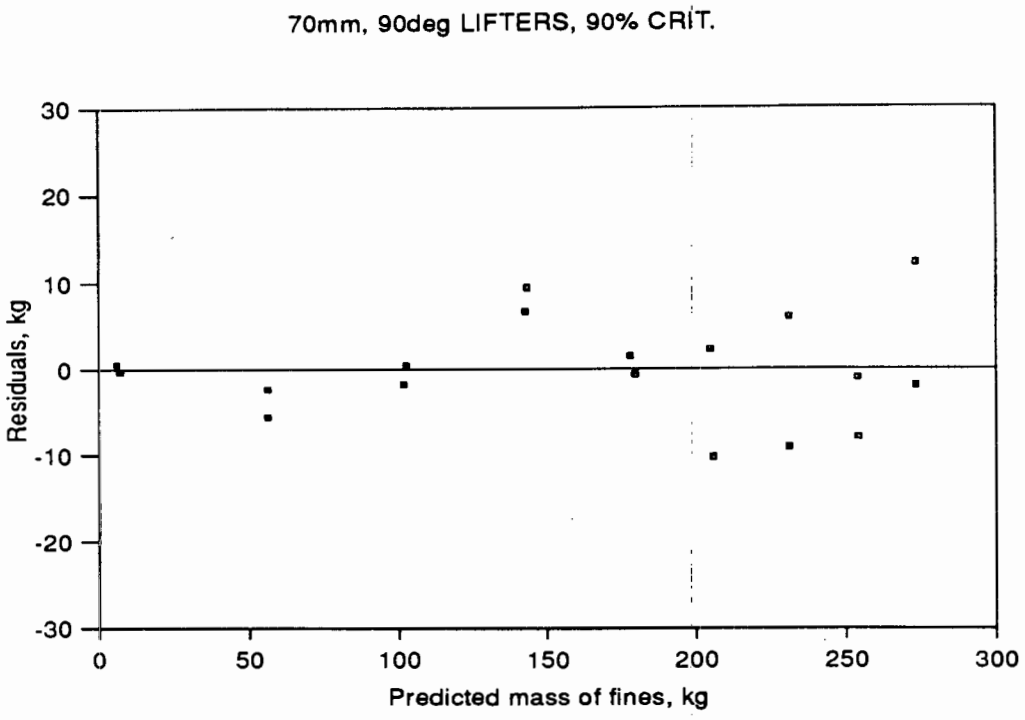

Figure 185. Residuals of test 5

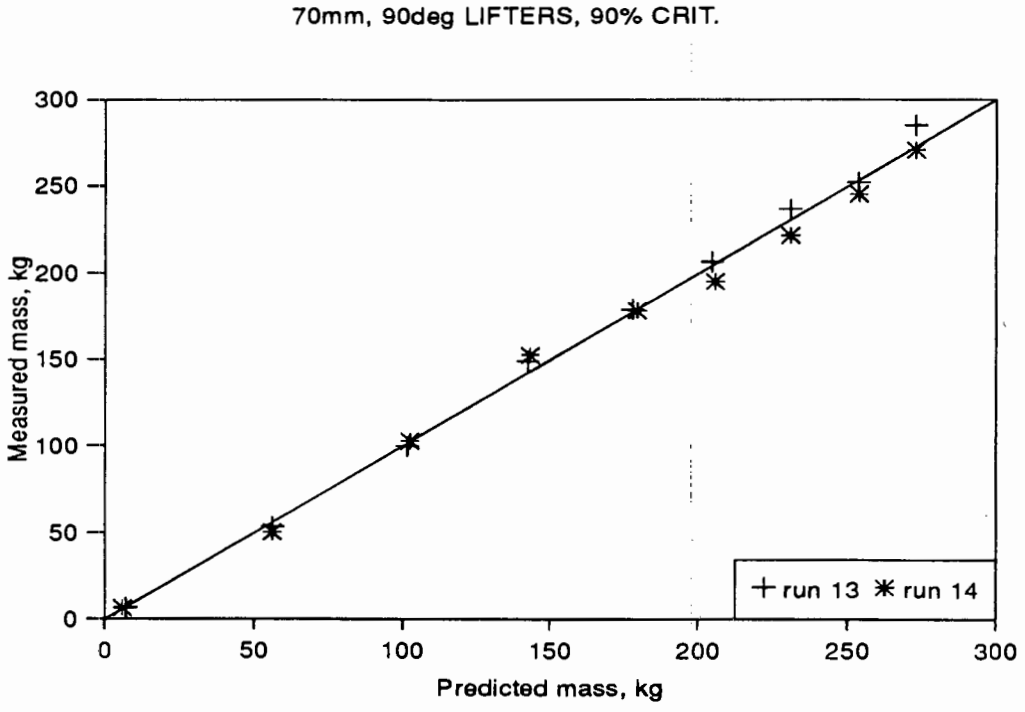

Figure 186. Comparison of experimental and predicted data, test 5

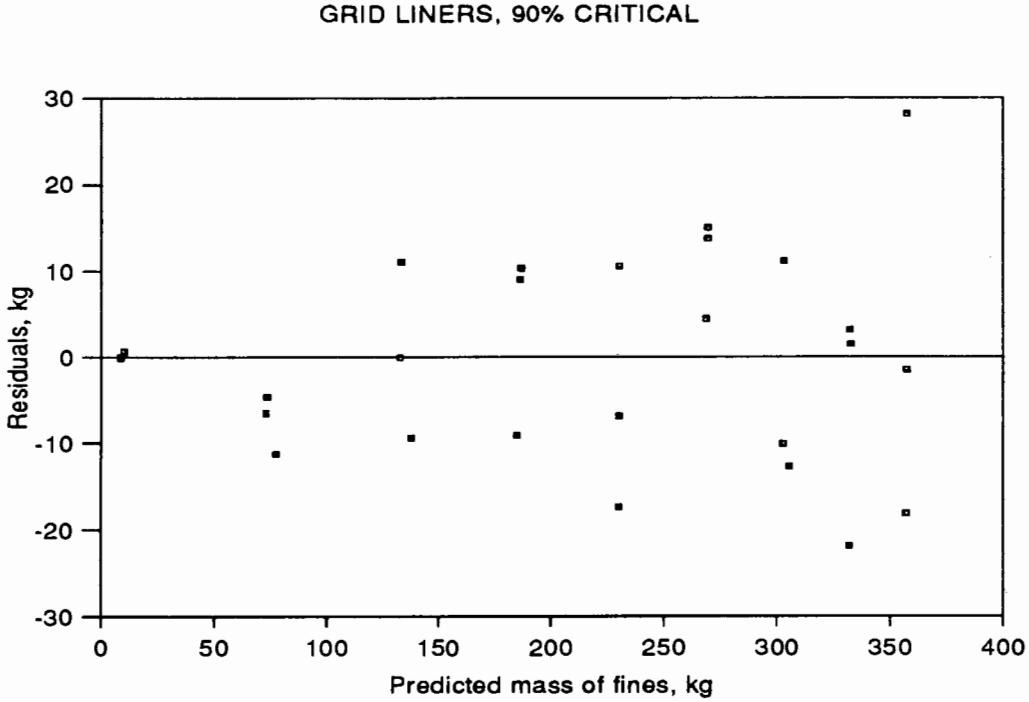

Figure 187. Residuals of test 6

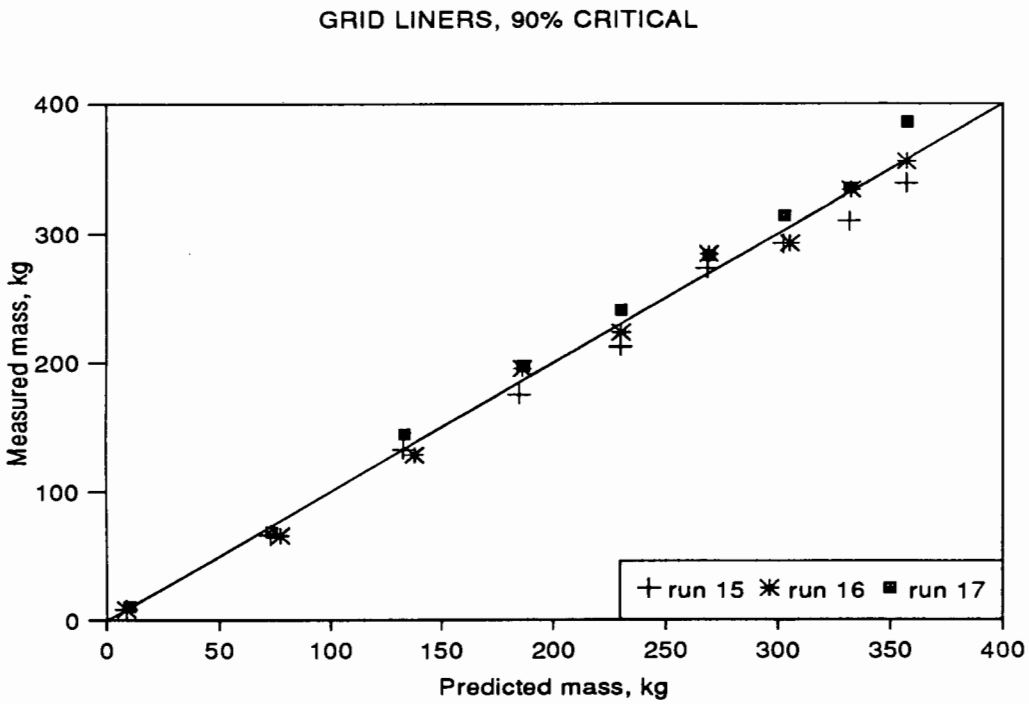

Figure 188. Comparison of experimental and predicted data, test 6

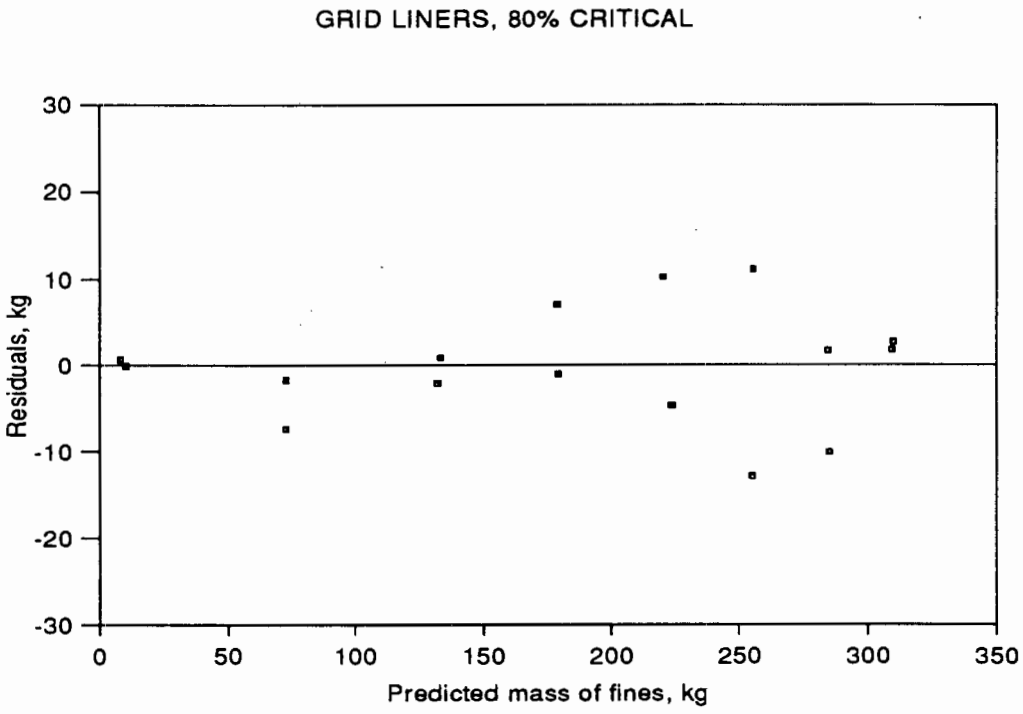

Figure 189. Residuals of test 7

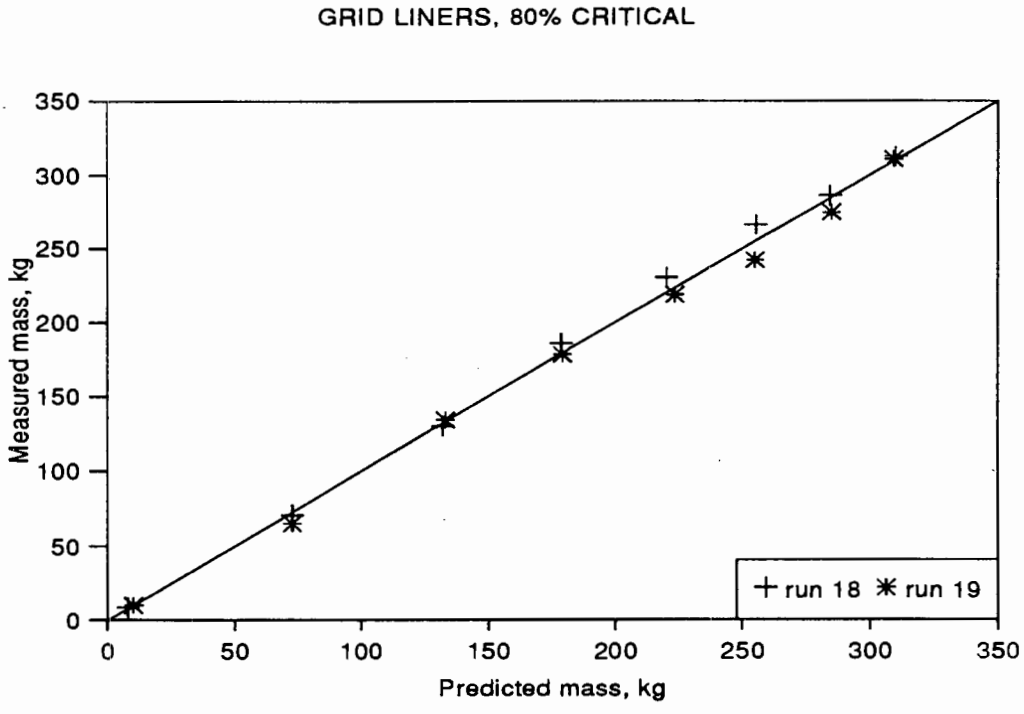

Figure 190. Comparison of experimental and predicted data, test 7

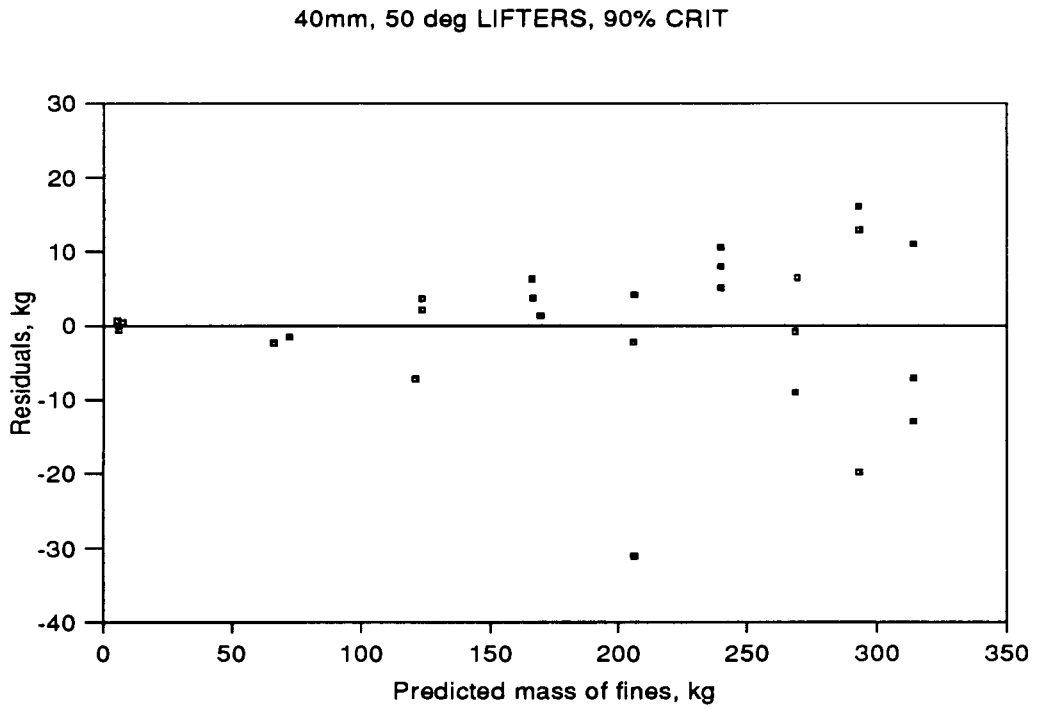

Figure 191. Residuals of test 8

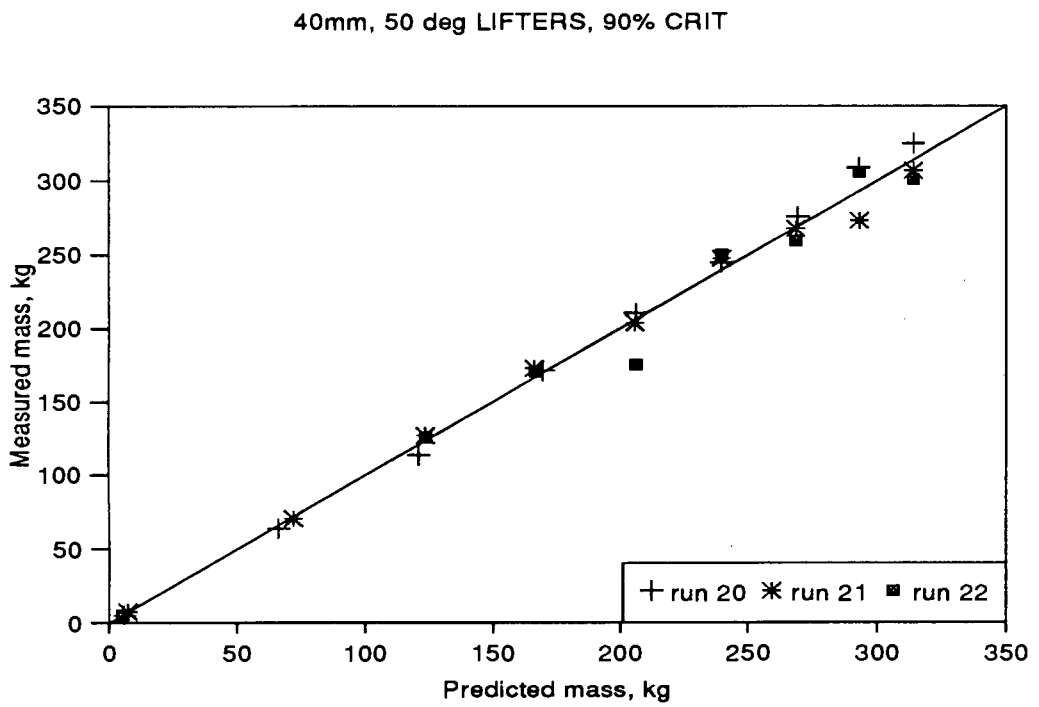

Figure 192. Comparison of experimental and predicted data, test 8

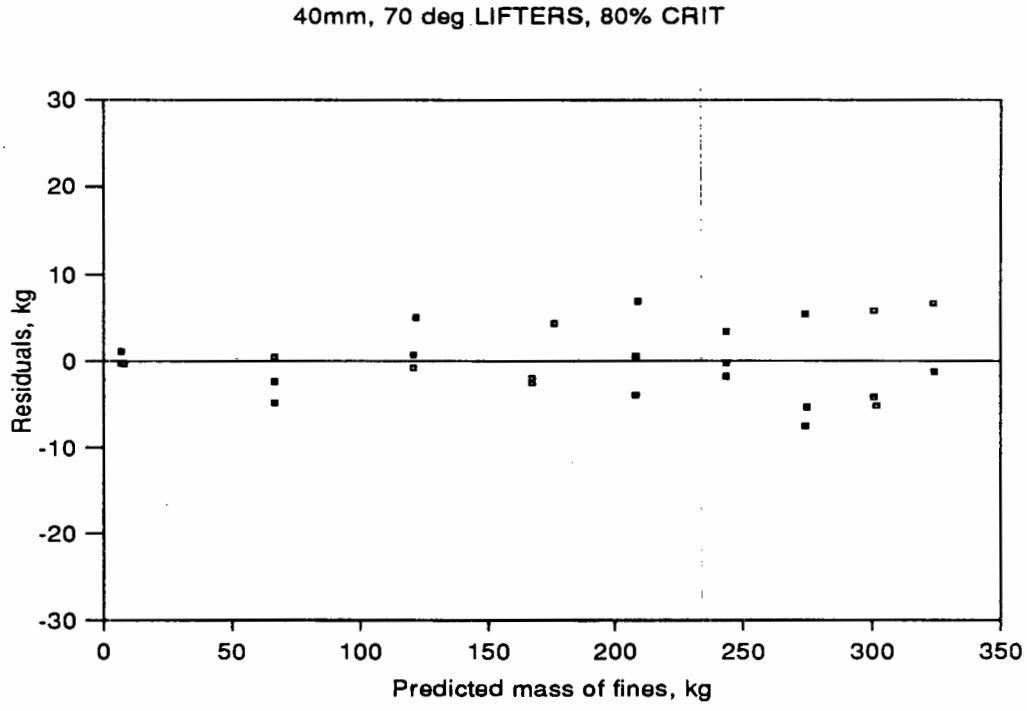

Figure 193. Residuals of test 9

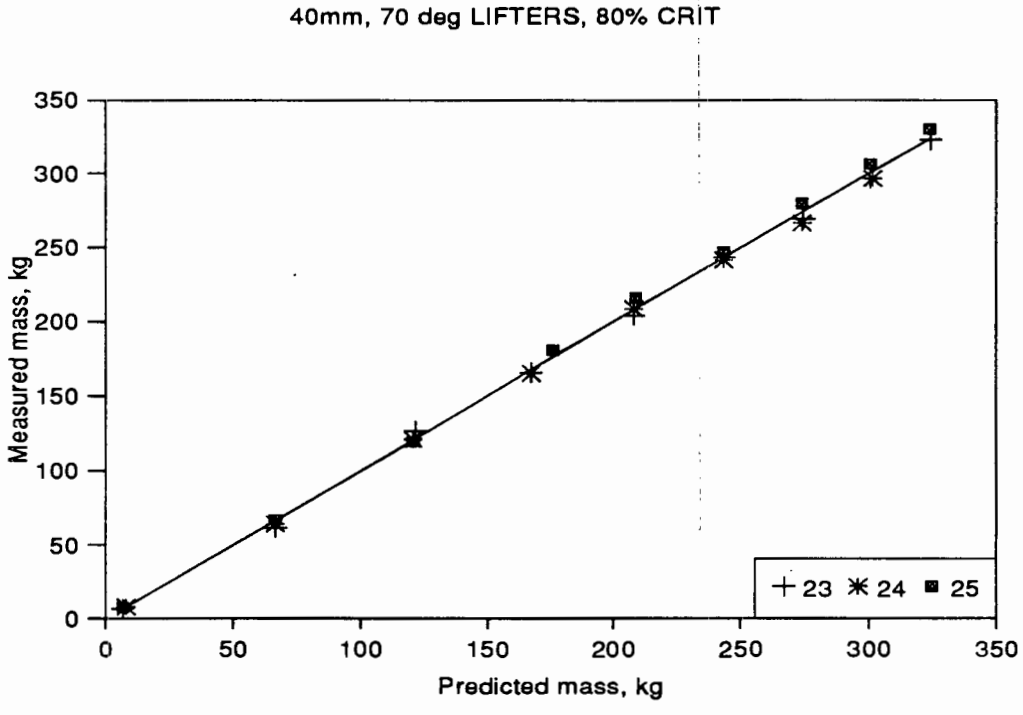

Figure 194. Comparison of experimental and predicted data, test 9